University of London

Imperial College of Science and Technology

COLLAPSE OF STRINGER-STIFFENED CYLINDERS

by

NICHOLAS AGELIDIS

A thesis submitted for the degree of Doctor of Philosophy

in the Faculty of Engineering of the University of London

and for the Diploma of Membership of Imperial College

Steel Structures Section

Civil Engineering Department

September 1984

to Lamya

ABSTRACT

This thesis considers the buckling behaviour of longitudinally-stiffened cylindrical shells under combinations of axial compression and external pressure.

The first part of the work deals with the testing of ten experimental models. These comprised a large-scale model loaded under axial compression and small-scale models loaded either axially or under combined axial load and pressure. In all cases detailed measurements were made of the initial shapes of the model surfaces, and of their deflections and stresses during loading. A range of failure modes, including both local panel buckling and orthotropic buckling, was observed.

All the cylinders were analysed using a finite element model consisting of a single stiffener and its associated shell. The analysis is capable of modelling the behaviour of cylinders that fail by local or axisymmetric buckling. For the experiments that failed in these modes it gave good predictions both of the collapse load and the stresses and displacements.

An extensive parametric study was then undertaken using the finite element analysis over a broad range of practical shell geometries that would also fail in these modes. The geometric variables, the type of loading, magnitude and shape of inital imperfections, stiffening ratio, residual stresses and shape of stiffeners were all varied.

The experimental and analytical results were compared with current design codes, which were critically reviewed. Recommendations were made for improved design formulations.

ACKNOWLEDGEMENTS

This work was carried out in the Steel Structures Section of Imperial College, under the supervision of Professor P. J. Dowling. His guidance, advice and encouragement throughout the project are most deeply and sincerely appreciated.

The project was funded by the UK Department of Energy and the Science and Engineering Research Council; one series of experiments was sponsored by Det norske Veritas.

I wish to thank the skilled staff of the Structures Laboratory, who in the pleasant atmosphere inspired by the expert supervision of the evercheerful Mr. J. Neale, made my period in the laboratory one of the most enjoyable parts of the work.

My thanks also go to Mr. N.D. Scott and Mr. P.J.D. Guile and their staff of craftsmen at R.M.E. who create models of the finest quality; to Professor A. C. Walker of Surrey University for making available the hyperbaric testing facility, and to Mr S. McCall for his assistance in its use. For the advice and help of Dr. J. E. Harding and Mr. W. Fahy, whose testing rigs I inherited, I am grateful.

I also wish to acknowledge the efforts of Dr. U. Trueb and Mr. D. N. Bates in developing their excellent program FINAS, and thank them for their patient assistance and advice in using it.

The photographic work was expertly carried out by Mr. R. Packer, Mr. A. Chipling and Mrs. J. Gurr; Mr. D. Rashid assisted in the data preparation for the plotting of the load-deflection curves of the parametric study. I am very grateful to Mr. M. Chryssanthopoulos, who

carefully proofread the entire text.

Finally, thank you to all my colleagues, whose advice was often sought and freely given, and whose friendship I hope will outlive my stay at Imperial College.

NOTATION

A_s cross-sectional area of stringer

a_s ratio of area of stringer to area of panel

d depth of stringer

E Young's modulus

e local deviation of shell from true circle

g gauge length for imperfection measurements

L length of cylinder

m number of axial waves

N number of stringers

n number of circumferential waves

n_5 number of circumferential waves in five panel F.E. analyses

P axial load

p external pressure

R radius

s panel breadth

t thickness of shell

t_s thickness of stringer

Z $\sqrt{1-\nu^2}\ L^2/Rt$

Z_s $\sqrt{1-\nu^2}\ s^2/Rt$

α σ_x/σ_θ

Δ initial imperfection

$\Delta R+$ maximum outward imperfection

$\Delta R-$ maximum inward imperfection

δ imperfection tolerance

η plasticity reduction

θ Koiter's curvature parameter

λ slenderness $(=\sqrt{\sigma_o/\sigma_e})$

$\bar{\lambda}_x$ slenderness $(=\sqrt{\sigma_o/\sigma_{ex}})$

$\bar{\lambda}_\theta$ slenderness $(=\sqrt{\sigma_o/\sigma_{e\theta}})$

ν Poisson's ratio

σ_e elastic critical stress

σ_x axial stress

σ_θ nominal hoop stress (=pR/t)

σ_o yield stress

$\bar{\sigma}$ von Mises equivalent stress

φ plasticity reduction factor

ψ imperfection sensitivity parameter ($=\sigma_{\Delta}/\sigma_{\Delta/2}$)

Subscripts

a,b "primary" or "secondary" peak (see Sect. 4.3.1)

c characteristic strength (elastoplastic)

exp experimental

FE finite element

l local

o overall

s stringer

u maximum load (not subsequently exceeded)

w web

x axial

Δ "standard" imperfection magnitude

$\Delta/2$ half of "standard" imperfection magnitude

θ circumferential

1 inital peak or change in slope (subsequently exceeded)

Superscripts

$\bar{}$ normalized with respect to: yield stress (for stresses)
shell thickness (for dimensions)

Other symbols are defined as they appear in the text

CONTENTS

ABSTRACT 3

ACKNOWLEDGEMENTS 4

NOTATION 6

CHAPTER ONE
INTRODUCTION AND LITERATURE SURVEY

1.1 INTRODUCTION 15
1.2 LITERATURE REVIEW 16
1.2.1 SHELL THEORIES 17
1.2.1.1 Linear Theories 17
1.2.1.1.1 First order 18
1.2.1.1.2 Higher order 18
1.2.1.2 Nonlinear Theories 18
1.2.1.2.1 Shallow shells 19
1.2.1.2.2 Non-shallow shells 19
1.2.2 AXIALLY-LOADED CYLINDERS 19
1.2.2.1 Isotropic cylinders 19
1.2.2.1.1 Linear or Classical analysis 20
1.2.2.1.2 Early modifications 20
1.2.2.1.3 Minimum postbuckling load 21
1.2.2.1.4 Initial postbuckling theory 23
1.2.2.1.5 Nonlinear prebuckling analysis 25
1.2.2.1.6 Form of buckling pattern 27
1.2.2.1.7 Influence of boundary conditions 27
1.2.2.1.8 Plastic buckling 29
1.2.2.2 Stringer-stiffened cylinders 32
1.2.2.2.1 Smeared stiffener theory 32
1.2.2.2.2 Eccentricity of stiffeners 33
1.2.2.2.3 Effect of boundary conditions 34
1.2.2.2.4 Effect of eccentricity of loading 35
1.2.2.2.5 Linear v's nonlinear analysis 35
1.2.2.2.6 Effect of initial imperfections 36
1.2.2.2.7 Lower bound approaches 37
1.2.2.2.8 Plastic buckling 38
1.2.2.2.9 Discrete stiffeners 38
1.2.2.2.10 Local panel buckling 40

1.2.2.2.11 Mode interaction 40
1.2.3 PRESSURE-LOADED CYLINDERS 41
1.2.3.1 Local shell buckling 42
1.2.3.2 General buckling 44
1.2.3.3 Effect of initial imperfections 45
1.2.3.4 Effect of plasticity 47
1.2.4 COMBINED AXIAL COMPRESSION AND EXTERNAL PRESSURE . . . 48
1.2.5 OFFSHORE-RELATED RESEARCH 50
1.2.6 EXPERIMENTAL INVESTIGATIONS 54
1.2.6.1 General 55
1.2.6.2 Fabricated steel specimens 56
1.2.6.3 Ring stiffened cylinders 57
1.2.6.4 Stringer-stiffened models 58
1.3 AIMS OF THESIS 58
1.4 LAYOUT OF THESIS 60

C H A P T E R T W O
E X P E R I M E N T A L T E S T S

2.1 GENERAL 61
2.2 LARGE-SCALE CYLINDER TEST 62
2.2.1 INTRODUCTION 62
2.2.2 MATERIAL TESTING 64
2.2.3 FABRICATION 64
2.2.4 RESIDUAL STRAINS 65
2.2.5 INITIAL IMPERFECTIONS 66
2.2.6 TEST RIG 69
2.2.7 INSTRUMENTATION 70
2.2.8 ELASTIC TEST 70
2.2.9 FAILURE TEST 72
2.2.9.1 Strain gauge results 73
2.2.9.2 Deflections 75
2.2.10 DISCUSSION 77
2.3 SMALL-SCALE MODELS 80
2.3.1 INTRODUCTION 80
2.3.2 MODEL DESCRIPTION AND MANUFACTURE 80
2.3.3 MATERIAL TESTING 81
2.3.4 IMPERFECTION MEASURING EQUIPMENT 82
2.3.4.1 Shell surface imperfections 82
2.3.4.2 Stiffener imperfections 83
2.3.5 IMPERFECTION RESULTS 84
2.3.6 INSTRUMENTATION 86

2.3.7 TEST RIG 87
2.3.8 SETTING UP OF MODELS 87
2.3.9 TEST PROCEDURE 88
2.3.10 DESCRIPTION OF TESTS 89
2.3.11 RADIAL DEFLECTION DATA 90
2.3.12 STRAIN GAUGE DATA 92
2.3.13 DISCUSSION 96
2.4 SLENDER SMALL-SCALE SERIES 97
2.4.1 INTRODUCTION 97
2.4.2 MANUFACTURE 98
2.4.3 MATERIAL TESTING 98
2.4.4 INITIAL IMPERFECTIONS 99
2.4.5 AXIALLY-LOADED MODELS 100
2.4.5.1 General 100
2.4.5.2 Description of tests 100
2.4.5.3 Radial deflection data 101
2.4.5.2 Strain gauge results 102
2.4.6 HYDROSTATIC AND COMBINED LOADING TESTS 104
2.4.6.1 Testing equipment and procedure 105
2.4.6.2 Strain gauging 106
2.4.6.3 Hydrostatically-loaded models 106
2.4.6.4 Combined axial compression and pressure loaded models 108
2.4.7 DISCUSSION 110

C H A P T E R T H R E E

N U M E R I C A L A N A L Y S I S

3.1 INTRODUCTION 223
3.2 COLUMN ANALOGY 224
3.3 DESCRIPTION OF FINITE ELEMENT PROGRAM 'FINAS' 227
3.3.1 FINITE ELEMENTS 227
3.3.2 SOLUTION 228
3.4 DESCRIPTION OF FINITE ELEMENT MODEL 230
3.4.1 GENERAL 230
3.4.2 NUMBER OF ELEMENTS 230
3.4.3 BOUNDARY CONDITIONS 231
3.4.4 LOADING 232
3.5 CONVERGENCE STUDY 233
3.6 ANALYSIS OF EXPERIMENTAL MODELS 235
3.6.1 INITIAL IMPERFECTIONS 235
3.6.1.1 Imperfection mode 235

3.6.1.2 Imperfection magnitude 237
3.6.1.3 Imperfection amplitudes for higher modes 237
3.6.2 DNV SERIES 238
3.6.3 LARGE-SCALE CYLINDER IC4 243
3.6.4 SLENDER SERIES 246
3.7 CONCLUSIONS 249

C H A P T E R F O U R
P A R A M E T R I C S T U D Y

4.1 INTRODUCTION 268
4.2 PRELIMINARIES 270
4.2.1 RANGE OF PARAMETERS 270
4.2.2 PRELIMINARY DETERMINATION OF EXTENT OF STUDY 271
4.2.3 MATERIAL PROPERTIES 273
4.2.4 BOUNDARY CONDITIONS AND LOADING 273
4.2.5 INITIAL IMPERFECTIONS 275
4.2.5.1 Imperfection magnitude 275
4.2.5.2 Imperfection mode 278
4.2.5.3 Eigenvalue study 279
4.2.5.4 Variation of amplitude with mode shape 282
4.2.5.5 Shortcomings of the eigenvalue study 282
4.2.6 PRESENTATION OF RESULTS 284
4.3 CYLINDER GEOMETRY STUDY 286
4.3.1 FORM OF LOAD-DEFLECTION GRAPHS 286
4.3.2 AXIAL LOAD 287
4.3.2.1 Load-deflection paths 287
4.3.2.2 First yield 288
4.3.2.3 Deflection modes 289
4.3.2.4 Effect of geometric parameters 291
4.3.2.4.1 Length of cylinder 291
4.3.2.4.2 Number of stiffeners 292
4.3.2.4.3 Radius to thickness ratio 293
4.3.3 PRESSURE LOAD 293
4.3.3.1 Load-deflection paths 293
4.3.3.2 Load capacity of pressure-loaded cylinders 294
4.3.3.3 First yield 295
4.3.3.4 Deflection modes 296
4.3.3.5 Effect of geometric parameters 297
4.3.3.5.1 Length of cylinder 297
4.3.3.5.2 Number of stiffeners 298
4.3.3.5.3 Radius to thickness ratio 298

4.3.4 AXIAL-DOMINANT COMBINED LOAD 298
4.3.4.1 Load-deflection paths 298
4.3.4.2 First yield 299
4.3.4.3 Deflection modes 299
4.3.4.4 Effect of geometric parameters 300
4.3.4.4.1 Length of cylinder 300
4.3.4.4.2 Number of stiffeners 300
4.3.4.4.3 Radius to thickness ratio 300
4.3.5 PRESSURE-DOMINANT COMBINED LOAD 301
4.3.5.1 Load-deflection paths 301
4.3.5.2 First yield 302
4.3.5.3 Deflection modes 302
4.3.5.4 Effect of geometric parameters 302
4.3.6 INTERACTION BEHAVIOUR 302
4.3.6.1 Definition of cylinder strength 303
4.3.6.2 Interaction curves 308
4.4 IMPERFECTION SENSITIVITY 309
4.4.1 GENERAL 309
4.4.2 AXIAL LOAD 311
4.4.2.1 Load-deflection paths 311
4.4.2.2 First yield location 311
4.4.2.3 Deflection mode 312
4.4.2.4 Imperfection sensitivity 312
4.4.3 PRESSURE LOAD 313
4.4.3.1 Load-deflection paths 313
4.4.3.2 First yield location 314
4.4.3.3 Deflection mode 314
4.4.3.4 Imperfection sensitivity 314
4.4.4 COMBINED LOAD 315
4.4.5 SUMMARY 315
4.5 STIFFENING RATIO STUDY 315
4.5.1 AXIAL LOAD 316
4.5.2 PRESSURE LOAD 317
4.5.2.1 First yield position 317
4.5.2.2 Deflection mode 317
4.5.2.3 Effect on strength 318
4.5.3 COMBINED LOAD 319
4.5.4 INTERACTION BEHAVIOUR 319
4.6 RESIDUAL STRESSES 320
4.6.1 GENERAL 320

4.6.2 RESIDUAL STRESS DISTRIBUTION 320
4.6.3 AXIAL LOAD 323
4.6.4 PRESSURE LOAD 323
4.6.5 COMBINED LOAD 324
4.6.6 SUMMARY 324
4.7 STIFFENER SLENDERNESS 325
4.7.1 AXIAL LOAD 326
4.7.1.1 Load-deflection paths 326
4.7.1.2 First yield location 326
4.7.1.3 Deflection mode 326
4.7.2 PRESSURE LOAD 327
4.7.2.1 Load-deflection paths 327
4.7.3 COMBINED LOAD 327
4.7.4 SUMMARY 328
4.8 FIVE PANEL ANALYSES 328
4.8.1 INITIAL IMPERFECTIONS 330
4.8.2 AXIAL LOAD 331
4.8.3 PRESSURE LOAD 333
4.8.4 CONCLUSIONS 334
4.9 SUMMARY 334
4.9.1 AXIAL LOAD 335
4.9.2 PRESSURE LOAD 336
4.9.3 COMBINED LOAD 337
4.10 CONCLUSION 338

CHAPTER FIVE
ASSESSMENT OF
CURRENT DESIGN RULES

5.1 INTRODUCTION 409
5.2 AXIALLY-LOADED CYLINDERS 409
5.2.1 LOCAL BUCKLING 409
5.2.2 IMPERFECTION SENSITIVITY 412
5.2.3 OVERALL BUCKLING 414
5.2.4 EXPERIMENTAL MODELS 417
5.2.5 RESIDUAL STRESSES 419
5.2.6 SUMMARY 420
5.3 PRESSURE-LOADED CYLINDERS 421
5.3.1 LATERALLY-LOADED BEAM MODE 423
5.3.2 EXPERIMENTAL MODELS 427
5.4 INTERACTION BEHAVIOUR 428
5.5 CONCLUSIONS 433

CHAPTER SIX
CONCLUSIONS AND SUGGESTIONS FOR FUTURE WORK

6.1 CONCLUSIONS 454
6.1.1 EXPERIMENTAL RESULTS 454
6.1.2 NUMERICAL RESULTS 457
6.2 SUGGESTIONS FOR FUTURE WORK 459

REFERENCES 462

APPENDIX A APPROXIMATE DETERMINATION OF MINIMUM STIFFENING RATIO FOR LOCAL BUCKLING MODE 477
A.1 GENERAL 477
A.2 AXIAL COMPRESSION 478
A.2.1 Local buckling 478
A.2.2 Overall buckling 478
A.2.3 Equate local and overall buckling stresses 478
A.3 EXTERNAL PRESSURE 479
A.3.1 Local buckling 479
A.3.2 Overall buckling 480
A.3.3 Equate local and overall buckling stresses 480

APPENDIX B LOAD-DEFLECTION CURVES FROM PARAMETRIC STUDY 481

APPENDIX C MATERIAL STRESS-STRAIN CURVES 545

CHAPTER ONE

INTRODUCTION AND LITERATURE REVIEW

1.1 INTRODUCTION

Steel cylindrical shells have been used in offshore structures for many decades. The original structural systems conceived for the shallow waters of the Mexican Gulf had to be modified for the deeper and more hostile North Sea. In particular, the more severe environment made the overload condition a more important design consideration than it had been for structures in calmer waters, for which fatigue had often governed the design.

Although concrete is often a viable alternative for fixed production platforms, steel continues to be the most commonly used material. In addition, mobile exploration and drilling structures are almost always made of steel.

One of the primary elements in all these structures is the cylindrical shell. The desire to minimize the structural weight, especially for bouyant structures, while improving the load capacity and response characteristics, has promoted the use of more slender stiffened cylinders. A major factor affecting the design of such elements is their collapse or buckling behaviour.

Research into the behaviour of cylindrical shells has recieved a strong impetus on several occasions in the past. The 1940's and 50's saw a large concentration of effort in the study of shells for airplane fuselages, which was later applied and extended to the design of aerospace vehicles. Widespread use has also been made of

cylindrical shells for submarines, storage tanks, nuclear containment vessels and many other structures.

The nature of cylindrical shells is such that the differences in the geometric proportions and material properties utilized in each application often produced significant changes in the structural behaviour. This has limited the extent to which extrapolation of results from different fields has been possible. The structural form, loading and environmental conditions, material properties and method of fabrication employed in offshore structures make them substantially different to the cylindrical shells used elsewhere. The lack of information specific to this area prompted major research efforts at various centres. In Britain, a large programme was funded by the Department of Energy and the Science and Engineering Research Council, of which this work is part.

1.2 LITERATURE REVIEW

Cylindrical shells combine the attributes of structural efficiency, simplicity of form and complexity of behaviour. This unique combination has, on the one hand, promoted their extensive use and, on the other, has necessitated considerable investigation, both from theoretical and practical standpoints. The inherent complexity of the subject has resulted in one of the most voluminous literatures of any engineering field. Consequently, a survey of this subject can only describe the more important and durable aspects of the theory, which has developed over seventy or so years.

The first section of this survey presents a very brief classification of various shell theories. The major part of the review has been somewhat arbitrarily subdivided for ease of presentation into research dealing with cylinders loaded by axial

compression, external pressure or combinations of both, even though much of this work was concurrent and closely related. Since the study of axially-loaded cylinders is presented first and more of the problems inherent in cylinder behaviour were encountered in its context, it is dealt with in somewhat greater detail.

Each of these sections presents the work establishing the current state of the theory of cylinder buckling. More recent investigations specifically for the offshore field and usually with an emphasis towards design is summarized in the next section. Finally, a brief review is presented of the evolution of experimental techniques used in cylinder buckling research.

1.2.1 SHELL THEORIES

The essence of any mathematical description of shell behaviour is judicious approximation, and all the theories which have been developed represent different compromises between mathematical exactness and ease (or possibility) of solution. Common to all of them is the reduction of the three-dimensional problem to one of a surface, from which the behaviour of any point in the shell can be inferred. The task, which can be approached with extreme mathematical formalism, is sufficiently complex to have occupied the minds of many applied mathematicians for decades. Little more than an overview is attempted here.

1.2.1.1 Linear Theories

Theories described as "linear" assume that displacements are small and occur without rotation of the shell. This is equivalent to the ommission of all higher order displacement terms from the equations.

1.2.1.1.1 First order

Many shell theories are of this type; they assume that the ratio of the thickness of the shell to its radius of curvature is negligible compared with unity. Love [1] invoked this approximation in conjunction with those applied by Kirchhoff in thin plate analysis: i) that normals to the reference surface remain straight and normal after deformation (i.e. the transverse shear resistance is infinite) and ii) that the transverse normal stress is negligible. Refinements of Love's theory have been presented by Budiansky and Sanders [2] and Koiter [3].

A useful simplification of the first order equations for the particular case of circular cylindrical shells was derived by Donnell [4] in a linear version of an analogous large displacement formulation.

1.2.1.1.2 Higher order

Some theories have been based on the assumption that only the terms containing the thickness to radius ratio to quadratic or higher order can be neglected. Flugge [5] developed such a theory. Koiter [6] showed that the accuracy is not improved by such a refinement unless an approximation of equivalent magnitude, the neglect of transverse shearing deformations, is also eliminated. Reissner [7], Mindlin [8] and Naghdi [9] have presented theories in which this ommission is not made.

1.2.1.2 Nonlinear Theories

Small, but finite, deflections of a shell will, in general, entail rotations. A theory which attempts to take account of these effects must contain nonlinear displacement terms. Because of their

complexity, nonlinear shell equations were first derived for specific shell geometries.

1.2.1.2.1 Shallow shells

A shell qualifies for inclusion in this category if the wavelength of its deformation mode is small relative to its radius of curvature. In this sense, not only truly "shallow" shells but even complete cylinders can, in many cases, be handled with accuracy by theories of this sort. Donnell [10] was the first to develop large-deflection shell equations, for the particular case of cylindrical shells. He included nonlinear terms similar to those in the von Karman equations for flat plates. Donnell's theory was subsequently extended by Vlasov [11] to shallow shells of otherwise general geometry. Reissner [12] presented a set of equations applicable to shells of revolution.

1.2.1.2.2 Non-shallow shells

A general, but incomplete, theory of shells was presented by Novozhilov [13]. Sanders [14], Budiansky [15] and Koiter [16], among others, have developed general nonlinear shell equations.

1.2.2 AXIALLY-LOADED CYLINDERS

1.2.2.1 Isotropic cylinders

Although this thesis is concerned with stringer-stiffened cylinders, it is convenient to begin the review with the work carried out on isotropic cylindrical shells, in which the direction of much of the later research was established.

1.2.2.1.1 Linear or "Classical" analysis

The problem of stability of a cylindrical shell under axial loading was first addressed by Lorenz [17] in 1911. Within a few years Southwell [18], Timoshenko [19] and von Mises [20] also presented solutions for this problem.

Essentially, these methods adopted the "classical" stability approach. By analogy with the previous studies of columns, it was assumed that the initial deviations from the perfect shape and the subsequent deformations were small. The point at which these deflections became indeterminately large, or at which the potential energy of the system became negative, represented a bifurcation point in the cylinder's behaviour: the mode of deflection was assumed to change suddenly from a linear prebuckling shape to some lateral mode. The load at which this occurred was termed the (classical) critical load.

In contrast to the behaviour of columns, however, the critical load was an extremely elusive quantity in practice. Experiments rarely attained more than half of this load and usually much less. Something was obviously wrong or inadequate in the linear theory, and several attempts were made to bring it into conformity with the experimental results.

1.2.2.1.2 Early modifications

Flugge [5] carried out tests on relatively stocky celluloid cylinders which failed at loads in the upper range of the experimental scatter. He suspected that the discrepancy was due to radial restraint at the ends of the cylinder and initial deviations from the perfect shape; he was able to show, in fact, that localized stresses beyond the yield limit of the material would be produced before the

critical load was reached, and thus to account for the differences he observed.

Later tests by Lundquist [21] and Donnell [10] on much thinner aluminium cylinders produced failure loads too low for Flugge's explanation to be adequate. Donnell [10] attempted to include the effects of initial imperfections by applying his nonlinear shallow shell equations to the problem. However, the analysis was oversimplified and the results were unsatisfactory.

Further attempts to explain the phenomenon were made along different lines in three key papers which influenced much of the subsequent research. One thing had become clear: linear stability theory was incapable of furnishing an acceptable solution to the problem, and refined theories would be required.

1.2.2.1.3 Minimum postbuckling load

In 1941, von Karman and Tsien [22] used Donnell's large-deflection equations to investigate the postbuckling behaviour of cylindrical shells. Their analysis, having been carried out for a perfect cylinder without end effects, predicted the same maximum load as the classical analysis. However, their results showed that for a large range of applied load three equilibrium positions were possible: they discovered that the load-deflection path fell suddenly at buckling, and, after reaching a minimum value of approximately one-third of the buckling load, began to rise again.

von Karman and Tsien interpreted the experimentally observed behaviour of shells as a "jump" from the prebuckling to the postbuckling path prior to the attainment of the bifurcation load, induced by small unavoidable external disturbances. Tsien [23] developed an "energy criterion", which stated that the transition

would occur at a stress for which the potential energies before and after the jump were equal. He predicted that the failure loads of cylinders loaded in a rigid testing machine and under gravity loading would be different.

von Karman and Tsien obtained solutions to the large-deflection equations by assuming an expression for the radial deflection which approximated the observed "diamond" pattern. The total potential energy, expressed in terms of wavelength and amplitude parameters, was minimized with respect to the amplitude terms, for assumed values of the wavelength ratios. Leggett and Jones [24] were able to carry out the minimization with respect to the wavelength parameters as well, and the procedure was further refined by Michielsen [25] and Kempner [26]. Each successive improvement produced a reduction in the minimum value of the postbuckling load.

Almroth [27] obtained computer solutions to the minimization problem for increasing numbers of terms in the displacement function. He came to the conclusion that the minimum postbuckling load for his ten term approximation, which was only about one-tenth of the buckling load, approached the true limiting value.

Initially, the interest in quantifying the minimum postbuckling load arose from the assumption that it represented a reliable and useful lower bound to the load-carrying capacity of a practical shell. It became apparent, however, that this was not the case: there was no logical reason why the postbuckling minimum should be related to the prebuckling peak load, and for high values of R/t the assumption was not always conservative, whilst for low R/t's it was overly so.

The whole exercise was shown to be a futile one by Hoff et al [28], who demonstrated that a completely accurate calculation would

yield a minimum postbuckling load which tended to zero for vanishing thickness to radius ratios. Although a real cylinder would have a non-zero minimum load, the significance attached to this minimum had been diminished.

Nevertheless, some investigators pursued the same general line of attack and produced refined estimates of postbukling load values; Esslinger and Geier [29], for example, suggested that the appropriate minimum is the one for a buckling mode consisting of square buckles.

A recent alternative lower bound approach was proposed by Batista and Croll [30]. They identified the components of the membrane stiffness of the shell which are, on the one hand a major stabilizing factor on the cylinder's initial behaviour, and on the other, severely eroded during buckling. They postulate that a useful lower bound solution is obtained by neglecting the contribution of this quantity to the stiffness of the cylinder.

1.2.2.1.4 Initial postbuckling theory

An alternative and elegant approach to the problem was proposed by Koiter [31]. This work was in Dutch and remained relatively obscure until a shorter English version appeared in 1963 [32]. Koiter was critical of the attempts to obtain a postbuckling minimum and argued that the relevant quantity from a logical and practical point of view was the maximum load that the structure could support before buckling. He restricted his attention to the behaviour in the vicinity of the bifurcation point, and was able to relate the initial stage of postbuckling behaviour to the stability or instability of equilibrium at the critical point itself.

The method is based on an analysis of the potential energy of the system. For the case of the perfect structure, the bifurcation load

is found, as in the classical analysis, by equating the second derivative of the potential energy to zero. Koiter showed that the secondary equilibrium path for the perfect system can have an upward or downward slope. The exact form, in the vicinity of the bifurcation point, is defined by the values of the third and fourth variations of the potential energy. The assumption that the incremental displacements are of the same shape as the buckling mode "linearizes" the problem and greatly simplifies its solution.

The cases in which the secondary equilibrium path slopes downward were recognized by Koiter to be imperfection sensitive. By appending a correction term for the effect of initial imperfections to the potential energy expression, it is possible to determine the limit load of a structure with small imperfections. The analysis in the case of several simultaneous or nearly simultaneous modes, as occur in cylindrical shells, is similar but considerably more complicated. Koiter found that the limit load for a cylindrical shell was extremely sensitive to initial imperfections and that the plot of limit load against imperfection magnitude has, in fact, a vertical tangent at zero imperfection.

Because higher order terms in the energy expressions were neglected, the analysis is strictly valid in an asymptotic sense only, that is, for small values of imperfection. In an alternative analysis, Koiter [33] considered imperfections of finite magnitude but axisymmetric shape and predicted similar, but even more imperfection-sensitive, behaviour.

The initial postbuckling technique has been applied to a large range of buckling problems by workers at University College and Harvard. An extensive review by Hutchinson and Koiter [34] outlines and references much of this work. Hutchinson [35] used a large-

deflection, Donnell-type analysis to study the effect of axisymmetric and asymmetric imperfections on the buckling load of internally pressurized, axially-loaded cylinders. He found that the axisymmetric type were generally more damaging and was able to account for the discrepancy between experimental and theoretical results. He also found that the considerably simpler Koiter analysis gave quite accurate results.

The best experimental confirmation of the initial postbuckling approach was obtained in a series of tests on an eccentrically loaded, two bay frame by Roorda [36]. Agreement between theory and experiment was excellent, due to the precision with which both the mathematical and physical problems can be handled.

The large number of parameters which influence the behaviour means that precise quantitative validation for an axially-loaded cylinder is not as easily established; nevertheless, encouraging correlation was obtained in a series of experiments by Tennyson and Muggeridge [37], in which known sinusoidal axisymmetric imperfections were machined or cast into test specimens. The experimental buckling loads were compared with an extended version of Koiter's general theory and with accurate numerical results obtained using a large-deflection numerical solution, which included the effects of nonlinear prebuckling and end conditions. A similar method was used by Hutchinson et al [38] in a study of more localized axisymmetric imperfections.

1.2.2.1.5 Nonlinear prebuckling analysis

A third type of approach was initiated by Donnell and Wan [39]. They included in their analysis the effect of an idealized form of initial imperfection, and obtained a nonlinear solution to the entire

load-deflection path. They assumed that the most detrimental form of imperfection is of the same shape as the deflection surface, and related to it through an empirical proportionality constant termed the "uneveness" factor, which depends on the method of fabrication of the shell. Unfortunately, the initial shape was not fixed, but followed the form of the constantly changing deflection mode during the minimization process.

Donnell and Wan used the nonlinear, large-deflection equations obtained previously by Donnell [10]. They assumed an initial deformation function similar to, but more general than, the one used by von Karman and Tsien, and arrived at an expression for the potential energy which they minimized, with considerable effort, with respect to the five displacement parameters. They obtained a family of load-deflection curves for various values of the uneveness factor, and an imperfection sensitivity plot similar to that obtained by Koiter [31].

Although Koiter's results were unknown to them, and would remain so for several more years, their entirely different method had yielded a quantitative desription of the buckling phenomenon similar to his, albeit with considerably greater computational effort.

Almroth et al [40] conducted a series of experiments to compare the hypotheses of von Karman and Tsien against those of Donnell and Wan. Thin aluminium and nickel cylinders were tested under dead weight loading and controlled end-shortening, for which von Karman and Tsien predicted different buckling loads. Because the models buckled elastically, they could be retested under different conditions and levels of external disturbance. The results showed that the same cylinder buckled at similar loads for the various test methods, but that nominally identical cylinders buckled at loads exhibiting

considerable scatter. The buckling load was influenced much more by the properties of the models themselves than by the loading arrangement, and the Tsien energy criterion was shown to be invalid.

The general philosophy of Donnell and Wan's method of following the load-deflection path up to, and perhaps beyond, the peak load is the approach of many current general computer programs, even though the numerical methods employed are completely different.

1.2.2.1.6 Form of buckling pattern

Yoshimura [41] suggested a geometrical explanation, which bears his name, for the observed buckling mode shapes. He discovered that a cylinder can be transformed into a polyhedral surface consisting of identical plane triangles without stretching of the midsurface. Small bending stresses are required to eliminate the initial curvature of the triangles, and bending stresses also arise along the ridge lines of the polyhedron. Since the extensional rigidity of the shell wall is proportional to the thickness whilst the bending rigidity is proportional to the cube of the thickness, a cylinder is more likely to buckle into the inextensional Yoshimura pattern as the shell becomes thinner; axisymmetric modes, involving less bending, are observed for stockier cylinders.

1.2.2.1.7 Influence of boundary conditions

The instigators of all three methods considered infinitely long cylinders, and the task of incorporating boundary effects was left to subsequent investigators. There are primarily two ways in which the presence of boundary conditions modifies the solution for the infinitely long cylinder. The first is that the various degrees of restraint will affect the allowable buckling mode shapes and, consequently, the classical buckling load. This effect can be

investigated, somewhat inconsistently, by assuming linear prebuckling, and this was the approach of Hoff and Soong [42]. They used the small deflection, Donnell-type equations to calculate the critical load for nine different edge support conditions. They found that rotational restraint at the ends had little effect on all but very short cylinders, and that only in the case of cylinders whose edges were free to move tangentially was there any significant change in the critical load; in those cases it was approximately one-half of that for simply supported cylinders.

The second effect is that the radial restraint at the ends of the cylinder will prevent any Poisson expansion at these positions, and hence produce a nonlinear, barrelling-type prebuckling deformation. Stein [43] used a Donnell-type analysis for a perfect shell of finite length with radial end restraints to illustrate the importance of the effect.

Almroth [44] used a finite difference computer analysis to solve the cases in which both effects are included. He confirmed the findings of previous investigators and showed that the neglect of radial restaints could result in buckling loads 20% greater than if they were included.

The extension of Koiter's initial postbuckling theory [31] to include the effects of nonlinear prebuckling deformations was carried out by Cohen [45].

The more recent developments in the study of elastic isotropic cylinders, most of which are concerned primarily with analytical refinements, will not be reviewed here. Since many of these have been modified and incorporated into the literature on stiffened cylinders, they will be encountered in the next section.

1.2.2.1.8 Plastic buckling

The buckling behaviour of cylinders in the plastic range has received much less attention than elastic buckling. Bijlaard [46] made use of the deformation theory of plasticity to investigate this problem and found that buckling into the asymmetric mode required a slightly higher load than into the axisymmetric mode. In a subsequent investigation Gerard [47] obtained similar results by using the small-deflection Donnell equations and assuming deformation theory and an axisymmetric buckling mode. Both Bijlaard and Gerard justified their use of deformation theory, which cannot represent material unloading, by suggesting that the existence of small unavoidable imperfections would produce simultaneous axial load and bending, and that a sudden bifurcation and strain reversal would not occur at buckling; however, neither one considered the effect of imperfections in his analysis. Their predictions agreed very well with available experimental results.

The more rigorous incremental, or flow, theory of plasticity was also used by Bijlaard [46] but, as had already been found in many other plastic buckling problems, it significantly overestimated the buckling load. Lee [48] attempted to bring the incremental theory predictions into closer agreement with test results by considering the effects of initial imperfections in a large-deflection analysis. However, once again, deformation theory gave the better estimates.

A discussion of this paradox, which is not yet fully resolved, is given by Hutchinson [49] in a review of plastic buckling theory. The explanation appears to be related to the existence of corners in the yield surface.

Batterman [50] conducted a series of tests on cylinders with

R/t's between 10 and 120. For quite stocky cylinders, Batterman was able to obtain accurate predictions from both deformation and incremental theories by assuming an axisymmetric hinge model for the buckled shape. For less stocky cylinders, the neglect of initial imperfections in the analysis may have been the cause of the overestimation of the experimental loads; for cylinders with R/t's greater than about 80 the observed mode was asymmetric and the predictions were poor.

Murphy and Lee [51] were the first to include the effects of radial edge restraint in plastic buckling calculations, and found that the incremental theory predictions were considerably improved. Most axially-loaded cylinders buckling in the plastic range develop localized axisymmetric bulges near one or both ends (e.g. Sobel and Newman [52]). This prebuckling deformation tends to be much more significant than initial imperfections for stocky cylinders. Gellin [53] found that an axially-loaded cylinder is less sensitive to imperfections if it buckles in the plastic range than if it had buckled elastically.

Tvergaard [54] and Hutchinson [49] reviewed the development of initial postbuckling analyses which include plasticity, a field to which they themselves are the main contributors. A major problem in applying such methods to imperfect cylinders is that the maximum load is some distance beyond the bifurcation point and elastic unloading will usually occur before it is reached. An asymptotic, Koiter-type expression for the peak load is, therefore, not strictly valid.

A different approach was used by Nimmer and Mayers [55], who represented the Yoshimura buckling pattern [41] by a mechanism model consisting of bars which resist extensional and shear deformations connected by nodes which resist the bending and twisting deformations.

The deformation theory of plasticity was used, and the results compared reasonably well with other theories. Nonlinear material effects were seen to have a diminishing but noticeable effect for R/t's up to 500.

In recent practice, an investigation of geometrically and materially nonlinear behaviour is usually carried out numerically using one of the general-purpose computer programs currently available.

Harding [57] used a finite difference, dynamic relaxation method which included the effects of plasticity to calculate complete load-deflection paths of imperfect cylinders under axial compression and pressure. He determined the large influence of the axial imperfection mode on the buckling load and pointed out that design codes, which place tolerances on the imperfection magnitudes but do not consider the mode shapes, can, in many cases, be unconservative.

Despite the development of a number of theoretical models for plastic buckling, methods allowing for plasticity in the design of shells are usually semi-empirical. In particular, two approaches are widely used.

The first, called the η-method, is most frequently used in structures that are only slightly affected by plasticity (e.g. Gerard and Becker [56]). η is a reduction factor relating the elastoplatic buckling strength to the elastic critical stress, for which expressions can be derived from theories of plasticity. Usually, however, an empirical formulation is used in design codes (e.g. ASME N-284 [156]).

The second method uses a parameter, φ, dependent upon the structural slenderness, to relate the elastoplastic strength to the

yield stress and is better suited to more stocky structures. This is the approach adopted by the DnV Rules [153], for example.

1.2.2.2 Stringer-stiffened cylinders

The strength of cylindrical shells can be enhanced, and their postbuckling behaviour tempered, by the addition of stiffeners. For the case of a cylinder stiffened by rings and stringers several types of buckling behaviour are possible:

i) the shell skin may buckle between stiffeners (local)

ii) the shell and stringer unit may buckle between rings (panel or overall)

iii) the shell, stringers and rings may buckle as a unit (general)

iv) the stiffeners may buckle locally (stiffener instability)

1.2.2.2.1 Smeared stiffener theory

The earliest analyses of stiffened cylinders were carried out using modified versions of methods that had been applied to isotropic cylinders. The discrete stiffeners were treated by "smearing" their properties throughout the shell, resulting in an equivalent orthotropic material. This technique is applicable to closely-stiffened cylinders in which the deflection mode will involve several stiffeners in conjunction with the shell. Such methods, therefore, are useful in the investigation of the general or panel buckling behaviour of cylinders. For the closely-stiffened cylinders used in the aerospace industry, this was often the controlling mode, and a large amount of work has been carried out using this method. Singer [58] presents a review of stiffened cylinder research, much of which was based on the smearing technique.

Becker and Gerard [59] and Gerard [60] developed a theory for cylinders with orthotropic properties. They used a linear, small

deflection analysis, and, by making simplifications applicable to different ranges of cylinder length, obtained buckling load predictions for axially-loaded cylinders. Milligan et al [61] tested the theory in a series of experiments on aluminium cylinders which had very shallow, integrally machined stiffeners, and therefore failed to highlight the theory's neglect of stiffener eccentricity. The correlation was reasonable, with the poorest agreement for cylinders in which the stiffening was approximately equal in both directions.

1.2.2.2.2 Eccentricity of stiffeners

As early as 1947, van der Neut [62] recognized the importance of taking account of the eccentricity of the stiffeners relative to the shell midsurface. However, little further work was done in this area until Baruch and Singer [63] formulated rigidity expressions in which the contributions due to the eccentricities of the stiffeners were incorporated. In a later paper, Singer et al [64] investigated the importance of this effect for axially-loaded cylinders. The modified force-displacement relations were substituted into the Donnell stability equations and a linear prebuckling pattern assumed. They obtained solutions for simple and clamped supports and found that, for all but very short cylinders, outside stiffening produced considerably higher buckling loads. They also investigated the influence of various stiffener cross-section parameters on the maximum load.

Block et al [65] used similar rigidity expressions in a classical buckling analysis of axially-loaded, simply supported, stiffened cylinders. Their analysis was also capable of considering a shell composed of genuinely orthotropic material, in addition to the stiffening. They neglected prebuckling deformations, and through the minimization of a potential energy function arrived at a buckling equation which is still often used today, (e.g. ECCS [155], ASME N-

284 [156]). Hedgepeth and Hall [66] used an alternative simplified method, in which the bending and twisting rigidities of the skin and the twisting rigidity of the stiffeners were neglected.

The significant effect that stiffener location was predicted to have on the buckling load of the shell was investigated experimentally by Card and Jones [67]. They tested six pairs of cylinders with integrally machined or Z-section stiffeners; in each pair one model had stiffeners attached to the inside and the other to the outside of the shell. The cylinders with external stiffeners carried up to twice the load of their internally-stiffened counterparts, as was predicted by the method of Block et al [65].

Burns [68], in an optimization study of stiffened cylinders, found that the optimum stiffener shapes may be different for internally and externally-stiffened cylinders; the effect of stiffener location for practical designs will therefore be less than that predicted by assuming the use of the same stiffeners in both cases.

1.2.2.2.3 Effect of boundary conditions

As in the case of isotropic cylinders, a rigorous incorporation of general boundary conditions requires a twofold refinement. The modified critical load can be calculated with linear theory and is discussed here. The effect of nonlinear prebuckling deflections is discussed in Section 1.2.2.2.5..

Soong [69] and Singer et al [70] showed that clamping produced a much more significant increase in the buckling load in axially-stiffened cylinders than in isotropic cylinders. Obviously, the increased bending rigidity provided by the stringers will extend the range over which the boundary conditions have an effect. In a series of experiments Card and Jones [67] observed the effect of clamping in

cylinders with lengths up to ten times their radius.

Singer and Rosen [71] found that, in contrast to the behaviour of isotropic shells, circumferential restraint had a minor effect on the buckling load of stiffened shells. However, constraining the loaded edges to remain straight increased the buckling load by up to 50% in some cases.

1.2.2.2.4 Effect of eccentricity of loading

The effect of axial load applied at an eccentricity to the shell-stiffener centroid was first analysed by Stuhlman et al [72] and Block [73]. Their findings, which were later confirmed by Weller et al [74], showed that eccentricity of loading produced a significant change in the buckling load, the magnitude and sign of which depended on the direction of eccentricity and location of stringers.

1.2.2.2.5 Linear v's nonlinear analysis

Little disagreement exists among researchers that an accurate investigation of isotropic cylinder buckling requires the consideration of nonlinear prebuckling effects. Many arguments have been put forward, however, claiming that for axially-stiffened shells a linear analysis is sufficient.

Van der Neut [75] and Hedgepeth and Hall [66] suggested that, because stiffened shells have a much larger effective thickness than unstiffened shells, initial imperfections play an insignificant role and a linear analysis is adequate. Also, because the buckling mode of stiffened cylinders is usually unique, the imperfection sensitivity produced in isotropic shells by the interaction of several simultaneous modes does not occur. Singer [76] claimed that linear theory is applicable to heavily and closely-stiffened cylinders, and

suggested a sufficiently narrow panel in terms of Koiter's [98] curvature parameter (see Sect. 1.2.2.2.10). Arbocz and Babcock [77] and Arbocz and Sechler [78] showed that a much larger effect resulted from the inclusion, in a linear analysis, of specific boundary conditions than the further effect due to the nonlinear prebuckling deformations that these would produce.

On the other hand, Stein [79], in an appraisal of recent research work, argued that it is both "consistent" and necessary to include both effects. Hutchinson and Frauenthal [80] showed that, although the trends in the behaviour of stiffened cylinders calculated in an earlier analysis by Hutchinson and Amazigo [81] were correct, inclusion of nonlinear prebuckling did modify the quantitative results. Sheinman and Simitses [82] found that the buckling mode shape calculated for the limit point of an imperfect cylinder will, in general, be different to that predicted by a linear analysis. Finally, Tennyson et al [83] demonstrated that an accurate investigation of the interaction between local and global modes requires the use of nonlinear theory.

The general conclusion seems to be that, although the peak load predicted using linear theory may be reasonably accurate for many cases, a detailed study including effects such as imperfections and interacting modes should be carried out using a nonlinear analysis. The preference for linear analyses was stronger before the widespread availability of general nonlinear computer codes.

1.2.2.2.6 Effect of initial imperfections

Hutchinson and Amazigo [81] studied the imperfection sensitivity of stiffened cylinders using Koiter's [31] postbuckling theory. They assumed linear prebuckling displacements and found that, whilst

considerably less than for isotropic cylinders, the imperfection sensitivity of stiffened cylinders was still considerable. They calculated that a sudden increase in the imperfection sensitivity occurs for relatively short shells. However, this effect had not been observed in tests, and a later refinement of the method which included nonlinear prebuckling by Hutchinson and Frauenthal [80] removed this discrepancy. They also showed that most effects that tend to increase the buckling load, such as stiffener eccentricity, load eccentricity and stiffener location, tend also to increase the imperfection sensitivity.

An alternative approach was followed by Arbocz and Babcock [84]. They used the so-called Multi-mode analysis, in which a number of Fourier components of the initial imperfect shape could be incorporated. The amplitudes of the imperfection modes were obtained from experimental measurements. The analytical failure loads could be made to agree reasonably well with the experiments by including a sufficient number of mode shapes. The selection of the appropriate modes is quite important and some guidance was given. The results were also compared by Arbocz and Sechler [78] with an extended analysis in which nonlinear prebuckling deflections were considered and found to be reasonably accurate. A useful assessment of these methods and the range of application of each is given by Arbocz and Babcock [85].

1.2.2.2.7 Lower bound approaches

Thielemann and Esslinger [86] pursued their minimum postbuckling approach [29] for the case of stringer-stiffened cylinders. They calculated the stable parts of the postbuckling curves for various buckling modes by looking at the sign of the second variation of the potential energy, and were thus able to arrive at a lower bound

estimate for the buckling load.

The reduced stiffness aproach of Batista and Croll [30] was extended by Ellinas et al [87] to the elastic overall buckling behaviour of stringer-stiffened cylinders. They incorporated the orthotropic shell properties into the analysis and found that the effect of using stringers was not always as advantageous to the strength or imperfection sensitivity of the shell as was often thought. In an extensive appraisal of experimental data and a comparison with the reduced stiffness approach, Ellinas and Croll [88] conclude that the imperfection sensitivity of elastically buckling stringer-stiffened cylinders is more significant than previously accepted. Also they suggest the use of clamped ends as more easily attainable and better defined boundary conditions for future testing.

1.2.2.2.8 Plastic buckling

A small number of papers extended earlier smeared stiffener theories into the plastic range. The first, by Gerard [89], incorporated the deformation theory of plasticity in the method of Becker and Gerard [59]. However, in common with that analysis, it oversimplified the representation of the stiffeners.

Jones [90], used the more appropriate theory of Block et al [65] in conjunction with the deformation theory of plasticity. However, even this analysis neglected prebuckling deformations and initial imperfections.

1.2.2.2.9 Discrete stiffeners

All the analyses described so far idealized the shell-stiffener cross-section as a uniform orthotropic shell. An alternative theory was developed by Block [73] and Singer and Haftka [91] to account for

the discreteness of the ring stiffeners, which even in the closely-stiffened aerospace shells were often too far apart for smearing to be valid. Singer and Haftka considered the stiffeners as linear discontinuities represented by the Dirac delta function. In a subsequent paper, Singer and Haftka [92] applied this method to axially-loaded stringer-stiffened cylinders, and analysed shells with the minimum number of stringers necessary to ensure general, rather than local, buckling, thus maximizing the discreteness effect for that mode. The maximum reduction in buckling load for the cases which they investigated was 14%, but this would probably be larger if the stringers were even more widely spaced to induce local buckling.

Wang and Lin [93] treated the stiffeners and the panels between them as individual components which were coupled by displacement continuity constraints along their intersections. They found that for very few stiffeners, when the local buckling of the shell panels was critical, the buckling load was insensitive to the number of stiffeners. Esslinger and Geier [94] reported the same effect in a series of experiments on Mylar cylinders.

Syngellakis and Walker [95] studied the critical and post-critical behaviour of perfect broad-panelled cylinders, in which the stiffeners were treated as narrow plates. From experimental evidence they assumed the deflected shape was antisymmetric about the stiffener. They found that a number of critical modes existed in close proximity to one another and postulated a high imperfection sensitivity. In a later paper [96] they also included the effect of initial imperfections of the same form as the critical mode. Reddy [97] extended the method to include plasticity and found that the critical stress of the stiffened cylinder may fall below that of the unstiffened cylinder if the torsional rigidity of the stringers is

low.

1.2.2.2.10 Local panel buckling

The most important contribution in this field is probably that by Koiter [98]. He applied his initial postbuckling theory [31] to the case of a simply supported curved panel under axial compression, and found that the postbuckling behaviour, and hence the imperfection sensitivity, was dependent upon the degree of curvature, or narrowness, of the panel. Flat panels have a stable postbuckling path, whilst strongly curved panels are unstable and significantly imperfection sensitive. Koiter defined a measure of the curvature and determined its magnitude at the transition between stable and unstable behaviour. His assumption of simply supported edges is not strictly valid for panels bounded by stiffeners with finite torsional rigidity. The analysis was modified to include this effect, as well as the presence of internal pressure, by Stephens [99].

Tvergaard [100] extended this analysis further by considering a panel buckling in the plastic range. He neglected the effect of elastic unloading, but a comparison with an incremental numerical solution showed that this did not lead to significant errors.

More recently, Dowling and Ho [101] used a finite differece method to study the elastoplastic behaviour of simply supported cylindrical panels, and found the imperfection sensitivity generally to be less than that of complete cylinders.

1.2.2.2.11 Mode interaction

The trend towards "optimum" designs in which local and overall buckling modes occur almost simultaneously has prompted some work on the imperfection sensitivity produced by the interaction of modes.

Byskov and Hutchinson [102] used the analyses developed by Hutchinson and Amazigo [81] for general buckling and Koiter [98] for local buckling to obtain postbuckling coefficients necessary for a multimode initial postbuckling analysis as desribed by Koiter [31]. The presence of mode interaction resulted in a much weaker dependence of the buckling load on the number of stiffeners than for either mode considered individually. A more refined analysis was carried out by Byskov and Hansen [103] in which the overall mode was calculated assuming discrete rather that smeared stringers and the torsional and bending rigidities of the stiffeners were incorporated as boundary conditions in the local shell buckling analysis.

By assuming that the wavelength of the overall modes is much larger that that of the local mode, Koiter [104] considered the interaction phenomenon as a modulation of the local mode amplitude due to the presence of the overall mode. His initial postbuckling solutions show mode interaction to always have a detrimental effect.

1.2.3 PRESSURE-LOADED CYLINDERS

In many respects the development of the theory for the buckling of cylinders under external pressure followed a similar sequence to that for axially-loaded cylinders. The two cases were studied concurrently, and several papers dealt with both. The review of pressure-loaded cylinder research will be relatively brief since many developments have already been discussed in the previous section. The following deals mainly with ring-stiffened shells since stringer-stiffened cylinders under external pressure have received far less attention. An extensive and useful review of the literature on cylindrical shells under external pressure has recently been compiled by Tsang and Harding [105].

1.2.3.1 Local shell buckling

Cylindrical shells under external pressure are often stiffened by rings which can considerably enhance their strength. This section will review the work carried out on the elastic buckling of unstiffened cylinders and the inter-ring buckling of stiffened cylinders.

An early solution for an infinitely long cylinder under external pressure was given by Levy [106], who considered a ring of unit width under a radial load. Von Mises [20] used small deflection theory to analyse a cylinder of finite length by assuming a deflection mode consistent with simple supports at the ends. In a later study [107] he added the effect of axial compression caused by hydrostatic loading.

Windenberg and Trilling [108] carried out a number of experimental tests and in a comparison of all the known experimental data and theoretical formulae found that agreement was reasonable for longer cylinders, but poor for short cylinders. They attempted to explain this by proposing a thinness parameter, and suggesting that buckling took place elastically when this was large, and inelastically when it was small. They also recommended a simplified expression, which over the range of applicability of the von Mises equation gave critical pressures within a few percent of it.

Nash [109] observed that the assumed deflection modes used in preceding analyses did not coincide with the experimental observations for ring-stiffened cylinders. He incorporated a more appropriate shell deflection pattern, which allowed for torsionally stiff rings, and also included a number of components of the strain energy of the rings, but obtained poor correlation with experimental strengths.

Nevertheless, Wenk et al [110], describing a series of tests on ring-stiffened cylinders, suggested that the fully clamped edge conditions assumed by Nash were essentially correct. Bijlard [111] allowed for the effect of rings by calculating a shell effective length based upon the torsional rigidity of the stiffeners.

Batdorf [112] used the Donnell shell equations to derive an expression for the critical buckling load similar to that of von Mises. He identified the geometric parameter, Z ($=\sqrt{1-\nu^2}\,\frac{L^2}{Rt}$), which bears his name, and was able to relate the buckling pressure to it. However, because of the shallow shell assumption that the wavelength is small compared to the radius, the theory is not applicable to short cylinders, which buckle with few circumferential waves.

An attempt to remove this limitation was made by Loo [113], who suggested that the problem stemmed from the neglect of transverse shear stresses. However, Armenakas and Hermann [114] criticized his addition of extra energy terms because it made the stiffness matrix unsymmetric. Soong [115] applied the more accurate shell equations derived by Sanders [14], which do not require that the number of circumferential waves is large. He found significant discrepancies between his and previous analyses for long, thick cylinders.

Yamaki [116] compared the buckling strengths obtained using the Donnell and the more accurate Flugge equations, and found the Donnell theory to be satisfactory if the number of circumferential waves is greater than five. He assumed linear prebuckling and considered the effect of boundary conditions only on the form of the allowable buckling mode. Sobel [117] had shown that rotational restraints at the ends of a cylinder had a significant effect on the buckling pressures only of short cylinders and that cylinders of intermediate length were more strongly influenced by the axial restraint along

their ends.

Stein [43] pointed out the inadequacy of considering the boundary restraints only in the selection of allowable displacement modes and that an accurate analysis would also require a consideration of the prebuckling deformations that these induce. In a later paper, Yamaki [118] included this effect and found major differences with his previous analysis for cylinders with Z less than approximately 10.

1.2.3.2 General buckling

If, in a ring-stiffened cylinder, the ring spacing is small and the ring strength inadequate, the development of a general buckling mode including the stiffeners is possible. An early approach to this problem is that of Tokugawa [119], whose solution was a summation of the strength of the ring and of the shell buckling separately. Using a different approach, and making more appropriate estimates of the shell-stiffener interaction, Bryant [120] arrived at similar results.

Salerno and Levine [121] adopted an energy approach, in which they assumed a buckling configuration that extended over the entire shell-frame assembly. They obtained a strain energy expression including shell and ring contributions and minimized the total potential to obtain the buckling load.

An omission in this work was discovered and corrected by Kendrick [122,123] in a three part set of design recommendations. In part I Kendrick assumed a smoothly-varying deflection mode along the cylinder, while in part III he superimposed local inter-ring deflections. His predictions were confirmed by a series of experimental models tested by Reynolds and Blumenberg [124].

Bodner [125] applied a "smeared stiffener" approach by analysing

an equivalent orthotropic shell, neglecting, however, the eccentricity of the stiffeners relative to the shell midsurface. Orthotropic shell properties including this effect were derived by Baruch and Singer [63], whose method subsequently found widespread use for axially-loaded cylinders.

1.2.3.3 Effect of initial imperfections

The strengths of moderately long elastic cylinders (Z>100) that buckled elastically agreed well with the simple theories, but shorter models buckled at loads considerably below the theoretical values. The discrepancy was much smaller than that which faced the analysts of axially-loaded cylinders, but nonetheless considerable.

Sturm [126] in 1941 realised the importance of initial imperfections as a source of this discrepancy and derived an expression for the allowable pressure of an unstiffened cylinder in terms of the amplitude of the initial out-of-roundness.

Bodner and Berks [127] presented a modified form of the Donnell equations which included initial imperfections. Their shell equations were used by Galletly and Bart [128] to study the effect of clamped boundary conditions in association with initial imperfections. They obtained expressions for the total principal stresses, which were then related through the von Mises yield criterion to give an estimate of the pressure at which yielding began. They found that although the effect of clamped boundaries had been considerable in previous analyses of perfect cylinders, it was less significant when inital imperfections were considered.

Holt [129] suggested that the most appropriate measure of out-of-roundness in real cylinders is the radial deviation of the shell from a perfect arc of length equal to the preferred buckling half-

wavelength. Galletly and Bart obtained the best correlation with experiments using this as the measure of initial imperfection in their calculations; it has remained the basis of out-of-roundness measurement in several current design codes.

Donnell [130] followed the procedure that he and Wan [39] had applied to axially-loaded cylinders to determine the effect of imperfections in elastic cylinders under hydrostatic pressure. The assumption of typical imperfection levels resulted in strengths significantly below those predicted by the von Mises theory and in good agreement with experimental results. An alternative approach, yielding similar conclusions, was also followed by Nash [131].

Kempner et al [132] investigated the postbuckling behaviour of cylindrical shells under hydrostatic pressure and found that, in contrast to the situation in axially-loaded cylinders, in many cases stable (i.e. rising) postbuckling paths existed. For small Z values, however, they found postbuckling equilibrium states at pressures less than the buckling value, and inferred that cylinders in this range were imperfection sensitive.

This was confirmed by Budiansky and Amazigo [133], who applied Koiter's initial postbuckling theory [31] and found that significant imperfection sensitivity can be expected in cylinders whose Z is less than 100. They had assumed an initial imperfection of the same form as the buckled shape, but in later papers Amazigo and Frazer [134] and Amazigo [135] obtained similar findings for localized dimple imperfections and random imperfections respectively.

Montague [136] conducted a series of tests on mild steel cylinders under external pressure and found three ranges of behaviour, which he distinguished approximately in terms of Windenberg and

Trilling's [108] thinness parameter: thin shells buckled elastically and could be analysed adequately by elastic buckling theories; thick shells buckled plastically and required the use of plastic theories; the strength of shells in the intermediate range, he found, could not be predicted accurately by either theory and required an analysis including the effects of initial imperfections.

1.2.3.4 Effect of plasticity

Sturm [126] had recognised the importance of plasticity in the buckling of cylinders in his 1941 paper and suggested that his theory could be applied to shells stressed beyond the elastic limit by the use of an effective modulus of elasticity. Hodge [137] developed a rigid plastic analysis using the Tresca yield criterion for the collapse pressure of short cylinders that failed by yielding rather than instability.

Two distinct modes of inter-ring buckling can occur in cylinders under external pressure that fail inelastically: axisymmetric collapse, in which the radial deflections along any circumference are uniform, and asymmetric or lobar buckling, in which alternate inward and outward lobes develop around the circumference of the shell.

In his experimental investigation of externally pressurized cylinders, Montague [136] observed that the axisymmetric mode occurred in short cylinders, while lobar buckling took place in the longer cylinders. He also found that the simple yield stress limit on the circumferential membrane stress was an acceptable estimate of the collapse pressure.

Axisymmetric buckling was investigated experimentally by Lunchick [138], who found that the use of the von Mises yield criterion gave better agreement with the tests than did a limit on the maximum normal

stress. He later developed an analysis [139] based on the deformation theory of plasticity for the case of short cylinders under hydrostatic pressure.

Reynolds [140] investigated the asymmetric mode of failure and derived expressions based on the differential equations of Gerard [47] for the buckling strength of cylinders of elastic-perfectly-plastic and elastic-strain-hardening material. Despite neglecting the effects of imperfections and prebuckling deformations, he obtained excellent agreement with a series of experimental tests.

Recently, Reis and Walker [141] studied the local buckling behaviour of ring-stiffened cylinders, considering both elastic and inelastic collapse. They confirmed the imperfection sensitivity behaviour found by Budiansky and Amazigo [133] and established the importance of nonlinear prebuckling effects on the occurrence of first yield.

Lunchick [142] developed an analysis based on the deformation theory of plasticity for the inelastic general buckling strength of ring-stiffened cylinders.

Ellinas and Croll [143] have also applied their reduced stiffness method to the elastoplastic analysis of the general buckling of ring-stiffened cylinders.

1.2.4 COMBINED AXIAL COMPRESSION AND EXTERNAL PRESSURE

Many combinations of applied loads are frequently encountered in shell structures, but one of particular interest to the offshore field is that of axial compression and external pressure.

Timoshenko [144] presented an analysis of this problem for

elastic simply-supported cylinders. Based on this equation, Sharman [145] suggested a linear interaction as a close lower bound for design, which was incorporated into several design recommendations (e.g. Gerard and Becker [57]).

Starting with the Donnell equations and an assumed displacement function, Lakshmikantham and Gerard [146] derived an expression for the axial buckling stress in terms of the loading ratio. A similar approach by Krishnamoorthy [147] yielded a solution for clamped boundary conditions.

Zyczkowski and Bucko [148] employed a generalized power series to determine the elastic buckling stress of a cylindrical shell under simultaneous loads. Using the von Mises yield criterion, they also determined the limiting slenderness, beyond which their elastic theory would not be valid.

Weingarten and Seide [149] carried out a series of elastic combined loading tests on Mylar cylinders and cones, and concluded that a linear interaction curve was an acceptable lower bound, but a more accurate description would involve the R/t ratio and probably the L/R ratio. Hutchinson [150] was able to account for the scatter in the axial-dominant loading range of their experimental results by applying Koiter's [31] analysis and considering axisymmetric imperfections.

Tennyson et al [151] obtained theoretical interaction curves for elastic isotropic cylinders by formulating the problem as an eigenvalue analysis. They found that the shape of the curves varied significantly depending on the Z of the cylinder. For the longer cylinders (Z>200) they found the curves to be reasonably uniform and suggested an approximate design curve. For very short cylinders

(Z<20) they calculated that the interaction curve was convex and will not be bounded by the simple linear interaction often used for design. They also tested a series of Mylar models which displayed a similar but less marked trend. However, steel cylinders of these proportions will not buckle elastically and this is not a phenomenon that structural engineers need consider.

Reis et al [152] obtained interaction curves for the elastoplastic collapse of cylindrical shells with axisymmetric imperfections. They observed that the initial imperfection modes causing the largest deterioration of strength were different if buckling was elastic or plastic.

1.2.5 OFFSHORE-RELATED RESEARCH

More recently, in the context of the cylindrical shells encountered in offshore structures, a number of papers have proposed simplified analytical methods with an emphasis towards the development of design procedures for such structures. Papers of this style often considered several forms of stiffening, types of loading and buckling modes, offering recommendations for each, and are difficult to summarize in detail. A brief review will, nevertheless, be attempted.

Several design codes are now available which deal with the buckling of stringer-stiffened cylinders (e.g. DnV Rules [153], DnV Classification Notes [154], ECCS Rules [155], ASME N-284 [156]), and a discussion of these is given in Chapter 5.

Samuelson and Vestergren [157] proposed a design method for axially-loaded, stringer-stiffened cylinders which became the basis for the ECCS Draft Rules [155]. Beginning with the elastic buckling stresses for a flat plate and a curved panel and the orthotropic theory of Block et al [65], the authors obtained predictions for the

strengths of cylinders by applying semi-empirical knockdown factors for plasticity and initial imperfections. In a comparison with experimental results, Samuelson [158] found the method gave acceptable design predictions.

On the basis of experimental observations, Walker and Sridharan [159] subdivided stringer-stiffened cylinders under axial load into broad-panelled and narrow-panelled geometries, and proposed simple design formulations for each. The former, which buckle locally, were analysed as simply supported flat plates. The latter fail in overall modes and were analysed by considering a column consisting of a stiffener and a flat plate resting on an elastic foundation representing the hoop stiffness of the shell. Interacting local buckling was included by using the effective width concept. Good agreement with experimental results was observed for both modes.

Faulkner et al [160] proposed limit state design criteria for stringer-stiffened cylinders under axial compression, external compression or both. The proposed method used an effective width approach in the calculation of the axial strength, and was shown to agree well with experimental results, although pressure loading was treated less comprehensively. A parabolic interaction was used to determine the cylinder strength for combined loading cases.

Croll and Ellinas [161] applied their reduced stiffness analysis to the study of stiffened cylinders under combined loading that fail in axisymmetric modes. Pressure-induced deformations, boundary effects and geometric imperfections were incorporated as an equivalent imperfection in a "column-type" bifurcation analysis.

Several workers at DnV have been involved in developing more accurate design procedures than those contained in the DnV Rules.

Valsgard and Steen [162] extended the flat plate Robertson approach of the DnV Rules to incorporate the effect of shell curvature. A beam-column on an elastic foundation was used to model the shell-stiffener combination, for which a first yield criterion was used to define failure.

The general buckling of orthogonally-stiffened cylinders subjected to axial compression, external pressure and shear was studied by Steen and Valsgard [163]. Recommendations were made regarding the sizing of rings to avoid general buckling using two methods. The first ensured an adequate margin between the characteristic buckling strengths in the general mode (including rings) and the panel mode (between rings). The second considered the most heavily loaded region of the shell and applied a yield criterion on the local stresses, into which amplified stresses were incorporated, reflecting the effect of initial imperfections and prebuckling deformations.

This method was extended by Steen et al [164] to stringer-stiffened cylinders under combined loading. Their proposed design method was compared by Harding et al [165] with the experimental results of the stocky small-scale series of cylinders described in this thesis, and is discussed in greater detail in Chapter 5.

Many aspects of cylinder buckling were considered by Odland [166] including various types of loading, stiffening and buckling modes. His approach is essentially that of the DnV Rules, although an interaction equation was proposed which was incorporated in the DnV Notes, and will also be discussed more fully in Chapter 5. Briefly, however, Odland was able to devise an interaction curve whose shape changed from linear to concave by including an effective stress term in the interaction equation; the interaction approaches a straight

line for elastic structures and the von Mises curve for stocky plastic structures.

A number of recent papers have realized the need for more data on the behaviour of cylinders under combined axial and pressure loading. Harding [167] used an elastoplastic large deflection analysis, employing the finite difference technique to calculate the strengths of ring-stiffened cylinders under combined loading and demonstrated the importance of initial imperfection mode and magnitude on behaviour.

Walker et al [168] carried out a series of tests on unstiffened cylindrical shells under combined loading and were unsatisfied with the correlation with codes and other analytical interaction curves. Tsang et al [169] reported a series of experiments on ring-stiffened cylinders, for which the code predictions were generally conservative.

A numerical approach was followed by Galletly and Pemsing [170], who employed the BOSOR 5 computer program to calculate interaction curves for unstiffened cylinders with axisymmetric imperfections. Although conservative, the linear interaction curve of the ECCS Rules was recommended as a suitable design approach. They also found the interaction curve suggested by Odland to be less conservative but still safe, but appeared wary of recommending it until more extensive experimental correlation is available. Their general findings were confirmed by the experimental study of Galletly et al [171] on small unstiffened models.

Miller [172] compared the strength predictions of the API Rules and ASME N-284. The latter neglect any interaction between axial and hoop compression when buckling is inelastic. He proposed instead to use the ASME elastic interaction equations to predict a buckling

stress for combined load, which is then reduced by the plasticity reduction factors used in the rules. Although an improvement, this procedure still yields curves suggesting significantly less interaction between the loads than is assumed by other design methods.

Miller et al [173] presented the results from part of a series of ring-stiffened and orthogonally-stiffened cylinders tested under combined loading. These were welded specimens of relatively large scale, some of which were stress-relieved before testing. The results, when available, should be valuable in assessing the interaction of axial and pressure load in stringer-stiffened cylinders and the effect of residual stresses.

Recently, Ellinas et al [198] have carried out a major and very valuable compilation of experimental results and code predictions for the buckling behaviour of many of the structural elements found in offshore structures. They also highlight many of the areas where further work in needed.

1.2.6 EXPERIMENTAL INVESTIGATIONS

In few fields of engineering research is experimentation such a vital part as in the study of shell buckling; the dependence of the behaviour of shells on such a large number of parameters means that frequent experimental verification of theoretical analyses is vital. Because it forms such an integral part of shell buckling research, experimentation has evolved almost as greatly as analysis. An excellent survey of this development is given by Babcock [174]. Some of the more important advances in experimental techniques, rather than a presentation of results, will be given here.

1.2.6.1 General

Since the early experiments by Flugge [5] on stocky celluloid and rubber cylinders, a wide variety of materials have been used for the fabrication of models. Because much of the research has been directed primarily towards aerospace applications, there has been a natural preference for the use of aluminium and lightweight alloys; the most common fabrication method has been to machine the specimen, be it isotropic or stiffened, from heavy gauge or solid stock: e.g. Singer and Rosen [71], Hedgepeth and Hall [66], Card and Jones [67] and many others.

Despite the apparent contradiction, plastics can be very useful for elastic tests and have the added advantage that they can be tested repeatedly without an appreciable loss of strength. Esslinger and Geier [94] carried out an interesting study of ring- and stringer-stiffened cylinders using Mylar models. Tsao and Chin [175] conducted an experimental parametric study by successively removing stringers from a cylinder, to which they had been attached using double-sided tape.

Thompson [176] introduced a method, which was later used by Babcock and Sechler [177], of electroplating a machined wax mandrel which was subsequently melted out. A spin-casting technique developed by Tennyson [178] has produced some of the most perfect shell specimens, and also allows cylinders to be made with accurately predefined imperfections; see, for example, Tennyson [178], Tennyson and Muggeridge [37], Hutchinson et al [38].

Rather than produce specimens with specified imperfections, several investigators have attempted to measure the imperfections in models produced by more or less conventional fabrication techniques.

This is usually accomplished by taking a series of axial or circumferential scans of the cylinder surface. In earlier work these scans were not all referred to a common datum. It appears that Coppa [179] was the first to introduce the mean cylinder concept, albeit in a crude fashion. In later work by Arbocz and Babcock [77] and Arbocz and Williams [180] all the readings were reduced to a common "best fit" reference cylinder. Prebuckling deflection readings were also taken during the tests. Both aspects are features of past and present experimental work on shell buckling at Imperial College; see, for example, Dowling et al [181] and Fahy [182].

Other specialized techniques include the use of high speed photography, for example Esslinger and Geier [29], to investigate the modal shape changes at buckling, and vibration methods as a nondestructive technique for determining boundary conditions and buckling loads, Singer [183].

Many experiments have been conducted on fairly stocky specimens in which yielding takes place before the peak load is reached. For example, Lee [48] and Batterman [50] carried out such a series of tests on aluminium cylinders with R/t's between 10 and 120, and Sobel and Newman [52] tested stocky stainless steel cylinders with R/t's of approximately 18.

1.2.6.2 Fabricated steel specimens

With the increasing recent interest in stiffened cylinders for structural engineering, and in particular for offshore applications, researchers realized that the importance of effects such as welding-induced residual stresses, imperfections and plasticity on the behaviour of cylinders would cast doubt on the extrapolation of results obtained from experiments which did not include these effects.

Relatively little work, however, has been carried out on steel cylinders. A large number of hydrostatic tests were carried out on unstiffened and ring-stiffened cylinders at the David Taylor Model Basin in the 1950's and 60's to investigate the behaviour of submarine hulls, e.g. Galletly et al [184] and Lundchick [138].

Wilson and Newmark [185] and Wilson [186] tested a series of steel cylinders covering a large range of R/t values between 36 and 990, intended to be representative of the geometries encountered in elevated water tanks. More recently several series of tests on large fabricated cylinders have been conducted by various workers at Lehigh University: Marzullo and Ostapenko [187] tested fairly short stocky cylinders; Chen and Ross [188] tested longer thick-walled columns; and Ostapenko and Gunzelman [189] a series of short cylinders. Miller [190,191] reviewed and tabulated this and other data.

1.2.6.3 Ring stiffened cylinders

All these test programmes were concerned with unstiffened cylinders, and in 1977, Miller [190] commented that none of the stiffened cylinder tests reported in the literature had been on models fabricated by rolling and welding. In the same reference he presented results from two series of tests, one on large-scale and the other on small-scale ring-stiffened cylinders under axial load and pressure.

The recent research programme funded by the U.K. Department of Energy, of which some of the work reported in this thesis is part, had a considerable experimental content, and much of the following work is from that programme.

Large-scale, ring-stiffened specimens were tested by Dowling and Harding [192]. The method of fabrication and testing of the models

was followed in the large-scale stringer-stiffened cylinder experiment reported in this thesis. Walker et al [193] tested a series of small-scale unstiffened and ring-stiffened models.

1.2.6.4 Stringer-stiffened models

Walker et al [193] also conducted several tests on small-scale stringer-stiffened cylinders. The models were fabricated from 0.8 mm steel sheet, following a rolling and welding procedure developed by Walker and Davies [194], in which individual curved panels and stringers were welded using T-butt welds. Using the same material but an alternative fabrication technique, Dowling et al [195] also produced and tested small-scale stringer-stiffened models. This was the fabrication method used for the small models presented in this thesis and will be described in detail in Chapter 2. Green and Nelson [196] tested three large-scale stringer-stiffened models under axial compression.

Meanwhile in the United States, Kinra [197] tested two large orthogonally-stiffened models under hydrostatic pressure; in a somewhat questionable procedure, one of these was subsequently straightened and retested under axial load.

1.3 A I M S O F T H E S I S

At the time of initiation of this project relatively little data existed on the behaviour of stringer-stiffened cylinders under axial and combined loading, relevant to the offshore field. The aim of this thesis has been to contribute detailed experimental and numerical information on the behaviour of such elements.

An experimental investigation was carried out on a number of cylindrical models covering a range of geometries and failure modes.

Detailed measurements were taken both before and during the tests to enable an accurate description of behaviour to be compiled and explanations for the observations to be established.

As a complement to the experimental tests, extensive numerical analyses were performed. The finite element technique has developed into a powerful tool for the stability analysis of shell structures and has the potential to investigate a greater number of the parameters affecting the behaviour than any previous numerical model. It has been applied by several workers to the analysis of specific geometries, but not, to the present author's knowledge, in a broad systematic study of the governing parameters. It was thought that such an exercise would provide information of a more detailed nature than could be established experimentally. The recent development of a powerful nonlinear finite element package at Imperial College, which is capable of handling shell stability problems comprehensively and efficiently made such an undertaking feasible.

Based upon the observations from the experimental tests, a broad class of practical problems were identified as being suitable for economic analysis by the finite element method. A simplified model was suggested, and its predictions validated against the experimental results. The model was then applied over a broad range of variables, the extent of which was established using a more general analysis.

In order that other research workers can take advantage of these results in their own studies, both the experimental and numerical results have been presented in considerable detail.

The ultimate aim of this type of research is to produce improvements in design formulations, and towards this end all the generated results were compared with available design codes.

1.4 LAYOUT OF THESIS

Chapter 2 describes and presents the results of the experimental tests of ten stringer-stiffened cylindrical shells.

The possibility of analysing these models using a moderately sized finite element analysis is investigated in Chapter 3. The assumptions and limitations of the method are discussed and the results are compared with the experimental observations.

Chapter 4 applies the method to a large number of cases, the results of which are presented in detail. Conclusions regarding the effects of the various parameters are drawn.

An assessment of the principal design rules for stringer-stiffened cylinders on the basis of the experimental and parametric results forms Chapter 5.

The thesis is concluded in Chapter 6.

Tables and figures are presented at the end of the relevant chapter, with the exception of the load-deflection curves from the parametric study, which are included in an appendix.

CHAPTER TWO

EXPERIMENTAL TESTS

2.1 GENERAL

It was mentioned in the previous chapter that, although it has been the subject of some extremely complex mathematical analysis, shell buckling research has always relied heavily on experimental testing. The behaviour is too complex for total reliance to be placed in mathematical analysis. A large number of tests were carried out for the aeronautics and aerospace industries, in which interest was primarily in the geometric parameters. In structural engineering where it is also necessary to deal with material nonlinearity, and fabrication-induced residual stresses and imperfections, the need for experimentation may be even stronger. Of course, being, in general, stockier cylinders than those which are required to fly, cylinders used in structural engineering tend to be imperfection-sensitive to a lesser degree, but sensitive nevertheless.

Experimentation allows the development of a general understanding of behaviour through observation, but also enables a more accurate and complete modelling of the various parameters than may be possible in an analysis. Paramount amongst its functions is to bridge the gap between the analysis and the full-scale structure by allowing the validation of analytical methods against a series of models where full-scale behaviour would be difficult or impossible to test. The experimental philosophy which has evolved has tended intuitively to subdivide further the area between analysis and full-scale behaviour, filled by experimentation, into two broad, overlapping areas according

to whether the primary aim is the representation of a full-scale structure or the validation of analytical methods. Large-scale models, which can be fabricated by conventional methods to simulate effects present in prototype structures fall into the former group; small-scale models with well defined, even if not typical, properties, into the latter. Both large- and small-scale models were tested by the author. The distinction between the aims of modelling, whilst by no means clearcut, guided the selection, for example, of realistic boundary conditions for the large-scale model, and well-defined, although untypical, clamped ends for the small-scale models.

The author tested a total of ten stiffened cylinder models, one of large scale and the remainder of small scale, the proportion being similar to the relative costs of each. Obviously, the small models allow a more systematic and thorough investigation of the governing parameters. Once an analytical approach can be devised and verified against such models, a yet cheaper and more convenient means of parametric investigation will be available.

In this chapter the tests on the large-scale model, and on two series of small-scale models will be discussed in separate sections.

2.2 L A R G E - S C A L E C Y L I N D E R T E S T

2.2.1 INTRODUCTION

This model, designated IC4, formed part of a substantial series of tests funded by the Department of Energy and carried out at a number of centres around the U.K. [199].

In the original testing programme drawn up by the D.En., model IC4 was specified as a quarter-scale, eccentrically-loaded cylinder, stiffened by forty stringers. This model would have had panels

between the stiffeners with a b/t of 31. A cylinder of that form would most probably fail at a load very near squash, and was considered, therefore, to be a rather uninformative model to test. In addition, a comparison of the proposed model with typical cylinder designs for fixed and tension leg platforms from a survey carried out by Lloyds Register of Shipping [200] showed that IC4 would have had much narrower panels than is common.

Therefore, to avoid the predictability of failure and the departure from conventional design, it was decided to modify the geometric parameters of the model by reducing the number of stiffeners to twenty.

Also, the value of a single eccentric load test, especially when so little data was available from concentric tests, was considered to be limited. It was thought that a test under concentric load would augment the results from the other large-scale, stringer-stiffened models tested at Glasgow [196]. IC4 was, therefore, loaded concentrically.

As had been done in the previous large-scale, ring-stiffened cylinders [195], a three bay model was tested, the central bay of which was designed to fail. The reason for this was to provide better defined and more representative boundary conditions for the central bay than would have been possible if it had been tested in isolation. It should be possible, in a model which will buckle plastically, to ensure that failure will occur in the central panel, whilst maintaining a constant elastic stiffness throughout, simply by using a higher strength steel of the same thickness in the outer bays. However, experience with one of the previous ring-stiffened cylinders tested at Imperial College, in which small variations in material thickness and initial imperfection magnitudes resulted in the failure

of an outer panel, suggested the cautious strategy of using slightly thicker, as well as stronger, plate for the outer panels. This was the approach adopted, and the final geometric parameters of the model are detailed in Table 2.1.

2.2.2 MATERIAL TESTING

The central bay of the cylinder was made from 3.5 mm thick grade 43 plate and the outer bays from 4.0 mm grade 50 plate. Tensile specimens were cut both along and across the direction of rolling and tested at low strain rate to obtain the upper and lower yield strengths. As compressive tests of thin plate material are almost impossible to control, the various centres participating in the testing programme agreed to use as the compressive lower yield stress the corresponding tensile value plus 10 N/mm^2, as recommended by TRRL [201]. Since the direction of rolling had no discernible effect on the behaviour of the specimens, only average values are tabulated in Table 2.2. A typical stress-strain curve for the material is given in Appendix C.

2.2.3 FABRICATION

Fig 2.1 shows the fabrication details of the model. The first stage in the fabrication sequence was the butt welding of the flat plate panels. Then the combined plate was rolled, butt welded along the longitudinal seam and re-rolled to enhance its circularity. Next, the end flanges were attached. The ring stiffeners were made up in sections of one quarter of the circumference and attached to the cylinder using intermittent fillet welds. Finally, the stringers were welded, again using relatively light intermittent welds. The central bay stiffeners were added first, and then those in the outer bays; in each case diametrically opposite stiffeners were attached alternately.

All the welding of the model was carried out using the MiG welding process.

2.2.4 RESIDUAL STRAINS

Residual strain readings were taken after each major stage of fabrication using an electrical extensometer of the type developed at Cambridge University [202]. The measurements were taken across 100 mm gauge lengths defined by small punch marks in corresponding locations on both sides of the plate. At each logging session readings were also taken of a dummy specimen to determine and allow for the strains produced by temperature variations.

In addition, residual strain measurements were made on small test pieces before the fabrication of the model to ensure that the final stress levels would be representative of full-scale construction.

The residual strains in the model, plotted in Figs 2.2 - 2.6, are the midplate values obtained by averaging the pairs of surface readings. A large increase in the circumferential strain readings occurred during rolling. This effect was primarily due to the reduction in the linear distance between gauge marks which occurs as a flat plate is bent to an arc, and produced readings of about 1000 $\mu\epsilon$. The remaining fabrication produced a further average change in the hoop strain of about 80 $\mu\epsilon$, although some individual readings increased by as much as 350 $\mu\epsilon$.

The longitudinal strain readings, on the other hand, were little affected by the rolling of the cylinder. By that stage the longitudinal strains averaged about 85 $\mu\epsilon$ and were probably due to a Poisson effect from both the butt welding of the flat plates and the rolling. As would be expected, the greater part of the longitudinal residuals was accumulated during the attachment of the stringers. At

completion of the model, the longitudinal strain was fairly uniform throughout the shell, with an average value of about 350 $\mu\epsilon$ or 21% of the yield strain.

Readings were also taken of the residual strains in the ring and stringer stiffeners, (Figs 2.4 - 2.6). In the rings, the largest increase in the residual strains occurred during the fabrication of the rings themselves. A substantial amount of bending was produced by the eccentricity of the weld; this can be seen in Fig 2.4. Subsequent fabrication tended to relax these strains slightly.

Three longitudinal stiffeners were gauged for residual strains before and after being welded to the cylinder (Fig 2.6). Two stiffeners, 7 and 15, behaved similarly: the maximum compressive strain occurred at the tip of the stiffeners at midheight, probably due as much to being forced into the barrel-like shape of the shell as to the residual strains produced by the welding. However, stiffener 1, which was located on the longitudinal butt weld, showed a very different residual pattern. It is possible that the imperfections and residual strains already produced at this location by the butt weld may have been relaxed by the subsequent stiffener weld, resulting in the almost purely tensile residual strains observed. Also, this area was moderately heated after completion in an attempt to reduce the local imperfections, and this too may have affected the residual strains.

2.2.5 INITIAL IMPERFECTIONS

Detailed readings of the initial imperfections of the shell surface were obtained by rotating the cylinder against a fixed bank of displacement transducers (Fig 2.8). The datum for the readings was determined using a straight edge positioned a known distance from the

centre of rotation of the model. A grid of 80 readings around the circumference and 19 along the length was obtained for the central bay of the model and analysed to obtain the best-fit perfect cylinder.

The readings were the deviations of the model surface from a perfect cylinder of known radius (the cylinder defined by the distance of the straight-edge from the centre of rotation, not the best-fit cylinder). The axis of the model, or rather of the perfect cylinder which most closely approximates it, will not be the axis about which the model was rotated, nor will the axes be parallel. Five variables are therefore needed to specify the best-fit cylinder and its location (Fig 2.7): the radius, the coordinates of the perfect cylinder axis at one end and the angles in two directions between the cylinder axes. A modified version of a program written by Green and Nelson [196], which minimized the sum of the squares of the deviations with respect to these five variables, was used to determine the best-fit cylinder and the imperfections of the real model from it. It also calculated the coefficients of the Fourier series:

$$w_0 = \sum_{M=1,2,} \sum_{N=0,1,} (A_{MN} \cos N\vartheta + B_{MN} \sin N\vartheta) \sin \frac{M\pi x}{L}$$

which approximates the imperfect surface. Neither a sine series nor a cosine series is capable of representing the imperfect shape completely: the sine series results in zero imperfections along the upper and lower circumferences, whereas the cosine series produces zero slopes at these positions. However, the former is the better approximation and was used in the analysis of the imperfections.

Fig 2.9 shows the imperfections of the cylinder surface along the nineteen, equally spaced circumferential sections. The largest imperfections occurred along the obvious inward kink produced by the longitudinal butt weld. Also clearly visible is the major

imperfection mode of four waves around the circumference. This mode appears to have been induced by the fabrication method employed: the rings were attached to the cylinder in four sections, and the shrinkage of the welds between these sections probably produced the observed circumferential imperfection mode.

The imperfection data are also plotted along forty vertical sections in Fig 2.10, in which the odd-numbered sections are the longitudinal stiffener positions and the even sections, the panel centrelines. Presented in this manner, the data reveal the predominant axial mode of one halfwave along the length. Also, small inward kinks can be seen adjacent to the rings, the combined result of the circumferential butt welds and the attachment of the rings.

Fig 2.11 is a pictorial representation of the cylinder surface, in which most of the important features are discernible; the longitudinal weld and the predominant mode shapes are obvious.

The maximum imperfection of the shell was an inward deviation of 2.90 mm at the longitudinal weld; the maximum outward imperfection was 2.15 mm at a point on the ridge approximately 45° around from the weld. The DnV rules specify an out-of-roundness tolerance for this cylinder of 3.0 mm, an allowable deviation of 3.4 mm on an arc length of 265 mm and an allowable local deviation of 1.5 mm on a gauge length of 180 mm along a straight generator. The corresponding measured values for the model were 2.9 mm, 1.7 mm and 1.2 mm.

The coefficients obtained from the Fourier analysis of the imperfections have been plotted in Figs 2.12 - 2.15. In the figures the coefficients have been non-dimensionalized by division by the plate thickness.

In the axial direction the odd-numbered coefficients,

representing barrel-shaped imperfections, predominate, and display significant values even at quite high wave numbers. In the circumferential direction the N = 2, 4 and 8 coefficients are the most important, verifying the observations made from the imperfection plots directly. Somewhat surprisingly perhaps, the presence of the stringers did not result in peaks at the N = 10, 20 or 40 coefficients.

Measurements were also taken of the initial lateral imperfections of the longitudinal stiffeners. Since the model was quite large and allowed two people to work comfortably inside it, the measurements were made simply by using a dial gauge travelling along a straight edge which was positioned against each stiffener. This method enabled the shape of the stiffener tip to be determined but could not describe its line of attachment to the shell nor the angle it made with it. However, these were considered to be parameters of little importance to the buckling behaviour which did not warrant the considerable effort involved in their measurement. The initial stiffener shapes are shown in Fig 2.16. The DnV tolerance on the straightness of these stiffeners is 1.0 mm, whereas the largest measured imperfection was 0.8 mm for stiffener 17.

2.2.6 TEST RIG

The model was tested under concentric compressive loading in the test rig shown in Fig 2.17, the major part of which had been developed for the series of ring-stiffened cylinder tests [195]. Twenty four jacks, each of 20 T rating, were equally spaced beneath the cylinder's circumference and were all fed from a common pressure supply to ensure a uniform concentric loading. Because the jacks were directly beneath the cylinder shell, a relatively light bottom platten was sufficient to distribute the load. At the top, however, the reaction against the

cross-frame was through a central spherical bearing and a substantial top platten was needed to minimize bending distortions. The cylinder was bedded onto the plattens using a sand and araldite mixture to ensure uniform contact and load application.

2.2.7 INSTRUMENTATION

Also visible in Fig 2.17 is the rotating transducer frame used to measure the radial deflections during the test. The frame, which carried two vertical banks of transducers, rotated on an accurately machined steel ring bedded onto the top platten, and could be located at twenty predetermined positions using a spring loaded plunger, giving a total of 40 readings around the circumference. Using this method, a repeatability of readings to within 0.1 mm was achieved.

The model was extensively strain gauged. The gauge types and locations are shown in Figs 2.18 and 2.19, together with the section reference names adopted in the presentation of the results which follow. Cross and rosette gauges were used predominately in the shell to determine the biaxial state of stress, with linear gauges employed primarily for the stringers and rings.

Using the variation in the ambient temperature of the laboratory over a complete 24 hour cycle, a temperature calibration of each gauge against a set of dummy (or "thermometer") gauges was obtained. This allowed a compensation for the temperature-induced strains to be made for each gauge throughout the following tests.

2.2.8 ELASTIC TEST

An elastic test was carried out in which the model was loaded to 160 tons (1595 kN), equivalent to approximately one third of the squash load, in order to check the correct working of the system and

the concentricity of loading. In addition it allowed the linear part of the model's behaviour to be investigated in some detail.

Figs 2.20 - 2.27 present the more important strain gauge results from the elastic test, a more complete description of which can be found in Ref 195. Figs 2.20 - 2.24 show the longitudinal strains around different circumferential sections of the model. At the locations shown in the first three graphs, the distribution of longitudinal strain was reasonably uniform and proportional to the load. There was no significant eccentricity of load, and the elastically-predicted longitudinal strain at 160 tons (1595 kN), drawn in these figures as a broken line, showed only minor variations from the observed results.

However, in the vicinity of the bottom weld, and to a lesser degree around the top weld (Figs 2.24 and 2.23), a nonlinear strain pattern began to develop at a load of about 100 tons (1000 kN). This is not surprising, since these gauges were located very near the welds, on material which had probably yielded during the butt welding of the flat plates, and was now in a state of high tensile prestress. Also, a considerable amount of bending occurred near the ring stiffeners due to the initial inward kinks in these areas. The most heavily-strained region was near the intersection on the longitudinal and circumferential butt welds. The localized areas of high stress can be seen more clearly in Fig 2.25, in which the longitudinal strains are plotted along four vertical sections.

The hoop strains along these same sections are plotted in Fig 2.26, and show the pinching effect of the ring stiffeners (the strain distribution along section 3 was distorted by a malfunctioning gauge). By restraining the radial Poisson expansion of the shell, the rings induced in their vicinity the relatively large compressive hoop

stresses which are apparent in Fig 2.27. Compressive stresses of up to one third of the average longitudinal stress were measured near the rings. Elsewhere, the hoop stresses were quite low (less than 7% of the longitudinal stress), indicating that an almost unrestrained Poisson expansion was taking place.

The radial deflections throughout this test remained very small and nowhere exceeded 0.3 mm.

2.2.9 FAILURE TEST

The failure test was carried out once the analysed results of the elastic test confirmed the correct working of the experimental system. Fig 2.28 is the autographic record of the testing machine - a continuous plot of the load against the deflection of the loading platten of the rig. After an initial "bedding in", the load-deflection behaviour was linear. Because the model had already been loaded to 160 tons in the previous test, and a small amount of plastic straining had occurred, on reloading a small change in slope was observed when this load was exceeded.

The first part of the test, up to 320 tons (3190 kN), was carried out under load control. After each load increment, a small amount of creep occurred, which is represented in Fig 2.28 by the short horizontal sections of the graph. At 320 tons the machine was changed to displacement control; beyond this load the short vertical sections of the graph represent the shedding of load as readings were taken at the end of each load increment.

Visual inspection of the model first revealed the imminence of failure at a load of 410 tons (4086 kN): a small buckle appeared near the top of a panel in the central bay of the cylinder almost diametrically opposite the longitudinal weld; a slightly larger load

fall-off can be seen on the autographic record. However, the model remained stable and testing continued until the load reached 420 tons (4185 kN) or 0.87 times the squash load. New buckles gradually formed at another position about 90° around from the first one and then linked up to form a "chequerboard" pattern of local panel buckles extending around approximately one third of the circumference. This process took one or two seconds to occur, by which time the load had dropped to 340 tons (3389 kN). The remainder of the unloading curve was obtained by applying further deflection increments, which increased both the magnitude and extent of the buckles.

2.2.9.1 Strain gauge results

The results from this test are presented in Figs 2.29 - 2.46. The plots of longitudinal strain in Figs 2.29 - 2.33 show that significant nonlinearities developed and increased at loads above about 240 tons (2400 kN), until, by the latter stages of the test, a very uneven strain distribution existed. In general the peak strain locations corresponded to areas of substantial bending, in which a significant part of the plate thickness had yielded, thus reducing the stiffness and resulting in the higher average strains.

The graphs of longitudinal strain along vertical sections, Fig 2.34, show clearly that the highest strains occurred a small distance within the centre panel. The deflection profiles (Figs 2.48 - 2.49) show these to be locations of concentrated bending. By the time failure occurred a large proportion of the model cross-section had yielded.

An interesting effect is illustrated in Fig 2.33. At high load levels the average longitudinal strain along part of the bottom butt weld dropped as the load was increased. A redistribution of stress

was taking place as sections higher up the cylinder began to absorb a larger proportion of the strain. However, in the vicinity of the longitudinal weld it was this bottom section which was strained most heavily.

The plots of hoop strain, Fig 2.35, show that the general pattern, evident in the elastic test, of low strains at the ring positions with higher strains a short distance from them and at the panel centreline were preserved. Nonuniformities in the hoop strains near the central part of the model became pronounced at higher load levels. This effect can also be seen in Fig 2.36, showing the hoop stress along the model length, in which the stresses alternately rise and fall. This is due to the multiwave mode in the axial direction into which the cylinder was deflecting and is consistent with the shapes of the deflection profiles shown in Figs 2.48 - 2.49.

Figs 2.37 and 2.38 present the average and surface strains in the stringer stiffeners. One of the gauges at the tip of the midsection of stiffener 1 was faulty and gave low readings for the entire test. These figures show the surprising fact that at 400 tons (3980 kN) all these stiffeners had yielded through virtually their entire cross-section at midheight. Premature stiffener tripping does not, therefore, appear to have been the mode triggering failure. An inspection of the cylinder after failure showed the stiffeners adjacent to the first panel buckle to have remained relatively straight. As has been mentioned above and will be discussed later, local panel buckling was the initiator of failure.

The lateral deflections of all the gauged stiffeners were in the same direction. The stiffeners were six panels apart, and in a mode containing twenty waves around the circumference would all be located similarly with respect to the inward and outward deflecting panels.

The identical intermittent weld pattern for each stiffener probably created similar initial imperfections and also helped to induce their common direction of deflections.

A explanation of the behaviour of the ring stiffeners (Figs 2.39 and 2.40) is difficult. At some locations the highest tensile strain was measured in the shell, whilst at others it occurred in the stiffener flange. The distribution of strains is influenced, amongst other things, by the initial imperfections of the shell, the flatness of the rings and the amount of bending restraint that the rings are called upon to provide to the shell, and hence its prediction is complex. In any case, the strains were relatively small (less than 200 $\mu\epsilon$) and did not play a major part in the overall behaviour of the model.

Figs 2.41 - 2.46 show the distribution of stress in the model. These are elastically-calculated stresses, and are not correct once a location begins to yield. Consequently, stresses have not been presented for the higher load levels, although some of the values which are plotted lie above the elastic range and are shown by dotted lines.

2.2.9.2 Deflections

It seems that the cylinder behaviour was strongly influenced by the initial imperfections of the model. Fig 2.47 presents the radial deflections of the cylinder at 390 tons (3890 kN) around two circumferential sections: the upper diagram shows the midheight circumference and the lower diagram a section about one quarter of the way up the centre panel. At midheight an overall deflection mode containing eight waves can be clearly seen. A comparison of this mode with the initial imperfections reveals a marked similarity in the

locations of peaks and troughs. Lower down the cylinder, where the proximity of the rings restrained the deflections of the stringers, this overall mode was broken up by the superimposed local panel mode. The stiffener deflections were almost invariably smaller than those of the plate panels they enclosed.

An inspection of the deflection profiles, plotted in Figs 2.48 - 2.49 is also useful. At the stiffener locations, which are the odd-numbered sections, the deflections were in a single halfwave, whereas the midpanel deflections were larger over more of their length and contained a short wavelength pattern superimposed upon the single halfwave. The stiffeners were reasonably effective in maintaining the straightness of their lines of support, and thus in limiting the magnitude of the short wavelength deflections. It should be noted that all the prebuckling deflections were small: at a load of 390 tons (3890 kN) the maximum radial deflection was 1.0 mm (0.3 times the plate thickness).

The plots show distinctly the growth of the small inward depression of section 12 into the buckle observed at 410 tons (4090 kN). At 420 tons (4190 kN) the small inward kink at the bottom of section 20 and the inward depression at section 22 increased and propagated until the final buckle pattern illustrated in Figs 2.50 and 2.51 was produced.

Both initiating areas were in "valleys" in the initial surface of the shell: section 12 was in the inward depression shown about one quarter of the way across the initial imperfection plots and section 22 was in the adjacent depression, near the centre of the plots. The reason that the failure was not initiated at the largest inward imperfection of all, the longitudinal weld, is obscure. Of course, many other factors, such as variations in thickness, material

properties and loading are also significant and make a precise quantification of failure shapes and locations difficult.

Fig 2.52 shows the model after testing, with the local failure mode clearly visible. Fig 2.53 is an internal view of the cylinder showing the buckled shapes of the stringers, which, in general, were sympathetic to the shell buckles. The buckle at the far end of the panel most centrally placed in the photograph was the first that formed. That the stiffeners adjacent to it remained straight indicates that stiffener tripping did not initiate failure. Rather, an interaction between the initial local panel buckles and subsequent sympathetic stiffener buckles seems to have been the mode through which failure progressed.

2.2.10 DISCUSSION

The relatively high failure load of the model must to some extent justify the decision not to test a 40 stringer cylinder, for it is likely that the ultimate load of that model would have approached the squash load. The local shell buckling preceding the overall collapse would have been absent in a narrow-panelled cylinder, and the behaviour would have been similar to the small-scale cylinders tested by Fahy [182].

The measurements of initial imperfections and welding residual strains enabled an accurate and detailed picture of the initial state of the model to be compiled. The model satisfied all the tolerance requirements of the DnV rules, but not by such a large margin as to have made it unrepresentative of full-scale construction. Similarly, the residual strains appear to have been of typical magnitude and distribution.

The Fourier analysis of the cylinder revealed the presence of

short wavelength axial imperfection modes as well as the primary barrel shape imperfection. The prebuckling deflections also contained higher modes in the axial direction, most apparent in the outward bulges adjacent to the end rings. The deflected shape can also be inferred from the alternate zones of high and low hoop stresses along the cylinder length. In the outwardly deflecting zones the tensile hoop stresses produced earlier yielding of the material, and failure was initiated by the formation of inward buckles adjacent to this area.

A common failure mode of cylinders is a series of predominantly inward buckles. In cylinders without stringers, this mode usually comes about by a sudden snap-through from the outward prebuckling deflections to the inward-lobe buckling configuration. Snap-through is less likely to occur in an axially-stiffened shell, and the inward lobes may develop more gradually. In a long cylinder these buckles may form in the concave region adjacent to the outward bulges that are induced by Poisson expansion near the end rings. The higher bending stiffness of an axially-stiffened shell pushes this region further from the rings, and the buckles may form at a greater distance from the ends of the cylinder than is observed in an unstiffened model. Finally, the buckle pattern may spread along the cylinder length; the plots of the final shape (Figs 2.50 - 2.51), in which the buckles are located fairly centrally in the panel, may therefore be misleading in that they obscure the position at which the failure was initiated.

A number of points can be made concerning the stability of the model and its components. First, it seems that the stringers, despite having yielded through a considerable part of their midheight cross-section, did not initiate failure. Of course, their reduced stiffness would have lessened their effectiveness in controlling the local panel

buckles which formed and therefore would have had some influence on the collapse load, but this is a secondary effect.

Secondly, the initial panel buckles were quite localized and did not trigger an overall failure. Although only a relatively small load margin existed between the appearance of the first buckle and the final collapse, the behaviour is nevertheless in sharp contrast to that observed in ustiffened models, in which the two effects cannot usually be differentiated.

Finally, the model had a considerable load capacity after failure. At collapse the load fell to about 80% of the peak load, and even after quite severe straining the model was able to support approximately 50% of its maximum load.

The DnV rules predict a failure load of 66% of the squash load for both the plate-initiated and stiffener-initiated modes of failure. That both modes should be predicted to occur at similar loads is appropriate, since in the test the panels buckled locally shortly before overall failure. However, the substantial underestimation of the failure load points out the shortcoming of a method such as this which neglects the often significant effect of curvature.

The stiffeners of the model did not meet the requirements of the DnV rules: the stringers were too slender (d/t = 13.6 c/f DnV: 10.6) and the rings were insufficiently stiff (I_{eff} = 5.9 x 10^5 mm^4 c/f DnV: 7.1 x 10^5 mm^4). Adherence to the stringer stiffener requirements may have resulted in a slight strengthening of the model. However, the rings were so lightly stressed during the test that the DnV rules seem to be overconservative in requiring more substantial rings than were present.

2.3 SMALL-SCALE MODELS

2.3.1 INTRODUCTION

The series of twelve small-scale cylinders was commissioned by Det norske Veritas and tested in a joint programme carried out at Imperial College and Surrey University. All the models had the same cross-section; the twelve tests consisted of the various combinations of three cylinder lengths with four different load types: pressure only, pressure + axial tension, pressure + axial compression, and axial compression only. The nine models under pressure or combined loading were tested at Surrey University [203], and although the tests will not be described here, the results will be used in the next chapter. The testing of the three remaining cylinders under axial load and the detailed measurement of the initial imperfections of all twelve models were carried out by the author [204]. The loading ratios and geometric parameters for the complete series are given in Tables 2.3 and 2.4. The original numbering system used for the testing programme will be retained here: accordingly, the short, medium and long axially-loaded cylinders are designated 1, 7 and 10 respectively.

2.3.2 MODEL DESCRIPTION AND MANUFACTURE

All twelve cylinders were of the same cross-section: a diameter of 320 mm with 40 internal stringer stiffeners of 6.7 mm depth, and were fabricated entirely from 0.84 mm steel sheet. Four specimens were made in each of three lengths (64, 128 and 192 mm) and the three I.C. tests comprised one from each group.

The welding used in the models, minute in size and of extremely high quality, was developed for the fabrication of a previous series of small-scale models. The first step in the manufacture of the

models was to TiG weld the stiffeners to a flat sheet which was subsequently rolled and seam-welded around a copper forming mandrel with copper inserts between stiffeners. An outer copper former was then clamped to the assembly and, in this tightly restrained condition, the model was stress-relieved in an inert atmosphere heat treatment oven. Once the assembly was dismantled, the ends of the cylinder were lapped parallel and flat in preparation for the attachment of end rings.

In previous small-scale tests clamping of the cylinder ends was achieved by embedding the shell using a sand/araldyte mixture in the annulus between two heavy steel rings (Fig 2.54(a)). The shell protruded beyond the end rings and, once lapped to the loading plattens, provided a uniform and direct load transfer. However, in this series the waterproofing requirements for the hyperbaric tests dictated the use of a single grooved end-ring (Fig 2.54(b)). Close tolerances on the overall circularity of the cylinders were achieved by fitting the ends against the small step machined into the bottom of the groove in the end rings. The cylinders were then cast in position using a mixture of sand and araldite epoxy resin.

2.3.3 MATERIAL TESTING

Thin sheet material does not generally possess mechanical properties similar to structural grade steels. The material used in the present series, however, was part of a large run of 0.84 mm sheet specially rolled for a major testing programme on box girder bridges conducted previously at Imperial College [205].

Each model was fabricated from a single sheet of material from which test coupons were also cut and subjected to heat treatment at the same time as the models. Tensile tests were carried out on these

specimens at Surrey University and the average values obtained for the material characteristics were:

$E = 202\ kN/mm^2$

$\sigma_o = 313\ N/mm^2$

It was assumed that the appropriate value for the compressive yield stress was 10% greater than the lower static tensile yield, giving a stress of $344\ N/mm^2$.

2.3.4 IMPERFECTION MEASURING EQUIPMENT

A very large number of imperfection measurements were made on the twelve cylinders making up this series. Because of the small modelling scale, care and precision was necessary, both in the taking of readings and in the design and manufacture of the measuring equipment itself.

2.3.4.1 Shell surface imperfections

The shell surface readings were obtained using a modified version of a measuring frame used previously in similar experimental work [182]. The frame is shown in Fig 2.55 located in the testing rig, in which it was also used to measure the radial deflections during the loading tests. The frame enclosed the model and supported a ring carrying forty transducers, equally spaced around the circumference and in contact with the cylinder. The ring could be raised and lowered by means of the threaded columns which supported it. All the columns could be turned simultaneously and by the same amount through a chain and gear mechanism using a winding handle. The vertical spacing of readings was established by rotating the winding handle a certain number of turns, allowing quick yet accurate vertical positioning of the transducers.

The frame could also be rotated about the vertical axis and positioned using a locating pin. By successively rotating the frame through a quarter of the angle between adjacent transducers, the number of readings around the circumference was increased to 160.

The radial projection of the end rings of the model beyond the cylinder surface exceeded the length of travel of the transducers. The transducer ring was therefore made in four quarter-circle segments, in order that it could be dismantled to allow the insertion of the cylinder and then relocated precisely using postioning dowels.

An accurately machined cylinder with a tolerance of ±.0025 mm on its diameter was used as a datum for the imperfection readings of all models. The procedure was to scan this cylinder and then record the differences of each model from it. In each case, the measuring sequence consisted of taking a full vertical series of readings from the top to the bottom of the cylinder, raise the transducer frame to the top and rotate it to the next position, repeating these steps four times in all. It is estimated that the results obtained using this equipment were accurate to within ±.05 mm.

The readings were then analysed using the imperfection program to determine the best-fit perfect cylinder and the imperfections and Fourier coefficients.

2.3.4.2 Stiffener imperfections

The equipment shown in Fig 2.56 was devised to measure the lateral imperfections of the stiffeners. It consisted of a spring loaded carriage, which could roll along a machined beam. The beam's cross-section was trapezoidal (see Fig 2.57); this shape and the spring loading ensured that the carriage was always in contact with the longer edge of the beam cross-section. Attached to the sliding

carriage was a transducer, bearing against one end of a pivoting right-angle mechanism whose other end was in contact with the side of the stiffener. By sliding the carriage along the beam to predetermined positions, readings of the stiffener imperfections could be obtained. The beam and the cylinder itself were mounted in end brackets; the beam height could be adjusted and the cylinder could be rotated on bearings to bring each stiffener into position and then locked.

The readings were analysed to obtain the best-fit straight line through them and the imperfections of the stiffener from this line. The equipment is estimated to be accurate to within ±.03 mm.

2.3.5 IMPERFECTION RESULTS

Table 2.5 presents for each model the radius of the best-fit cylinder, the maximum inward and outward shell imperfections and the maximum stiffener imperfections.

The most notable observation which can be made about the imperfections is that they were very small and well within the DnV tolerances. Table 2.5 shows the maximum deviation of any point from the corresponding perfect cylinder was 0.41 mm, compared with the allowable out-of-roundness DnV tolerance of 0.80 mm. The tolerances on the local deviation from the straight generators and from circular arcs were also easily satisfied.

Also presented in Table 2.5 are the maximum stiffener imperfections, calculated as the sum of the maximum positive and negative deviations from the best-fit straight line. This is a conservative approximation to the stiffener imperfection measurement specified in the DnV rules, because the "straight-edge" from which the DnV imperfections should be measured will not generally be parallel to

the best-fit straight line. The relatively high readings shown for stiffeners 11 and 14 of model 1 were due to a problem with the measuring equipment and should be disregarded.

All the models satisfied the DnV tolerances for the stiffeners. The slight amount by which cylinder 4 exceeded the specified tolerance is more than compensated by the conservatism in the approximation of the imperfection measurements.

The entire series of imperfection figures is available in Ref 204. Here, the most relevant graphs for the three axially-loaded cylinders will be presented, following the numbering system presented in Fig 2.58.

The plots of imperfections along the circumferential sections (Figs 2.59, 2.67 and 2.76) do not reveal any marked features common to all the cylinders. Often, a particular panel was found to have considerably larger imperfections than any other part of the cylinder: this suggests that for this form of fabrication the welding of the stiffeners to the shell plate is one of the most critical stages and highly dependent upon the skill of the welder. The overall circularity was well maintained during the subsequent rolling, seam welding, heat treatment and end ring attachment.

When plotted along vertical sections, Fig 2.60, 2.68, 2.69, 2.77 and 2.78 the data show that the cylinders were extremely straight along their lengths. This is also revealed in the graphs of the Fourier coefficients, Figs 2.63 - 2.66, 2.72 - 2.75 and 2.81 - 2.84, where the lowest axial mode, M = 1, was always predominant. In the circumferential direction the N = 2 or 3 mode was often important, and a small peak was usually observed around N = 40.

2.3.6 INSTRUMENTATION

All three models were strain gauged before testing. Since length was the main variable in the series, the variation in the distribution of strain along the length of the cylinders was of primary interest. In order to determine this distribution in some detail while limiting the number of gauges, only the top half of each cylinder was strain gauged. This was considered to be justified by the assumption that the behaviour was symmetric about the midheight circumference, which, at least below the elastic limit of the material was probably not severely violated.

Figs 2.85 - 2.87 show the precise locations of the gauges for the three models. In each case two diametrically opposite panels and a stiffener adjacent to each were strain gauged. In addition, a pair of gauges were also located at the two other quarter points of the midheight circumference so that the concentricity of load could be checked.

The axial shortening of the models was determined by averaging the readings from three displacement transducers located within the model and symmetrically positioned about its centre. The transducers measured the relative displacement of the two end plattens in contact with the cylinder.

Radial deflection readings of the cylinder surface were taken at regular intervals during the tests with the same rig as was used to measure the initial imperfections. Although for the initial imperfection scans 160 readings were taken around the circumference, for the load tests, where deflections rather than imperfections were being measured, this degree of detail was considered unnecessary, and readings were taken along the lines of stiffeners and mid-panels (i.e.

80 readings around the circumference).

2.3.7 TEST RIG

The models were tested in a circular frame 2.5 m high and 1.0 m in diameter (Figs 2.88 and 2.89). The frame consisted of four 125 mm thick plates (the top one of which is not shown in Fig 2.89) acting as a multiple sandwich for the model, load cells and screw jack. The screw jack was located between the two bottom plates and load was applied by reaction against the upper plate through six 50 mm diameter tension rods. The load was transferred directly through three load cells, which provided the only support to the plate carrying the model and transducer frame. The intermediate plates were supported laterally by three 75 mm diameter columns, clamped to the second plate and free to move vertically through roller bearings in the top and bottom plates.

Although self-reacting, the rig was also anchored to the laboratory strong floor by means of a 200 ton capacity cross-frame (again not shown in Fig 2.89) which considerably increased its stiffness and allowed the post-collapse path of the models to be followed with greater control. The screw jack was driven by a variable-speed electric motor through a low ratio gearbox, which enabled a very slow loading rate to be achieved.

2.3.8 SETTING UP OF MODELS

After each cylinder was strain gauged and all the contact surfaces of the end rings and plattens were cleaned, it was lowered onto its supporting platten. The internal transducers were positioned and the internal strain gauges were wired up to the data logger through holes in the top platten and tube.

Next, the top platten of the machine was located on the columns and supported by nuts on the threaded rods in a position slightly above the top of the model/end platten assembly. Then the crosshead was placed over the rig and bolted down to the floor, again allowing a small clearance between it and the bearing on the top of the upper platten. Two theodolites were used to locate the model, end plattens and top bearing on the centre-line passing through the ram of the jack.

While the load cells were carefully monitored, the model was raised using the screw jack until it carried the top platten and just brought it into contact with the crosshead. At this point the nuts on the six tension rods which react against the top platten were screwed down by hand. By using the model as a guide in setting up the top platten and crosshead even contact was achieved between all surfaces. The test was then ready to commence.

2.3.9 TEST PROCEDURE

For each model an elastic test was first carried out to check the line of action of loading and the correct working of the test setup. Once satisfactory concentricity was established the models were loaded to failure. Initially the load was applied in increments of approximately 2 tons (20 kN) which were reduced to 1 ton (10 kN) as the models approached failure. The strain gauges and axial displacement transducers were logged after each load increment, and the radial displacements were measured every two or three increments. The models were loaded considerably beyond the peak load to determine the post-buckling response.

2.3.10 DESCRIPTION OF TESTS

The load-deflection plots for the three cylinders are shown in Figs 2.90, 2.91 and 2.92 and are very similar in appearance. Initially, the response was nonlinear as the "bedding in" of the contact surfaces took place. From then until approximately 90% of the failure load the behaviour was linear. Beyond that point the response departed smoothly from linear behaviour until, at a load approximately equal to squash, a fairly gradual failure was observed in all cases.

For each cylinder, the peak load was accurately determined, since the load was continuously monitored throughout each test. The axial shortening, however, was measured only after each loading increment. Only in the case of cylinder 1 did the end of an increment coincide with the peak in the curve. For the other two cylinders the precise value of the axial shortening at the peak load could only be estimated, and the upper parts of Figs 2.91 and 2.92 have been drawn with a broken line.

The fall-off in load capacity after failure, although fairly gradual in all cases, was slightly more rapid for the longer cylinders. This is to be expected, since a longer cylinder would have absorbed, and therefore released at failure, a larger amount of strain energy. It appears that all models were approaching very similar values of post-buckling strength.

In all three cylinders the failure mode was a ring of outward buckles which spread around the entire circumference very near the bottom end ring of each model. Figs 2.93 - 2.96 show the three models after failure. Unfortunately, it appears likely that this mode was influenced by the end ring detail adopted for these tests, although it is not clear by what mechanism this was brought about. This problem

was not encountered in the combined loading tests, in which the external pressure dominated the mode of failure.

Being so close to squash, the failure loads could not have been significantly reduced by this end condition mode. This is also demonstrated by the behaviour of the longest cylinder, in which an overall mode consisting of buckles, each spanning approximately five panels, appears to have occurred virtually independently of and simultaneously with the end condition mode. Only one of these buckles was apparent during the test, and it is visible in the right portion of Fig 2.95. However the entire pattern can be seen in a plot of the radial deflection data presented in the next section.

The ultimate loads of the three cylinders were quite similar: 0.93 σ_o, 0.99 σ_o and 1.00 σ_o for the short, medium and long cylinders respectively. The perhaps surprising fact that the failure load increased with cylinder length, which was thought to be simply a consequence of experimental scatter, was shown in the numerical analysis of the next chapter to be the expected result.

2.3.11 RADIAL DEFLECTION DATA

A large amount of data was collected on the growth of radial deflections during the tests. This can be divided into the "pre-buckling" information, which showed the steady, gradual increase of deflections as the tests progressed and the "post-buckling" data, illustrating the failure mode shapes. In order to simplify the presentation of this information, only the last of the pre-buckling and the first of the post-buckling data sets are plotted. The information that has been ommitted is generally proportional to one or other of these curves. Fig 2.97 gives the precise vertical locations of the readings taken for each cylinder. Deflection readings were

taken to within 3 or 4 mm of the end rings and very localized behaviour, nearer to the ends than this, could not be measured.

Two figures are presented for each cylinder (Figs 2.98 - 2.103). The first shows radial deflections along eight vertical sections: an adjacent midpanel and stiffener at four quarter points of the cylinder. The second plots the radial deflections around two circumferential sections for each cylinder. The lower diagram shows the circumferential set of readings, usually the bottom or next-to-bottom section, which was closest to the peaks in the end buckles. The upper plot shows whichever section best illustrates the deflected shape of the central part of the cylinder. The gaps in these diagrams correspond to positions at which strain gauges or wires were located and readings could not be taken.

The vertical plots (Figs 2.98, 2.100 and 2.102) show the rapid growth and localized nature of the end buckles, features which were apparent, in any case, in the tests. Prior to the formation of these buckles the deflections were generally of a barrel form. However, in the case of cylinder 1, reasonably large deflections were measured prior to failure quite close to the bottom ring, and it seems that the end conditions had a more marked effect than in the longer models. This can also be seen in the graphs for all three models of the pre-buckling deflections around the lower circumferential section, which show that the magnitudes and curvatures of this form of deflection decreased with increasing cylinder length. The vertical distribution of pre-buckling deflections along section 1B of cylinder 10 shows that the overall buckling mode was developing prior to failure and was not generated as a consequence of the end buckles.

The graphs of the deflections around circumferential sections (Figs 2.99, 2.101 and 2.103) also reveal a number of interesting

features. The lower plots clearly illustrate the buckling pattern near the end rings, in which the midpanel and stiffener readings are easily recognized as the peaks and troughs respectively; in cylinder 10 the ring of buckles was not as straight as in the other models and the peaks are not all contained in a single circumferential line of readings, resulting in the less uniform pattern shown.

In the upper plots, on the other hand, much more gradually varying deflections are evident. In these, stiffener and midpanel readings are not readily distinguishable, as the entire cross-section was deflecting in an overall mode. The upper diagram for cylinder 10 reveals the formation of an eight wave overall mode, of which only the largest buckle was apparent during the test. The beginnings of a similar overall buckling mode can just be discerned in the upper diagram for the medium length cylinder, but appear to be absent in the short cylinder.

A correlation between the mode or point of initiation of failure and the form of the initial imperfections is not possible or relevant due to the localized end condition failures which occurred. In the case of the overall mode of cylinder 10, however, it may be significant that the largest buckle occurred in a location of relatively large adjacent inward and outward imperfections in the vicinity of the longitudinal seam weld.

2.3.12 STRAIN GAUGE DATA

The strain and stress results are presented in Figs 2.104 - 2.121. Unless stated otherwise, midplate (membrane) strains and stresses are plotted; in all diagrams compressive strains and stresses are negative. Unfortunately, some elements of the cross gauges on cylinder 1 did not function properly. Consequently, the only data

presented for cylinder 1 are Figs 2.104 and 2.119, the circumferential distribution of longitudinal strain and the longitudinal strains in the stiffeners. In addition, due to a fault in the logging equipment all the strain readings for cylinder 1 were about 30% too low, although their relative magnitudes appear to have been unchanged. These faults were corrected before the two other tests, for which the full series of plotted data is presented.

Figs 2.104 - 2.106 show the distribution of longitudinal strain around the midheight circumference for each model. The strains were reasonably uniform and the small nonuniformities which did exist around each model were established in the first load increment and remained substantially unchanged for most of the test; they were, therefore, probably due to a slight uneveness in the contact between the cylinder and end rings, and between the end rings and plattens. The least uniform distribution occurred in the shortest model, cylinder 1. A small imperfection in the end bearing surfaces would represent a larger proportion of the applied end shortening for this model and would also produce a more detectable effect at the centre of the cylinder since a shorter distance is available for the stresses to even out. In addition, the change in the strain distribution during the tests was greater in cylinder 1 than in the other models, suggesting that the loading may have been slightly eccentric.

The longitudinal stress distributions around cylinders 7 and 10 (Figs 2.107 and 2.108) were quite uniform and regular. Stresses presented in these figures are calculated on an elastic basis and should be disregarded once the elastic limit of the material is exceeded.

At peak load, the largest strains in all three models were measured at the longitudinal weld, although this was initially the

least strained area. This may be coincidental, or it could reflect a possible weakening produced by the longitudinal weld. Figs 2.111 - 2.114 present the axial distributions of longitudinal strains and stresses, which were relatively uniform along both models and did not show any unexpected features.

The hoop strains around models 7 and 10 were also relatively constant (Figs 2.109 and 2.110). Graphs showing the circumferential distributions of hoop stress have not been included because at midheight the hoop stresses remained very small throughout the tests.

The hoop strains along the length of cylinders 7 and 10 are shown in Figs 2.115 and 2.116 and are regular in form: the maximum tensile hoop strains occurred at the midheight of the models, with much smaller strains near the radially-restrained ends. Substantial compressive hoop strains were recorded near the ends of cylinder 7, the consequence, perhaps, of the initial imperfection shape. The longitudinal strains in these locations were larger on the outer surface of the shell, indicating that localized inward bending was occurring; the circumferential shortening that must accompany such a deflection would explain the compressive hoop strains observed at these points.

The hoop stresses are plotted in Figs 2.117 and 2.118. In both cases, the radial restraints produced relatively large compressive stresses near the ends. At the centre of the model, the hoop stresses were approximately zero for cylinder 7, while in the longer cylinder 10 they were tensile. By interpolating some of the missing strain readings for cylinder 1, it was confidently estimated that the hoop stresses in the centre of that model were compressive. These observations are consistent with the expected effect of the distance from the radial restraint: as the model length increases, the

restraint to barrelling near the centre decreases and the hoop stresses at that point become more tensile.

The final set of diagrams (Figs 2.119 - 2.121) gives the longitudinal strains in two stiffeners for each model. An outline of each stiffener and the adjacent shell is drawn and the strain readings are plotted in the approximate positions at which they were measured. The strain readings obtained from the gauges on the outside of the shell along the lines of the stiffeners are included on these plots to give an indication of the distribution of strain through the stiffener depth. In the left pair of figures the longitudinal strains along each side of the stiffener tip have been averaged; in the other diagrams the surface strains at the tip were plotted separately to indicate the amount of lateral bending in the stiffeners.

Near the rings, the longitudinal strains are larger in the shell, whilst at the model centreline the larger strains are at the stiffener tip. Both observations correspond to the curvatures produced by the barrelling form of deflections. The surface strain plots give a measure of the lateral deflection of the stiffeners. The central gauge on the front face of stiffener 1 of cylinder 1 and also, possibly, the lower gauge on the rear face of stiffener 21 were faulty and have distorted the graphs at these points. It is interesting to note the low strain readings obtained at the top of stiffener 21, most probably due to a localized uneven end bearing in this area. The corresponding plots for cylinder 7 show the gauged stiffeners to have remained remarkably straight throughout the test. In the longer cylinder 10, which was undergoing substantial deflections in an overall mode, significant lateral deflections occurred in the stringers, especially in stiffener 1 which was near the largest buckle.

2.3.13 DISCUSSION

Using now well-established techniques, high quality models were fabricated, which despite their small size had imperfection levels of only about one half of the DnV specifications for full-scale structures.

Although the end ring detail necessitated by the hyperbaric tests seems to have influenced the mode of failure of the axially-loaded models, it did not produce a significant reduction in the failure loads, which in all cases were close to squash.

The different lengths of the three specimens produced failure modes which spanned the transition between local and overall buckling. The longest model buckled in an overall mode simultaneoulsy with the end mode. The deflections of the midlength model appeared to contain an overall mode which did not finally predominate, while in the short model little evidence of any overall mode was found.

Another interesting effect of length was seen in the axial distribution of hoop stresses. At the midheight of the short model the hoop stresses remained compresssive due to the proximity of the radial restraint of the end rings. As the length increased, however, the central hoop stress became less compressive and finally tensile. Nevertheless, in all cases the hoop stress varied smoothly along the cylinder length (unlike unstiffened and lightly-stiffened cylinders).

The overall behaviour of the models was very smooth: failure was gradual, load fall-off was relatively slow and the postbuckling strength considerable; all resulted from the stocky proportions of the cylinders and the presence of a large number of stiffeners.

2.4 SLENDER SMALL-SCALE SERIES

2.4.1 INTRODUCTION

Upon completion of the previous series of small-scale tests, all the stiffened cylinders tested at Imperial College, both by the author and previously by Fahy [182], had failed at a load above 95% of the squash load in the case of the small-scale models and 86% for the large-scale model in the presence of residual stresses. With the possible exception of the longest small-scale cylinder described above, the failure mode, in all cases, consisted of a series of local panel buckles. It was thought that the testing of cylinders with more slender geometries, by broadening the range over which experimental results were available, would provide useful information.

The substantial amount of forming and clamping equipment which was required in the manufacture of the cylinders, and the limitations imposed by the dimensions of the testing rig and measuring frame meant that models of a different radius could not be manufactured and tested without great additional expense. More slender geometries had to be achieved, therefore, through the use of thinner shell plate material. As mentioned earlier, thin plate does not generally display the same behaviour as structural steel. Fortunately, however, it was possible to obtain specially-rolled 0.63 mm sheet which had similar properties to structural steel, and the models of the current series were fabricated entirely from it.

Preliminary calculations showed that although the reduction in the R/t ratio would produce a significant weakening effect, it was likely that the failure mode would still consist of single panel buckles. Orthotropic buckling was induced by decreasing the relative stiffness of the stringers through the use of flats of depth only six

times their thickness.

The series consisted of six models, three of which had twenty, and the other three, forty, stringers, but whose lengths and cross-sectional dimensions were otherwise identical. One model from each set was tested under axial load, one under hydrostatic pressure and the third under combined axial load and pressure. The relevant geometric and loading parameters are set out in Tables 2.6 and 2.7.

2.4.2 MANUFACTURE

The models were fabricated making use of the same equipment and techniques used in the previous series. Since the forming mandrel was designed for 0.84 mm material, it was necessary, in order to limit distortions during the heat treatment, to insert beside each stiffener thin sheet of thickness equal to the difference between the thickness of the material being used (0.63 mm) and that for which the mandrel had been designed.

The doubt in the performance of the end rings used in the previous series prompted their replacement, for the axially-loaded models of this series, by the original annulus type illustrated in Fig 2.54(a). The single ring had worked well in the pressure and combined loading cases and was retained for those models of this series.

2.4.3 MATERIAL TESTING

Using the procedure adopted for the previous series, the following properties were determined for the sheet material after heat treatment.

$E = 210\ kN/mm^2$

$\sigma_o = 365\ N/mm^2$

A typical stress-strain curve is given in Appendix C.

2.4.4 INITIAL IMPERFECTIONS

Once again, the initial imperfections of both the shell and stiffeners were determined in detail for each cylinder; 160 readings around the circumference were taken at 21 positions along the cylinder length, and the stiffener imperfections were determined at 12 points along each. The considerable resulting data are plotted in detail in Ref 204 and summarized in Table 2.8. In order to limit the quantity of plotted information but still convey an impression of the type and magnitude of imperfections, only a projected view of the imperfect surface of each cylinder is given here, Figs 2.122 - 2.127.

The first set of numbers in Table 2.8, referring to the radius of the best-fit perfect cylinder, although consistent, are all below the corresponding values for the first small-scale series. This is simply because using the same forming mandrel with thinner sheet material resulted in a smaller outside radius.

The maximum inward and outward imperfections, given in the next two lines, are all significantly larger than for the first series. This appears to be due to the poorer restraint which the outer clamping mandrel could impose on the cylinders of thin material. Hence, during heat treatment larger imperfections of long circumferential wavelength formed than in the first series. This can be seen in a comparison of the projected imperfection surfaces of the current models, which all show a prominent two or three wave mode around the circumference, with those of the previous series, Figs 2.61, 2.70 and 2.79, which do not. The Fourier coefficients, although not presented here, all display a marked peak at the N = 2 or 3 modes.

On the other hand, the deviation from a perfect circle, e, measured over a short arc length, is of the same order as was observed

previously. This is a local imperfection produced by the welding of the stiffeners to the shell and is, therefore, unaffected by the poorer clamping. Also the out-of-straightness, which seems to be adequately restrained by the stiffeners, is as small as in previous models. The lateral imperfections of the stiffeners are dependent upon the quality of restraint during heating, and are, in general, larger in the present group.

Despite the fact that the imperfections were larger in the current series of cylinders, they were all within the DnV tolerances, albeit by a smaller margin than in previous models.

2.4.5 AXIALLY-LOADED MODELS

2.4.5.1 General

The test rig and setting up procedure were identical to the previous series. Use of the annulus end rings enabled the model ends, which projected slightly beyond the rings, to be lapped against the loading plattens, producing a superior uniformity of contact.

2.4.5.2 Description of tests

The load-deflection paths for the axially-loaded cylinders are shown in Figs 2.128 and 2.129. In both cases the prebuckling curve was fairly linear up to the peak load, at which point a sudden and dramatic drop in load was observed. In the case of the 40 stiffener model, E, the behaviour was unremarkable until at a load of 28.8 tons (289 kN), and with an audible bang, the cylinder buckled in an overall mode consisting of nine circumferential waves. In the 20 stiffener cylinder test, A, a single panel between stiffeners "popped" into an inward mode at a load of 17.7 tons (176 kN). The load dropped only slightly and was subsequently increased to 19.2 tons (191 kN) before

the cylinder failed in a ten wave overall mode. The ultimate loads of the two cylinders correspond to average applied stresses of 399 and 281 N/mm^2 respectively.

It can be seen that the applied stress in the forty stringer model exceeded the compressive yield stress by approximately 9%. The maximum variation in the yield stress of the seven tensile specimens from the average value was 2%, making it unlikely that the experimental strength was high as a consequence of differences in the material properties. It may, however, reflect an inaccuracy in the method used to predict the compressive yield stress from the measured tensile value.

The failure shapes of the two cylinders, shown in Figs 2.130 and 2.131, are similar, despite the differences in the number of stiffeners and failure load of each. The postbuckling strengths of the two cylinders were also similar (about 8 - 10 tons) although the 40 stiffener model underwent a much larger fall off in load capacity to reach this level.

2.4.5.3 Radial deflection data

As before, readings of the shell surface deflections were taken throughout the tests. In Figs 2.132 and 2.133 the radial deflections have been plotted along a circumferential section near the centrelines of the 40 and 20 stiffener cylinders respectively, at loads just before and after the peak.

In the 40 stiffener model (Fig 2.133) the prebuckling shape at 27.1 tons (270 kN) displayed only vague signs of the nine wave mode into which it was about to buckle. The postbuckled shape exhibits a uniformity of wavelength and amplitude which is quite remarkable. The occurrence of a nine wave mode in a 40 stiffener cylinder suggests

that the stiffener locations were unimportant and that the shell behaved in an orthotropic manner.

The failure mode of the 20 stiffener model was less uniform, but clearly distinguishable as one containing ten waves. The displacements at 14.2 tons (142 kN), although very small, already exhibited the inwardly-deflecting zones, in the left of the diagram, which later initiated the local buckles in this area. These buckles formed at 17.7 tons (176kN) and were each confined to a single panel; at this stage the stiffeners were effective in maintaining the straightness of the shell along their lines of connection to it. The buckles were only apparent in part of the cylinder but were clearly part of the ten wave mode which was about to form.

As the load was increased further, the local buckles suddenly increased in amplitude and extent to the almost complete ten wave mode shown by the solid line. The largest lobes were in the locations which had buckled originally; however, their form had changed significantly: instead of the gradually-varying waves, there were now larger inward buckles enclosed within sharp, clearly-defined yield lines (Fig 2.130). Diamond-shaped buckles extended between the centrelines of every second panel, and, consequently, each stiffener was involved in the buckling mode.

Since the stiffeners buckled in conjunction with the shell, it would be easy to classify this failure as an orthotropic one, similar to the 40 stiffener case. However, it was seen above that the final buckled shape grew out of a prebuckling local deformation mode which was a result of the precise number of stringers.

2.4.5.4 Strain gauge results

The strain gauge results are presented in Figs 2.137 - 2.150.

The variation of the longitudinal strain around the circumference is shown in Figs 2.137 and 2.138 for cylinders A and E respectively. In both the initial strain distribution was reasonably uniform. The predominance of buckles in one area of cylinder A is reflected in the non-uniformity of longitudinal strains which developed above 18 tons (Fig 2.137). When plotted along vertical sections in Figs 2.139 and 2.140, the longitudinal strains are relatively constant, and the small deviations which did occur appear to have been random. The corresponding longitudinal stress plots (Figs 2.141 - 2.144) are very similar in shape to the strain plots discussed above. The comparison between the experimental stresses and the analytically predicted value at 12 tons, shown by the broken line, is good.

An interesting effect can be seen in the distribution of circumferential strain along the length of the models, Figs 2.145 and 2.146, in which the plotted strains were measured along the centrelines of two diametrically opposite panels. In the 40 stiffener cylinder the hoop strains vary smoothly from low values near the rings to the almost constant values over the central part of the cylinder, the type of behaviour observed in the previous small-scale series of tests (e.g. Fig 2.116).

In the 20 stiffener model, where the panels were wider and the shell more closely resembled an isotropic cylinder, the hoop stresses are alternately tensile and compressive, indicating the presence of a prebuckling deflection mode containing several axial waves. This effect was observed in the only other 20 stiffener axially-loaded cylinder, the large-scale model IC4, and in the longitudinally unstiffened cylinders tested by Dowling et al [195]. In Fig 2.134 the radial deflections of the cylinder shell along four vertical sections are plotted. Of these, section 1B best illustrates the form of

prebuckling deflections, containing seven halfwaves, which gave rise to the observed hoop strain distribution. The circumferential strain varied by up to 200 $\mu\epsilon$ at a load of 20 tons. The differential radial displacement necessary to produce such a variation is 0.03 mm, which is of the same order of magnitude as appears in the deflection profiles.

The behaviour of the 20 and 40 stiffener models can also be contrasted by reference to Figs 2.147 and 2.148, showing the hoop stress along the cylinders. The more heavily-stiffened cylinder had sufficient orthotropic stiffness to restrict the radial deflections to a smoothly-varying form, producing the low compressive hoop stresses in the middle of the cylinder. The lightly-stiffened model, on the other hand, behaved more like an unstiffened cylinder and took up a multiwave mode in the axial direction.

Finally, the longitudinal strains in two stiffeners are shown in Figs 2.149 and 2.150. In the 40 stiffener model the single wave, barrelling mode produced compressive stresses at the midheight of the stiffener which were highest at the tip, whilst at the ends clamping resulted in higher stresses in the shell.

Four gauges in the 20 stiffener model were faulty and distorted the strain results of Fig 2.149. Neglecting these, however, the strain distribution through the stiffener depth appears to be considerably more uniform than in the 40 stiffener model. There appears to be no clear reason why this should be so and it may simply be the result of experimental scatter.

2.4.6 HYDROSTATIC AND COMBINED LOADING TESTS

The four remaining cylinders of the series were tested in the hyperbaric facility at Surrey University.

2.4.6.1 Testing equipment and procedure

The testing equipment is described in detail by McCall and Walker [203] and will only be briefly outlined here.

The arrangement is shown schematically in Fig 2.151. The bottom end ring of the model was bolted to the flange of the pressure chamber, and the loading platten and shaft assembly passed through the model and bolted to its upper end ring. Both connections were made water-tight through the use of rubber O-rings.

The bell chamber was then held in position above the model while the wires from the external strain gauges were passed through the manifold and soldered to small conducting rods passing through an insulating diaphragm which provided the waterproof seal. Wires soldered to the other ends of these rods were then connected to the logging equipment. The wires from the internal gauges passed through the opening in the flange of the chamber and were connected directly to the logger.

The bell was then lowered to its final position and bolted down to the flange, and the vessel filled with water through the central opening. When the chamber was filled to the top the water level rose only a short way up the manifold, and electrical insulation of the soldered strain gauge wires was achieved by topping up the manifold with non-conducting transformer oil. The small positive displacement pump, which applied the test pressure, was then connected to the system and both ball valves of the chamber were closed.

At this point a hydrostatic test was ready to begin. For the combined axial compression and pressure tests, the central loading shaft was connected through a 500 kN load cell to a hydraulic

actuator, driven by a servo-controlled loading machine.

2.4.6.2 Strain gauging

The strain gauges on the inside of the cylinder, which remained dry throughout, were of the same type and applied in the same manner as in previous tests. On the outside, however, (the wet side of the model) more sophisticated materials and techniques had to be used to ensure operation under pressure.

"Micromeasurements" gauges and sealing materials were used according to the manufacturer's recommendations. After the gauges were bonded to the steel and the lead wires soldered to tags, a sealing agent was applied. Special low resistance wires with waterproof insulating material were connected to the tags. A thin polyurethane film was placed over each gauge and a substantial mastic coating was formed over the gauge, tags and around a short length of the lead wires. The whole area was then covered by an adhesive foil to complete the watertight seal.

The time and expense involved in this form of strain gauging and, more importantly, the limit on the number of wires which could be passed through the waterproof diaphragm and manifold restricted the number of gauges which could be used. The strain gauge arrangement adopted for the hyperbaric tests consisted of an internal and external cross gauge at the quarter positions of the cylinder's midheight circumference.

2.4.6.3 Hydrostatically-loaded models

The first models to be tested in the hyperbaric chamber were the 20 and 40 stiffener cylinders under hydrostatic pressure, models B and F. Similar behaviour under load was observed for both models: as

water was pumped into the chamber the pressure increased uniformly until a load plateau was reached. A relatively large volume of water had then to be added before any significant change in pressure was observed, and even beyond the peak the load fall-off was very gradual.

The 20 stiffener model resisted a pressure of 31.8 psi (0.219 N/mm^2), while the 40 stiffener model achieved 34.2 psi (0.236 N/mm^2). These pressures are respecively 15% and 16% of the pressure to produce a nominal hoop stress equal to yield and illustrate the weakness of this type of stiffening arrangement in resisting external pressure.

The modes of failure can be seen in the photographs of the models after testing (Figs 2.152 and 2.153) and from the plots of postbuckling radial deformations around the midheight circumference (Figs 2.154 and 2.155). The failure modes, which extended around a portion of the circumference, consisted of a series of alternate inward and outward deflecting panels, while the stiffeners remained straight. Sharp yield lines were formed along the centrelines of several panels, especially in the wider panelled model.

An approximate calculation of the critical buckling mode of an unstiffened cylinder using the formula given by Roark and Young [206] predicts eleven waves around the circumference. It is not surprising, therefore, that even light stiffeners were sufficient, in the 20 stiffener model, to limit the shell deflections along their lengths and to induce the ten wave mode observed in the experiment.

The local buckling mode for the 40 stiffener model would contain twenty circumferential waves. Because this mode is far removed from the preferred buckling mode of the unstiffened cylinder, very heavy stiffeners would be necessary to produce it. The cylinder, in fact, failed in an orthotropic mode: the buckles which formed can be seen in

Fig 2.155 to be part of a mode containing approximately eleven circumferential waves.

The longitudinal and circumferential membrane stresses are plotted against applied pressure in Figs 2.156 and 2.157. In both diagrams the stresses at location A were distorted by the readings obtained from a malfunctioning gauge. Neglecting these results, the stresses in the remaining positions of the 20 stiffener cylinder (Fig 2.156) are uniform and closely follow the analytically predicted stresses. In the other model the hoop stresses are, once again, uniform around the circumference, but the longitudinal stresses show a degree of scatter which is difficult to account for. Since the longitudinal compressive stress is applied by the pressure acting on the sealed ends of the cylinder and not by a loading ram, an eccentricity in the line of application of the load cannot arise. The nonuniform stress distribution must have been due to uneven contact between the end rings of the model and the loading plattens, or, more likely, between the end rings and the shell itself.

In both models the stresses remained linear until a pressure of approximately 24 psi (0.17 N/mm^2) was applied, above which the longitudinal stresses became increasingly nonlinear; their gradual departure from linearity is consistent with the soft buckling behaviour of the models.

2.4.6.4 Combined axial compression and pressure loaded models

By the time the axial and hydrostatic loading tests had been carried out, and two points obtained on the axial-pressure interaction curves for each cylinder, it was reasonably clear approximately what ratio of axial load to pressure for the remaining models would be most useful in defining the shape of the interaction curves. The loading

ratio was simply chosen as approximately equal to the ratio of the axial failure load to the hydrostatic failure pressure. Since the cylinders were relatively far stronger under axial load, the combined loading consisted primarily of axial compression with a small amount of pressure. The ratios of nominal axial stress to hoop stress σ_x/σ_θ were 6.65 and 6.15 for the 20 and 40 stiffener models respectively.

Load was applied so that at the end of each increment the required ratio of loading was obtained precisely, whilst during the increments themselves the ratio was maintained approximately correct by applying axial and pressure loading concurrently.

The combined loading at which the 20 stiffener cylinder failed consisted of an axial load of 154 kN (15.5 tons) and a pressure of 21.5 psi (0.145 N/mm^2); the 40 stiffener model reached 160 kN (16.1 tons) and 22.3 psi (0.154 N/mm^2). Allowing for the extra axial stress produced in the models by the pressure acting on their ends, the applied axial stresses at failure were 246 and 240 N/mm^2 for the 20 and 40 stiffener models respectively. Because it had a slightly smaller cross-sectional area, the 20 stiffener model was subjected to the higher value of applied stress even though its ultimate load was less.

However, the surprising fact still remains that a relatively small amount of pressure produced a far greater strength deterioration in the 40 stiffener cylinder. Although under axial load the more heavily stiffened model was stronger by 42%, under combined loading the strengths were almost identical. In fact, the axial-pressure interaction curves for the two sets of models, given in Fig 3.15, show that the ultimate loads of the cylinders were virtually unaffected by the number of stiffeners except under axial load.

Of course, experimental scatter may be a factor in the distribution of observed results, and before any conclusions could be drawn with certainty more corroborative results would be desirable.

In both experiments the failure was sudden and audible, as it had been in the axial tests. Figs 2.158 and 2.159 show that in the mode of buckling the cylinders also resembled their axially-loaded counterparts. The plots of radial deformations around the midheight circumference, Figs 2.160 and 2.161, clearly show that the buckling modes contained ten waves, even though they were not fully developed around the model.

The graphs of longitudinal and hoop stresses against applied axial load, Figs 2.162 and 2.163, show that for both models the behaviour was linear until very near the failure load.

2.4.7 DISCUSSION

The techniques used in the fabrication of the earlier small-scale cylinders were succesfully applied in the manufacture of the present set of more slender models. All the DnV tolerances were met, although the imperfection levels were higher than in previous models. This was due to the use of forming equipment which was modified rather than tailor-made to suit the thinner sheet material, and not due to any limitations of the manufacturing process itself. There appears to be no reason to prevent the use of yet thinner sheet other than the difficulty of obtaining representative mechanical properties.

The sudden and precipitous buckling behaviour of the axial and combined loading tests was the result of the slender shell properties and the small stringers. In the axially-loaded, wide-panelled model the stringers, due to their small size, were capable of only temporarily limiting the growth of the elastic local shell buckles.

In the narrow-panelled cylinder this mode was prevented completely and a much higher load was supported before the model finally failed in an orthotropic mode.

Under external pressure the cylinders were extremely weak. The model bay length was too large to produce an efficient design for resisting external pressure and would be reduced in practice by inserting intermediate ring stiffeners. This weakness under external pressure meant that in the combined loading tests low pressures were sufficient to produce a significant deterioration in axial load-carrying capacity.

Since radial deflections could not be measured during the hyperbaric tests, clues to the behaviour of the combined loading models must be sought in the more complete descriptions of the axial specimens. It was seen that under axial load the prebuckling deflections of the 20 and 40 stringer models were significantly different in shape. In the more heavily stiffened model the prebuckling mode contained a single half wave in the axial direction. In the combined loading test the external pressure reduced the outward deformations so that there was less difference between this mode and the inward postbuckling mode, and snap through took place at a lower load.

The 20 stiffener cylinder, by contrast, deformed under axial load in a mode containing several waves along the length of the model, and it initially buckled in a localized mode of similar shape. The addition of external pressure would superimpose a single axial halfwave deflection which would have little effect on the overall behaviour.

This discussion has been highly conjectural, and it would have

been useful to have detailed deflection readings to establish its validity. However, it is supported by the fact that the reduction in axial load carrying capacity was, in fact, much greater in the 40 stiffener model than in the 20 stiffener model.

Table 2.1 GEOMETRIC PARAMETERS OF IC4

Shell	Center panel	Outer panels
Radius, R (mm)	599.2	600
Thickness, t (mm)	3.53	4.0
R/t	170	150
Length, L (mm)	666	666
L/R	1.11	1.11
No. of stringers, N	20	20
Panel width, s (mm)	188	188
s/t	53.3	47.1
L/s	3.54	3.54
Stringers		
Depth, d_s (mm)	48	48
Thickness, t_s (mm)	3.53	4.0
d_s/t_s	13.6	12.0
Rings		
Depth of web, d_w (mm)	60	
Thickness of web, t_w (mm)	3.53	
d_w/t_w	17.0	
Width of flange, b_f (mm)	30	
Thickness of flange, t_f (mm)	3.53	
b_f/t_f	8.5	

Table 2.2 MATERIAL PROPERTIES OF IC4

Grade	Upper Yield $(t)_2$ N/mm^2	Lower Yield $(t)_2$ N/mm^2	Ultimate $(t)_2$ N/mm^2	Lower Yield $(c)_2$ N/mm^2	Young's Modulus kN/mm^2
43	292	279	433	289	205
50	359	334	470	344	213

(t) tension (c) compression

Lower Yield (c) = Lower Yield (t) + 10 N/mm^2

Table 2.3 GEOMETRIC PARAMETERS OF SMALL-SCALE SERIES

Cylinder	1-4	5-8	9-12
Radius, R (mm)	160	160	160
Thickness, t (mm)	0.84	0.84	0.84
R/t	190	190	190
Length, L (mm)	64	128	192
L/R	0.40	0.80	1.20
No. of stringers, N	40	40	40
Panel width, s (mm)	25.1	25.1	25.1
s/t	30	30	30
L/s	2.55	5.10	7.65
Depth of stringers, d_s (mm)	6.72	6.72	6.72
d_s/t_s	8.0	8.0	8.0

Table 2.4 EXPERIMENTAL FAILURE LOADS

Cylinder	1	2	3	4	5	6	7	8	9	10	11	12
σ_x (N/mm^2)	327	136	39	336	65	0.6	347	290	46	365	0.1	184
σ_θ (N/mm^2)	0	346	363	237	165	184	0	148	116	0	121	92
σ_x/σ_θ	-	.396	.11	1.42	.396	.004	-	1.96	.396	-	.002	2.0

Table 2.5 INITIAL IMPERFECTIONS - SMALL-SCALE SERIES

Cylinder	1	2	3	4	5	6	7	8	9	10	11	12
Perfect radius, R	159.99	159.99	159.95	159.97	159.89	159.83	159.90	159.90	159.87	159.91	159.89	159.95
Max outward reading, ΔR+	0.10 (0.80)	0.22 (0.80)	0.16 (0.80)	0.09 (0.80)	0.22 (0.80)	0.14 (0.80)	0.17 (0.80)	0.17 (0.80)	0.16 (0.80)	0.24 (0.80)	0.28 (0.80)	0.23 (0.80)
Max inward reading, ΔR-	-0.22 (0.80)	-0.24 (0.80)	-0.23 (0.80)	-0.22 (0.80)	-0.28 (0.80)	-0.41 (0.80)	-0.31 (0.80)	-0.23 (0.80)	-0.20 (0.80)	-0.32 (0.80)	-0.30 (0.80)	(0.80)
Out-of-straightness, δ_g	0.10 (0.39)	0.08 (0.39)	0.13 (0.39)	0.17 (0.39)	0.10 (0.39)	0.16 (0.39)	0.20 (0.39)	0.10 (0.39)	0.19 (0.39)	0.17 (0.39)	0.17 (0.39)	0.10 (0.39)
Deviation from circle, e	0.21 (0.44)	0.23 (0.44)	0.17 (0.44)	0.21 (0.44)	0.24 (0.53)	0.22 (0.53)	0.26 (0.53)	0.19 (0.53)	0.32 (0.59)	0.31 (0.59)	0.32 (0.59)	0.31 (0.59)
Stiffener out-of-straightness, w_g	0.07 (0.10)	0.07 (0.10)	0.08 (0.10)	0.11 (0.10)	0.12 (0.19)	0.12 (0.19)	0.12 (0.19)	0.09 (0.19)	0.16 (0.29)	0.24 (0.29)	0.20 (0.29)	0.14 (0.29)

Figures in brackets are allowable DnV tolerances

Table 2.6 GEOMETRIC PARAMETERS OF SLENDER SERIES

Cylinder	A-C	E-G
Radius, R (mm)	160	160
Thickness, t (mm)	0.63	0.63
R/t	254	254
Length, L (mm)	160	160
L/R	1.0	1.0
No. of stringers, N	20	40
Panel width, s (mm)	50.3	25.1
s/t	80	40
L/s	3.2	1.6
Depth of stringers, d_s (mm)	3.6	3.6
d_s/t_s	6.0	6.0

Table 2.7 EXPERIMENTAL FAILURE LOADS - SLENDER SERIES

Cylinder	A	B	C	E	F	G
σ_x (N/mm^2)	281	26	246	399	26	240
σ_θ (N/mm^2)	0	56	37	0	60	39
σ_x/σ_θ	-	0.46	6.65	-	0.43	6.15

Table 2.8 INITIAL IMPERFECTIONS - SLENDER SERIES

Cylinder	A	B	C	E	F	G
Perfect radius, R	159.61	159.63	159.60	159.57	159.62	159.61
Max outward reading, ΔR+	0.44 (0.80)	0.54 (0.80)	0.49 (0.80)	0.47 (0.80)	0.40 (0.80)	0.66 (0.80)
Max inward reading, ΔR-	-0.54 (0.80)	-0.50 (0.80)	-0.49 (0.80)	-0.45 (0.80)	-0.36 (0.80)	-0.44 (0.80)
Out-of-straightness, δ_g	0.18 (0.33)	0.23 (0.33)	0.12 (0.33)	0.10 (0.33)	0.14 (0.33)	0.12 (0.33)
Deviation from circle, e	0.35 (0.63)	0.23 (0.63)	0.27 (0.63)	0.31 (0.63)	0.33 (0.63)	0.31 (0.63)
Stiffener out-of-straightness, w_s	0.14 (0.24)	0.15 (0.24)	0.22 (0.24)	0.25 (0.24)	0.22 (0.24)	0.24 (0.24)

Figures in brackets are allowable DnV tolerances
All dimensions in mm

CYLINDER IC4 - FABRICATION DETAILS

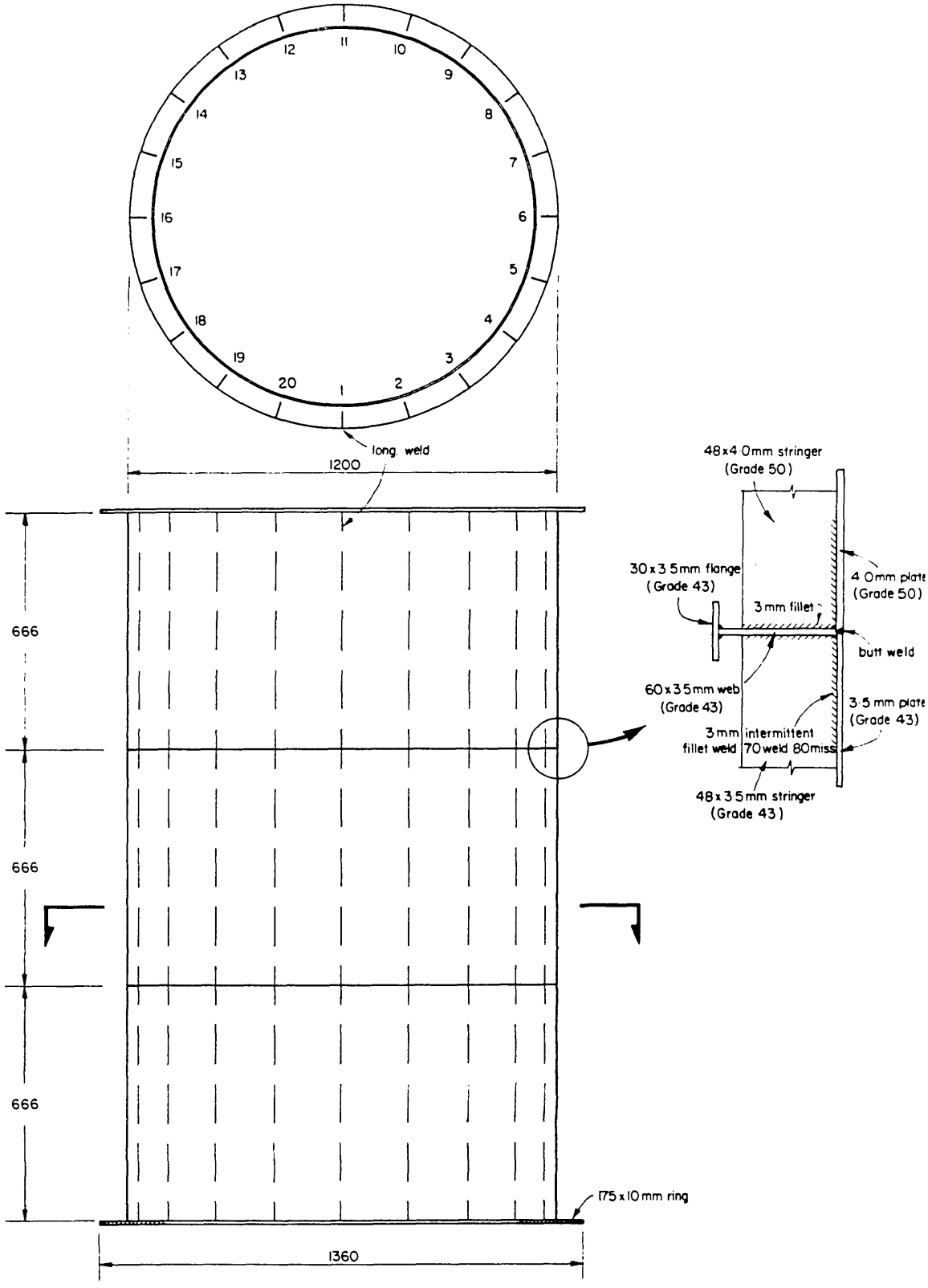
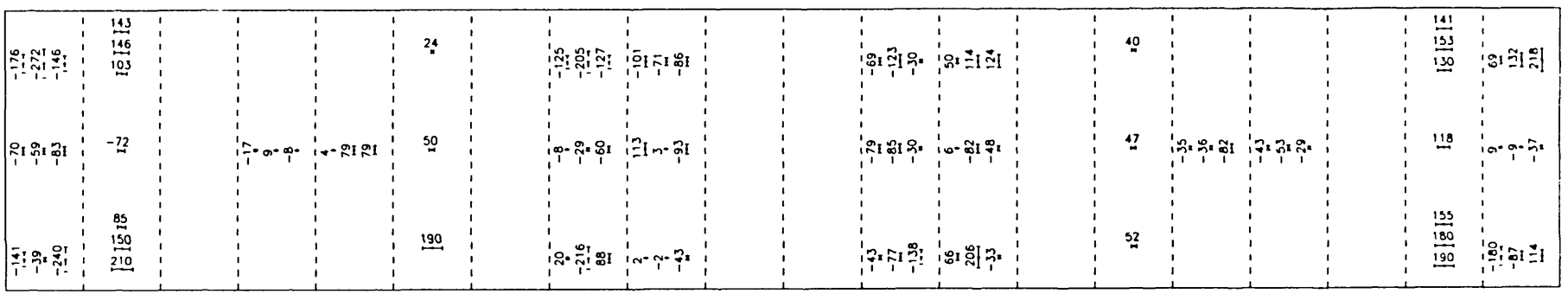


Fig. 2.1

CYLINDER IC4 – RESIDUAL STRAINS

Positive strains are compressive

After butt welding of plates



After rolling and long. butt weld

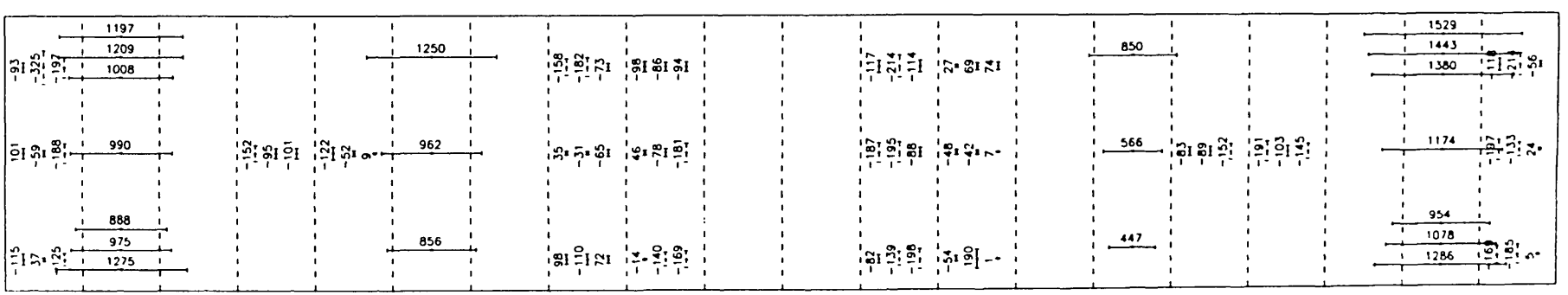
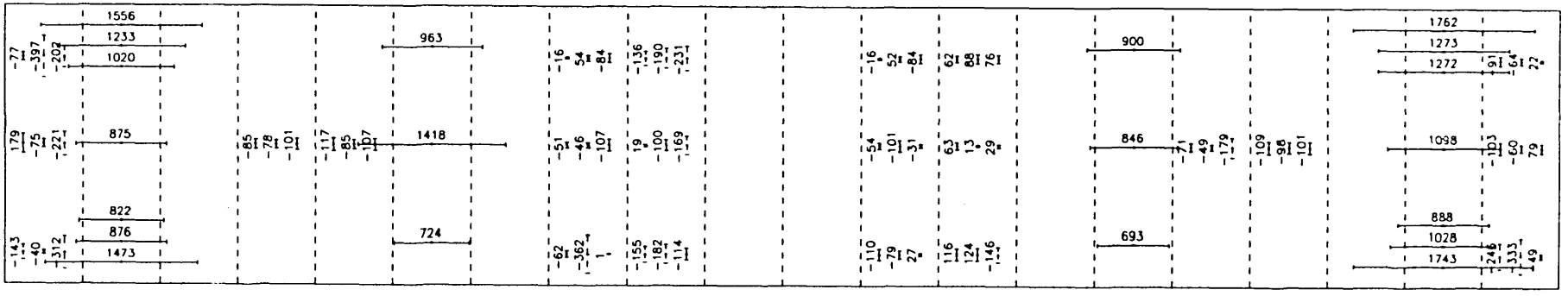


Fig. 2.2

CYLINDER IC4 – RESIDUAL STRAINS

Positive strains are compressive

After welding of ring stiffeners



After completion

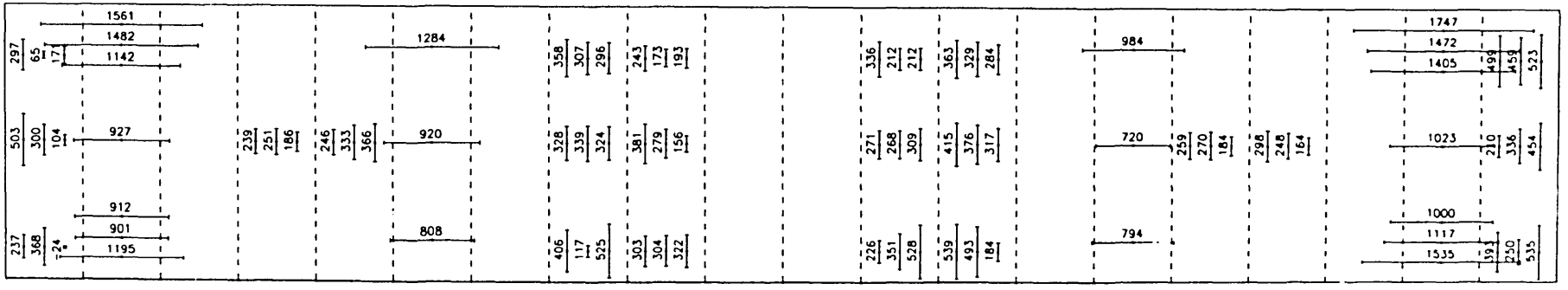
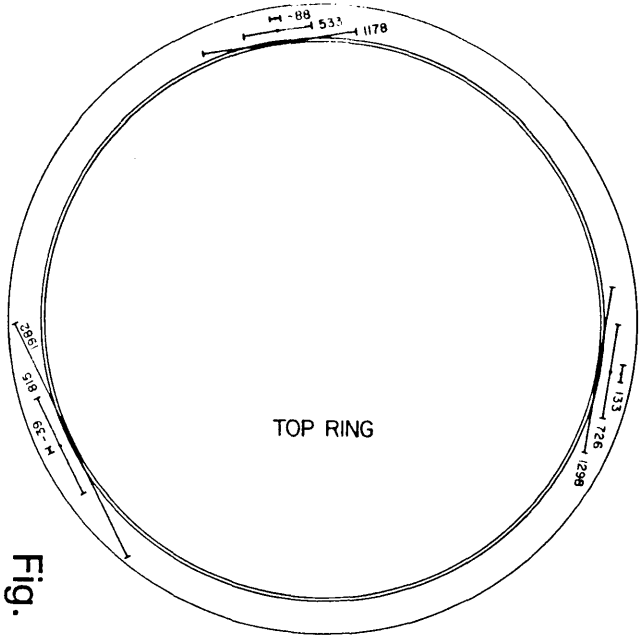


Fig. 2.3

CYLINDER IC4 - RESIDUAL STRAINS

After fabrication of rings



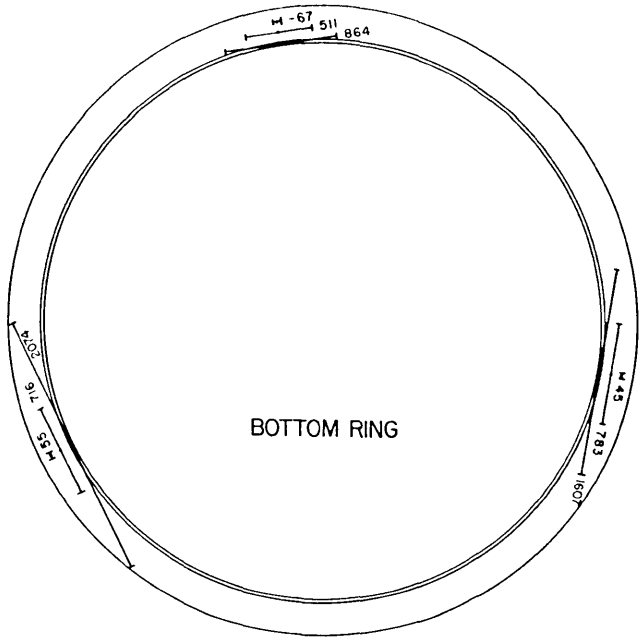
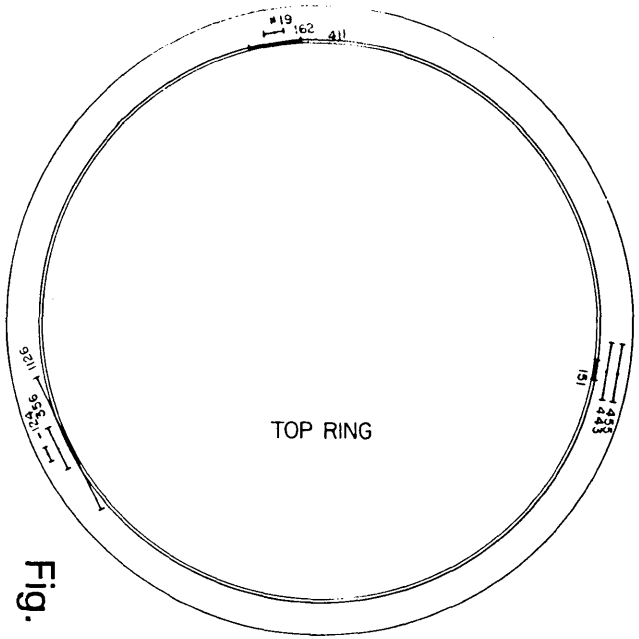


Fig. 2.4

Positive strains are compressive

CYLINDER IC4 - RESIDUAL STRAINS

After welding of rings



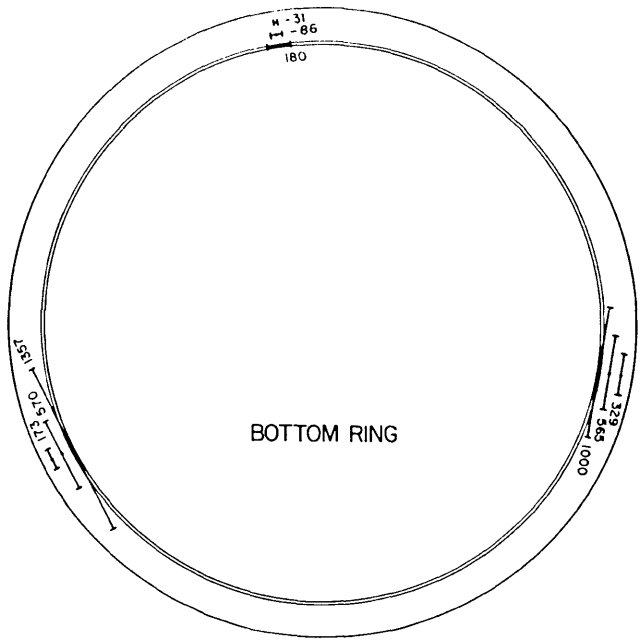
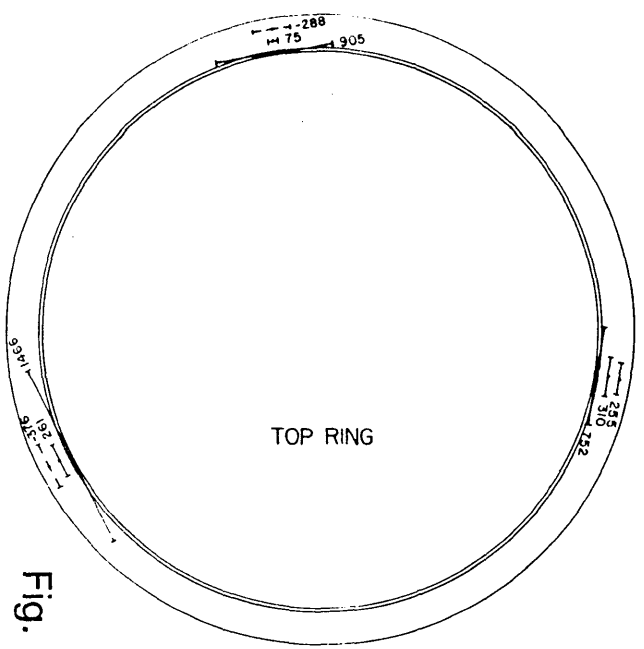


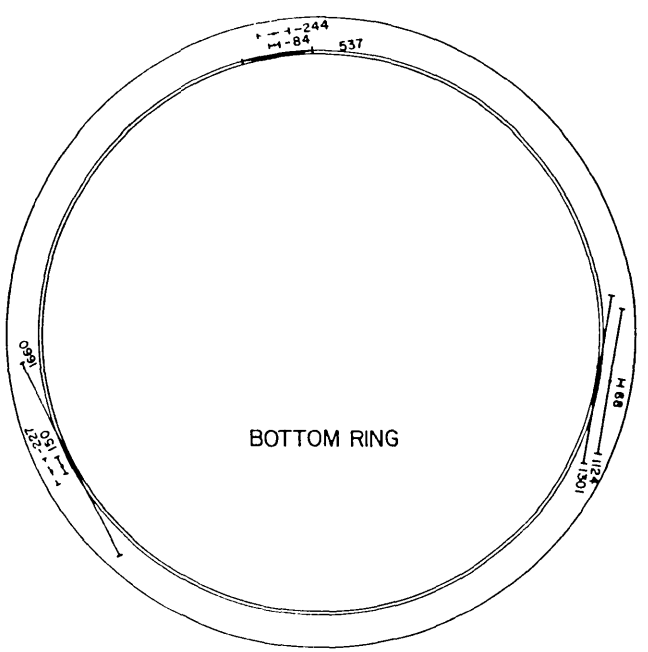
Fig. 2.5

Positive strains are compressive

CYLINDER IC4 - RESIDUAL STRAINS

After Completion





Positive strains are compressive

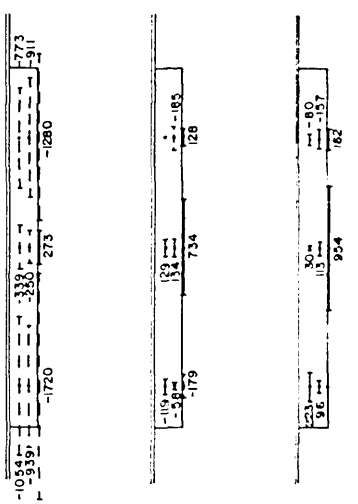
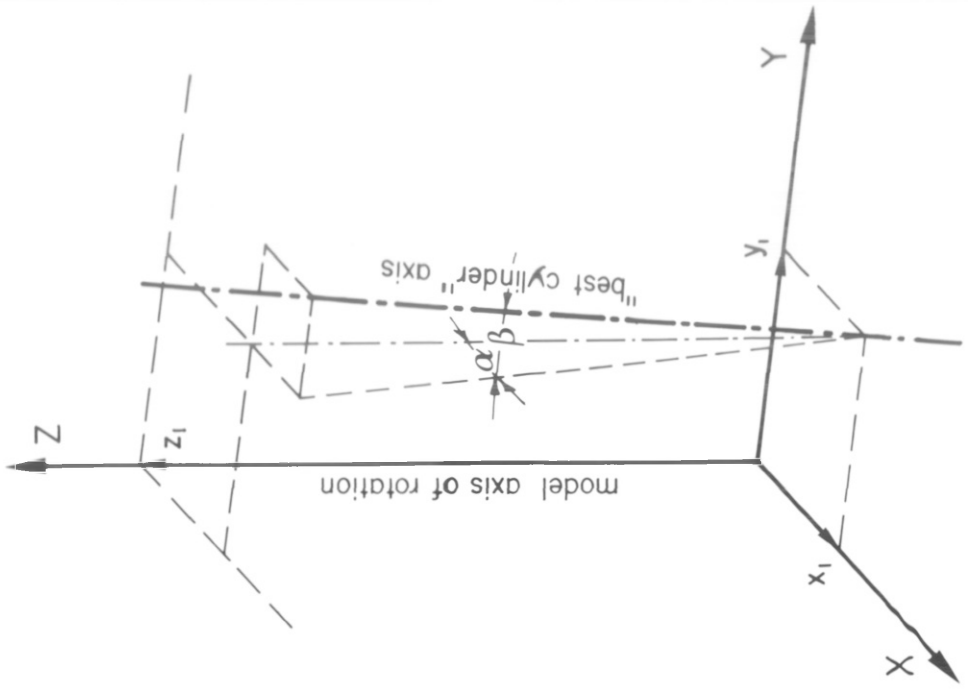
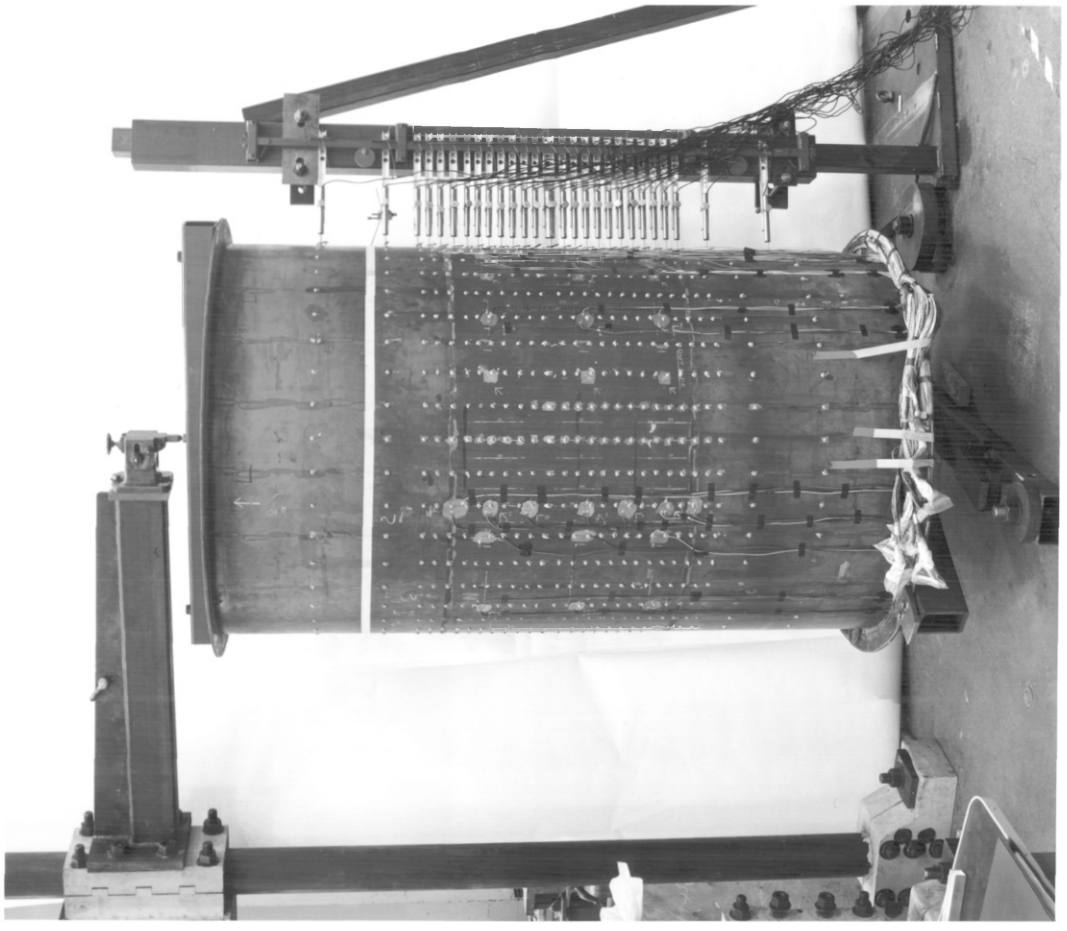


Fig. 2.6



DEFINITION OF BEST-FIT CYLINDER

Fig. 2.7



SETUP FOR IMPERFECTION MEASUREMENTS

Fig. 2.8

CYLINDER IC4 – INITIAL IMPERFECTIONS
Circumferential Sections

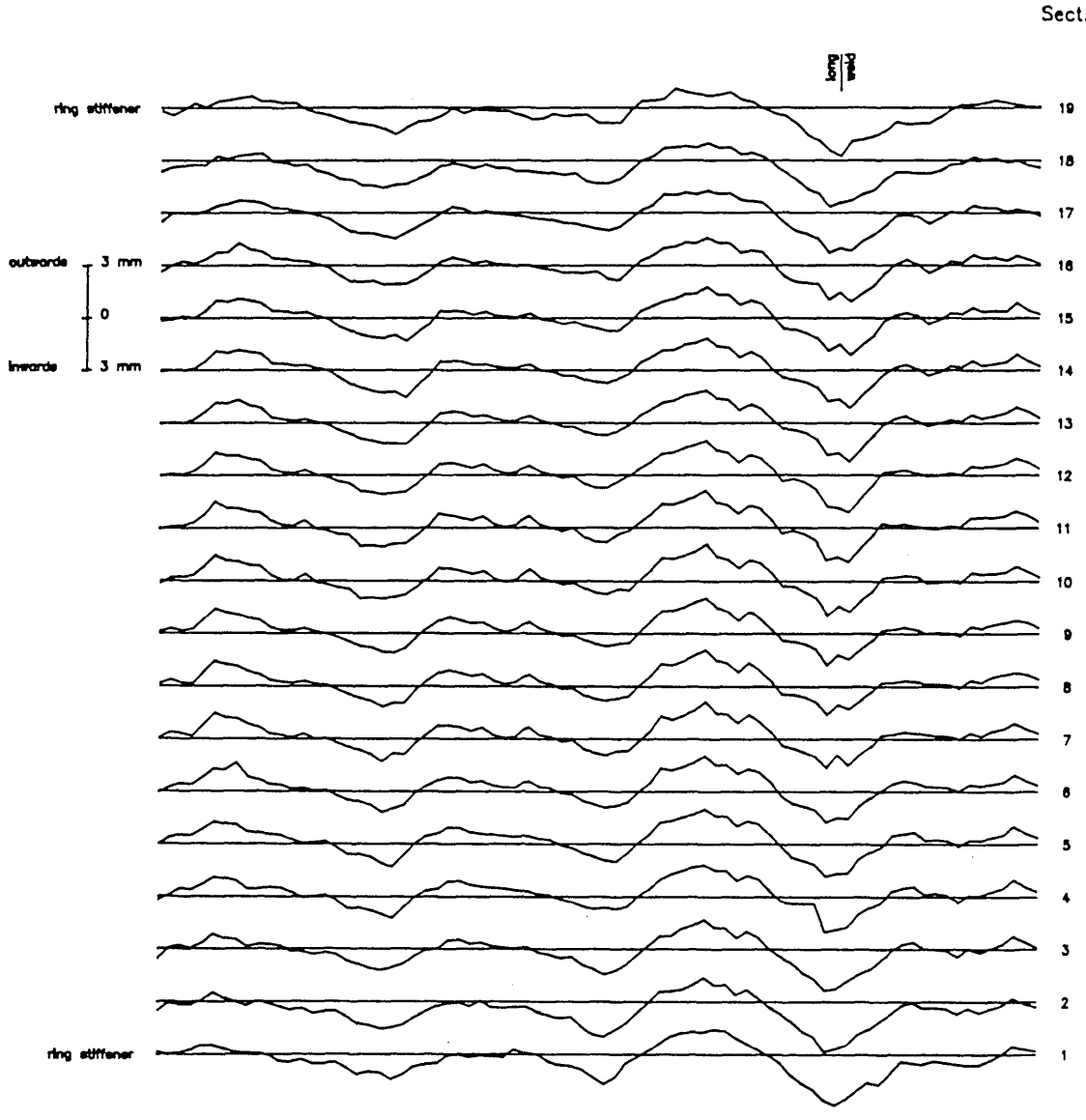


Fig. 2.9

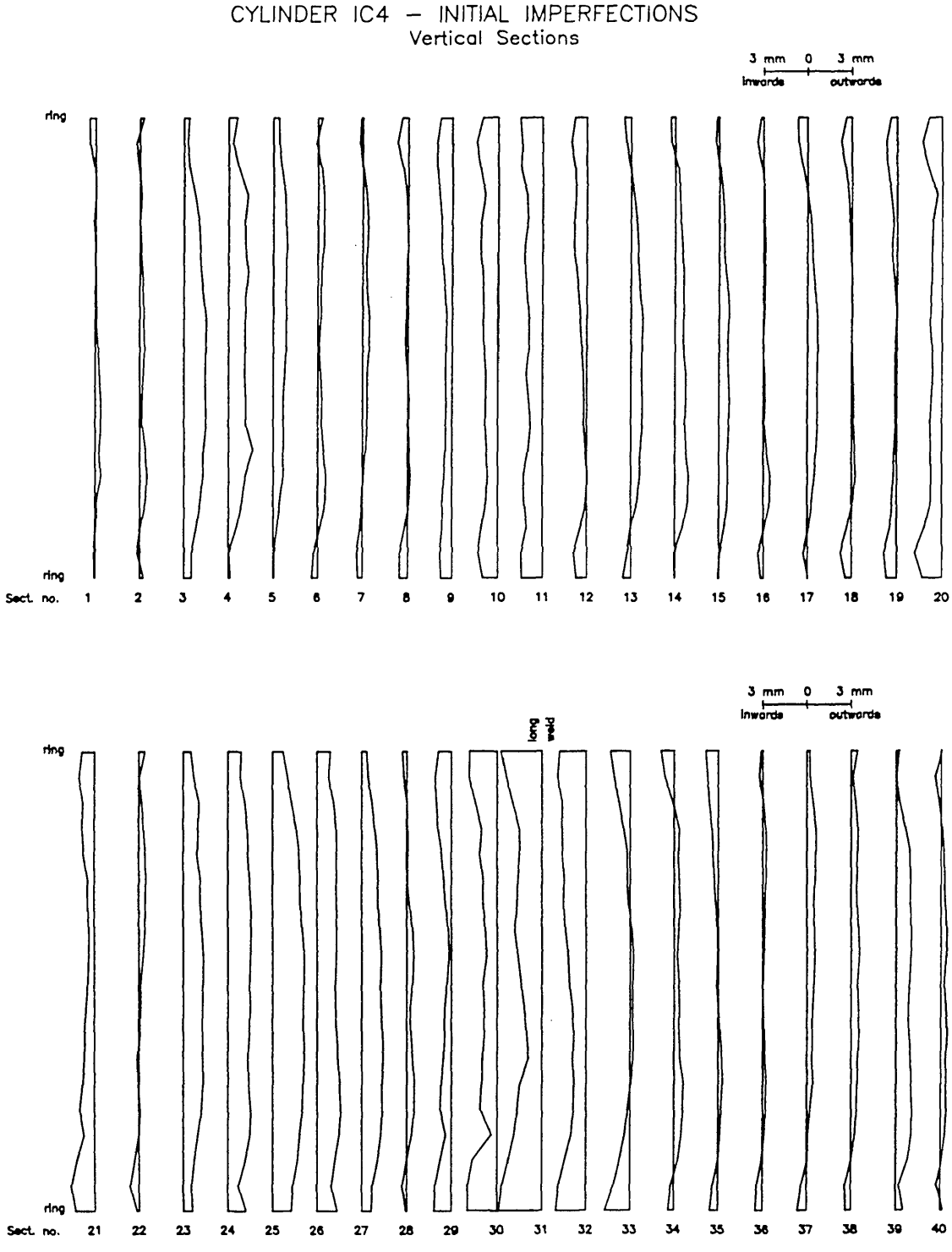

CYLINDER IC4 – INITIAL IMPERFECTIONS
Vertical Sections
3 mm 0 3 mm
inwards outwards
ring
ring
Sect. no. 1 2 3 4 5 6 7 8 9 10 11 12 13 14 15 16 17 18 19 20
3 mm 0 3 mm
inwards outwards
long weld
ring
ring
Sect. no. 21 22 23 24 25 26 27 28 29 30 31 32 33 34 35 36 37 38 39 40

Fig. 2.10

CYLINDER IC4 – INITIAL IMPERFECTIONS

Projection of imperfection surface

Fig. 2.11

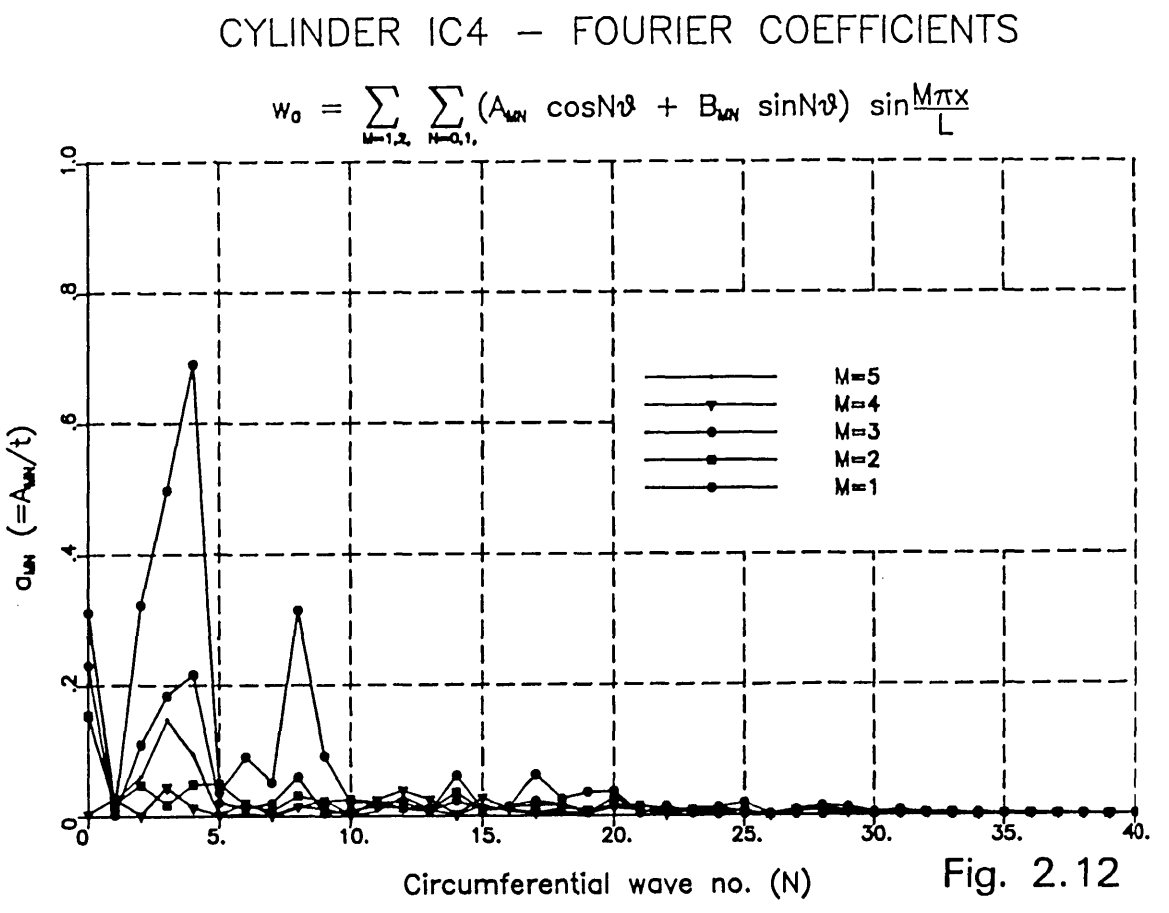


Fig. 2.12

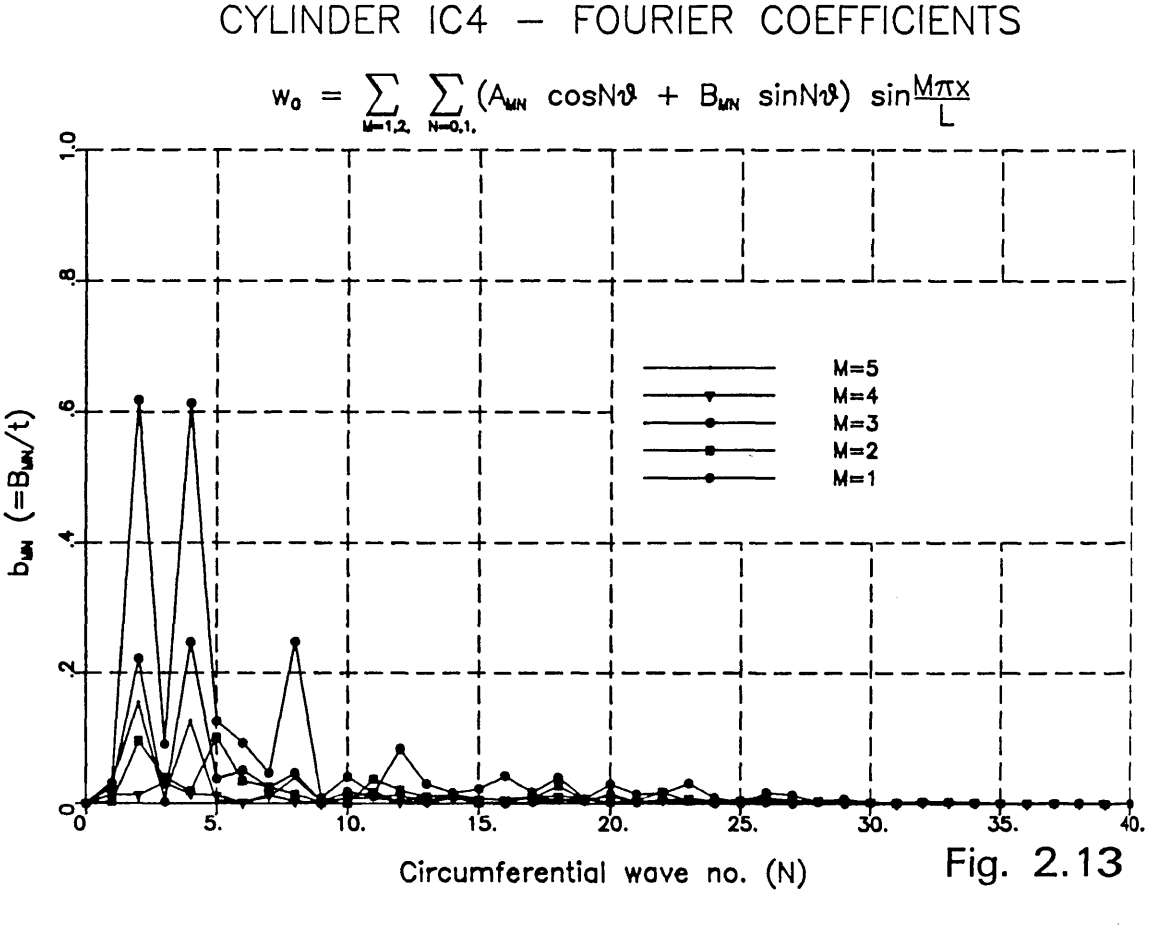


Fig. 2.13

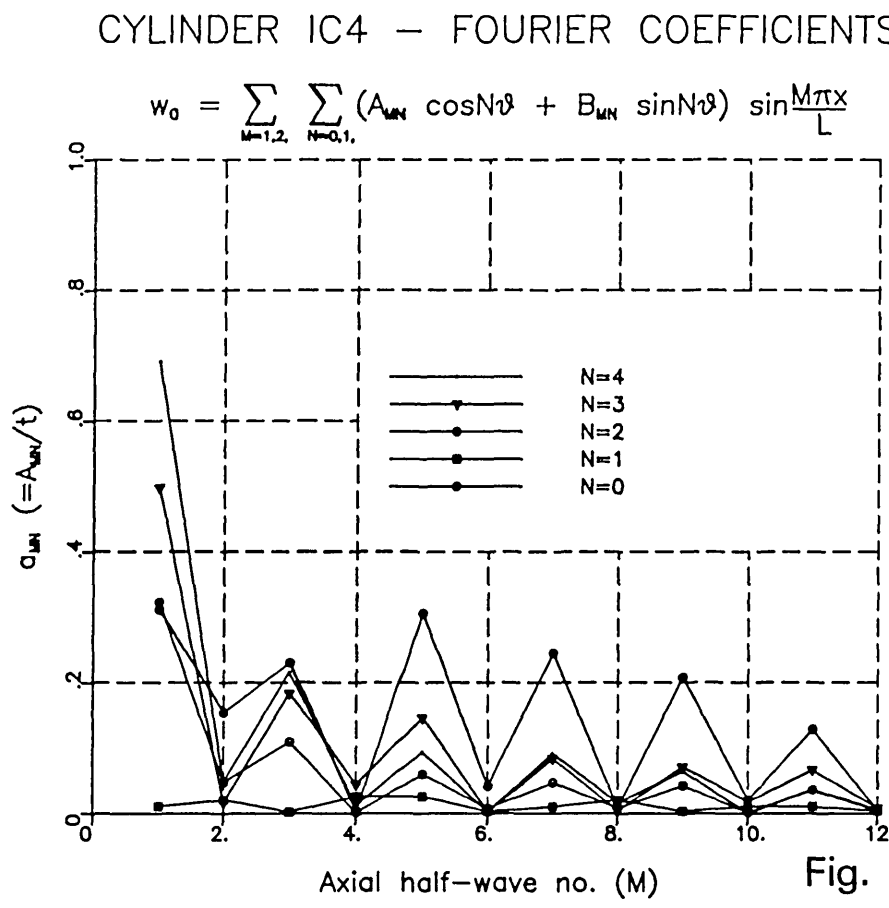


Fig. 2.14

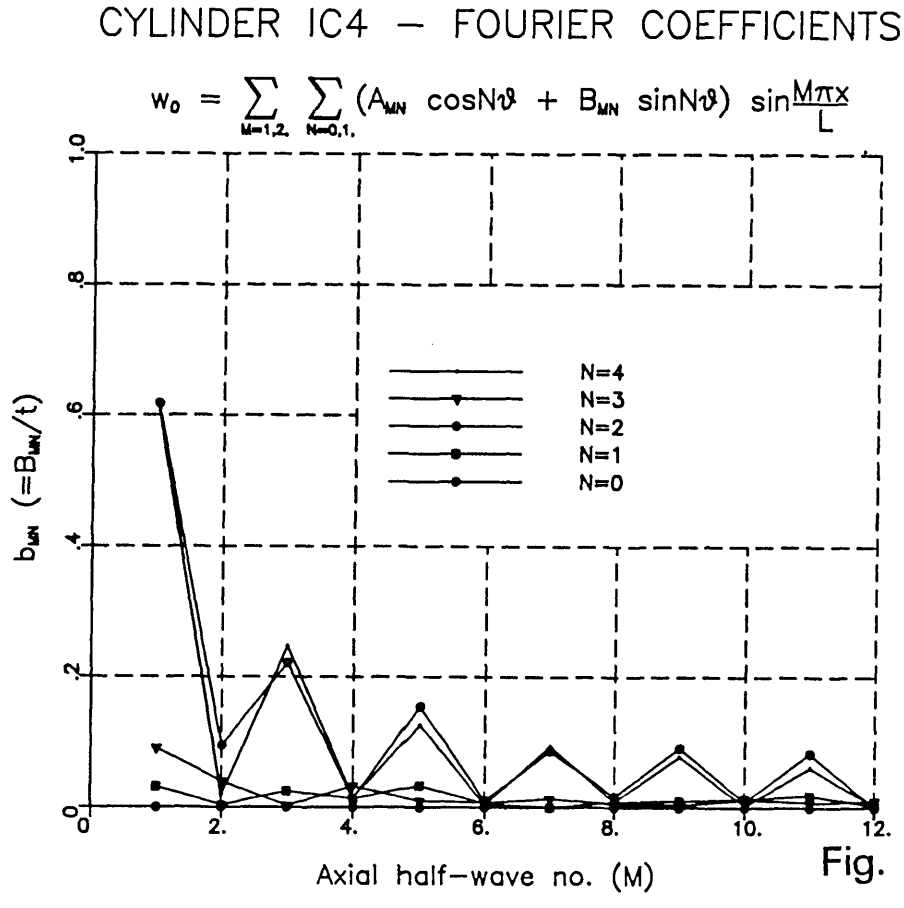


Fig. 2.15

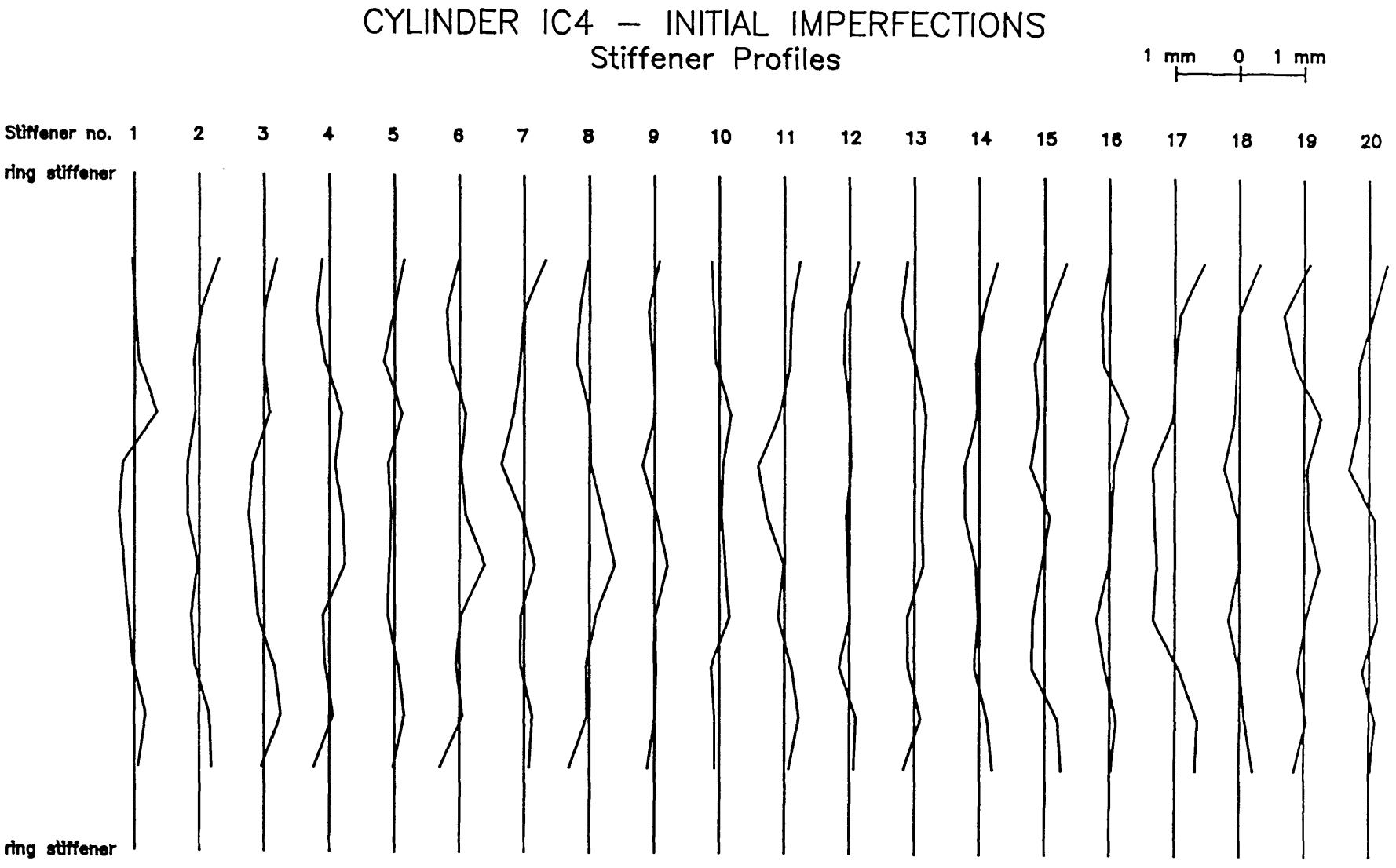
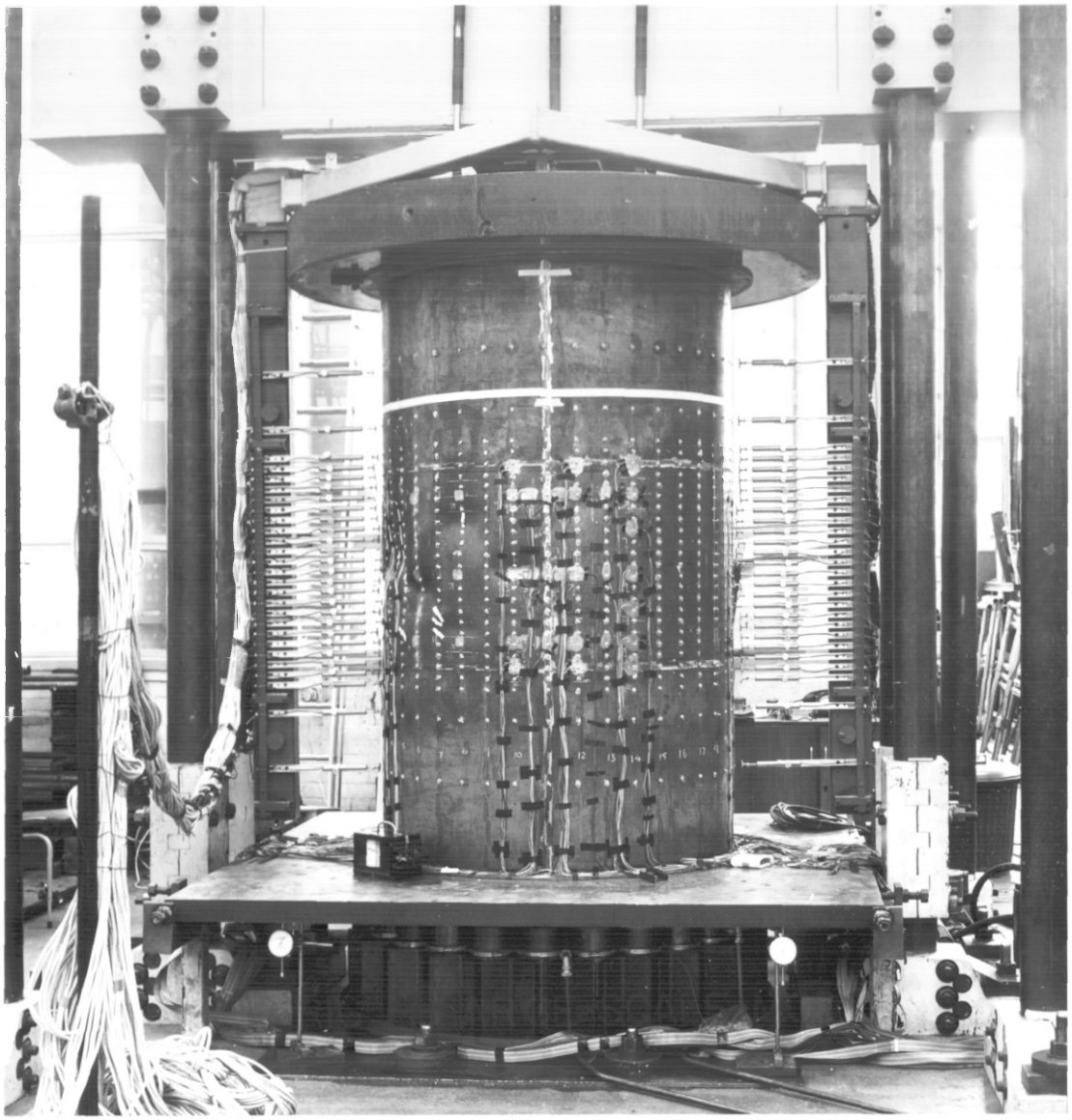

CYLINDER IC4 – INITIAL IMPERFECTIONS
Stiffener Profiles
1 mm 0 1 mm
Stiffener no. 1 2 3 4 5 6 7 8 9 10 11 12 13 14 15 16 17 18 19 20
ring stiffener
ring stiffener

Fig. 2.16



TEST RIG - LARGE-SCALE MODEL

Fig. 2.17

CYLINDER IC4 - STRAIN GAUGE LOCATIONS

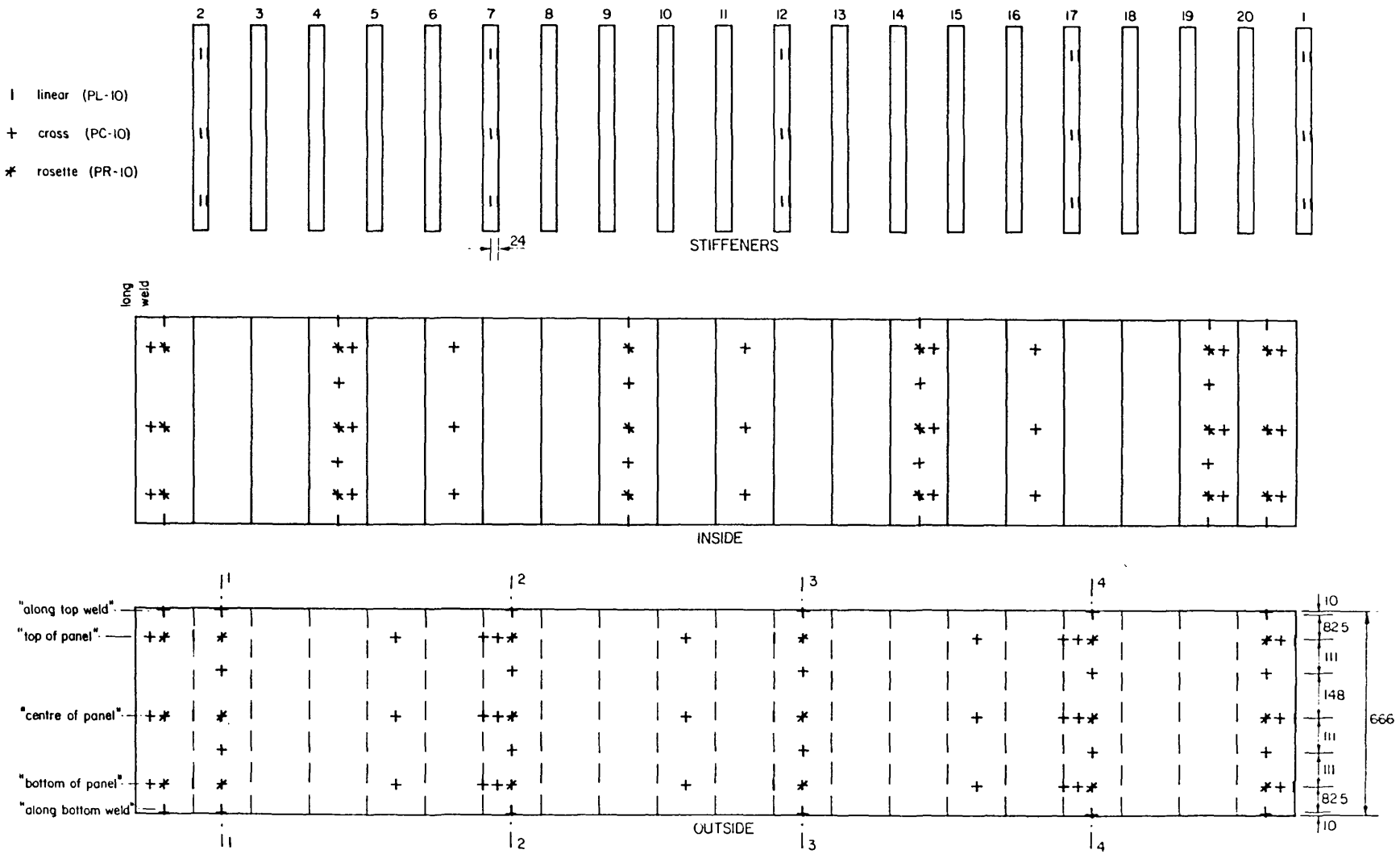


Fig. 2.18

CYLINDER IC4 - STRAIN GAUGE LOCATIONS

Ring Stiffeners

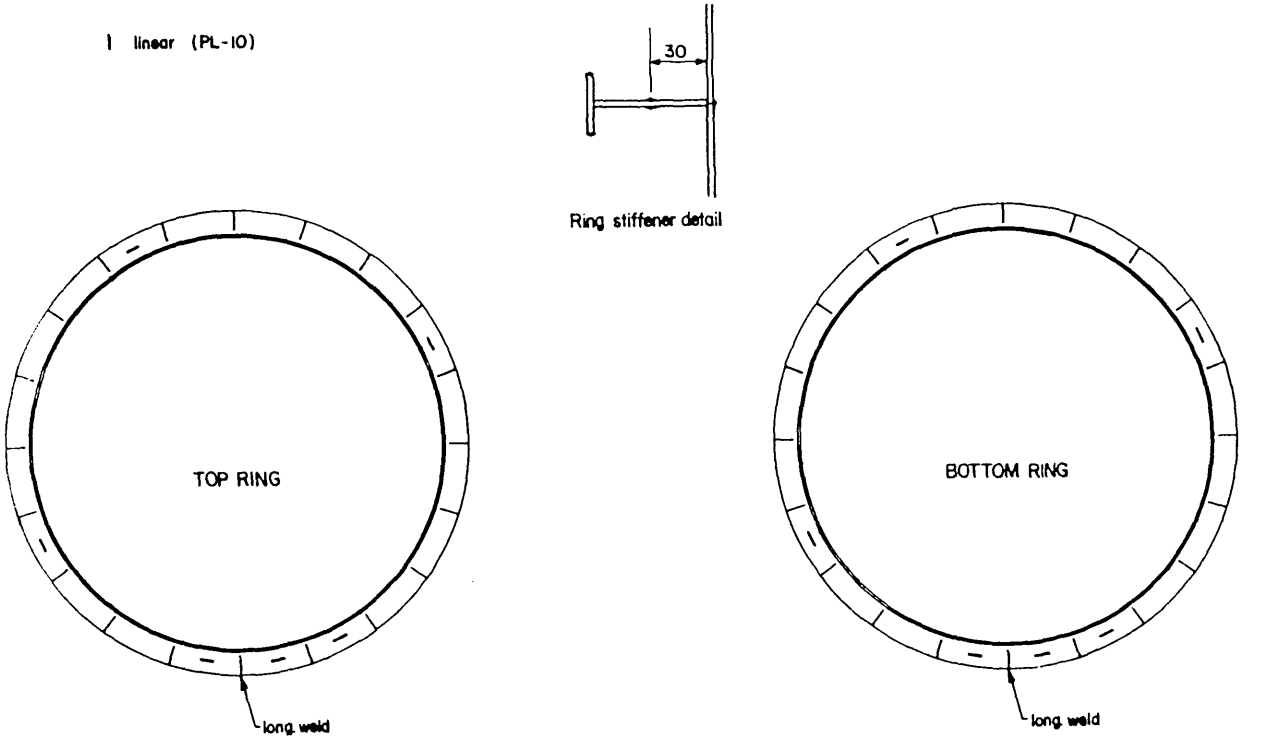


Fig. 2.19

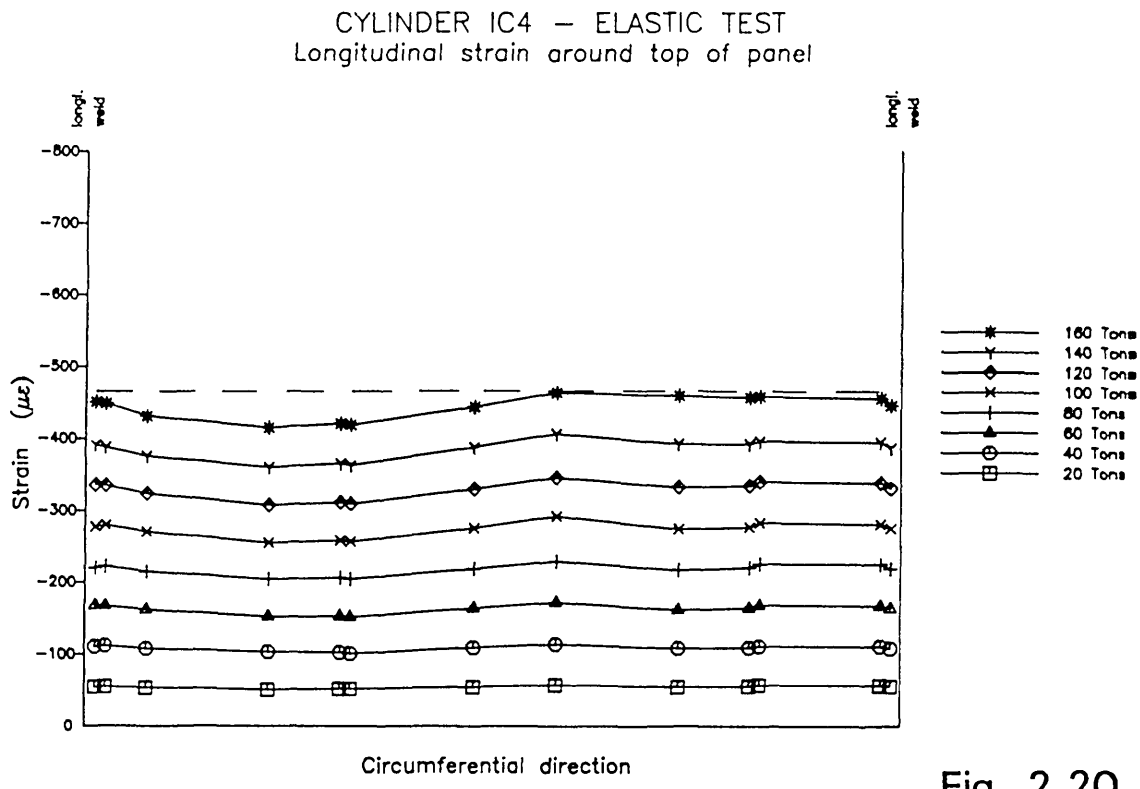


Fig. 2.20

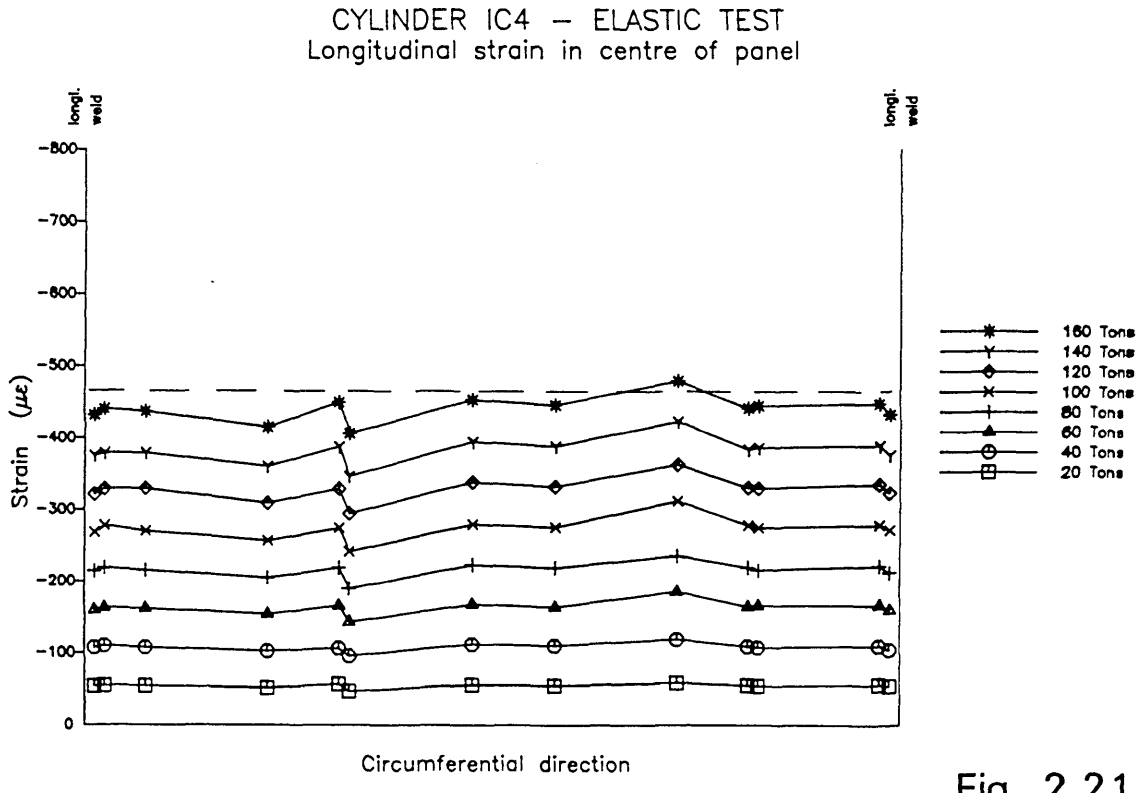


Fig. 2.21

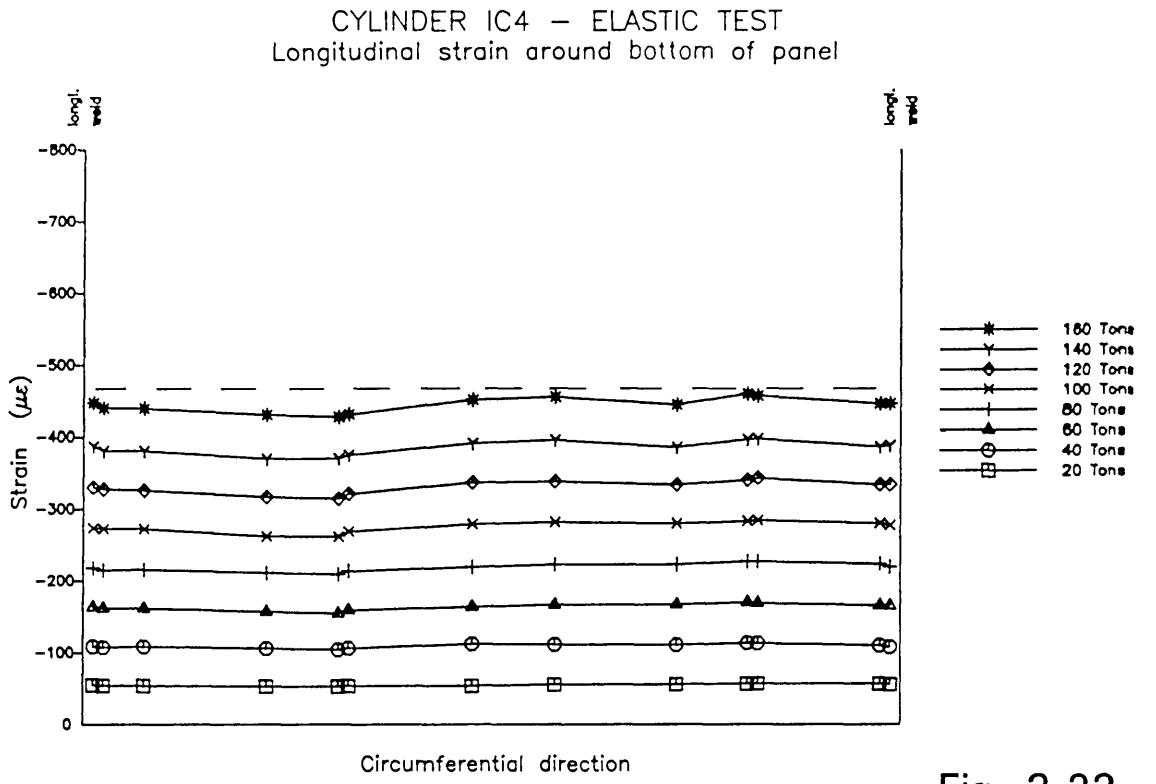


Fig. 2.22

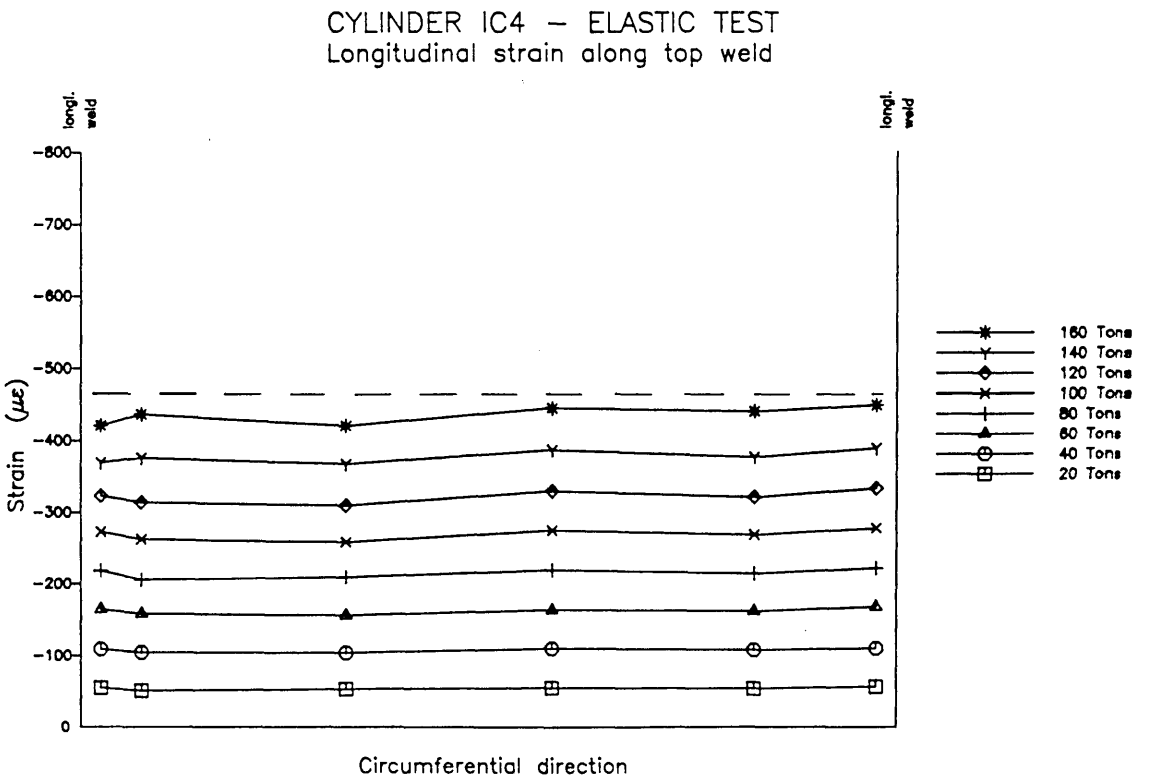


Fig. 2.23

CYLINDER IC4 – ELASTIC TEST
Longitudinal strain along bottom weld

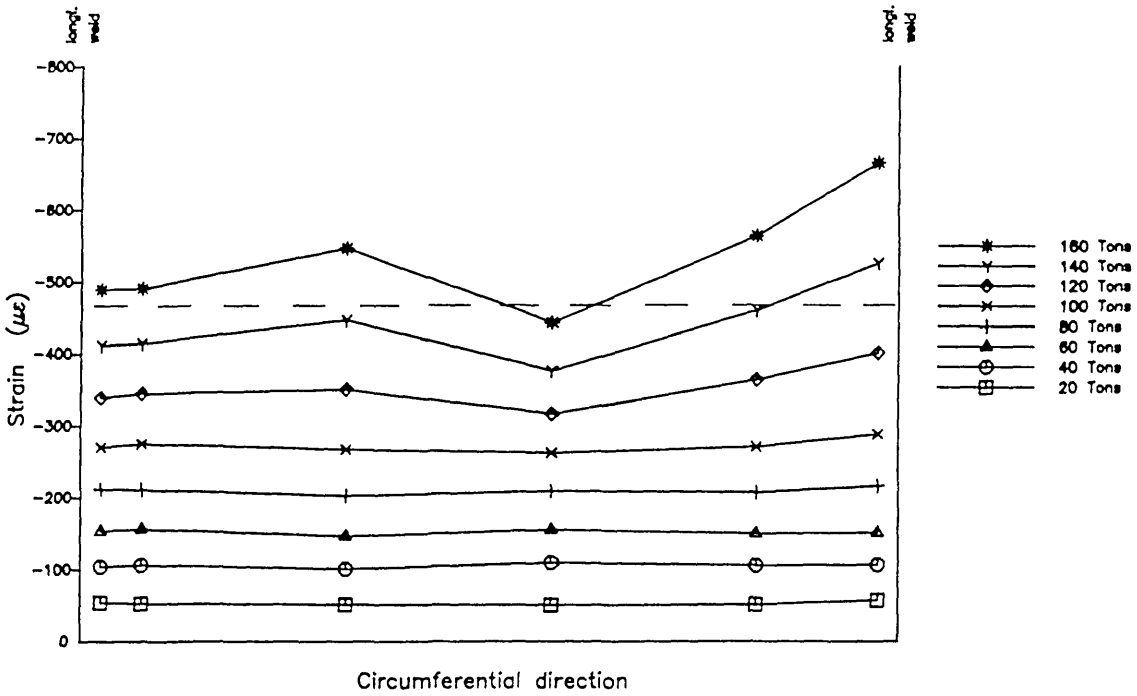


Fig. 2.24

CYLINDER IC4 – ELASTIC TEST
Longitudinal strain down centre panel

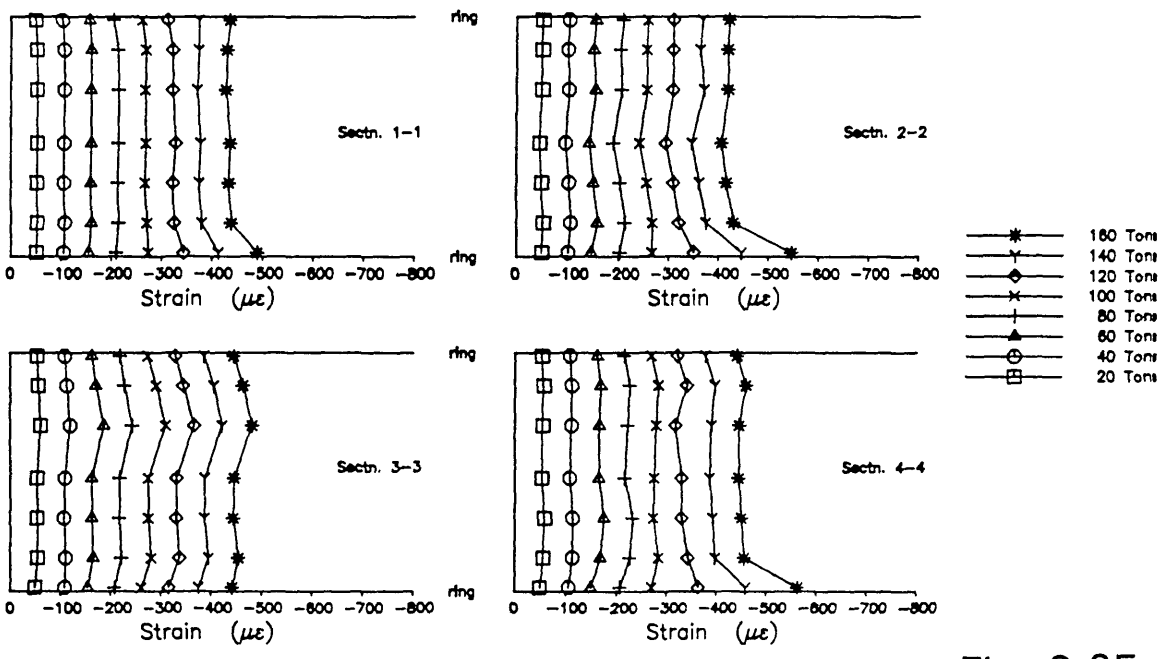


Fig. 2.25

CYLINDER IC4 – ELASTIC TEST
Hoop strain down centre panel

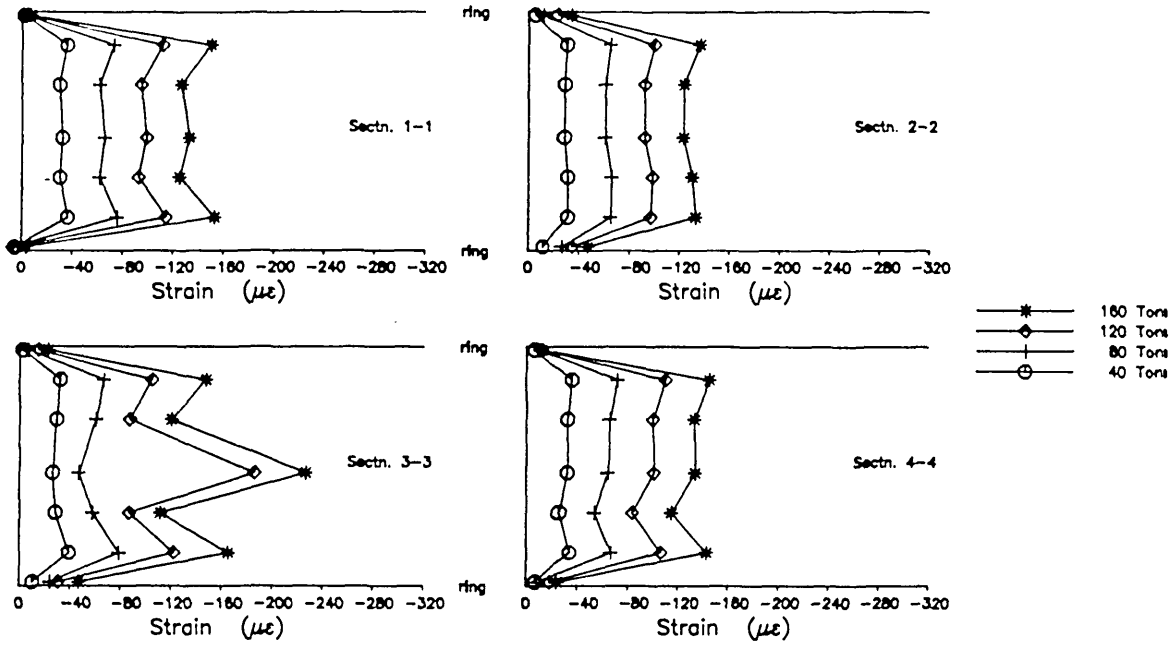


Fig. 2.26

CYLINDER IC4 – ELASTIC TEST
Hoop stress down centre panel

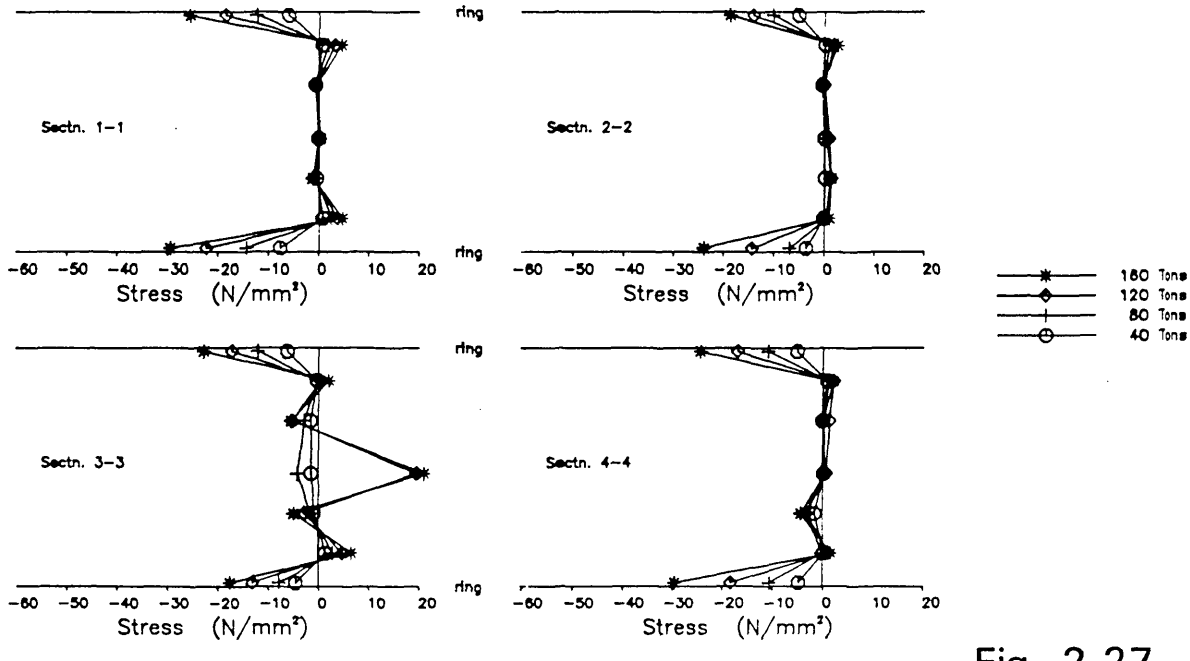


Fig. 2.27

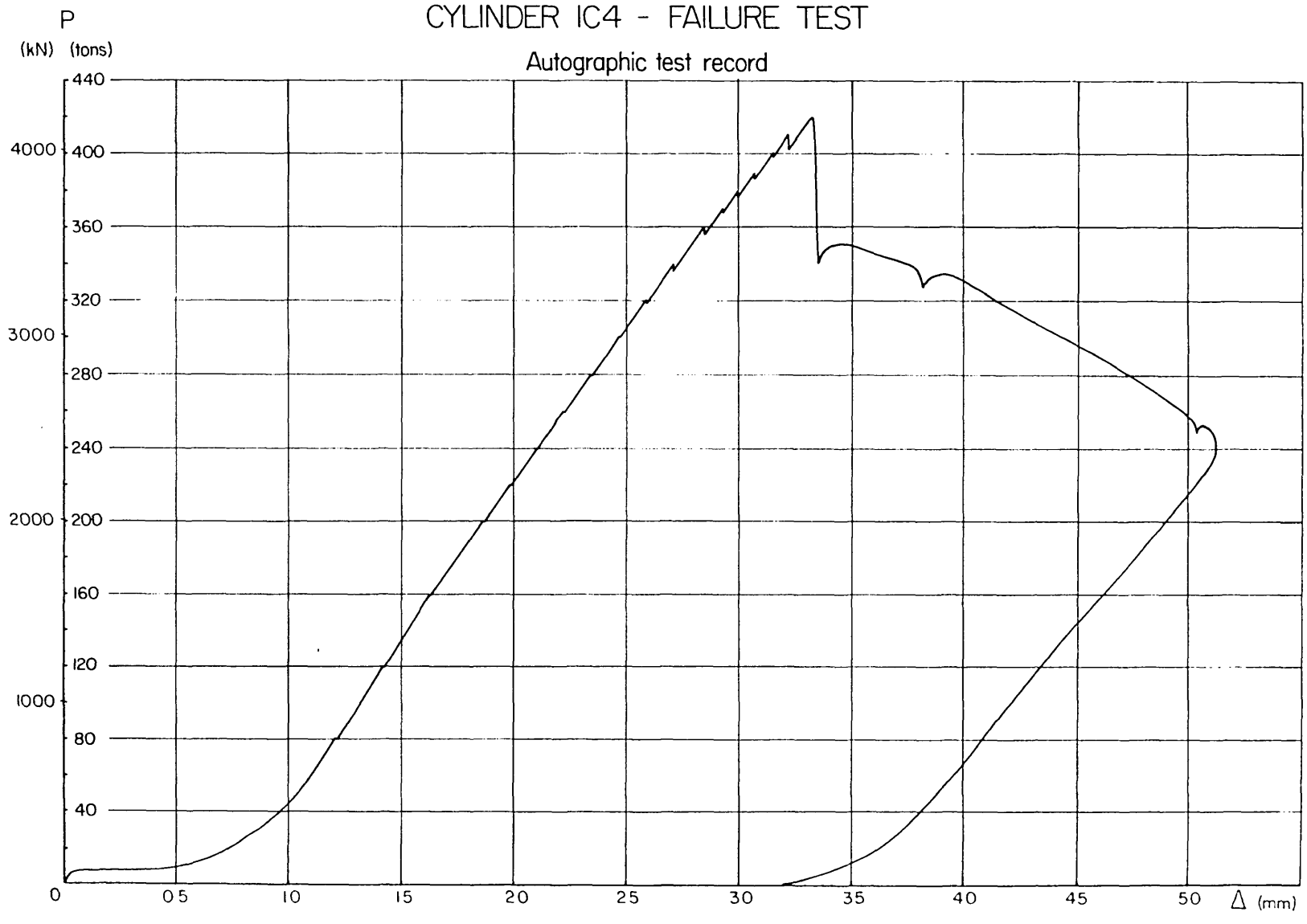

CYLINDER IC4 - FAILURE TEST
Autographic test record
P
(kN) (tons)
440
4000
400
360
320
3000
280
240
2000
200
160
120
1000
80
40
0
05
10
15
20
25
30
35
40
45
50
Δ (mm)

Fig. 2.28

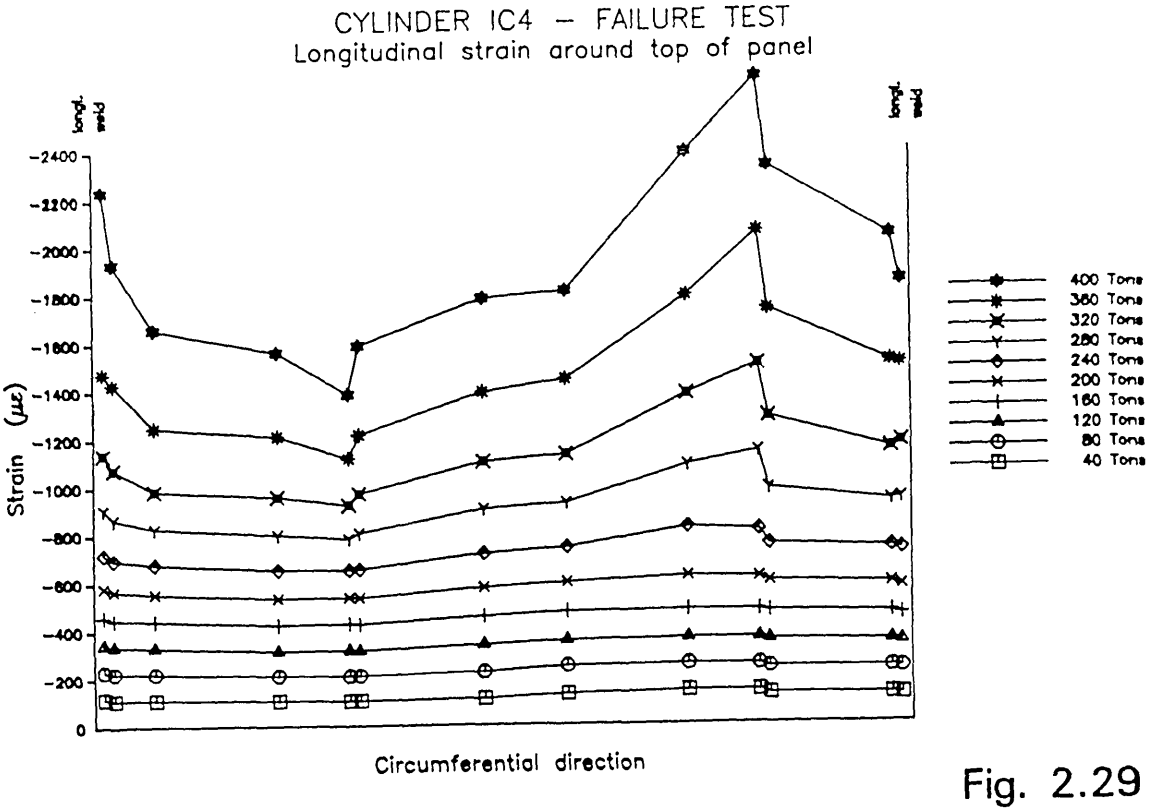


Fig. 2.29

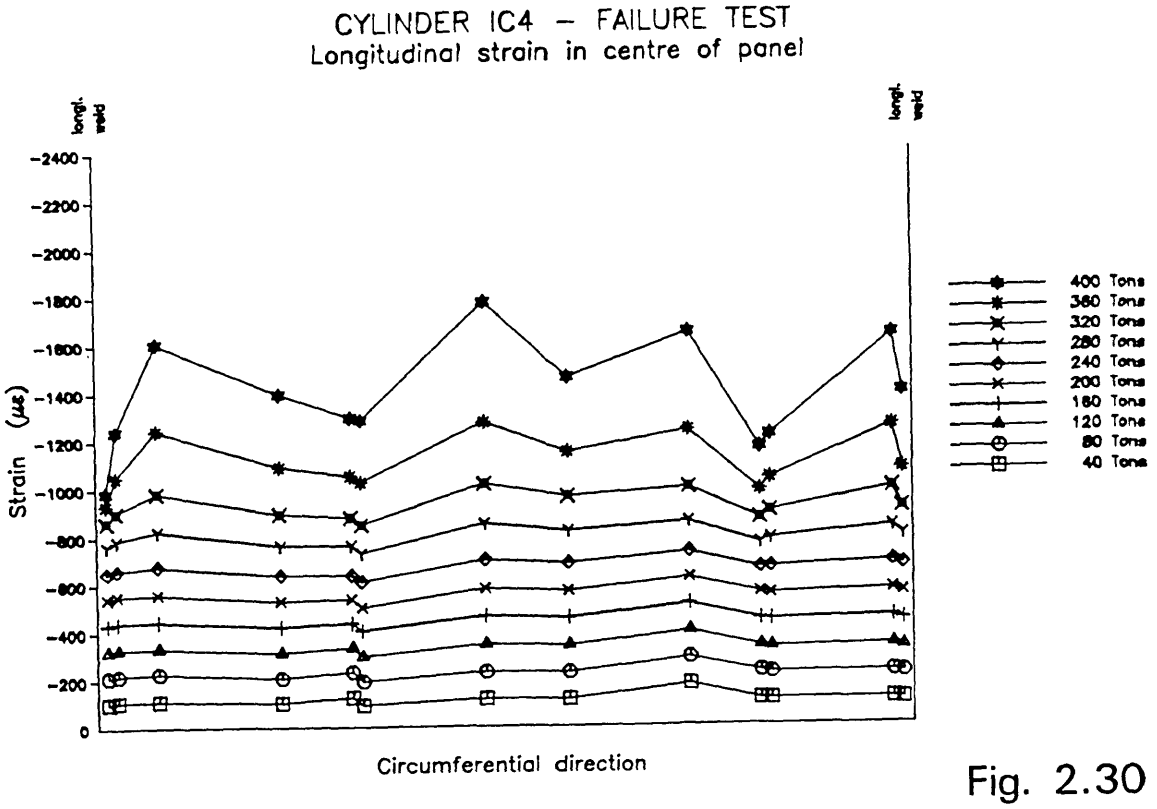


Fig. 2.30

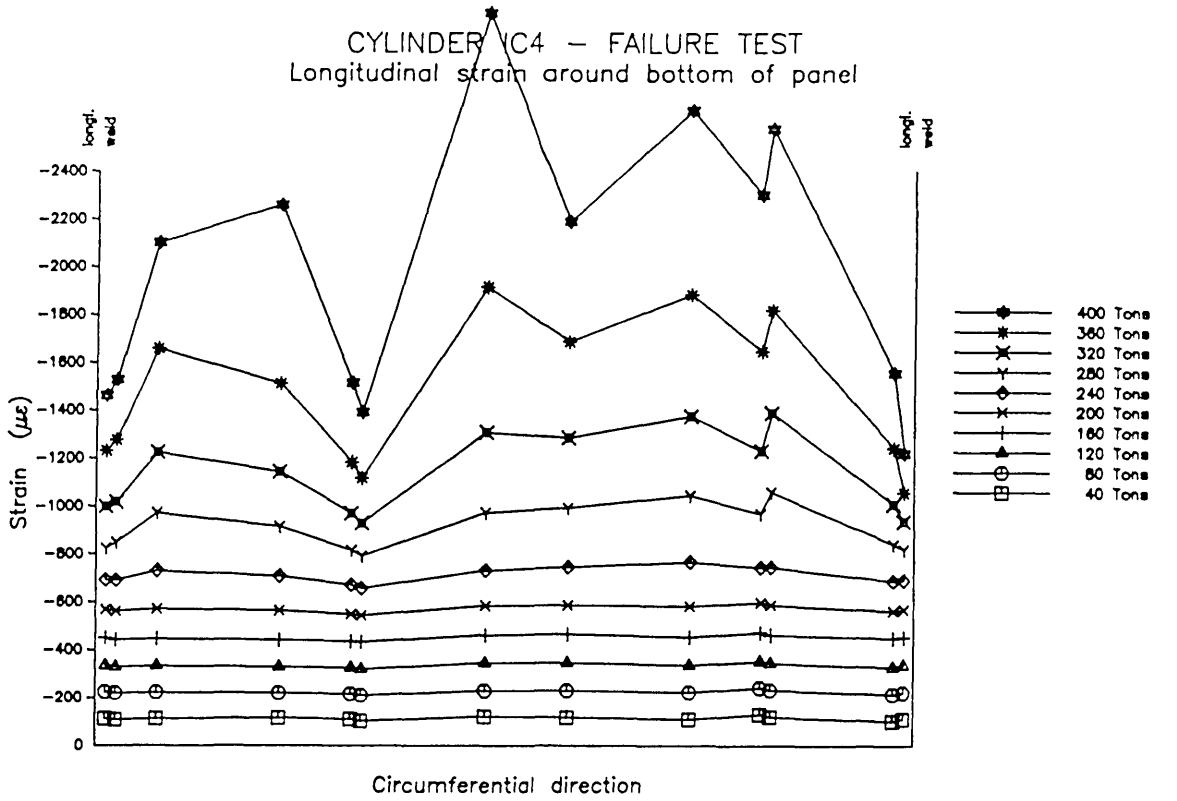


Fig. 2.31

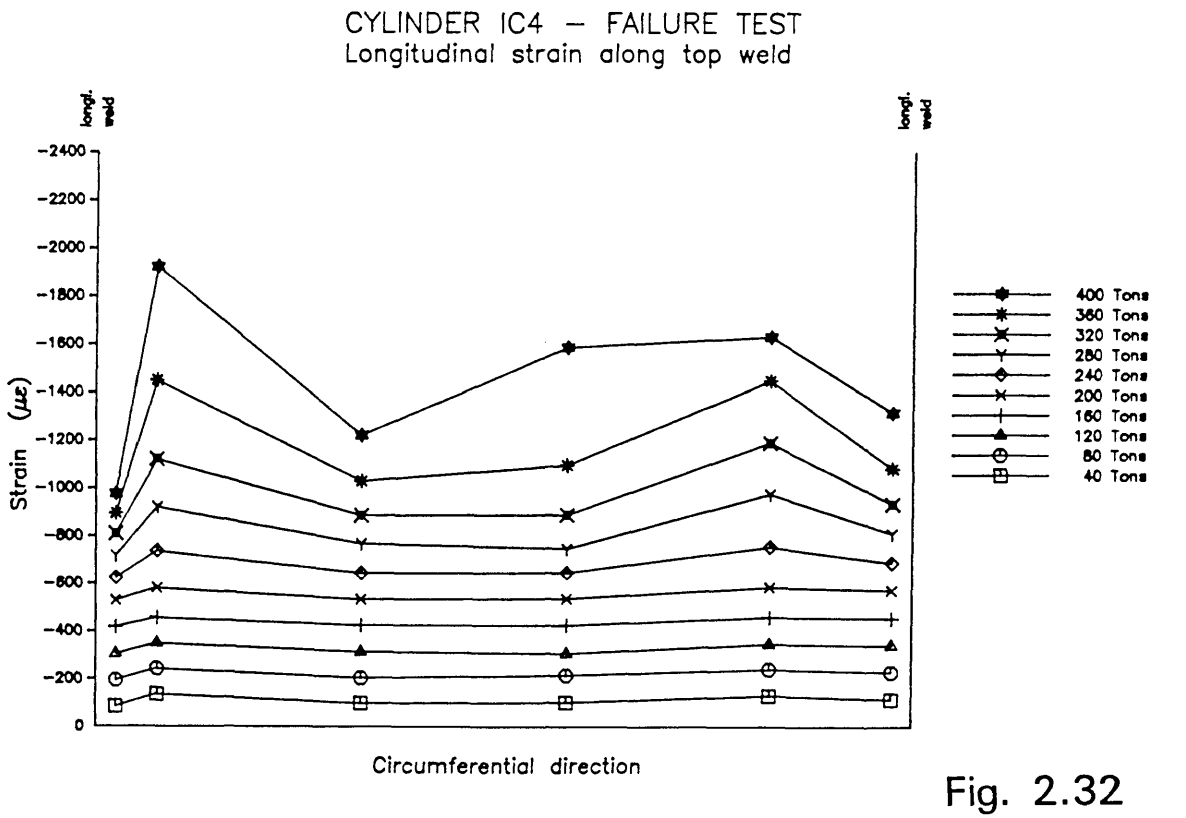


Fig. 2.32

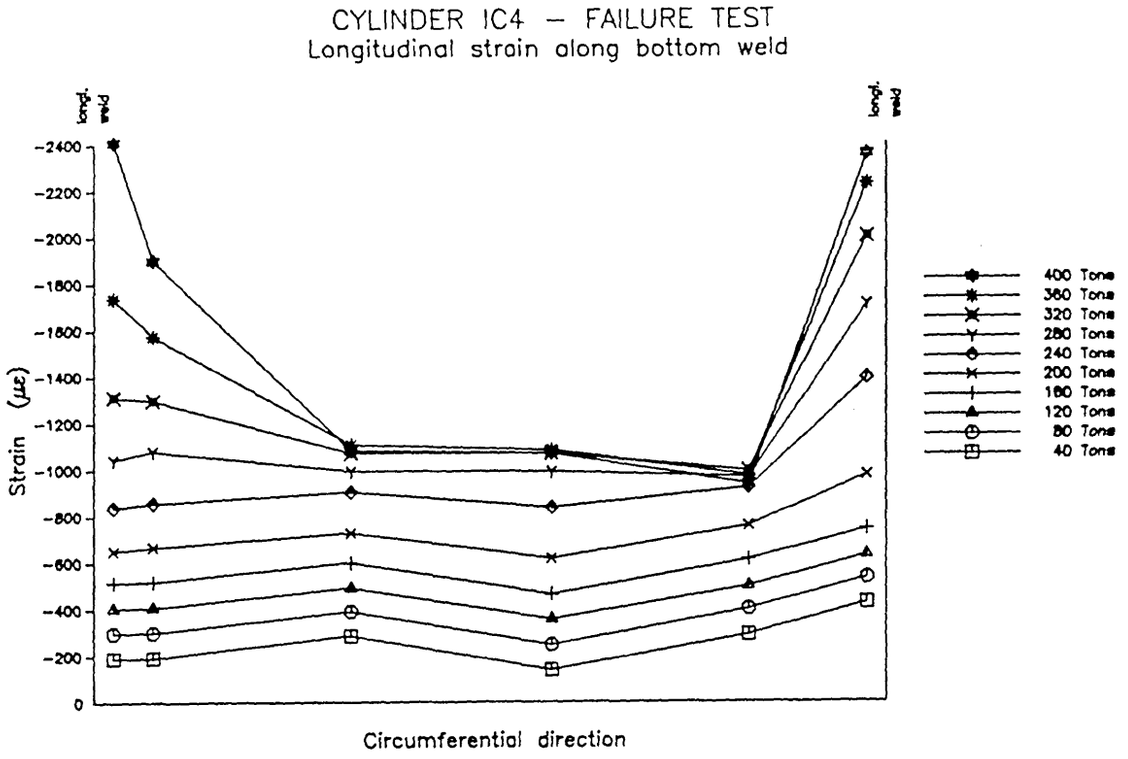

CYLINDER IC4 – FAILURE TEST
Longitudinal strain along bottom weld
longi. weld
longi. weld
-2400
-2200
-2000
-1800
-1600
-1400
-1200
-1000
-800
-600
-400
-200
0
Strain (με)
Circumferential direction
400 Tons
360 Tons
320 Tons
280 Tons
240 Tons
200 Tons
160 Tons
120 Tons
80 Tons
40 Tons

Fig. 2.33

CYLINDER IC4 – FAILURE TEST
Longitudinal strain down centre panel

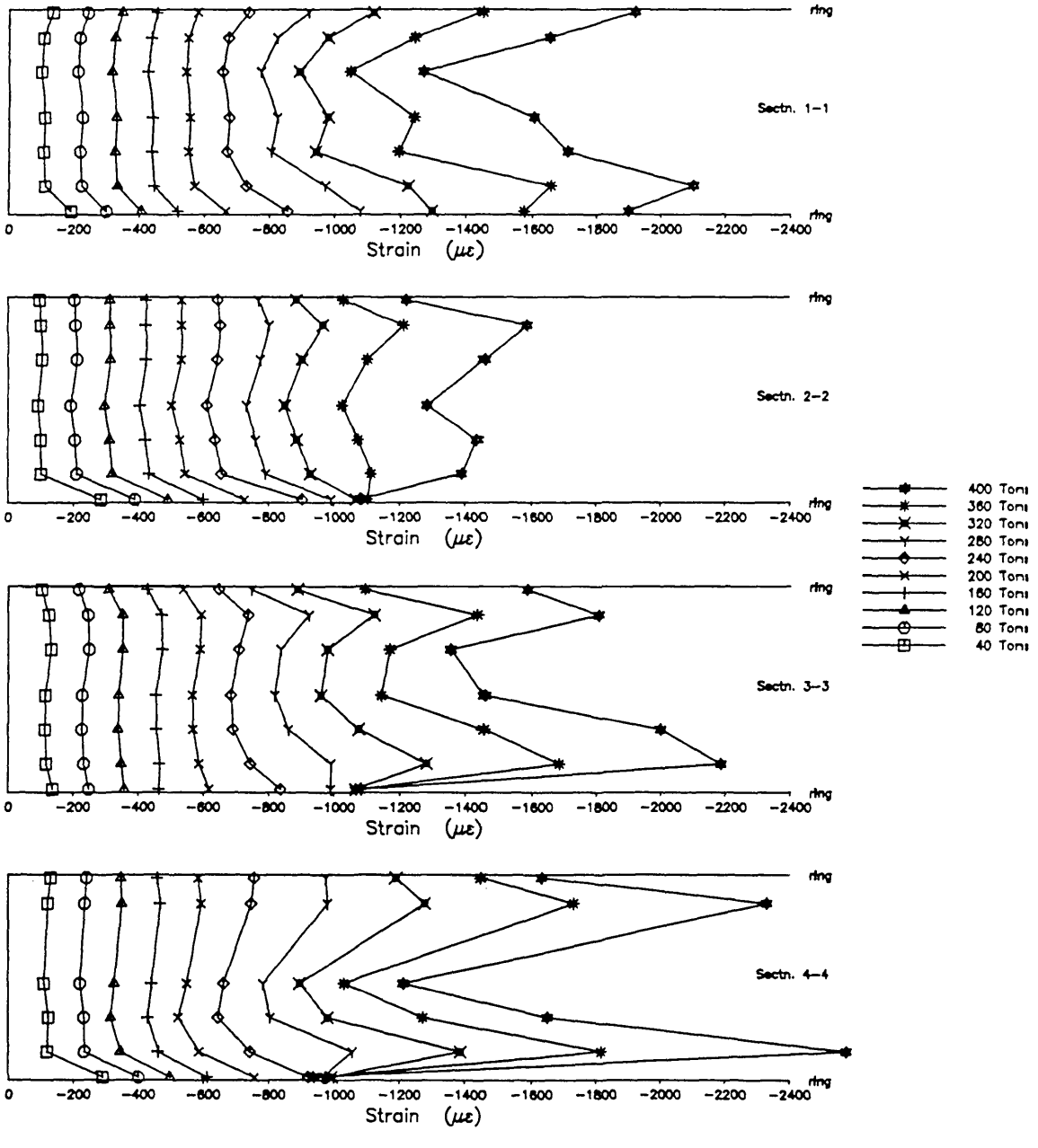


Fig. 2.34

CYLINDER IC4 – FAILURE TEST
Hoop strain down centre panel

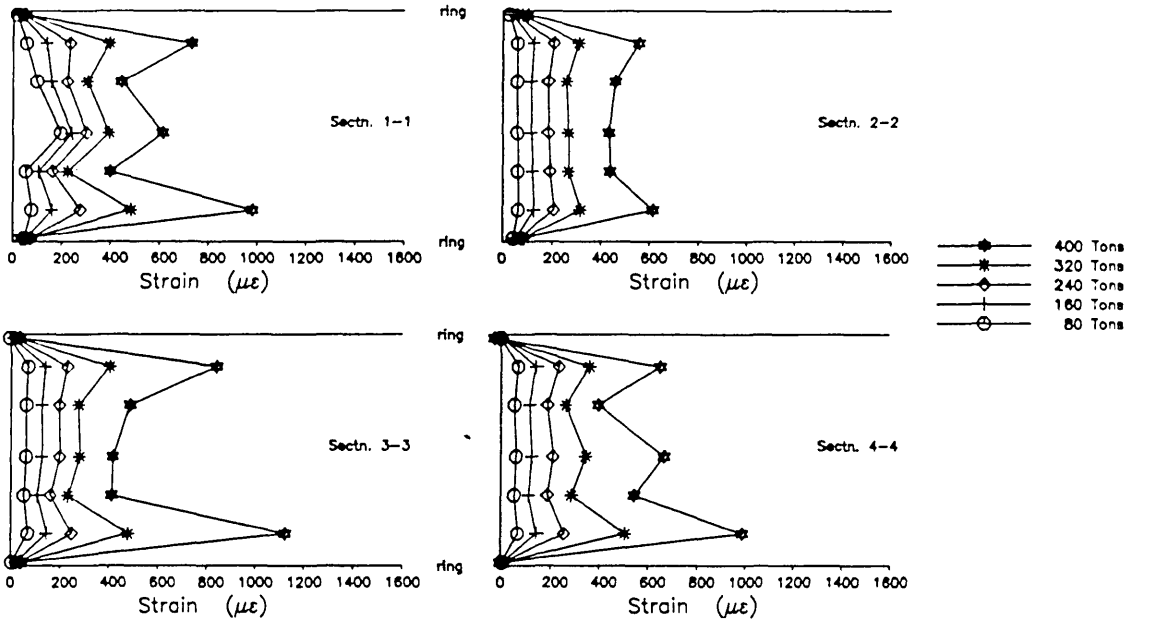


Fig. 2.35

CYLINDER IC4 – FAILURE TEST
Hoop stress down centre panel

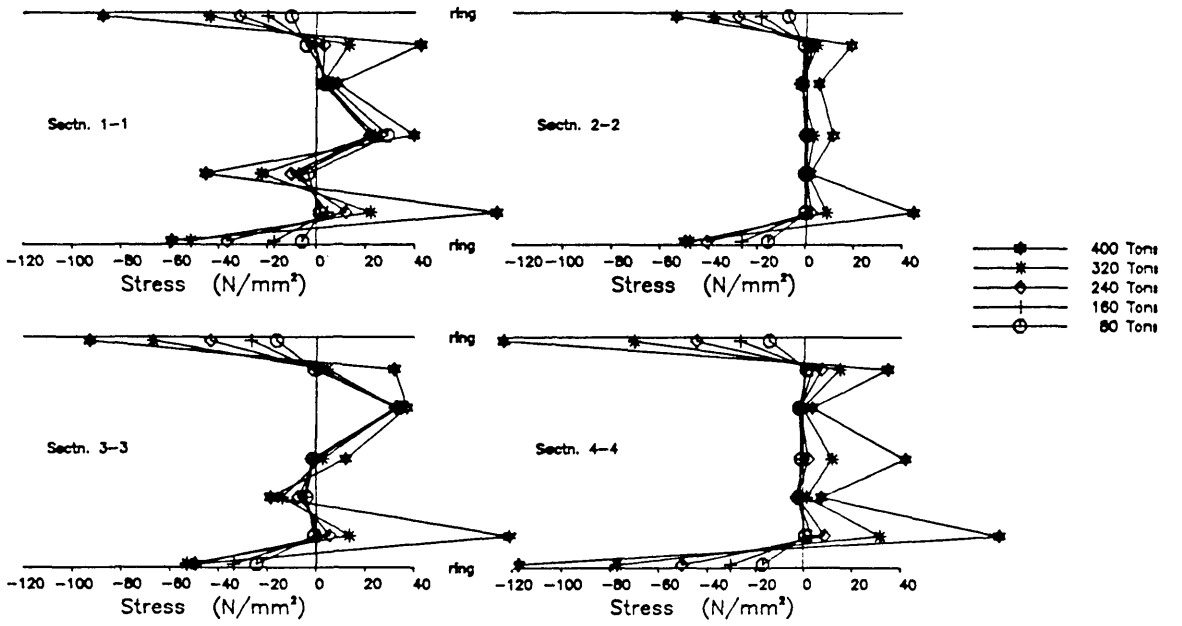


Fig. 2.36

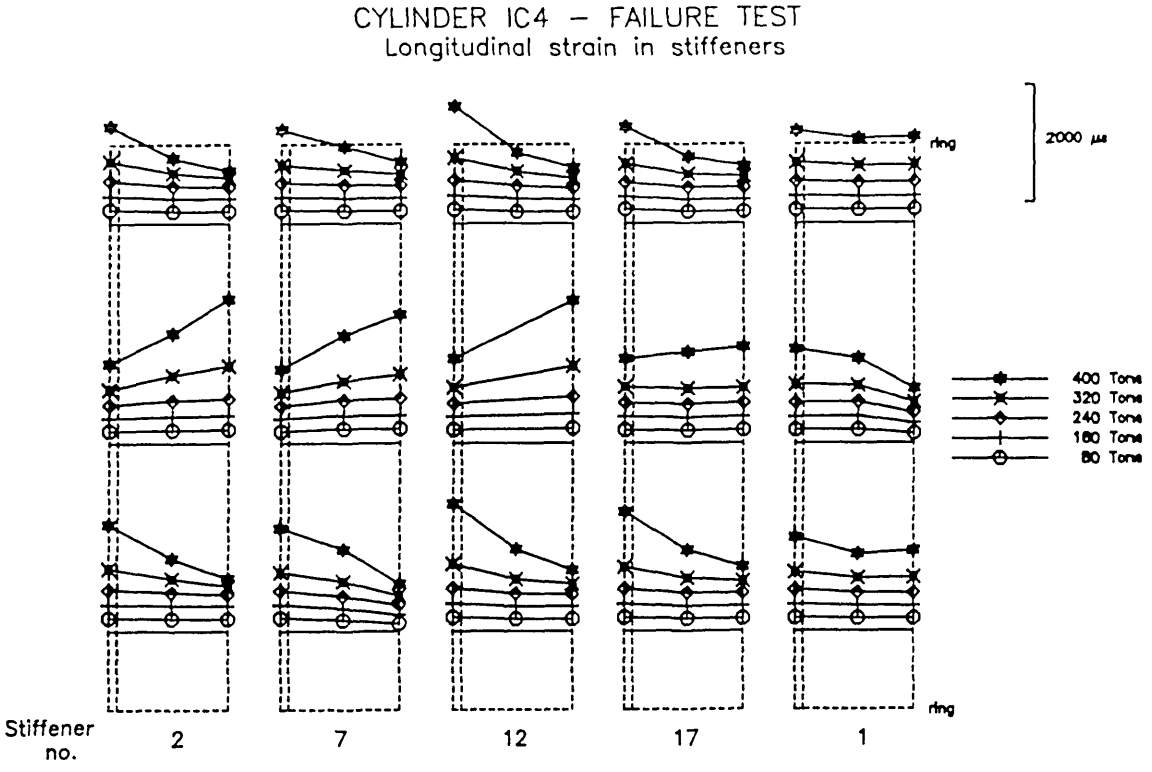


Fig. 2.37

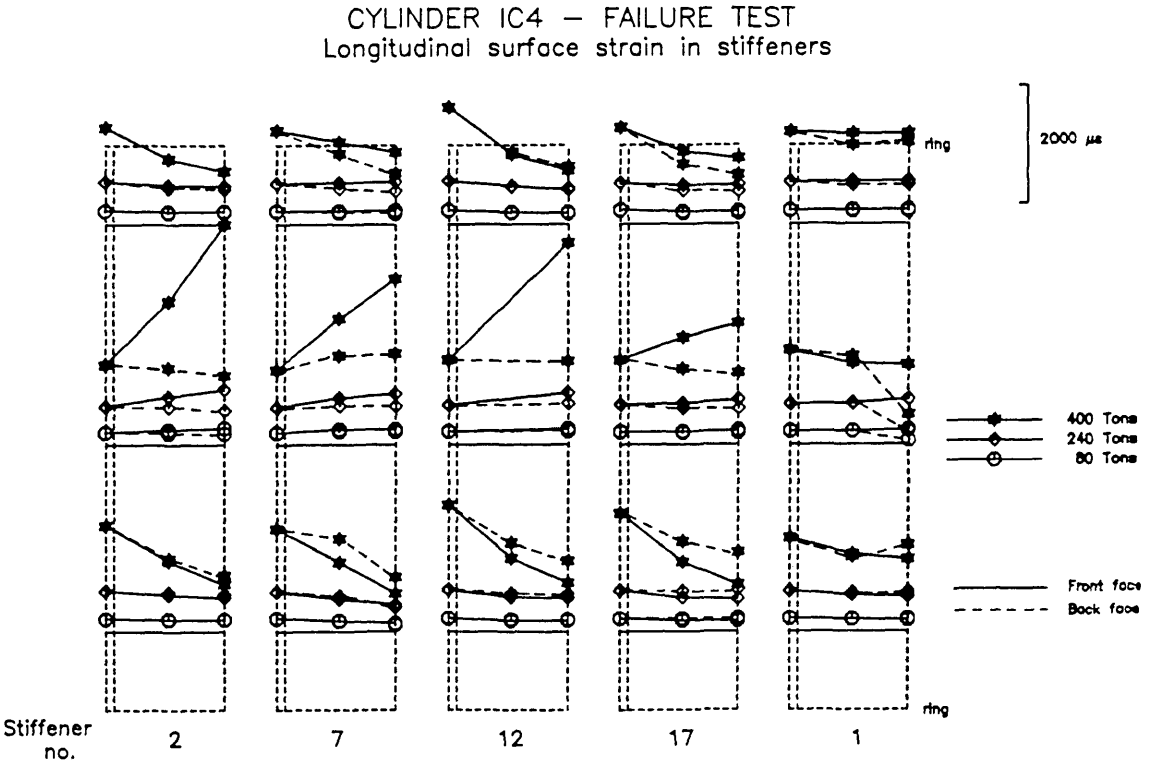


Fig. 2.38

CYLINDER IC4 – FAILURE TEST
Hoop strain in ring stiffeners

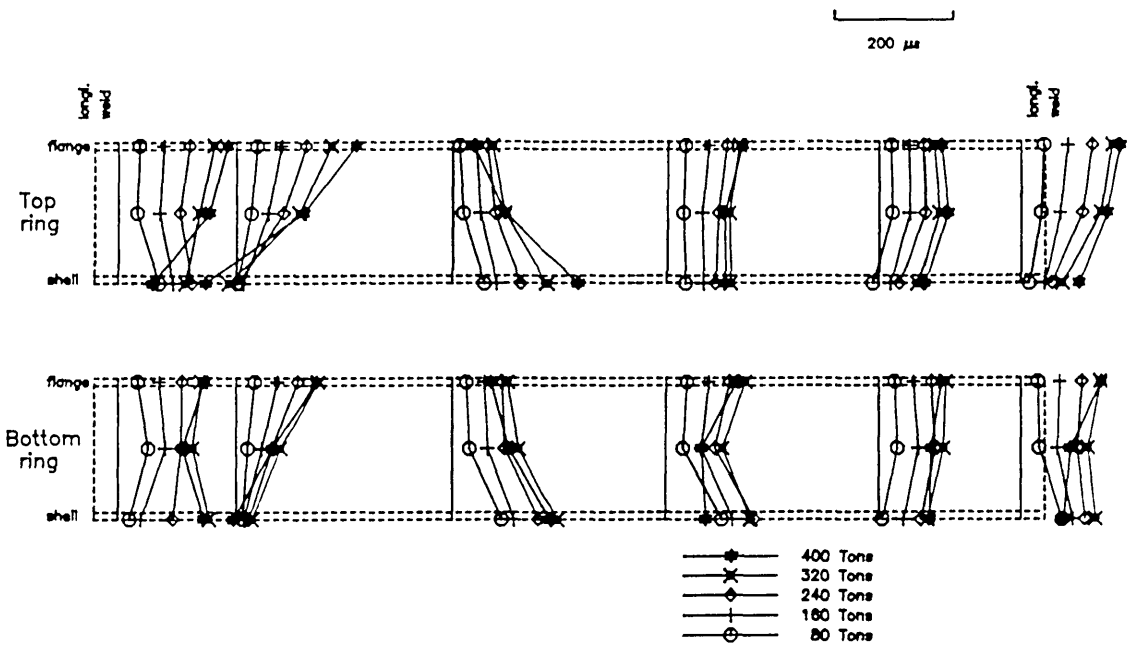


Fig. 2.39

CYLINDER IC4 – FAILURE TEST
Hoop surface strain in ring stiffeners

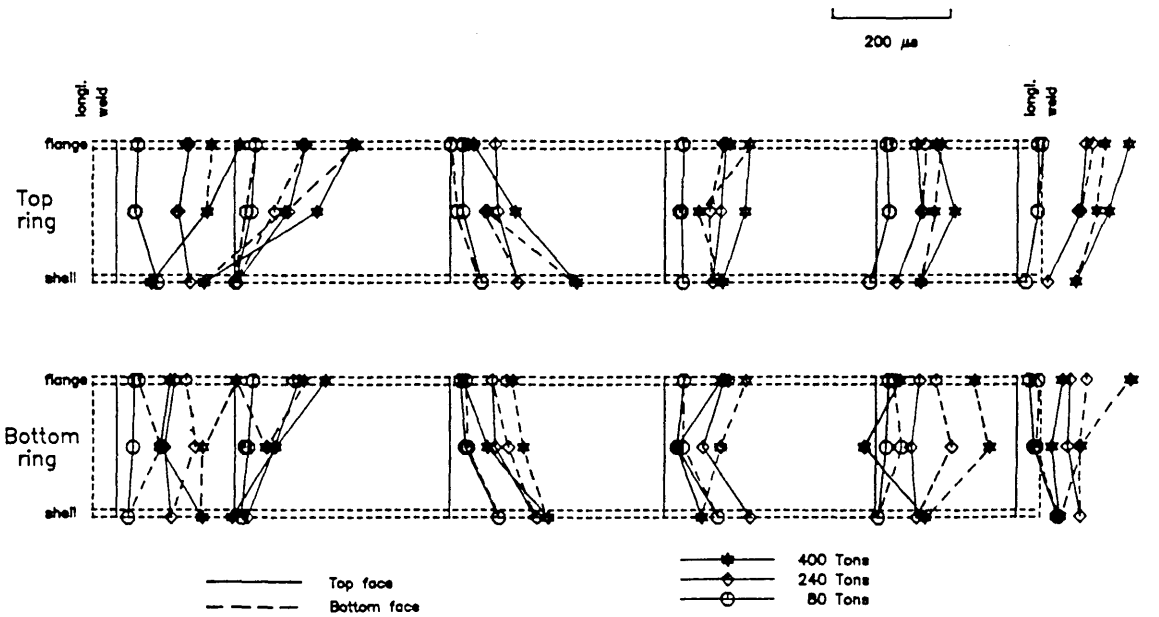


Fig. 2.40

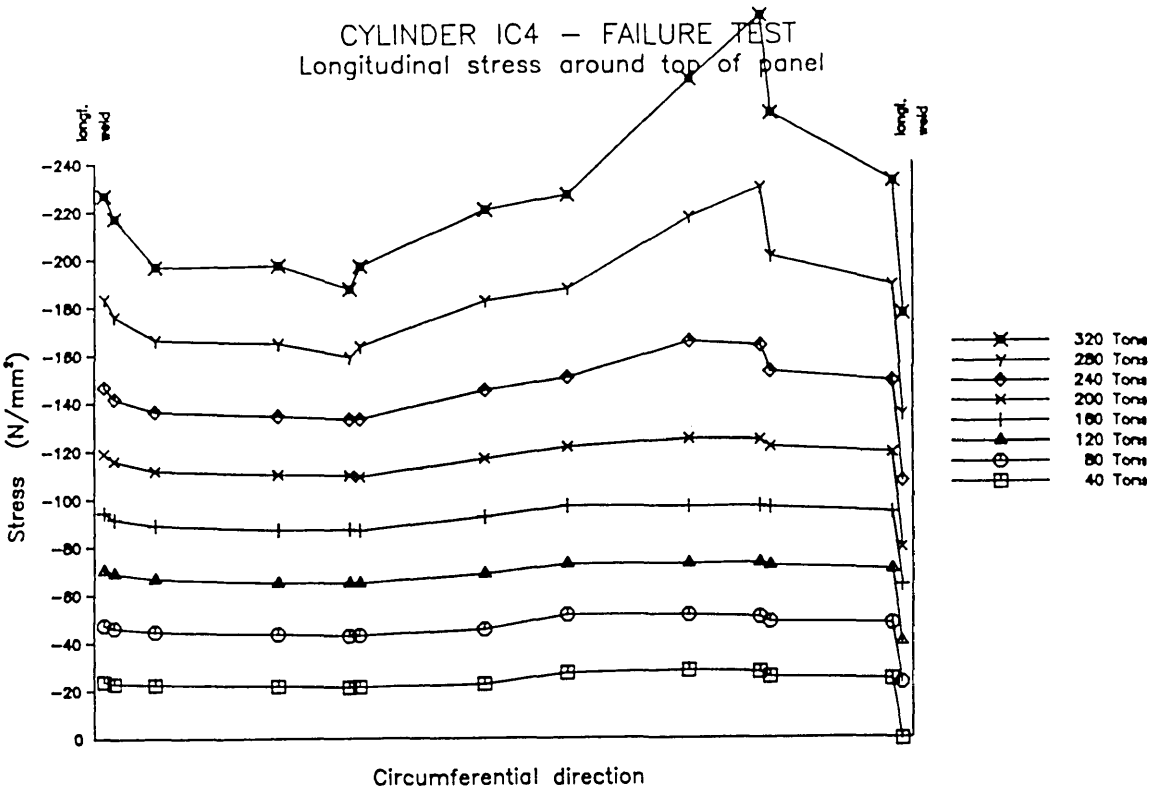


Fig. 2.41

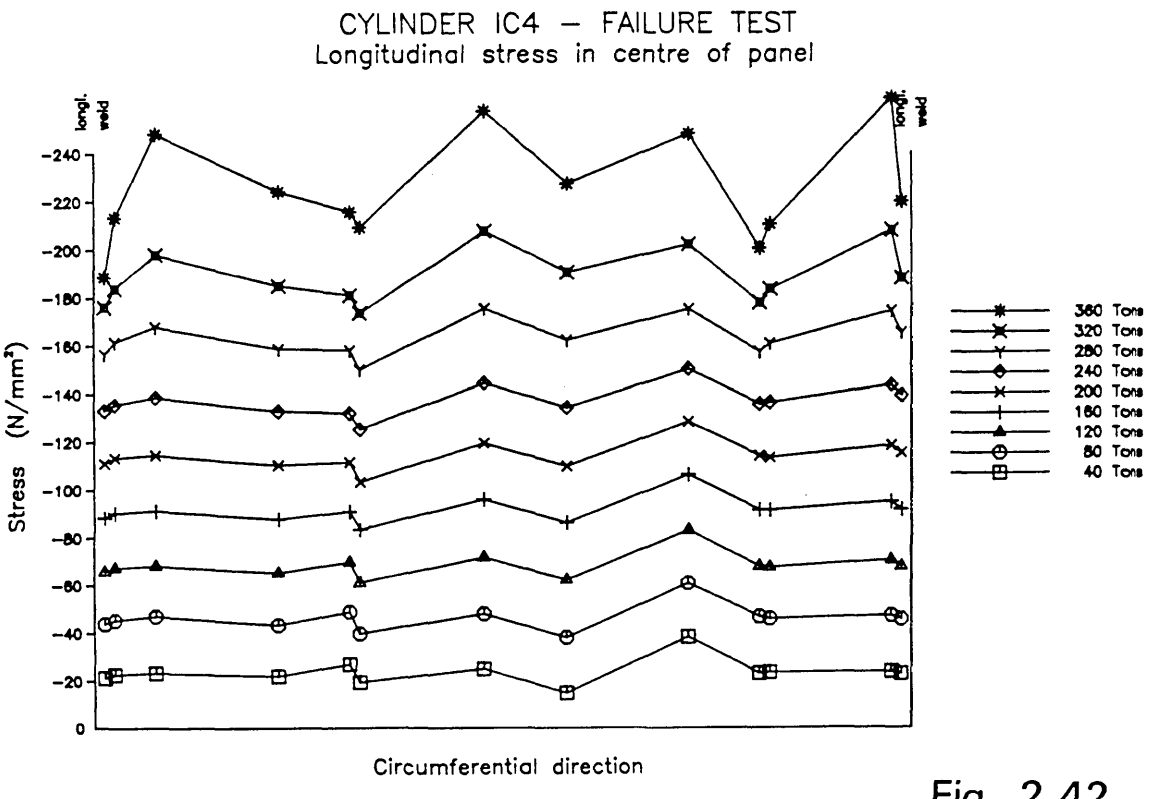


Fig. 2.42

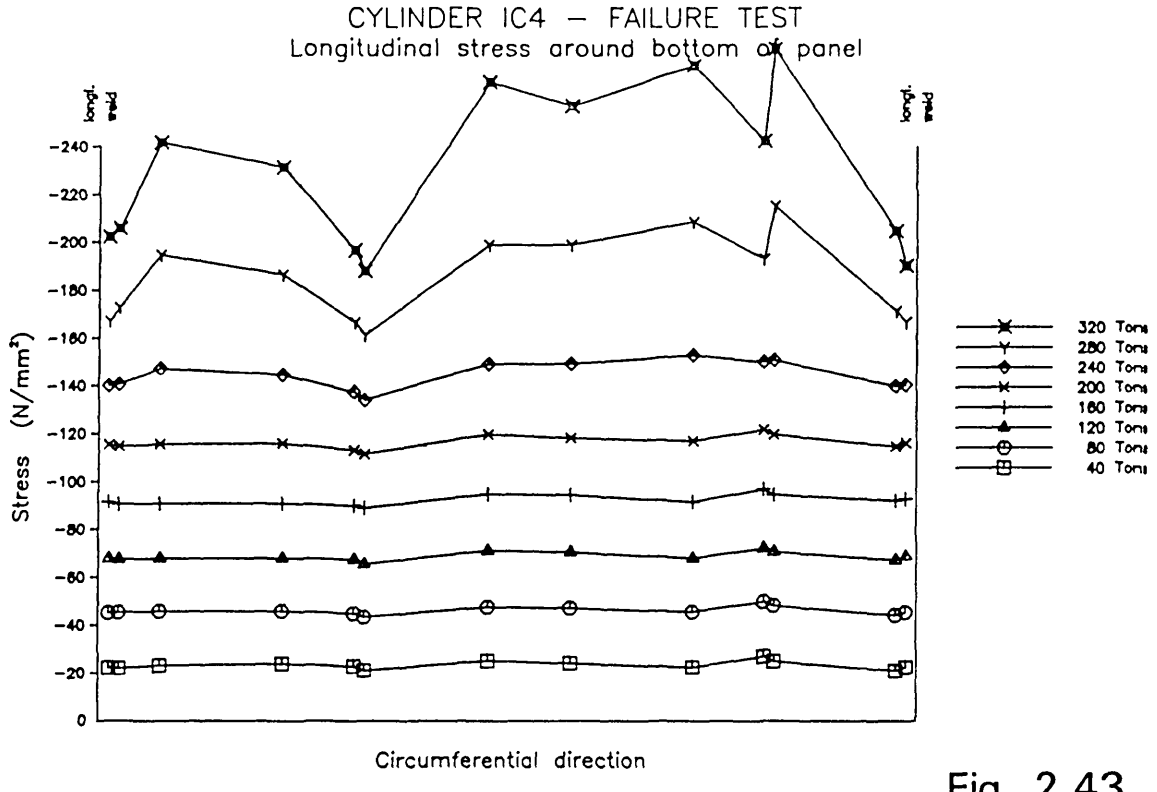


Fig. 2.43

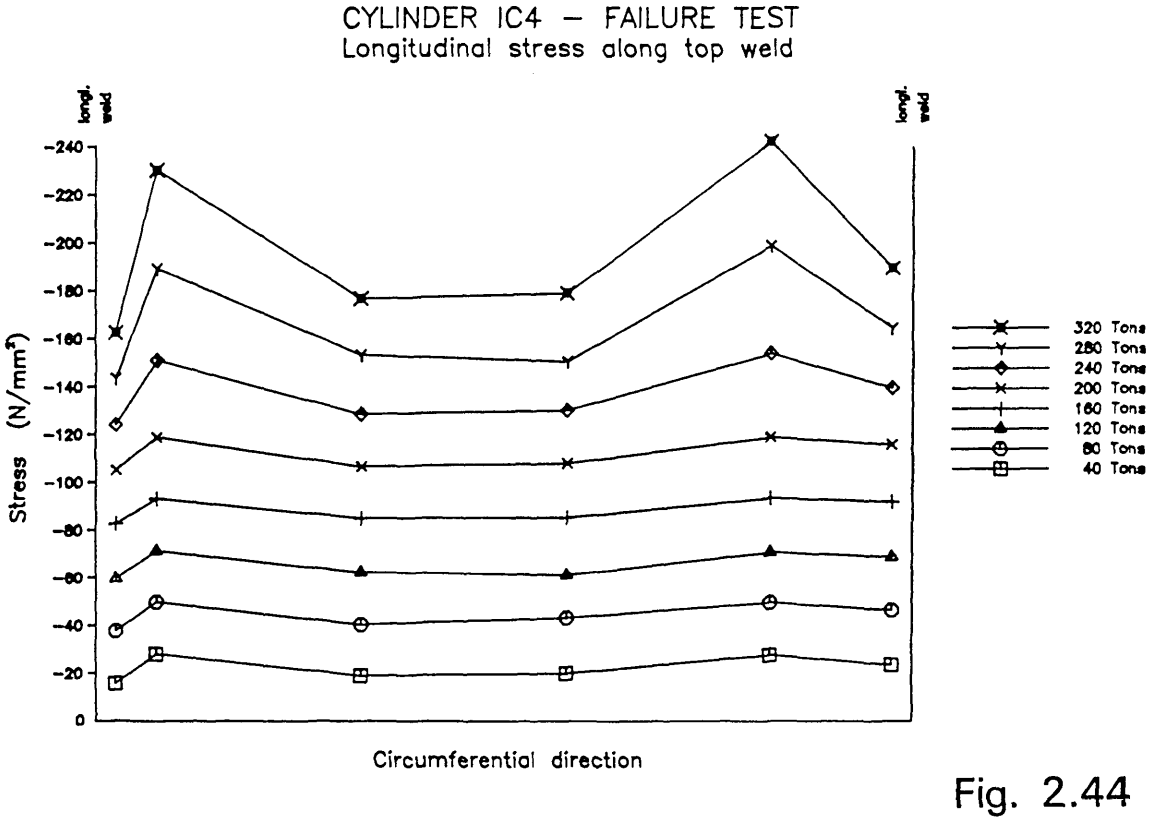


Fig. 2.44

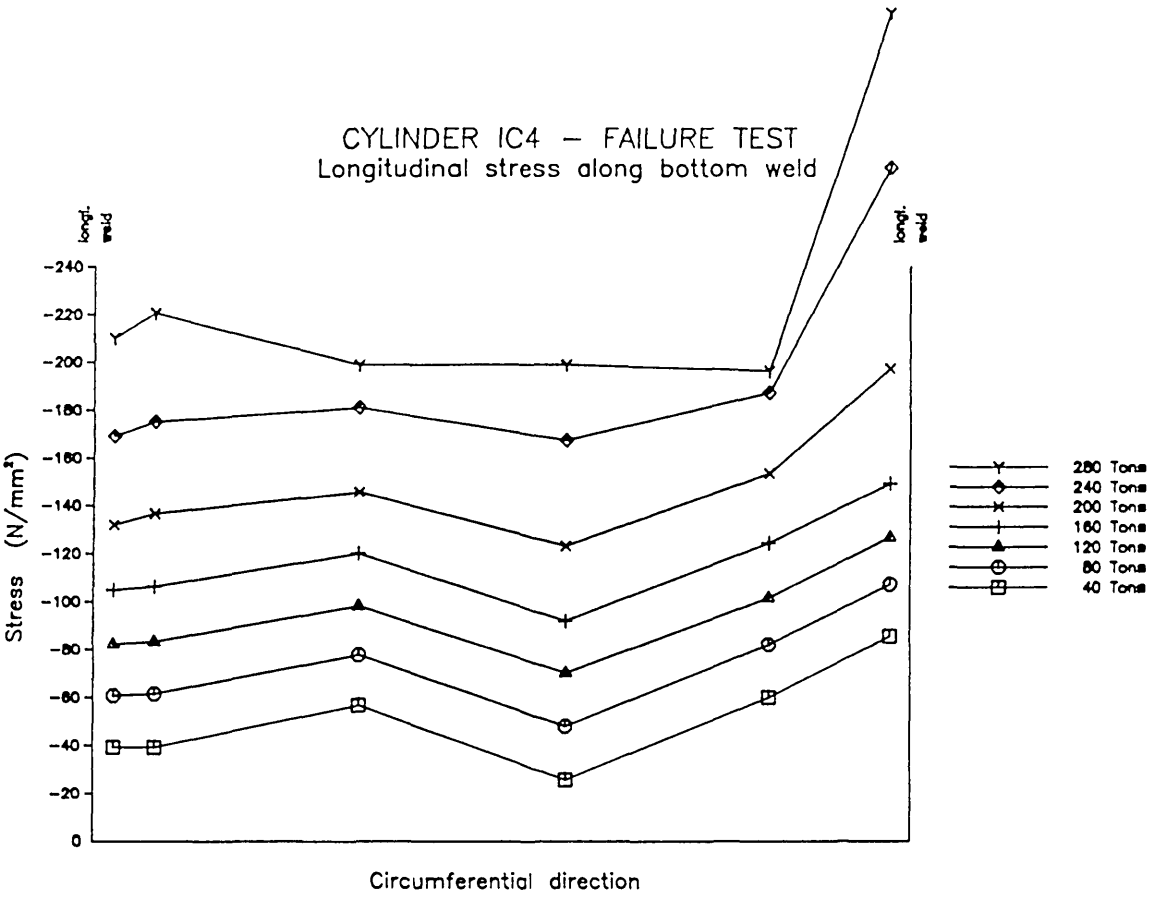

CYLINDER IC4 – FAILURE TEST
Longitudinal stress along bottom weld
longi. weld
longi. weld
Stress (N/mm²)
-240
-220
-200
-180
-160
-140
-120
-100
-80
-60
-40
-20
0
Circumferential direction
280 Tons
240 Tons
200 Tons
160 Tons
120 Tons
80 Tons
40 Tons

Fig. 2.45

CYLINDER IC4 – FAILURE TEST
Longitudinal stress down centre panel

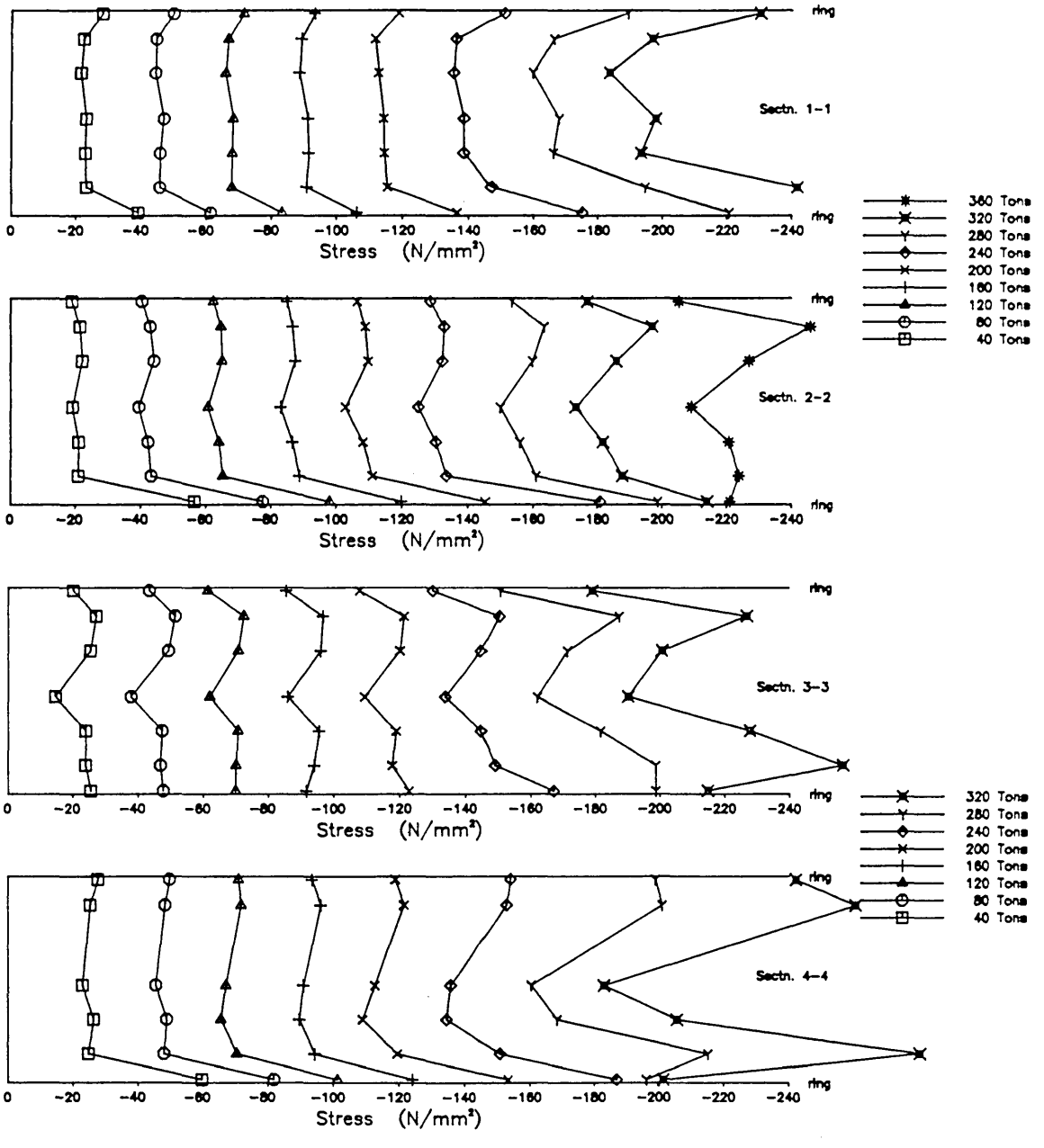
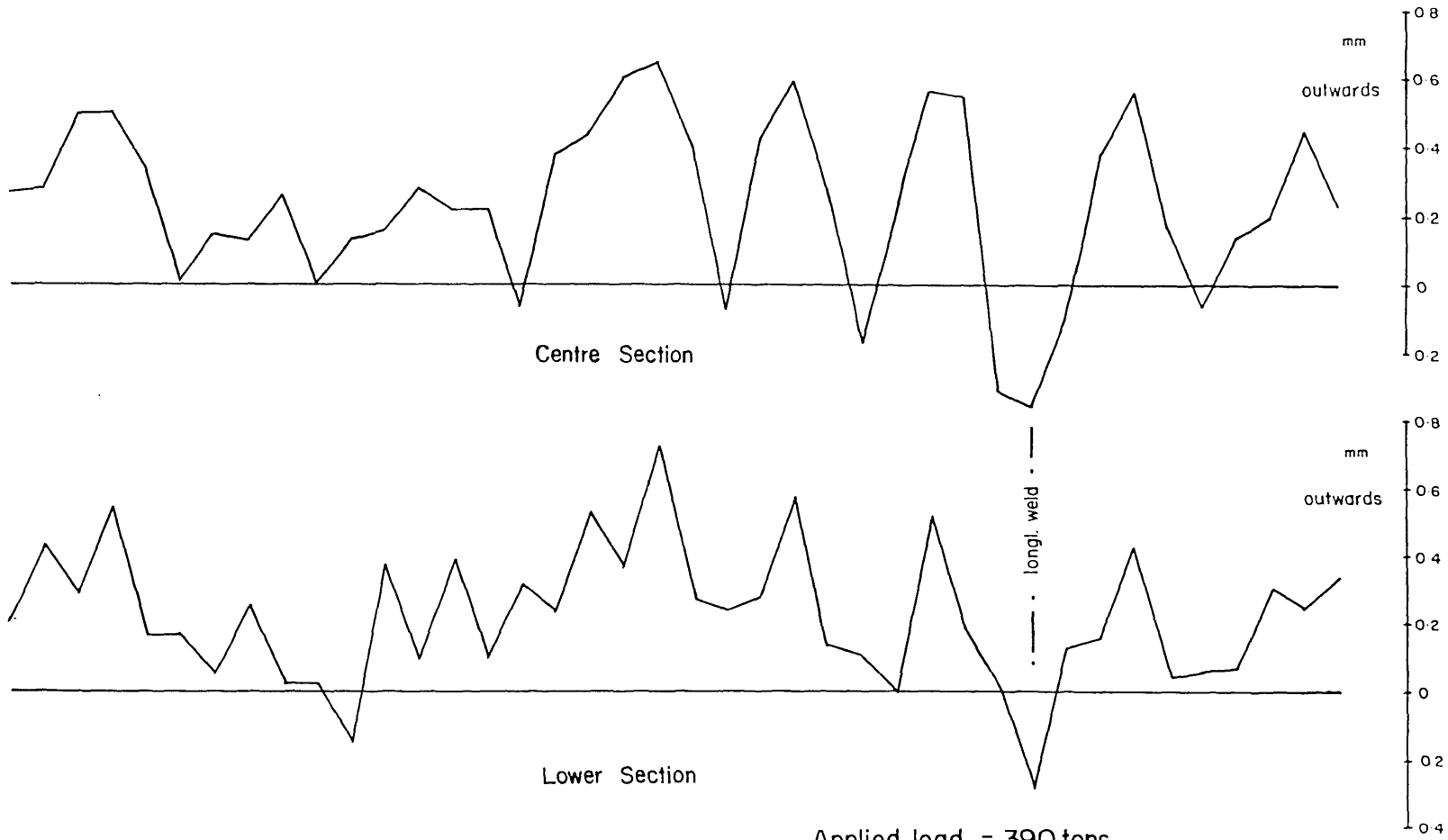


Fig. 2.46

CYLINDER IC4 - RADIAL DEFLECTIONS

Circumferential sections



Applied load = 390 tons

Fig. 2.47

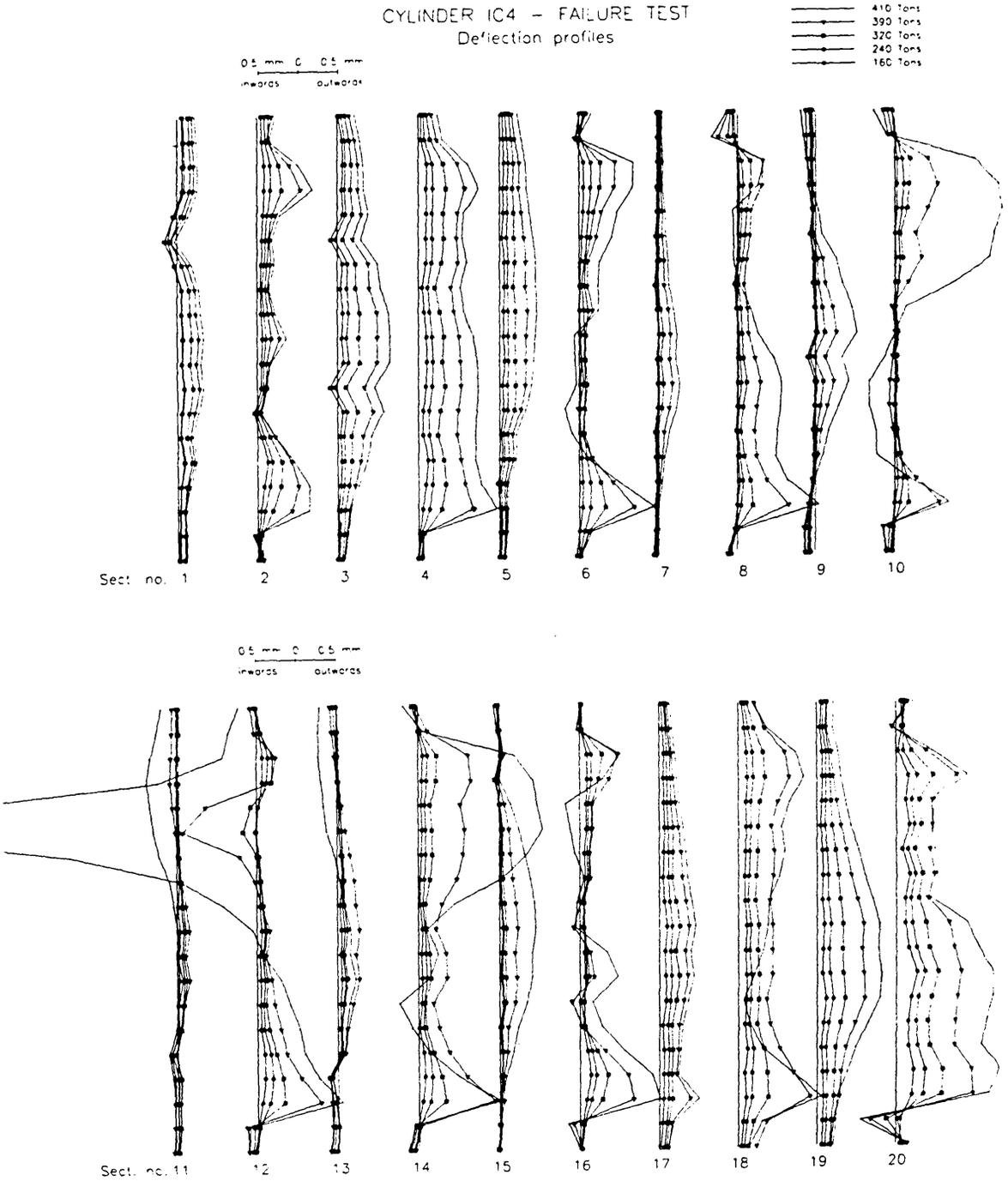

CYLINDER IC4 – FAILURE TEST
Deflection profiles
410 Tons
390 Tons
320 Tons
240 Tons
160 Tons
0.5 mm 0 0.5 mm
inwards outwards
Sect. no. 1 2 3 4 5 6 7 8 9 10
0.5 mm 0 0.5 mm
inwards outwards
Sect. no. 11 12 13 14 15 16 17 18 19 20

Fig. 2.48

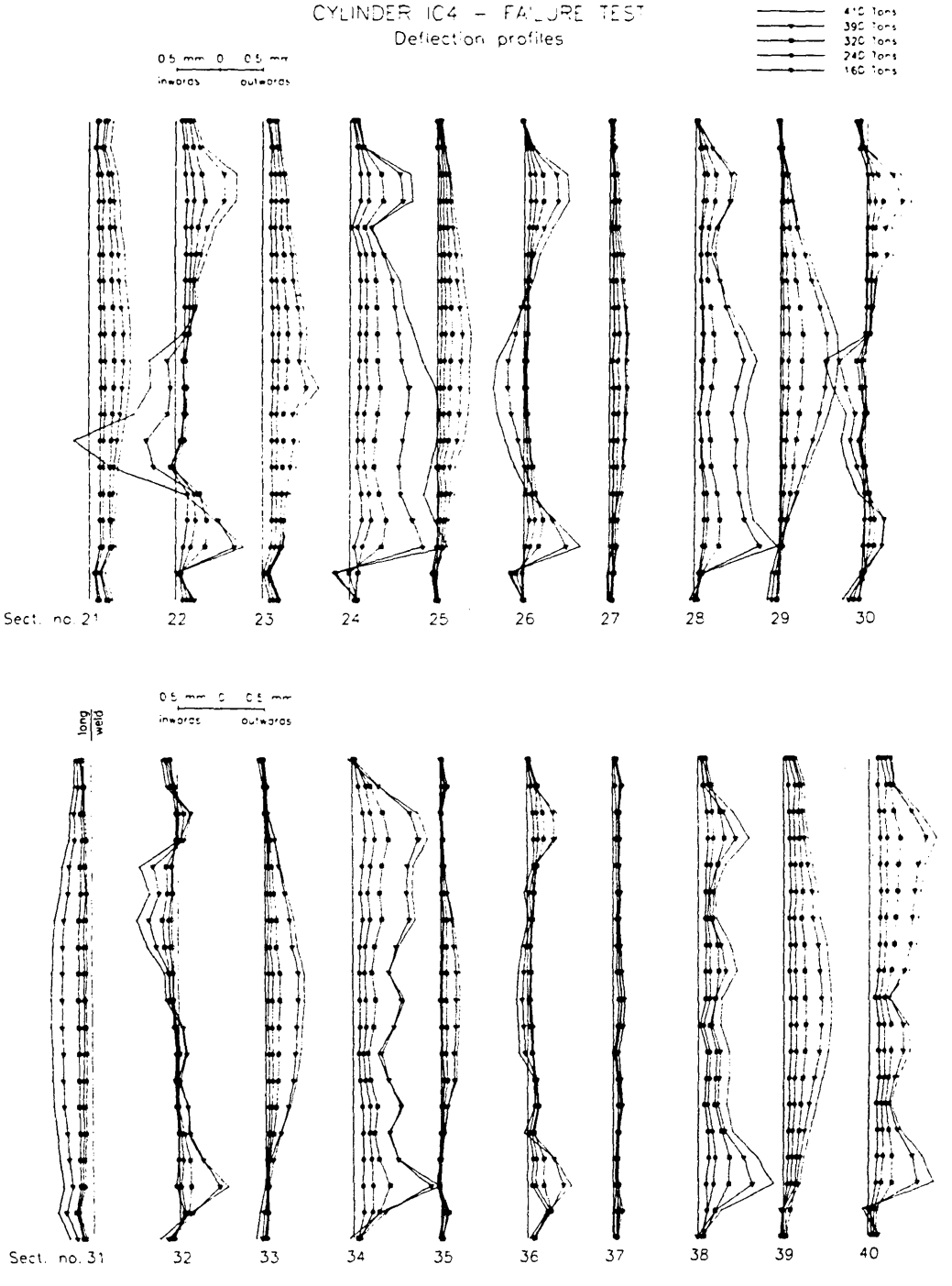

CYLINDER IC4 - FAILURE TEST
Deflection profiles
0.5 mm 0 0.5 mm
inwards outwards
long weld
Sect. no. 21
22
23
24
25
26
27
28
29
30
31
32
33
34
35
36
37
38
39
40

Fig. 2.49

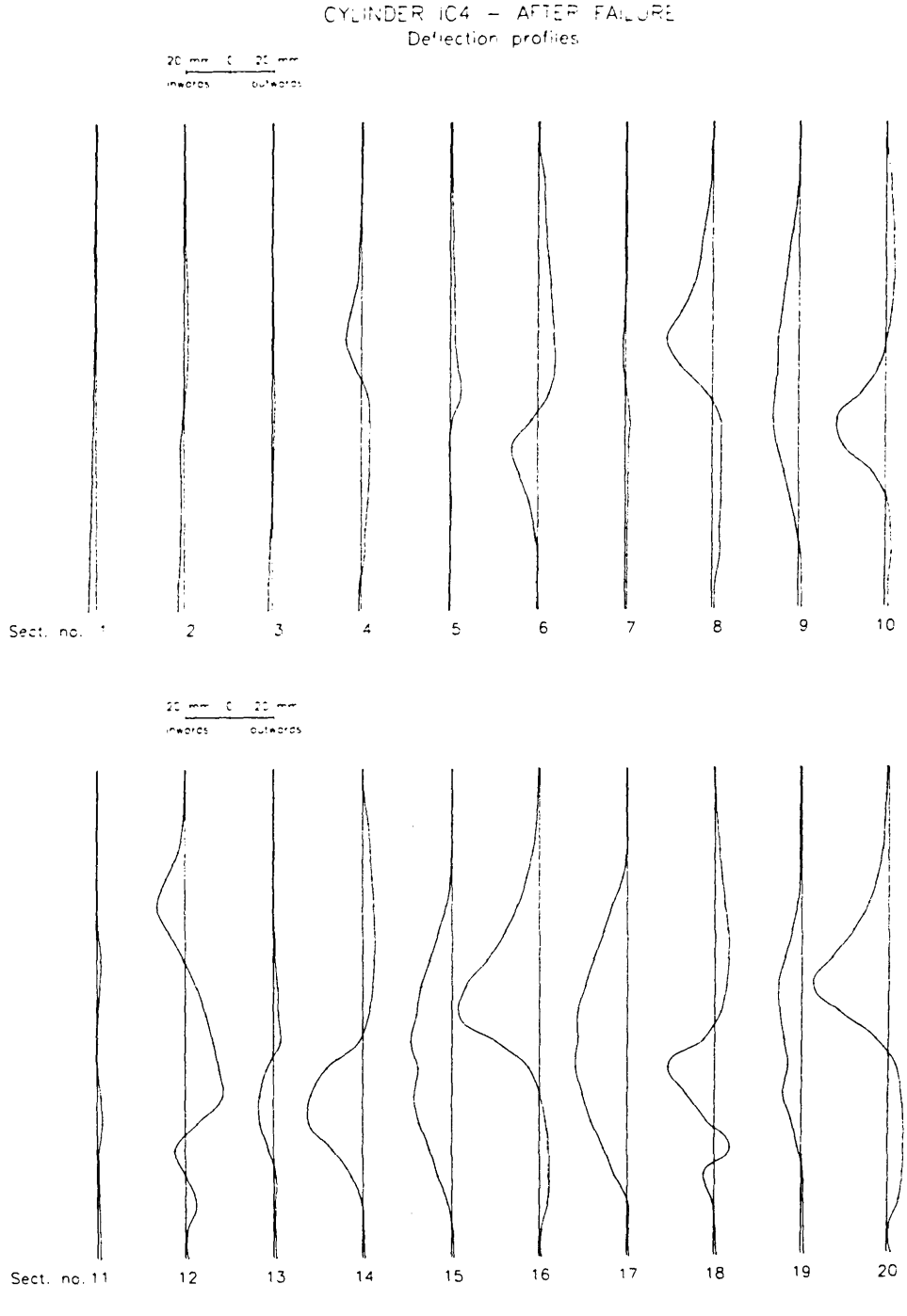

CYLINDER IC4 – AFTER FAILURE
Deflection profiles
20 mm 0 20 mm
inwards outwards
Sect. no. 1 2 3 4 5 6 7 8 9 10
20 mm 0 20 mm
inwards outwards
Sect. no. 11 12 13 14 15 16 17 18 19 20

Fig. 2.50

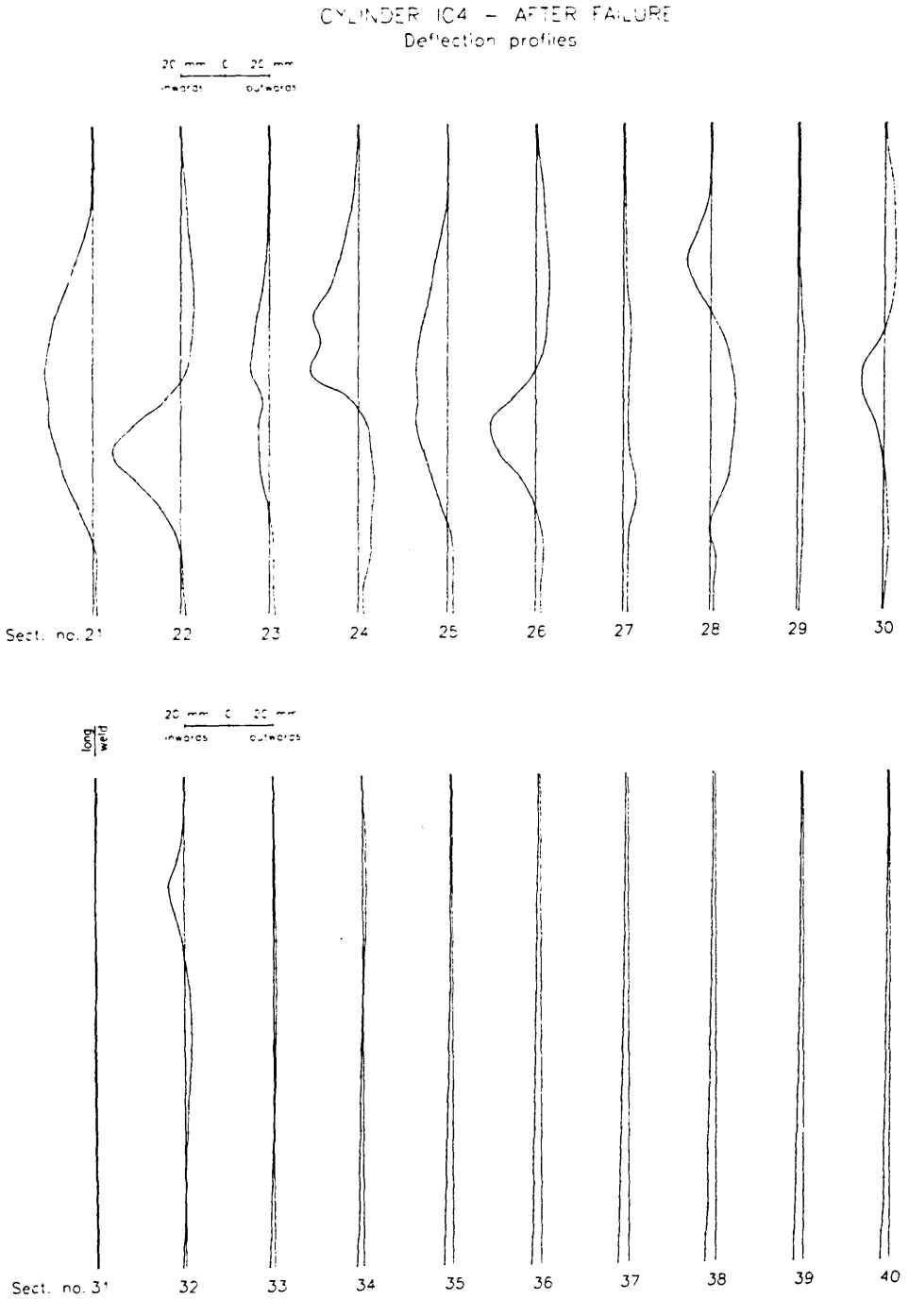

CYLINDER IC4 – AFTER FAILURE
Deflection profiles
20 mm 0 20 mm
inwards outwards
Sect. no. 21
22
23
24
25
26
27
28
29
30
long weld
20 mm 0 20 mm
inwards outwards
Sect. no. 31
32
33
34
35
36
37
38
39
40

Fig. 2.51

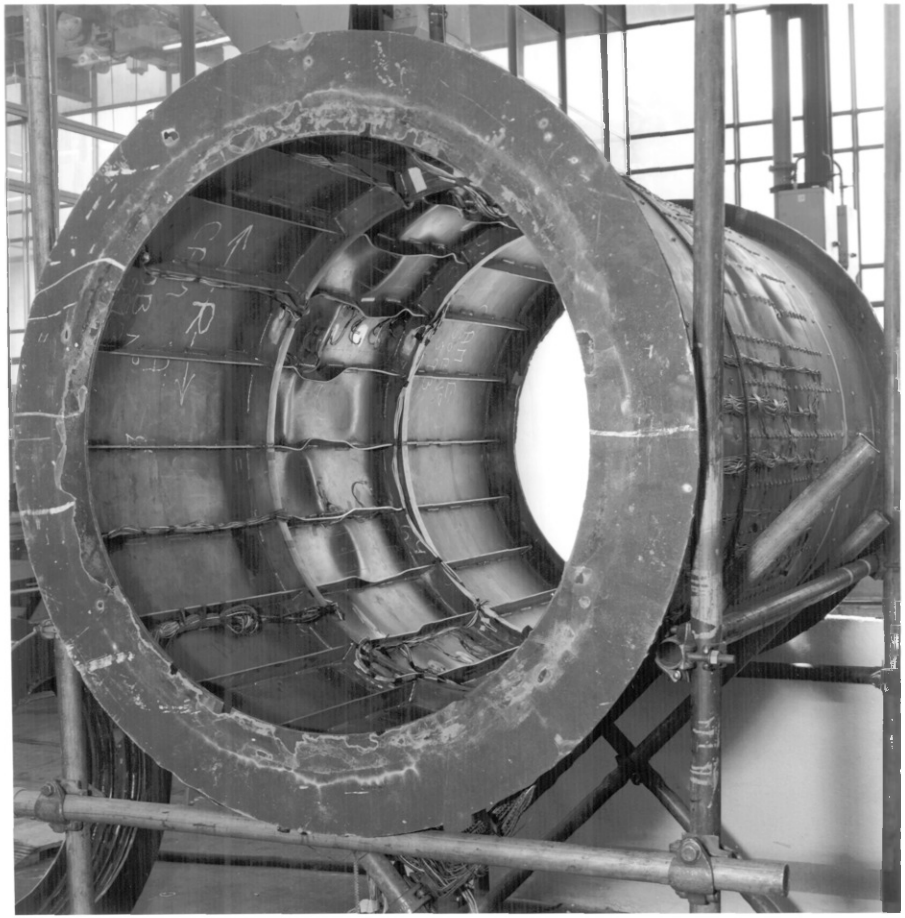


Fig. 2.53 INTERNAL VIEW AFTER FAILURE

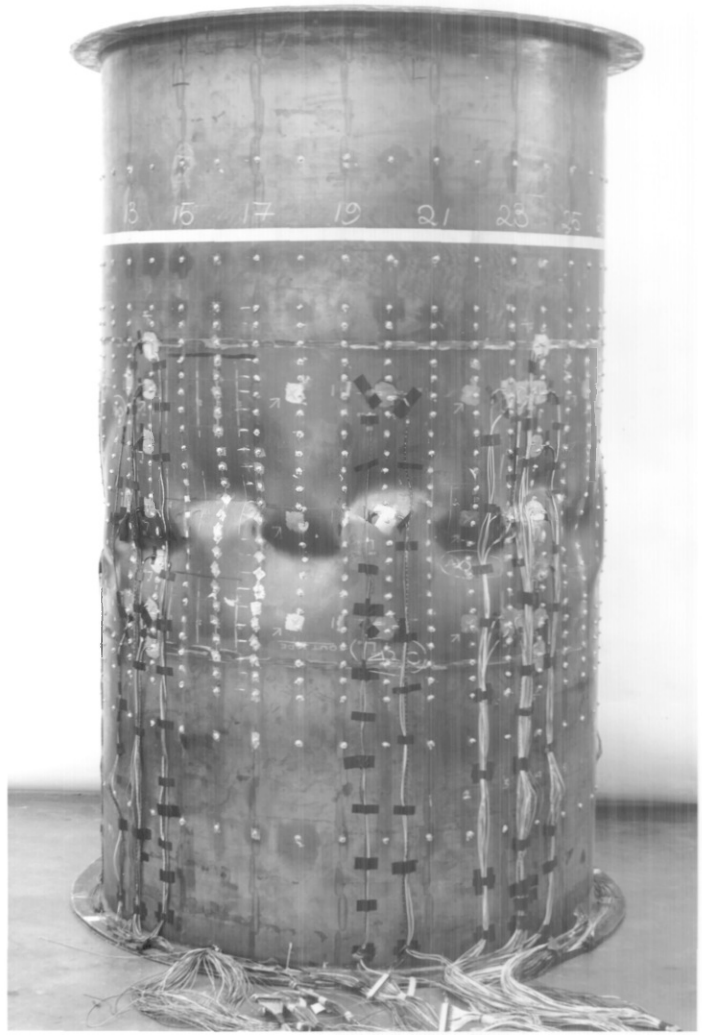
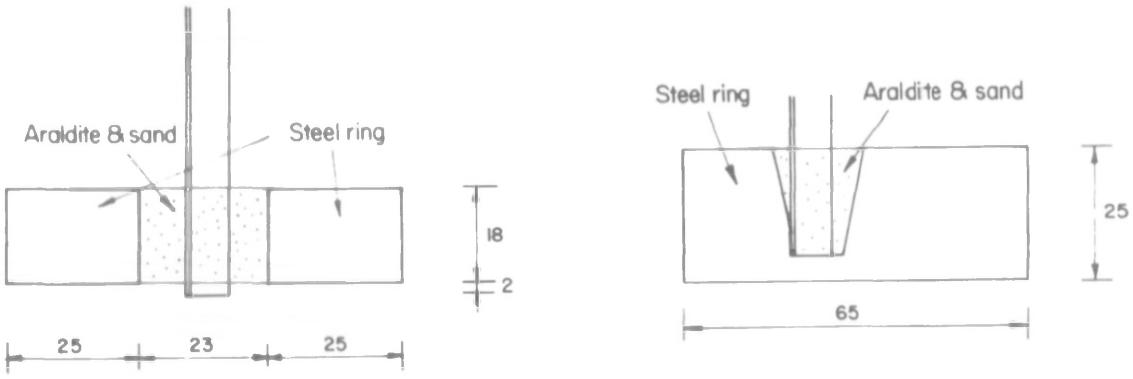
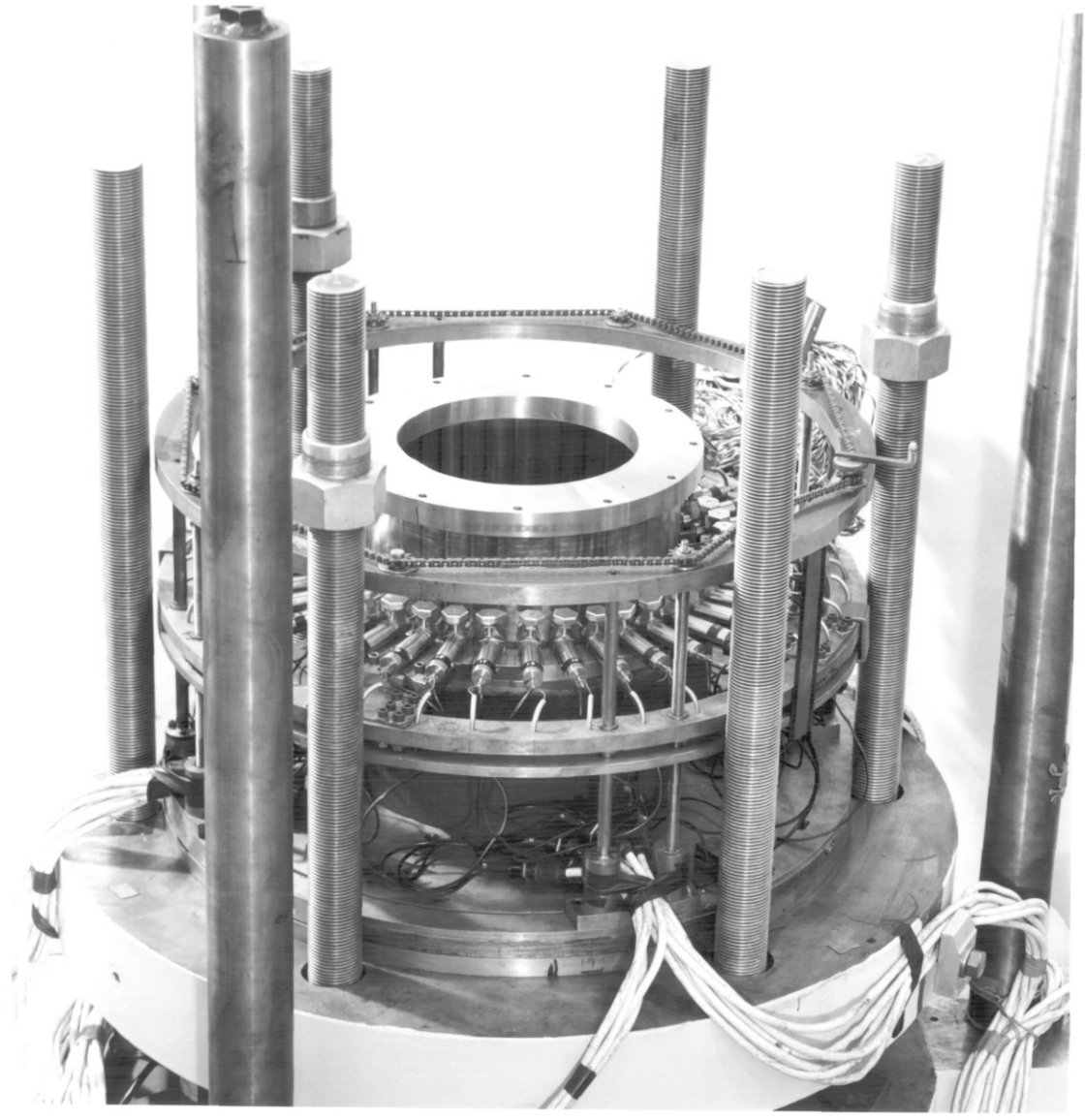


Fig. 2.52 EXTERNAL VIEW AFTER FAILURE

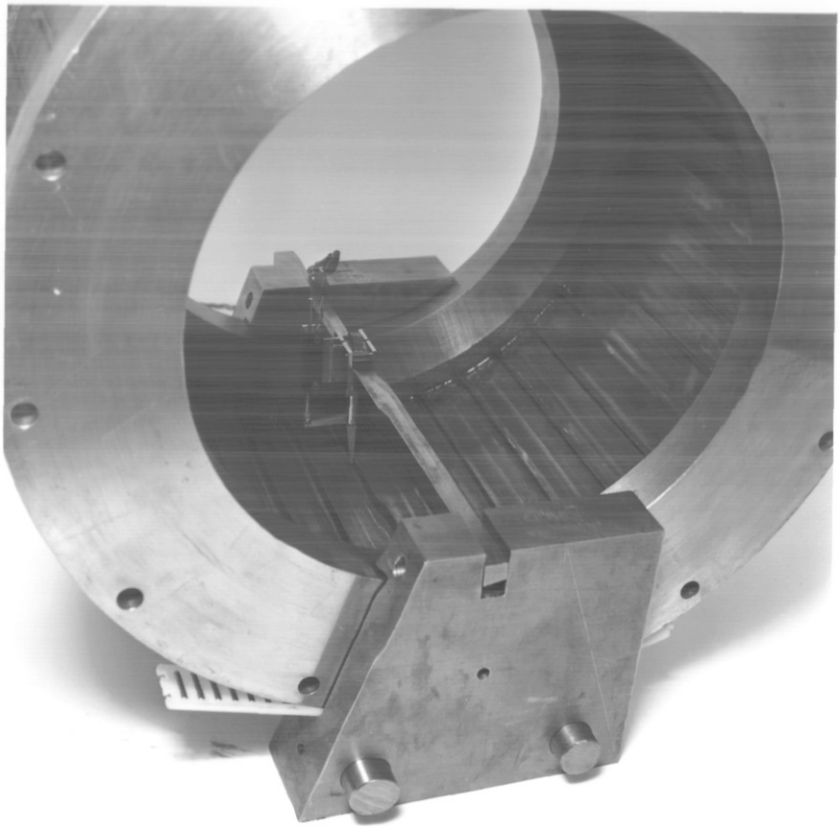


END RING DETAIL

Fig. 2.54

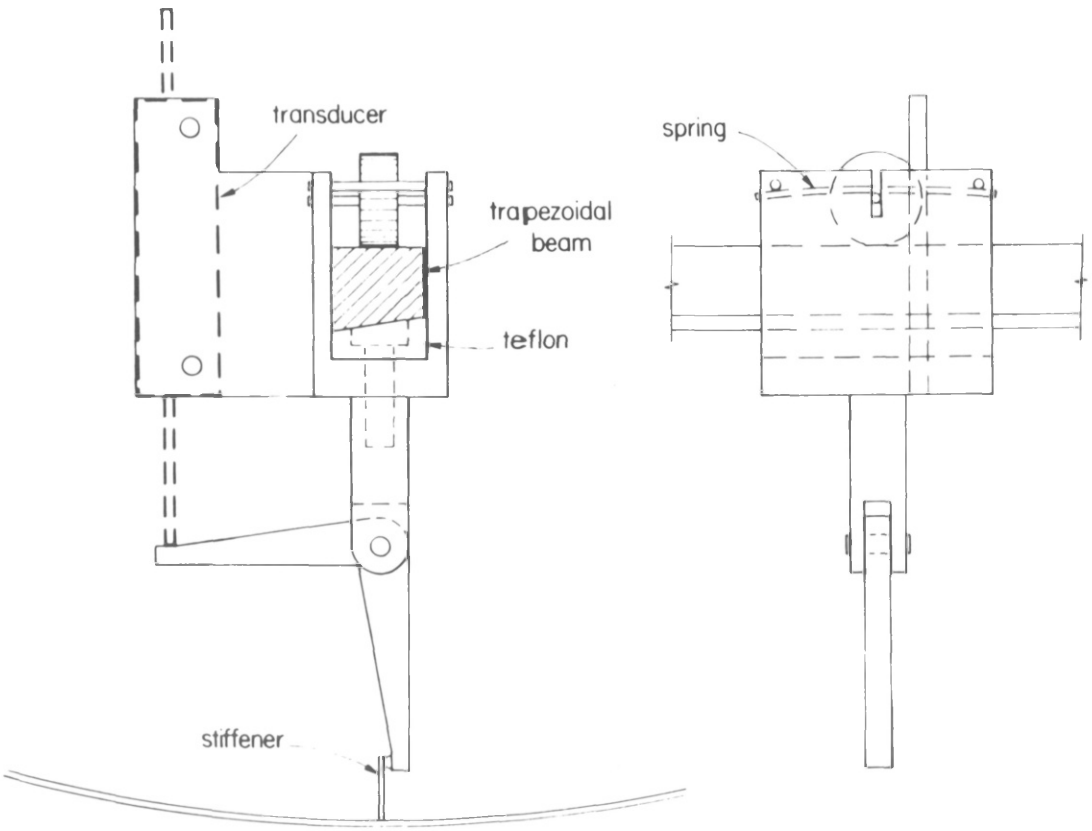


IMPERFECTION MEASURING RIG Fig. 2.55



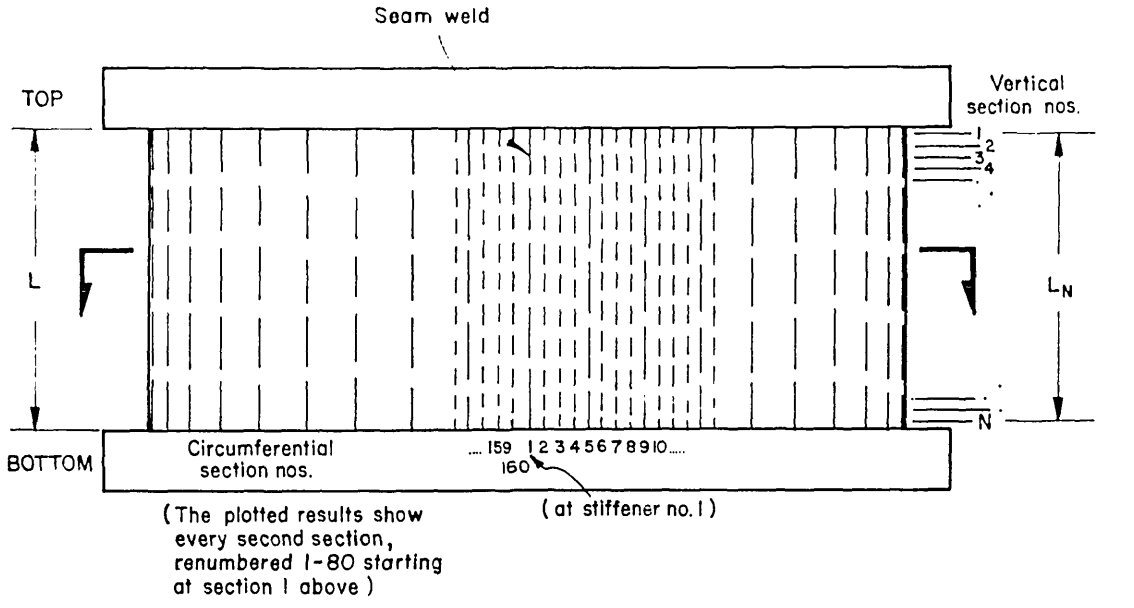
STIFFENER IMPERFECTION MEASURING EQUIPMENT

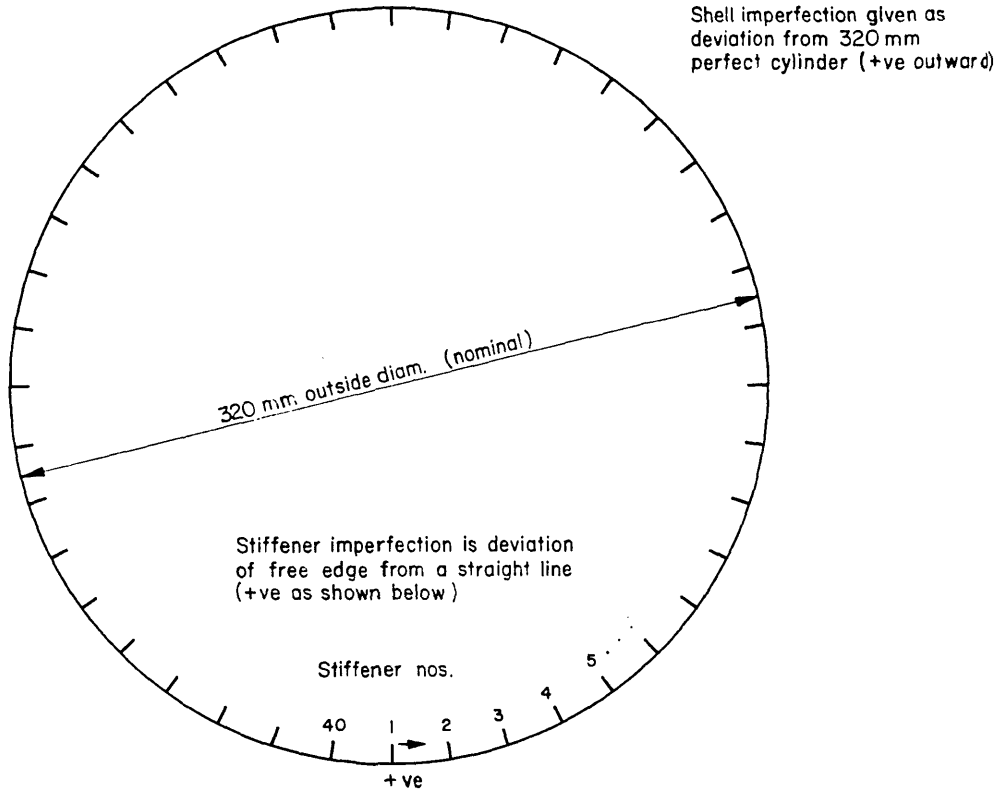
Fig. 2.56



STIFFENER IMPERFECTION MEASURING EQUIPMENT

Fig. 2.57





CYLINDER No.	1 – 4	5 – 8	9 – 12
L	64	128	192
L_N	59	123	187
N	16	20	25

Fig. 3 Explanatory diagram for presentation of imperfection results.

Fig. 2.58

CYLINDER 1 – INITIAL IMPERFECTIONS
Circumferential Sections

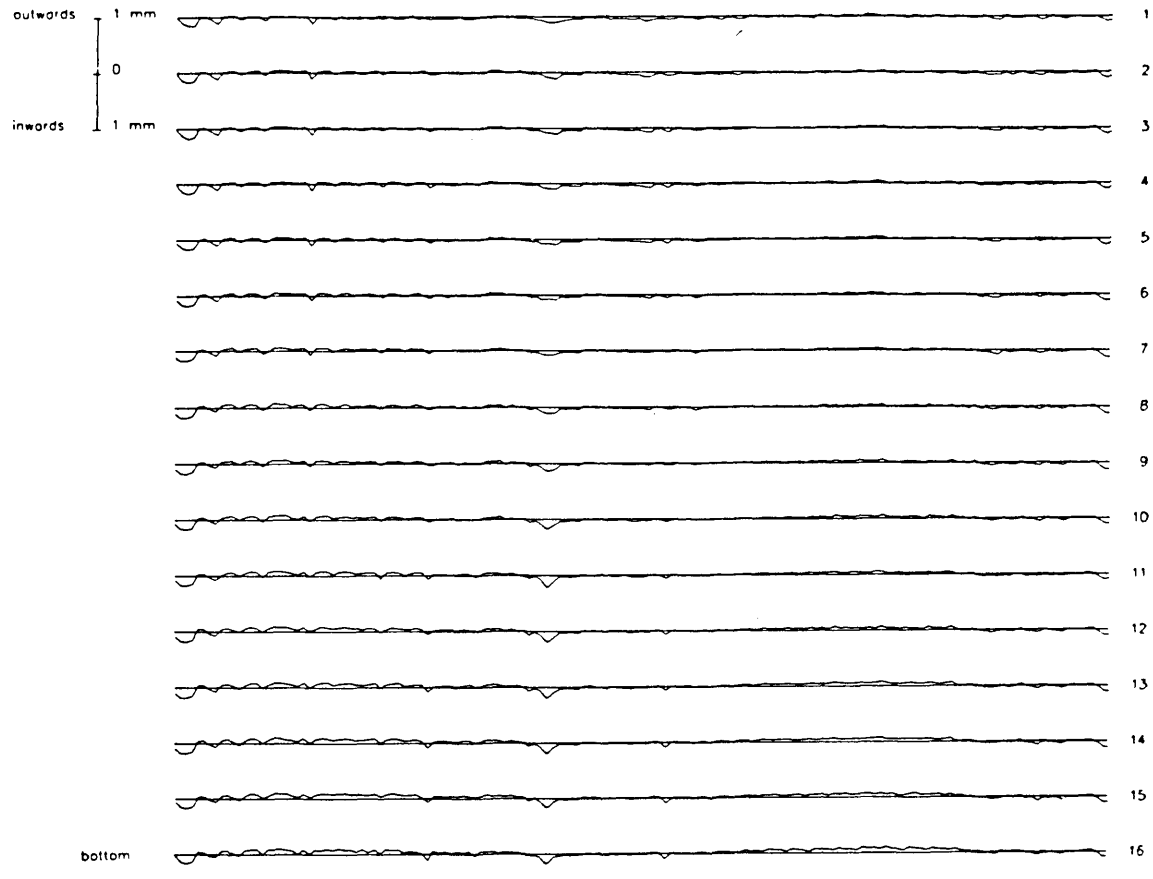


Fig. 2.59

CYLINDER 1 – INITIAL IMPERFECTIONS
Vertical Sections

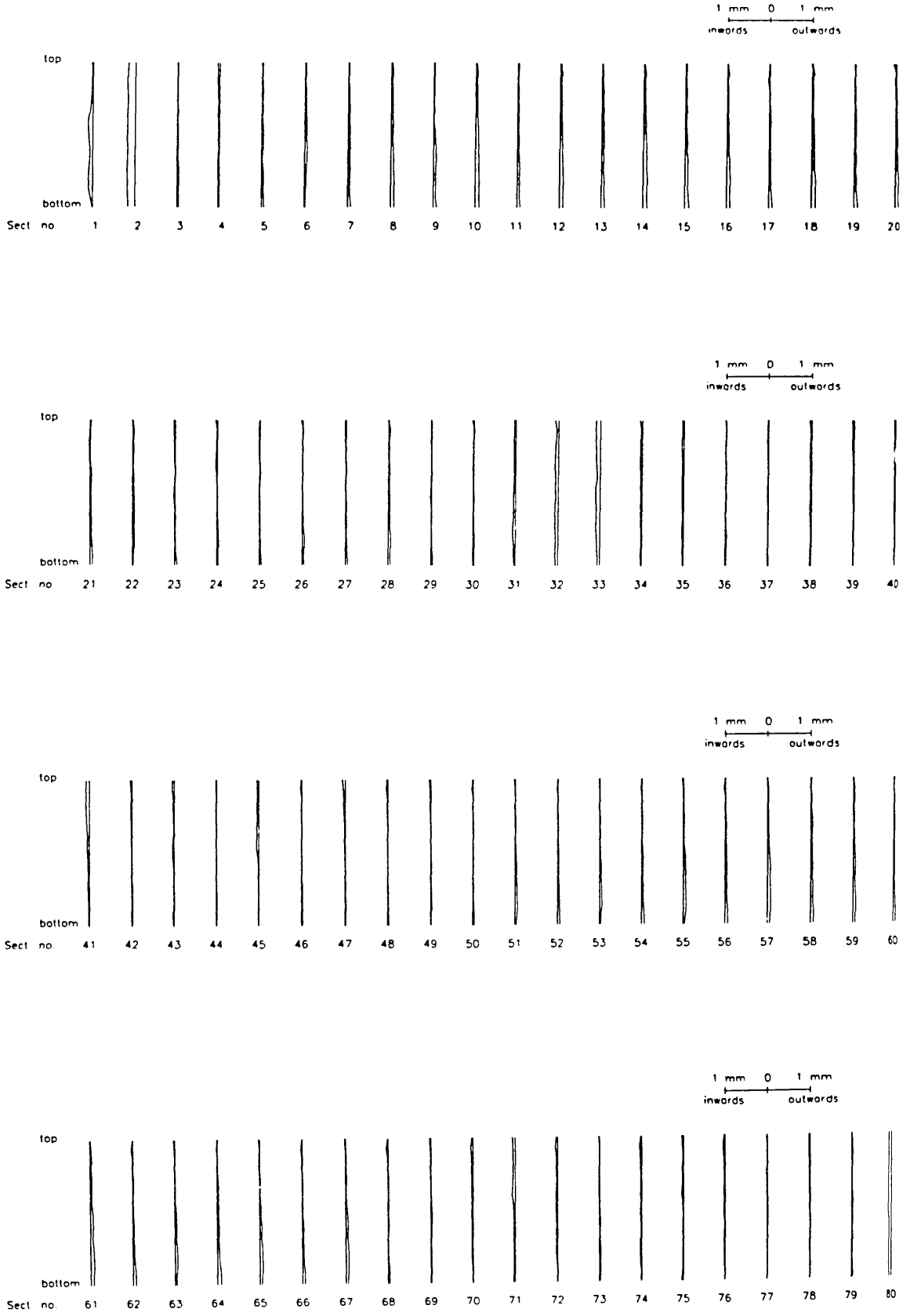


Fig. 2.60

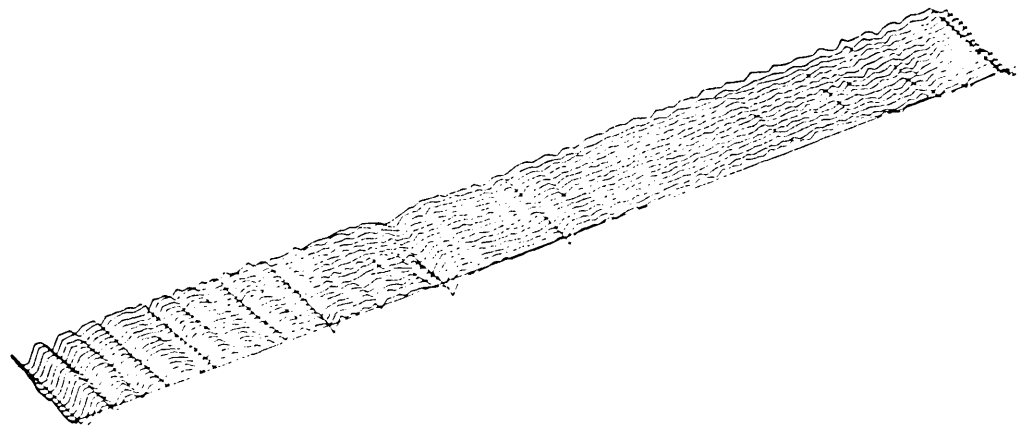


Fig. 2.61

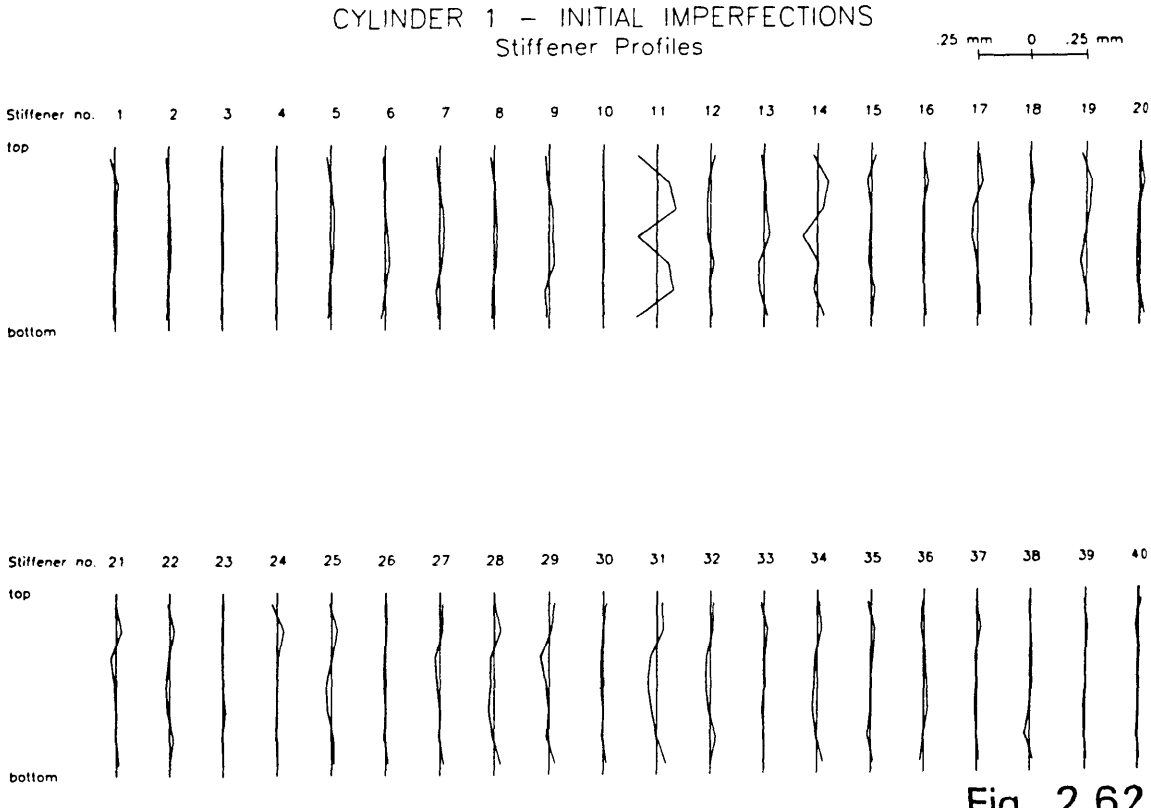


Fig. 2.62

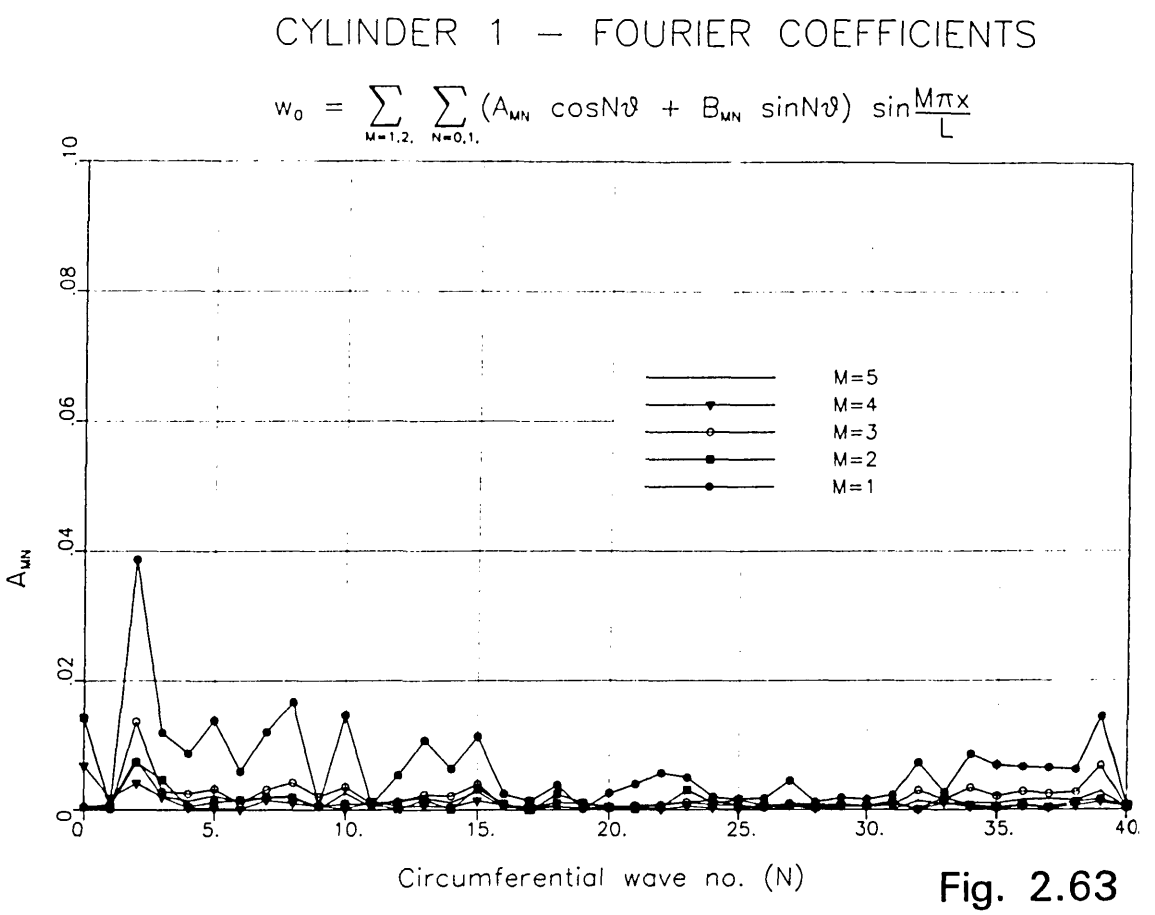


Fig. 2.63

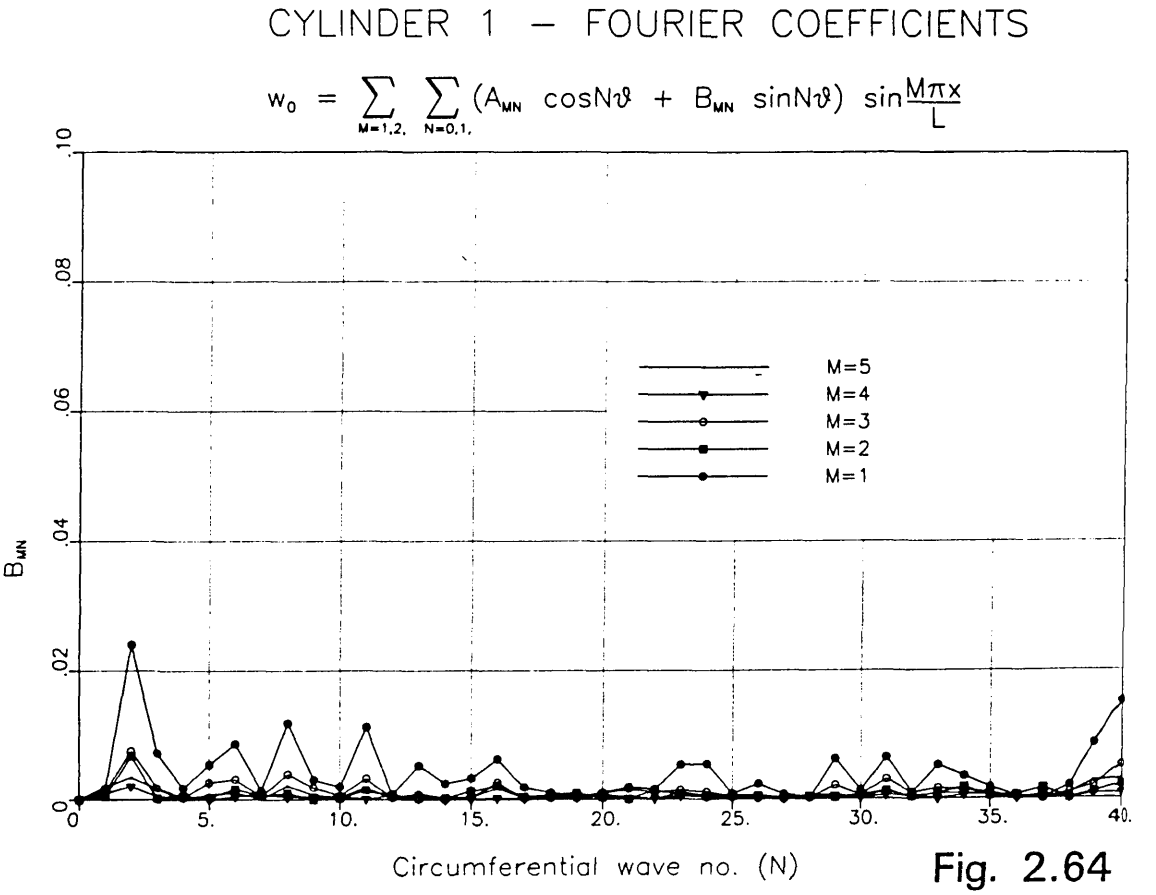


Fig. 2.64

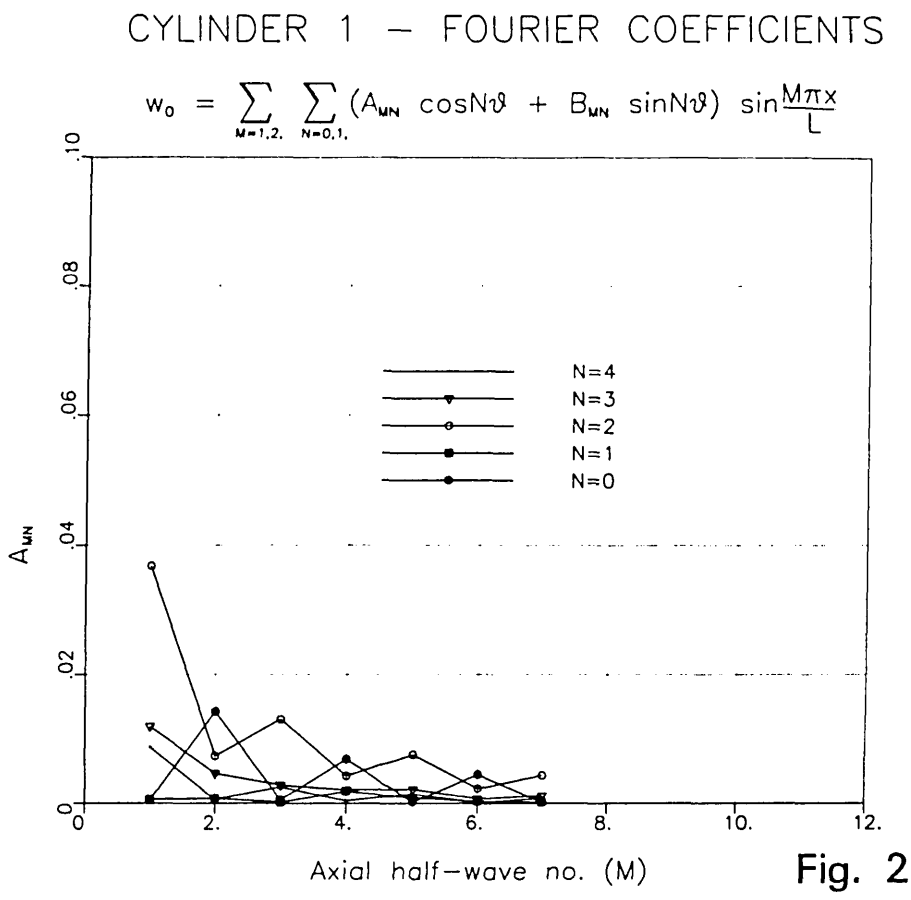


Fig. 2.65

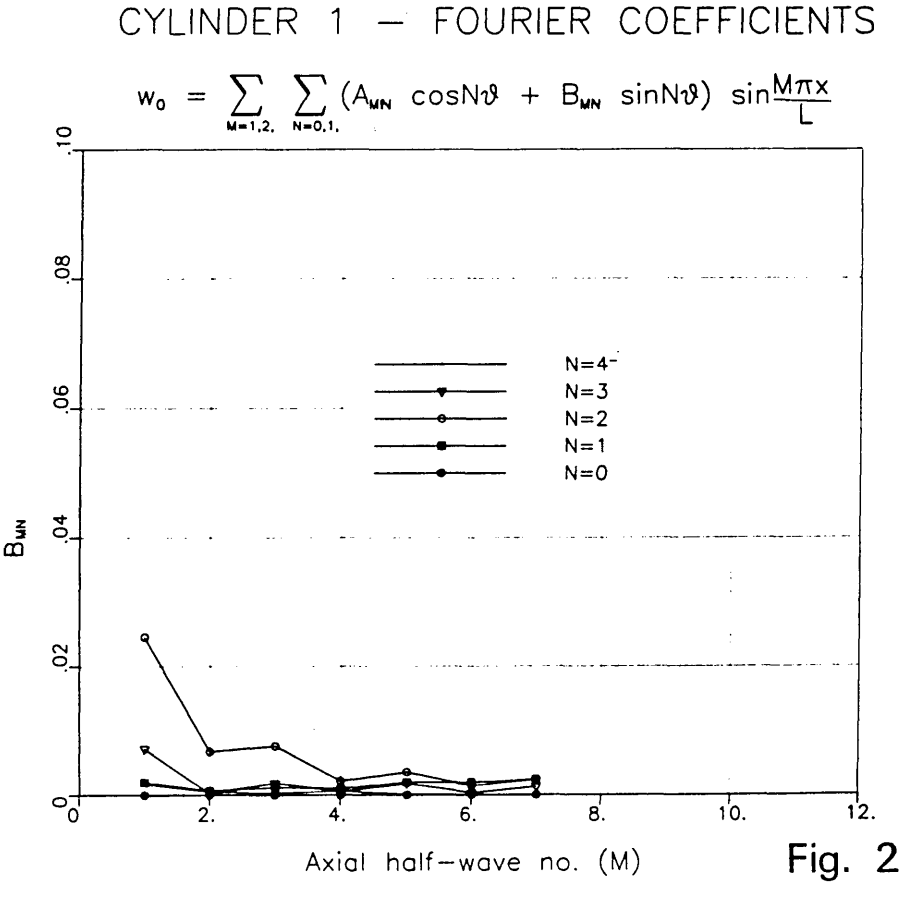


Fig. 2.66

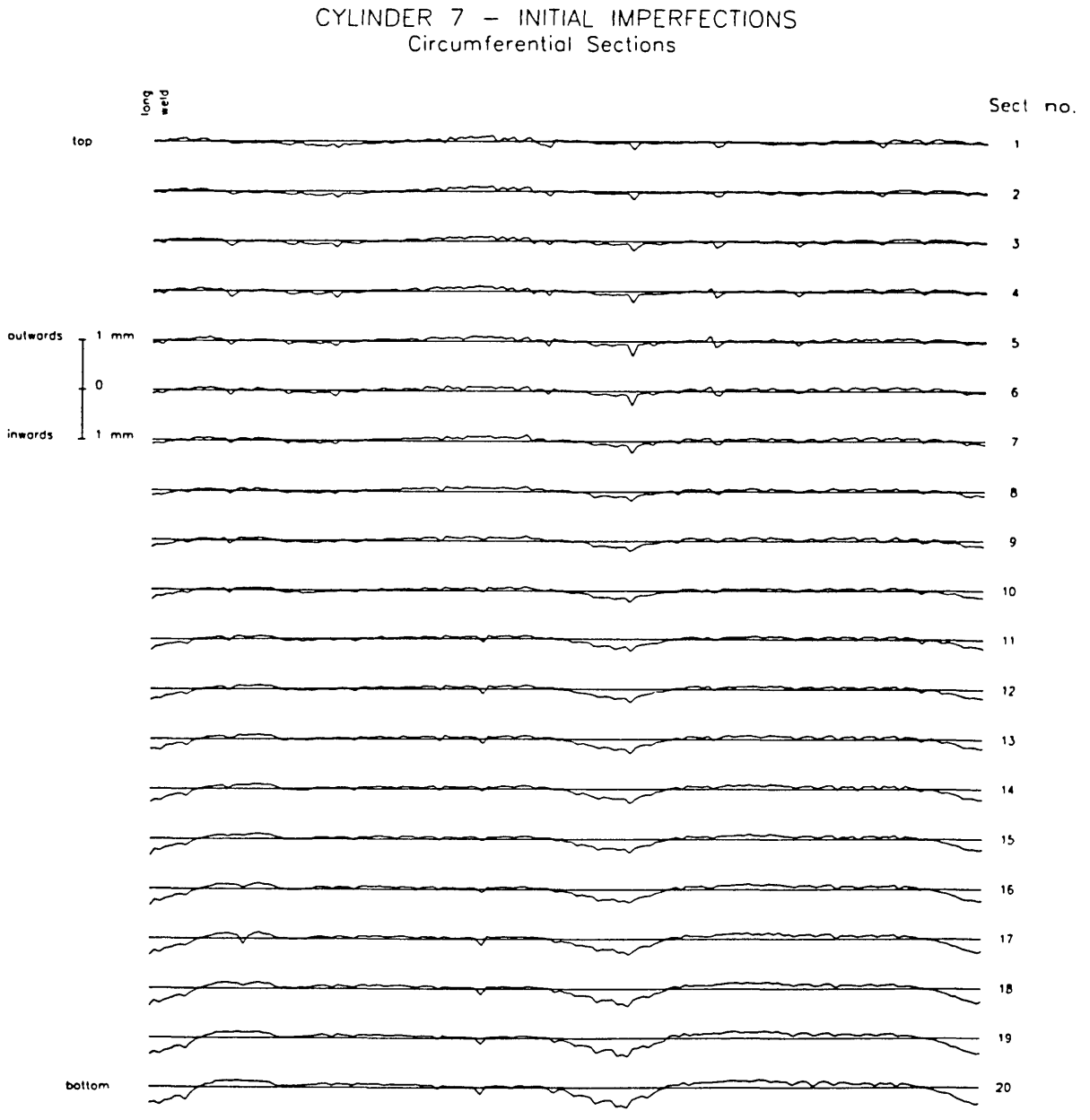

CYLINDER 7 – INITIAL IMPERFECTIONS
Circumferential Sections
long weld
Sect no.
top
outwards
1 mm
0
inwards
1 mm
bottom
1
2
3
4
5
6
7
8
9
10
11
12
13
14
15
16
17
18
19
20

Fig. 2.67

CYLINDER 7 – INITIAL IMPERFECTIONS
Vertical Sections

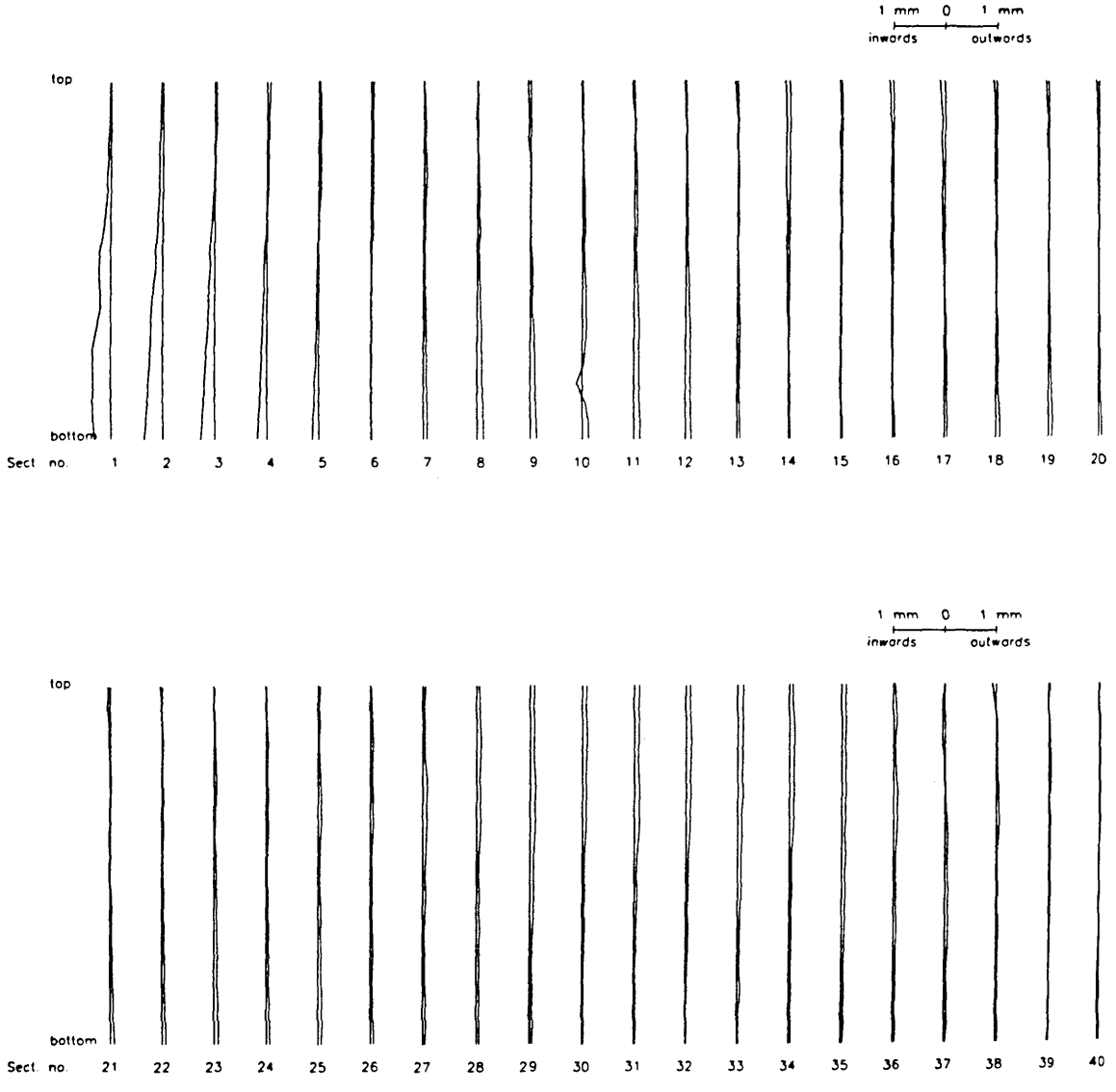


Fig. 2.68

CYLINDER 7 – INITIAL IMPERFECTIONS
Vertical Sections

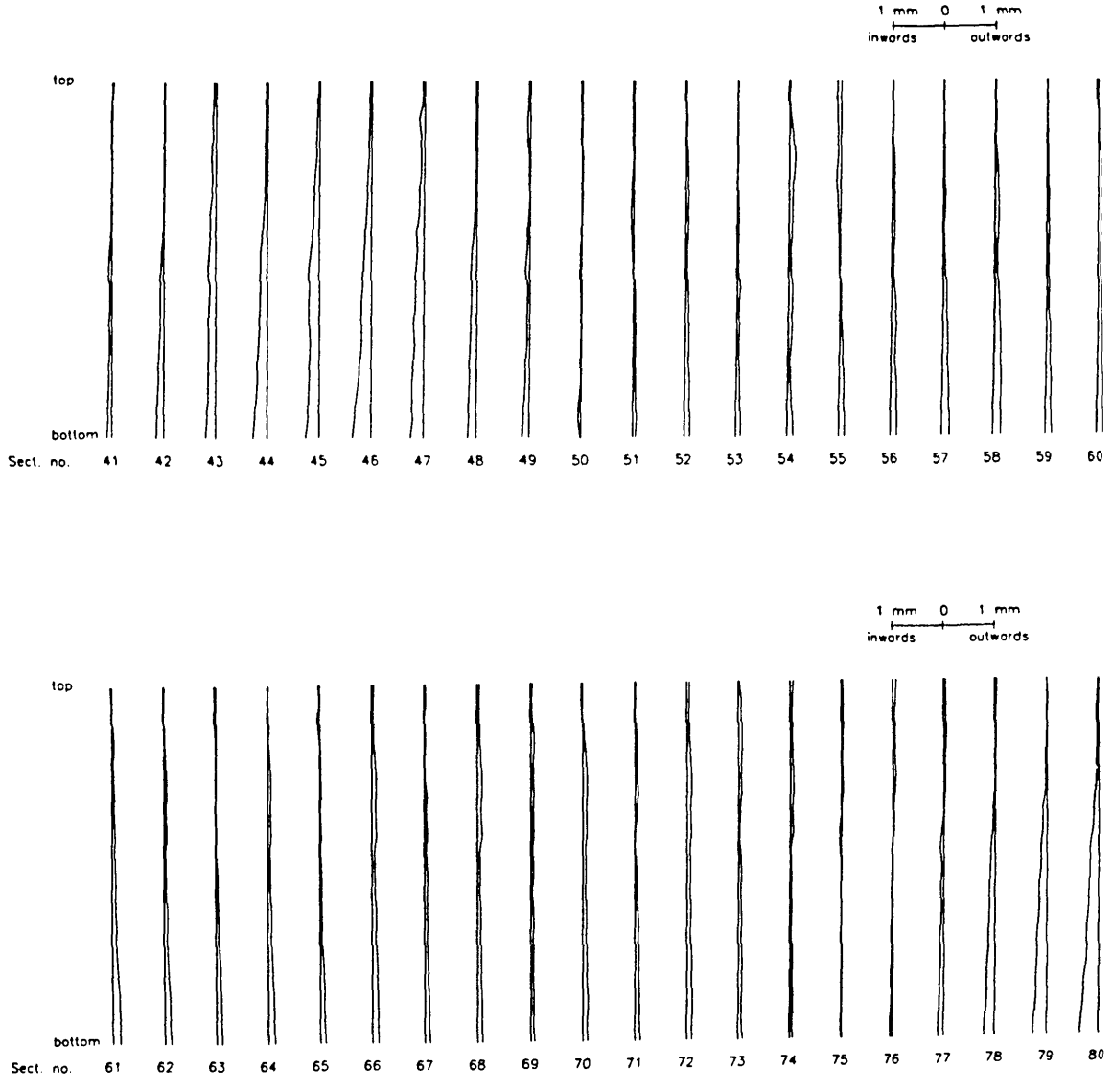


Fig. 2.69

CYLINDER 7 – INITIAL IMPERFECTIONS

Projection of imperfection surface

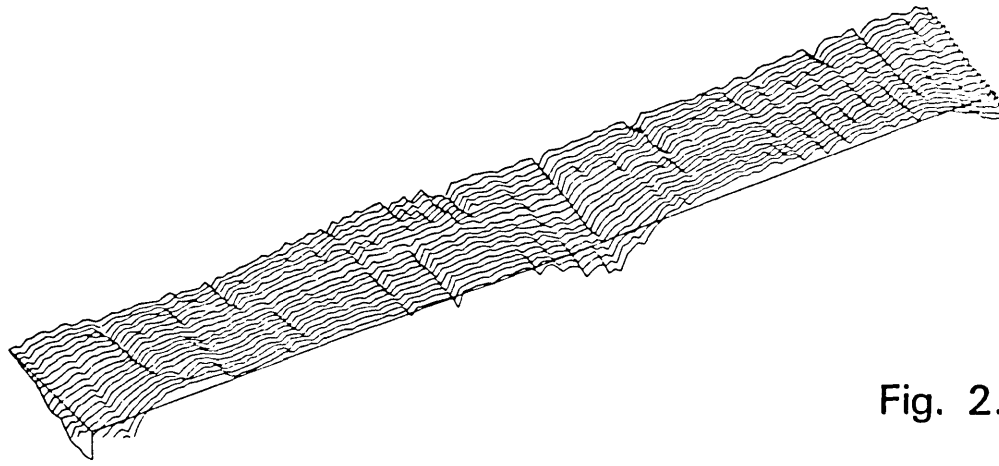


Fig. 2.70

CYLINDER 7 – INITIAL IMPERFECTIONS

Stiffener Profiles

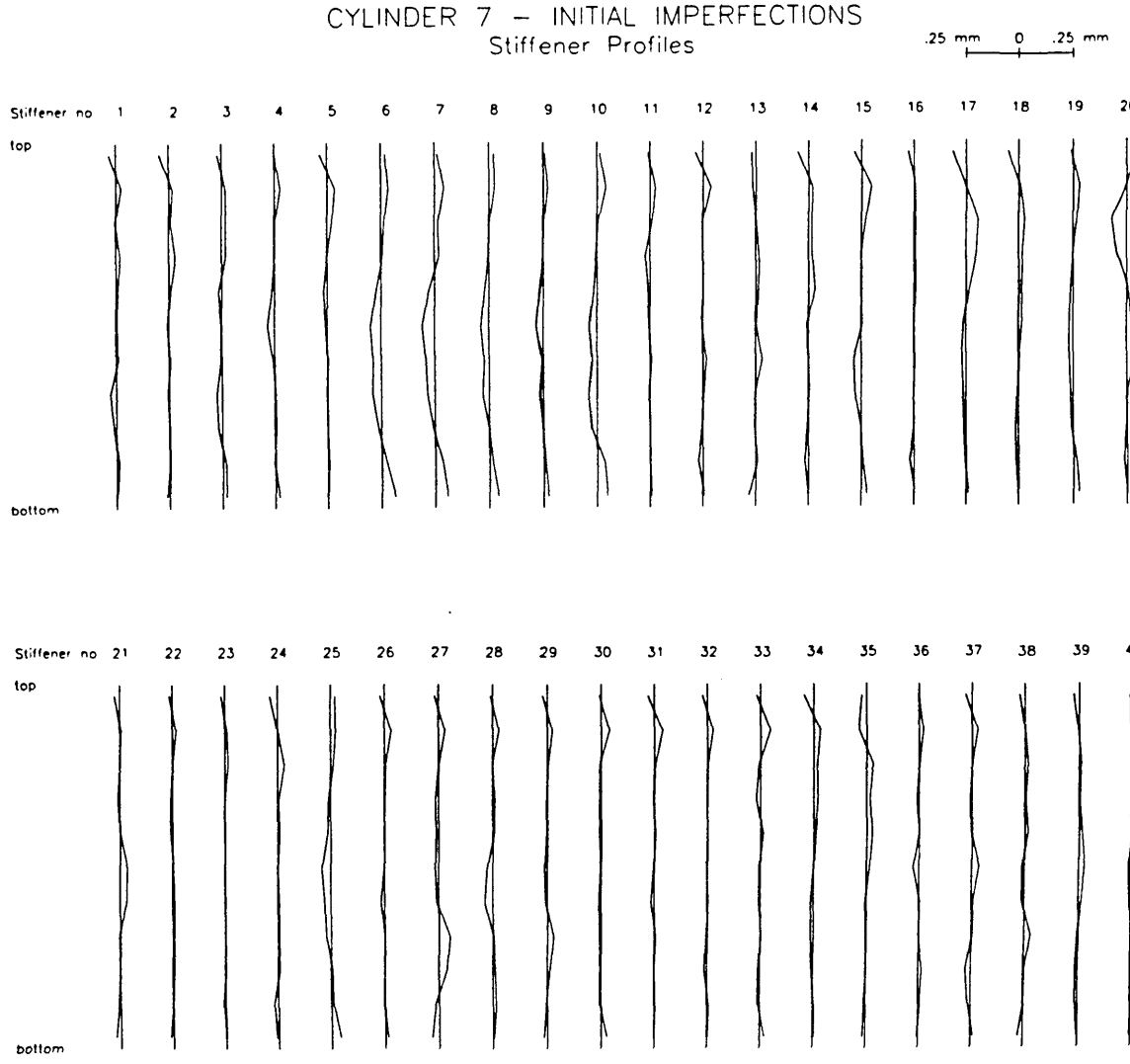


Fig. 2.71

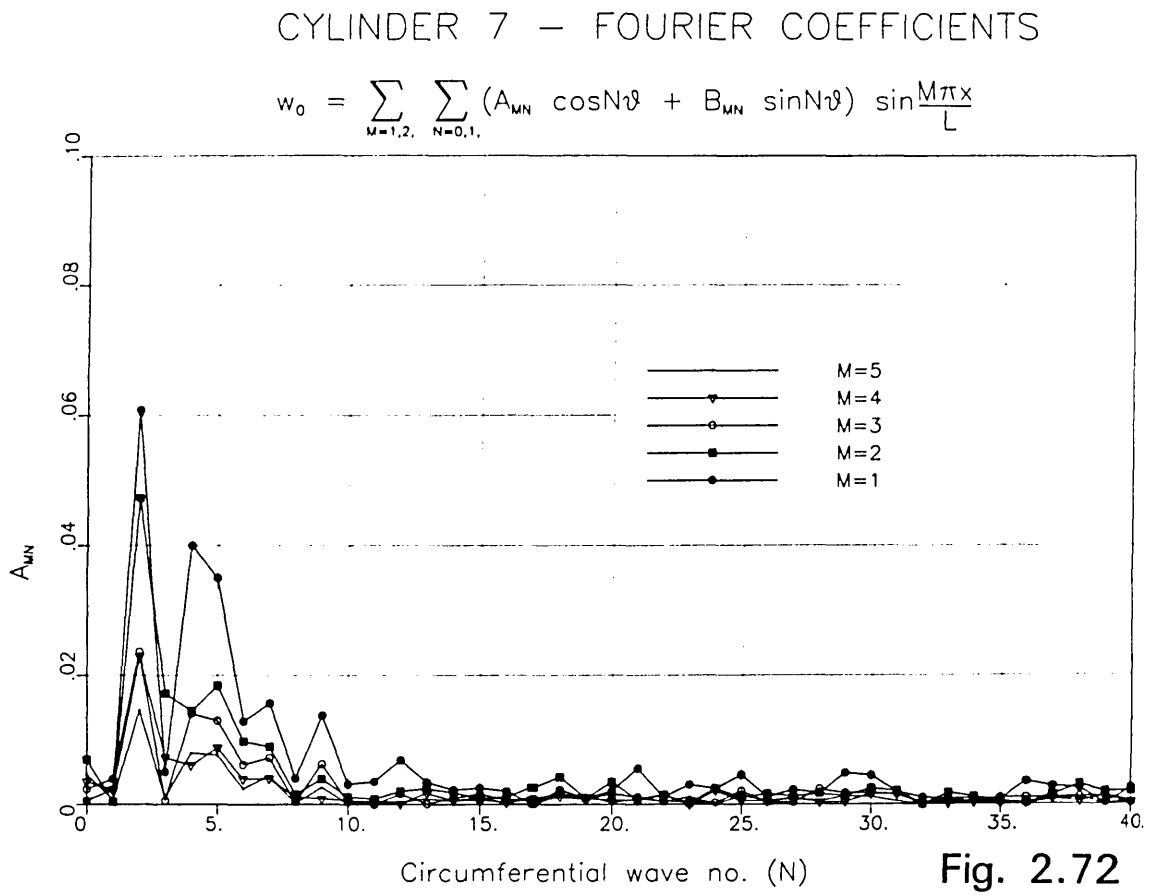


Fig. 2.72

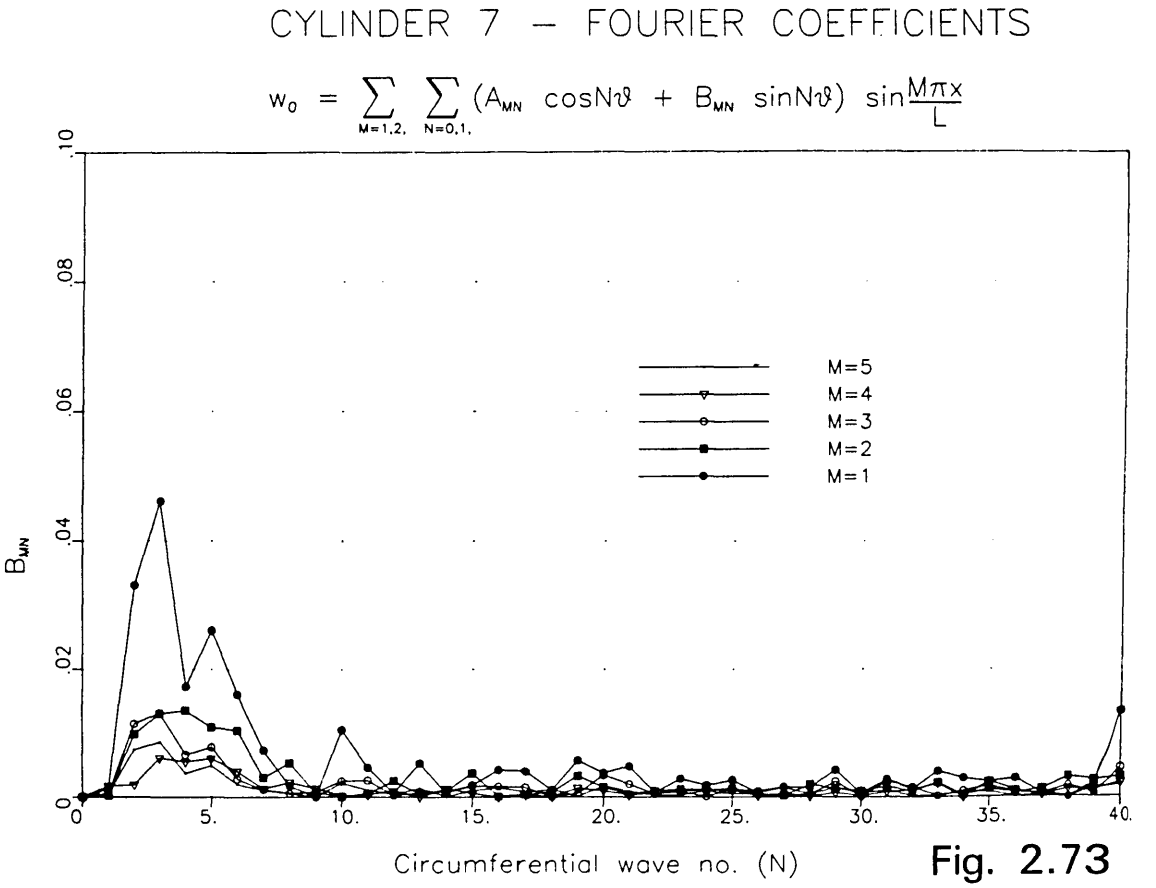


Fig. 2.73

CYLINDER 7 — FOURIER COEFFICIENTS

$$w_0 = \sum_{M=1,2,} \sum_{N=0,1,} (A_{MN} \cos N\vartheta + B_{MN} \sin N\vartheta) \sin \frac{M\pi x}{L}$$

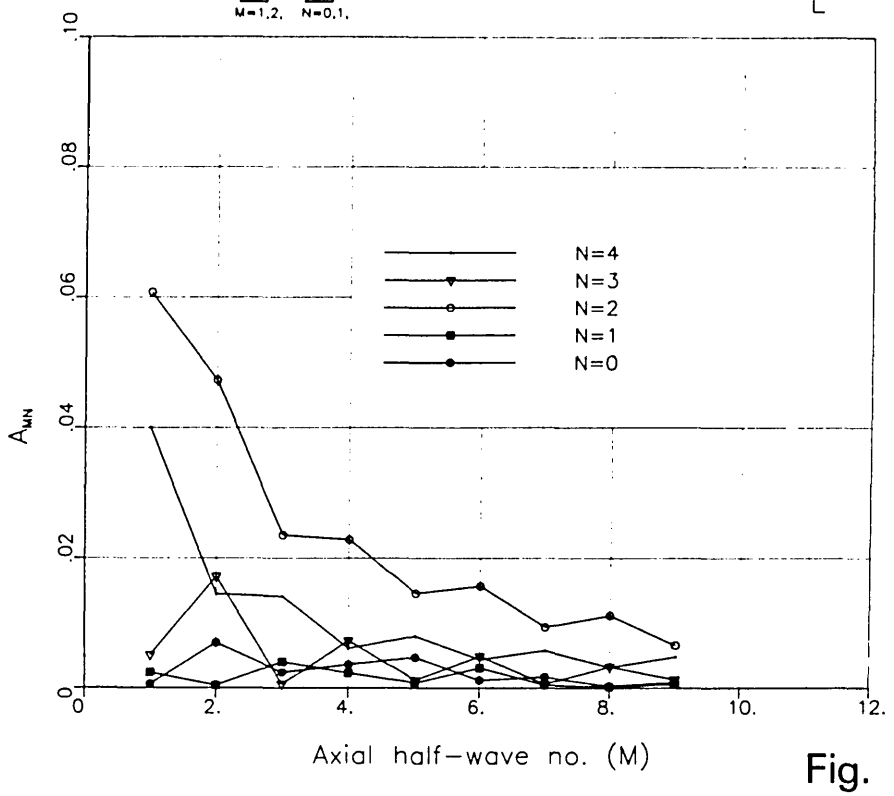


Fig. 2.74

CYLINDER 7 — FOURIER COEFFICIENTS

$$w_0 = \sum_{M=1,2,} \sum_{N=0,1,} (A_{MN} \cos N\vartheta + B_{MN} \sin N\vartheta) \sin \frac{M\pi x}{L}$$

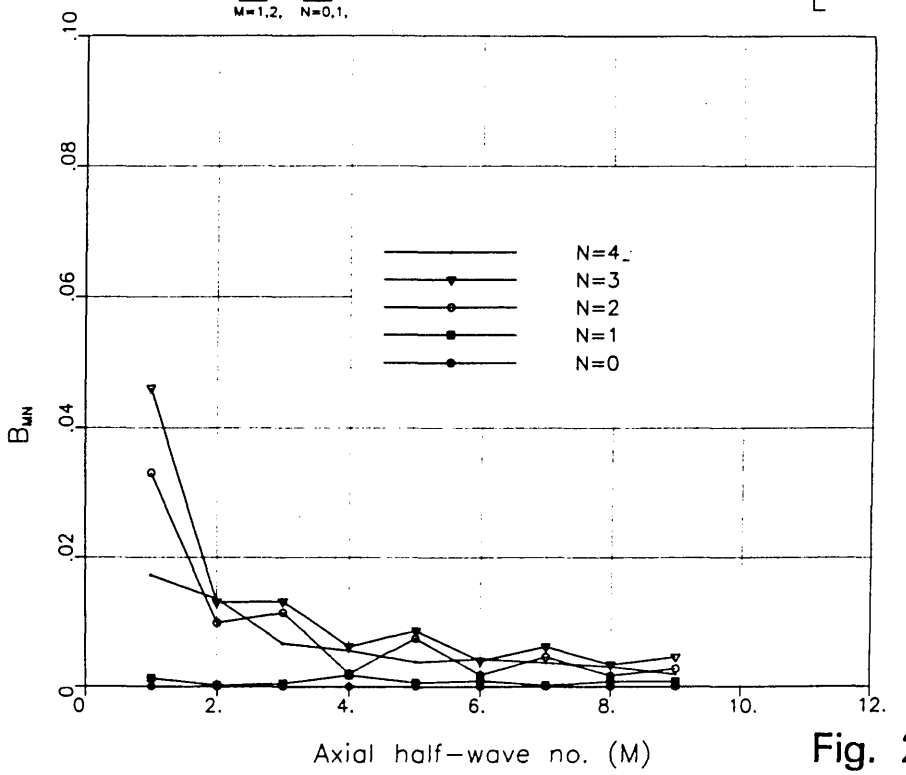


Fig. 2.75

CYLINDER 10 – INITIAL IMPERFECTIONS
Circumferential Sections

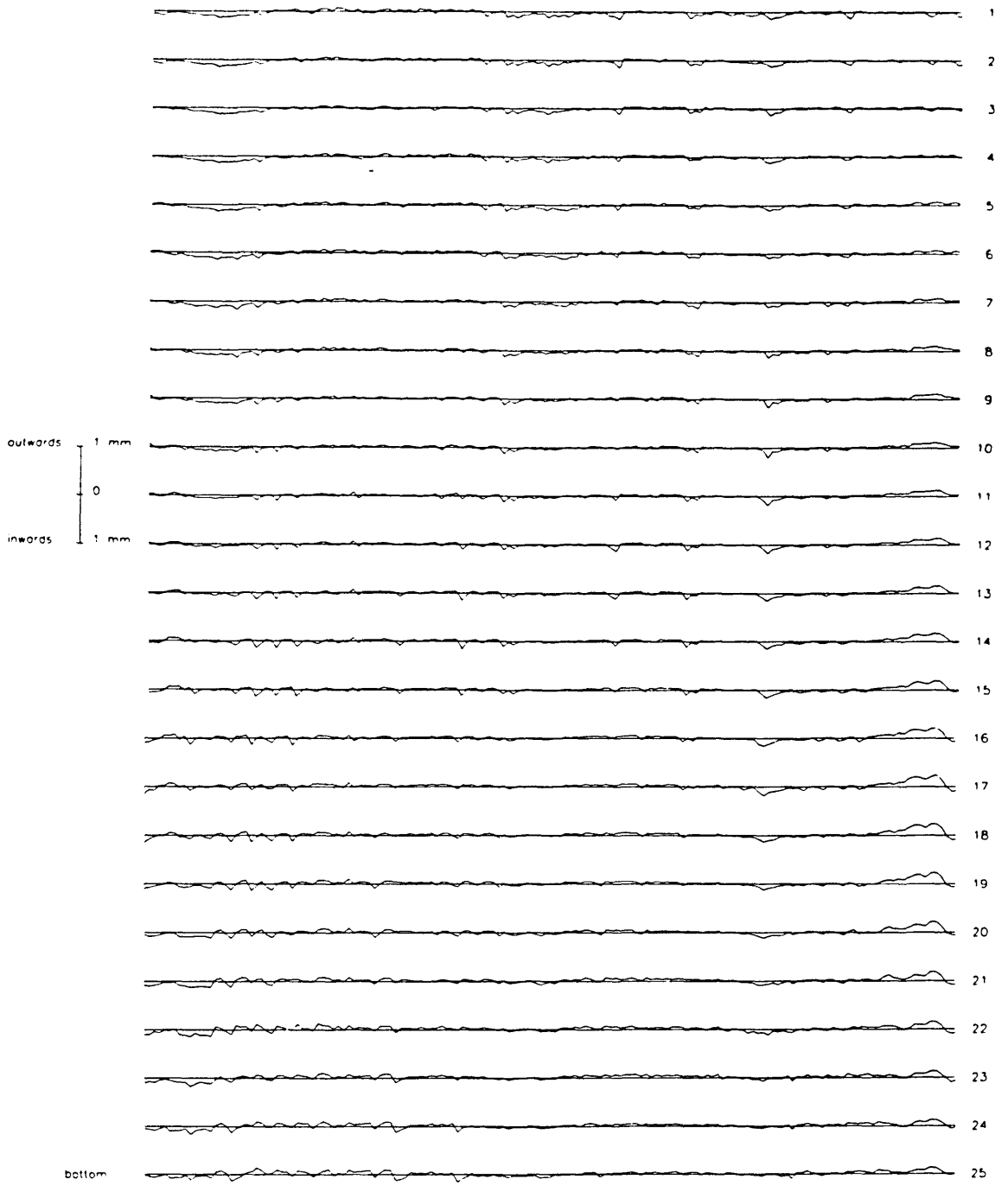


Fig. 2.76

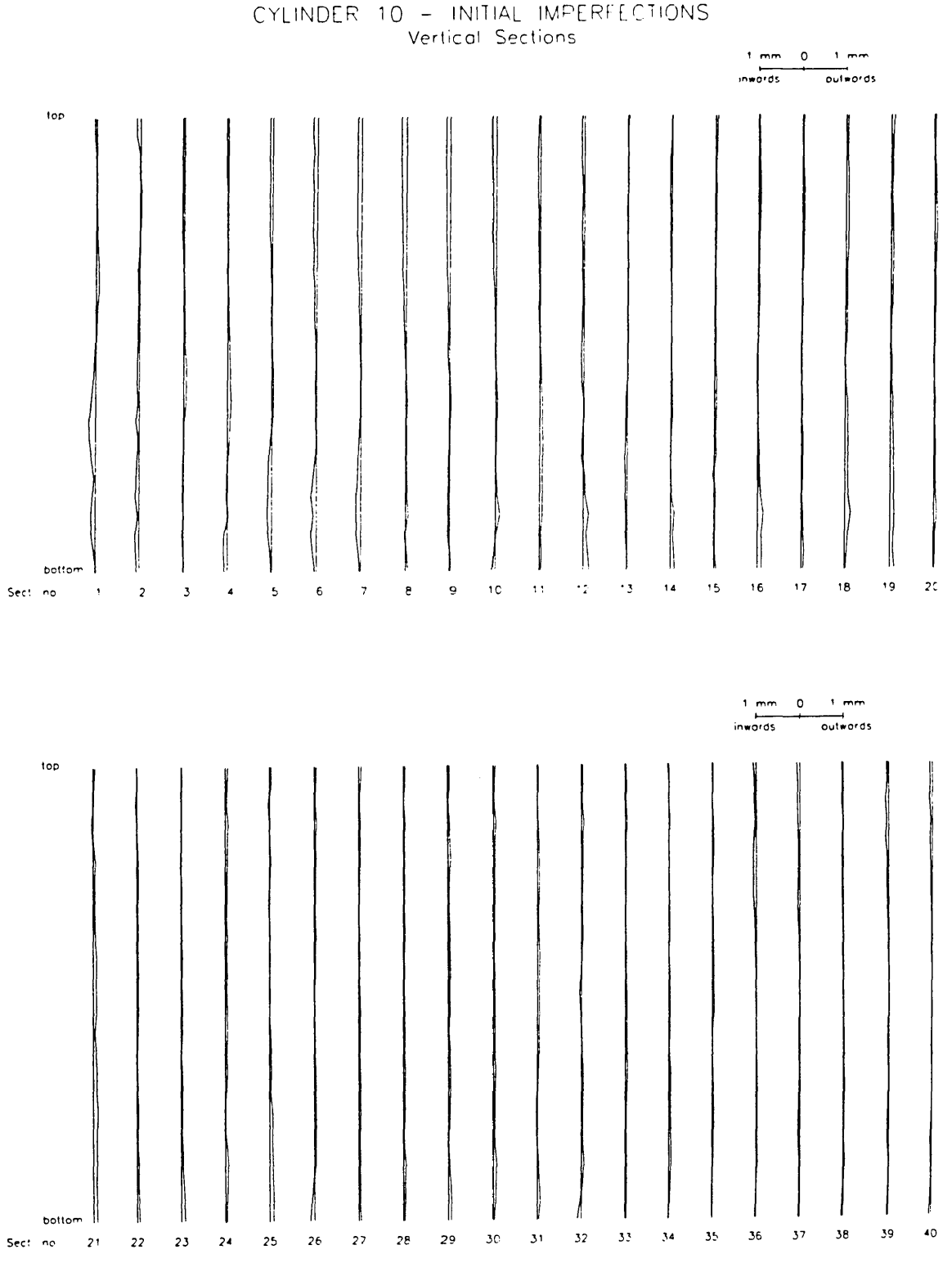

CYLINDER 10 - INITIAL IMPERFECTIONS
Vertical Sections
1 mm 0 1 mm
inwards outwards
top
bottom
Sect no 1 2 3 4 5 6 7 8 9 10 11 12 13 14 15 16 17 18 19 20
1 mm 0 1 mm
inwards outwards
top
bottom
Sect no 21 22 23 24 25 26 27 28 29 30 31 32 33 34 35 36 37 38 39 40

Fig. 2.77

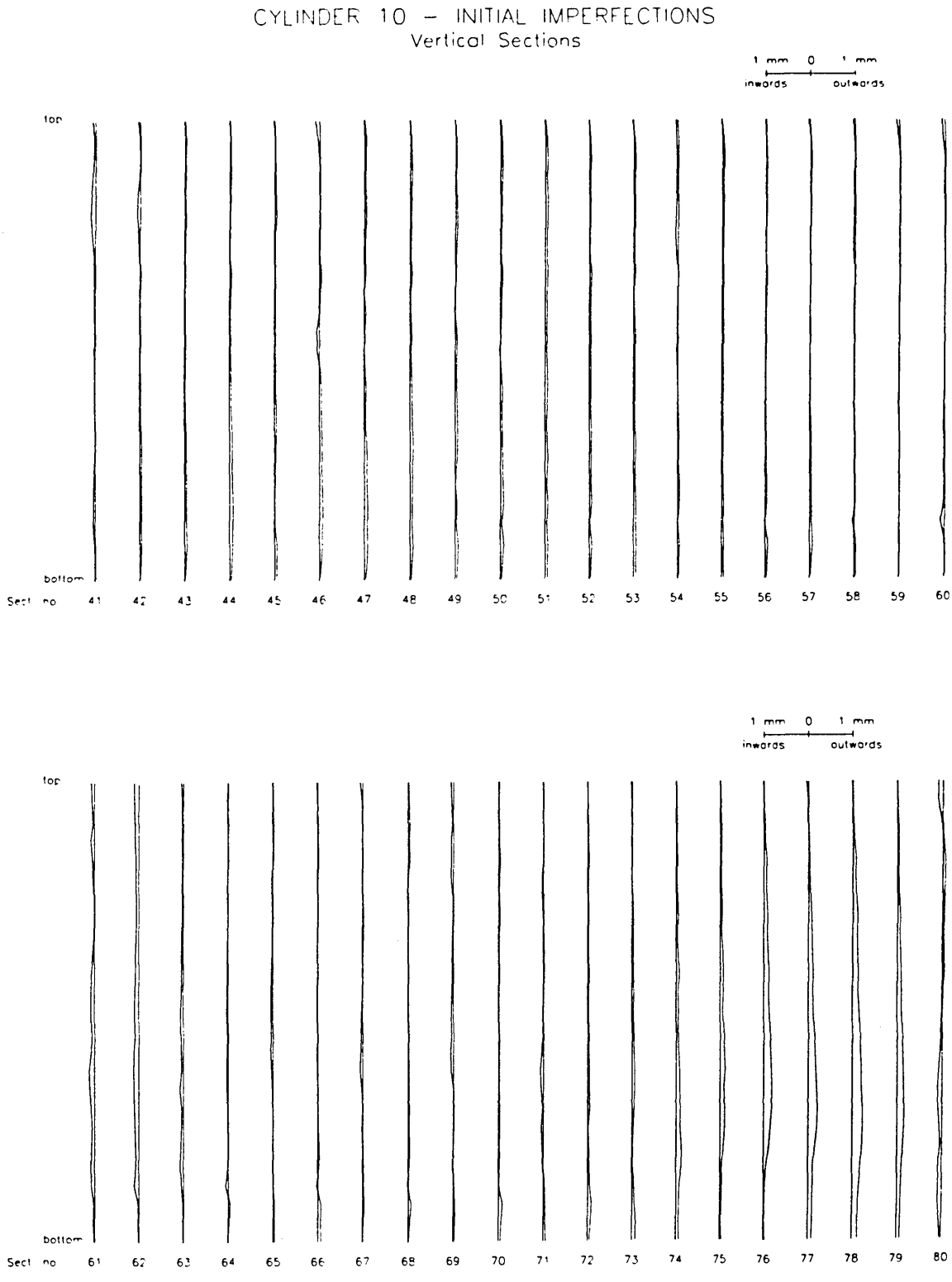

CYLINDER 10 – INITIAL IMPERFECTIONS
Vertical Sections
1 mm 0 1 mm
inwards outwards
top
bottom
Sect no 41 42 43 44 45 46 47 48 49 50 51 52 53 54 55 56 57 58 59 60
1 mm 0 1 mm
inwards outwards
top
bottom
Sect no 61 62 63 64 65 66 67 68 69 70 71 72 73 74 75 76 77 78 79 80

Fig. 2.78

CYLINDER 10 – INITIAL IMPERFECTIONS

Projection of imperfected surface

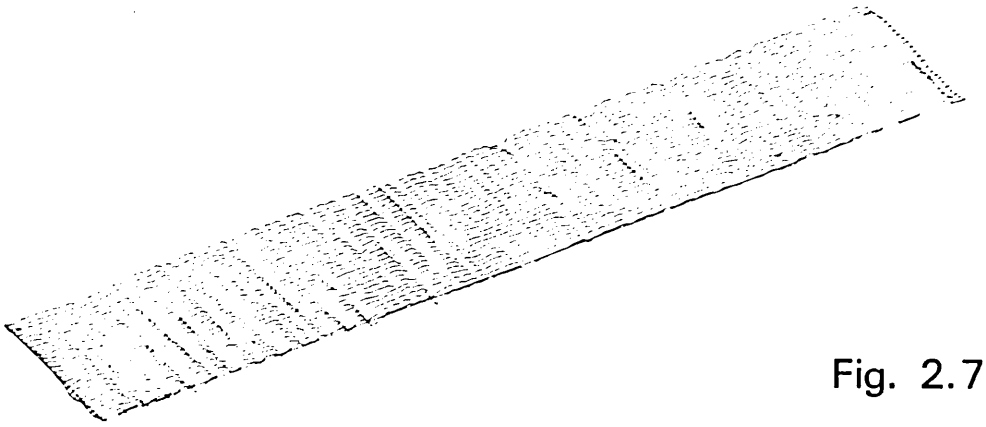


Fig. 2.79

CYLINDER 10 – INITIAL IMPERFECTIONS

Stiffener Profiles

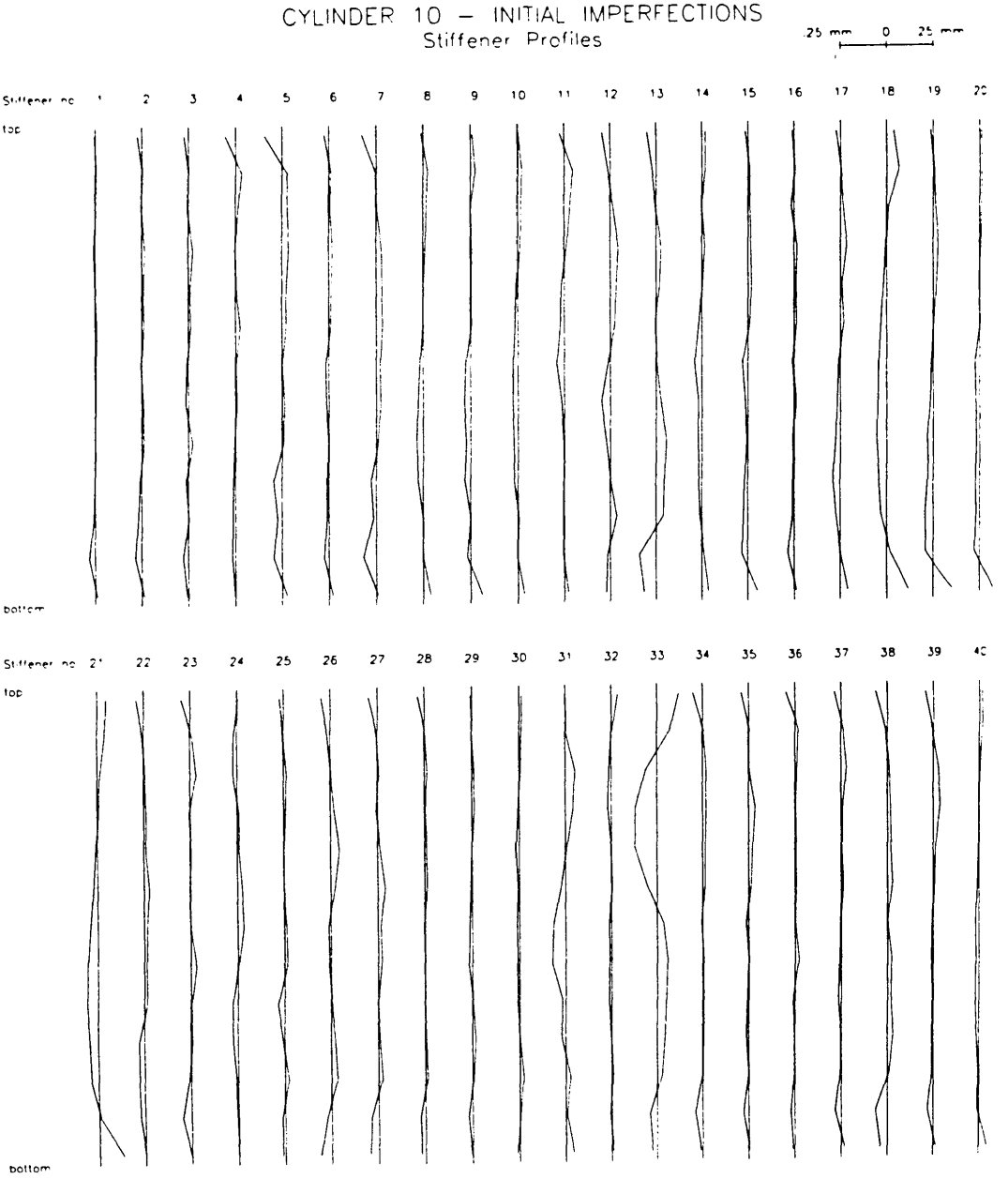


Fig. 2.80

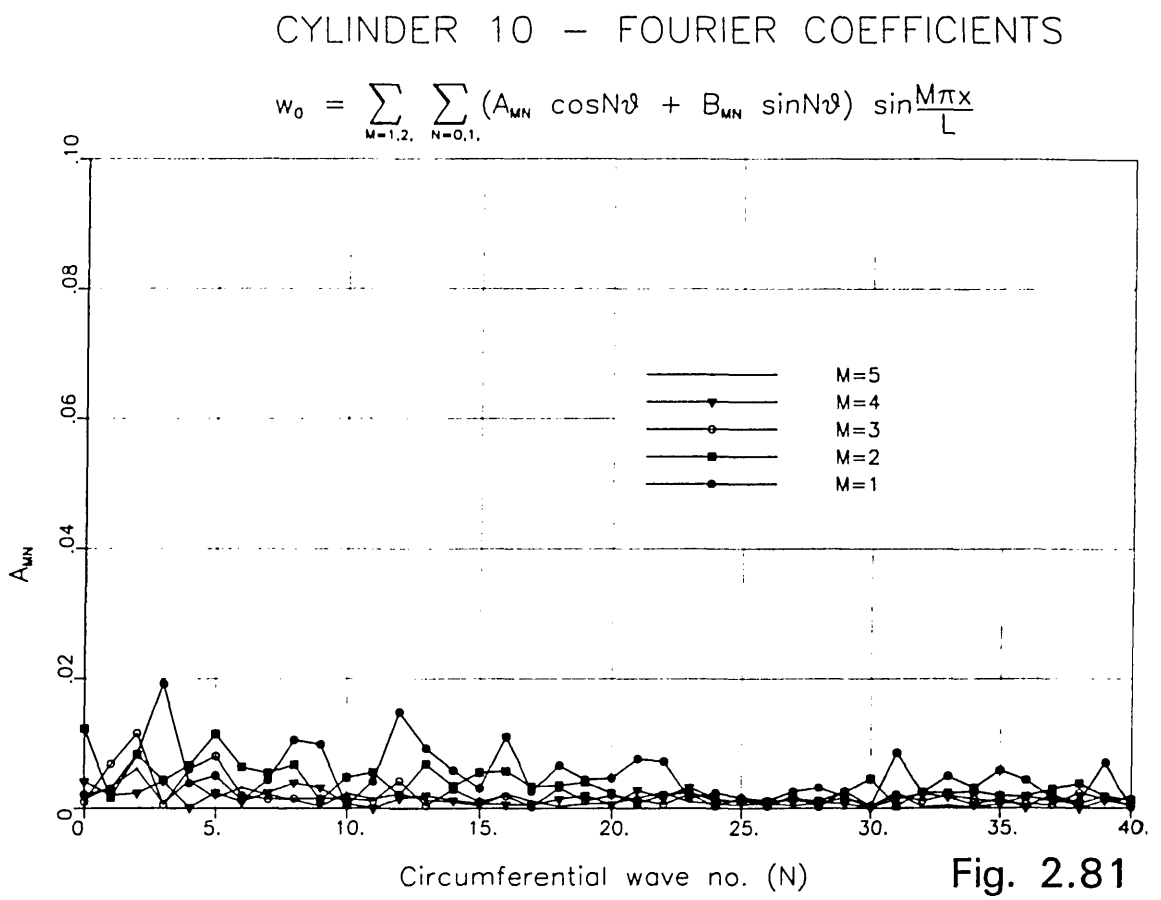


Fig. 2.81

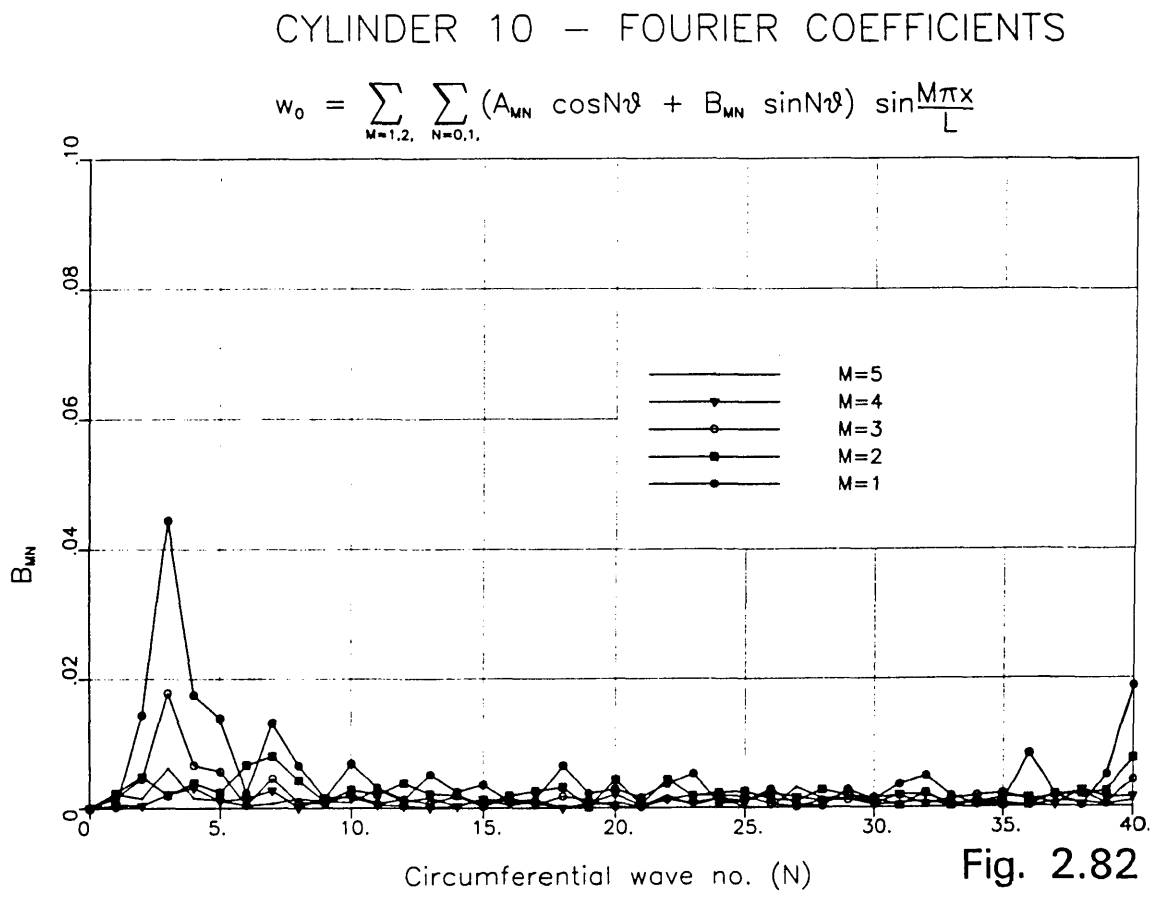


Fig. 2.82

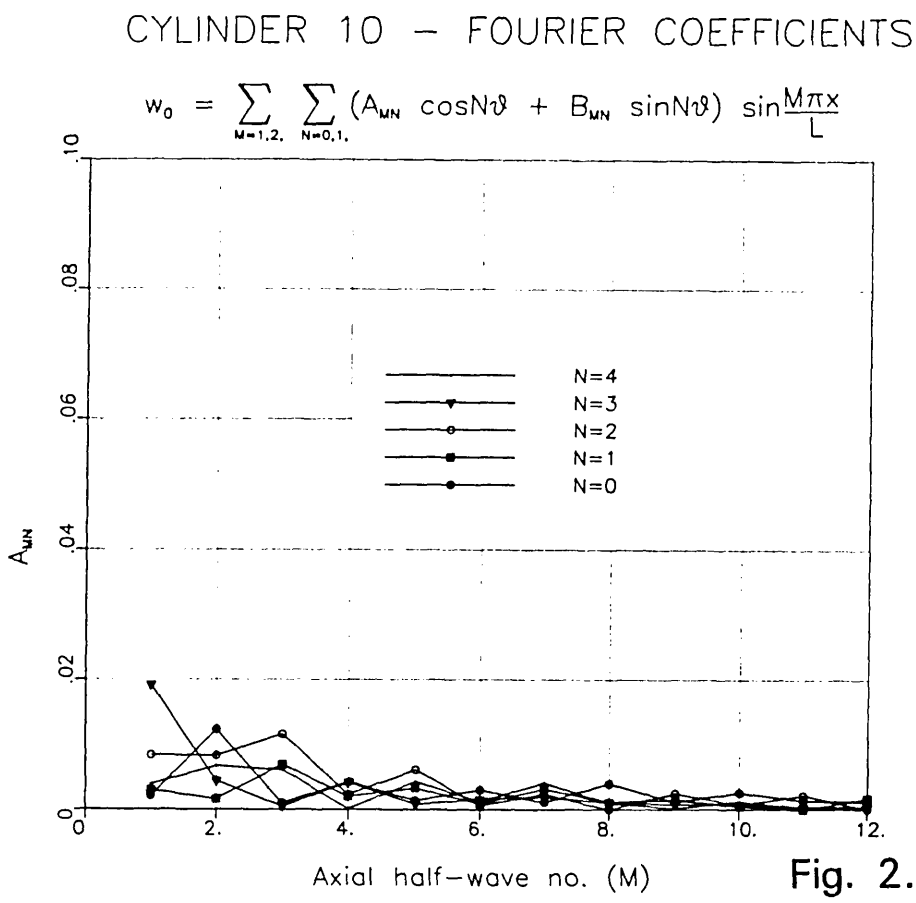


Fig. 2.83

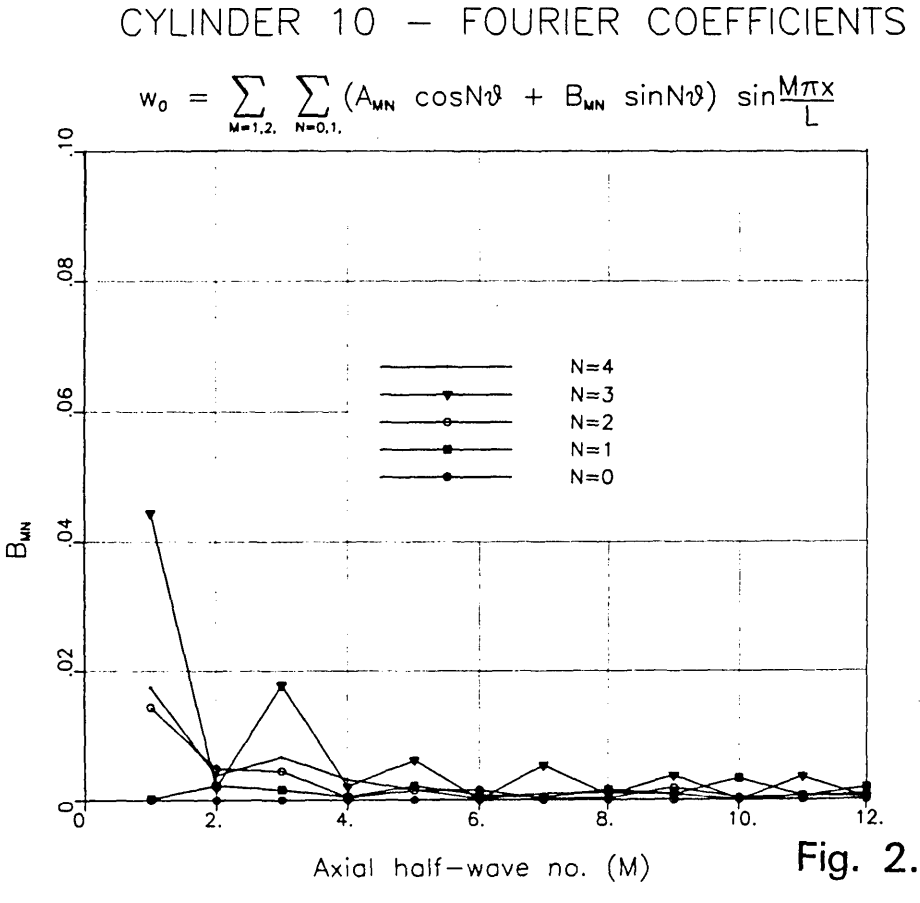


Fig. 2.84

CYLINDER I - STRAIN GAUGE LOCATIONS

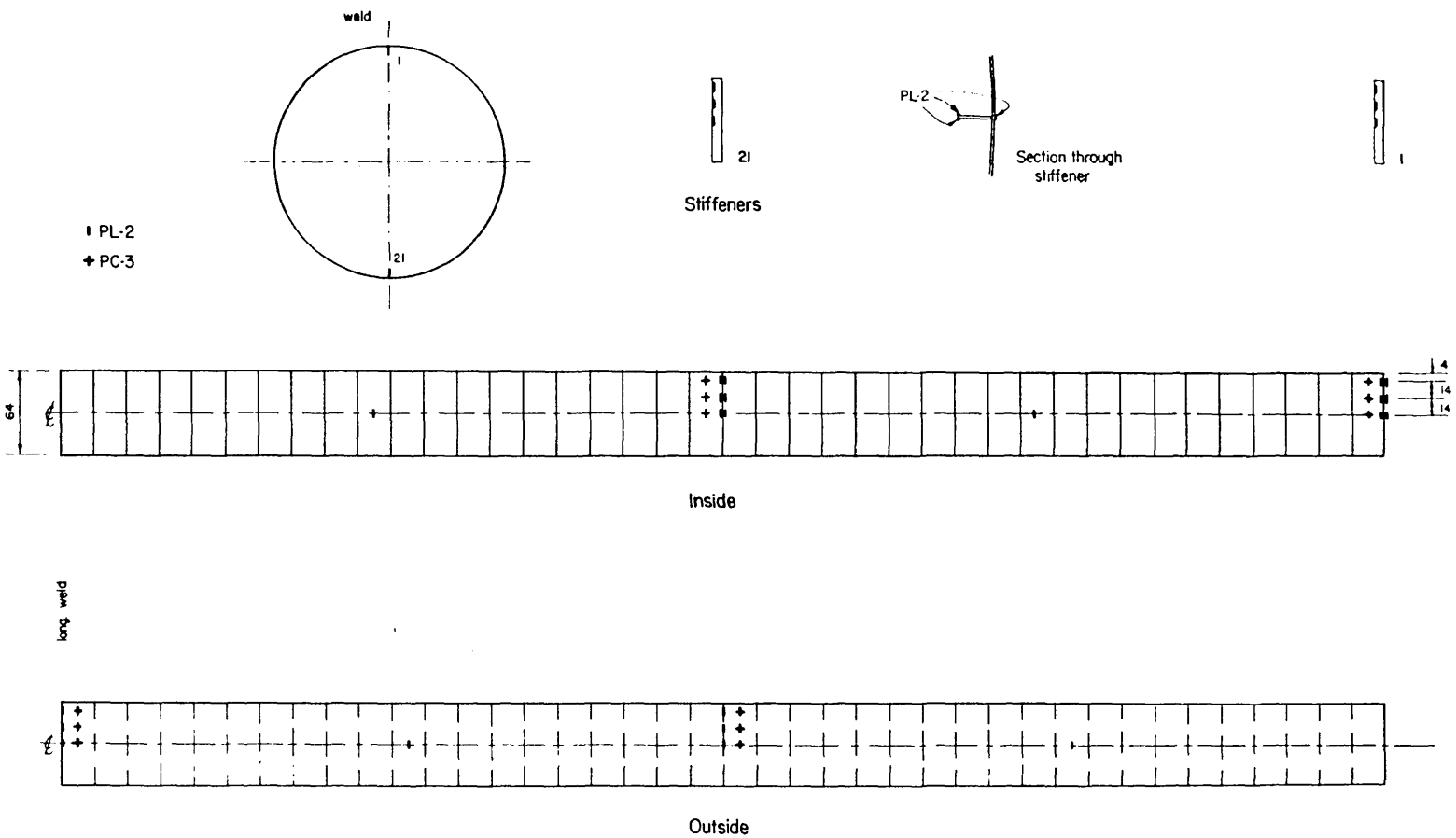


Fig. 2.85

CYLINDER 7 - STRAIN GAUGE LOCATIONS

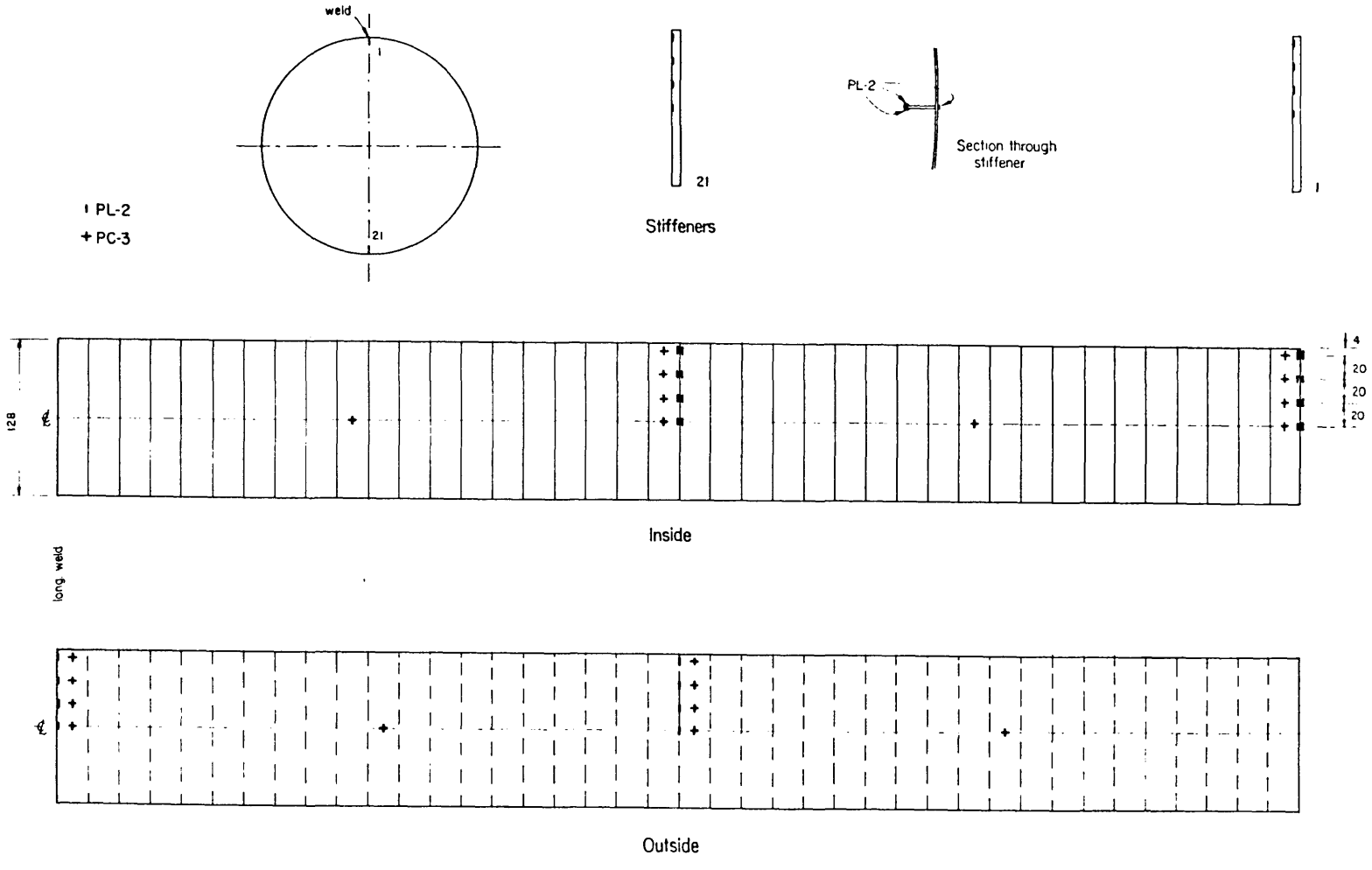


Fig. 2.86

CYLINDER IO - STRAIN GAUGE LOCATIONS

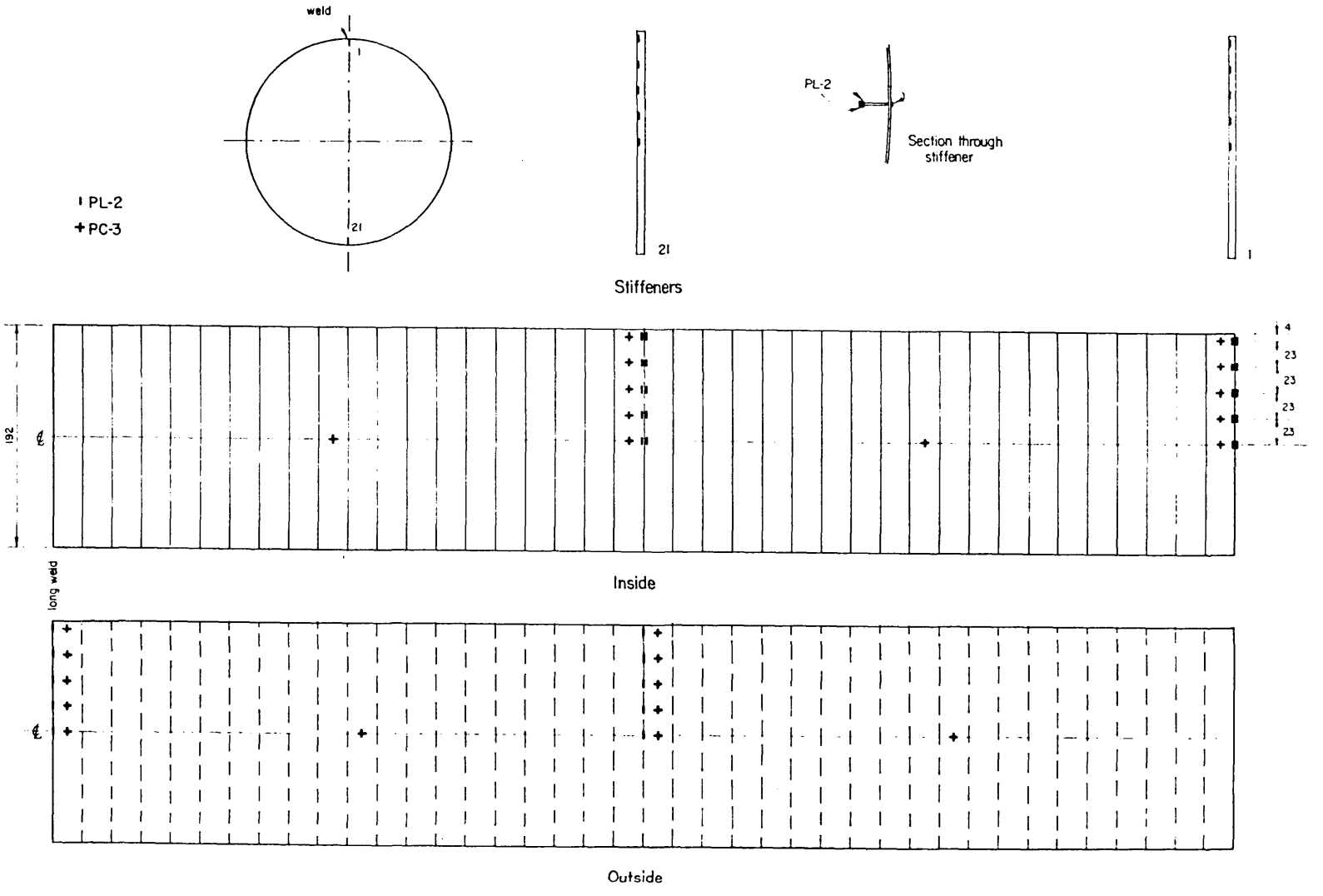


Fig. 2.87

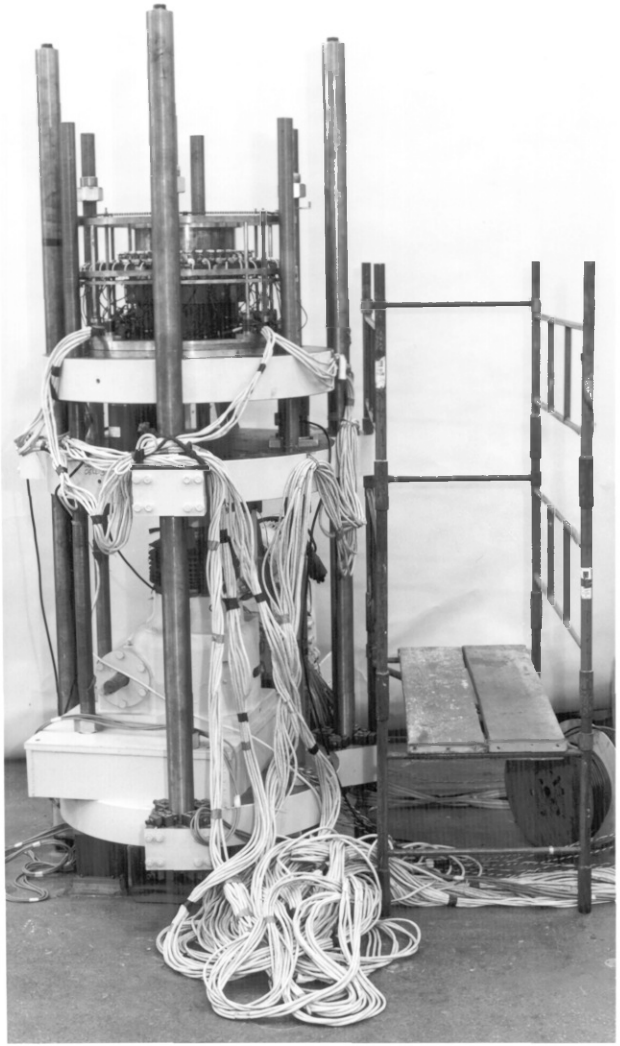


Fig. 2.89

TEST RIG

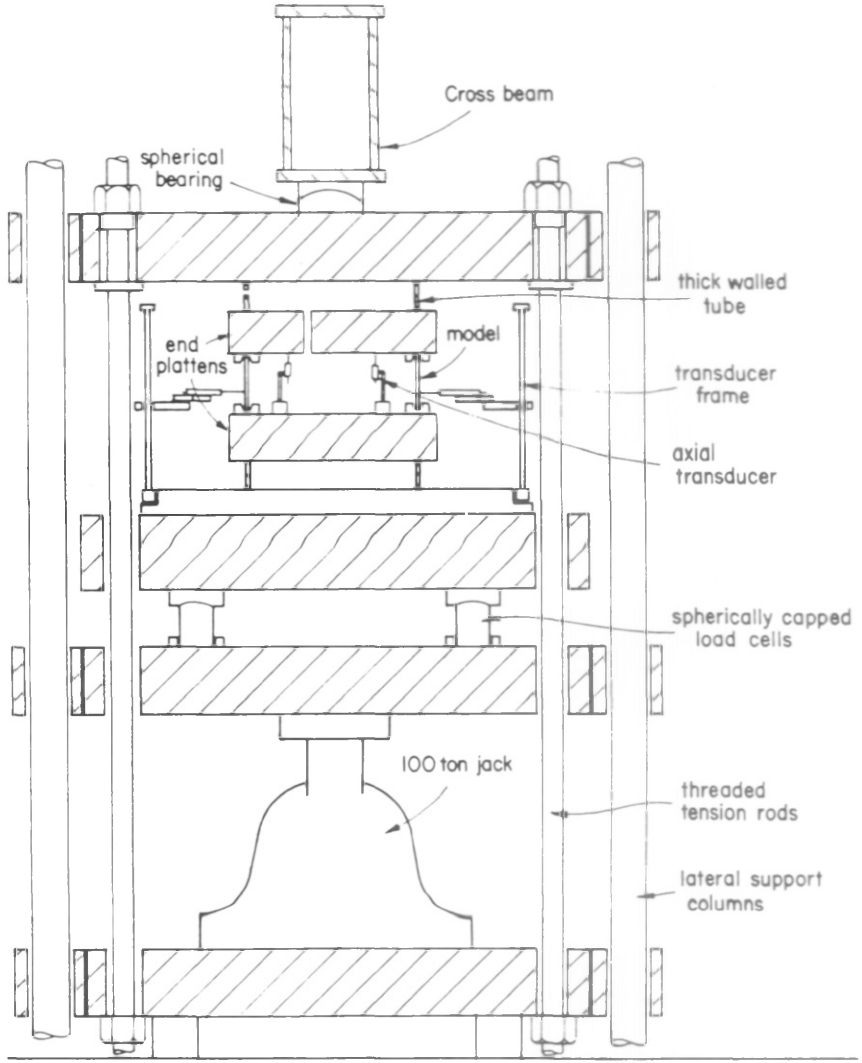


Fig. 2.88

TEST RIG - SCHEMATIC

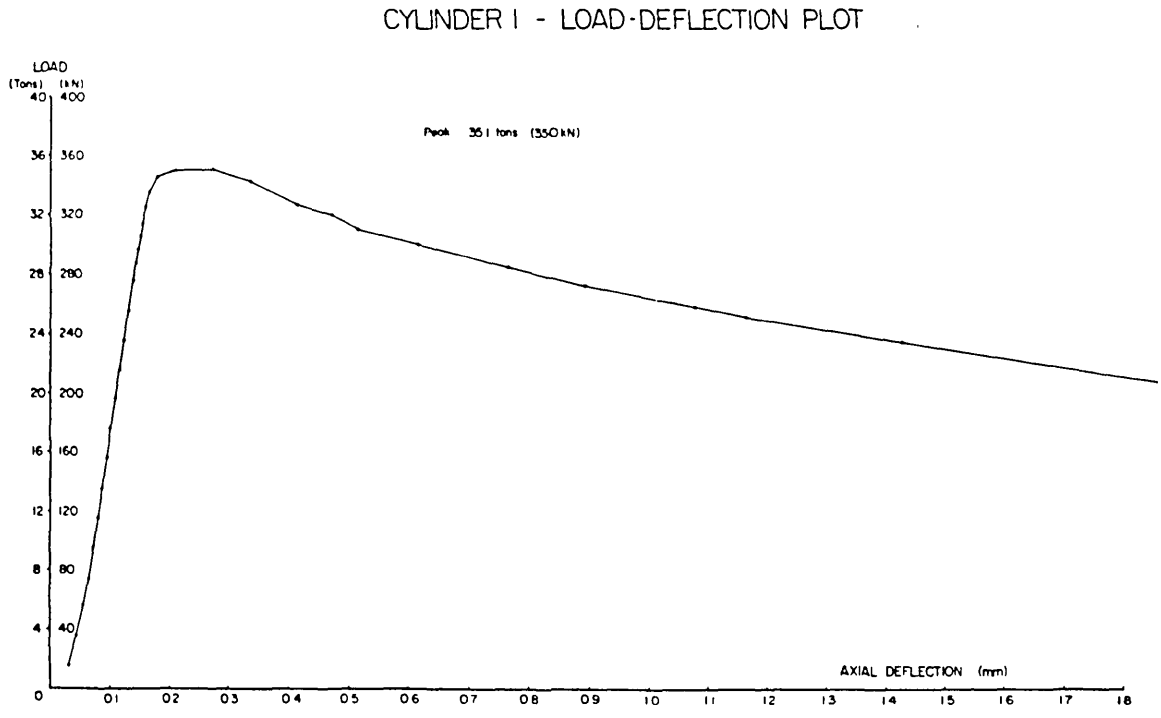

CYLINDER I - LOAD-DEFLECTION PLOT
LOAD
(Tons) (kN)
40 400
36 360
32 320
28 280
24 240
20 200
16 160
12 120
8 80
4 40
0
Peak 351 tons (3510 kN)
AXIAL DEFLECTION (mm)
01 02 03 04 05 06 07 08 09 10 11 12 13 14 15 16 17 18

Fig. 2.90

CYLINDER 7 - LOAD-DEFLECTION PLOT

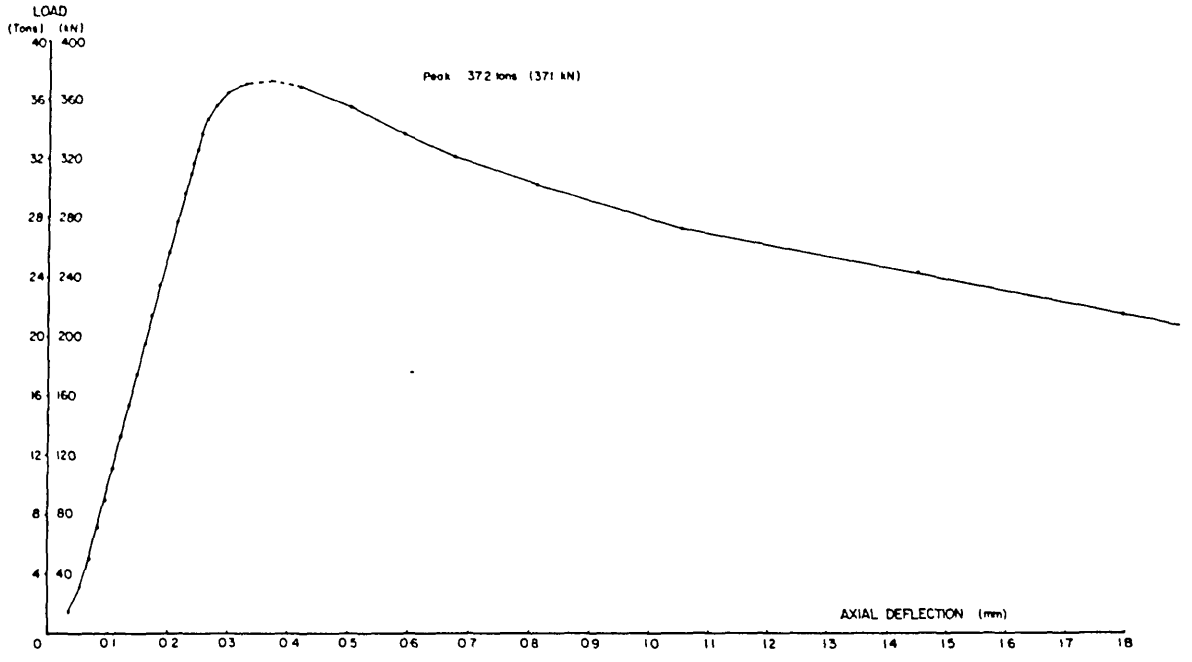


Fig. 2.91

CYLINDER 10 - LOAD DEFLECTION PLOT

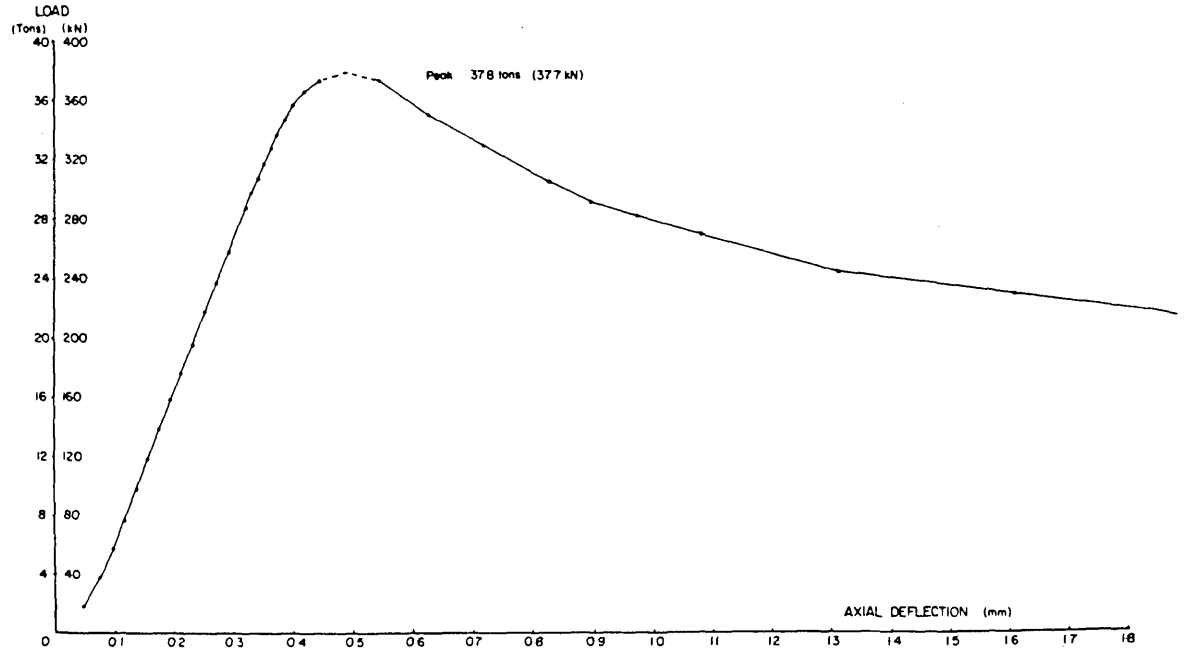


Fig. 2.92



CYLINDER I - BUCKLED SHAPE

Fig. 2.93



CYLINDER 7 - BUCKLED SHAPE

Fig. 2.94



CYLINDER 10 - BUCKLED SHAPE

Fig. 2.95



CYLINDER 10 - BUCKLED SHAPE

Fig. 2.96

VERTICAL LOCATION OF DEFLECTION READINGS

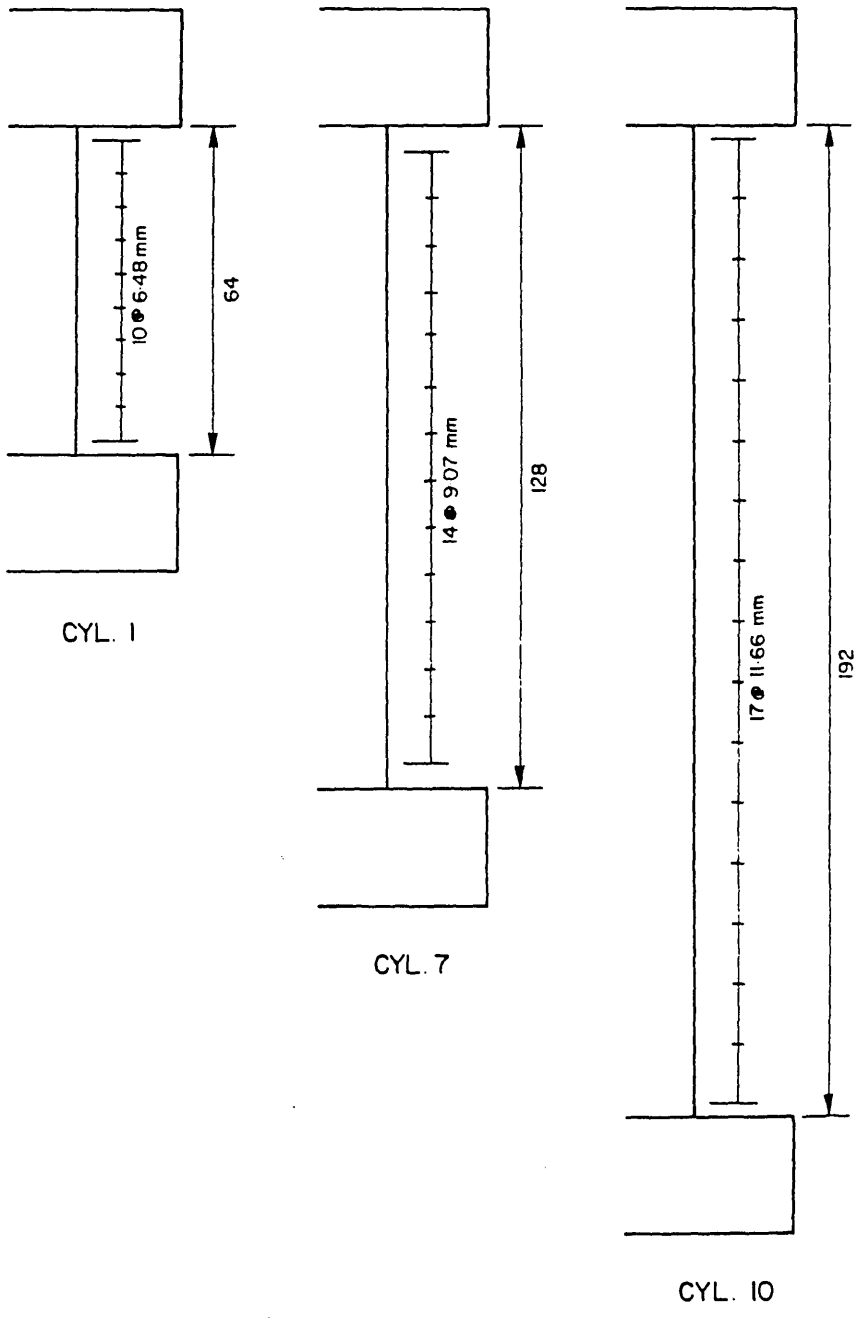
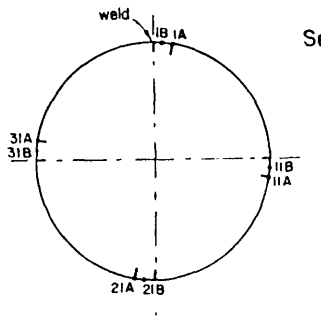
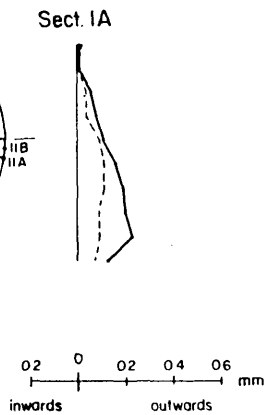


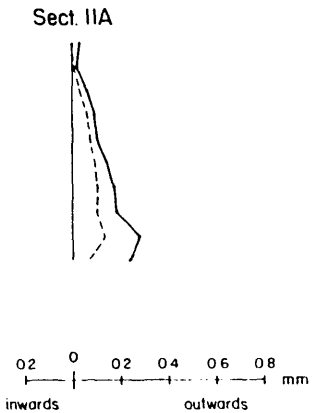
Fig. 2.97

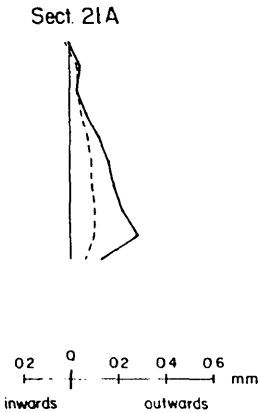
CYLINDER I – RADIAL DEFLECTIONS

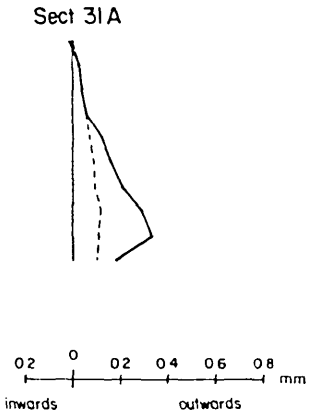
Vertical Sections

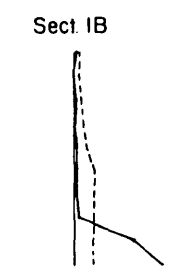


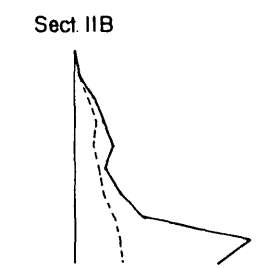


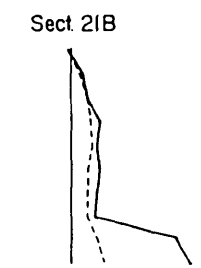












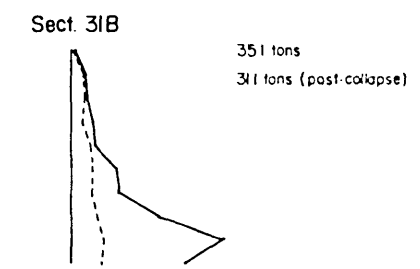


Fig. 2.98

CYLINDER I – RADIAL DEFLECTIONS

Circumferential Sections

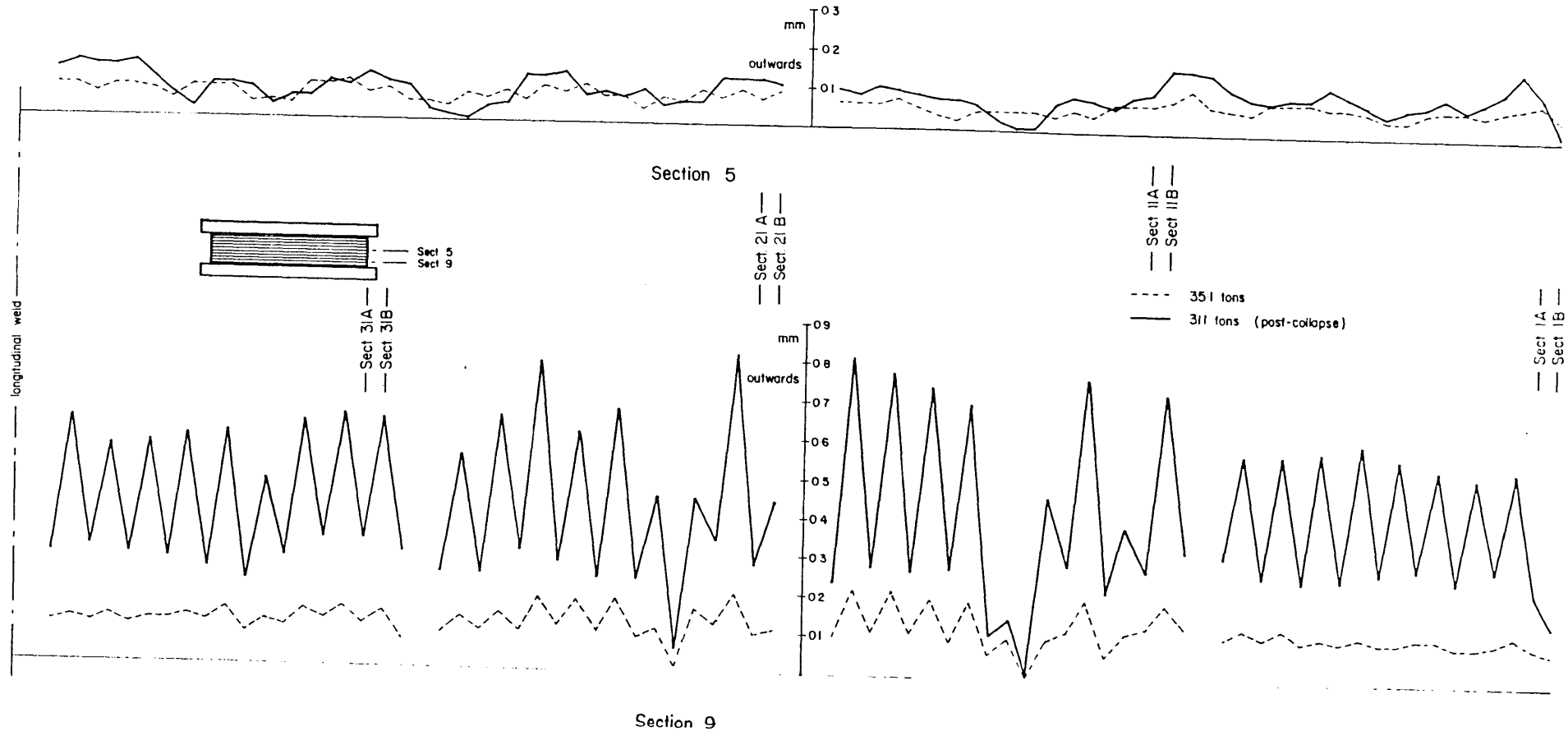


Fig. 2.99

CYLINDER 7 - RADIAL DEFLECTIONS

Vertical Sections

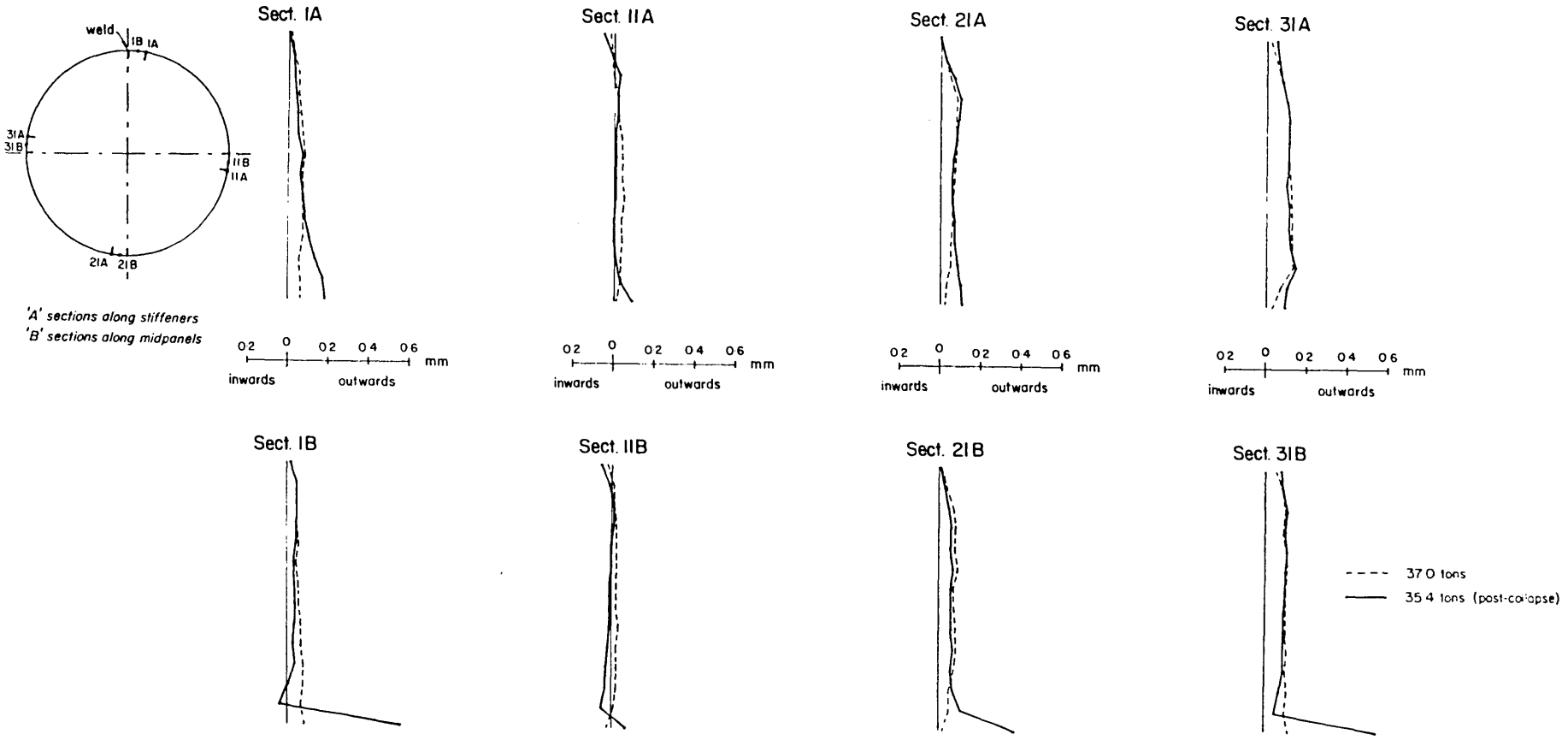


Fig. 2.100

CYLINDER 7 – RADIAL DEFLECTIONS

Circumferential Sections

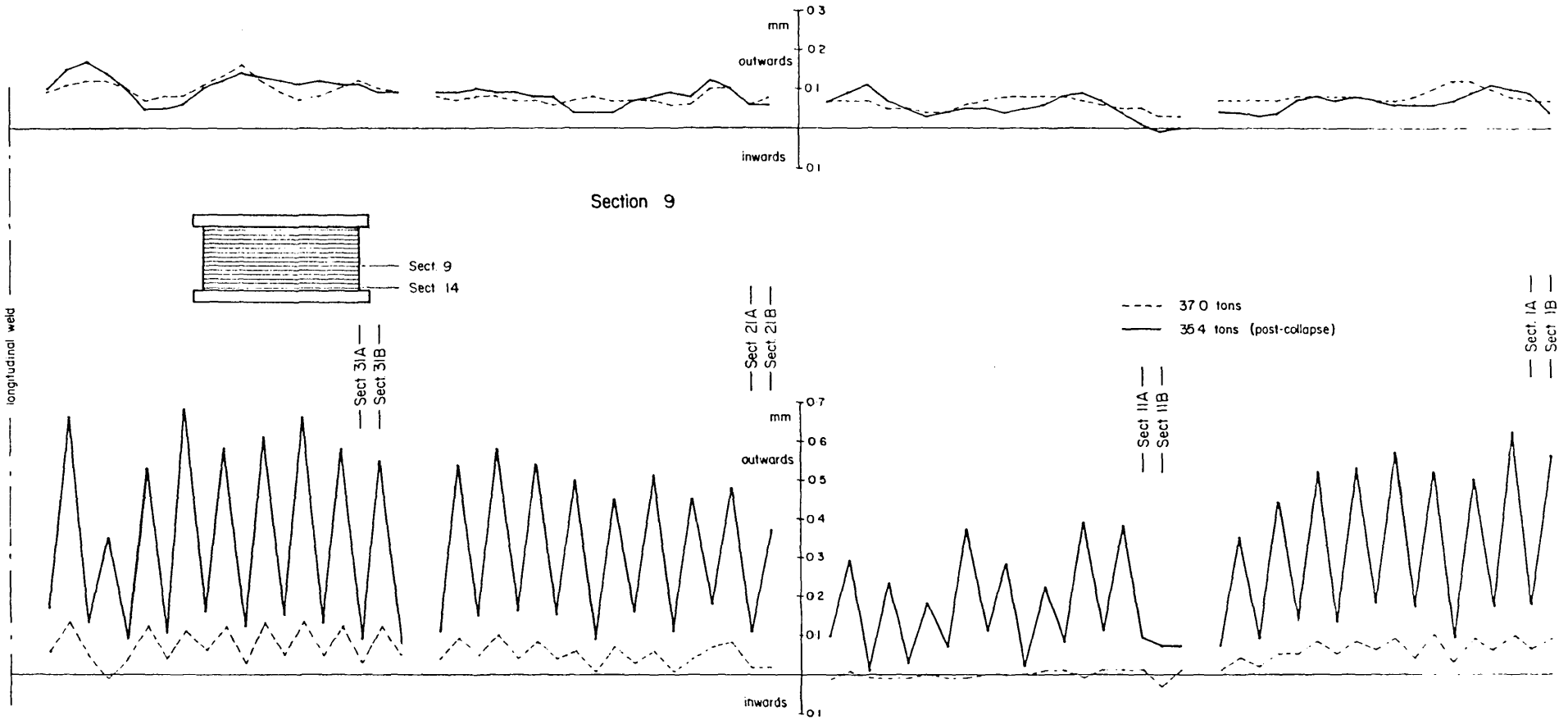


Fig. 2.101

CYLINDER 10 - RADIAL DEFLECTIONS

Vertical Sections

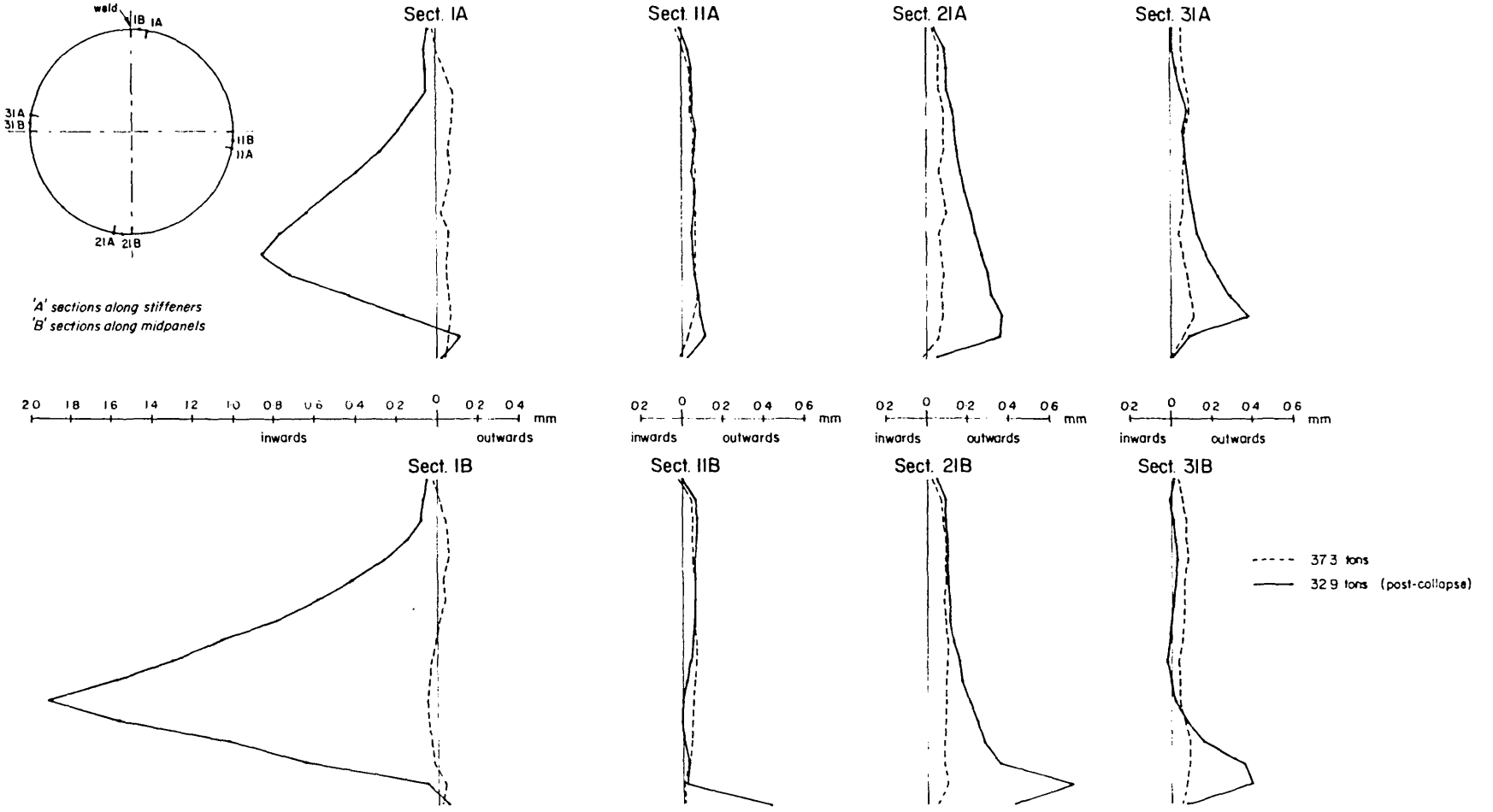


Fig. 2.102

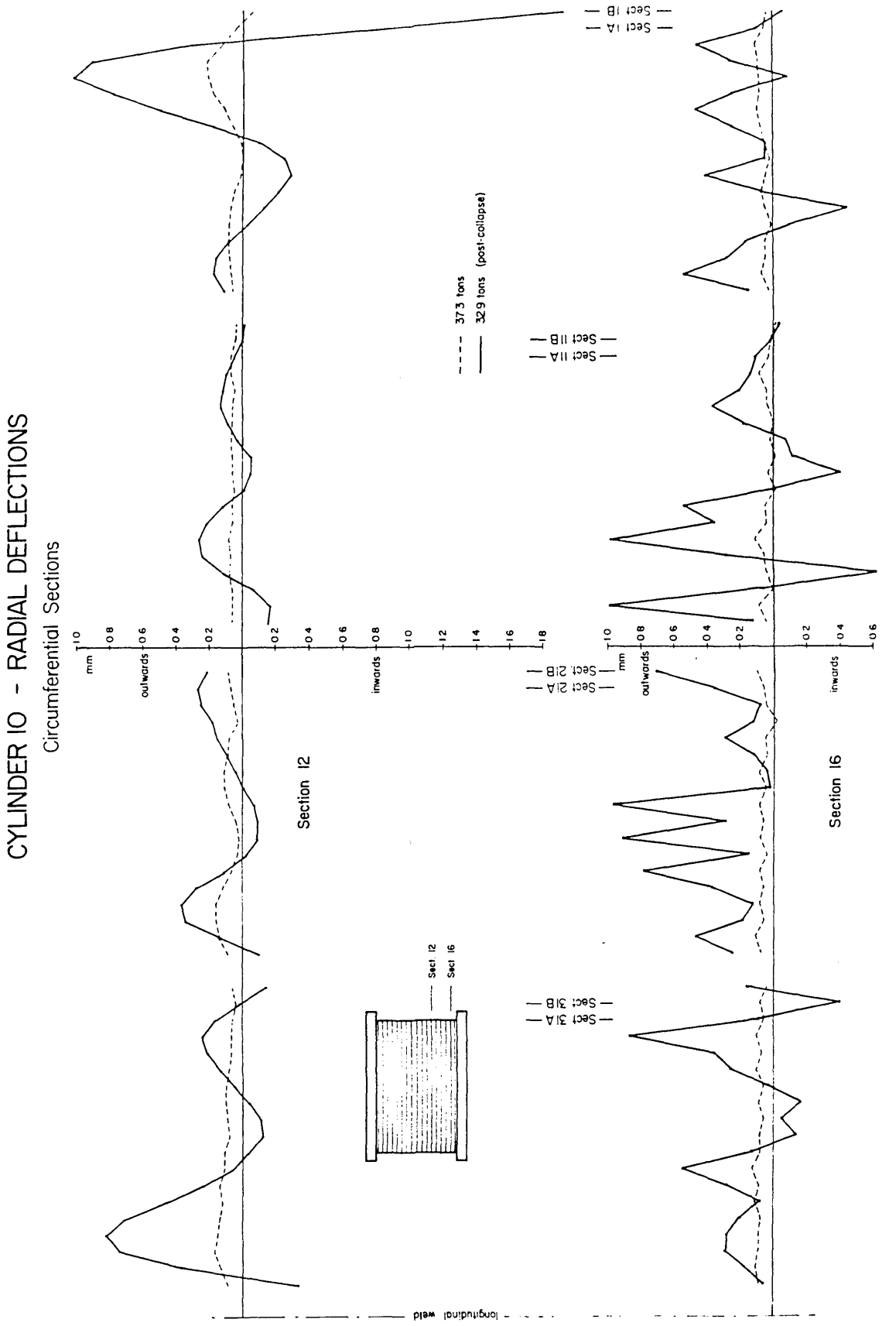

CYLINDER IO - RADIAL DEFLECTIONS
Circumferential Sections
373 tons
329 tons (post-collapse)
Sect IA
Sect IB
Sect IIA
Sect IIB
Sect 2IA
Sect 2IB
Sect 3IA
Sect 3IB
Section I2
Section I6
mm
outwards
inwards
longitudinal weld
Sect I2
Sect I6

Fig. 2.103

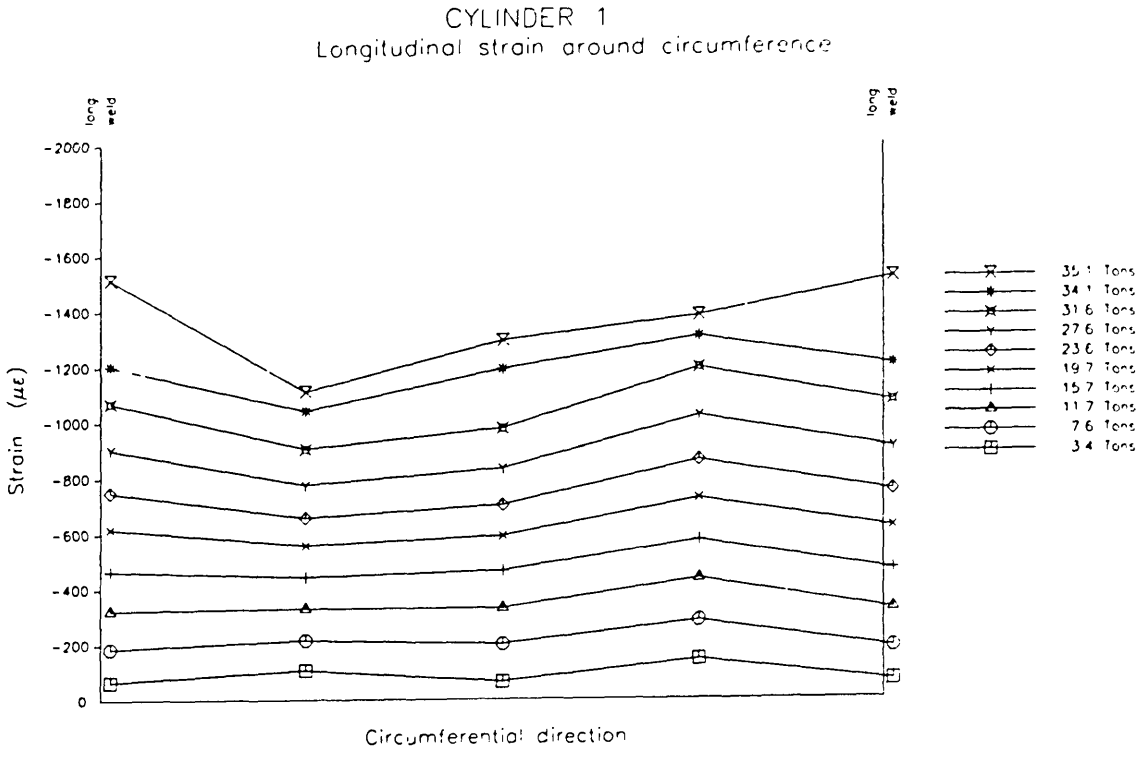

CYLINDER 1
Longitudinal strain around circumference
long weld
long weld
-2000
-1800
-1600
-1400
-1200
-1000
-800
-600
-400
-200
0
Strain (με)
Circumferential direction
35 1 Tons
34 1 Tons
31 6 Tons
27 6 Tons
23 6 Tons
19 7 Tons
15 7 Tons
11 7 Tons
7 6 Tons
3 4 Tons

Fig. 2.104

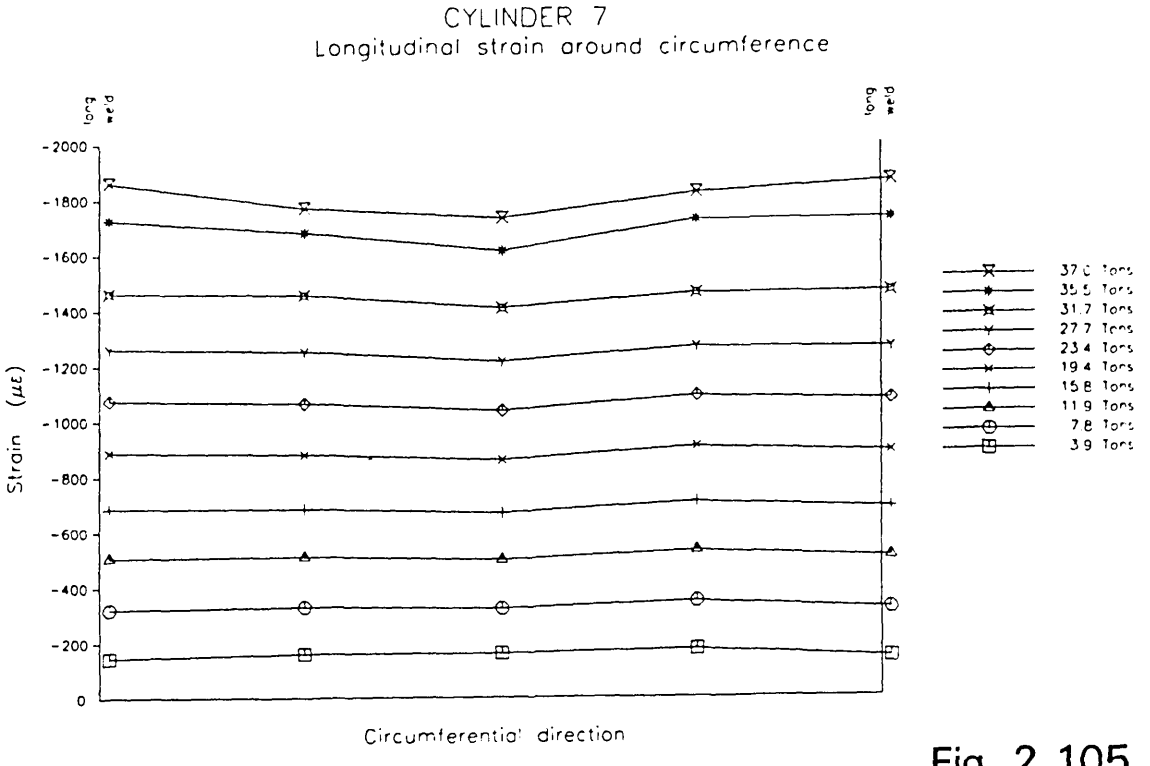


Fig. 2.105

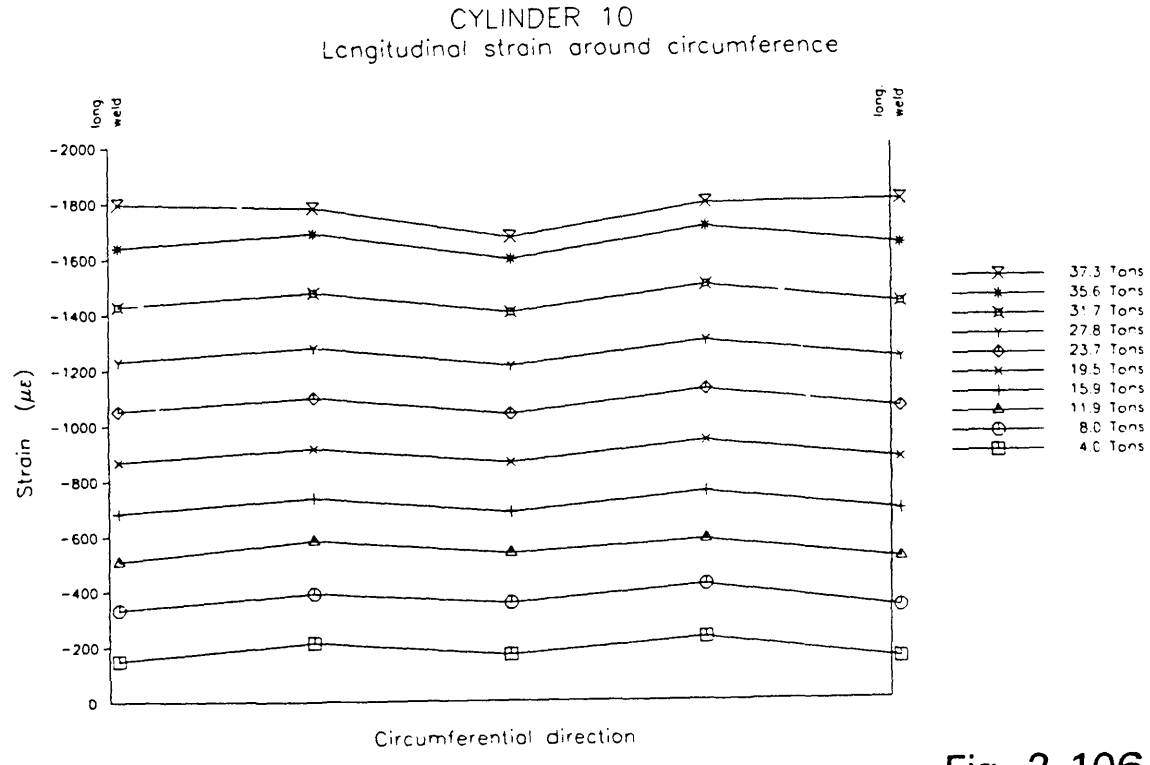


Fig. 2.106

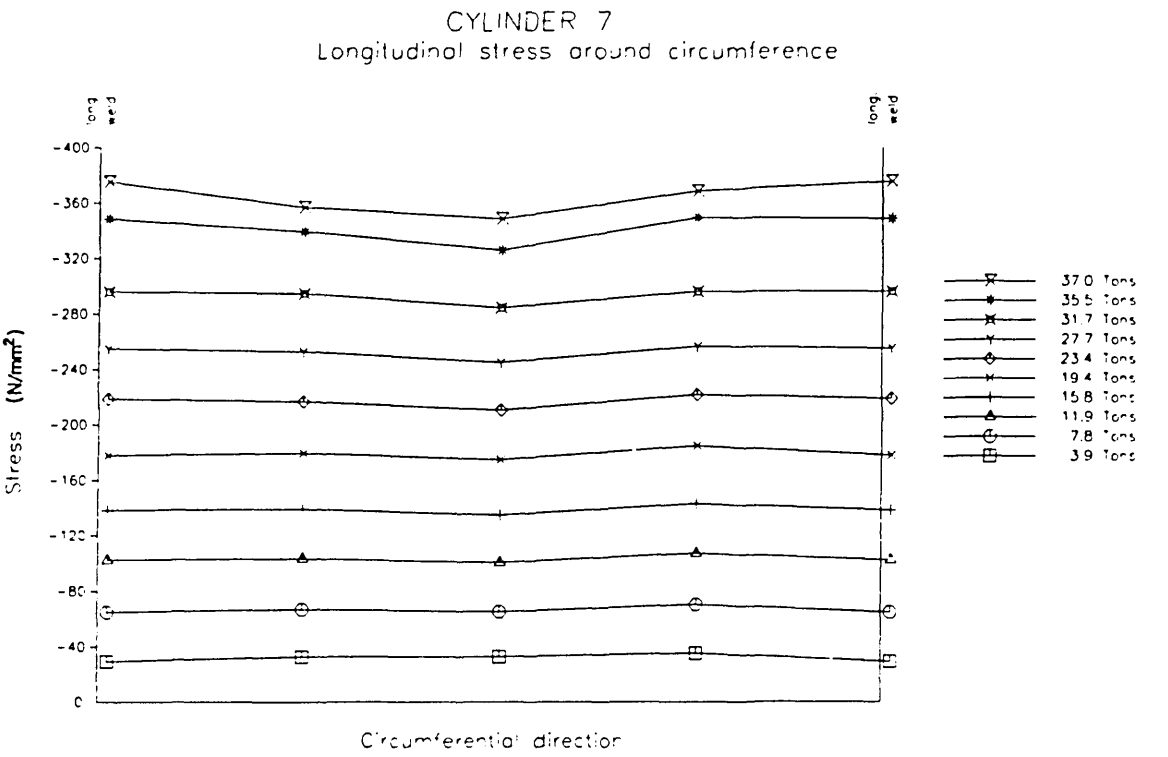


Fig. 2.107

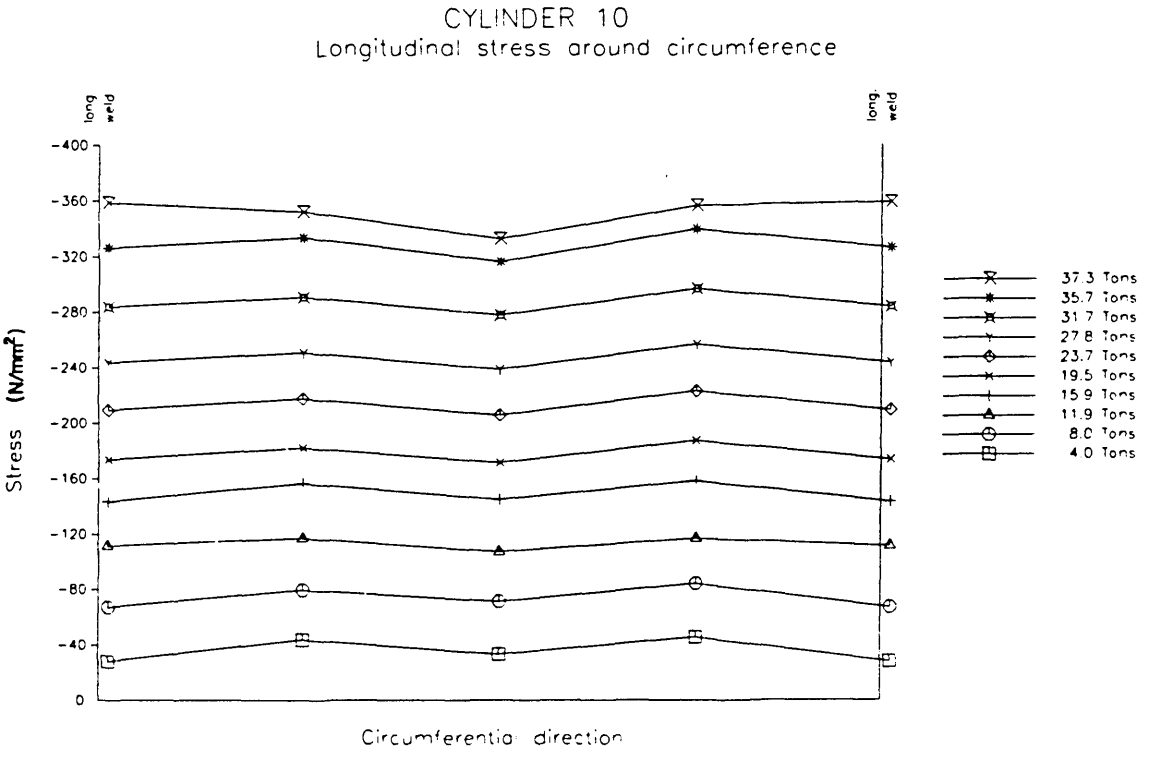


Fig. 2.108

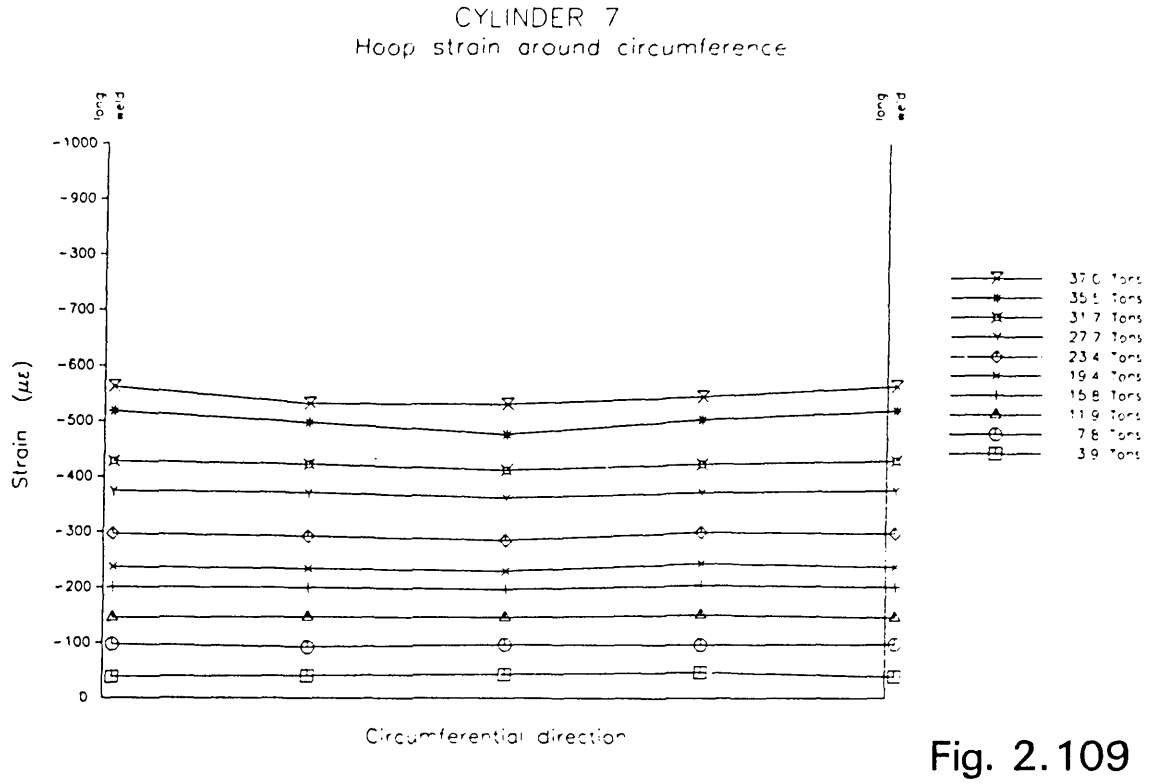


Fig. 2.109

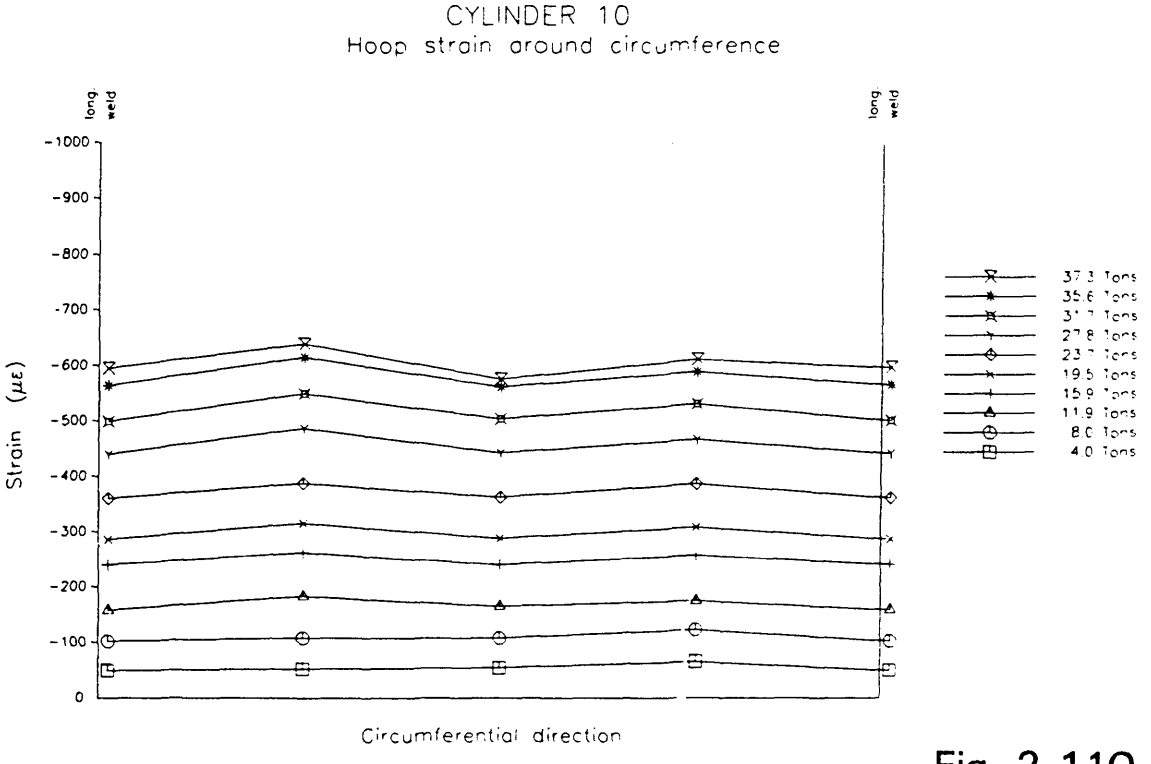


Fig. 2.110

CYLINDER 7
Longitudinal strain down length

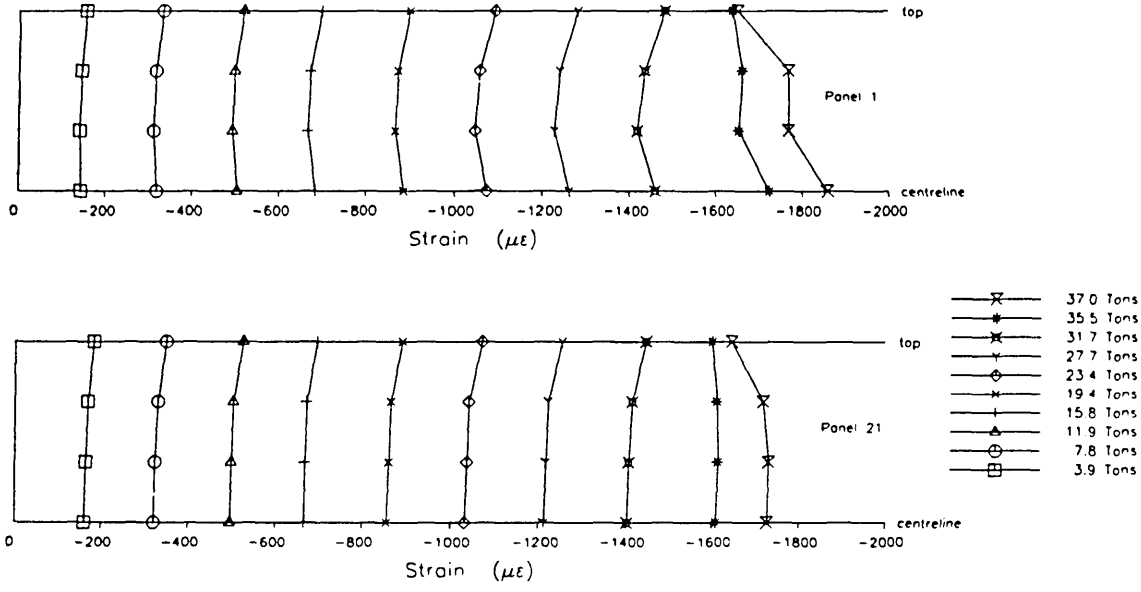


Fig. 2.111

CYLINDER 10
Longitudinal strain down length

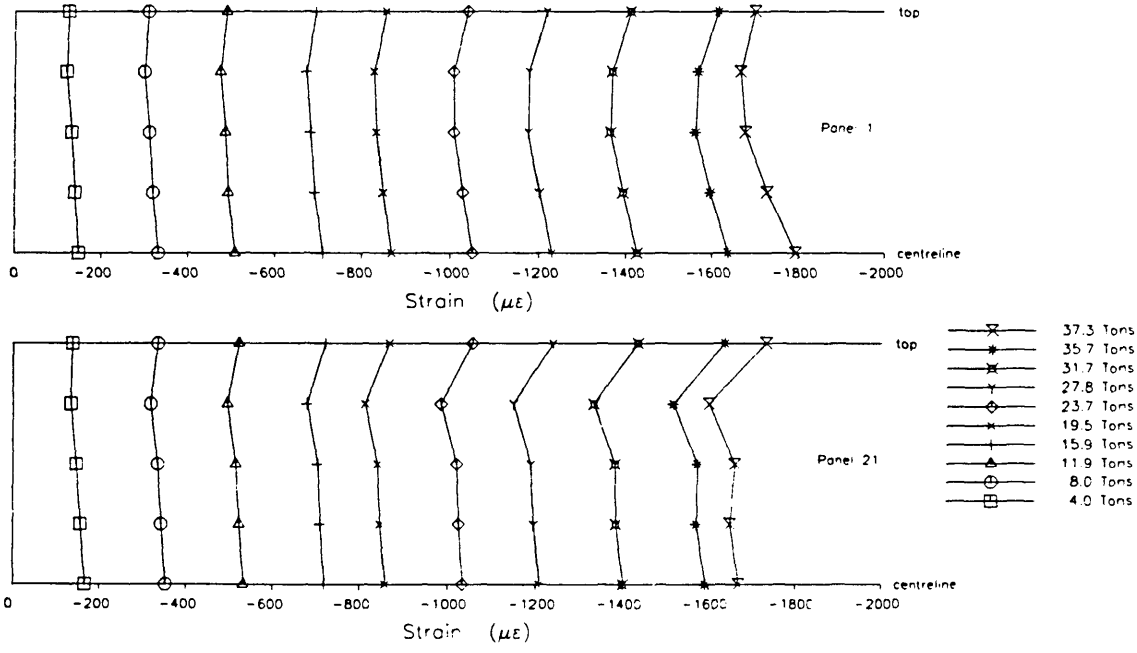


Fig. 2.112

CYLINDER 7
Longitudinal stress down length

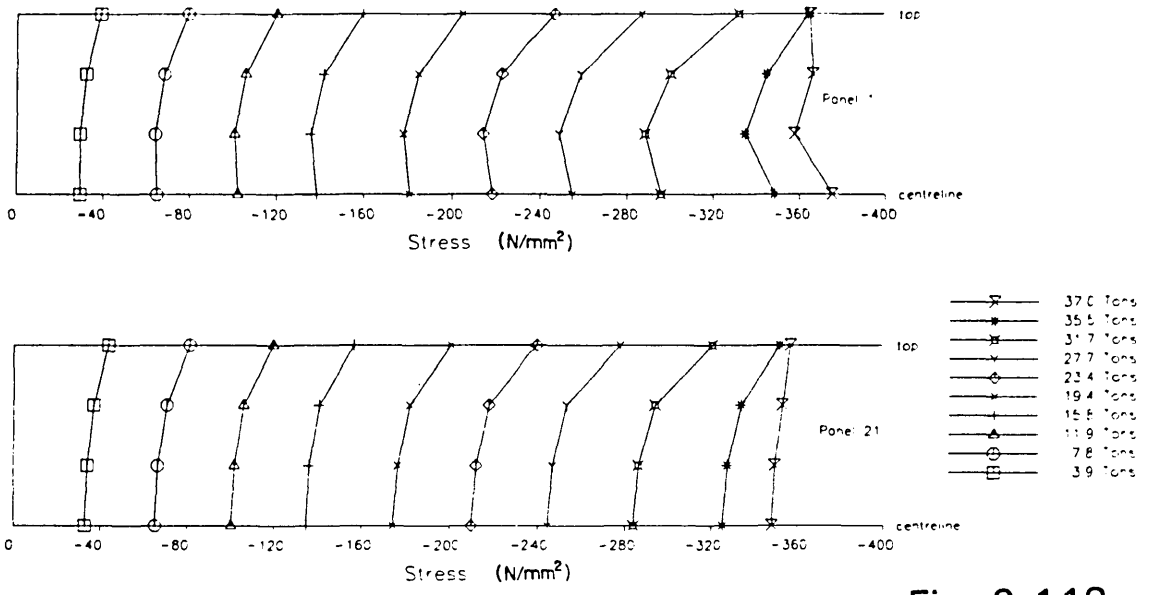


Fig. 2.113

CYLINDER 10
Longitudinal stress down length

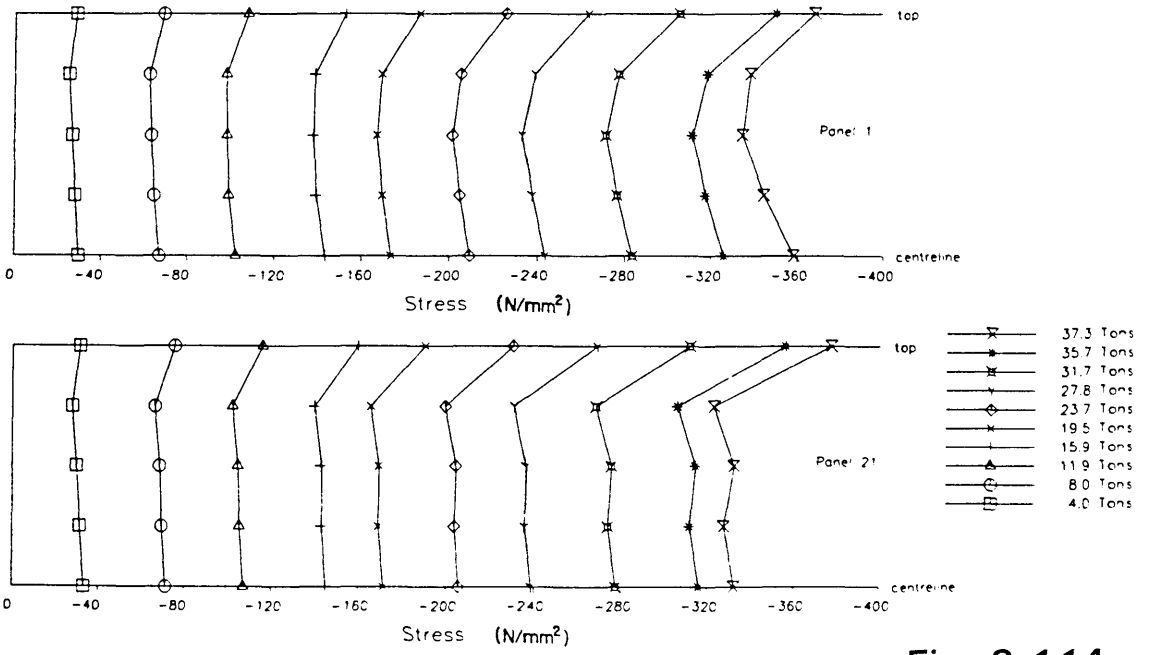


Fig. 2.114

CYLINDER 7

Hoop strain down length

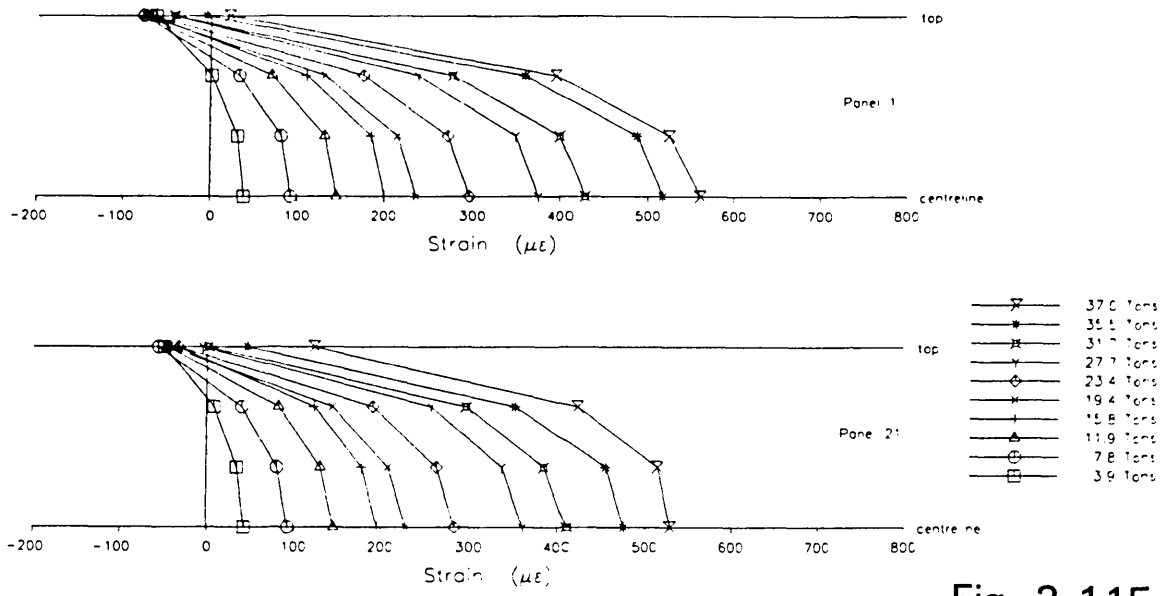


Fig. 2.115

CYLINDER 10

Hoop strain down length

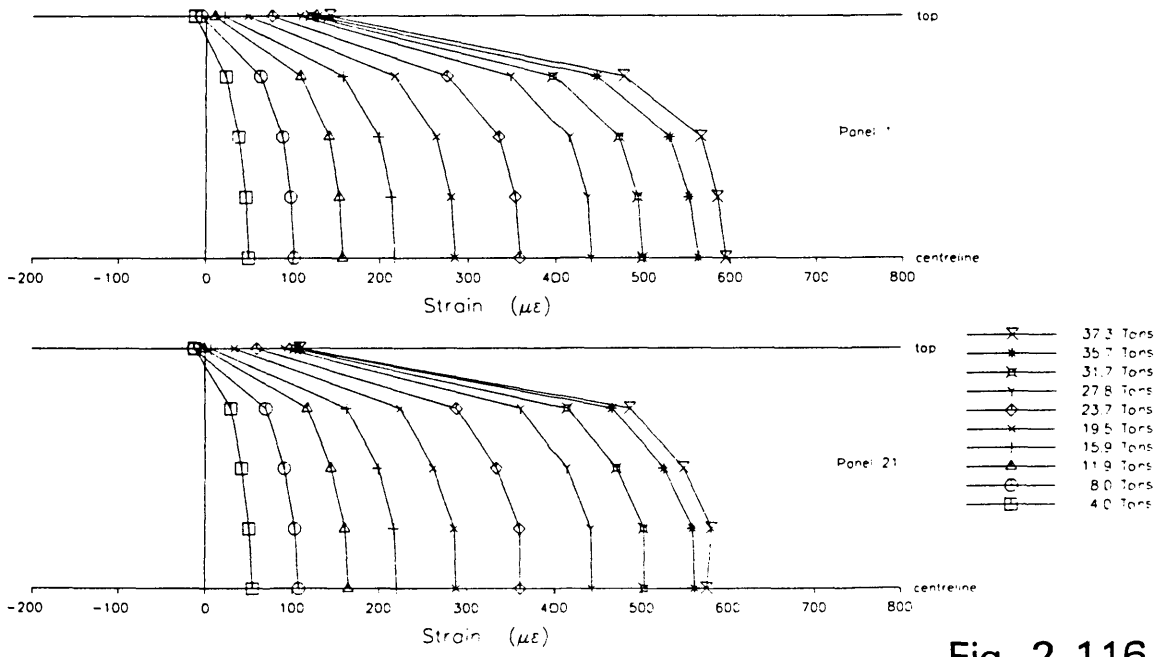


Fig. 2.116

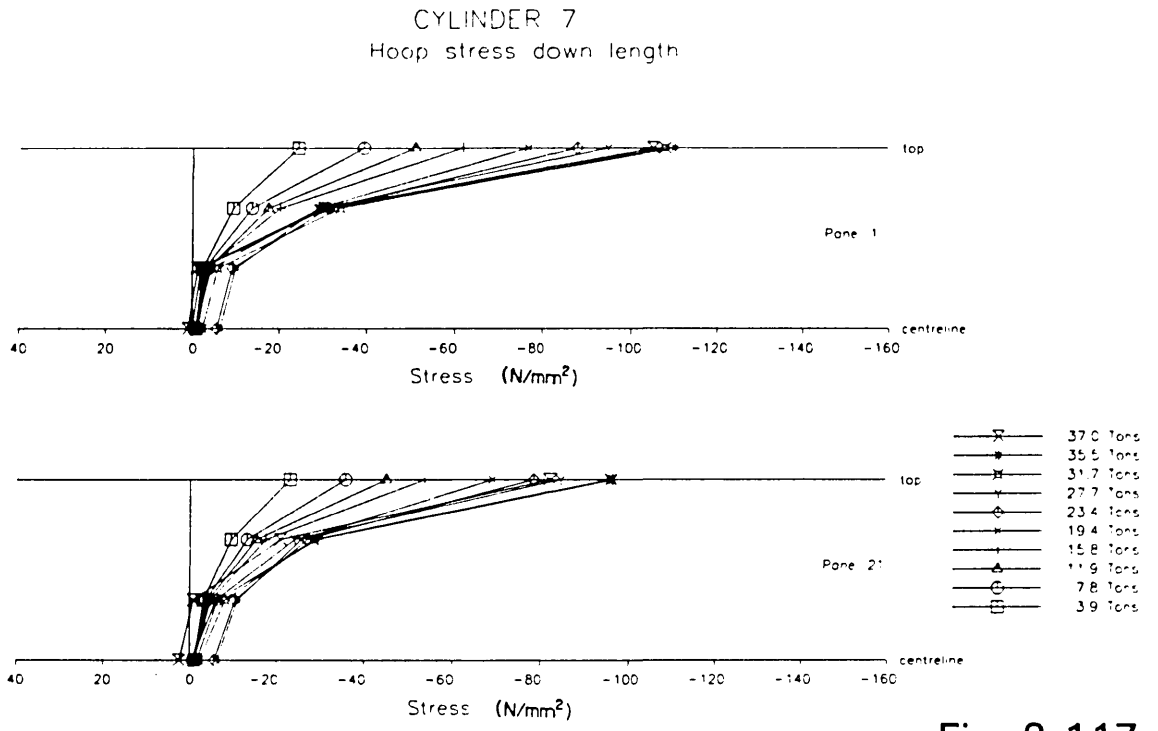


Fig. 2.117

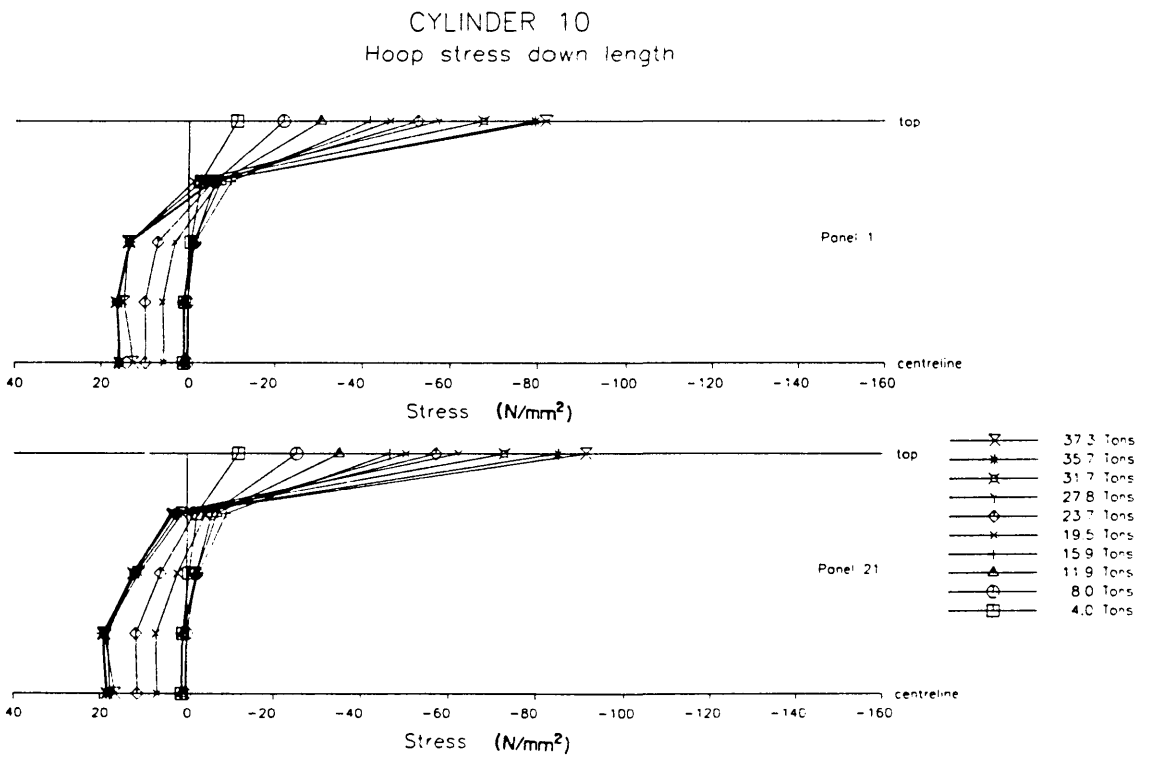


Fig. 2.118

CYLINDER 1
Longitudinal strain in stiffeners

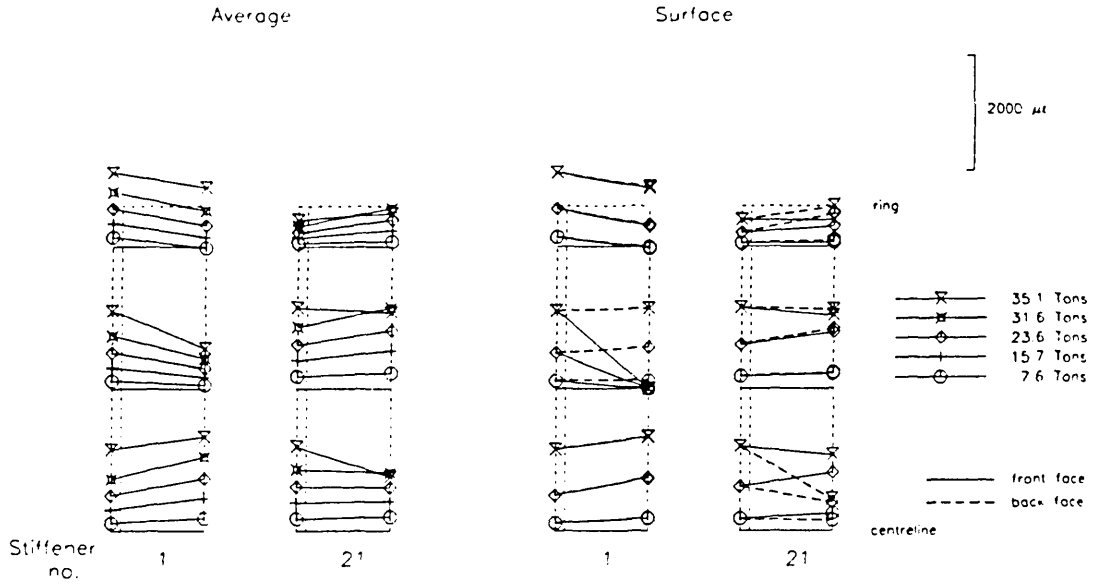


Fig. 2.119

CYLINDER 7
Longitudinal strain in stiffeners

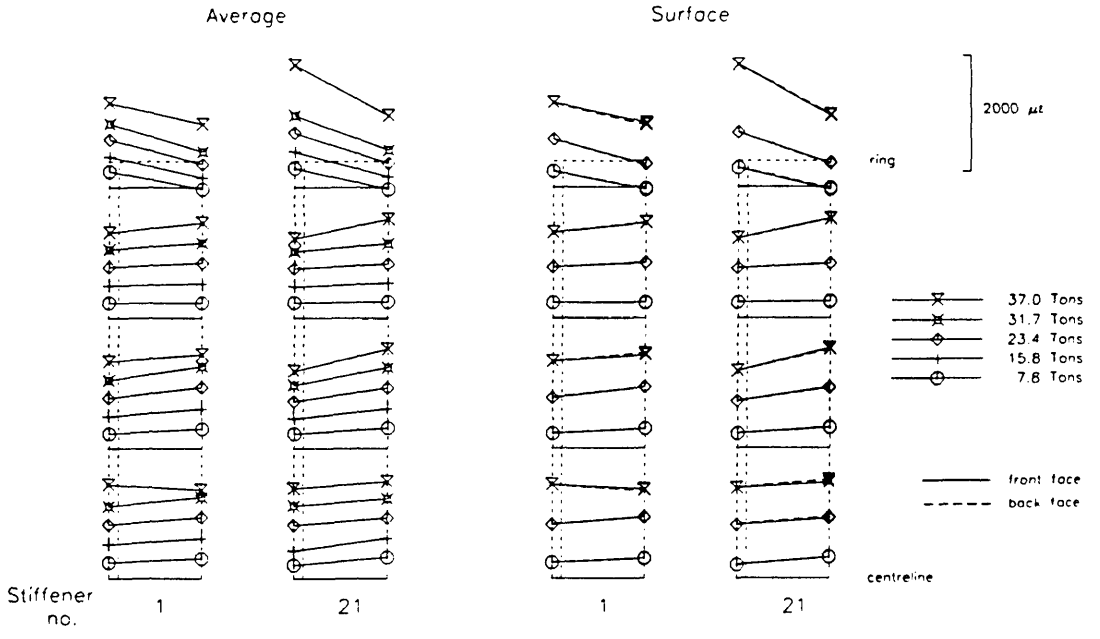


Fig. 2.120

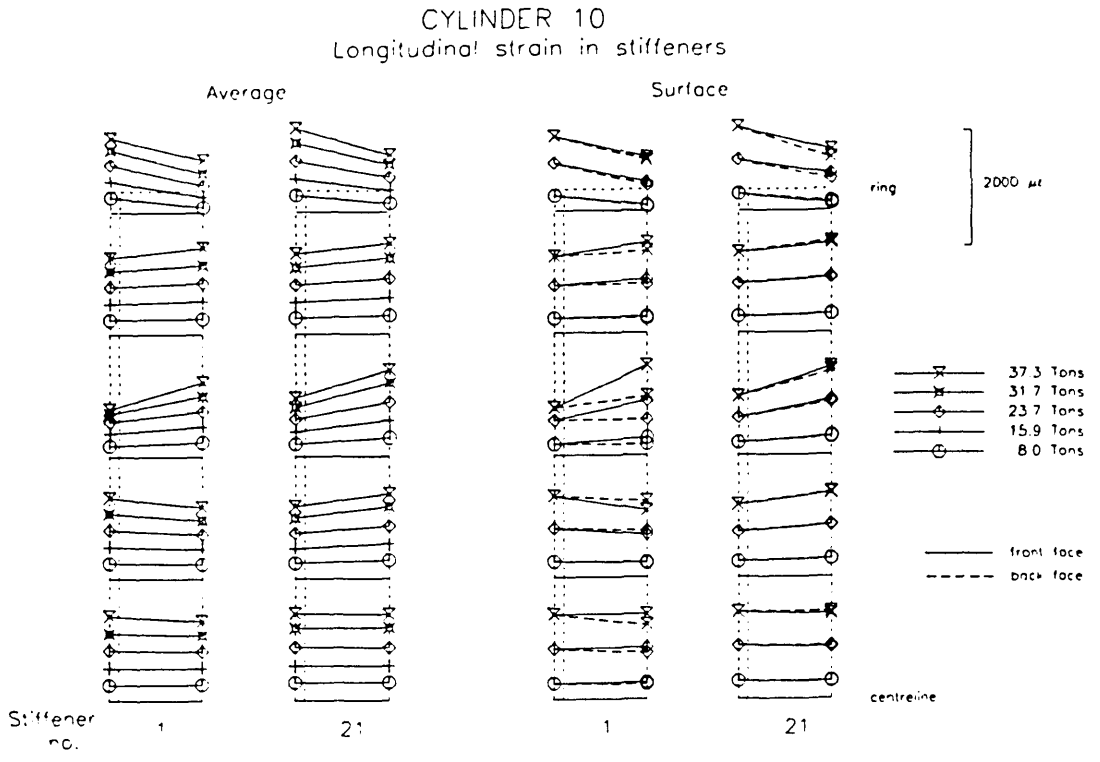

CYLINDER 10
Longitudinal strain in stiffeners
Average
Surface
ring
2000 με
37.3 Tons
31.7 Tons
23.7 Tons
15.9 Tons
8.0 Tons
front face
back face
centreline
Stiffener no.
1
21
1
21

Fig. 2.121

CYLINDER A – INITIAL IMPERFECTIONS

Projection of imperfection surface

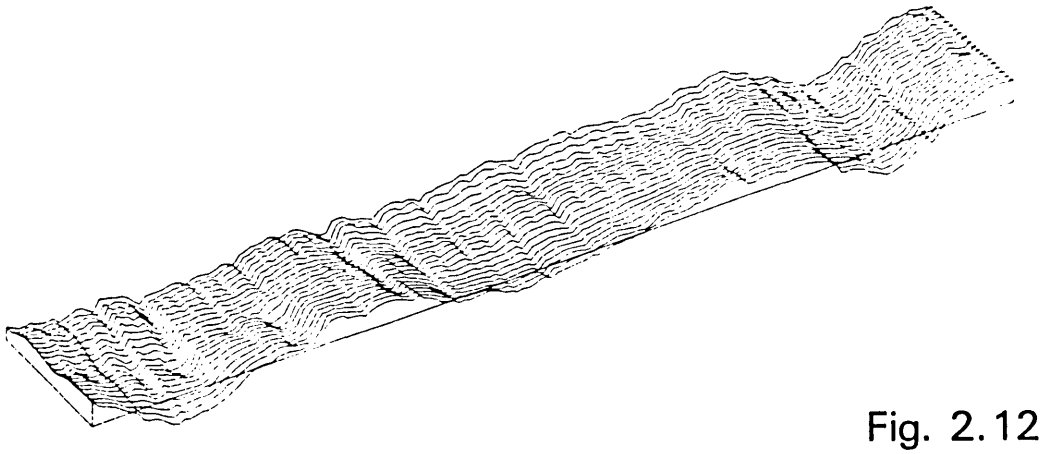


Fig. 2.122

CYLINDER B – INITIAL IMPERFECTIONS

Projection of imperfection surface

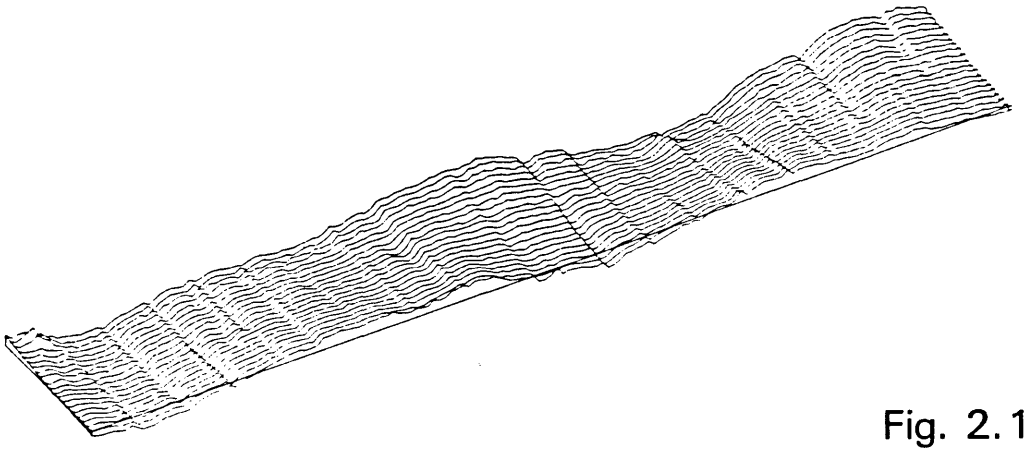


Fig. 2.123

CYLINDER C – INITIAL IMPERFECTIONS

Projection of imperfection surface

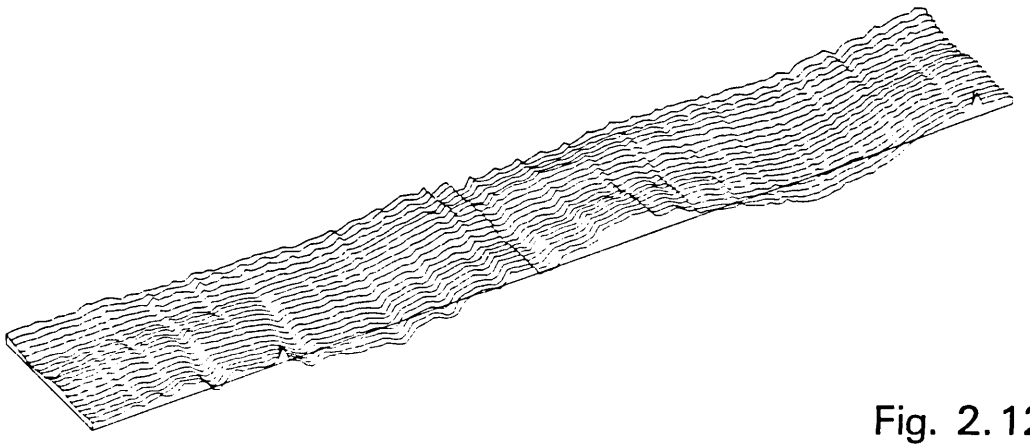


Fig. 2.124

CYLINDER E – INITIAL IMPERFECTIONS

Projection of imperfection surface

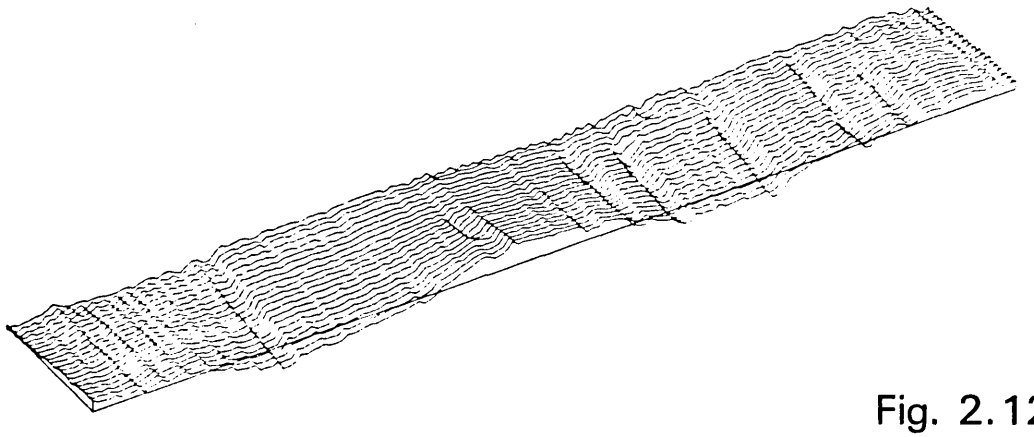


Fig. 2.125

CYLINDER F – INITIAL IMPERFECTIONS

Projection of imperfection surface

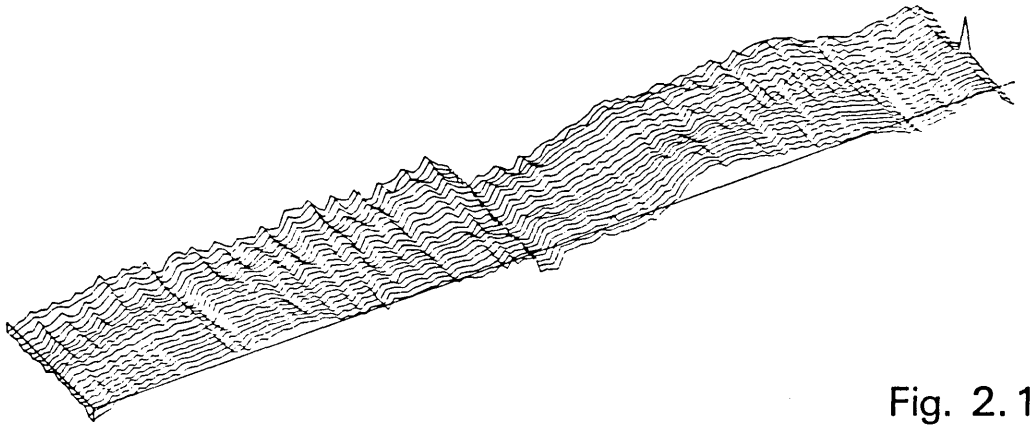


Fig. 2.126

CYLINDER G – INITIAL IMPERFECTIONS

Projection of imperfection surface

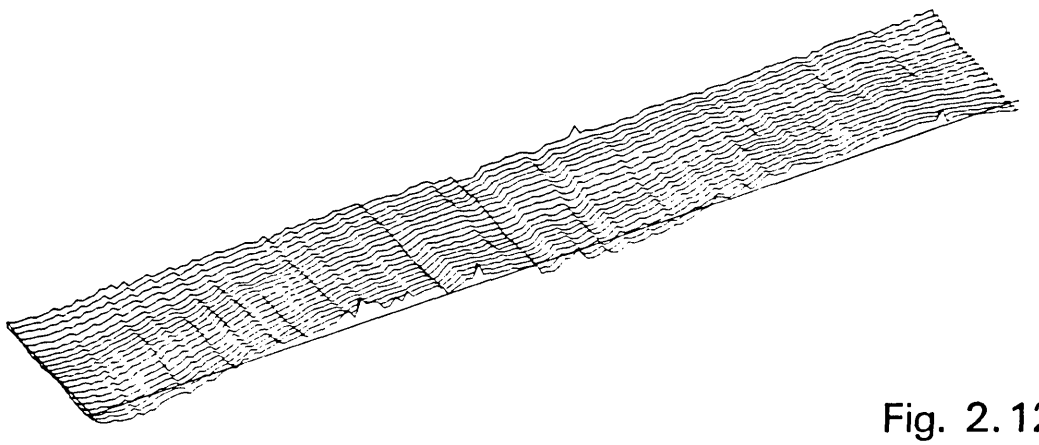


Fig. 2.127

CYLINDER E - LOAD-DEFLECTION PLOT

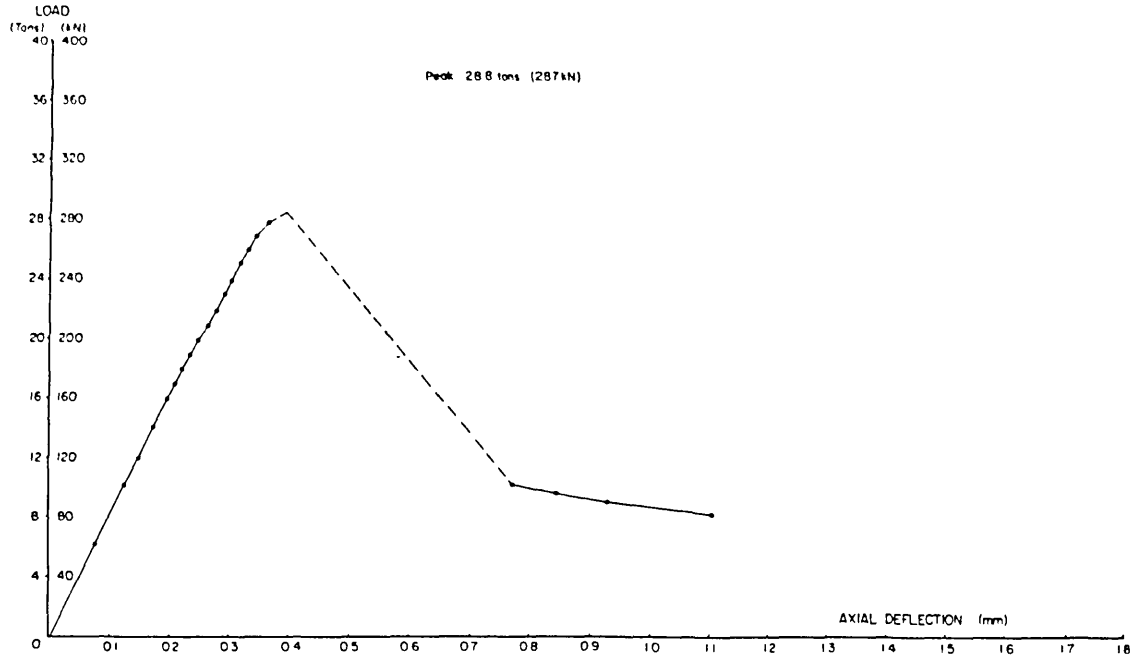


Fig. 2.128

CYLINDER A - LOAD-DEFLECTION PLOT

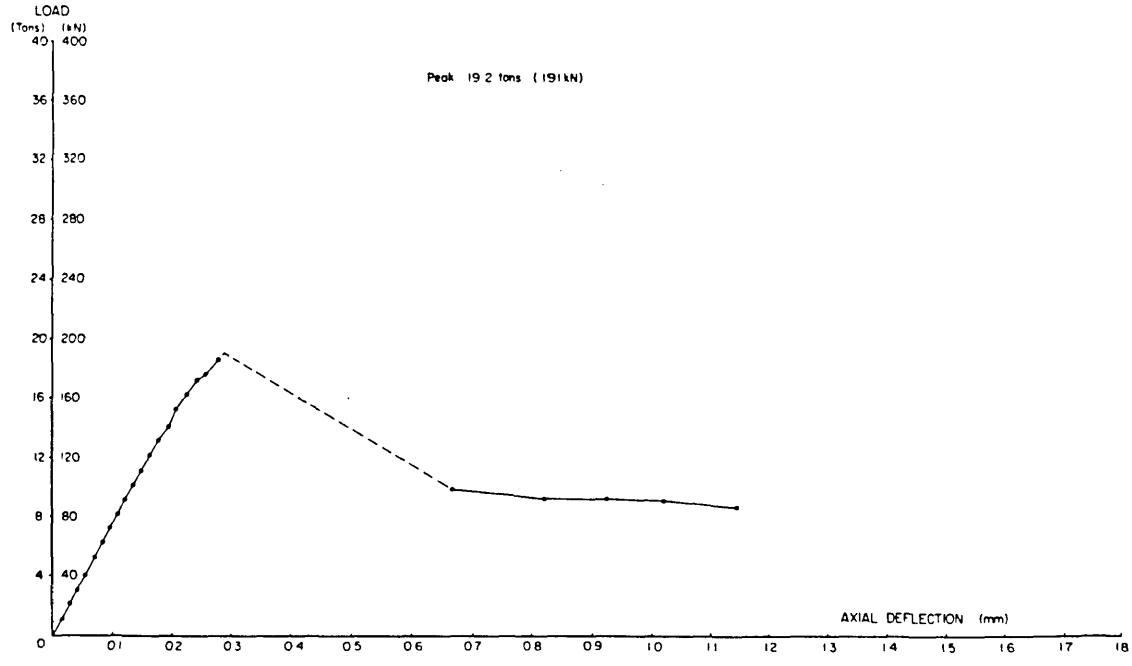
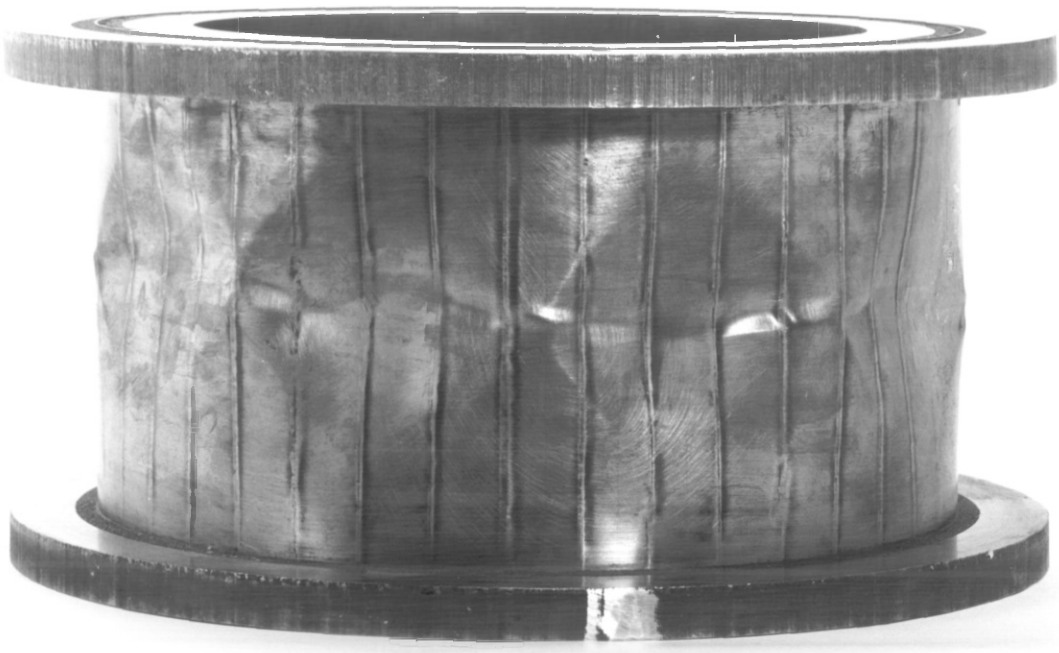


Fig. 2.129



CYLINDER A

Fig. 2.130



CYLINDER E

Fig. 2.131

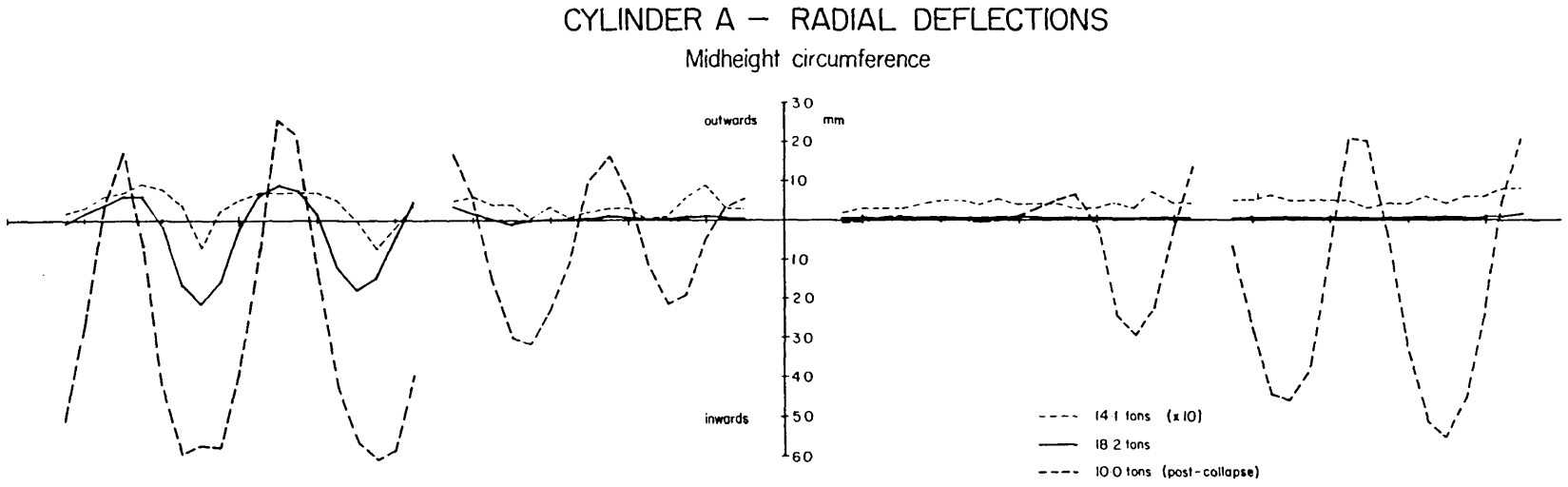


Fig. 2.132

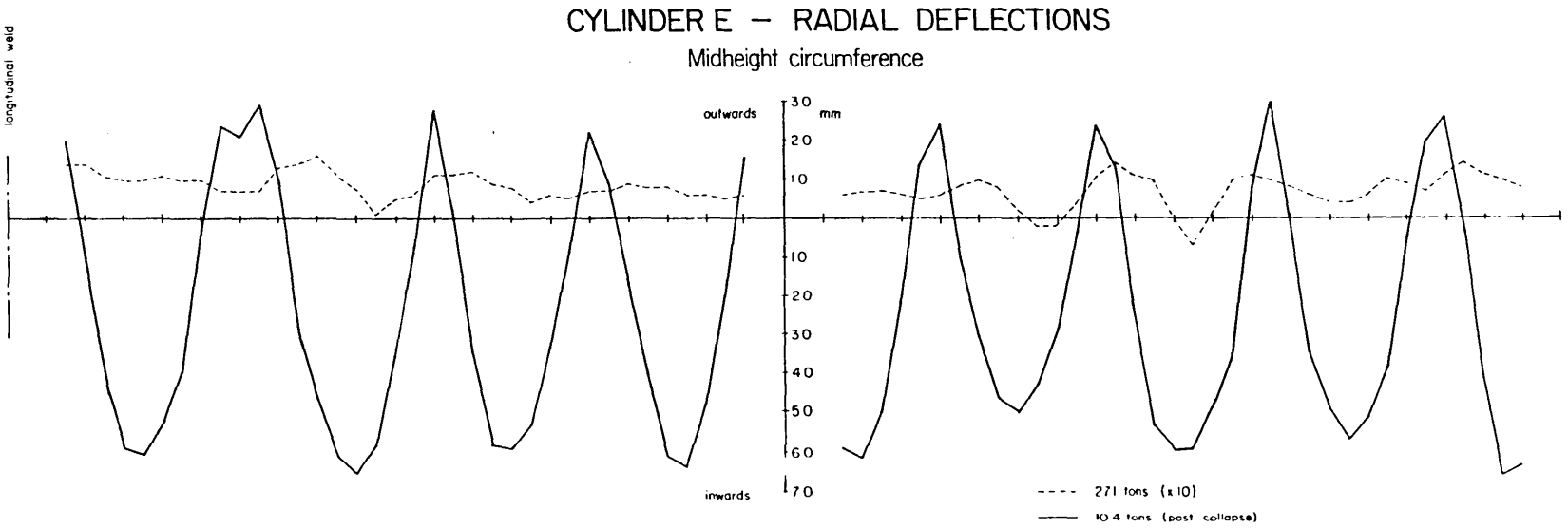
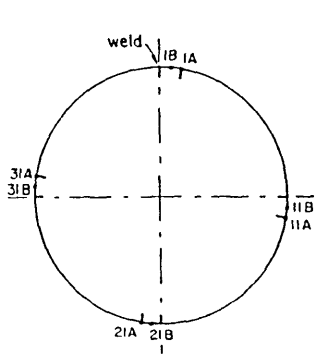


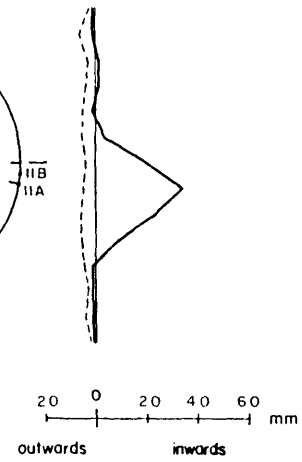
Fig. 2.133

CYLINDER A - RADIAL DEFLECTIONS

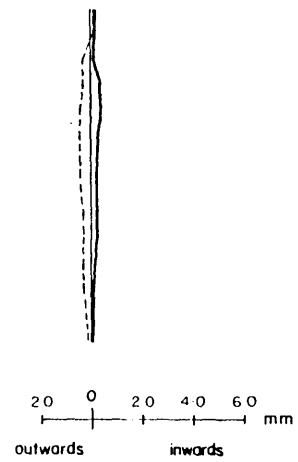
Vertical Sections



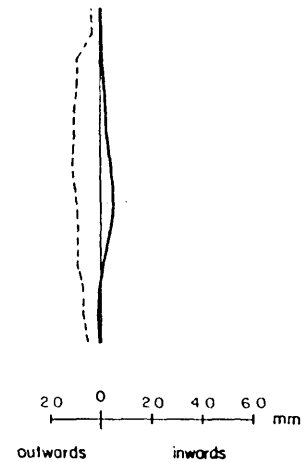
Sect. 1A



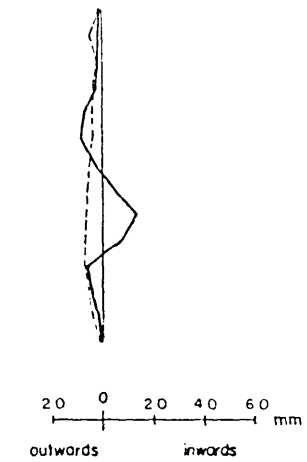
Sect. 11A



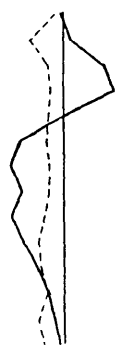
Sect. 21A



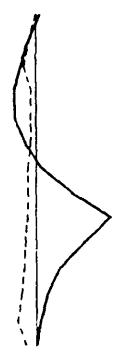
Sect. 31A



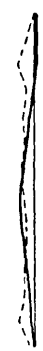
Sect. 1B



Sect. 11B



Sect. 21B



Sect. 31B

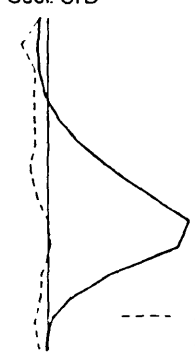


Fig. 2.134

CYLINDER E - RADIAL DEFLECTIONS

Vertical Sections

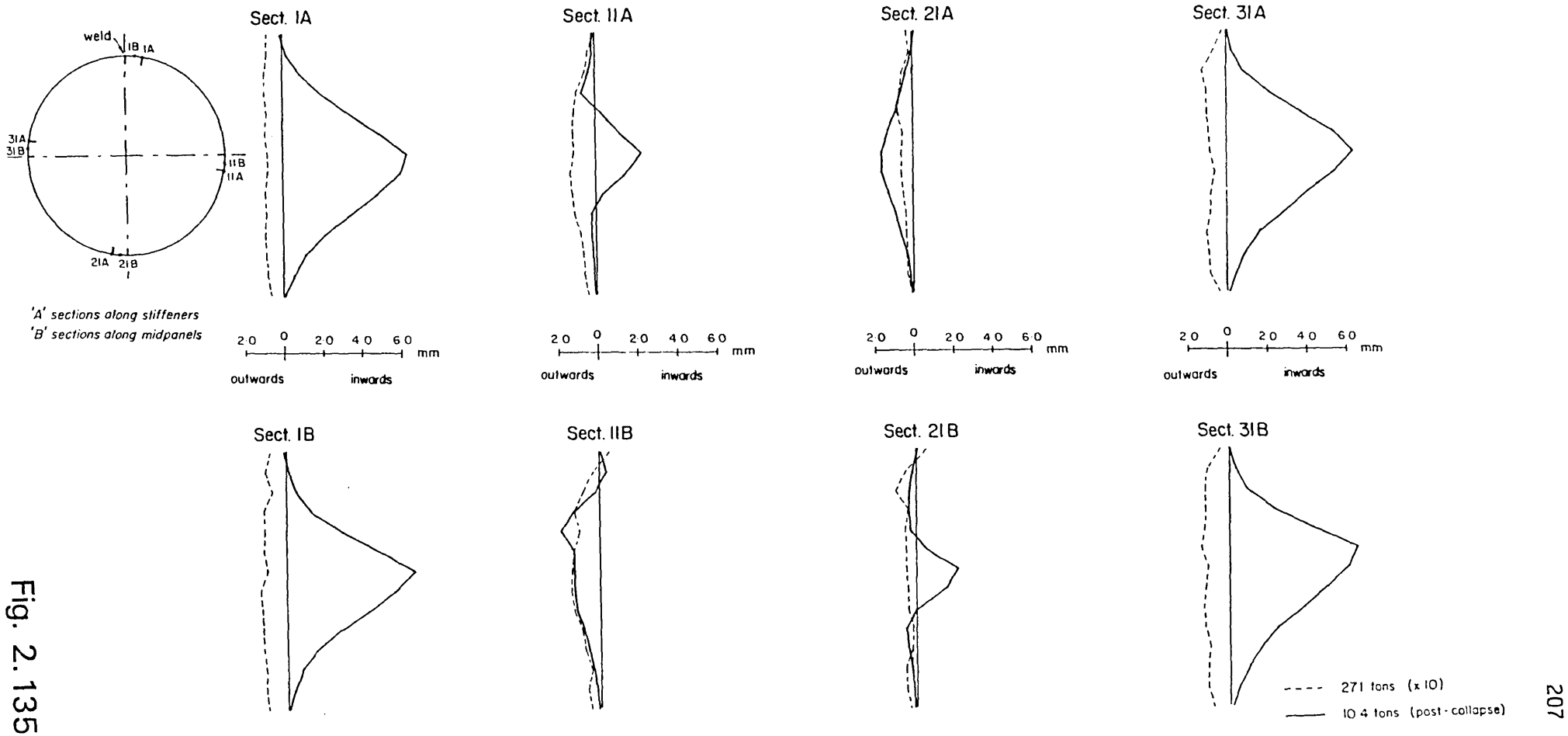


Fig. 2.135

CYLINDERS A & E - STRAIN GAUGE LOCATIONS

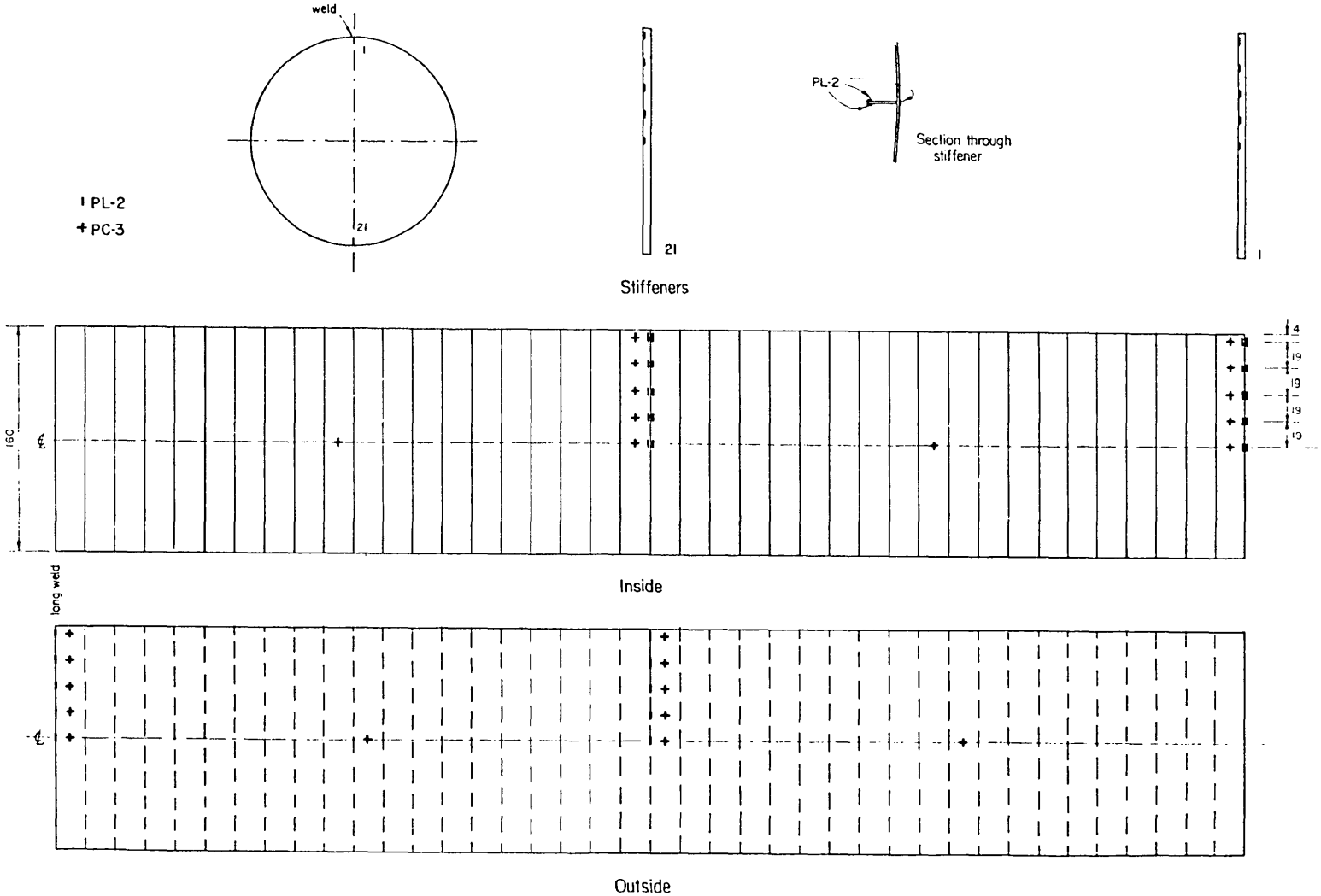


Fig. 2.136

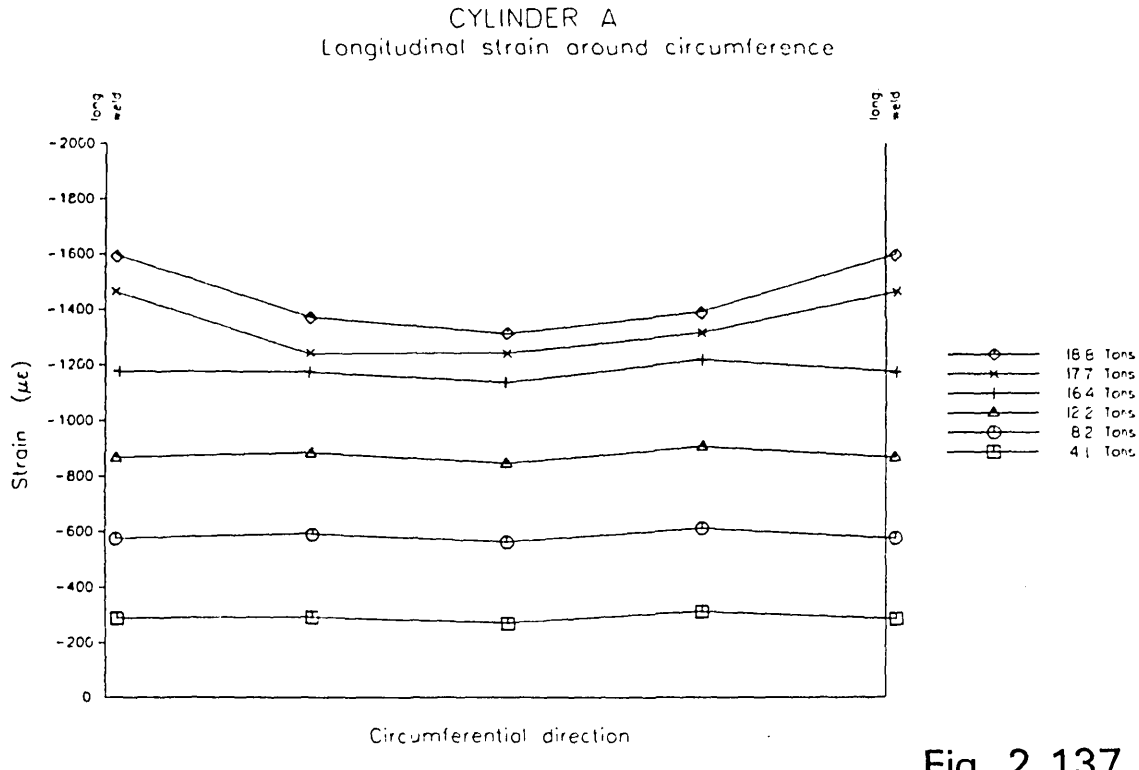


Fig. 2.137

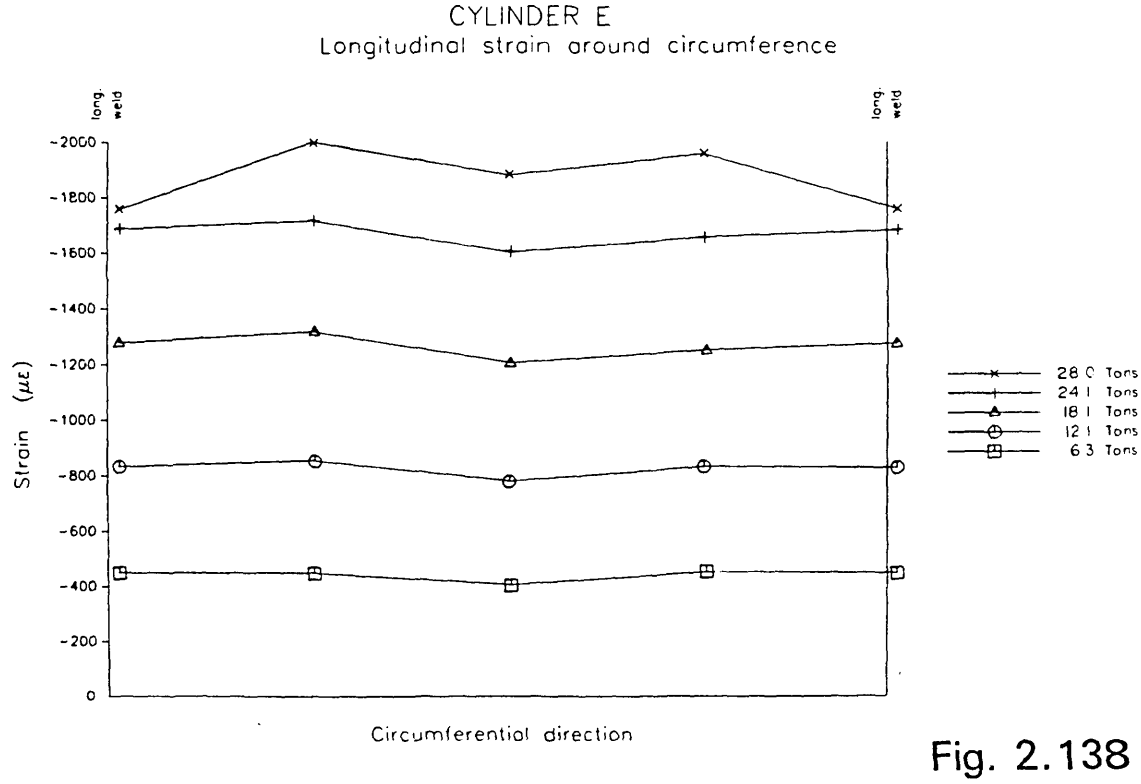


Fig. 2.138

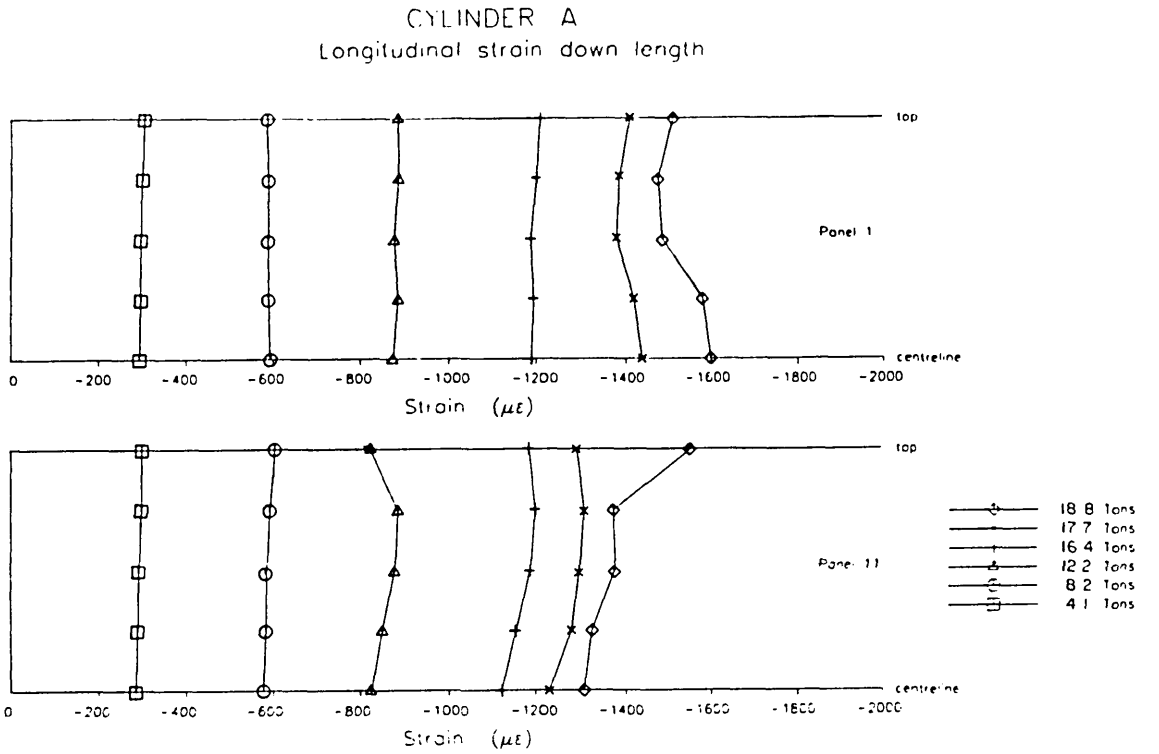


Fig. 2.139

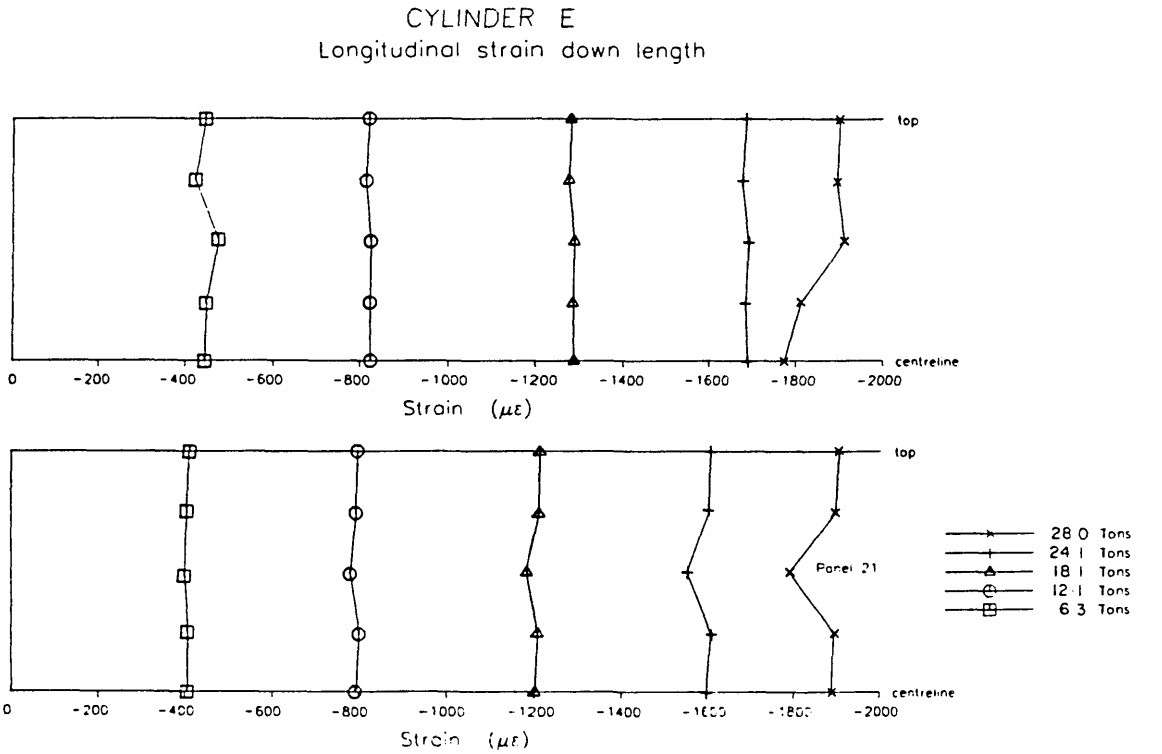


Fig. 2.140

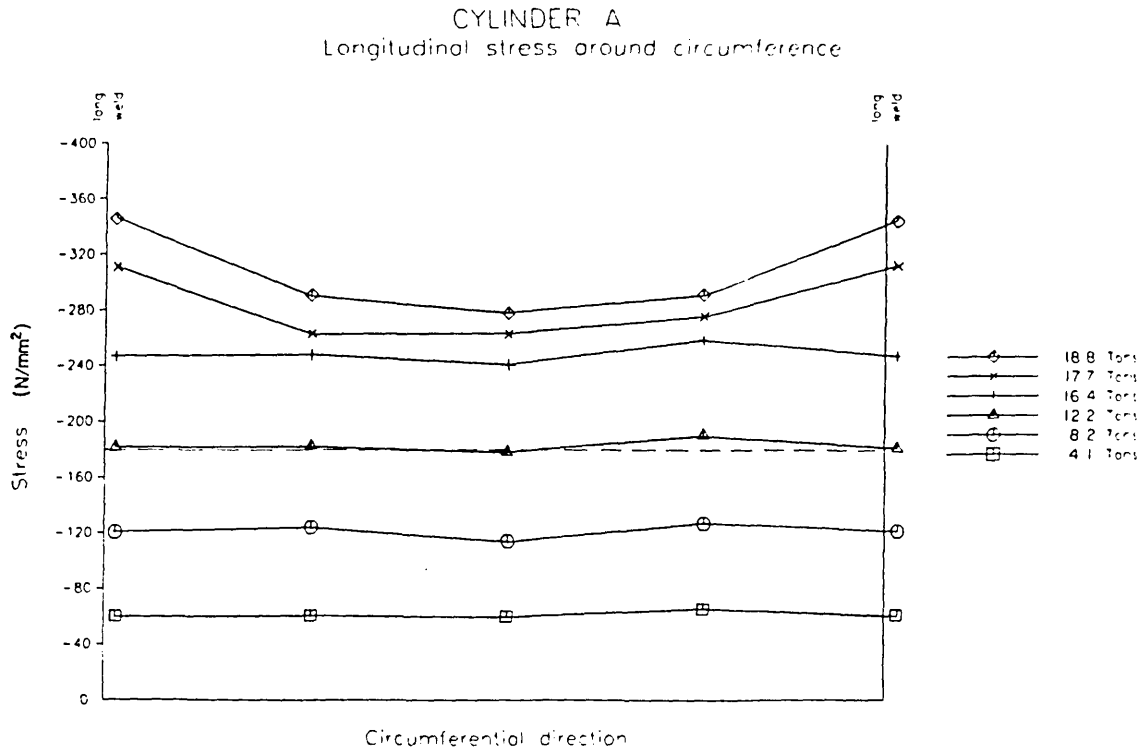


Fig. 2.141

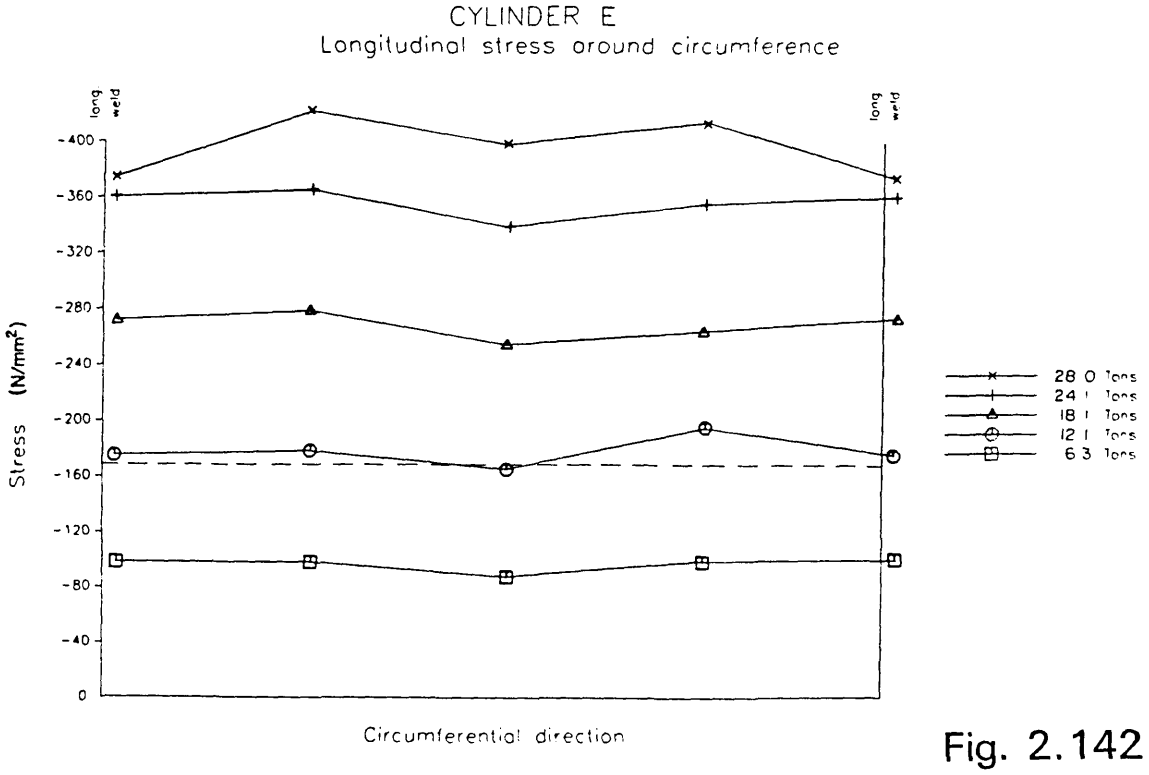


Fig. 2.142

CYLINDER A
Longitudinal stress down length

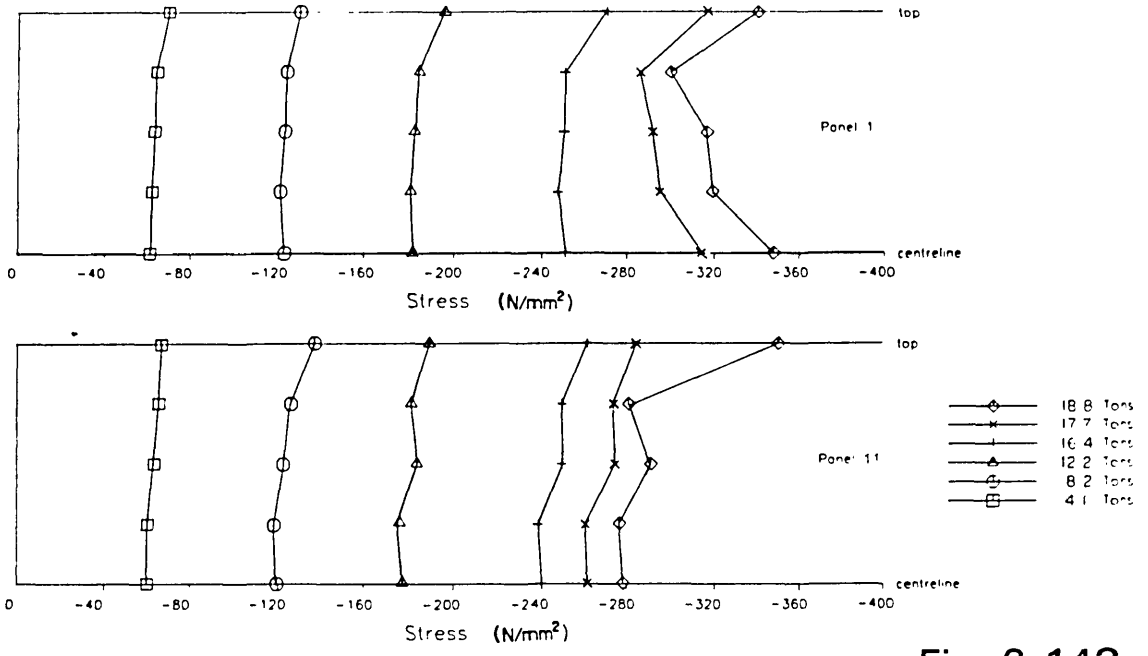


Fig. 2.143

CYLINDER E
Longitudinal stress down length

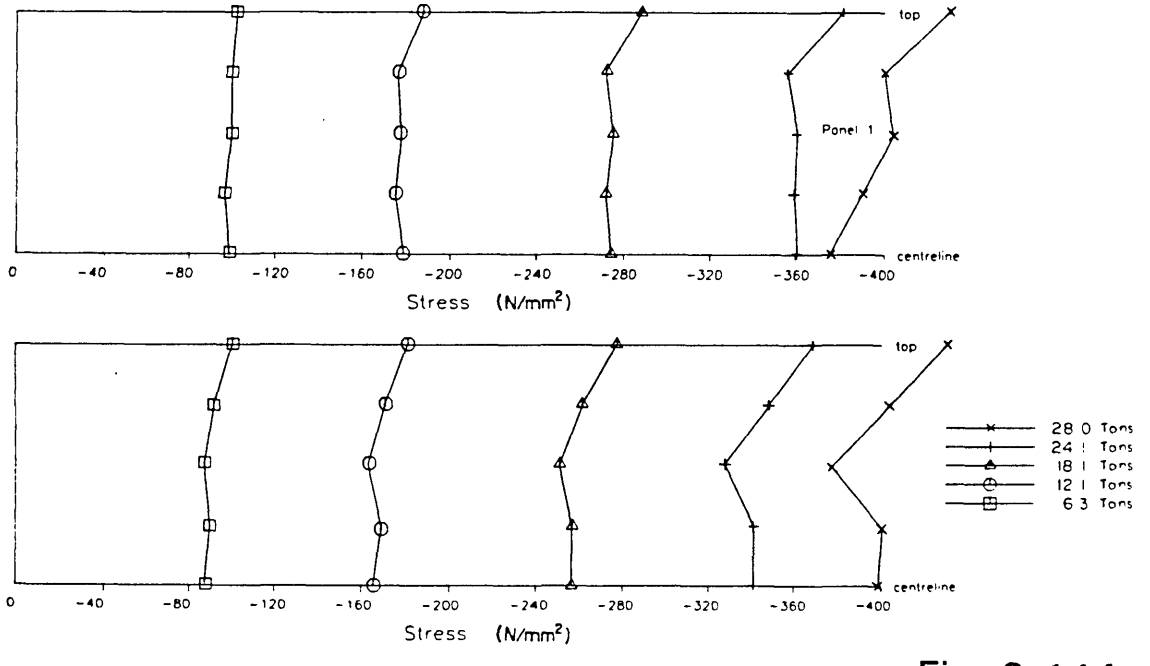


Fig. 2.144

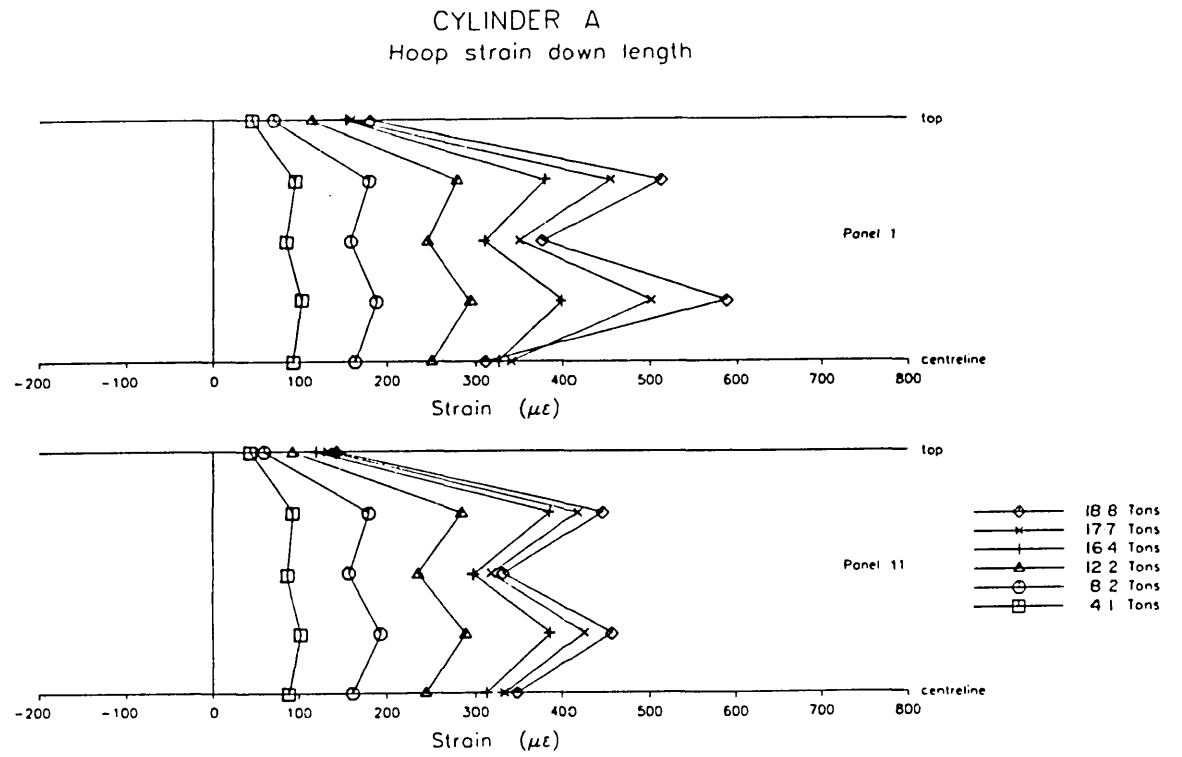


Fig. 2.145

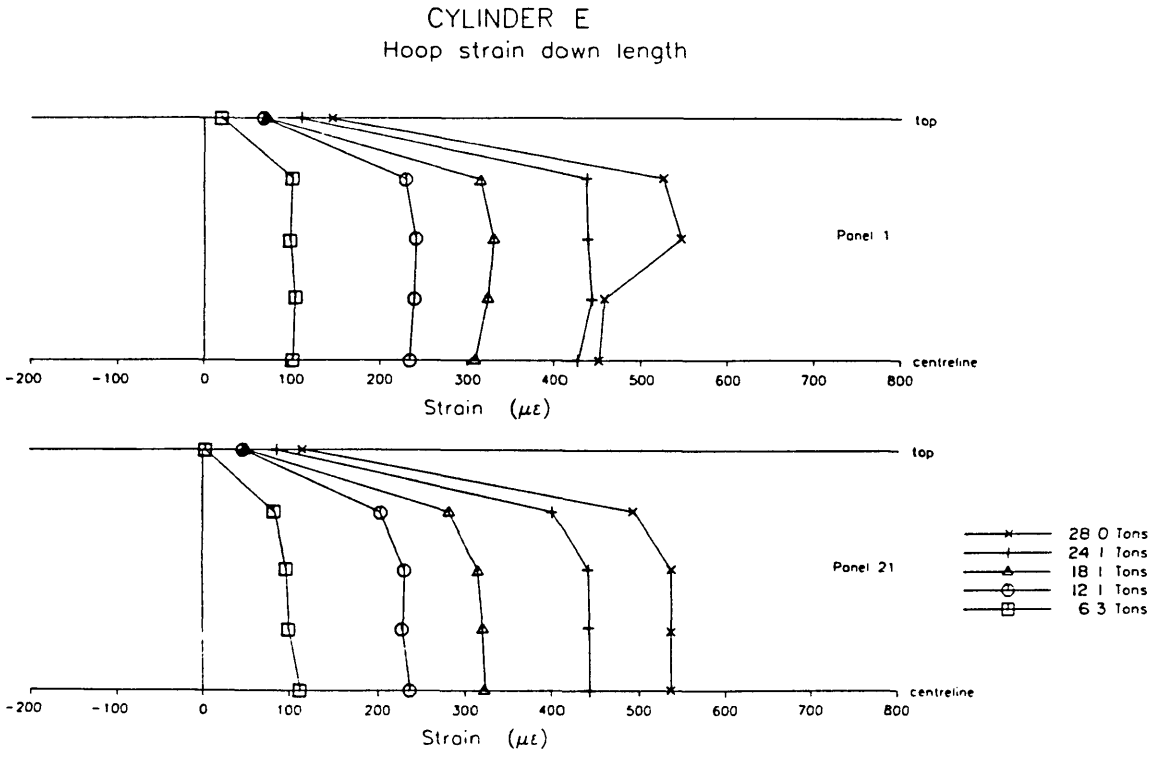


Fig. 2.146

CYLINDER A
Hoop stress down length

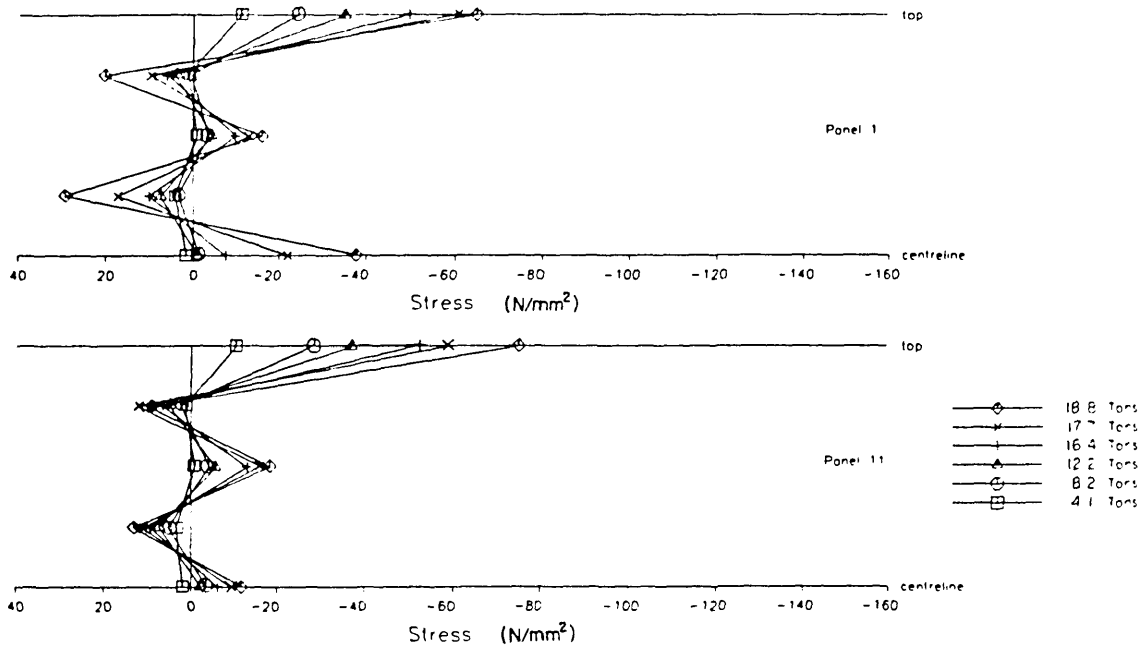


Fig. 2.147

CYLINDER E
Hoop stress down length

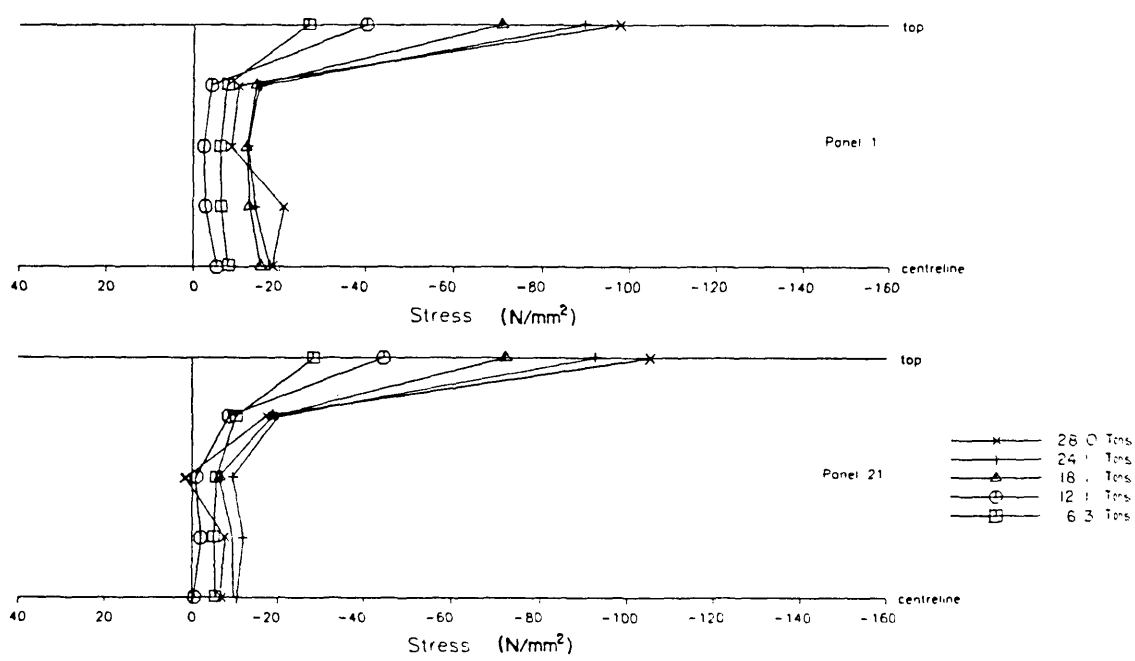


Fig. 2.148

CYLINDER A
Longitudinal strain in stiffeners

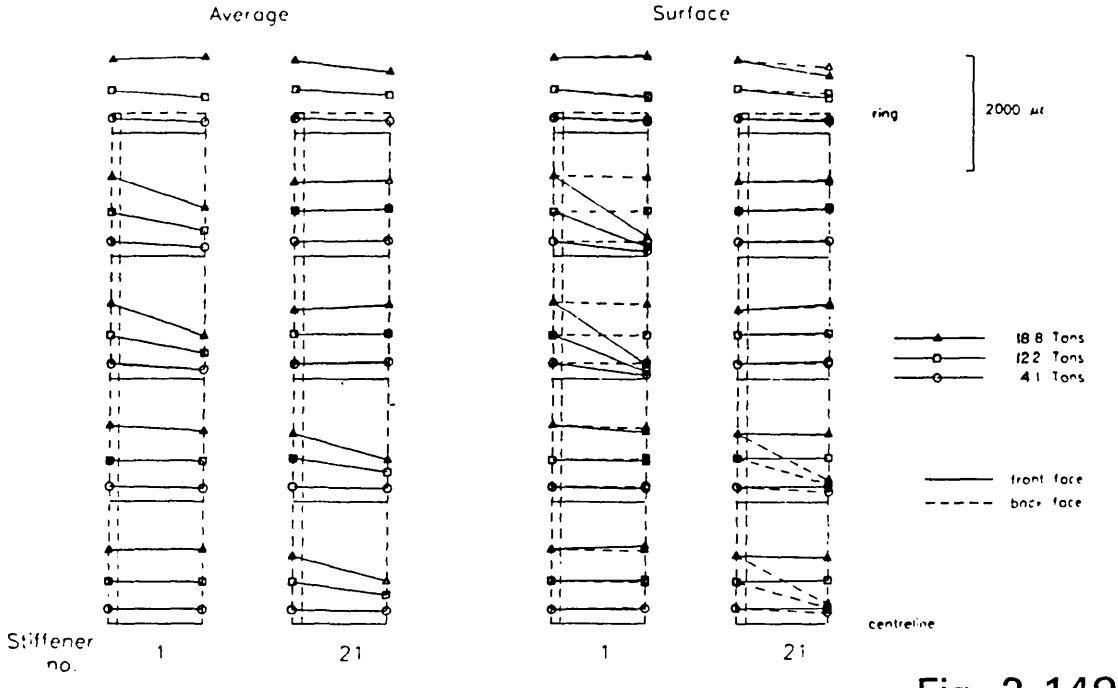


Fig. 2.149

CYLINDER E
Longitudinal strain in stiffeners

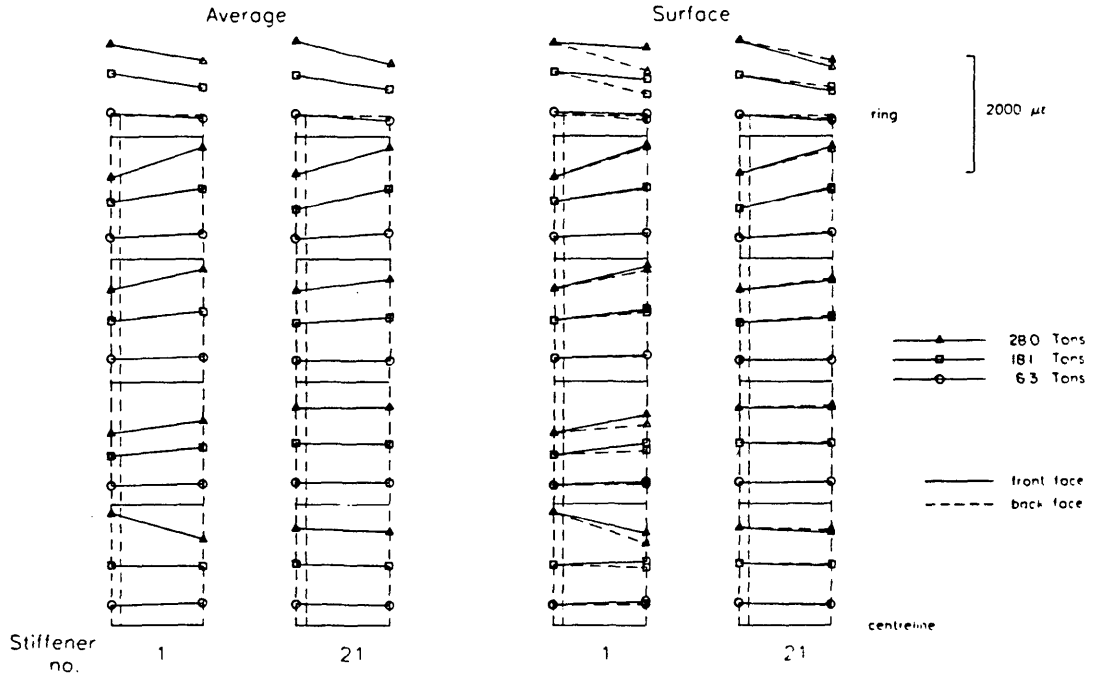
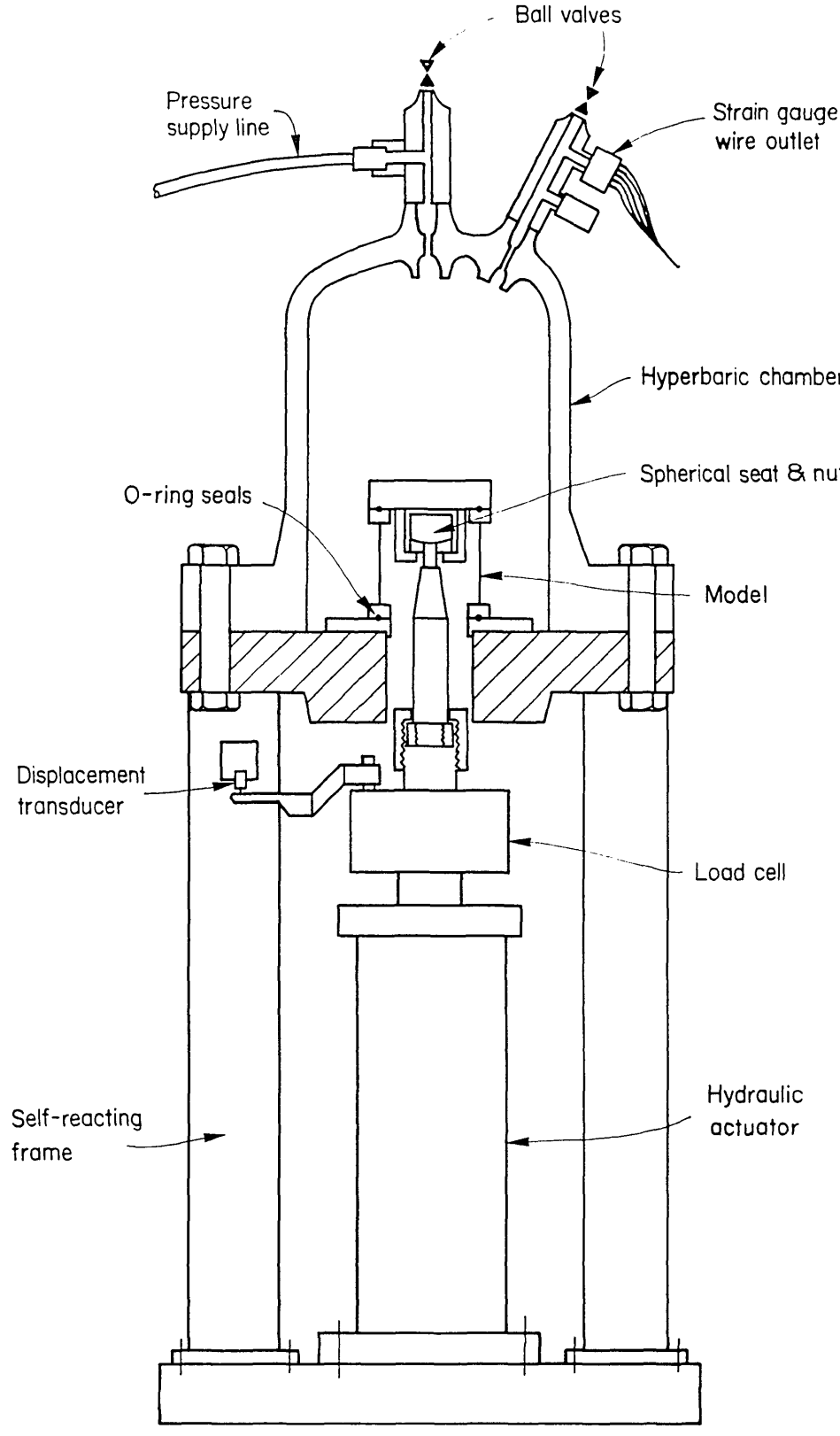


Fig. 2.150



Hyperbaric test rig

Fig. 2.151



CYLINDER B

Fig. 2.152



CYLINDER F

Fig. 2.153

CYLINDER B - BUCKLED SHAPE

Midheight circumference

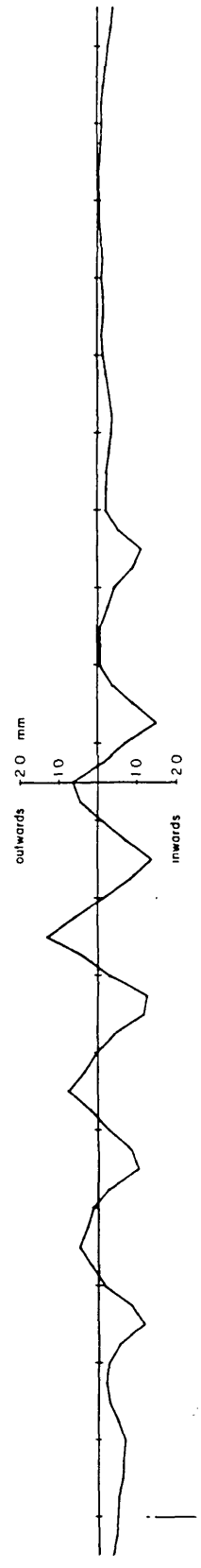


Fig. 2.154

CYLINDER F - BUCKLED SHAPE

Midheight circumference

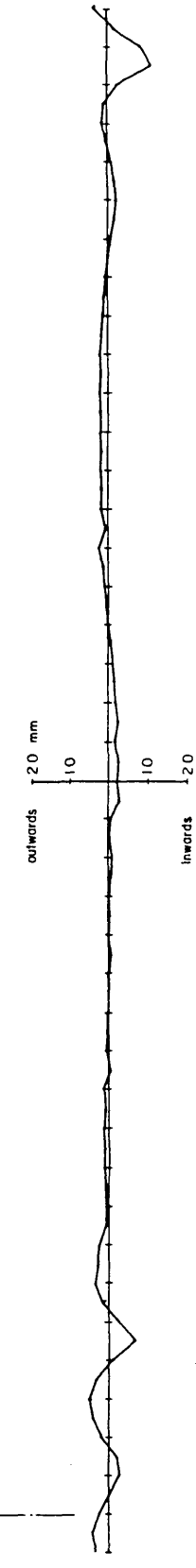


Fig. 2.155

CYLINDER B - EXTERNAL PRESSURE vs MEMBRANE STRESS

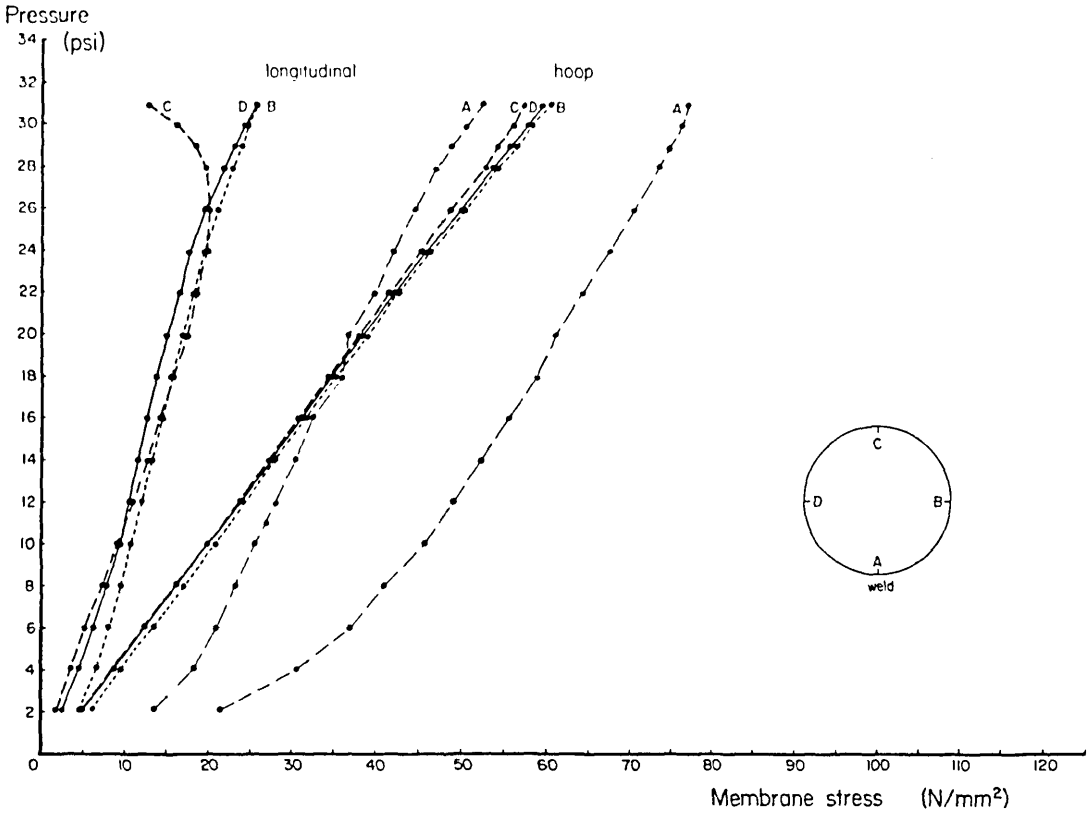


Fig. 2.156

CYLINDER F - EXTERNAL PRESSURE vs MEMBRANE STRESS

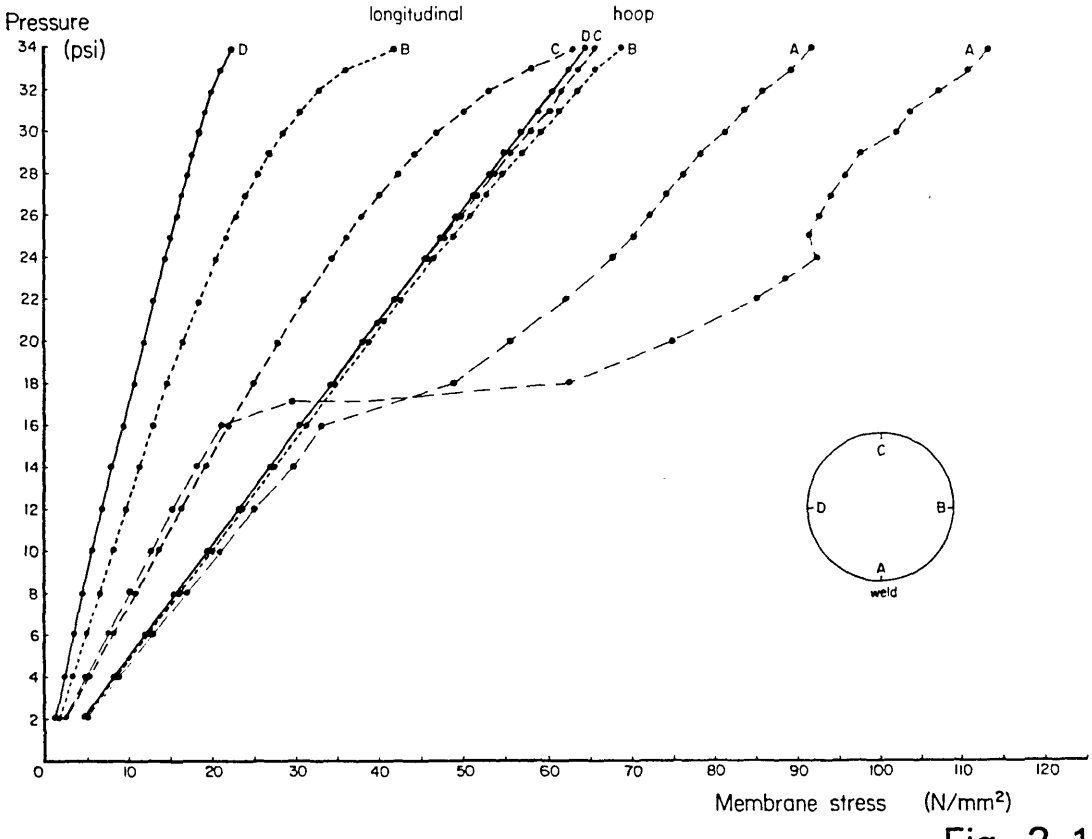
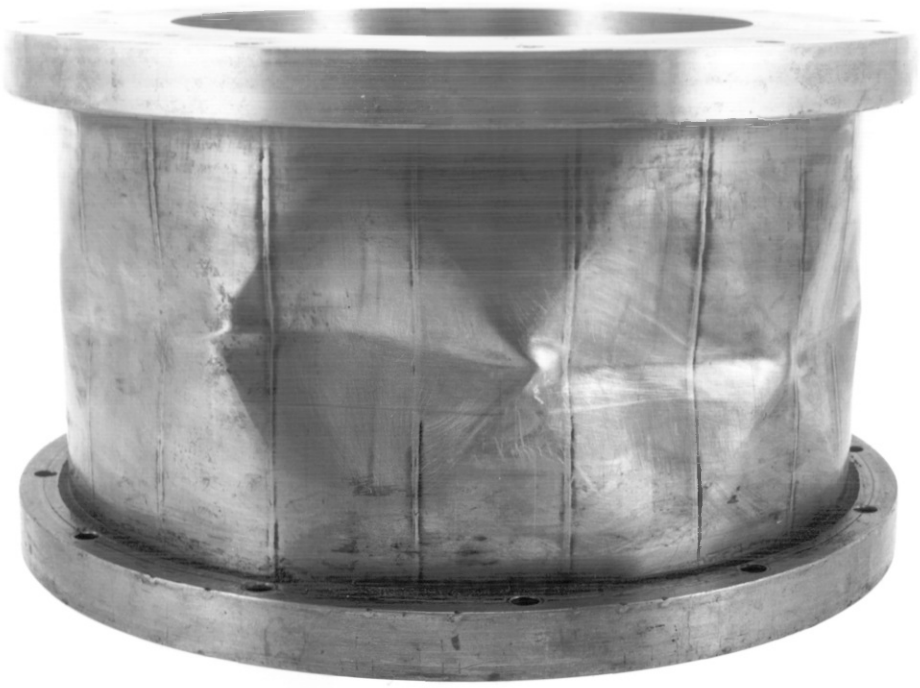


Fig. 2.157



CYLINDER C

Fig. 2.158



CYLINDER G

Fig. 2.159

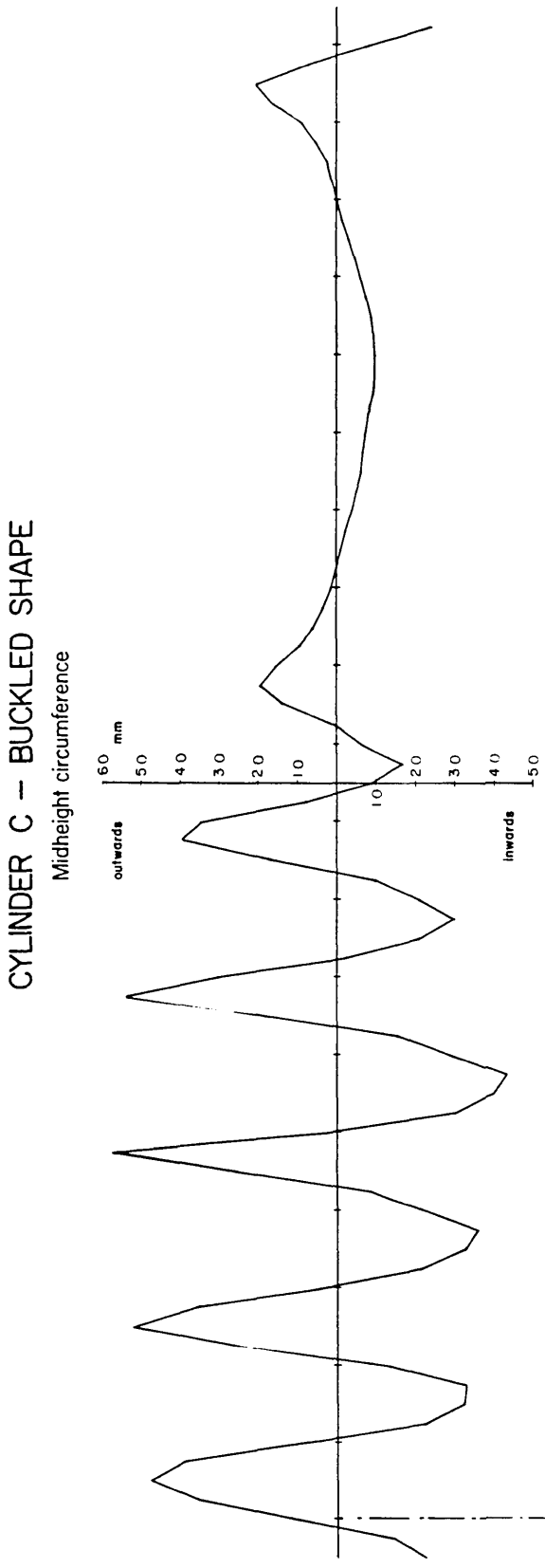


Fig. 2.160

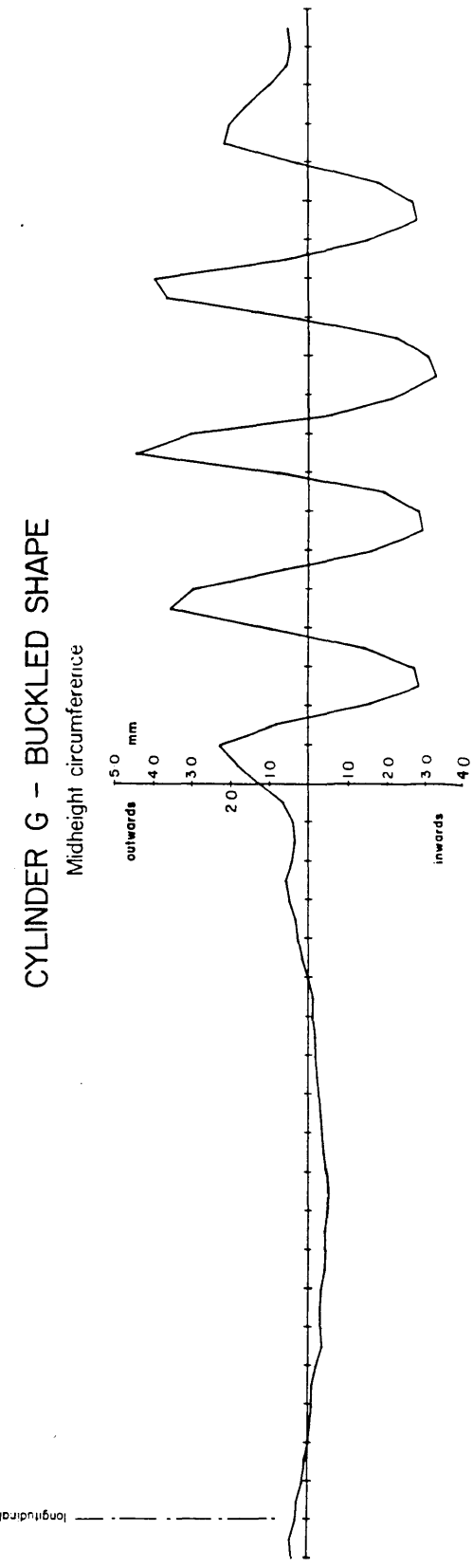


Fig. 2.161

CYLINDER C - AXIAL LOAD vs MEMBRANE STRESS

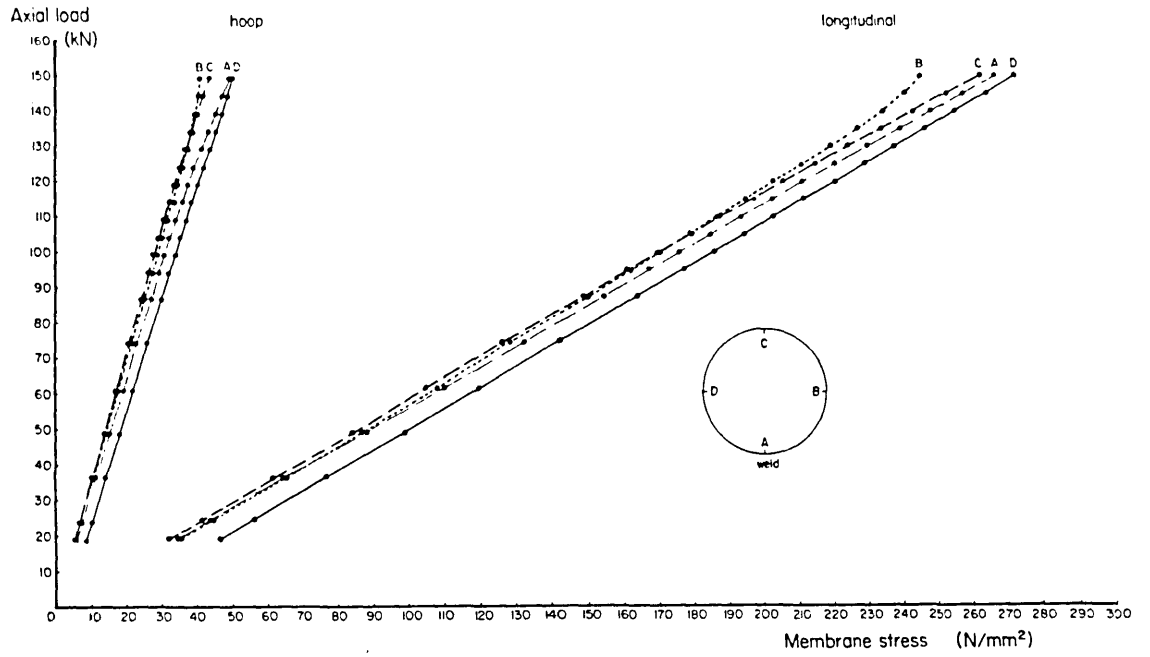


Fig. 2.162

CYLINDER G - AXIAL LOAD vs MEMBRANE STRESS

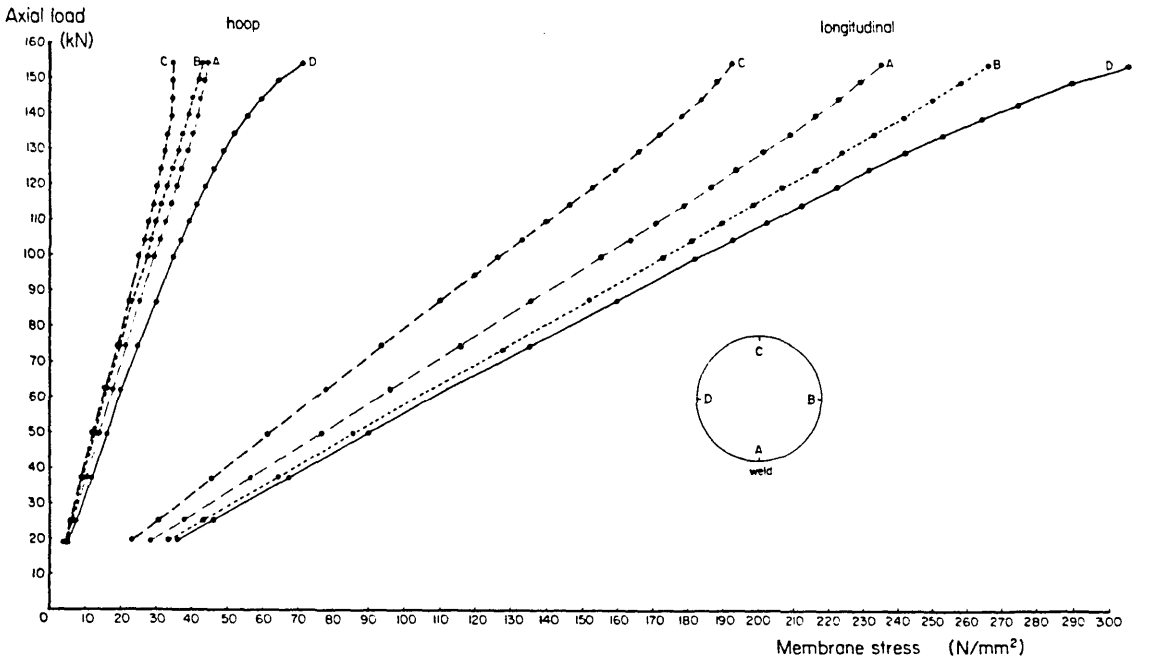


Fig. 2.163

CHAPTER THREE

NUMERICAL ANALYSIS

3.1 INTRODUCTION

Many of the experimental models, in particular the shorter and more heavily-stiffened cylinders, failed in modes consisting of buckles, which each extended over one panel only. In fact, the models that failed in overall modes were either longer or more lightly-stiffened than is common in practice.

The aerospace industry, for example, uses slender cylinders that are stiffened by a large number of light stringers and are prone to overall buckling. In structural engineering, where the consideration of minimum weight is not as crucial, it is more common for a smaller number of heavier stringers to be used. More stiffeners would mean higher fabrication costs, which may outweigh any savings in material.

In addition, angle or tee sections are often employed as stringers in preference to flat bars for a number of reasons: they are unlikely to buckle locally; they increase the inertia of the shell-stiffener cross-section and therefore enhance the behaviour under lateral load, e.g. pressure or slam loading; and they are more effective in limiting the damage produced by impact against the shell. On the other hand, only the material cost, and not the cost of fabrication, is increased by their use.

The presence of relatively few heavy stringers often makes the cylindrical shells used in offshore structures more likely to buckle in a local rather than an overall mode. This form of behaviour

suggests that the analysis of an appropriate component of the cylinder may be sufficient for the determination of the structure's response.

The first part of this chapter describes a means of analysis using the finite element method, which can be used to model economically the behaviour of stringer-stiffened cylinders. In the next chapter the method will be used in an extensive parametric study. The first step towards the confident application of the finite element model to a range of problems is to verify its predictions against experimental results. To this end, all the experimental cylinders reported in this thesis were analysed using the finite element model; this will form the second part of this chapter.

3.2 COLUMN ANALOGY

The idea of analysing a representative component of a larger repetitive structure is not new; it was originally applied to longitudinally-stiffened flat plates (e.g. Moolani and Dowling [207]). It relies on the assumption that the stiffened plate is composed of a large number of repetitions of a single stiffener and its associated plating, and that the behaviour of the entire structure can be accurately represented by that of a single component. It is further assumed that bending occurs in one direction only, and that under axial load no transverse stresses are produced.

For cylindrical shells this assumption cannot be made, as even under purely axial load hoop stresses will be produced. The hoop stiffness will reduce the lateral (radial) deflection of the column, and can be represented by attaching lateral springs to the flat plate unit: in effect placing the column on an elastic foundation.

This approach was used by Walker and Sridharan [159] to analyse

axially-loaded cylinders that fail in deflection modes that contain a number of panels within each buckle. Their implicit assumption was not that each shell-stiffener unit in the cylinder behaves identically, but rather that the cylinder behaviour is governed by what happens to the shell-stiffener unit in the middle of an overall buckle. The method was applied to narrow-panelled cylinders failing in overall modes.

It would be useful to apply a similar model to stringer-stiffened shells that fail locally and fulfil the requirement of symmetry along the boundaries of the model. However, the column analogy cannot be used in its simple form for a number of reasons.

Because an initially straight column under axial load will remain straight up to the buckling load, the method cannot predict the prebuckling radial deformations of the cylinder induced by Poisson expansion, but can only account for the amplification of initial imperfections. The two effects will usually produce deflections in different modes, and very often the former will be the more significant. This will be particularly so in short, stocky cylinders. Whilst Walker and Sridharan used this method to obtain good correlations with their experimental tests, extending its use to a broader range of geometries may be less appropriate.

The method also neglects the hoop stresses in the shell. For axially-loaded shells this will produce errors in the prediction of the onset of yielding and the radial stiffness of the shell. More significantly, it makes the analysis of pressure and combined loading cylinders impossible.

Finally, the use of a constant spring stiffness will not reflect the reduction in the stiffness of the shell as it begins to yield.

The analysis described above is the product of two simplifying assumptions: first, that the behaviour of the cylinder can be studied by looking at a small representative part of it and, second, that this portion can then be analysed by reducing it to a beam-column on an elastic foundation. Whilst the first assumption reduces the problem to a small fraction of its original size and is supported in many cases by experimental observations, the second assumption is one which, with the present availability of high-speed computing capability, is neither necessary nor desirable. In fact, all the shortcomings mentioned above can be eliminated by analysing the single panel shell/stiffener assembly using a finite element analysis. The curvature of the shell can be incorporated directly without the need to use an artificial spring stiffness. The Poisson expansion and hoop stiffness of the shell are then both predicted correctly.

The experimental cylinders to be modelled in this chapter, and also those in the parametric study to follow usually buckled elastoplastically. The analysis must, therefore, take account of the geometric and material nonlinearity in the structural response. Since plasticity is path dependent, a full nonlinear, incremental, iterative solution is required, in which small increments of load or displacement are applied to the model and the entire load-deflection response is calculated.

Diack and Ramm [208] independently of the present author carried out a similar analysis of an experimental model tested by Walker and Sridharan [159]. Their method of modelling was similar, although, being less concerned with the computing costs of their more moderate study, they used a greater number of elements.

3.3 DESCRIPTION OF FINITE ELEMENT PROGRAM "FINAS"

The finite element analyses were carried out using a general-purpose nonlinear finite element program, FINAS, developed at Imperial College by Trueb [209], and incorporating shell and stiffener elements developed by Bates [210]. Their work, directed primarily toward shell applications, resulted in a program capable of very efficient analysis of nonlinear plate and shell problems that includes many features not commonly found in commercially available finite element packages. The references cited above should be consulted for a full exposition of the program and the finite elements, but a brief description of the features relevant to the present study will be given here.

3.3.1 FINITE ELEMENTS

A number of element types are available, all of which are isoparametric, and apart from the shell element used throughout this work and described below, they include a 3-D beam element, a plane stress and plane strain membrane element, a membrane plate, an axisymmetric element and a 3-D continuum element.

In all the single panel analyses of this and the next chapter shell elements were used to model both the shell and the stiffeners. The shell elements are doubly-curved, eight-noded isoparametric elements which have the full six degrees of freedom per node and allow both smooth and discontinuous shell structures to be analysed. The element formulation is based on Mindlin shell theory [8], which assumes that:

(a) the transverse direct stress is zero,

(b) a normal to the shell midsurface remains straight but not necessarily normal during deformation, i.e. the transverse

shear stress is constant.

It is, therefore, well suited to both thin and thick plate and shell analysis.

Gauss numerical integration at a user specified number of integration stations in each direction is employed to generate the element stiffness matrices. Because the shear rigidity is proportional to the shell thickness while the flexural rigidity is proportional to its cube, the global stiffness matrix may become ill-conditioned for very thin shells whose linear dimensions are much larger than their thickness. It has been found, e.g. [210], that this problem, termed "shear locking", can be overcome by the use of reduced Gauss integration, and throughout this work 2 x 2 integration was used across each shell.

Since the element formulation is based on a nonlinear strain-displacement relationship, it includes large displacement and rotation effects through the coupling of membrane and bending terms. A penalty function approach, in which the rotation of the normal to the shell is expressed in terms of the in-plane displacements, was used by Bates to avoid the spurious modes which may arise in continuous shells with six degrees of freedom per node.

Material nonlinearity is included through an elastoplastic multilayer technique, using the von Mises yield criterion and its associated flow rule, in which the number of layers through the thickness of the element is specified by the user. For the analyses in this thesis five layers were used.

3.3.2 SOLUTION

The solution of the resulting set of simultaneous equations is based on Gauss elimination and is not restricted to positive-definite

matrices; this enables load-deflection paths to be followed into the unloading range. Only the non-zero coefficients in the upper triangular part of the stiffness matrix are stored. To further increase efficiency, automatic node renumbering may be carried out prior to assembly to minimize the bandwidth of non-zero terms in the stiffness matrix. The stiffness matrix is automatically divided into a number of blocks, which, if necessary, are stored on mass storage devices during execution, thus virtually freeing the problem from any in-core storage limitations.

An eigenvalue analysis can be carried out at any load level to solve a nonlinear buckling eigenvalue problem including large displacement and elastoplastic effects, although in the present work only linear initial eigenvalue problems were solved. The subspace iteration technique is employed for the eigenvalue solution.

A number of nonlinear solution strategies are available, based on the Newton-Raphson technique. The solution proceeds in a series of steps, at each of which equilibrium iterations may be performed to re-establish equilibrium to a given tolerance. The stiffness matrix can be recalculated at a user specified frequency to produce a full Newton-Raphson, modified Newton-Raphson or alternative solution scheme. The loading steps are specified as increments of the vector of applied loads or of a displacement, the latter being necessary if the unloading part of the load-deflection path is to be obtained.

The program is extremely efficient on crossing limit points in the load response. Several strategies are available, but the one used in this work was to specify increments to be applied to whichever is the fastest growing displacement at each stage of loading, which the program will select. This is extremely useful in snap-through problems, in which the area of the structure deflecting most rapidly

changes during the loading history. Should equilibrium not be reached within a preset number of iterations, the program will automatically reduce the step size, move to a more powerful solution scheme (e.g. modified N-R, full N-R, etc) and retake the step. Conversely, if equilibrium is reached quickly the program can increase the step size, up to a preset limit, to maintain efficiency. In this way the required loading input data is minimized, consisting only of the first displacement increment and the maximum factor by which it may be multiplied in subsequent steps.

This degree of automation meant that in the majority of cases one run was sufficient to obtain the fully nonlinear load-deflection path including the postbuckling range. This feature, possibly more than any other, made the undertaking of the large parametric study of the next chapter feasible.

3.4 DESCRIPTION OF FINITE ELEMENT MODEL

3.4.1 GENERAL

The finite element model consisted of a single longitudinal stiffener and its associated curved shell. The longitudinal edges of the shell, which are the centrelines of two adjacent panels, were assumed to be lines of symmetry. Symmetry was also invoked along the circumferential centreline to reduce the problem to one half of the bay length.

3.4.2 NUMBER OF ELEMENTS

The mesh refinement needed to achieve a certain degree of accuracy was the subject of a convergence study, reported later in Sect 3.5. However, an initial estimate for the mesh, which proved

sufficient for most cases, was made by using as a guide the requirement derived from experience that an acceptable mesh usually contains two eight-noded elements for each halfwave of the deflected shape. A single halfwave across the width of the panel with possibly several halfwaves along its length was the expected deflection mode, and a 6x2 mesh of elements was adopted for the shell in most cases.

Modelling of the stress variation through the stiffener and the representation of localized stiffener deflections suggested the use of two elements through the stiffener depth. This gave rise to the arrangement of elements shown in Fig 3.1.

3.4.3 BOUNDARY CONDITIONS

Fig 3.1 also illustrates the directions along which movement was prevented at the boundary nodes of the finite element model. Because of the curvature of the shell, the local directions normal and tangential to the shell in which the boundary restraints should be imposed do not correspond to the global coordinate system. It is necessary to specify the boundary conditions in local coordinates aligned with the shell surface.

The facility for incorporating boundary conditions in a local axes system was not available in the finite element package, and it was necessary, before commencing the analysis, to develop and implement routines to carry out these transformations. The equilibrium equations were expressed and solved in the local coordinate systems and the results transformed back into the global system before output.

Along the longitudinal (straight) edges, conditions of symmetry were applied by preventing tangential displacement and rotation about the edge. The curved edge along the cylinder centreline was also

assumed to be a line of symmetry, and was allowed to move in the radial direction only.

At the remaining loaded edge, restraints were applied to simulate as closely as possible the experimental boundary conditions produced by the sand/araldyte end fixtures. All degrees of freedom other than the longitudinal displacement were eliminated along this edge. Unfortunately, because the facility did not exist to specify a uniform displacement of all the loaded nodes, it was possible for the nodes along the loaded edge of the stiffener to deflect nonuniformly and for the stiffener end to rotate (see Fig 3.2(a)). Maintaining the end of the stiffener parallel to its original position while free to move longitudinally was achieved by the somewhat artificial, but nonetheless effective, method of restraining the radial displacement of the two nodes nearest the end (Fig 3.2(b)).

3.4.4 LOADING

The situation in the axially-loaded experimental models would be best represented by a uniform strain loading, in which all the loaded nodes are displaced by the same amount. As mentioned above, it was not possible to do this with the current version of the program, and a uniform stress loading was used. Since most models to be analysed were relatively narrow-panelled, this would probably have little effect on the predicted peak load in most cases, but could sometimes reduce the degree of stress redistribution possible as one area of the model began to buckle. Nevertheless, it should be conservative in all cases, and was adopted for the experimental correlation studies and for the subsequent parametric analysis (see Sect 4.2.4).

For the combined loading cases the ratio of axial to pressure load was constant throughout the loading history.

3.5 CONVERGENCE STUDY

A number of convergence studies were carried out on models of various dimensions to determine suitable element meshes and to gain experience in using the analysis. A mesh of 6x2x2 elements, where the numbers refer to the elements along the length of the model, across the width of the shell and through the depth of the stiffener respectively, was chosen as the starting point for all these studies (see Table 3.1). Attention was focused on axially-loaded models since it is in these that the shortest wavelength buckles are usually found; they therefore require the greatest number of elements in order to be modelled accurately.

Two perfect models were studied first: one, a stocky cylinder (R/t=200, L/R=1, N=40), the other, considerably more slender (R/t=500, L/R=1, N=40). The first geometry was analysed using a 3x2x2, a 6x2x2 and a 12x2x2 mesh of elements, for which the peak average applied stresses of 240.6, 239.4 and 239.9 N/mm^2 differed by a maximum of 0.5%. The results for the second case, although not exhibiting the same degree of precision, were still acceptable. For the same three meshes the stresses were 229.9, 224.3 and 214.2 N/mm^2, giving in this case a maximum variation of 7.0%.

The 3x2x2 and 6x2x2 meshes were also used to analyse the same geometries with initial imperfections in a single halfwave mode (see Fig 3.3(c)) of amplitude equal to the shell thickness; the results were similar to those obtained above, in that changes in the peak load of 0.2% and 3.2% were obtained by refining the mesh from 3x2x2 to 6x2x2 elements for the stocky and slender cases respectively.

These runs provided a feel for the precision to be obtained using

typical meshes, but a more systematic bounding of the expected inaccuracies was obtained by analysing a short wide-panelled model, a long narrow-panelled model and a short narrow-panelled model. These cases maximized the effect of the shell width, the shell length and the stiffener depth respectively. Each was analysed using the 6x2x2 mesh as a datum and subsequently with a mesh in which the number of elements in the direction of interest was doubled (Table 3.2). It was possible in this way to investigate the effect of mesh refinement more economically and systematically than if the number of elements in all directions were increased simultaneously.

The short, wide-panelled cylinder (R/t=200, L/R=0.25, N=20) gave peak stresses of 285.4 and 271.5 N/mm^2 for the 6x2x2 and 6x4x2 meshes, (i.e. a difference of -4.9%). The long, narrow-panelled model (R/t=600, L/R=1, N=60) was analysed using a 6x2x2 and a 12x2x2 mesh, for which results of 307.8 and 290.0 N/mm^2 were obtained, (i.e. a difference of -5.8%). Finally, the short, narrow-panelled cylinder (R/t=200, L/R=0.25, N=60) was analysed with 6x2x2 and 6x2x4 meshes. These gave the almost identical results of 326.9 and 326.8 N/mm^2, indicating the adequacy of using two elements through the stiffener depth.

These three models bounded the geometries analysed in the parametric study described in the next chapter and, therefore, represented the worst geometries to be considered. In most cases the improvement in accuracy to be derived from using a refined mesh would be less significant. Given the inherent inaccuracy of the single panel simplification, errors of up to about 5% in its numerical analysis are quite acceptable, and the 6x2x2 mesh was adopted as the standard model throughout this work.

3.6 ANALYSIS OF EXPERIMENTAL MODELS

It was now possible to proceed to the analysis of the experimental cylinders. All the models described in the previous chapter and, in addition, those tested at Surrey University [203] and constituting the remainder of the DnV series were analysed.

3.6.1 INITIAL IMPERFECTIONS

The detailed initial imperfection readings taken for each cylinder provided the data base from which suitable imperfections for the finite element model were chosen. Obviously, if the whole cylinder were being analysed the entire measured imperfect geometry could be used. However, as only a small part of the cylinder was modelled, it was necessary to extract from the data a severe yet reasonably representative imperfection mode and amplitude. To be compatible with the single panel model, the imperfect shape could not include modes spanning more than one panel.

3.6.1.1 Imperfection mode

A preliminary study was carried out in which a number of the models from the DnV series were analysed using various initial imperfection shapes. Fig 3.3 illustrates the types of imperfections considered. These were (a) a symmetric outward "barrel" mode, (b) a symmetric inward "barrel" mode, (c) an antisymmetric mode and (d) a combined mode, the superposition of (a) and (c). In the symmetric modes the stiffener was left flat, whereas in the antisymmetric modes it was given a torsional imperfection.

Cylinder 11, the longest pressure-loaded cylinder, was analysed in its perfect state and with each imperfection mode, and the results of the analyses are summarized in Table 3.3. The outward barrel mode

produced virtually no reduction in the peak load compared with the perfect case, whilst the inward barrel produced a numerical instability at about two thirds of the perfect cylinder's peak load and a snap through into the antisymmetric mode. The antisymmetric mode was critical and produced a reduction of the peak load to approximately one third of the value for the perfect case. The subsequent superposition of the barrel and antisymmetric modes produced very little further change in the load capacity.

This set of results illustrated the importance of including some degree of asymmetry in the initial geometry. An asymmetric structure can approach a symmetric deflected shape if this is its preferred mode. A symmetric model, however, must rely on numerical round-off errors to induce an asymmetric mode and gives a totally erroneous description of the structural response.

Predicted values for some of the corresponding cases for cylinders 7 and 8, the medium length axial and combined loading models, are also given in Table 3.3. These confirm the finding that the barrel imperfection is not a critical one. In fact, only in cylinder 7, the axially-loaded model, is the peak load for the combined mode d) even marginally less than that for the panel mode only. The reason for this is probably that relatively large barrel-shaped imperfections are produced by Poisson expansion as the model is loaded, outweighing the small initial imperfections in this mode.

Although it was clear that an antisymmetric mode should be used, the question still remained as to how many longitudinal waves it should contain. As in the parametric study which follows, this problem was addressed by carrying out eigenvalue analyses for each geometry investigated and, in some cases, by performing nonlinear load-deflection runs using different initial imperfection modes. The

single wave antisymmetric mode was the lowest eigenmode for most of the small-scale models. It was not the critical mode for the large-scale model and for the longer, closely-stiffened, cylinders under axial load, i.e. models 7, 10 and E. In those cases modes containing a number of halfwaves in the axial direction were critical.

3.6.1.2 Imperfection magnitude

In general, single halfwave antisymmetric imperfections were incorporated in the analytical model, but for the cases mentioned above analyses were carried out both for the single wave and multiple wave imperfections. When the single wave, antisymmetric imperfection mode was used, its amplitude was determined by selecting the largest imperfection across the width of one panel from the circumferential plots of the initial imperfections (e.g. Fig 2.59). The line of connection of the stiffener was straight but a sympathetic torsional mode was applied by shifting the tip of the stiffener laterally by an amount determined from the stiffener initial imperfection plots (e.g. Fig 2.62).

3.6.1.3 Imperfection amplitudes for higher modes

For the analyses with a higher mode imperfection a reduced amplitude would be appropriate. The initial imperfection readings of the experimental models were examined to see if a relationship existed between axial wave number and amplitude. For the predominant circumferential mode, the Fourier coefficients for different axial wave numbers were expressed as a proportion of the single halfwave coefficient.

The relationship between magnitude and wave number was very similar in all cylinders, regardless of modelling scale or geometry. The average of all models, in Fig 3.4, shows that the magnitude of

each Fourier coefficient was almost exactly inversely proportional to the axial wave number. This relationship was used to determine the magnitude of the initial imperfections when higher mode shapes were used. This point is discussed further in Sect 4.2.5.4.

3.6.2 DNV SERIES

The initial eigenvalue analyses showed that for all but the two longer axially-loaded cylinders the single halfwave mode was critical. All cylinders were analysed with this as their initial shape, and the two cylinders above were also analysed using a reduced amplitude imperfection in the higher mode. In both cases the single halfwave imperfection provided the lower value of peak load and has been used throughout this series to define the cylinder strength.

Similar values of the imperfection magnitudes were obtained from the experimental readings for cylinders of each length, and average values were used in the analyses for each group (Table 3.4).

The experimental and analytical peak load values are presented in Table 3.5 and plotted in the form of axial-pressure interaction curves in Fig 3.5.

The correlation is extremely good for the long cylinders but slightly poorer as the cylinder length decreases. Nevertheless, the maximum error was 16%, which, given the nature of the problem and the degree of simplification, is very reasonable.

That the correlation became poorer for the shorter cylinders was probably due to the changing aspect ratio of the shell panels. The short models have relatively broader panels, whose strength is more affected by the constant stress loading. It is not surprising that the two poorest correlations were both for cylinders under combined

axial and low pressure loading; this is the most imperfection-sensitive range of behaviour, since the outward barrelling produced by the axial load is counteracted by the external pressure and only small prebuckling deformations are produced.

In almost all cases the finite element analysis underestimated the experimental failure load. This is to be expected, since the complete cylinder to which the analytical model is equivalent would contain initial imperfections of the maximum amplitude and critical mode in each panel, and would be incapable of load redistribution between the panels. In addition, the constant stress loading used in the analysis is a more severe means of load application than the experimental condition.

The analyses were carried out for all the models irrespective of the experimental failure modes; these have been included in Table 3.5. It can be seen that all the short and several of the longer models buckled in local modes. The analysis is directly applicable in these cases.

The longest axially-loaded model failed in an overall mode containing 16 circumferential halfwaves simultaneoulsy with the local end failure. The failure load was very near squash both for the experimental and for the analytical models and the precise buckling mode was relatively unimportant. This, therefore, was not a difficult test for the finite element model.

The remaining cylinders failed with deflection modes which, if complete, would have contained approximately 24 - 26 halfwaves around the circumference. Each halfwave spanned approximately one and a half panels, and the analytical assumption that each buckle was contained within one panel was not a significant limitation. The analysis,

therefore, gave good predictions for all these cases.

As experimental load-deflection paths and detailed strain readings were obtained only for the axially-loaded cylinders (the models tested by the author) the following discussion concentrates on them.

A comparison of the experimental and analytical load-deflection paths for these cylinders (Figs 3.6, 3.7 and 3.8) shows their general shape to be similar but that, after collapse, the analytical model tends to shed load more gradually than the real cylinder. There are two reason for this: first, a mesh which is sufficiently refined for the prebuckling behaviour of the cylinder may not be totally adequate in the postbuckling range, in which larger and more localized deflections may occur; secondly, the assumed symmetry lines along the panel centrelines may be a good approximation in the prebuckling range but probably over-restrain the model after buckling. However, neither effect should have a major influence on the predicted peak load, which is the result of primary interest. The more gradual load fall-off of the analytical model is encouraging in one respect: if the constant stress loading were far from appropriate a more rapid unloading than in the experiments would be expected.

The linear part of the predicted load-deflection path should fall between two limits: a simple calculation of the stiffness of the cylinder can be made assuming either that the hoop strain is zero (i.e. imposing the situation existing at the ends of the cylinder to the entire length), or that the hoop stress is zero (i.e. assuming that the situation at the centre of a long cylinder exists throughout). The lines labelled "1" and "2" in Figs 3.6, 3.7 and 3.8 give the stiffnesses calculated for the two cases, and they do bound the finite element solution. The numerical curve is closer to line 2

in all cases, suggesting that the effect of radial restraint at the ends is rather localized in practice and has little effect on the overall axial stiffness. As expected, the numerical curve comes closer to line 2 as the cylinder length increases.

Despite this agreement, the numerical model is in all cases considerably stiffer than the experiments. The length of the finite element model was taken to be the distance between the end rings and an allowance should be made for the axial shortening of the enclosed sections of the shell. Again, two simple cases can be easily assessed: in the first the load transfer between the shell and the end ring is accomplished entirely by a uniform shear stress along the length of the enclosed section, requiring no end bearing between the shell and the metal ring; in the other case all the load is transferred through end bearing with no shear transfer through the sand/araldyte; in both, full radial restraint was assumed.

The additional deflections produced in the enclosed sections of the shell were calculated for the two cases and, when added to the predicted finite element deflections, yielded curves 3 and 4 respectively. Curve 4 (end bearing only) was calculated assuming a constant stress along the entire length of the enclosed section, and must therefore be an upper bound estimate of the deflections. The other situation assumed a linear variation in the axial stress from the nominal value at the top of the end ring to zero at the end; it is not necessarily a lower bound, since the transfer of load could occur even more rapidly and produce yet smaller deflections. However, this curve does approach quite closely the experimental curve. It is possible, therefore, to account quantitatively for the differences between the experimental and analytical stiffnesses.

The stresses predicted by the analytical model and those measured

in the experimental tests were compared at a load level approaching the peak load. Because of the incompleteness of the strain gauge measurements obtained for cylinder 1, this comparison was based on the results for cylinders 7 and 10 only.

Three sets of figures are presented for each cylinder in Figs 3.9 and 3.10. The first two show the variation along the length of the cylinder of the axial and hoop stresses in the shell, and the third the longitudinal stress in the stiffener tip. The shell stresses were measured experimentally at locations along two vertical midpanel sections for each model (e.g. Figs 2.113 and 2.117), both of which are replotted here to give an indication of the degree of experimental scatter. Inner surface, outer surface and midplate values are shown. The finite element program calculates stresses at the element Gauss points, and the values plotted in these figures are for the longitudinal line of Gauss points nearest the midpanel centreline.

The longitudinal stress plots show that the midplate values are almost constant in all cases and that there is good agreement between experiment and analysis. The surface stresses predicted by the finite element analysis were consistent with the measured values, given the degree of experimental scatter and the spacing of strain gauges.

The midplate hoop stresses also agree well. The surface stresses are somewhat less comparable, with the experimental inner and outer surface stresses crossing nearer to the centre of the model in cylinder 10 and not at all in cylinder 7. However, these differences are relatively minor and depend upon the precise shape of the initial imperfections.

The stiffener tip stresses also displayed good agreement between experiment and analysis. Slightly higher stresses were predicted in

the analytical model, suggesting the presence of more severe outward bulging than occurred at either of the instrumented locations in the experiments. The kink in the stress plot near the end of the finite element model was the localized stress due to the artificial radial restraint of the nodes in the stiffener adjacent to the ring.

3.6.3 LARGE-SCALE CYLINDER IC4

The large-scale cylinder was analysed in a similar fashion to the previous cases, except that for this model residual stresses had also to be included in the analysis. From the residual strains measured at completion of the model (see Fig 2.3) a value of 60 N/mm^2 (i.e. 21% of yield) was selected as a representative compressive residual stress in the longitudinal direction. Although residual stresses in the circumferential direction could also have been easily included in the analysis, it was not considered necessary since these were compressive and would have had little effect under the tensile hoop stresses induced by the axial loading. A constant compressive stress of 20 N/mm^2 was selected for the stiffener.

In order to represent accurately the distribution of stress across the width of the panel, the number of elements in this direction was doubled, resulting in a mesh of 6x4 elements for the shell. This provided four Gauss points on either side of the stiffener at which the initial stress values were to be specified. A residual stress distribution consisting of a constant compressive stress at the six outermost Gauss points balanced by a larger tensile stress at the two central Gauss point was selected. The compressive stress of 60 N/mm^2 in the shell and 20 N/mm^2 in the stiffener required a tensile stress of 175 N/mm^2 at the central Gauss points to maintain internal equilibrium, and produced the residual stress distribution shown in Fig 3.11. A further discussion of residual stresses is given

in Sect 4.7 of the parametric study.

Only the central bay of the three-bay experimental model was analysed, for which simply-supported boundary conditions were assumed at the ring positions. The finite element analysis was performed twice: in the first analysis an imperfection with a single halfwave in the axial direction was used, the amplitude of which was determined from the experimental imperfection measurements. This gave almost exact agreement with the experimental failure load. However, the failure shape suggested that a three halfwave imperfection may have been critical, and the model was re-analysed with an initial imperfection of this form. According to the relationship described in Sect 3.6.1.2, a reduced amplitude equal to one third of the original magnitude was used in this case. A lower peak load was obtained and this was taken to be the cylinder strength predicted by the analytical model. The load-deflection paths of both finite element analyses are shown in Fig 3.12.

During the experiment the end shortening was measured over the entire cylinder length, but by factoring this deflection in the proportion of the flexibilities of the three bays, it was possible to obtain an estimate of the shortening of the central bay. The experimental load path calculated by this method is also shown in Fig 3.12. Although the agreement with the experimental result is virtually exact for the single wave analysis, the lower, three wave result must be accepted as the predicted strength. Nevertheless, this value is only 8.0% below the actual strength and justifies the claim of good agreement.

The distributions of the longitudinal and hoop stress along the cylinder length measured during the test and predicted by the analysis are presented in Fig 3.13. These stresses were measured in most

detail along four vertical sections of the model, and both the inner and outer surface stresses for each section are presented in the figure. The plotted analytical stresses are the differences between the total stresses at the selected load and the initial stress state at zero load (i.e. after the residual stresses are subtracted) and correspond to the experimentally measured values. Stresses have been plotted for the lines of Gauss points nearest the longitudinal edges of the finite element model.

In the longitudinal stress plots, the general trend appears to be that the surface stresses are approximately equal at the centre of the model, where the curvature is small, and that the inner surface stresses reach a peak near the rings, indicating the presence of an outward bulge. The analytical plots mirror this general behaviour, but the stresses rise to smaller peaks, which occur nearer to the end of the model. This is a consequence of the assumed simple supports at the ends whilst in reality there was continuity across the rings; the experimental stress plots show the reversal of bending near the rings which this produced.

The analytical results predicted a larger difference between the inner and outer surface stresses at the cylinder midlength and a more frequent variation of stress along the cylinder due to the assumed initial imperfection mode. Although the experimental model contained a significant three wave mode, which governed the behaviour, it was superimposed upon other modes. This created a shape which had relatively large bulges near the rings but was reasonably flat in the middle. This shape was reflected in the distribution of longitudinal surface stresses, which differed most at the ends. In the analytical model, in which only a single mode has been included, the surface strains cross more frequently in response to the modulations in the

assumed initial shape.

The hoop stresses are also influenced by the same phenomenon. The midplate stresses are accurately predicted, but the surface values vary more rapidly due to the initial shape.

The stiffener tip stresses are relatively uniform both in the experimentally measured locations and in the analytical model, and agree well.

Fig 3.14 compares the finite element prediction of the buckling mode with the observed buckled shape of the section of the model at which the failure was initiated. As the finite element model is symmetric about the circumferential centreline of the cylinder, only half of the panel length has been drawn. However, the experimental results for the entire length of the central bay of the cylinder are presented for comparison. Although the experimental shape is not as symmetric as assumed by the finite element analysis, the agreement is excellent. The general features of an antisymmetric buckling mode, with inward lobes at the centre of one panel and near the ends of the adjacent one, are present in both figures. The continuity of the shell plating in the experimental cylinder pushed the inward bulge further from the end of the model.

3.6.4 SLENDER SERIES

The cylinders in this series were of two different cross-sections; one contained twenty, and the other forty, stringers. The cylinders with twenty stiffeners failed in local modes, for which the single panel analysis should provide good results. The cylinders with forty stringers, however, failed in overall modes, and in these cases the analytical model should overestimate the strength. Although not strictly applicable in the latter cases, the analysis was applied to

both groups of models.

The initial imperfection magnitudes extracted from the experimental readings and used in the finite element analyses are given in Table 3.4. The analytical and experimental peak loads are summarized in the two axial-pressure interaction diagrams, Fig 3.15, and in Table 3.5.

The predicted strengths for the forty stiffener cylinders under combined and pressure loading exceeded the experimental values. This was not unexpected, since in the experimental cylinders an overall mode developed prior to the local mode to which the analytical model is restricted. For the corresponding axially-loaded cylinder the experimental strength was greater than the analytical result. The analytical model predicted a strength very near the squash load, while the experimental cylinder exceeded it. The difference was relatively small (9.5%) and may have been due to a variation in the value of yield stress.

Better predictions are to be expected for the twenty stiffener cylinders. Fig 3.16 shows the analytical and experimental load-deflection curves for the axially-loaded model. Correlation is excellent, with the analytical result overestimating the experimental strength by less than 3%. In addition, the violent unloading behaviour was also predicted.

The difference between the initial slopes of the analytical and experimental curves of both cylinders (Figs 3.16 and 3.17) can be accounted for, as before, by the different lengths of the experimental and analytical models. Lines 1 and 2 correspond to those described in Sect 3.6.2. Because of the different end rings, the axial stress in the enclosed section of the shell was constant and equal to the

applied stress. This correction has been calculated assuming constant axial stress and zero circumferential strain, and when added to the finite element results gives Line 3, which agrees closely with the experimental stiffness.

Unfortunately, the strength predictions for the two remaining twenty stringer models were poorer. Under hydrostatic loading the difference between the analytical and experimental results was small in absolute terms (0.06 σ_o), but large as a proportion of the experimental value (0.34 σ_{exp}). The combined loading results differed substantially by both measures (0.30 σ_o or 0.44 σ_{exp}).

The discrepancy may be partly due to differences between the initial imperfections in the experiment and the analysis. A more significant cause, however, may be the use of constant stress loading. Under axial loading, the shortening of the loaded curved edge was relatively uniform. The radial deflections of the shell panels grew in the directions of the initial imperfections. Because the cylinder was long and slender, the Poisson bulging effect was relatively minor.

The addition of external pressure superimposed inward radial deflections of the shell. When an inwardly imperfect shell panel deflects further inward the distance between its ends decreases. A panel which is initially bowed outwards, on the other hand, will become longer as it deflects inward. This difference creates the nonuniform end shortening in the broad-panelled cylinders under combined and hydrostatic loading, and is probably the reason for the lower predicted strengths in these cases. In the experimental models this difference is not allowed to develop by the heavy experimental end rings and a constant strain loading would be a closer approximation to the boundary conditions.

Once again, a detailed comparison of the stress distribution was carried out for the two axially-loaded models. The results are presented in Figs 3.18 and 3.19 for the twenty and forty stiffener models respectively. As before, the midplate stresses agree well in both cases, although the surface stresses do not correlate as closely. In particular, the surface hoop stresses in the broad-panelled model are significantly overestimated by the analysis. This was due to the initial shape of the analytical model, which did not correspond precisely with that of the experimental cylinder. Nevertheless, the lowest value of peak load was obtained with this single halfwave imperfection rather than with a higher mode of reduced amplitude. The stiffener stresses agree very well if the dubious experimental readings for cylinder A are discounted.

3.7 C O N C L U S I O N S

In this chapter the finite element method has been applied to the analysis of stringer-stiffened cylindrical shells. By limiting attention to those geometries in which failure occurs in a local deflection mode, it was possible to reduce the problem size to that of a single stiffener and shell panel. This enabled the relatively inexpensive analysis of the experimental models of the previous chapter to be carried out.

The finite element discretization of the structure can be carried out to any degree of refinement to produce the required detail, both in the definition of the problem and in the description of the results. However, since the aim was eventually to use the analysis for a large parametric investigation, economy was always an important consideration. Convergence studies were carried out which showed that a moderate mesh of eight-noded isoparametric shell elements would

provide results of acceptable accuracy.

All the experimental models described in the previous chapter were analysed using the model. Very good correlation was obtained for the entire DnV series of small-scale models. Good predictions were obtained even for those cylinders that failed in overall modes for two main reasons. Firstly, the overall buckling modes usually contained a large number of circumferential halfwaves, which meant that the analytical assumption of one halfwave per panel was not grossly in error. Secondly, the models were quite strong and failed after plasticity had spread considerably. In such cases the failure load is governed more by the loss of material stiffness than by geometrically nonlinear behaviour. Consequently, the allowable deflection modes, provided they are not too far in error, will not significantly affect the predicted behaviour.

The large-scale cylinder was analysed by modelling a panel in the central bay of the cylinder and incorporating residual stresses. Its behaviour was predicted accurately, both in terms of peak strength and deflection mode.

The poorest correlation was obtained for the cylinders of the slender series. The narrow-panelled experimental models had failed in overall modes and good correlations with the analysis was not expected. The strength of the axially-loaded model was predicted quite accurately for the reasons given above. The pressure and combined loading cylinders, however, failed elastically, and in these cases modelling the precise deflection mode is important if accurate strength predictions are to be made. The single panel analysis imposed too severe a limitation on the allowable deflected shapes and overestimated the strength of these cylinders.

The broader-panelled experimental cylinders failed in local modes, for which modelling of a single panel was more appropriate. Once again, the strength of the axially-loaded cylinder was predicted accurately, but the combined and pressure loaded analyses underestimated the strength of the models. The reason in this case was the use of the more conservative constant stress loading, which did not represent the experimental end conditions accurately. Nevertheless, for reasons to be discussed in the next chapter (Sect 4.2.4), it was selected in the parametric study for representing the boundary conditions in an internal bay of a long cylinder.

Comparisons were carried out, wherever possible, on the basis of deflected shape and stress distribution. The agreement was usually good, but could have been improved by using initial shapes for the analytical models closer to the experimental imperfections. Instead, a single mode imperfection was incorporated in each analysis. This produced a somewhat oversimplified distribution of surface stresses and radial deflections compared to the experimental models, in which a number of modes were superimposed. However, it was the procedure to be adopted in the parametric study and was also used here in order that its effect could be assessed.

In general, the method produced close agreement with the experimental results. In those cases for which the agreement was poorer the reasons for the discrepancy were established. Provided it is applied only to cylinders which do not fail in an overall mode, the analysis should provide accurate and detailed results for the parametric investigation.

An important observation was made when the experimental imperfection results were re-examined for guidance in the selection of magnitudes for higher mode imperfections. It was found that in all

models an inverse proportionality existed between each axial wave number and its Fourier coefficient.

Table 3.1 PRELIMINARY CONVERGENCE STUDY

R	L/R	N	Imperf.	Elements	Peak stress (N/mm^2)
200	1	40	Perfect	3x2x2	240.6
"	"	"	"	6x2x2	239.4
"	"	"	"	12x2x2	239.9
500	1	40	Perfect	3x2x2	229.9
"	"	"	"	6x2x2	224.3
"	"	"	"	12x2x2	214.2
200	1	40	t (anti)	3x2x2	237.2
"	"	"	" "	6x2x2	236.5
500	1	40	t (anti)	3x2x2	193.8
"	"	"	" "	6x2x2	187.7

Table 3.2 CONVERGENCE STUDY

R	L/R	N	Imperf.	Elements	Peak stress (N/mm^2)
200	0.25	20	t (anti)	6x2x2	285.4
"	"	"	" "	6x4x2	271.5
600	1.0	60	t (anti)	6x2x2	307.8
"	"	"	" "	12x2x2	290.0
200	0.25	60	t (anti)	6x2x2	326.9
"	"	"	" "	6x2x4	326.8

Table 3.3 IMPERFECTION MODE STUDY

Cylinder	DnV11	DnV8	DnV7
Imperfection	Peak loads (N/mm^2)		
Perfect	337.7	377.8	
Outward barrel	336.4		
Inward barrel	236.4		
"Panel" (antisymmetric)	110.5	242.7	341.3
"Panel" + outward barrel	111.5	250.1	339.2

Imperfection magnitude in all modes: cylinder 11 0.40 mm
cylinders 7 & 8 0.27 mm

Table 3.4 IMPERFECTIONS USED IN THE ANALYSIS

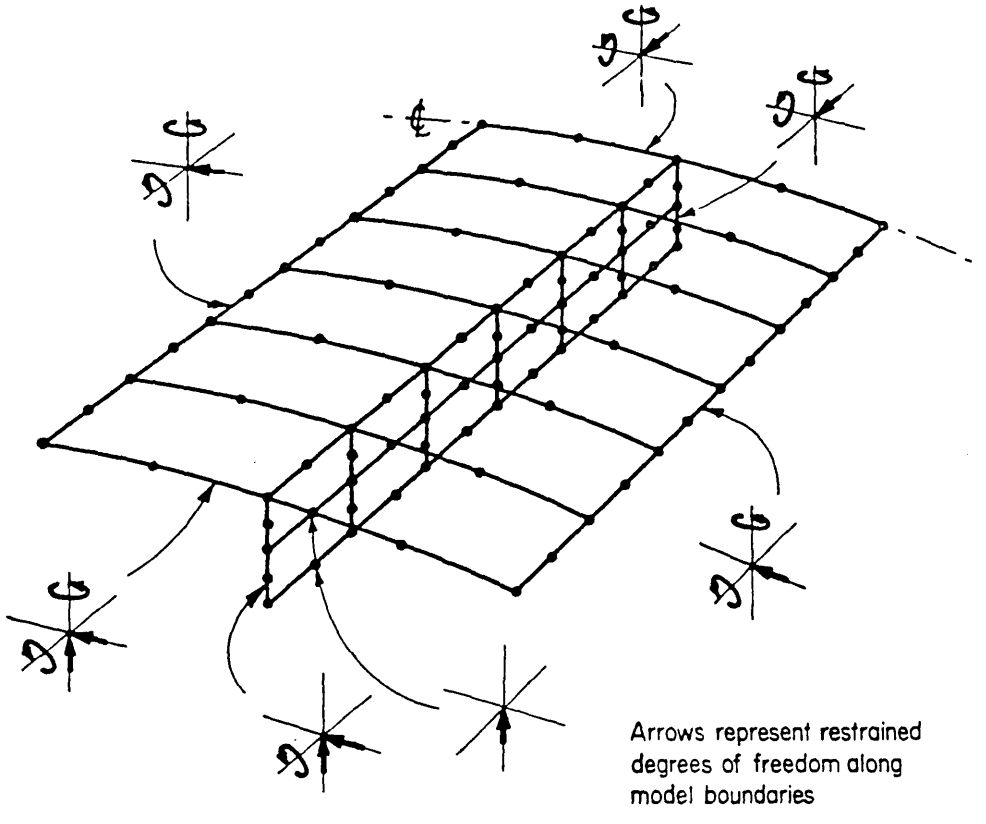
Cylinder	Shell	Stiffener
IC4	3.00	0.75
1-4	0.20	0.10
5-8	0.24	0.12
9-12	0.40	0.24
A	0.30	0.14
B	0.24	0.15
C	0.28	0.22
E	0.30	0.25
F	0.24	0.22
G	0.30	0.24

All dimensions in mm

Table 3.5 EXPERIMENTAL AND ANALYTICAL FAILURE LOADS

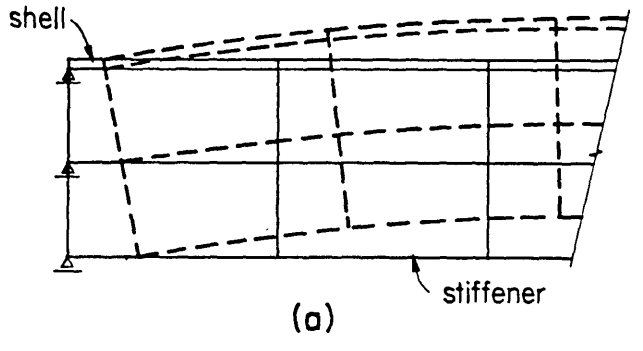
Cylinder	1	2	3	4	5	6	7	8	9	10	11	12	IC4	A	B	C	E	F	G
Experimental																			
σ_x (N/mm^2)	327	136	39	336	65	0.6	347	290	46	365	0.1	184	251	284	26	246	400	26	240
σ_θ (N/mm^2)	0	346	363	237	165	184	0	148	116	0	121	92	0	0	56	37	0	60	39
Failure mode	(l)	(l)	(l)	(l)	(l)	(o)	(o)	(l)	(l)	(o)	(l)	(l/o)	(l)	(l)	(l)	(l)	(o)	(o)	(o)
(n)						13	12			13		8					9	11	10
Analytical																			
σ_θ/σ_x	0	2.52	∞	.703	2.52	∞	0	.511	2.54	0	∞	.498	0	0	2.17	.150	0	2.38	.167
σ_x (N/mm^2)	338	123	0	285	62	0	341	234	42	193	0	193	231	297	17	137	362	36	327
σ_θ (N/mm^2)	0	311	360	201	156	161	0	124	108	0	111	96	0	0	37	21	0	84	53
% Difference	3.4	-9.6	-0.8	-15.2	-4.6	-12.5	-1.7	16.2	-8.7	-3.7	-8.3	4.9	-8.0	4.6	-34	-44	-9.5	40	36

Failure mode: (l) local
(o) overall
n approximate number of circumferential halfwaves

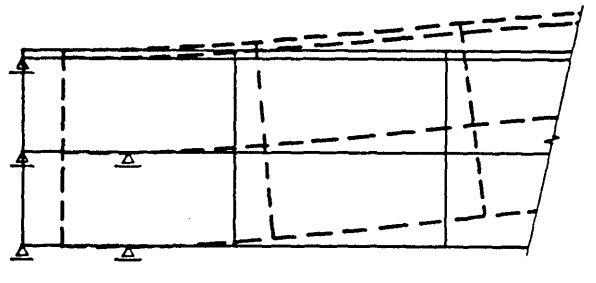


Finite element model
(experimental correlation)

Fig. 3.1



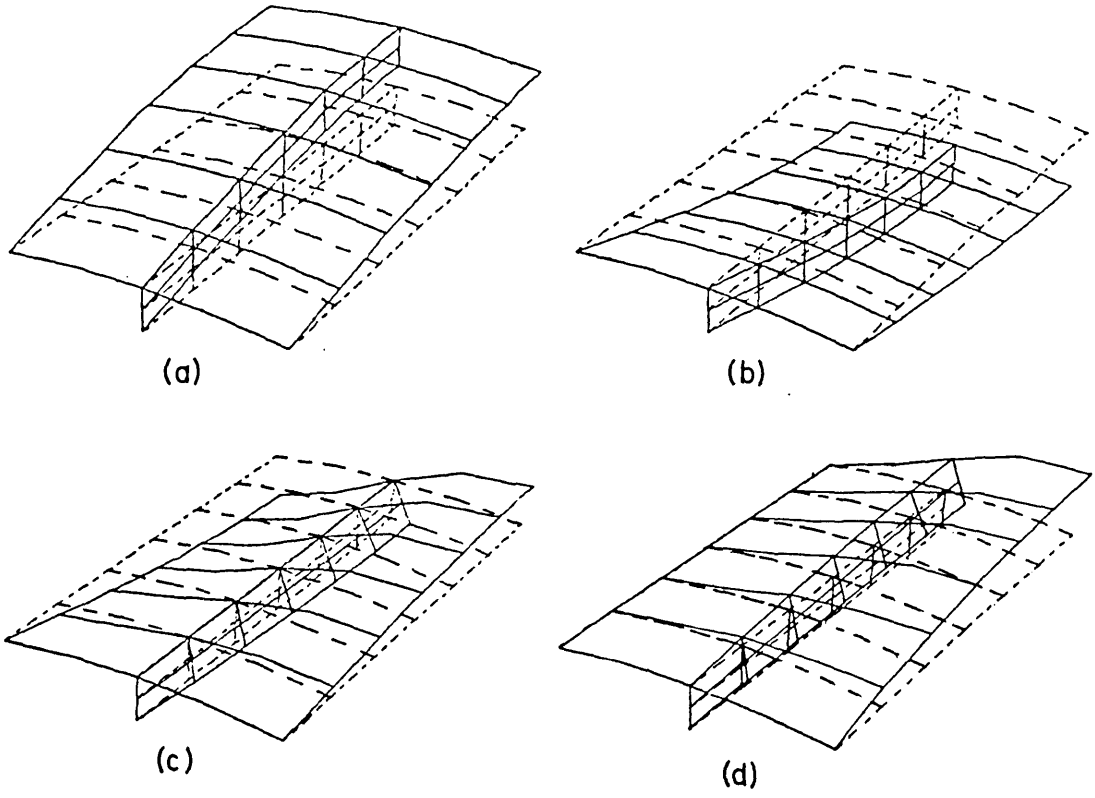
(a)



(b)

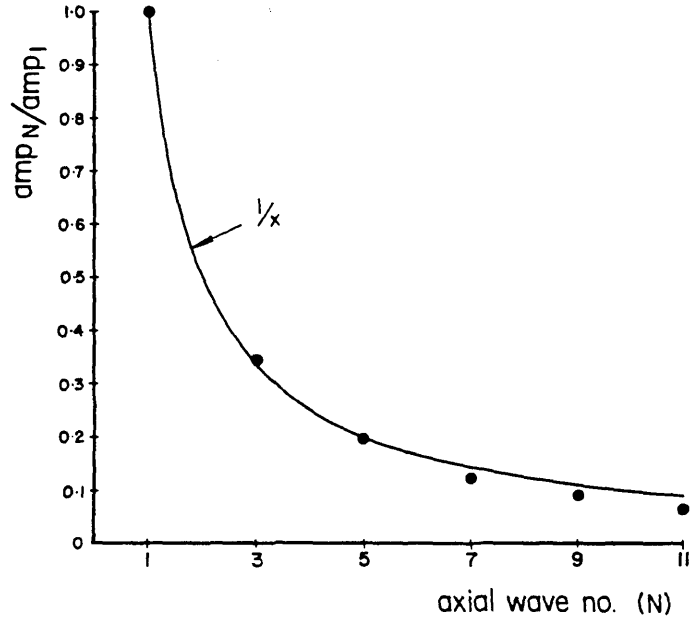
Boundary conditions at end of model

Fig. 3.2



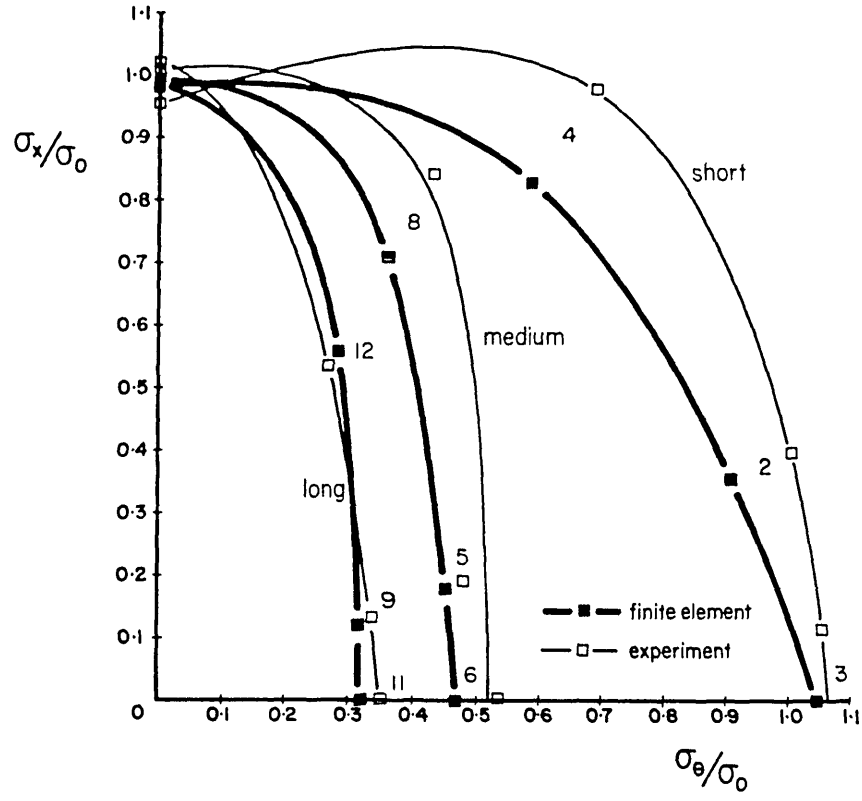
Initial imperfection modes

Fig. 3.3



Imperfection amplitude v's wave number

Fig. 3.4



Interaction curves
DnV series

Fig. 3.5

Load-deflection paths for cylinder 1

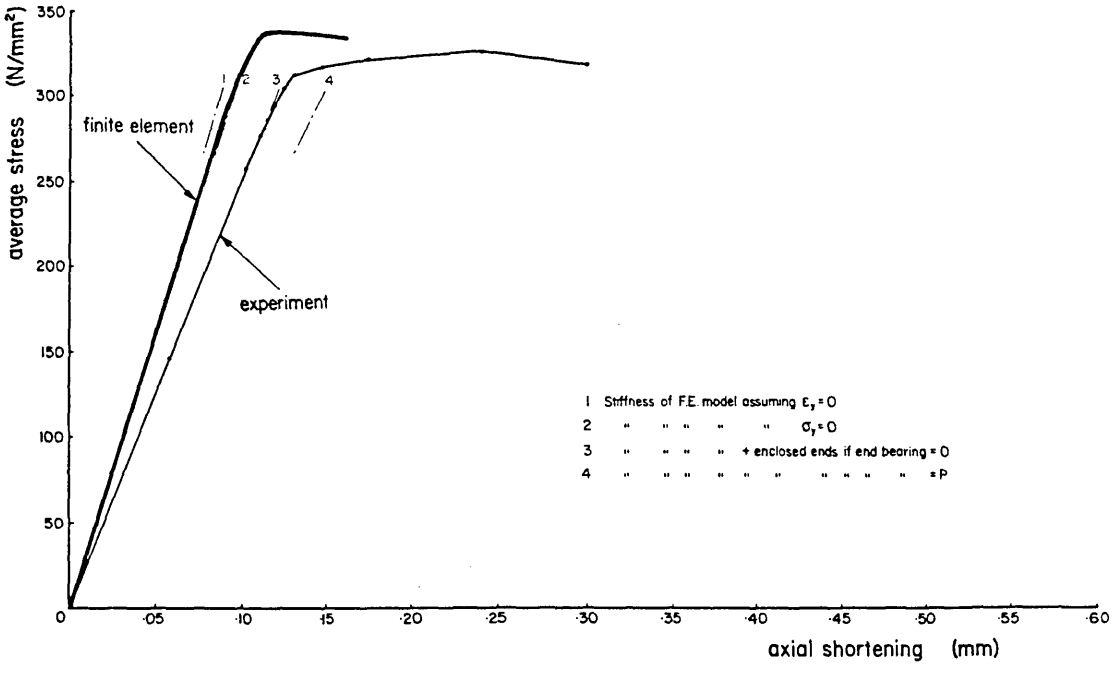


Fig. 3.6

Load - deflection paths for cylinder 7

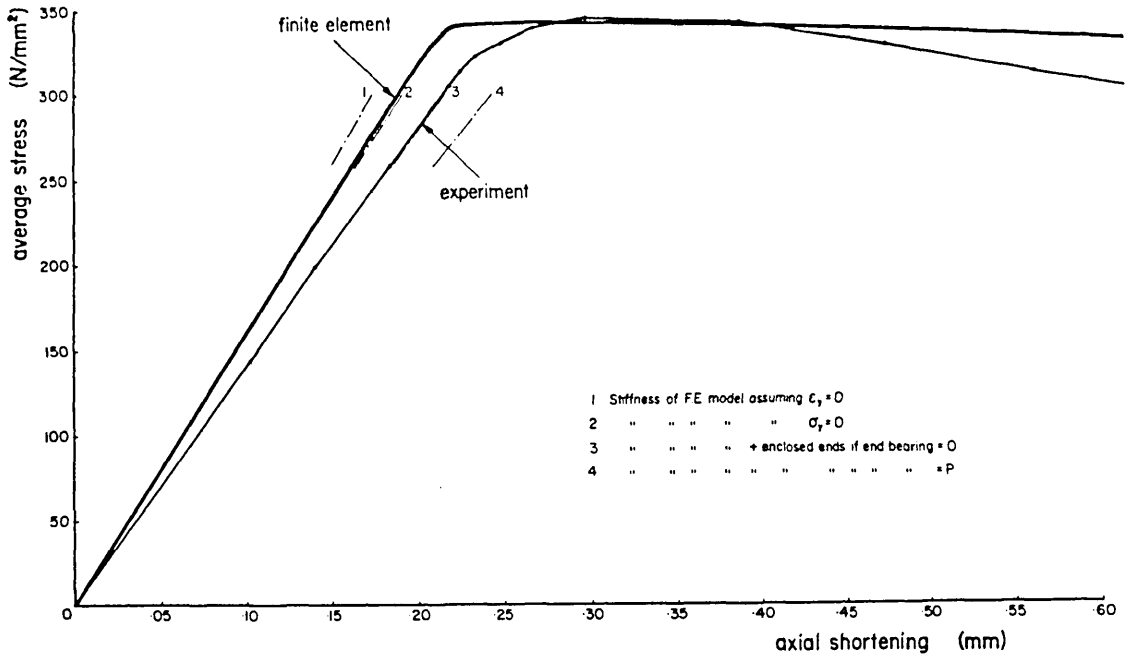


Fig. 3.7

Load - deflection paths for cylinder 10

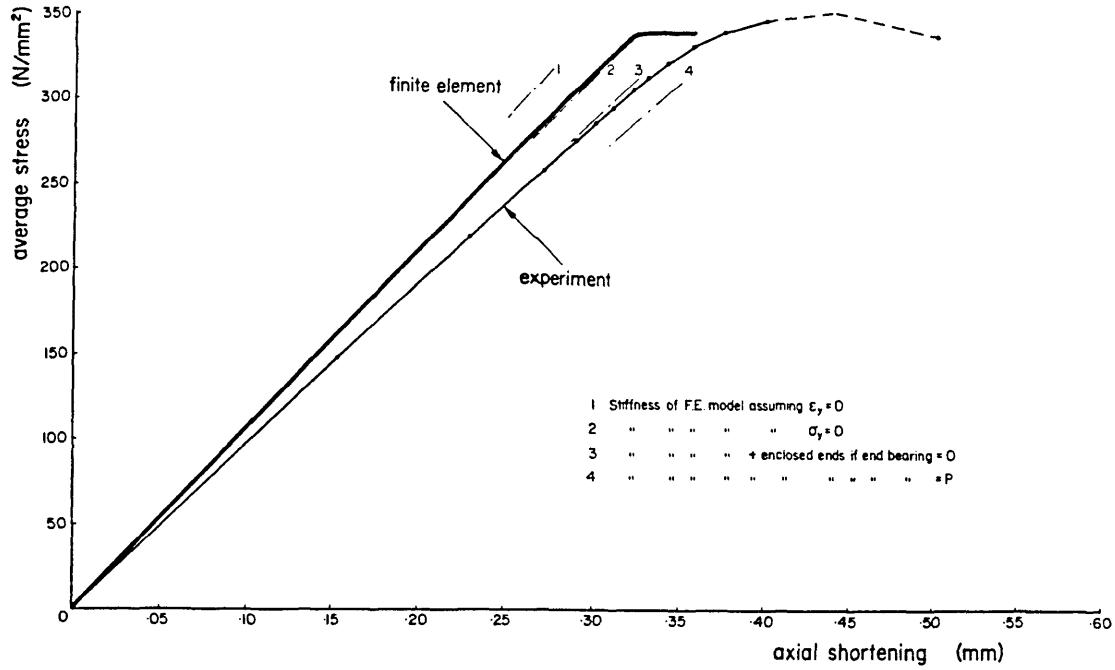
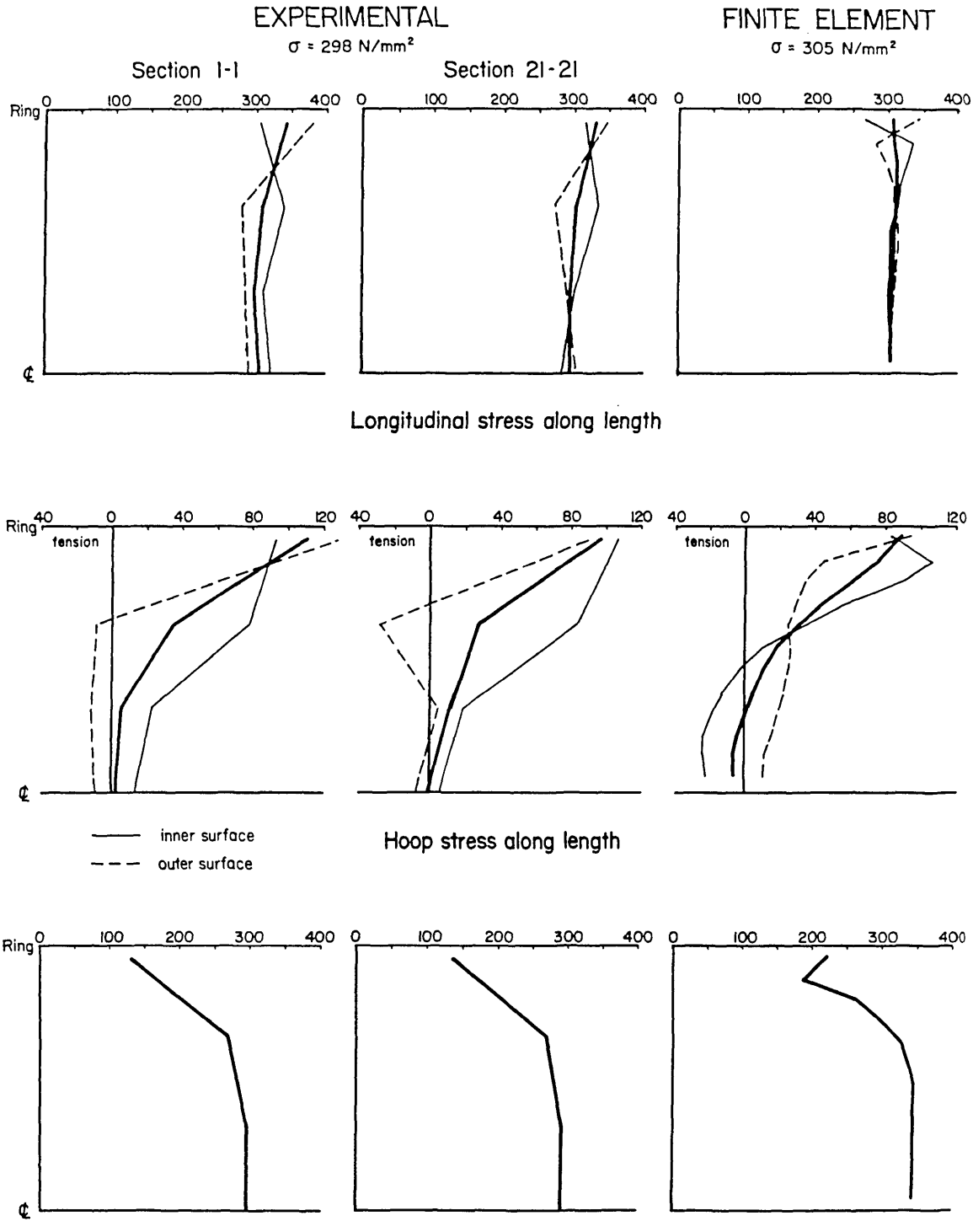
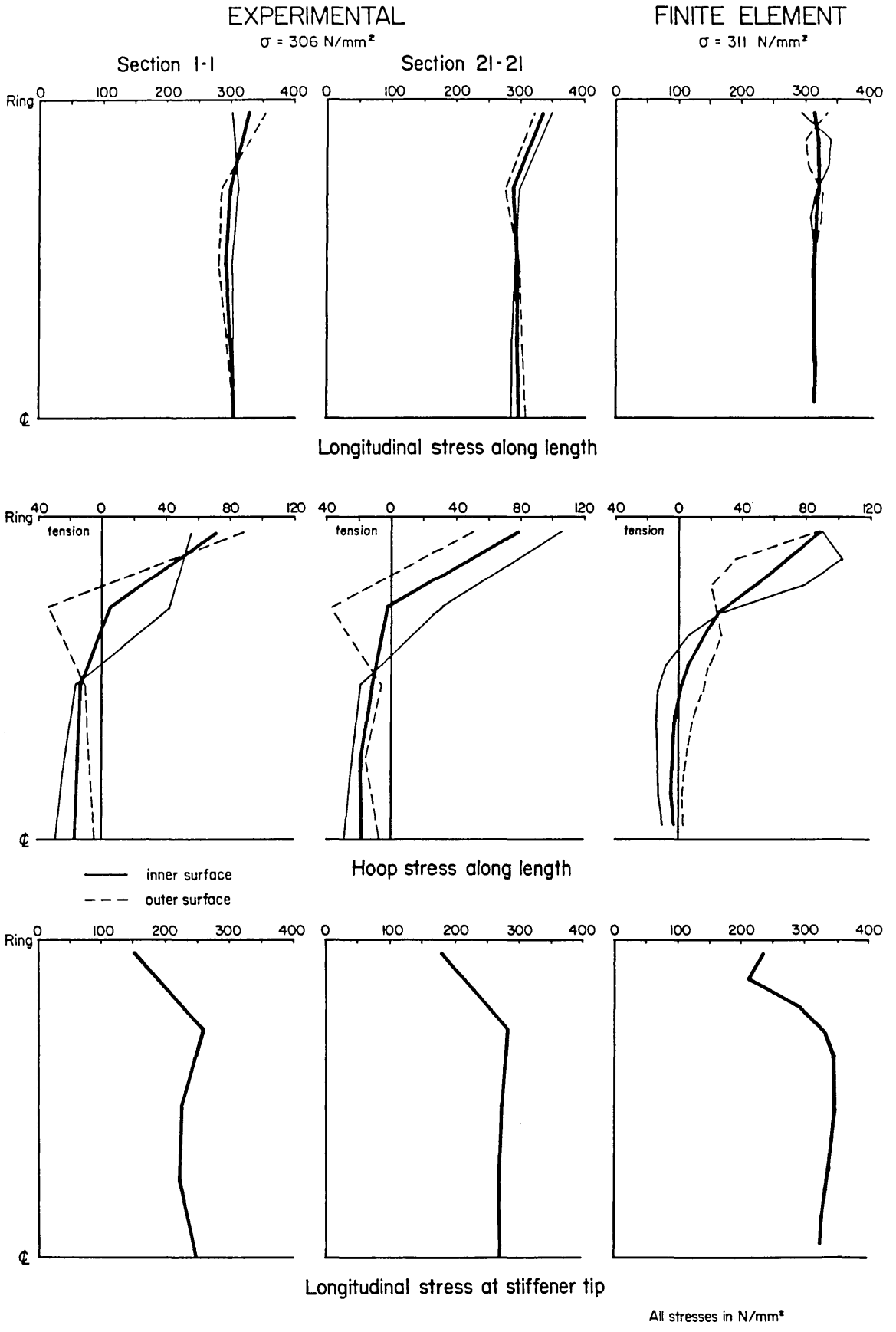


Fig. 3.8



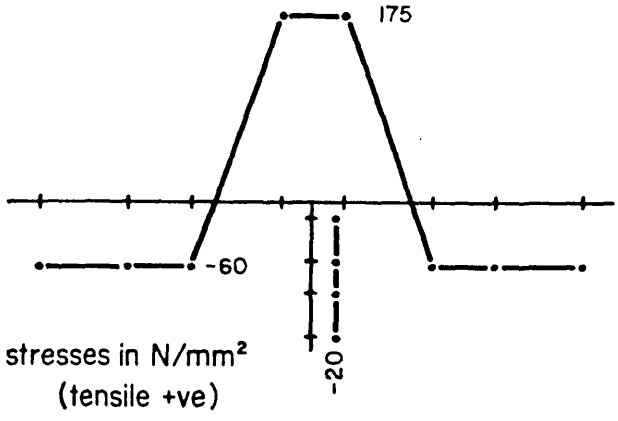
Experimental and analytical stress distribution for model 7

Fig. 3.9



Experimental and analytical stress distribution for model 10

Fig. 3.10



Assumed residual stress distribution for analysis of model IC4

Fig. 3.11

Load-deflection paths for cylinder IC4

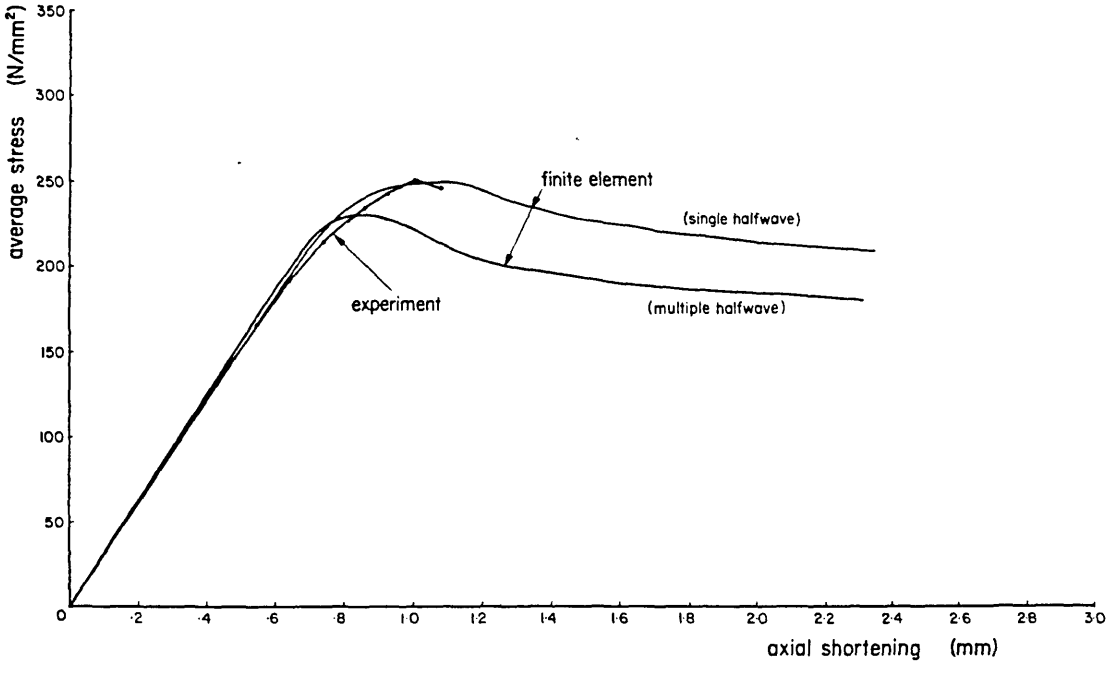


Fig. 3.12

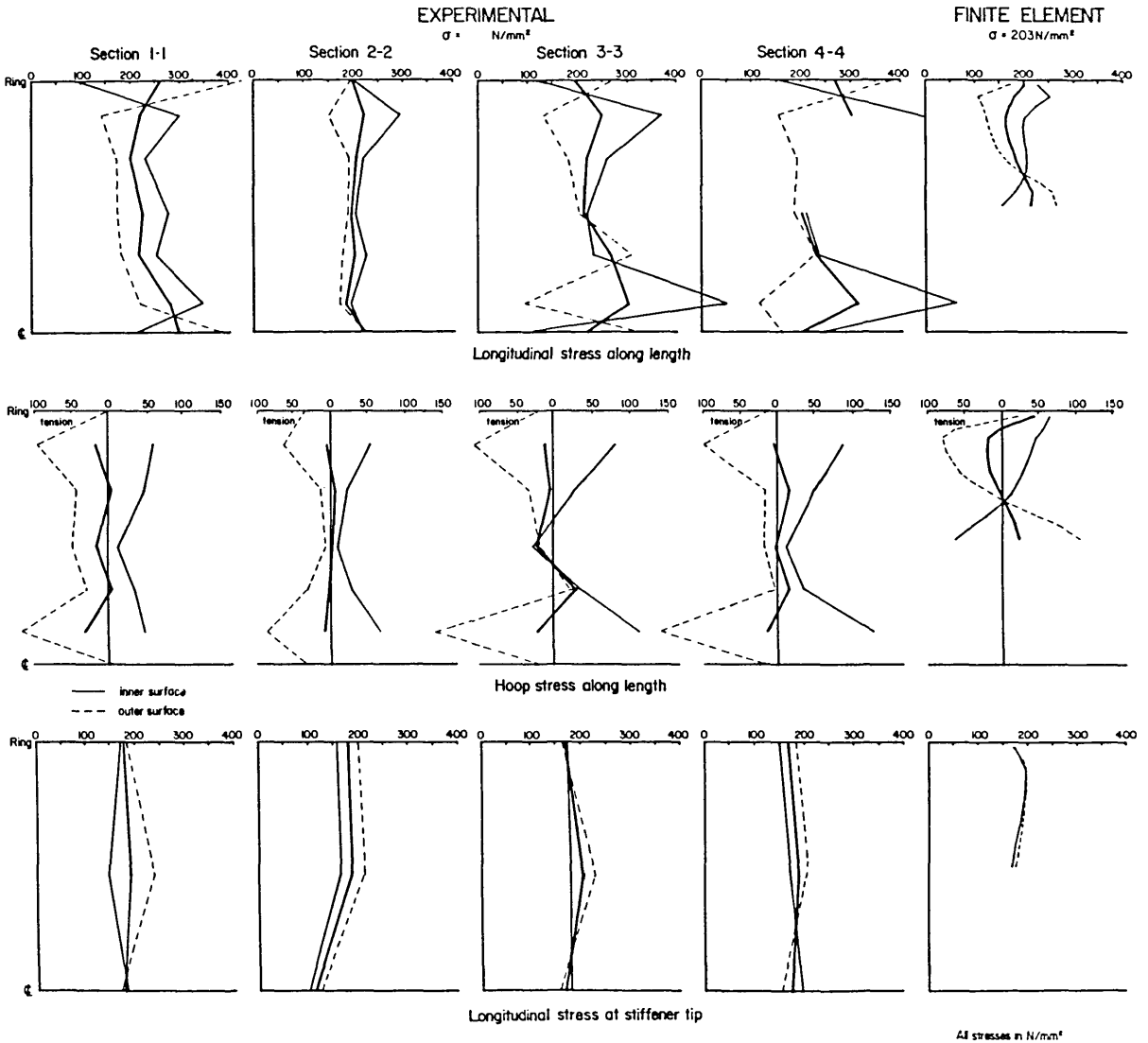
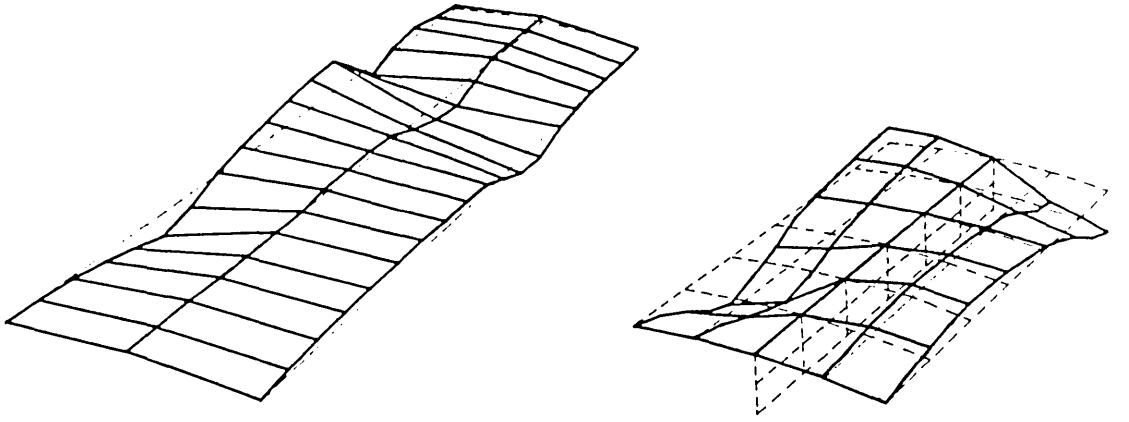


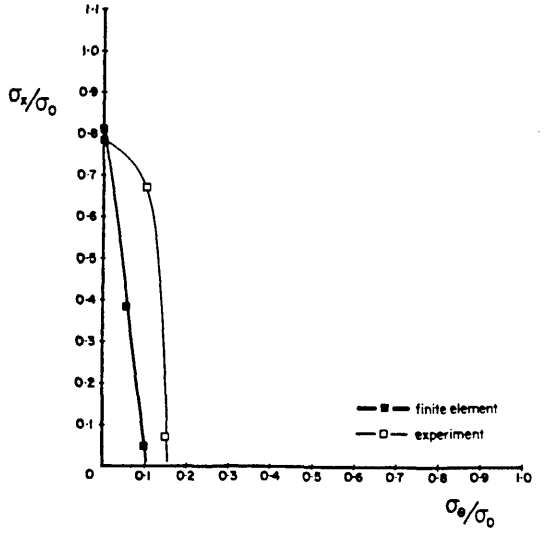
Fig. 3.13 Experimental and analytical stress distribution for model IC4



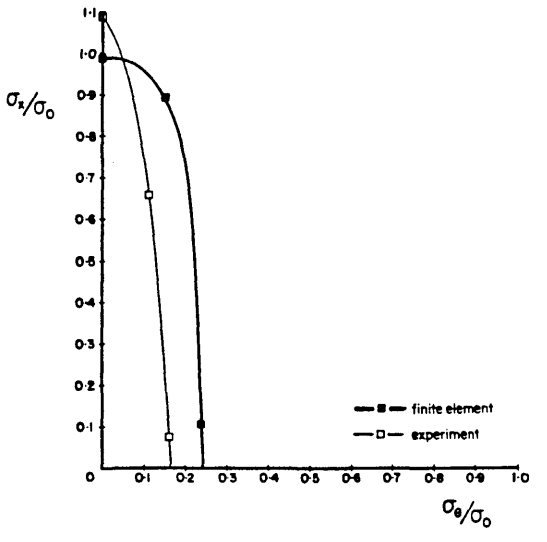
Experimental Analytical

Deflected shape of model IC4

Fig. 3.14



Interaction curves
slender series (N=20)



Interaction curves
slender series (N=40)

Fig. 3.15

Load-deflection paths for cylinder A

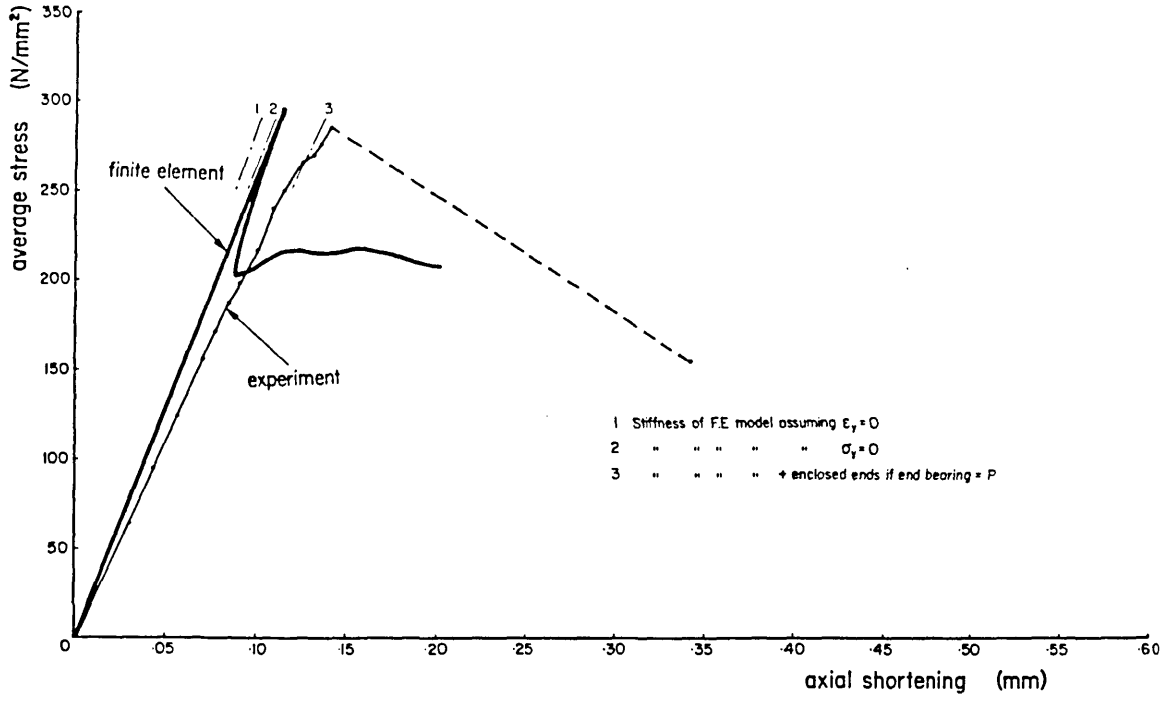


Fig. 3.16

Load-deflection paths for cylinder E

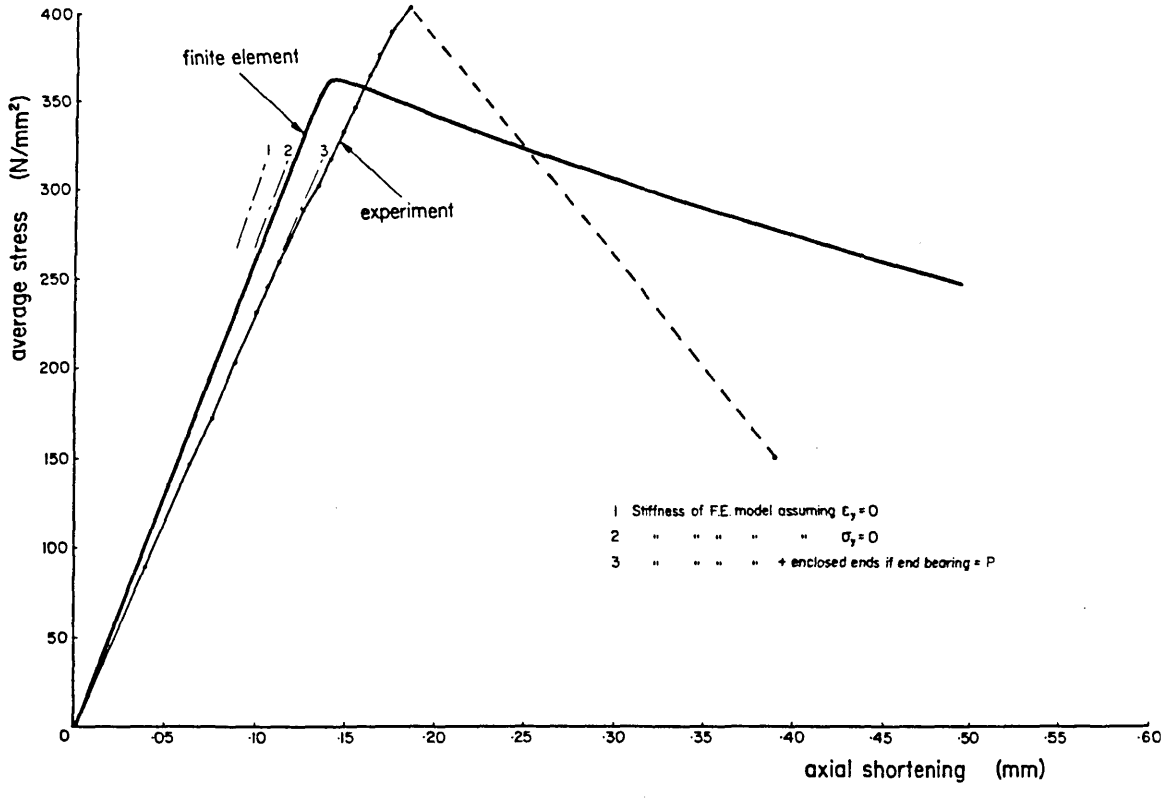
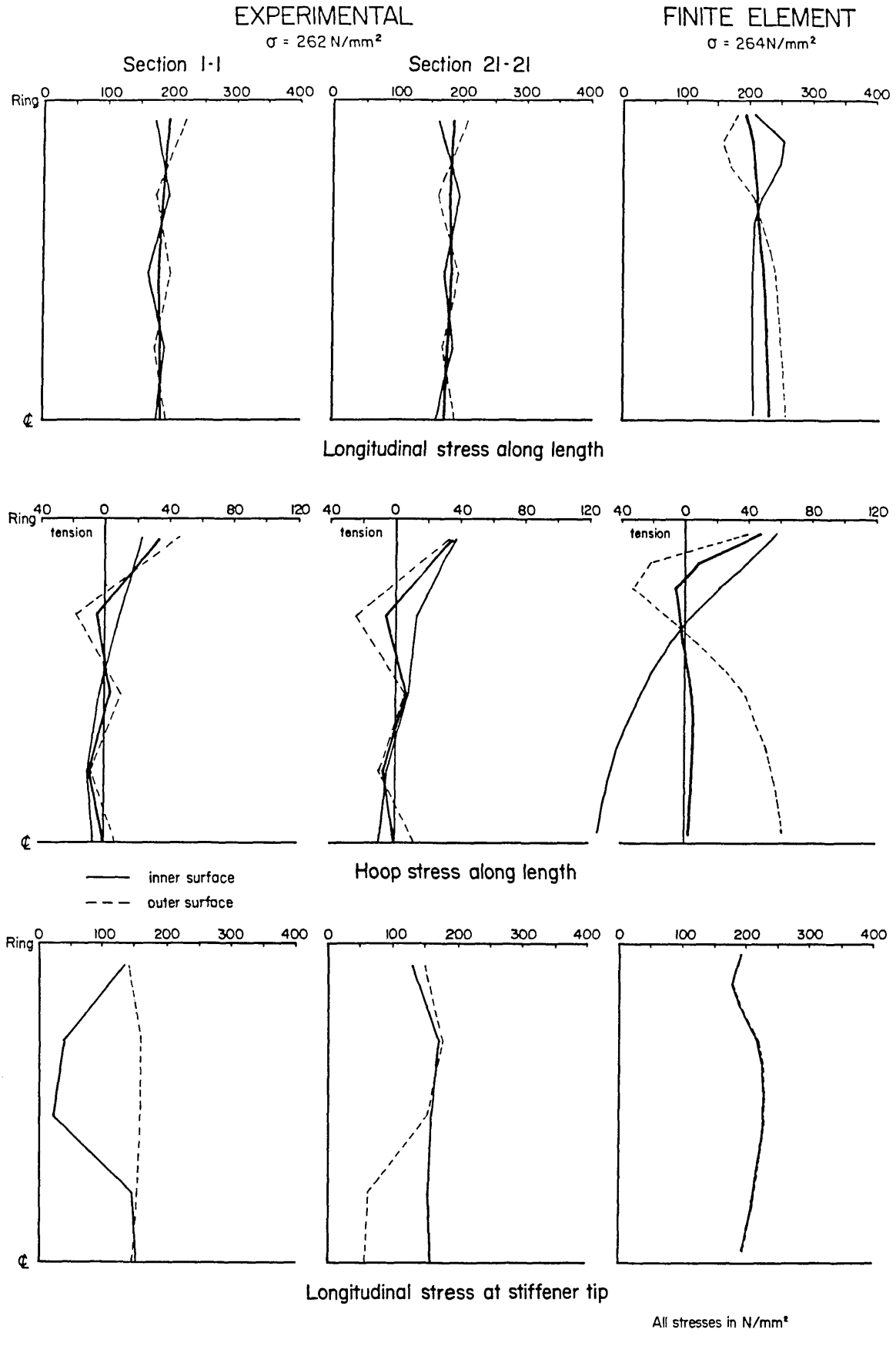
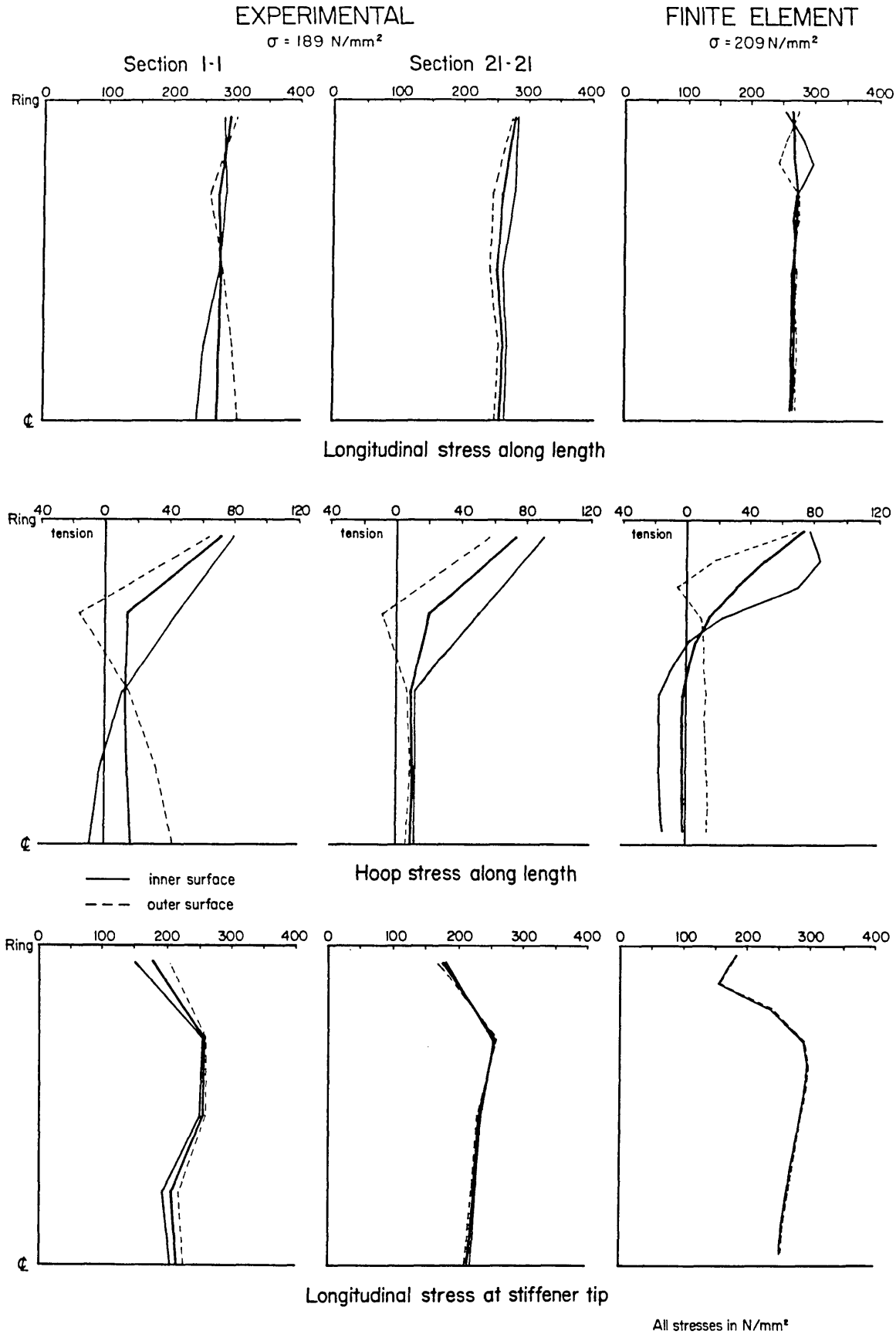


Fig. 3.17



Experimental and analytical stress distribution for model A

Fig. 3.18



Experimental and analytical stress distribution for model E

Fig. 3.19

CHAPTER FOUR

PARAMETRIC STUDY

4.1 INTRODUCTION

The experience and confidence gained from the correlation between the numerical and experimental results suggested the possibility of proceeding to a systematic investigation of cylinder behaviour over a wider range of parameters. It should be possible to include in the study all cylinders that fail in modes which are repeated in each panel (in practice, these modes may only develop in a small number of panels of the cylinder). The allowable deflections will include not only local buckling of the shell and of the stiffener, but a number of other modes. Because no constraints are placed upon the deflection of the shell-stiffener intersection, interacting modes, axisymmetric modes, and "hungry horse" modes are all possible.

The method cannot handle overall buckling in which several stiffeners are contained within each lobe. It is of paramount importance, therefore, to determine the range of parameters over which the method can be successfully applied. The range will be fairly broad in offshore engineering, where the tendency is to minimize the number of stringers and to use cross-sections of moderately high inertia (e.g. angles and tees). Both effects result in the buckling stresses for overall modes being higher than for local modes.

It is also general practice in offshore structural design to use heavy ring stiffeners which will not participate in the buckling mode of the cylinder. This feature, by confining the buckles to the inter-ring spacing, makes the analysis of a single bay of the stiffener

adequate. Of course, the shell plating is continuous over the ring and a carryover effect exists between adjacent bays, but the neglect of this relatively minor effect by the assumption of simple supports at the rings should produce moderately conservative results.

For the cases to which it is applicable, the analysis should provide an accurate and detailed description of cylinder behaviour. It relies only on a few basic assumptions, the more important of which relate to the symmetry of deflections. These are supported by observation and do not impose any significant restrictions on the allowable deflections of the structure. The major advantage of the analysis lies in its ability to model many aspects of behaviour and to include effects such as imperfection mode and magnitude, and residual stresses.

Alternative analytical or mechanistic approaches require more significant assumptions to be made, and are limited either in their range of application or in the descriptive detail that they can furnish. This is not to belittle their usefulness; it is not proposed that the finite element analysis replaces them as a design method. But it is an extremely valuable research tool, providing data at far more moderate expense than the alternative of experimental testing.

The objective in this chapter is to conduct a large parametric study covering as broad a range as possible of the geometries used in offshore structural engineering. The results will be described and assessed in detail. However, comparisons with design rules will be the subject of the following chapter.

4.2 PRELIMINARIES

4.2.1 RANGE OF PARAMETERS

An extensive study was undertaken, in which geometric variables, type of loading, magnitude and form of initial imperfections and level of residual stresses were varied. The values of the geometric parameters were selected to be typical of offshore structural designs. Surveys of currently employed geometries in Refs 200 and 211 proved useful in this respect.

All models had a unit shell thickness; the radius was 200, 400 or 600 and the length equal to 1/4, 1/2 or 1 times the radius. Each model had 20, 40 or 60 stringers. Although in practice angle or tee stiffeners are often used, it was assumed for this study that the stringers were flat bars in order to reduce the number of variables. For the type of steel used in these analyses (Sect 4.2.3), the maximum stringer d/t allowed by the DnV [153] and draft ECCS [155] rules is 9.7 and 8.6 respectively; in the major part of this study a constant value of 10 was adopted. The actual dimensions of the stringers were chosen to give a stiffening ratio, a_s, equal to either 0.1, 0.3 or 0.5. The effect of using more slender stringers (d/t = 20) was also briefly investigated.

The models were analysed under axial load, lateral pressure (i.e. no axial compression) and combined loading, in which the pressure-induced hoop stress was usually equal to 0.4 times the average axial stress (i.e. $\sigma_\theta/\sigma_x = 0.4$). The factor 0.4 was selected because in most cases it gave a convenient point for the interpolation of interaction curves. For several geometries an additional load case with $\sigma_\theta/\sigma_x = 2.5$ was also investigated.

Most analyses were carried out for initially stress-free models;

however, some cylinders with residual compressive stresses equal to 30% of yield were also analysed.

4.2.2 PRELIMINARY DETERMINATION OF EXTENT OF STUDY

Not all combinations of the geometric parameters were investigated; many were omitted for economy and because they would provide little additional information which could not be gleaned from elsewhere; however, other cases were eliminated because they represented cylinders in which an overall buckling mode would predominate.

At the outset of the study, it was necessary to obtain an estimate of the range of geometric parameters over which the single panel model would be applicable. This would be checked later using finite element runs, but at this stage a simple analytical estimate was needed.

In a stiffened shell of given geometry (i.e. R, L and N), the buckling mode can be altered by changing the stiffness of the stringers. With light stringers overall buckling is likely; using progressively heavier stiffeners will increase the overall buckling stress and eventually induce local shell buckling. It is useful to bound the range of parameters over which local buckling is likely to occur by determining, for a shell of given radius, length and number of stringers, the size of the stiffeners required to produce equal buckling stresses in the local and overall modes. Of course, mode interaction may complicate behaviour in this region, but this need not be of concern, since all that is required at this point is a preliminary estimate of which cases to exclude. A more precise verification of the range of validity of this analysis will be obtained later using the finite element method.

Expressions for the elastic critical stresses for local and overall buckling of stringer-stiffened cylinders under axial compression and external pressure were derived by Steen et al [164] using the principle of stationary potential energy. Since in the present study the stringers were of given proportions (d/t = 10) the stiffener section properties and, finally, the buckling stress expressions could be formulated in terms of the stiffening ratio a_s. Equating the local and overall buckling stresses gave expressions for a_s, in terms of the other geometric variables, at which the two forms of buckling would occur simultaneously. The expression in the case of axial compression could be solved explicitly, whilst for pressure, an iterative solution was necessary. Appendix A outlines the derivation of these expressions.

For each geometry and type of loading the value of the stiffening ratio for which the local and overall buckling stresses were equal provided a bound to the extent of the parametric study: combinations of geometries with stiffening ratios less than the calculated value were excluded from the investigation.

Fig 4.1 illustrates on a single chart the range of principal variables in the current study. The shaded areas are the cases eliminated by the procedure described above. As would be expected, the inappropriate geometries were the longer cylinders with a large number of light stringers.

It is significant to note that none of the thirteen stringer-stiffened cylinders described in the survey of Ref 211 fall into this excluded region. The frequent use in practice of angle or tee stiffeners increases the inertia of stringers, thereby reducing the stiffening ratio below which overall buckling predominates and

extending the range of geometries for which the present method of analysis may be suitable.

4.2.3 MATERIAL PROPERTIES

Properties typical of grade 50 steel, the material most commonly employed in offshore structures, were adopted for all the finite element runs. The values used were:

$$E = 210 \text{ kN/mm}^2$$

$$\sigma_o = 350 \text{ N/mm}^2$$

$$v = 0.30$$

4.2.4 BOUNDARY CONDITIONS AND LOADING

In general, the boundary conditions were similar to those used in the previous study of the experimental models. However, the curved loaded edge which was previously clamped to simulate the effect of the heavy experimental end rings, was simply supported for the parametric study, Fig 4.2. This more conservative boundary condition was used to model more closely the situation at an internal panel of a long stiffened cylinder.

In the experimental models the end rings restrained the radial deflections at the ends of the shell. In an orthogonally-stiffened cylinder, small radial deflections of the rings are possible. However, since it was assumed that the rings do not participate in the failure mode, it is more demanding on the shell to apply complete radial restraint, rather than elastic support, along the curved loaded edge. As well as avoiding the selection of specific properties for the ring, the former situation will produce more severe bulging of the shell, and was the one adopted here.

In Sect 3.4.4 it was mentioned that a uniform stress, as opposed

to uniform strain, loading would be used both for the experimental correlation and for the parametric study. Whilst the difference between the two usually was small, there was no doubt that the constant strain loading would have been a better approximation of the experimental boundary conditions. For the parametric study, however, where the intention was to model an internal bay of a cylinder, the choice was less clear.

For example, as an axially-loaded shell panel that initially has an outward imperfection bulges outward due to the Poisson effect the distance between is curved ends will decrease. If the initial imperfection is inward the length will decrease by less or may even increase. Under external pressure the situation is reversed, with an outwardly imperfect panel tending to get longer and an inwardly imperfect one tending to shorten. A "chequerboard" pattern of inward and outward imperfections may, therefore, induce an in-plane waviness of the circumferential cross-sections. The stiffness of the rings in opposing this mode is small. It may be unconservative, therefore, to assume that the circumferential cross-section at the ring will remain plane throughout the loading history, which is the implication of a constant strain loading.

It cannot be claimed that the constant stress loading is an exact representation of the real situation; only that it is a conservative one, whereas the constant strain loading is unconservative. The most accurate approach would be to analyse a multibay model, in which the edge of the outer panel is loaded under constant strain. This would then enable the edges of the inner bay to deflect as required. However, such a modification more than doubles the cost of the analysis and is, therefore, unattractive, if not prohibitive. In any case, the difference in behaviour is probably small up to the peak

load, beyond which the constant stress loading will underestimate the degree of load redistribution possible.

Under pure pressure, the curved edges of the model were free to pull in along the length of the panel. The alternative produces a tension field in the shell, which is neither representative of real behaviour nor consistent with the other loading cases.

In the combined loading cases proportional loading was used, in which the axial and pressure components of the load remained in the same ratio throughout the load path.

4.2.5 INITIAL IMPERFECTIONS

4.2.5.1 Imperfection magnitude

Of primary importance in the behaviour of cylindrical shells is the magnitude of initial imperfections. It is difficult, however, to formulate a standard measure of imperfection to be applied over the entire range of parameters to be considered. For example, if the imperfection amplitude were defined in terms of the shell thickness, it would be relatively larger in short, stocky cylinders than in long, slender ones. Alternatives using other geometric variables encounter similar problems.

For this reason, it was decided to base the initial imperfection magnitudes to be used in the study on the tolerances specified in the DnV rules. These are widely used specifications, which, through the use of several tolerance measurements, give an indication of what is currently accepted as a good level of workmanship. It would be useful to obtain predictions of the strengths of the poorest cylinders which still comply with these requirements.

The DnV Rules [153], in their specification of tolerances, make

no distinction between stiffened and unstiffened cylinders. The 1982 DnV Classification Notes [155] offer a more detailed assessment of tolerances specifically for stiffened cylinders, and will be used here. Tolerances are given for the local out-of-roundness and out-of-straightness of the shell, the radial misalignment of the stringer stiffeners and the out-of-straightness of the stringers. The tolerances are specified as allowable imperfections over certain gauge lengths, and are summarized in Fig 4.3. These gauge lengths will not generally be equal to the corresponding cylinder dimensions. In particular, a cylinder can have an imperfection of larger amplitude than the corresponding tolerance, provided the tolerance is to be measured over a gauge length less than the wavelength of the imperfection. It is necessary, therefore, to "scale up" (or scale down) the tolerance to find the equivalent imperfections across the corresponding model dimensions.

Throughout this study the initial imperfections were assumed to be of a sinusoidal shape, and the "scaling up" therefore involved finding the largest amplitude sine wave, which, when measured over the particular gauge length, would meet the specified tolerance. This is illustrated in Fig 4.4 (a) for a single halfwave imperfection. Fig 4.4 (b) deals with the case, to be considered in a later section, in which a higher mode imperfection is used.

With the method established by which specified tolerances are extrapolated to imperfection amplitudes, it was necessary to determine the maximum imperfection, of whichever mode was to be used, which would still satisfy all the tolerance requirements. The imperfection amplitudes for the various cylinders were determined assuming the single wave antisymmetic mode (Fig 3.3(c)) to be the form of initial imperfections; the validity of this assumption was investigated more

fully later (Sect 4.2.5.2).

Three types of shell tolerance are specified in the Notes. The first is the out-of-straightness of a meridional section, illustrated in Fig 4.3 (a). The tolerances are scaled up to the full cylinder length as appropriate.

The second tolerance concerns the radial misalignment of adjacent stiffeners (Fig 4.3 (b)). The worst case will occur when the stiffeners on either side of the stiffener of interest, are each out of alignment with it by the maximum possible amount, but in opposite directions. In this situation the maximum imperfection over one panel is equal to the tolerance; no scaling is necessary since the gauge length is equal to the panel width.

The third tolerance is a local out-of-roundness specified across an arc gauge length (Fig 4.3(c)). In the worst situation adjacent panels will deflect in opposite directions by the maximum amount. Scaling up will be necessary in those cases where the gauge length is not equal to the panel width.

The basic cylinder imperfection was the smallest value derived from the three tolerances. Fig 4.5 shows the magnitude extrapolated from the DnV Notes for a single halfwave imperfection in each of the cylinders considered in the parametric study. In the longer and more closely-stiffened cylinders the out-of-roundness requirement governs, whilst it is only for the short or sparsely-stiffened cylinders that misalignment or out-of-straightness is important.

If the imperfections are plotted against length for the various values of radius, Fig 4.6, it is clear that in all but the broad-panelled models the imperfections remain fairly constant for all cylinders of a particular cross-section. The reason is simply that

the governing tolerances on out-of-roundness and misalignment of stiffeners are almost independent of length.

It can be seen, however, that an increase in the allowable imperfections is possible as the cylinder becomes shorter; although the specified tolerance is reduced, so too is the gauge length over which it is measured, and when the imperfection is extrapolated to the full panel width an increase results.

For the sparsely-stiffened models, all three tolerance specifications govern at some point. The out-of-straightness and out-of-roundness tolerances need extrapolation to the full cylinder length and panel width respectively and are rapidly varying. The result is that the imperfection magnitudes obtained for the various lengths of each cross-section differ significantly.

The stiffener imperfections, for both the in-plane and out-of-plane modes, are specified as a proportion of the cylinder length and measured over it, and therefore need no extrapolation.

4.2.5.2 Imperfection mode

Within the framework of the DnV tolerance requirements, it is possible to incorporate the calculated imperfection magnitudes in the form of a number of realistic mode shapes. For example, models with an antisymmetric panel mode, or an inward or outward barrel mode, with an amplitude equal to the calculated imperfection would all satisfy the DnV requirements. In addition, higher wave modes are possible, although in some cases the imperfection magnitudes which would meet the DnV tolerances may change. It was neccessary to determine the form of initial imperfections which would produce the lowest cylinder strengths. To this end, an eigenvalue analysis was employed.

4.2.5.3 Eigenvalue study

The mathematical condition defining stability of a finite element assemblage is given by:

$$([K_o]+[K_u]+[K_g])\ \underline{U} = [K_t]\ \underline{U} = 0$$

where K_o is the small displacement stiffness matrix,

K_u is the initial displacement matrix,

K_g is the geometric matrix,

whose sum is the tangential stiffness matrix, K_t, and

$\underline{U}$ is an infinitesimal displacement vector.

In a linear initial stability analysis the deformations up to the critical point are neglected and the stresses are assumed to vary in proportion to a load factor β. The equation above can thus be simplified to:

$$([K_o]+\beta[K_g])\ \underline{U} = 0.$$

This is the typical eigenvalue problem, in which β is the load factor and $\underline{U}$ an infinitesimal displacement vector defining the buckling mode.

Solving this equation gives a series of associated loads and mode shapes at which instability will occur. It is common practice to use the lowest eigenmode as the form of the initial imperfections in a nonlinear analysis in order to guide the deflected shape into what should ultimately become its buckling mode. Since it is relatively inexpensive to solve the initial eigenvalue problem using the finite element technique, it was carried out for all geometries in the parametric study. In most cases, the first four eigenvalues were calculated in order to observe the variation in the eigenmodes as the geometric parameters were changed.

The imperfections used in the nonlinear analyses were assumed to be in the form of a regular sine wave. The principal information which was extracted from the eigenvectors was, therefore, not the

precise shape, but the number of halfwaves in each direction.

In Figs 4.7, 4.8 and 4.9 the eigenvalues are plotted against length in separate graphs for each radius, number of stiffeners and type of loading, and are joined by tentative "iso-modal" lines. Too few points are available for these curves to be drawn precisely; however, even the approximate shapes are useful in organizing the large quantity of data.

For any geometry, the eigenvalue in a particular mode will either be known or it will be greater than the highest calculated eigenvalue. This information is usually sufficient for the general shape of the curve to be drawn.

In referring to the eigenmode shapes a shorthand notation has been used consisting of up to two numbers and a letter. The first number refers to the halfwaves in the longitudinal direction, and is always given. The second is the number of halfwaves across the panel width, and is omitted from the figures if it is one, the most common value. Finally, the letter, A or S, depends on whether the mode is antisymmetric or symmetric about the stiffener line, and to save space in the figures is only shown if it is "S".

The antisymmetric halfwave mode (i.e. the 1,1,A mode) was critical in the majority of cases. It was the lowest mode in all the pressure loaded-models but one: the broad-panelled slender cylinder (R/t = 600, L/R = 0.25, N = 20) for which a mode containing three halfwaves across the panel width was found to be critical.

For the axially-loaded cases, closely spaced eigenvalues were more common. A series of modes was often obtained, in which the longitudinal wave number increased with increasing cylinder length; however, in all cases the critical mode was antisymmetric, with one

halfwave across the panel. In the longest (L/R = 1), broad-panelled (N = 20) cylinders the single halfwave mode reappeared in preference to the higher mode shapes. A later study (see Sect 4.8) showed that in these models the overall buckling mode for the complete cylinder contains approximately the same number of halfwaves as the number of stringers. This n = 1 mode is, therefore, an approximation of the overall buckling mode.

Under combined loading, the single halfwave mode was critical for all models with more than twenty stiffeners. In general, the graphs for the combined loading cases were very similar to the lower bounds obtained by overlapping the corresponding figures for axial load and pressure.

In the nonlinear analyses an initial imperfection of the same form as the lowest eigenmode should generally be used. Originally, it was decided that, for any mode shape, the amplitude should be the largest which would still satisfy the DnV tolerances. The imperfection derived from the out-of-straightness tolerance would be automatically reduced for the higher mode shapes as the ratio of wavelength to gauge length diminished. The scaling of the tolerance was accomplished using the equation shown in Fig 4.4 (b). The other tolerance requirements, however, were unaffected by the shorter longitudinal wavelength.

In many cases reduced imperfection amplitudes were obtained by using the extrapolation procedure of Fig 4.4 (b). Since the out-of-straightness tolerance often governed in the shorter, broad-panelled models, the maximum allowable imperfections were significantly reduced for the higher mode shapes. However, the magnitude of the reduction varied, and in some cases none was produced.

For example, in narrow-panelled models in which the out-of-straightness tolerance was far from critical both for the single and multiple halfwave modes there was very little or no reduction in amplitude despite the use of a much shorter wavelength imperfection.

4.2.5.4 Variation of amplitude with mode shape

From a practical point of view, it is extremely severe to incorporate in a higher wave mode an imperfection amplitude similar to that used in a single halfwave mode; some reduction in amplitude would be appropriate. It was decided to base the imperfection magnitude on the relationship between amplitude and axial wave number found in the experimental models and discussed in Sect 3.6.1.2.

It would be extremely useful to obtain corresponding relationships for large-scale structures from detailed measurements during fabrication. Unfortunately, very little information of this type exists, and where it does it is jealously guarded by the commercial organisation that produced it.

The experimental information suggests the type of variation to be expected in practical shells and demonstrates the harshness of using similar amplitudes for higher modes. In the absence of additional data, the inverse proportionality relationship was employed in this study to determine the amplitudes of the higher mode imperfections.

4.2.5.5 Shortcomings of the eigenvalue study

All cylinders in the parametric study were analysed with an imperfection in the single antisymmetric mode of magnitude equal to that derived from the DnV tolerances. In addition, those models for which a higher wave eigenmode was predicted were re-analysed using the eigenmode imperfection with an amplitude equal to the basic amplitude

divided by the wave number of the eigenmode. The lower peak load was taken to be the strength of the cylinder.

Unfortunately, this procedure was found to be inadequate. In the subsequent nonlinear analyses several geometries when loaded in axial compression, and some also under combined loading, developed deflections whose shape suggested that the critical initial imperfection should have been a multiwave mode, even though the lowest eigenmode contained only a single halfwave. The deflected shapes, instead of being smooth curves, varied rapidly near the ends of the cylinder and were relatively flat along the central part of the model. The phenomenon became even clearer when the location of first yield was noted. This was often not in the centre of the model, as one would expect in a single halfwave mode, but near the ends of the cylinder.

Most of these models, when re-analysed using a three halfwave imperfection, with a reduced amplitude, failed at a lower load. They will be discussed further in the appropriate sections of the parametric study, in which both sets of results will usually be presented.

It is perhaps disconcerting that the rigorous procedure of carrying out an eigenvalue analysis for each case and applying initial imperfections in the nonlinear analysis similar to the lowest eigenmode often failed to yield the lowest peak load. It is clear that the assumption of linear response and the neglect of deflections in the prebuckling range is an oversimplification which may often lead to significant errors in the eigenvalue analysis. However, discrepancies between imperfection mode and buckled shape could usually be detected by an inspection of the predicted behaviour, and were eliminated by re-analysing the model with a modified imperfection

shape.

An improvement may have been to obtain the lowest eigenmode using a much costlier analysis, in which the initial displacement matrix K_u is not assumed to be zero, and both it and the geometric matrix K_g are recomputed as the load is increased in an iterative, incremental procedure. This analysis is comparable in cost to the full nonlinear incremental solution and is, therefore, to be avoided if possible. An alternative is proposed in the conclusions to this chapter.

4.2.6 PRESENTATION OF RESULTS

A vast quantity of data was obtained from the computer analyses comprising the parametric study. To present this in detail for each case would be tedious and unhelpful. Tables, graphs and charts have been used wherever possible, not only to convey the information concisely, but also to allow easier comparison of results and the identification of general trends in behaviour, which is one of the principal aims of such a study.

The cases that were analysed in the principal sections of the parametric study are set out in graphical form in the chart of Fig 4.1, which gives the parameters for each case and the name by which each cylinder is referred to. Tables 4.1 - 4.5 present in tabular form the parameters for all the cases investigated. A prime after the cylinder name indicates that a higher mode imperfection was used.

To enable easier comparison between the results for different cylinders it would be useful to collect all of them on a single chart. Two primary variables affecting the cylinder behaviour were found to be the aspect ratio of the shell panel and the column slenderness of the shell-stiffener unit, i.e. L/s and L/r_y. An informative way of presenting the load-deflection curves is on a chart in which the panel

aspect ratio increases in one direction and column slenderness in the other (e.g. Fig 4.10).

The various combinations of the geometric parameters which were studied gave rise to four different values of the panel aspect ratio and seven different model lengths. Using length (L) rather than slenderness (L/r_y) leaves the relative positions of the models unchanged, but simplifies the presentation by reducing the number of distinct values in the chart. The position corresponding to a particular cylinder on this table will move towards the right as the number of stiffeners is increased. Moving downwards is equivalent to increasing the radius while maintaining a constant L/R. Increasing the length causes movement roughly along the diagonal downwards and towards the right.

Because these charts are used extensively in the presentation which follows, it is important to set out the objectives for which they were constructed in order that their applicability is not overestimated. At the most basic level, they enable a compact presentation of a considerable amount of information. Secondly, they allow a qualitative description of general trends in the behaviour of cylinders as they are affected by various parameters to be given. However, they do not contain all relevant variables and should not be used as design charts to be consulted for specific geometries.

The sequence to be followed in the presentation of the results will begin in each case with a general description of the overall behaviour of the models with reference to the load-deflection paths. This will then be followed by a more detailed discussion, in which the location of first yield and the deflection mode will be studied in an attempt to deduce the physical reasons for the observed behaviour. Finally, the influence of various parameters on the behaviour will be

examined. Wherever possible, groups of models which possess similar characteristics will be identified, and in this respect the charts and tables will prove useful. The load-deflection paths for all the finite element analyses are presented in Appendix B.

4.3 CYLINDER GEOMETRY STUDY

The initial and most substantial part of the parametric study dealt with the influence of the major geometric variables. The range of geometric parameters R, L and N, and the types of loading, defined by the ratio σ_θ/σ_x, for which analyses were performed are set out in Table 4.1. The imperfection magnitude, the stiffener slenderness and the level of residual stresses were all held constant in this investigation but varied in later studies. An asterisk is placed against the models that were analysed with a higher mode imperfection not based on the eigenmode analysis.

4.3.1 FORM OF LOAD-DEFLECTION GRAPHS

The load-deflection plots for all the runs performed in this part of the parametric study are presented in Figs B.1 - B.36. To save space, they are usually grouped into sets of three for each figure: the three different lengths of a particular cross-section and type of loading. Length was chosen as the variable parameter in the grouping of the figures, firstly, because it is the most easily visualized variation between models, and, secondly, so that on a single plot the cylinder cross-section would be unchanged. In some cases additional load paths are given for alternative initial imperfection shapes.

For the analyses with axial loading or combined loading in which the axial component predominates (σ_θ/σ_x = 0.4) the vertical axis gives the average applied axial stress, σ_x, normalized with respect to the

yield stress. The displacement plotted along the horizontal axis is, unless noted otherwise, the axial shortening of the node at the intersection of the shell and stiffener at the loaded edge. In cases with pressure only or pressure-dominant combined loading ($\sigma_\theta/\sigma_x = 2.5$) the vertical axis is the nominal hoop stress, σ_θ, again normalized with respect to yield, and the horizontal axis is the radial displacement of a node at the shell centreline.

If strains are plotted, the initial parts of the curves overlap and are difficult to distinguish. Deflections (normalized with respect to the shell thickness) have been plotted throughout to separate the initial load paths on each plot, and so to clarify each and simplify their identification as the short, medium and long models. The deflections always refer to the full panel length, rather than the half panel computer models.

In general, the curves were taken a considerable distance beyond the peak load. However, if the peak load had been clearly defined, analyses were not repeated simply to extend the post-buckling path.

4.3.2 AXIAL LOAD

4.3.2.1 Load-deflection paths

The load-deflection paths for the axially-loaded cylinders are presented in Figs B.1 - B.9. Once plotted on the chart of Fig 4.10, the load-deflection curves fall neatly into categories. The short, narrow-panelled models (i.e. those in the top right of the table) exhibited smooth load-deflection paths. The initially linear response deviated slowly into a well rounded peak followed by a gradual fall-off in load. The drop in load was slowest in the narrowest models, in which the shell panel was least curved and the shell-stiffener unit behaved most like a stiffened flat plate.

The slender models, at the bottom of the table, behaved very differently. In these, the peak was sharp and an abrupt drop in load occurred immediately. Subsequently, however, the load increased and post-buckling capacities above the initial buckling loads were reached. The shorter the cylinder, the broader its individual panels had to be for it to fall into this category.

Between these two zones of the table, was an intermediate range of behaviour, in which characteristics of the other two were combined. The peak was still fairly sharp and the loss in load capacity significant; however, neither effect was as severe as in the slender models, and the initial peak load was not subsequently exceeded.

4.3.2.2 First yield

All the finite element analyses were studied to identify the load and location within the model at which yielding began. Fig 4.11 shows the different initiating areas which were identified and plots this information for each cylinder in a table of the same form as used above. Close correlation between the first yield position and the shape of the load-deflection path can be identified by comparing this table with that in Fig 4.10.

In the stocky, narrow-panelled models first yield always took place in the stiffener at midlength. This was followed by progressive yielding through the cross-section to produce the gradual reduction in load capacity and the relatively soft failure. The slender cylinders failed elastically, exhibiting the sharp-peaked loading curves associated with elastic snap-through behaviour. Post-buckling peaks occurred only in these models, since the loss of stiffness accompanying plastic failure would preclude a subsequent increase in load-carrying capacity.

In the intermediate zone, yielding began in the inwardly deflecting shell panel, usually at the cylinder midlength. The consequent loss of stiffness then allowed a fairly rapid change in the deflected shape of the structure and a sudden drop in load. However, the presence of plasticity usually produced a more rounded peak than in the elastic models.

Of the cylinders in which first yield occurred in the shell, several of the more slender began to yield at locations away from the cylinder midlength. The deflected shape of these narrow-panelled models was in a higher mode, which produced the largest curvatures at locations near the ends of the cylinders.

Also shown in Fig 4.11 is the load, expressed as a fraction of the peak load, at which yielding began. There does not appear to be a very distinct trend, but, in general, the ratio increases with increasing slenderness until the elastic cases are reached, for which it is no longer meaningful. This general tendency is as one would expect: the stockier models were capable of sustaining load long after their stiffness had begun to be eroded by the spread of plasticity; the more slender models needed all the stiffness they had, and buckling followed very soon after yielding began.

4.3.2.3 Deflection modes

A number of categories of deflection shapes were identified from the computer results. These are illustrated in Fig 4.12 and noted in the corresponding table. Each cylinder is given the letter which best characterizes its deflected shape, although in some cases the mode combined features from two categories and both are noted.

In this and subsequent discussions of the deflected shapes, the

terms "symmetric" and "antisymmetric" will be frequently used. In the eigenvalue study these terms were used precisely; however, here they will be used more loosely to convey the general characteristics rather than the exact shape of the deflection modes.

The short, narrow-panelled models deflected in axisymmetric modes despite the antisymmetry in the initial imperfections which they possessed. The deflected shape in most cases contained a single halfwave. The narrowest model took up a shape containing a strong three halfwave component, but was so insensitive to imperfections that very little change in its behaviour was produced by using a higher mode inital imperfection. In all these models the deflection magnitudes were amplified near the peak but the axisymmetric mode was maintained.

All the remaining models deflected into antisymmetric modes from the outset. The deflected shape of most contained a single axial halfwave, although for some of the more slender models higher modes were obtained. Usually the prebuckling deflections in the inward and outward deflecting regions of the shell were of comparable magnitude. Beyond the peak, however, and with varying rates of rapidity, the mode changed to one in which the inward buckle became much larger. This was often associated with an inward movement of the stiffener, which until that point had remained relatively straight.

For all the models that deflected into a multiple wave antisymmetric shape (mode "B" in Fig 4.12) the lowest value of peak load was produced when they were analysed with a higher mode imperfection. However, the eigenvalue analysis failed to predict the higher buckling mode for the four broader-panelled cylinders, and it was inferred from the deflected shapes that the models assumed when analysed with a single halfwave imperfection.

Several other models were also re-analysed using higher mode imperfections. These cases are included in Table 4.1, but did not yield lower buckling load predictions.

4.3.2.4 Effect of geometric parameters

In the following sections the effect of the various geometric variables on the peak load will be discussed.

4.3.2.4.1 Length of cylinder

In Fig 4.22(a) the peak load is plotted against the cylinder L/R for the various values of radius and number of stiffeners. Complete curves are available only for the sparsely-stiffened models and these will be discussed first. In the stockier cylinders (R = 200 & 400) the midlength models were found to be the weakest. This unexpected behaviour was due to the use of relatively large imperfection tolerances in these particular models. Fig 4.6, the plot of imperfection magnitude against length, shows that a consequence of the changing critical tolerance type is that the largest imperfections occur in the L/R = 0.5, N = 20 cylinders. An estimate of the peak load for a reduced imperfection magnitude can be obtained by reference to Fig 4.40, one of the imperfection sensitivity plots to be presented later. In fact, using an imperfection magnitude similar to that in the other cylinders with the same number of stiffeners would increase the peak load sufficiently to produce a monotonic variation in the strength vs length curves.

In the more slender models the load decreased slightly with increasing length. In the stocky cases, with either a smaller radius or a larger number of stiffeners, it was the shortest model that was weakest. This was probably due to the significant Poisson bulging

that will occur in short, stocky cylinders and the consequent earlier initiation of yielding.

Neglecting the artificially low results for the cases mentioned above, a 20% reduction in strength is the maximum produced by a doubling of length, and in most cases it is much less. Length is, therefore, of relatively minor importance in the behaviour of these models, which fail by local buckling. Of course, it will be more important for models which fail in overall modes.

4.3.2.4.2 Number of stiffeners

The graphs of peak load against the number of stiffeners (Fig 4.23(a)) show this to be a variable whose effect is both considerable and fairly consistent. Not surprisingly, it is least significant in in the stockiest cylinders (R = 200), which can manage reasonably well with little stiffening. In these cases 40 stiffeners were sufficient to develop approximately 95% of the squash load, and little advantage is gained by adding more stiffeners. Because a constant stiffening ratio is assumed, using more stiffeners reduces the size of each. In short, stocky models which fail by yielding of the stiffener a reduction in strength may, therefore, result from an increase in the number of stiffeners.

In the more slender cylinders, which fail in the shell, the relationship between strength and number of stiffeners is almost linear. Considerable advantage is usually derived from the use of more stiffeners, provided they are strong enough not to fail themselves, since they enhance the local buckling strength of the shell panel by reducing its unsupported width.

For a constant amount of material, i.e. a constant stiffening ratio, strength increases of up to 100% are possible by doubling the

number of stiffeners. The minor variations due to changes in imperfection magnitude described in the previous section all but disappear when superimposed on the much stronger effect of the number of stiffeners.

4.3.2.4.3 Radius/thickness ratio

This variable also has a major effect on the cylinder strength (Fig 4.24(a)), especially when the number of stiffeners is not too large. With 60 stiffeners present, little reduction in strength occurs until the radius is increased beyond 400t. (The strength reduction observed in the R = 200, L/R = 0.25 cylinder is due to the severe Poisson effect in this particularly short, stocky cylinder.) On the other hand, in the sparsely-stiffened cylinders (N = 20) a major part of the load capacity of the cylinder has been eroded by the time the radius has been increased to 400t.

4.3.3 PRESSURE LOAD

4.3.3.1 Load-deflection paths

Radial external pressure loading (i.e. $\sigma_x = 0$) was applied to all geometries in the study. In general, the load-deflection paths were much smoother than for the axially-loaded cylinders. When compressed axially, the cylinders usually failed after deviating only slightly from the initial linear portion of the load-deflection path. The pressure-loaded models, however, often moved a very long distance away from the initial path before reaching their peak load.

The difficulty in estimating the deflections at which the peak would be reached made the running of these cases more difficult than the axially-loaded models. In particular, there was often a very large variation in the size of the displacement increments which could

be successfully applied at various stages of the loading path. In several cases no decrease in the load capacity was observed despite the application of radial deflections of over 50 times the shell thickness. The magnitude of the deflections in these cases reduces to some extent the confidence which can be placed in the finite element results, the accuracy of which may deteriorate at such large strains. More important, however, is that the significance of a "peak" as a measure of load capacity for design is questionable if it is accompanied by such large deflections. An alternative measure of strength is required in these cases, and this point is reconsidered in the next section.

The load-deflection paths for the pressure loaded cylinders are shown in Figs B.19 - B.27 and grouped in the chart of Fig 4.13. The radial displacements are plotted for the node at the centre of the inwardly-imperfect panel and at the shell-stiffener intersection.

Most often, a two-stage behaviour could be identified in the load-deflection response. After an initial, fairly straight section, a rapid change took place, beyond which the slope was significantly reduced. The curve then continued for a considerable length before a drop in load was observed, if, indeed, it was at all. The slender, narrow-panelled models possessed particularly long flat curves, in which peaks were often not reached. The load-deflection paths of the broader-panelled cylinders usually had a peak, beyond which a moderate loss of strength took place fairly suddenly.

4.3.3.2 Load capacity of pressure-loaded cylinders

The difficulty in selecting a single quantity which will provide a consistent measure of load capacity led to the use of two criteria in the quantification of strength. The first was simply the peak load

as used previously: the point at which the first drop in load occurred. The second was the load at which the abrupt change in slope, common to all the load-deflection curves, took place. Since the curve before and after this "knee" was fairly straight, the load at this point was determined by intersecting the best fit straight lines on either side. This gave a more consistent estimate than alternative methods defined in terms of loss of initial stiffness or magnitude of applied strain. In one case, 24E, although a small drop in load occurred at a low value of external pressure, this point clearly corresponds to the knee load of the other curves, and the peak is taken to be at the second, more substantial, drop in load.

4.3.3.3 First yield

The location of first yield in the pressure-loaded models, Fig 4.14, was very consistent. In almost all cases plasticity began at the midlength of the cylinder on the outer surface of the inwardly-deflecting shell panel. The inward deflections amplified the compressive hoop stresses and promoted yield in this area. Only in the shortest, closely-stiffened cylinder did tensile yield of the stiffener precede yielding of the shell (in another, they began almost simultaneously). By the time the peak load was reached extensive yielding had occurred through both the shell and the stiffener.

The longest narrow-panelled model (24H) yielded not at the midlength of the cylinder, but near its end, for in this geometry the largest curvatures were produced near the supports. Another model (24E) was still elastic when the first decrease in load took place at a plateau in its load-deflection path, but subsequently yielded in the shell at the same location.

The load at which yielding began is also shown in Fig 4.14, as a

proportion of the "knee" load. For a given panel aspect ratio, this load ratio increased with the length of the model, and for the longer models substantially exceeded unity. The large variation in this ratio implies that the change in slope at the knee of the load-deflection curves was induced by geometric rather than material nonlinearities.

4.3.3.4 Deflection modes

As the chart of Fig 4.15 shows, the deflected shapes of all the cylinders contained a single halfwave in the axial direction. In the circumferential direction two types of behaviour were found.

The first category contained most of the broad-panelled models ($L/s \leq 1.59$). Initially the deflections, although larger in the panel with inward imperfections, increased roughly in proportion throughout the structure. At the knee point the deflections began to grow rapidly in the inwardly imperfect panel, while remaining relatively constant in the other panel; the deflections along the stiffener line remained small. Near the peak the mode changed once again, as the other panel deflected inwards to produce a mode almost symmetric about the stiffener. Beyond the peak, membrane action in the shell predominated, resulting in the very stiff behaviour which can be seen in those cases for which the response beyond the peak was obtained.

In the narrow-panelled models ($L/s = 3.18$) the antisymmetric shape of the initial imperfections was maintained throughout the load path. The stiffener line initially remained straight, while each shell panel deflected in the direction of the initial imperfections. Once the flatter part of the load-deflection path was reached and the stiffener yielded, the cross-section ceased to distort further but began to deflect inwards as a beam. The absence of a subsequent snap-

through produced the long, slowly rising load response observed for these models.

There was a transition zone in between containing the models whose L/s was 2.39 and the shortest of the slightly narrower models. In these cases the antisymmetric deflection mode, typical of the narrow geometries, continued for a considerable part of the load path, but eventually both panels began to deflect inwards. However, the deflections from then on were not as symmetric as in the broader-panelled models and were accompanied by significant radial deflections of the stiffener.

4.3.3.5 Effect of geometric parameters

In the graphs which follow two curves are plotted for each set of variables: the broken line joins the peak loads, and the solid line the "knee" loads; both curves follow similar trends. For cylinders where a drop in load capacity was not observed, the maximum value attained is plotted with a small upward arrow to indicate that the peak lies somewhere beyond this load, and is joined to the other points by a dotted line.

4.3.3.5.1 Length

Very pronounced changes in strength were produced by variations in the length (Fig 4.22(c)). This was especially true of the shorter and more closely-stiffened models, in which a significant proportion of the strength was developed through the bending action of the shell-stiffener unit spanning between the ends of the cylinder. For the particularly short models, strengths far in excess of the nominal pressure to cause circumferential yield were achieved through this mode of action.

4.3.3.5.2 Number of stiffeners

As in some axially-loaded models, there appears to be an optimum number of stiffeners for a pressure-loaded cylinder of given geometry and stiffening ratio (Fig 4.23(c)). With too few stiffeners the shell is supported at a wide spacing and local buckling governs; too many and each stiffener becomes very light and, unable to restrain the movement of the shell, fails in a laterally-loaded beam mode or in an orthotropic mode.

For most of the geometries investigated, using 40 instead of 20 stiffeners usually produced a dramatic increase in strength, in many cases of more than 100%.

4.3.3.5.3 Radius/thickness ratio

Fig 4.24(c) shows that, once again, the cylinder slenderness had a major and straightforward effect on cylinder strength: increasing the R/t ratio reduced the strength.

4.3.4 AXIAL-DOMINANT COMBINED LOAD [$\sigma_\theta/\sigma_x = 0.4$]

All the cylinder geometries were analysed under a loading combination of axial compression and external pressure, in which the ratio σ_θ/σ_x was 0.4.

4.3.4.1 Load-deflection paths

As expected, the behaviour of these models combined characteristics from both the axially-loaded and pressure-loaded cases (Fig B.10 - B.18 and 4.16). Since the axial load was dominant, in most cases the load-deflection curves closely resembled those of the axially-loaded models. However, the long, narrow geometries, which had been particularly weak under pressure, behaved more like the

pressure-loaded cylinders.

Usually, the critical imperfection mode was found to be the same as for the corresponding axially-loaded cylinder. In some long, narrow-panelled models, however, the use of a three wave mode produced a response, which, although it fell slightly at one point, was generally stronger and stiffer than the single wave case. Usually the first drop in load has been adopted as the strength of the cylinder; but for reasons which are discussed in Sect 4.3.6.1 (in which this situation corresponds to case (f)) the single halfwave result has been selected as the appropriate one in these cases.

4.3.4.2 First yield

Under combined loading the location of first yield was almost invariably in the shell (Fig 4.17). The radial deflections due to pressure in all but the shortest, narrow model opposed the Poisson bulging sufficiently to prevent failure of the stiffeners and to induce first yield in the inwardly-deflecting panel of the shell.

4.3.4.3 Deflection modes

Fig 4.18 shows that the deflected shapes of the models can be grouped into two main categories.

The broad-panelled models, i.e. $L/s \leq 1.59$, deformed in a similar mode to the axially-loaded cylinders. The deflections were antisymmetric, with the stiffener remaining straight. However, the magnitude of the outward bulge in the shell was reduced by the external pressure. As in the axially-loaded models, failure was accompanied by the rapid growth of deflections in the inwardly-deflecting panel.

The closely-stiffened models, $L/s \geq 2.39$, displayed the same mode

as the pressure cylinders. The deflections were initially antisymmetric, but, at the flatter part of the load path, began to grow uniformly as the entire cross-section deflected inwards.

Some of the intermediate geometries with higher mode imperfections deflected into modes combining both single and multiple wave characteristics. The deflections began as a three wave mode, to which was later added a significant single wave component. This created the mode shape "I", in which the deflections throughout one panel were all inwards, but largest near the end of the cylinder.

In the shortest, narrow-panelled model the Poisson bulging due to the axial component was so severe that it dominated the behaviour and produced an axisymmetric failure.

4.3.4.4 Effect of geometric parameters

4.3.4.4.1 Length of cylinder

The strength of the sparsely-stiffened models was always eroded by an increase in length (Fig 4.22(b)). The narrow-panelled cylinders had been weakened by an increase in length when loaded under pressure and strengthened when loaded axially. In the combined loading cases these two opposing effects resulted in the strength being insensitive to variations in length. This is a coincidental result, dependent upon the precise value of the loading ratio. The axial-pressure interaction diagrams to be discussed later (Figs 4.27 - 4.29) show that the strength variation will be more significant for other loading combinations.

4.3.4.4.2 Number of stiffeners

The effect was similar to that found in the axially-loaded models, with substantial strength enhancement resulting from the use

of more stiffeners (Fig 4.23(b)).

4.3.4.4.3 Radius/thickness ratio

The weakening effect produced by an increase in the R/t ratio was, once again, similar to its effect in axially-loaded models (Fig 4.24(b)).

4.3.5 PRESSURE-DOMINANT COMBINED LOAD [$\sigma_\theta/\sigma_x = 2.5$]

Finally, to complete the cylinder geometry study and to provide additional information for the axial-pressure interaction behaviour a number of cylinders were analysed under pressure-dominant combined loading. The value of 2.5 was selected for the ratio of nominal hoop stress to axial stress as a convenient point in the interaction curves. It corresponds very nearly to hydrostatic loading in a longitudinally-stiffened cylinder with a stiffening ratio of 0.3 (for which the precise value is 2.6).

The longer, broad-panelled models, being weak under external pressure, have steep interaction diagrams whose definition is not significantly improved by an additional point near the pressure axis. Consequently, not all geometries were analysed under this loading combination. Table 4.1 details the models for which this load case was investigated.

4.3.5.1 Load-deflection paths

Shown in Figs B.28 - B.36 and 4.19, the load-deflection diagrams are generally very similar to those of the pressure-loaded models. However, the addition of a small proportion of axial load produced peaks in all cases, which even in the long, narrow-panelled geometries were reached with little difficulty.

4.3.5.2 First yield

In all cases yielding began in the shell at midlength (Fig 4.20). The Poisson bulging caused by the small proportion of axial load prevented tensile yield of the stiffener and caused first yield to occur in the shell.

4.3.5.3 Deflection modes

These are summarized in Fig 4.21, and generally follow the trend of the pressure-loaded cylinders. The broader-panelled models deformed in a symmetric mode in which both panels deflected inwards, with very little movement of the stiffener. The slightly narrower models also deflected in a relativley symmetric mode, but one in which the stiffener also participated. The narrow models maintained an antisymmetric shape throughout the load path, to which in the latter stages were added substantial radial deflections of the entire shell-stiffener cross-section. These modes had all occurred in the pressure-loaded cylinders, but in narrower-panelled models than were observed here. The addition of the axial component, tended to promote the growth of the initial antisymmetric imperfections and to extend the range of geometries over which the antisymmetric modes were observed.

4.3.5.4 Effect of geometric parameters

The influence of each geometric variable was so similar to what it had been in the pressure-loaded models that the graphs, presented in Fig 4.25, need no additional comments.

4.3.6 INTERACTION BEHAVIOUR

It should now be possible, with the information available, to

construct axial-pressure interaction diagrams which summarize the data. It quickly becomes apparent that the choice of a characteristic strength and its consistency for different load cases and shapes of load paths is crucial: widely varying shapes of interaction curves can be drawn according to the definition adopted. It would be unwise to complete this section without a further discussion of this point.

4.3.6.1 Definition of cylinder strength

Previous parametric studies, for example of stiffened plates, were simplified by the fact that each case possessed a load-deflection path more or less similar to the rest. The great diversity in the types of response of stringer-stiffened cylinders creates difficulties in comparing results from different geometries and loading types. The problem, trivial in most structures, becomes significant in cylinders, since it is possible that misleading trends may be inferred following an unwise definition of characteristic strength.

It may be worthwhile to look briefly at a sequence of load-deflection types and assess the various choices for the cylinder strength. It should be remembered that what is sought is not an academic definition of a failure load but a practically useful measure of strength: i.e. at what point on the load-deflection path would a designer or operator feel that his structure had failed, based either on a strength or serviceability criterion.

The simplest case, shown in Fig 4.26(a), is obviously trivial; all deflections remain small until the peak is reached; the load capacity then falls and never exceeds its prebuckling value. The sharp-peaked case shown in Fig 4.26(b) is almost as simple. The deflections remain small along the prebuckling path, but then increase dramatically as a large reduction in load capacity occurs almost

instantaneously. Although a higher load may be carried in the postbuckling range, there is little doubt that at the first peak the structure has failed.

Changing the proportions, rather than the basic form, of the curve creates a less straightforward situation. The curve of Fig 4.26(c), for example, also displays the same general features: a linear initial path terminated by a sudden drop in load at a peak which is subsequently exceeded in the next stage of the curve. Consistency with the previous case requires that the first small peak be taken as the strength of the cylinder. Indeed, when two cases such as (b) and (c) must be joined by an interaction curve or a curve showing the effect of some parameter, it becomes apparent that the first, albeit small, peak is the consistent choice. However, if one could be assured that a structure would behave as shown in Fig 4.26(c), which value should be taken as the strength? This, in fact, is the basic question and it should be answered in two stages.

In a localized analysis such as this, in which a small component is selected to be representative of the behaviour of a much larger structure, the assumption must be made that the deflection and failure modes of the small component are repeated throughout the structure. One can determine, perhaps from experimental observations or alternative analyses, the range of parameters for which this condition is met. While the analytical model retains its original stiffness and shape one can, therefore, be reasonably confident of the validity of the results. After a drop in load and a snap-through to an alternative shape, with a consequent loss of stiffness, one can no longer be sure that an overall mode would not now be triggered. It is the author's opinion that reliance on the analytical predictions of the component behaviour leaves little alternative but acceptance of

the first drop in load as the characteristic strength.

It should also be noted that, although the axial displacement shown in the load-deflection curves does not move far from the initial curve, other displacements, usually radial, will have increased significantly, perhaps to several times the shell thickness. Hence, if another deflection component were to be plotted a much less "peaky" response may be obtained.

Of course, small localized drops in the loading path have often been observed (in model A, for example, and by other researchers e.g. [159]). At first a local panel buckle formed, which the analysis should predict accurately, followed at a higher load by an overall failure, which the method cannot be expected to detect. However, it is unlikely that in any major structure even a small localized buckle could be accepted passively, without repairs and strengthening being undertaken. Once again, it is the first drop that should be taken as failure of the structure.

Unfortunately, however, this is not the end of the story. Fig 4.26(d) shows a curve in which only one drop in load occurred, but a sudden change in slope took place at a lower load. When families of curves are superimposed (e.g. 14B,14E,14H where the number of stiffeners is varied, or 14D,14E,14F where the imperfection magnitude is changed) it becomes clear that this change in slope corresponds to the first peak in the other curves. Although the small drop in load is not present, the change in stiffness and the rapid growth of radial deflections are both observed, and suggest, again from considerations of consistency and serviceability, that the load at the change in slope is the strength value that should be used.

It may seem somewhat inconsistent that part of the load capacity

of a cylinder which fails relatively gradually, such as (d), should be neglected while the entire capacity of a shell with a much more violent unloading, such as (b), should be retained. This discrepancy is best handled through the use of different values of safety factor, selected to reflect the difference in the behaviour of the two structures and the consequences of slightly exceeding the predicted strength; in one case the result is catastrophic, in the other it may only be unsightly. In addition, the variability in the strengths due to uncertainties in the initial geometry will be very different for the two structures, and will be discussed in the next section.

A further complication arose in some cases in which alternative imperfection modes were investigated. Fig 4.26(e) shows the simple case, in which no confusion can arise, and for which there is no alternative but to accept the lower peak load, for the higher mode imperfection, as the strength of the cylinder. Fig 4.26(f) illustrates a more complex situation, in which the model with a higher mode imperfection is initially stiffer, but after one or two snaps it approaches the load path of the single halfwave model.

The higher mode response on its own would suggest that the cylinder strength should be the first drop in load. However, this model was always stronger, and, except in the region of the snap, stiffer, than the single wave cylinder. What has happened here is that the higher mode initial imperfection shape is an inappropriate one and has caused a snap-through early in the loading to the alternative mode.

It is important to distinguish between the two types of snap-through that are possible. The first is the type discussed earlier, in which the shape of the prebuckling and postbuckling deflections are different, and the change from one to the other takes place as a

sudden jump (e.g. under axial load the prebuckling deflections will be outward, whereas the buckling mode may be predominantly inward). The second snap-through is from an inappropriate initial imperfection shape to the preferred prebuckling mode. For example, if a cylinder is analysed with initial imperfections in a mode other than the preferred one it may deform in the initial shape until, at some point, it snaps into its preferred prebuckling mode. From this point it will behave in a manner similar to what it would if it originally had initial imperfections in the preferred mode. The load at which such a snap is predicted by the analysis could probably be altered by using an initial imperfection mode still further removed from the preferred shape. It is a fictitious phenomenon, which is a consequence of an incorrect selection of initial imperfection mode and will not occur in a real cylinder, in which all imperfection modes will be present.

Yet another problem may arise when the imperfection magnitudes are varied; it is unique to this situation and is discussed in Sect 4.3.1.

In the pressure-dominant regime a more fundamental problem arises regarding the selection of a strength value: there may not be a peak at all. This problem was addressed in Sect 4.3.3.2, and the approach was adopted of using two values, the peak (when it occurred) and the load at which the slope changed rapidly. When the interaction diagrams were plotted it became clear that the load at the change of slope was the consistent value to use in combination with the loads selected for the axial cases.

For the longer and more slender models, in whose response there was a sudden change in slope followed by a very long, straight loading path that eventually rose to a considerably higher load (Fig 4.26(g), the "knee" load is the only sensible value to use. In shorter,

broader models, the slope of the load-deflection curve is not reduced as greatly (Fig 4.26(h), and it could be argued that the peak load would be attained without the prior violation of serviceability requirements. However, even in the shortest models, the maximum radial deflection prior to the peak was about three times the shell thickness, and for the remaining models, between five and ten times. These are not small deflections; they are easily distinguished by eye, and are best avoided by neglecting the strength of the cylinders beyond the point at which the change in slope occurs.

To summarize, in this section an examination has been attempted in a systematic fashion of the various forms of load-deflection response obtained. Failure has been defined as the first occurence of either the strength or serviceability limit state. The aim throughout has been to select strength values that will give as true a picture of the general trends in behaviour as possible. These quantities were used primarily in the description of the effects of the various parameters investigated. They were not intended to be the single value defining the behaviour of each cylinder. This cannot be accomplished by a single number, and for this reason all the load-deflection paths have been presented. These should be consulted when information about the general load response is required and when making decisions regarding appropriate factors of safety for the various limit states.

4.3.6.2 Interaction curves

Now, finally, the axial-pressure interaction diagrams can be drawn, and they are presented in Figs 4.27 - 4.29. They vary significantly, from straight to strongly concave.

The most significant influence on their shape was imposed by the

number of stiffeners. All the cylinders with twenty stringers have fairly straight interaction diagrams, with forty stringers they are curved, while with sixty they are even more so. In addition, the interaction became less linear as the radius was reduced. Both effects tend to increase the cylinder strength.

If the models in which buckling occurred elastically are noted, Fig 4.30, it becomes apparent that it is for these cases that the linear interaction curves were obtained. The short narrow-panelled models, in which yielding often occurred long before the peak load was reached, possess the most strongly curved interaction diagrams.

4.4 IMPERFECTION SENSITIVITY

4.4.1 GENERAL

The aim of this section was to investigate the extent to which a change in the magnitude of inital imperfections will affect the behaviour of the cylinders. The procedure was to use the critical imperfection mode found in the previous section, but to change its magnitude to one half and twice the original value. The study involved many cases, the basic parameters of which are set out in Table 4.2. The load-deflection curves, grouped into sets comprising the three imperfection levels for each geometry, are presented in Figs B.36 - B.58.

A complication arises in the presentation of the imperfection sensitivity figures, in which peak load is plotted against imperfection magnitude. In many slender models a high postbuckling peak occurs after the initial buckling load. For such models increasing the imperfections may remove the initial drop in load, and produce a load path rising smoothly to what, in the more perfect

models, was the postbuckling strength. This situation is different to any of the cases discussed in Sect 4.3.6.1. Defining the peak load as the first drop in strength results in the unlikely imperfection sensitivity graphs which suggest that the models become stronger as the imperfections increase.

To avoid this inconsistency two curves have been plotted. The first, a solid line, joins the initial buckling loads, and is continued as a dotted line from the imperfection level beyond which it is estimated that this initial drop in load will no longer occur. For models with imperfections larger than this the first reduction in strength will take place at the broken line, which joins the secondary peaks of the models. The term "secondary" peak must be thought of in the context of the series of load paths; it could refer to the only peak a model may display, but one which corresponds to the second peak of its more perfect counterparts.

Even though the apparent paradox has been avoided by the use of two curves, it is still necessary to define the strength value to be used for imperfect models with only a secondary peak. Can they be designed to carry a higher load than the more perfect cylinders? The answer, of course, must be no, and the most reasonable approach would be to limit their capacity to the lowest load at which a peak is observed, i.e. the lower end of the solid line, (e.g. Fig 4.41).

As discussed in the next section, this is the value of the secondary peak that cylinders buckling elastoplastically approach in any case. However, the secondary peaks of imperfect cylinders buckling elastically often substantially exceed this value.

Of course, many models have only one peak, irrespective of imperfection magitude, and for these such a procedure is unnecessary.

4.4.2 AXIAL LOAD

4.4.2.1 Load-deflection paths

Although less fully populated in this and subsequent studies, the aspect ratio-length chart will be retained for the presentation of results. Fig 4.31 collects the information for the axially-loaded models (Figs B.37 - B.46). The simplest behaviour is found once again in the top right of the table, amongst the short narrow cylinders. Of these, that furthest to the right, which failed in the stiffener with an axisymmetric deflection mode, was insensitive to the imperfection level. The slightly broader model adjacent to it also failed in an axisymmetric mode, but one in which yielding began in the shell. The imperfection magnitude had a small effect on the peak load through its initiation of earlier yielding in the shell.

In the remaining models more significant strength variations were produced by changes in the imperfection magnitude. When buckling took place elastoplastically, an approximate upper bound to the secondary curves was set by the lowest of the primary peaks. Put another way, the prebuckling strength of an imperfect model could not significantly exceed the postbuckling strength of a more perfect cylinder if substantial yielding took place. In the cylinders buckling elastically this limitation did not apply and imperfect models often carried a higher load than that required to initiate buckling in the more perfect cylinders.

4.4.2.2 First yield location

The location of first yield in the cylinders of each imperfection level is entered in Fig 4.32. The most imperfect versions of the slender cylinders, which had previously buckled elastically, are now

seen to yield before the peak. This change was caused by the disappearance of the initial drop in load, resulting in an apparently higher value of the peak, rather than by a major change in the load at which plasticity began.

Of the short models, the most perfect examples sometimes started to yield away from the cylinder midlength. The deflection mode began as a multiple wave shape, but soon returned to a single halfwave mode. Both effects were of little importance to the overall behaviour.

4.4.2.3 Deflection mode

A significant change in the deflection modes occurred only in the most perfect of the short cylinders (Fig 4.33). As mentioned above, the tendency to deflect into a higher wave mode grew as the imperfection magnitude was reduced.

In one of the short narrow-panelled cylinders the reduced imperfection amplitude was insufficient to induce antisymmetric deflections, and a barrelling mode resulted. Otherwise, the deflection modes retained their basic shape regardless of imperfection magnitude.

4.4.2.4 Imperfection sensitivity

Figs 4.40(a), 4.41(a) and 4.42(a) summarize the information in graphs of load against imperfection magnitude. It can be seen that the sensitivity to imperfections decreased significantly as more stiffeners were added. The importance of this effect can be gauged by comparing the curves for the three values of N in the R = 400, L/R = 0.25 cylinder. Equally important was the radius of the cylinder, which can be seen in the N = 40, L/R = 0.50 curves for the three values of R. In general, as the model slenderness was increased,

whether by an increase in radius or length or by a reduction in the number of stiffeners, the imperfection sensitivity rose, as did the likelihood of a two peak loading curve.

For the geometries studied here the imperfection sensitivity was relatively small unless N was 20. In quantifying the "sensitivity" to imperfections it is convenient to consider the percentage strength increase produced by halving the imperfection magnitude, as this avoids the change from the primary to the secondary peak that often occurred when the imperfection was doubled. The largest strength improvement produced by halving the imperfection for a cylinder with 40 stiffeners was about 21%, for the most slender model (R = 600). For the N = 20 models the corresponding increase was as high as 90%.

4.4.3 PRESSURE LOAD

4.4.3.1 Load-deflection paths

Six pressure-loaded geometries were looked at. Their loading paths, presented individually in Figs B.53 - B.58 and collected in Fig 4.34, fall into two main categories. The narrow-panelled models, in which failure was gradual and accompanied by large radial deflections, displayed very little imperfection sensitivity. The three curves are distinguishable for only a short distance along the initial loading path. The imperfection differences were eventually swamped by the much larger displacements which developed. In the shortest narrow-panelled model, in which the knee in the curve was sharpest, a small variation in the load capacity is observed in the two more perfect cases. Beyond this point all three curves converge once again.

Markedly different behaviour was observed in the broad-panelled models. Two sets of peaks were obtained; as the imperfection was increased the first peak load was reduced until, beyond a certain

imperfection magnitude, it no longer occurred. The load capacity at the second peak, however, was enhanced as the imperfection was increased. The reason appears to be that in the more perfect models the changes that accompanied the first drop in load were more substantial and created a situation from which it was easier for the cylinder to find its final buckled shape. The perfect models assumed relatively symmetric deflections to begin with, and at the first peak snapped into the antisymmetric mode into which the imperfect models had deflected from the outset. It is uncertain whether the variation in load capacity at the second peak would be observed experimentally, and to place any practical significance on it is unwise.

4.4.3.2 First yield location

Only minor variations in the position of initial yield were produced by the changes in imperfection magnitude (Fig 4.35). In the more slender models yielding was induced by the imposition of large deflections rather than by high levels of applied load. The smaller prebuckling deflections in some of the more perfect models, therefore, delayed yielding until after the peak load was reached.

4.4.3.3 Deflection mode

The deflected shapes remained substantially unchanged (Fig 4.36); unlike the situation in axially-loaded models, the deflections under pressure are in the same direction as the applied load, and are, therefore, less affected by the magnitude of initial imperfections.

4.4.3.4 Imperfection sensitivity

The imperfection sensitivity curves, Figs 4.40(c), 4.41(c) and 4.42(c), show the number of stiffeners to be the primary variable, with radius relatively unimportant. In other words, the panel breadth

is the significant parameter in determining the imperfection sensitivity under pressure loading.

4.4.4 COMBINED LOAD

The same six geometries were studied (Figs B.47 - B.52 and 4.37), and, as before, they fell into two distinct groups. The narrow models behaved very much like the corresponding pressure-loaded cylinders, displaying very little reaction to imperfection magnitude, while the broad models exhibited the families of sharp-peaked load paths found in the axially-loaded cylinders. The imperfection sensitivity graphs, Figs 4.40(b), 4.41(b) and 4.42(b), also reflect these similarities.

The changes to first yield location, Fig 4.38, and deflection mode, Fig 4.39, produced by variations in the imperfection level were very minor.

4.4.5 SUMMARY

Under all the loading types investigated, the reaction of the cylinders to the level of inital imperfections was most dependant upon the number of stiffeners. The entire spectrum of imperfection sensitivity was observed, from the extremely sensitive behaviour similar to that of unstiffened cylinders to insensitive behaviour similar to stocky columns. The narrower the shell panels the less sensitive the cylinder was to the magnitude of imperfections.

4.5 S T I F F E N I N G R A T I O S T U D Y

The limitation imposed in the initial study of a constant stiffening ratio of 0.3 was removed in this section, and more heavily and lightly stiffened cylinders were investigated. A number of cases were studied in which the stiffening ratio was increased to 0.5. An

earlier series of analyses, in which the actual dimension of the stiffener were held constant at 10 x 1 and the stiffening ratio varied between 0.080 and 0.159, provided data for the lightly-stiffened cross-sections. The parameters are set out in Table 4.3.

4.5.1 AXIAL LOAD

The load-deflection paths can be seen in Figs B.59 - B.67 and 4.43. In short, narrow-panelled models, which failed by yielding of the stiffener, the use of a higher stiffening ratio produced an increase in both the peak load and the postbuckling response.

The slender models had failed elastically, and the stiffener played little part other than to restrain the edges of the panels; as a result, the change in response was usually minor. In fact, in one case the larger stiffener did no more than increase the total cross-sectional area, thus reducing the average applied stress at failure.

The general form of the load-deflection paths remained unchanged by the stiffening ratio variations. The first yield locations, Fig 4.44, and the deflection modes, Fig 4.45, were also substantially unaltered.

The strength variation is plotted in Figs 4.52(a), 4.53(a) and 4.54(a). What little effect the stiffening ratio had became larger as the radius was reduced and as the number of stiffeners was increased; i.e. as the shell panel became stronger. This left the stiffener as the weaker part of the assemblage and made the use of heavier stringers of some value. Even in the stockiest cases, however, a doubling of the stiffening ratio produced only a 15% increase in the strength of the cylinder.

4.5.2 PRESSURE LOAD

The load-deflection curves are shown in Figs B.78 - B.88 and 4.46. Once again, the largest strength variation was produced in the short, narrow models, in which failure was often initiated in the stiffener. Even the longer narrow-panelled models became significantly stronger, at least initially, as the stiffening ratio was increased. These models resist the applied pressure in a laterally-loaded beam mode, which is strengthened by an increase in the stiffener size.

The broad-panelled models, on the other hand, failed in a local shell buckling mode, which was not affected to any great degree by a change in the stiffening ratio.

In contrast to these general trends, there are some geometries, especially amongst the narrower models, whose more heavily stiffened representatives display significantly different behaviour from the rest. These are best discussed with reference to the first yield position and deflection modes.

4.5.2.1 First yield position

Fig 4.47 shows the position of first yield in each model. The stiffening ratio variation produced no change in the broader models, in which yielding always began in the shell. In some of the narrower models, once the stiffening ratio fell below a certain value, first yield took place in the, now much weaker, stiffener.

4.5.2.2 Deflection mode

Several interesting trends can be distinguished in the variation of deflection mode with stiffening ratio (Fig 4.48).

Many of the models, when lightly stiffened, deflected into the antisymmetric mode with superimposed radial deflections (i.e. mode G'), but when stiffened more substantially deflected into one of the symmetric modes E or E'. The reason was either that the stringer became stiff enough to prevent radial movements and mode E resulted, or it was strong enough for the model to reach a higher load and develop a mode which it could not previously attain, mode E'.

The longer, narrow-panelled models fall into this category. When lightly stiffened they possessed long, flat load-deflection curves; the stiffener was relatively weak and, as plasticity progressed through the section, large deflections developed in the inward antisymmetric mode, G'. With larger stringers the cylinder was both stronger and stiffer; the shell became more highly stressed and less distorted than before and was able to snap suddenly into the symmetric mode, E', causing the sudden drop in the load-deflection curves of these models.

In the broader models (L/s = 1.59) a similar, though less severe, effect took place. The stiffer cases possessed a fairly sharp peak, at which they changed suddenly into the symmetric mode. The weaker models ignored this mode and deflected in preference in the radial mode, G'.

4.5.2.3 Effect on strength

The effect of the stiffening ratio can be seen more clearly when plotted against strength in Figs 4.52(c), 4.53(c) and 4.54(c). The difference between its influence on broad-panelled and narrow-panelled cylinders is quite plain.

The magnitude of the effect was often far larger than it had been in the axially-loaded models. This is to be expected, for in narrow-

panelled cylinders under pressure the stringers are major loadbearing elements, rather than stabilizing elements as they are in axially-compressed cylinders. In many cases an increase in the stiffening ratio produced an almost proportional increase in strength.

4.5.3 COMBINED LOAD

The combined loading cases are summarized in Table 4.3, and plotted in Figs B.68 - B.77. Fig 4.49, in which the load-deflection paths have been assembled, shows the effect of stiffening ratio to be minor in broad-panelled models, as it had been in axially-loaded cylinders. The narrow models, whose behaviour resembled that of pressure-loaded cylinders, are more sensitive to the stiffening ratio.

The first yield locations were virtually unchanged by the stiffening ratio (Fig 4.50). Not surprisingly, as the stiffening ratio was increased the deflections tended towards modes in which the stringer deflections were reduced (Fig 4.51).

The effect of the stiffening ratio on strength in Figs 4.52(b), 4.53(b) and 4.54(b) shows most clearly the distinction between the models with high and low panel aspect ratios. The narrowest models are the N = 40 cases, the two more slender of which display a strength variation similar to the pressure-loaded cylinders. All other models exhibit a much smaller reaction to the stiffening ratio.

4.5.4 INTERACTION BEHAVIOUR

It is useful to summarize the effect of stiffening ratio in the form of interaction curves plotted in the aspect ratio-slenderness chart. Fig 4.55 shows the interaction curves available both for the more lightly-stiffened and for the heavily-stiffened cylinders. A comparison of these charts with Fig 4.30 shows that only the shorter

and more sparsely-stiffened models display any reaction to the value of stiffening ratio. Even in these cases, the effect is significant only in the pressure-dominant loading regime.

4.6 RESIDUAL STRESSES

4.6.1 GENERAL

All the models analysed so far have been initially stress-free. In practice the cylinder will contain residual stresses built up from the cutting, rolling and welding of the shell. Of major importance in a stringer-stiffened cylinder will often be the longitudinal residual stresses due to the welding of the stringers.

In this section a brief study was undertaken of models with an initial distribution of longitudinal stresses typical of what may be found in a full-scale structure. The aims of this study were to demonstrate the use of the analysis in this situation and to identify some general trends in behaviour, rather than to accumulate a large quantity of results. Five geometries were analysed under each loading type, and each with one level of residual stress (Table 4.4).

4.6.2 RESIDUAL STRESS DISTRIBUTION

The distribution of residual stresses in a plate or shell due to the attachment of longitudinal stiffeners is, by now, well established e.g. [212,213]. The large heat input which occurs during the welding process causes the metal in the vicinity of the weld to yield in tension upon cooling. The tensile force developed in this region is balanced by a relatively uniform distribution of compressive stress in the remainder of the shell. The width of the yielded material and hence the magnitude of the balancing compressive stress depend primarily upon the heat input per unit length of weld. For design

purposes most researchers have suggested an idealised stress distribution, in which a step joins the area of tensile yield to the uniform compressive stress block, rather than the more gradual transition that will occur in practice.

The residual stress measurements of the large-scale model showed the distribution within the stiffeners to be less consistent. A stress variation which produced in some cases tensile and in others compressive stresses at the stiffener tip was found. White and Dwight [214], in an experimental and analytical study of the residual stresses present in large stiffened cylinders, identified two opposing effects creating a stress gradient through the stiffener; the eccentricity of the weld tends to bow the stiffener inwards, while wrap up of the weld produces the opposite effect. They found the second usually to be the dominant effect, and their experimental results showed the presence of a stress gradient producing compressive stresses at the tip and tensile stresses at the root, each approximately equal to the average compressive stress in the shell.

In the finite element analysis, stresses are calculated at the Gauss points of each element. Initial stresses can be specified at these points, to produce a residual stress pattern such as that shown in Fig 4.56. The spacing of Gauss points is such that, for a self-equilibrating stress distribution of this form with n elements across the width, it was found that the height of the tensile block will be n-1 times the value of the compressive block. In modelling the cylinder behaviour, the important parameter is the compressive stress value; this is chosen as required and balanced by the appropriate value of tensile stress, which clearly, can not exceed yield.

A constant value of compressive residual stress of 30% of yield was selected for all the models as a realistic but substantial effect.

If the cylinders to be analysed were, in fact, fabricated using the same welding process they would all develop the same tensile force in the material surrounding the weld. Since the cross-sectional areas of the models vary, so too would the compressive residual stresses required to balance these forces. It should be noted, therefore, that the same value of σ_r represents different levels of weld heat input in different models.

The geometries investigated in this section are placed in their appropriate positions in the chart of Fig 4.57, for example. Assuming that the residual stress level is inversely proportional to the cross-sectional area of the shell gives the relative magnitudes of the residual stresses that would be produced in the various models by the same fabrication method. Hence, the broader-panelled models towards the bottom and left of the group would contain much lower residual stresses than the narrower models at the top right. Despite this difference, the most systematic way to proceed is to assume a constant value of residual stress in all analyses.

The use of four elements across the panel width allowed the residual stress distribution to be defined accurately and resulted in a reasonable tensile stress value of 90% of yield.

The residual stresses satisfy the simplistic condition of longitudinal equilibrium precisely, and moment equilibrium about the centroid of the cross-section approximately. However, the stresses will produce deformations throughout the structure which will alter the stress state. It is necessary, therefore, in the finite element analysis to iterate in order to obtain the equilibrium state, either at zero load or at the first loading increment.

4.6.3 AXIAL LOAD

The presence of residual stresses produced changes in the load-deflection paths in one of two ways (see Figs B.89 - B.93 and Fig 4.57). The short narrow-panelled cylinders, when stress-free, had smooth, rounded load-deflection curves and failed by yielding in the stiffener. The residual stresses induced first yield in the shell (Fig 4.58) and produced more widespread and rapid plastification than had occurred previously. This reduced the slope of the load-deflection curve at a load below the stress-free peak. The maximum load capacity was only slightly reduced and the postbuckling curve approached that of the stress-free cylinder.

In the remaining models failure was initiated in the shell, either through the onset of plasticity or by the rapid growth of elastic deflections. Failure usually took place at a similar value of membrane stress regardless of whether the models contained residual stresses. However, the cylinders with residual stresses reached this stress level at a lower value of applied load.

Once the yield stress was reached in the shell and buckling of the shell panel took place, a further increase in load capacity occurred, since the remainder of the shell, initially stressed in tension could still carry more load. The load-deflection curve approached the postbuckling response of the initially stress-free cylinder with a considerably reduced slope.

Fig 4.59 shows that the buckling mode shapes were generally unchanged by the residual stresses.

4.6.4 PRESSURE LOAD

The load-deflection curves for the pressure-loaded cylinders are

given in Figs B.99 - B.102 and 4.60. In general, the presence of the longitudinal residual stresses produced a slightly earlier change of slope in the load response and a weaker behaviour from then on. In all cases yield was initiated at the shell-stiffener intersection at the cylinder midlength (Fig 4.61). The tensile longitudinal stresses combined with the compressive hoop stresses to produce an earlier onset of yielding. The deflected shapes (Fig 4.62) remained the same as in the stress-free cases.

4.6.5 COMBINED LOAD

The summary of the load-deflection curves (Fig B.94 - B.98) given in Fig 4.63 shows that, as has often been found before, the combined loading cylinders resemble either their axially-loaded or pressure-loaded counterparts. The short, closely-stiffened cylinders were similar to the axially-loaded models. The effect of the residual stresses was to reduce the load at which a change in slope took place and to produce a small reduction in the peak load.

The broad-panelled cylinders, which failed in the shell, also resembled the axially-loaded cases. The residual stresses reduced the failure load, although the postbuckling response approached the maximum load of the stress-free cylinder.

Finally, the longer of the narrow-panelled cylinders displayed load-deflection curves similar to those of the pressure-loaded cylinders. However, first yield occurred in the same location with and without residual stresses and only a small change in the response was produced.

4.6.6 SUMMARY

In general, the effect of the residual stresses was to reduce the

load at which there was a change in the cylinder response. The load-deflection path in the vicinity of this change of slope was round or sharp depending on the shape of the stress-free response. Beyond this point the curve was more rapidly rising than the postbuckling response of the initially stress-free models, due to the presence of the tensile zones which could still carry load; the postbuckling strengths of models with and without residual stresses were similar.

4.7 STIFFENER SLENDERNESS

Finally, the parametric study was completed by briefly studying the effect of changing the slenderness of the stiffener cross-section. An insight into the effect of using stringers of different cross-sections can be gained from the stiffening ratio study (Sect 4.5). In axially-loaded models, replacing flat stiffeners by angles or tees of the same cross-sectional area would produce little change provided the stiffening ratio was high enough to prevent an overall buckling mode with the flat stiffeners. In pressure-loaded models the additional inertia provided by the angles or tees would significantly strengthen the shorter and more narrow-panelled cylinders, but the broader-panelled models failing in the shell would be virtually unaffected.

This study, however, did not attempt to investigate cylinders with stringers of alternative cross-sectional shapes. Instead, it was sought to establish the type of behaviour induced in the various models by increasing the d/t of the stringers to a value where local stiffener buckling may be a problem. The d/t ratio was increased to 20, this being sufficiently high to induce local buckling in many cases. Five geometries were analysed, each under the three principal loading conditions (Table 4.5). Obviously, the stiffener slenderness will have the greatest effect in those geometries that are highly

stressed, i.e. in the shorter, closely-stiffened models, and it was towards these that most attention was directed.

4.7.1 AXIAL LOAD

4.7.1.1 Load-deflection paths

The load-deflection paths are given in Figs B.103 - B.107 and assembled in Fig 4.66. Increasing the slenderness of the stiffeners had an effect only on those models whose strength was higher than a certain value; otherwise the failure was still governed by local buckling of the shell. In the three strongest models, the shorter and more closely-stiffened cross-sections, a significant change in behaviour resulted. In all cases the cylinder strength was limited to approximately 0.65 σ_y, at which point local buckling of the stiffener took place.

In the shorter cylinders using more slender stiffeners not only reduced the peak load, but also resulted in a far more violent shedding of load in the post-buckling range.

4.7.1.2 First yield location

Little change in the position of first yield was produced by the slender stringers (Fig 4.67). In the shorter, narrow-panelled models the first yield position moved further along the stiffener towards the cylinder end, where local buckling took place.

4.7.1.3 Deflection mode

Superficially, the deflected shapes of the cylinders were unchanged by the stiffener slenderness variation (Fig 4.68). The general shapes of the shells were as they had been, except for the shortest, narrow-panelled cylinder, in which the deeper stringers,

being initially stiffer, forced a single rather than a multiple wave axisymmetric mode.

The delections of the stiffener, however, were significantly different in the local buckling cases. Previously the stiffener had deflected gradually during the loading, usually simply following the deflected shape of the shell. When local stiffener buckling took place a sudden and very rapid change in the stiffener shape occurred. Prior to the buckling load the stiffener deflections were in the single halfwave mode of the initial imperfections; in fact, in the shortest cylinder platicity began at the stiffener midlength.

As buckling occurred a sharp localized bulge was formed near the end of the stiffener and grew quickly. The very large erosion in the strength and stiffness of the stringer that resulted produced the sudden and complete collapse of the cylinder.

4.7.2 PRESSURE LOAD

4.7.2.1 Load-deflection paths

The load-deflection paths of Figs B.113 - B.117 are collected in Fig 4.69, which shows that the use of more slender stiffeners produced either little change (in the broad-panelled, shell buckling cases), or a significant strengthening (in the narrower-panelled models). Of course, the stringers were in tension and were not prone to local buckling.

Little change was produced in the location initiating yield, Fig 4.70, or in the general shapes of the deflections, Fig 4.71.

4.7.3 COMBINED LOAD

Figs B.108 - B.112 and 4.72 present the load-deflection paths and

Figs 4.73 and 4.74 the influence of stringer slenderness on first yield and deflection mode. In all respects the behaviour was very similar to that observed in the axial cases.

4.7.4 SUMMARY

This brief study has highlighted the potentially catastrophic consequences of using stringers prone to local buckling in axial-dominant loading situations. Little effect was produced in the weaker cylinders, whose strength was governed by local buckling of the shell. However, cylinders whose load capacity had previously exceeded the local buckling strength of the stringer, not only had their strength limited to the stringer capacity, but also their postbuckling characteristics dramatically and undesirably changed. Obviously, local stringer buckling is to be avoided at all costs.

4.8 FIVE PANEL ANALYSES

It has often been stated that the single panel analysis relies on the assumption that an overall mode, containing fewer circumferential halfwaves than the number of stringers, will not develop prior to the predicted collapse load.

An assessment of the geometries which meet this requirement was undertaken in this section by carrying out finite element analyses on a larger portion of the cylinder than had been considered previously. In order that all circumferential modes can be represented, the finite element model would have to be extended to one half of the cylinder (although the n = 2 mode can be represented in one quarter of the circumference, superposition of the n = 3 mode requires one half).

If one is to be sure that a different failure load predicted by the multipanel analysis was due to the model's ability to deflect in

more general modes, the same element types and arrangement as were used in the single panel analysis should be maintained. This would require that the new finite element meshes contain between ten and thirty times the number of elements of the single panel cases. These would be enormous analyses and a more moderate alternative was needed.

A reiteration of the objective suggests the course to be followed. The principal aim is to determine the validity of the single panel results and not to replace them in the inappropriate cases. This could be accomplished using an analysis of more moderate proportions. If a five panel analysis, for example, did not predict a lower failure load, one could be reasonably confident that the single panel failure mode was critical. If the five panel analysis did predict a lower load then it is possible that even this is insufficiently general and a yet lower load may be found if half the cylinder were analysed; but this is not of concern.

A number of axial and pressure cylinders were re-analysed using the five panel mesh shown in Fig 4.75. A constant mesh size was used even though this represented different proportions of the cylinder, depending upon the total number of stiffeners. The mesh refinement was identical to that used in the single panel cases and the boundary conditions and loading were also unchanged.

If the number of cases to be reanalysed using the large finite element model is to be kept to a minimum the selection of geometries must be made systematically. Two principles guided the choice of cylinders for reanalysis. First, the geometries most likely to fail in overall modes are the longer and more narrow-panelled cylinders, i.e. those near the bottom right of the aspect ratio-slenderness chart. Presumably, if they can be analysed successfully using the single panel model, so too can the shorter and broader-panelled

cylinders.

Secondly, the stiffening ratio calculated for each geometry by equating the elastic local and overall buckling stresses, according to Appendix A, was always less than the stiffening ratio of the cylinders analysed in the parametric study. Overall buckling would be most likely when the stiffening ratio used in the study was nearest to the calculated value. Using these two criteria a small number of geometries were selected for analysis. Their geometric parameters are listed in Table 4.6.

4.8.1 INITIAL IMPERFECTIONS

Since the overall buckling behaviour was to be studied, the appropriate initial imperfection mode was the lowest overall buckling mode. This would always contain one axial halfwave and a number of circumferential waves. The circumferential wave number for the complete cylinder, n, was determined from the expressions of Steen et al [164], given in Appendix A. The number of waves in a five panel portion of a cylinder with N stiffeners was then the nearest integer to 5n/N. The imperfection amplitude was unchanged from the single panel analyses.

Fig 4.76 tabulates the number of halfwaves in the five panel model corresponding to the overall buckling mode under axial and pressure load. Looking first at the axial loading cases and remembering that n = 5 corresponds to the mode shapes used in the single panel analyses shows that in many cylinders the local and overall modes have approximately the same number of circumferential waves. This is an encouraging result since it means that in these cases both the overall mode (with m = 1) and the local mode (with m $\geq$ 1) can be represented by the single panel model.

The single panel model is most likely to be unsatisfactory in those cases where the local and overall mode shapes differ most. This occurs in the short, narrow-panelled models at the top right of the table and in the longer, broad-panelled models towards the bottom left. The former failed in an axisymmetric mode in the single panel analysis (n = 0), and were so insensitive to initial imperfections that it seems unlikely that their behaviour will be significantly different in the five panel study. The broader-panelled cylinders have predicted overall modes containing more waves than the number of stiffeners. In practice, the radial restraint provided by the stringers produces local prebuckling deflections which bias the shell towards a local failure mode; models containing more than one circumferential halfwave per panel are not observed in practice unless they have very few stringers. It seems quite likely, therefore, that all the axial results obtained in the single panel parametric study will pass the five panel test.

The pressure-loaded cylinders rarely had overall modes with fewer circumferential waves than the number of stiffeners. Once again, it seems that the single panel analyses will be satisfactory in these cases.

4.8.2 AXIAL LOAD

The load-deflection paths for the axially-loaded, five panel models are presented in Figs B.118 - B.122, in each case with the curve from the corresponding single panel analysis. Three categories of behaviour can be distinguished and these will be discussed individually.

The longest cylinder, Fig B.120, when analysed by the single panel model, deflected into a single axial halfwave. As was mentioned

earlier (Sect 4.2.5.3), although representable within a single panel, this deflection was, in reality, an overall-type mode. Moving, therefore, to a five panel analysis, in which the number of circumferential halfwaves per panel is still one or very close to it and the number of axial halfwaves is also one should produce little change in peak load. In fact, for the longest cylinder the six halfwave overall mode required the bending of the stringers and produced a higher failure load than the five halfwave mode into which the real cylinder would buckle in preference.

The two midlength cylinders, Figs B.121 and B.122, had very different deflection modes when analysed using the two models. In the single panel analysis the local deflection mode contained several axial halfwaves while in the five panel model there was only one. The local mode was clearly critical, producing a failure load between 10% and 25% lower than the overall mode.

Lastly, in the case of the two shortest models, which failed in axisymmetric modes and were relatively insensitive to imperfections, similar load deflection curves were predicted by both analyses (Fig B.118 and B.119). The peak strengths predicted by the five panel analyses were only slightly below those from the single panel model (0.7% and 3.0%). These differences are very minor and, since the first yield location and deflected shape remained basically unchanged, the single panel results were retained.

All these analyses were carried out on cylinders with a stiffening ratio of 0.3. The more heavily-stiffened geometries are more likely to fail in a local mode and will all pass the five panel test; but it is not certain that the more lightly-stiffened cylinders would do so. Of the six geometries analysed above only two were included in the parametric study in their lightly-stiffened form.

These were the two midlength cylinders, for which the largest difference between the local and overall buckling loads was found. The model for which this difference was smaller, 17N, was re-analysed in its lightly-stiffened geometry. Its five panel and single panel load-deflection curves are given in Fig B.123.

This time the five panel analysis predicted a slightly lower failure load than the single panel model (224 N/mm^2 compared with 237 N/mm^2). Even in this case, which is the worst among the axially-loaded cylinders, the difference is relatively small (5%). Although the single panel analysis is not strictly correct in this case, the result has been retained in the parametric study, because it is only slightly at variance with the five panel result.

To summarize, then, the single panel results are applicable to all the axially-loaded geometries investigated in the parametric study.

4.8.3 PRESSURE LOAD

The load-deflection paths for the pressure-loaded cylinders are presented in Figs B.124 - B.126. In each case the radial deflection has been plotted for the node which corresponds most closely to that used in the single panel graphs, namely, a midpanel node at the central circumference that is also at the centre of an inward buckle. This enables the five and single panel results to be compared. Nevertheless, due to the nature of the problem, the apparent radial stiffness of the cylinder is dependent upon the initial shape. In a longitudinally compressed model all the loaded nodes deflect axially by approximately the same amount; in a pressure loaded cylinder the radial deflections may be inward or outward depending upon the initial imperfections. Therefore, it is best to rely upon the cylinder

strength value for comparison.

Once again, the results are encouraging. In two of the long cylinders the single panel and five panel models predicted almost identical behaviour. The longest model, which had a seven halfwave imperfection in the five panel analysis, was considerably stronger than it had been in the single panel study.

The strengths of the short cylinders were found to be slightly reduced when analysed by the five panel model (2% and 4%). As in the corresponding axially-loaded cylinders, the deflection mode and first yield location remained unchanged and the single panel results were retained.

4.8.4 CONCLUSIONS

The procedure of equating the local and overall buckling stresses (Appendix A) has provided acceptable limits to the range of applicability of the single panel study. On the one hand, all the geometries satisfied the single panel assumptions, and, on the other, it appears that the analysis has been applied across almost the full extent of its validity.

4.9 S U M M A R Y

It may be useful, in conclusion, to summarize in a concise tabular form the major findings of the parametric study. One table has been presented for each loading case, in which a brief qualitative description of the various effects is given for the different categories of cylinders.

	P-A	First yield	Deflection mode	Effect on strength of an increase in: Length	Number of stiffeners	Radius	Imperfection magnitude	Stiffening ratio	Residual stresses	Stiffener slenderness
short, narrow-panelled	rounded, gradual unloading (single peak)	stiffener	axisymmetric	minor increase	minor reduction (each stiffener is small & therefore weak)	minor reduction	little change	moderate increase	minor reduction	major reduction very violent unloading
long	very sharp peak (subsequent postbuckling peak)	elastic	local shell panel deflections (antisymm.)	moderate reduction	moderate increase	major reduction	minor reduction (initial peak in P-A may disappear)	little change	major reduction	minor change
short, broad-panelled	sharp peak no postbuckling peak	shell (midlength)	local shell panel deflections (antisymm.) (single wave)	moderate reduction	major increase	major reduction	major reduction	little change	major reduction	little change
intermediate	sharp peak no postbuckling peak	shell (near end of cylinder)	local shell panel deflections (antisymm.) (multiple wave)	moderate increase	major increase	major reduction	moderate reduction	little change	major reduction	moderate reduction more rapid unloading

	P-A	First yield	Deflection mode	Effect on strength of an increase in: Length	Number of stiffeners	Radius	Imperfection magnitude	Stiffening ratio	Residual stresses	Stiffener slenderness
narrow-panelled	long flat	shell	(antisymm.) with inward movement of stiffener	major reduction	moderate increase	major reduction	minor reduction	major increase	minor reduction	moderate increase
broad-panelled	bi-linear	shell	"hungry horse" (symmetric) (stiffener straight)	major reduction	major increase	major reduction	moderate reduction	minor increase	moderate reduction	little change
intermediate	bi-linear	shell (in stiffener for short cylinders)	"hungry horse" (symmetric) stiffener deflects inwards)	major reduction	little change (decrease when many stiffeners)	major reduction	moderate reduction	major increase	minor reduction	moderate increase

	P-A	First yield	Deflection mode	Effect on strength of an increase in: Length	Number of stiffeners	Radius	Imperfection magnitude	Stiffening ratio	Residual stresses	Stiffener slenderness
short, narrow-panelled	sharp peak no postbuckling peak	stiffener	axisymmetric	little change	little change	major reduction	moderate reduction	moderate increase	minor reduction	major reduction
moderate to long narrow-panelled	long flat	shell	(antisymm.) with inward movement of stiffener	moderate reduction (Little effect if many stiffeners)	major increase (moderate in shorter cylinders	major reduction	little change	major increase	minor reduction	moderate increase
long, broad-panelled	sharp peak (subsequent postbuckling peak)	elastic	local shell panel deflections (antisymm.)	moderate reduction	major increase	major reduction	minor reduction	little change	major reduction	little change
short, broad-panelled	shape varies	shell	local shell panel deflections (antisymm.)	moderate reduction	major increase	major reduction	moderate reduction	little change	major reduction	little change

4.10 CONCLUSIONS

The single panel analysis has been applied successfully to a large number of cases, and has provided data on the behaviour of stringer-stiffened cylinders, which, both in extent and detail, was not previously available. The effects of the various geometric parameters, the mode and magnitude of inital imperfections and the value of stiffening ratio have been investigated in detail. In addition, the influence of residual stresses and stiffener slenderness have been briefly studied.

General trends in behaviour were identified, for which a physical interpretation was always sought. The results have been plotted and tabulated in detail to allow their use by other workers in the field of cylinder buckling. The results will form the basis in the next chapter of an assessment of the current design rules for stringer-stiffened cylinders.

An important part of the investigation was to establish the appropriate shapes of the initial imperfections. The linear initial eigenvalue analysis was found to be of limited value in determining the shape of the buckling mode and hence of the critical imperfection mode to be incorporated in the analyses. Its neglect of prebuckling deformations led to significant errors in several cases. The alternative of a nonlinear, incremental eigenvalue analysis is a much more expensive and, therefore, unwelcome approach.

An alternative to using a single mode inital imperfection, which requires the determination of that mode, would be to always use a superposition of a number of principal modes. Assuming the relationship between imperfection amplitude and axial wave number found in the experiments to be a general one would allow the relative

magnitudes of the various modes to be established; their absolute magnitudes could be scaled to produce whatever total imperfection is required. The advantages are apparent: the need for a preliminary analysis to determine the buckling mode is eliminated; the analytical model will approximate the physical situation more closely; and the deflections are freeer to develop in whichever mode is preferred.

Considerable attention was given to the selection of a characteristic strength value from response curves of different shapes. It is hoped that the importance and non-triviality of this point were conveyed.

The assumption upon which the single panel analysis depends were verified for the geometries investigated by carrying out five panel analyses of the more extreme geometries. These showed that all the results obtained in the parametric study had been valid.

This work has produced an extensive set of data which covers a broad range of geometries encountered in practice. However, it cannot hope to be comprehensive; several variables were either only briefly looked at or held constant. For example, a more detailed assessment of the effect of residual stresses, especially including hoop stresses due to circumferential butt welds and the attachment of rings would be useful. Alternative material strengths could also be investigated. Shell continuity across the rings in multibay cylinders is another effect which could be studied using a two or three bay analytical model similar to that used in this work.

Despite these and other inevitable omissions, the results should be a useful addition to the experimental data available on the behaviour of stringer-stiffened cylindrical shells.

NAME	R	N	L	a_s	d/t	σ_r	LOAD	IMPERFECTION SHELL	IMPERFECTION STIFF	MODE	σ_{xu}	σ_{x1}	$\bar{\sigma}_{xu}$	$\bar{\sigma}_{x1}$
13B	200	20	50	.300	10	0	AXIAL	.4000	.075	1	277.7		.793	
13E	200	20	100	.300	10	0	AXIAL	.6283	.150	1	229.4		.655	
13H	200	20	200	.300	10	0	AXIAL	.4888	.300	1	322.8		.922	
13H'	200	20	200	.300	10	0	AXIAL	.1629	.100	3*	331.7		.948	
13K	200	40	50	.300	10	0	AXIAL	.2768	.075	1	329.7		.942	
13N	200	40	100	.300	10	0	AXIAL	.2715	.150	1	339.0		.969	
13N'	200	40	100	.300	10	0	AXIAL	.0905	.050	3	337.7		.965	
13T	200	60	50	.300	10	0	AXIAL	.1896	.075	1	307.8		.879	
13T'	200	60	50	.300	10	0	AXIAL	.0632	.025	3	308.0		.880	
17B	400	20	100	.300	10	0	AXIAL	.9648	.150	1	150.6		.430	
17B'	400	20	100	.300	10	0	AXIAL	.3216	.050	3	168.8		.482	
17E	400	20	200	.300	10	0	AXIAL	1.2566	.300	1		117.6		.336
17E'	400	20	200	.300	10	0	AXIAL	.2513	.060	5		195.6		.559
17H	400	20	400	.300	10	0	AXIAL	1.1383	.600	1		122.4		.350
17H'	400	20	400	.300	10	0	AXIAL	.2277	.120	5*		220.7		.631
17K	400	40	100	.300	10	0	AXIAL	.6283	.150	1	260.6		.745	
17K'	400	40	100	.300	10	0	AXIAL	.2094	.050	3*	213.0		.609	
17N	400	40	200	.300	10	0	AXIAL	.5430	.300	1	291.6	285.8	.833	.817
17N'	400	40	200	.300	10	0	AXIAL	.1780	.100	3	243.7		.696	
17T	400	60	100	.300	10	0	AXIAL	.3792	.150	1	341.1		.975	
17T'	400	60	100	.300	10	0	AXIAL	.1246	.050	3*	313.5		.896	
21B	600	20	150	.300	10	0	AXIAL	1.7482	.225	1	104.3		.298	
21B'	600	20	150	.300	10	0	AXIAL	.5827	.075	3	113.3		.324	
21E	600	20	300	.300	10	0	AXIAL	1.8850	.450	1	152	92.02	.434	.263
21E'	600	20	300	.300	10	0	AXIAL	.2693	.064	7	145.4		.415	
21H	600	20	600	.300	10	0	AXIAL	1.8783	.900	1		74.77		.214
21H'	600	20	600	.300	10	0	AXIAL	.6261	.300	3*		175.4		.501
21K	600	40	150	.300	10	0	AXIAL	.9425	.225	1	158.4		.453	
21K'	600	40	150	.300	10	0	AXIAL	.3142	.075	3*	149.7		.428	
21N	600	40	300	.300	10	0	AXIAL	.8145	.450	1	245.9	144.1	.703	.412
21N'	600	40	300	.300	10	0	AXIAL	.2715	.150	3*	187.4	139.0	.535	.397
21T	600	60	150	.300	10	0	AXIAL	.5688	.225	1	252.7		.722	
21T'	600	60	150	.300	10	0	AXIAL	.1896	.075	3*	221.8		.634	

Table 4.1 PARAMETRIC STUDY OF CYLINDER GEOMETRY (continued)

NAME	R	N	L	a_s	d/t	σ_r	LOAD	IMPERFECTION SHELL	IMPERFECTION STIFF	IMPERFECTION MODE	σ_{xu}	σ_{x1}	$\bar{\sigma}_{xu}$	$\bar{\sigma}_{x1}$
14B	200	20	50	.300	10	0	0.4	.4000	.075	1	194.2		.555	
14E	200	20	100	.300	10	0	0.4	.6283	.150	1	174.3	132	.498	.377
14H	200	20	200	.300	10	0	0.4	.4888	.300	1	141.8	110	.405	.314
14K	200	40	50	.300	10	0	0.4	.2768	.075	1	316.9		.905	
14N	200	40	100	.300	10	0	0.4	.2715	.150	1	312.9		.894	
14T	200	60	50	.300	10	0	0.4	.1896	.075	1	327.0		.934	
18B	400	20	100	.300	10	0	0.4	.9648	.150	1	103.9		.297	
18B'	400	20	100	.300	10	0	0.4	.3216	.050	3	143.8		.411	
18E	400	20	200	.300	10	0	0.4	1.2566	.300	1	104.1	58.39	.297	.167
18H	400	20	400	.300	10	0	0.4	1.1383	.600	1	98.78	32	.282	.091
18K	400	40	100	.300	10	0	0.4	.6283	.150	1	196.7		.562	
18K'	400	40	100	.300	10	0	0.4	.2094	.050	3*	176.6	168	.505	.480
18N	400	40	200	.300	10	0	0.4	.5430	.300	1	176.1		.503	
18N'	400	40	200	.300	10	0	0.4	.1810	.100	3*	180.3	145.1	.515	.415
18T	400	60	100	.300	10	0	0.4	.3792	.150	1	292.7		.836	
18T'	400	60	100	.300	10	0	0.4	.1264	.050	3*	284.1		.812	
22B	600	20	150	.300	10	0	0.4	1.7482	.225	1	75.54		.216	
22B'	600	20	150	.300	10	0	0.4	.5827	.075	3	102.1		.292	
22E	600	20	300	.300	10	0	0.4	1.8850	.450	1	80	42.40	.229	.121
22E'	600	20	300	.300	10	0	0.4	.2693	.064	7	112.7		.322	
22H	600	20	600	.300	10	0	0.4	1.8783	.900	1		17.87		.051
22K	600	40	150	.300	10	0	0.4	.9425	.225	1	152.0		.434	
22K'	600	40	150	.300	10	0	0.4	.3142	.075	3*	142.3	85	.407	.243
22N	600	40	300	.300	10	0	0.4	.8145	.450	1	139.6		.399	
22N'	600	40	300	.300	10	0	0.4	.2715	.150	3*	141.0	69.44	.403	.198
22T	600	60	150	.300	10	0	0.4	.5688	.225	1	216.7		.619	
22T'	600	60	150	.300	10	0	0.4	.1896	.075	3*	207.2		.592	

Table 4.1 PARAMETRIC STUDY OF CYLINDER GEOMETRY (continued)

NAME	R	N	L	a_s	d/t	σ_r	LOAD	IMPERFECTION SHELL	IMPERFECTION STIFF	IMPERFECTION MODE	$\sigma_{\theta u}$	$\sigma_{\theta 1}$	$\bar{\sigma}_{\theta u}$	$\bar{\sigma}_{\theta 1}$
15B	200	20	50	.300	10	0	2.5	.4000	.075	1	253.0	183	.723	.523
15K	200	40	50	.300	10	0	2.5	.2768	.075	1	417.0	365	1.191	1.036
15N	200	40	100	.300	10	0	2.5	.2715	.150	1	208.3		.595	
15T	200	60	50	.300	10	0	2.5	.1896	.075	1	525.8	490	1.502	1.400
19B	400	20	100	.300	10	0	2.5	.9646	.150	1	166.9	90	.477	.257
19K	400	40	100	.300	10	0	2.5	.6283	.150	1	266.0		.760	
19N	400	40	200	.300	10	0	2.5	.5430	.300	1	161.9	100	.463	.286
19T	400	60	100	.300	10	0	2.5	.3792	.150	1	303.0	275	.866	.786
23B	600	20	150	.300	10	0	2.5	1.7482	.225	1	119.4	63	.341	.180
23K	600	40	150	.300	10	0	2.5	.9425	.225	1	185.9		.531	
23N	600	40	300	.300	10	0	2.5	.8145	.450	1	125.4	88	.358	.250
23T	600	60	150	.300	10	0	2.5	.5688	.225	1	249.1	212	.712	.606
16B	200	20	50	.300	10	0	PRESS	.4000	.075	1	310.5	225	.887	.643
16E	200	20	100	.300	10	0	PRESS	.6283	.150	1	243.0	100	.694	.286
16H	200	20	200	.300	10	0	PRESS	.4885	.300	1	>182	75	>.52	.214
16K	200	40	50	.300	10	0	PRESS	.2766	.075	1	538.6	450	1.539	1.286
16N	200	40	100	.300	10	0	PRESS	.2715	.150	1	>346	212.6	>.99	.607
16T	200	60	50	.300	10	0	PRESS	.1896	.075	1	556.7	520	1.591	1.486
20B	400	20	100	.300	10	0	PRESS	.9648	.150	1	212.2	110	.632	.314
20E	400	20	200	.300	10	0	PRESS	1.2566	.300	1	142.0	42	.406	.120
20H	400	20	400	.300	10	0	PRESS	1.1383	.600	1	>109	17	>.31	.049
20K	400	40	100	.300	10	0	PRESS	.6283	.150	1	>510	300	>1.46	.857
20N	400	40	200	.300	10	0	PRESS	.5430	.300	1	271.9	100	.777	.286
20T	400	60	100	.300	10	0	PRESS	.3792	.150	1	414.9	255	1.186	.729
24B	600	20	150	.300	10	0	PRESS	1.7482	.225	1	175.8	65	.502	.186
24B'	600	20	150	.300	10	0	PRESS	1.7482	.225	3+	294.4		.841	
24E	600	20	300	.300	10	0	PRESS	1.8850	.450	1	105.0	30	.300	.086
24H	600	20	600	.300	10	0	PRESS	1.8783	.900	1	99.0	9	.283	.026
24K	600	40	150	.300	10	0	PRESS	.9425	.225	1	198.6		.567	
24N	600	40	300	.300	10	0	PRESS	.8145	.450	1	>248	85	>.71	.243
24T	600	60	150	.300	10	0	PRESS	.5688	.225	1	319.8	205	.914	.586

Table 4.1 PARAMETRIC STUDY OF CYLINDER GEOMETRY

σ_x = nominal axial stress (P/A)
σ_θ = nominal hoop stress (pr/t)
subscripts: u - maximum load (not subsequently exceeded)
1 - initial peak or change in slope (subsequently exceeded)
underlined value taken as cylinder strength
* not eigenmode + circumferential waves

NAME	R	N	L	a_s	d/t	σ_r	LOAD	IMPERFECTION SHELL	IMPERFECTION STIFF	IMPERFECTION MODE	σ_{xa}	σ_{xb}	$\bar{\sigma}_{xa}$	$\bar{\sigma}_{xb}$
13D	200	20	100	.300	10	0	AXIAL	.3142	.075	1	304.3		.869	
13E	200	20	100	.300	10	0	AXIAL	.6283	.150	1	229.4		.655	
13F	200	20	100	.300	10	0	AXIAL	1.2566	.300	1	232.9		.665	
13M	200	40	100	.300	10	0	AXIAL	.1358	.075	1	338.7		.968	
13N	200	40	100	.300	10	0	AXIAL	.2715	.150	1	339.0		.969	
13O	200	40	100	.300	10	0	AXIAL	.4530	.300	1	338.8		.968	
17A	400	20	100	.300	10	0	AXIAL	.4842	.075	1	213.6		.610	
17B	400	20	100	.300	10	0	AXIAL	.9648	.150	1	150.6		.430	
17C	400	20	100	.300	10	0	AXIAL	1.9296	.300	1	111.9		.320	
17D	400	20	200	.300	10	0	AXIAL	.6283	.150	1	226.6		.647	
17E	400	20	200	.300	10	0	AXIAL	1.2566	.300	1	117.6		.336	
17F	400	20	200	.300	10	0	AXIAL	2.5132	.600	1		186.0		.531
17G	400	20	400	.300	10	0	AXIAL	.5692	.300	1	177.8		.508	
17H	400	20	400	.300	10	0	AXIAL	1.1383	.600	1	122.4		.350	
17I	400	20	400	.300	10	0	AXIAL	2.2766	1.200	1	152.4		.435	
17J'	400	40	100	.300	10	0	AXIAL	.1047	.025	3	261.8		.748	
17K'	400	40	100	.300	10	0	AXIAL	.2094	.050	3	213.0		.609	
17L'	400	40	100	.300	10	0	AXIAL	.4186	.100	3	192.5		.550	
17M'	400	40	200	.300	10	0	AXIAL	.0890	.050	3	288.3		.824	
17N'	400	40	200	.300	10	0	AXIAL	.1780	.100	3	243.7		.696	
17O'	400	40	200	.300	10	0	AXIAL	.3560	.200	3	222.3		.635	
17S'	400	60	100	.300	10	0	AXIAL	.0623	.025	3	331.2		.946	
17T'	400	60	100	.300	10	0	AXIAL	.1246	.050	3	313.5		.896	
17U'	400	60	100	.300	10	0	AXIAL	.2492	.100	3	295.5		.844	
21D	600	20	300	.300	10	0	AXIAL	.9425	.225	1	173.2		.495	
21E	600	20	300	.300	10	0	AXIAL	1.8850	.450	1	92.02	152	.263	.434
21F	600	20	300	.300	10	0	AXIAL	3.7700	.900	1		136.3		.401
21M'	600	40	300	.300	10	0	AXIAL	.1358	.075	3	169.8		.485	
21N'	600	40	300	.300	10	0	AXIAL	.2715	.150	3	139.0	187.4	.397	.535
21O'	600	40	300	.300	10	0	AXIAL	.5430	.300	3		185.5		.530
14D	200	20	100	.300	10	0	0.4	.3142	.150	1	181.2		.518	
14E	200	20	100	.300	10	0	0.4	.6283	.300	1	132	174.3	.377	.498
14F	200	20	100	.300	10	0	0.4	1.2566	.600	1		170.3		.487
14M	200	40	100	.300	10	0	0.4	.1358	.075	1	338.9		.968	
14N	200	40	100	.300	10	0	0.4	.2715	.150	1	312.9		.894	
14O	200	40	100	.300	10	0	0.4	.5430	.300	1	285.9		.817	

Table 4.2 PARAMETRIC STUDY OF IMPERFECTION SENSITIVITY (continued)

NAME	R	N	L	a_s	d/t	σ_r	LOAD	IMPERFECTION SHELL	IMPERFECTION STIFF	MODE	σ_{xa}	σ_{xb}	$\bar{\sigma}_{xa}$	$\bar{\sigma}_{xb}$
18D	400	20	200	.300	10	0	0.4	.6283	.150	1	104.3		.289	
18E	400	20	200	.300	10	0	0.4	1.2566	.300	1	58.39	104.1	.167	.297
18F	400	20	200	.300	10	0	0.4	2.5132	.600	1		106.9		.305
18M	400	40	200	.300	10	0	0.4	.2715	.150	1	177.2		.506	
18N	400	40	200	.300	10	0	0.4	.5430	.300	1	176.1		.503	
18O	400	40	200	.300	10	0	0.4	1.0860	.600	1	174.6		.499	
22D	600	20	300	.300	10	0	0.4	.9425	.225	1	85.38		.244	
22E	600	20	300	.300	10	0	0.4	1.8850	.450	1	42.40	80	.121	.229
22F	600	20	300	.300	10	0	0.4	3.7700	.900	1		81.16		.232
22M	600	40	300	.300	10	0	0.4	.4073	.225	1		140.3		.401
22N	600	40	300	.300	10	0	0.4	.8145	.450	1		139.6		.399
22O	600	40	300	.300	10	0	0.4	1.6190	.900	1		140.4		.401
											$\sigma_{\theta a}$	$\sigma_{\theta b}$	$\bar{\sigma}_{\theta a}$	$\bar{\sigma}_{\theta b}$
16D	200	20	100	.300	10	0	PRESS	.3142	.075	1	139.8	220.8	.399	.631
16E	200	20	100	.300	10	0	PRESS	.6283	.150	1	100	238	.286	.680
16F	200	20	100	.300	10	0	PRESS	1.2566	.300	1	75	291.4	.214	.833
16M	200	20	100	.300	10	0	PRESS	.1358	.075	1	225.2	>340	.643	>.97
16N	200	20	100	.300	10	0	PRESS	.2715	.150	1	212.6	>346	.607	>.99
16O	200	20	100	.300	10	0	PRESS	.5430	.300	1	195	>340	.567	>.97
20D	400	20	200	.300	10	0	PRESS	.6283	.150	1	67.80	131.8	.194	.377
20E	400	20	200	.300	10	0	PRESS	1.2566	.300	1	42	142.0	.120	.406
20F	400	20	200	.300	10	0	PRESS	2.5132	.600	1	10	180.0	.029	.514
20M	400	40	200	.300	10	0	PRESS	.2715	.150	1	100	>270	.286	>.77
20N	400	40	200	.300	10	0	PRESS	.5430	.300	1	100	271.9	.286	.777
20O	400	40	200	.300	10	0	PRESS	1.0860	.600	1	100	>280	.286	>.80
24D	600	20	300	.300	10	0	PRESS	.9425	.225	1	49.47	101.0	.141	.289
24E	600	20	300	.300	10	0	PRESS	1.8850	.450	1	30	105.0	.086	.300
24F	600	20	300	.300	10	0	PRESS	3.7700	.900	1	10	131.4	.029	.375
24M	600	40	300	.300	10	0	PRESS	.4073	.225	1		>209		>.60
24N	600	40	300	.300	10	0	PRESS	.8145	.450	1	85	>248	.243	>.71
24O	600	40	300	.300	10	0	PRESS	1.6290	.900	1		>219		>.63

Table 4.2 PARAMETRIC STUDY OF IMPERFECTION SENSITIVITY

σ_x = nominal axial stress (P/A)
σ_θ = nominal hoop stress (pr/t)
subscripts: a - "primary" peak (Sect 4.3.1)
b - "secondary" peak (Sect 4.3.1)

NAME	R	N	L	a_s	d/t	σ_r	LOAD	IMPERFECTION SHELL	IMPERFECTION STIFF	IMPERFECTION MODE	σ_{xu}	σ_{x1}	$\bar{\sigma}_{xu}$	$\bar{\sigma}_{x1}$
01B	200	20	50	.159	10	0	AXIAL	.4000	.075	1	285.4		.815	
13B	200	20	50	.300	10	0	AXIAL	.4000	.075	1	277.7		.793	
01E	200	20	100	.159	10	0	AXIAL	.6283	.150	1	226.5		.647	
13E	200	20	100	.300	10	0	AXIAL	.6283	.150	1	229.4		.655	
25E	200	20	100	.500	10	0	AXIAL	.6283	.150	1	230.6		.659	
13N	200	40	100	.300	10	0	AXIAL	.2715	.150	1	339.0		.969	
25N	200	40	100	.500	10	0	AXIAL	.2715	.150	1	350.9		1.003	
13T	200	60	50	.300	10	0	AXIAL	.1896	.075	1	307.8		.879	
25T	200	60	50	.500	10	0	AXIAL	.1896	.075	1	337.1		.963	
05B	400	20	100	.080	10	0	AXIAL	.9648	.150	1	122.8		.351	
17B	400	20	100	.300	10	0	AXIAL	.9648	.150	1	150.6		.430	
05E	400	20	200	.080	10	0	AXIAL	1.2566	.300	1	121.5	103.8	.347	.297
17E	400	20	200	.300	10	0	AXIAL	1.2566	.300	1		117.6		.336
29E	400	20	200	.500	10	0	AXIAL	1.2566	.300	1		115.8		.331
05N'	400	40	200	.159	10	0	AXIAL	.1780	.100	3	237.4		.678	
17N'	400	40	200	.300	10	0	AXIAL	.1780	.100	3	243.7		.696	
29N'	400	40	200	.500	10	0	AXIAL	.1780	.100	3	252.2		.721	
17T'	400	60	100	.300	10	0	AXIAL	.1246	.050	3	313.5		.896	
29T'	400	60	100	.500	10	0	AXIAL	.1246	.050	3	311.6		.890	
21E	600	20	300	.300	10	0	AXIAL	1.8850	.450	1		92.02		.263
33E	600	20	300	.500	10	0	AXIAL	1.8850	.450	1		88.30		.252
09N'	600	40	300	.106	10	0	AXIAL	.2715	.150	3	177.5	134.0	.507	.383
21N'	600	40	300	.300	10	0	AXIAL	.2715	.150	3	187.4	139.0	.535	.397
33N'	600	40	300	.500	10	0	AXIAL	.2715	.150	3	181.1	145.3	.517	.415
09T'	600	60	150	.159	10	0	AXIAL	.1896	.075	3	221.0		.631	
21T'	600	60	150	.300	10	0	AXIAL	.1896	.075	3	221.8		.634	
33T'	600	60	150	.500	10	0	AXIAL	.1896	.075	3	215.5		.616	

Table 4.3 PARAMETRIC STUDY OF STIFFENING RATIO (continued)

NAME	R	N	L	a_s	d/t	σ_r	LOAD	IMPERFECTION SHELL	IMPERFECTION STIFF	MODE	σ_{xu}	σ_{x1}	$\bar{\sigma}_{xu}$	$\bar{\sigma}_{x1}$
02B	200	20	50	.159	10	0	0.4	.4000	.075	1	189.9		.543	
14B	200	20	50	.300	10	0	0.4	.4000	.075	1	194.2		.555	
02E	200	20	100	.159	10	0	0.4	.6283	.150	1	142.2	120	.406	.343
14E	200	20	100	.300	10	0	0.4	.6283	.150	1	174.3	132	.498	.377
26E	200	20	100	.500	10	0	0.4	.6283	.150	1	180	140	.514	.400
14N	200	40	100	.300	10	0	0.4	.2715	.150	1	312.9		.894	
26N	200	40	100	.500	10	0	0.4	.2715	.150	1	319.1		.912	
14T	200	60	50	.300	10	0	0.4	.1896	.075	1	327.0		.934	
26T	200	60	50	.500	10	0	0.4	.1896	.075	1	366.3		1.047	
06B	400	20	100	.080	10	0	0.4	.9648	.150	1	93.60		.267	
18B	400	20	100	.300	10	0	0.4	.9648	.150	1	103.9		.297	
06E	400	20	200	.080	10	0	0.4	1.2566	.300	1	70	51.5	.200	.147
18E	400	20	200	.300	10	0	0.4	1.2566	.300	1	104.1	58.39	.297	.167
30E	400	20	200	.500	10	0	0.4	1.2566	.300	1		60.76		.174
06N	400	40	200	.159	10	0	0.4	.5430	.300	1	132.0		.377	
18N	400	40	200	.300	10	0	0.4	.5430	.300	1	176.1		.503	
30N	400	40	200	.500	10	0	0.4	.5430	.300	1	208.0		.594	
18T	400	60	100	.300	10	0	0.4	.1246	.050	3	284.1		.812	
30T	400	60	100	.500	10	0	0.4	.1246	.050	3	288		.823	
22E	600	20	300	.300	10	0	0.4	1.8850	.450	1	80	42.40	.229	.121
34E	600	20	300	.500	10	0	0.4	1.8850	.450	1		43.60		.125
10N	600	40	300	.106	10	0	0.4	.8145	.450	1	99.42		.284	
22N	600	40	300	.300	10	0	0.4	.8145	.450	1	139.6		.399	
34N	600	40	300	.500	10	0	0.4	.8145	.450	1	168.4		.481	
22T'	600	60	150	.300	10	0	0.4	.1896	.075	3	207.2		.592	
34T'	600	60	150	.500	10	0	0.4	.1896	.075	3	196.4		.561	

Table 4.3 PARAMETRIC STUDY OF STIFFENING RATIO (continued)

NAME	R	N	L	a_s	d/t	σ_r	LOAD	IMPERFECTION SHELL	IMPERFECTION STIFF	MODE	$\sigma_{\theta u}$	$\sigma_{\theta 1}$	$\bar{\sigma}_{\theta u}$	$\bar{\sigma}_{\theta 1}$
04B	200	20	50	.159	10	0	PRESS	.4000	.075	1	286	226	.817	.646
16B	200	20	50	.300	10	0	PRESS	.4000	.075	1	310.5	225	.887	.643
04E	200	20	100	.159	10	0	PRESS	.6283	.150	1	>246	100	>.70	.286
16E	200	20	100	.300	10	0	PRESS	.6283	.150	1	238	100	.680	.286
28E	200	20	100	.500	10	0	PRESS	.6283	.150	1	219.2	125	.626	.357
16N	200	40	100	.300	10	0	PRESS	.2715	.150	1	>346	212.6	>.99	.607
28N	200	40	100	.500	10	0	PRESS	.2715	.150	1	>330	301.9	>.94	.863
16T	200	60	50	.300	10	0	PRESS	.1896	.075	1	556.7	520	1.591	1.486
28T	200	60	50	.500	10	0	PRESS	.1896	.075	1	785.9	760	2.243	2.717
08B	400	20	100	.080	10	0	PRESS	.9648	.150	1	169.1	100	.483	.286
20B	400	20	100	.300	10	0	PRESS	.9648	.150	1	221.2	110	.632	.314
08E	400	20	200	.080	10	0	PRESS	1.2566	.300	1	66.80	35	.191	.100
20E	400	20	200	.300	10	0	PRESS	1.2566	.300	1	142.0	42	.406	.120
32E	400	20	200	.500	10	0	PRESS	1.2566	.300	1	154.1	45	.440	.129
08N	400	40	200	.159	10	0	PRESS	.5430	.300	1	>206	40	>.59	.114
20N	400	40	200	.300	10	0	PRESS	.5430	.300	1	271.9	100	.777	.286
32N	400	40	200	.500	10	0	PRESS	.5430	.300	1	212.6	160	.607	.457
20T	400	60	100	.300	10	0	PRESS	.3792	.150	1	414.9	255	1.186	.729
32T	400	60	100	.500	10	0	PRESS	.3792	.150	1	497.6	410	1.422	1.171
24E	600	20	300	.300	10	0	PRESS	1.8850	.450	1	105.0	30	.300	.086
36E	600	20	300	.500	10	0	PRESS	1.8850	.450	1	123.2	33	.352	.094
12N	600	40	300	.106	10	0	PRESS	.8145	.450	1	>150	15	>.43	.043
24N	600	40	300	.300	10	0	PRESS	.8145	.450	1	>248	55	>.71	.157
36N	600	40	300	.500	10	0	PRESS	.8145	.450	1		139.0		.397
12T	600	60	150	.159	10	0	PRESS	.5688	.225	1	>300	85	>.86	.243
24T	600	60	150	.300	10	0	PRESS	.5688	.225	1	319.8	205	.914	.586
36T	600	60	150	.500	10	0	PRESS	.5688	.225	1	>400	325	>1.14	.929

Table 4.3 PARAMETRIC STUDY OF STIFFENING RATIO

σ_x = nominal axial stress (P/A)
σ_θ = nominal hoop stress (pr/t)
subscripts: u - maximum load (not subsequently exceeded)
1 - initial peak or change in slope (subsequently exceeded)
underlined value taken as cylinder strength

NAME	R	N	L	a_s	d/t	σ_r	LOAD	IMPERFECTION SHELL	IMPERFECTION STIFF	IMPERFECTION MODE	σ_{xu}	σ_{x1}	$\bar{\sigma}_{xu}$	$\bar{\sigma}_{x1}$
13E	200	20	100	.300	10	0	AXIAL	.6283	.150	1	229.4		.655	
37E	200	20	100	.300	10	.300	AXIAL	.6283	.150	1	219.0	149.9	.626	.428
13N	200	40	100	.300	10	0	AXIAL	.2715	.150	1	339.0		.969	
37N	200	40	100	.300	10	.300	AXIAL	.2715	.150	1	336.4		.961	
13T	200	60	50	.300	10	0	AXIAL	.1896	.075	1	307.8		.879	
37T	200	60	50	.300	10	.300	AXIAL	.1896	.075	1	291.5		.833	
17E	400	20	200	.300	10	0	AXIAL	1.2566	.300	1		117.6		.336
41E	400	20	200	.300	10	.300	AXIAL	1.2566	.300	1		48.43		.138
17N'	400	40	200	.300	10	0	AXIAL	.1780	.100	3	243.7		.696	
41N'	400	40	200	.300	10	.300	AXIAL	.1780	.100	3	197.1	155.9	.563	.445
14E	200	20	100	.300	10	0	0.4	.6283	.100	1	174.3	132	.498	.377
38E	200	20	100	.300	10	.300	0.4	.6283	.100	1	165.3	87	.472	.249
14N	200	40	100	.300	10	0	0.4	.2715	.150	1	312.9		.894	
29N	200	40	100	.300	10	.300	0.4	.2715	.150	1	267.9		.765	
14T	200	60	50	.300	10	0	0.4	.1896	.075	1	327.0		.934	
29T	200	60	50	.300	10	.300	0.4	.1896	.075	1	323.5		.924	
18E	400	20	200	.300	10	0	0.4	1.2566	.300	1	104.1	58.39	.297	.167
42E	400	20	200	.300	10	.300	0.4	1.2566	.300	1		24.50		.070
18N	400	40	200	.300	10	0	0.4	.5430	.300	1	176.1		.503	
42N	400	40	200	.300	10	.300	0.4	.5430	.300	1				
											$\sigma_{\theta u}$	$\sigma_{\theta 1}$	$\bar{\sigma}_{\theta u}$	$\bar{\sigma}_{\theta 1}$
16E	200	20	100	.300	10	0	PRESS	.6283	.150	1	238.0	100	.680	.286
40E	200	20	100	.300	10	.300	PRESS	.6283	.150	1	208.6	70	.596	.200
16N	200	40	100	.300	10	0	PRESS	.2715	.150	1	>346	212.6	>.99	.607
40N	200	40	100	.300	10	.300	PRESS	.2715	.150	1	>261	196.3	>.75	.561
16T	200	60	50	.300	10	0	PRESS	.1896	.075	1	556.7	520	1.591	1.486
40T	200	60	50	.300	10	.300	PRESS	.1896	.075	1	540.8	500	1.545	1.429
20E	400	20	200	.300	10	0	PRESS	1.2566	.300	1	142.0	42	.406	.120
44E	400	20	200	.300	10	.300	PRESS	1.2566	.300	1	>83	19.07	.237	.054
20N	400	40	200	.300	10	0	PRESS	.5430	.300	1	271.9	100	.777	.286
44N	400	40	200	.300	10	.300	PRESS	.5430	.300	1	296.9	95	.848	.271

Table 4.4 PARAMETRIC STUDY OF RESIDUAL STRESSES

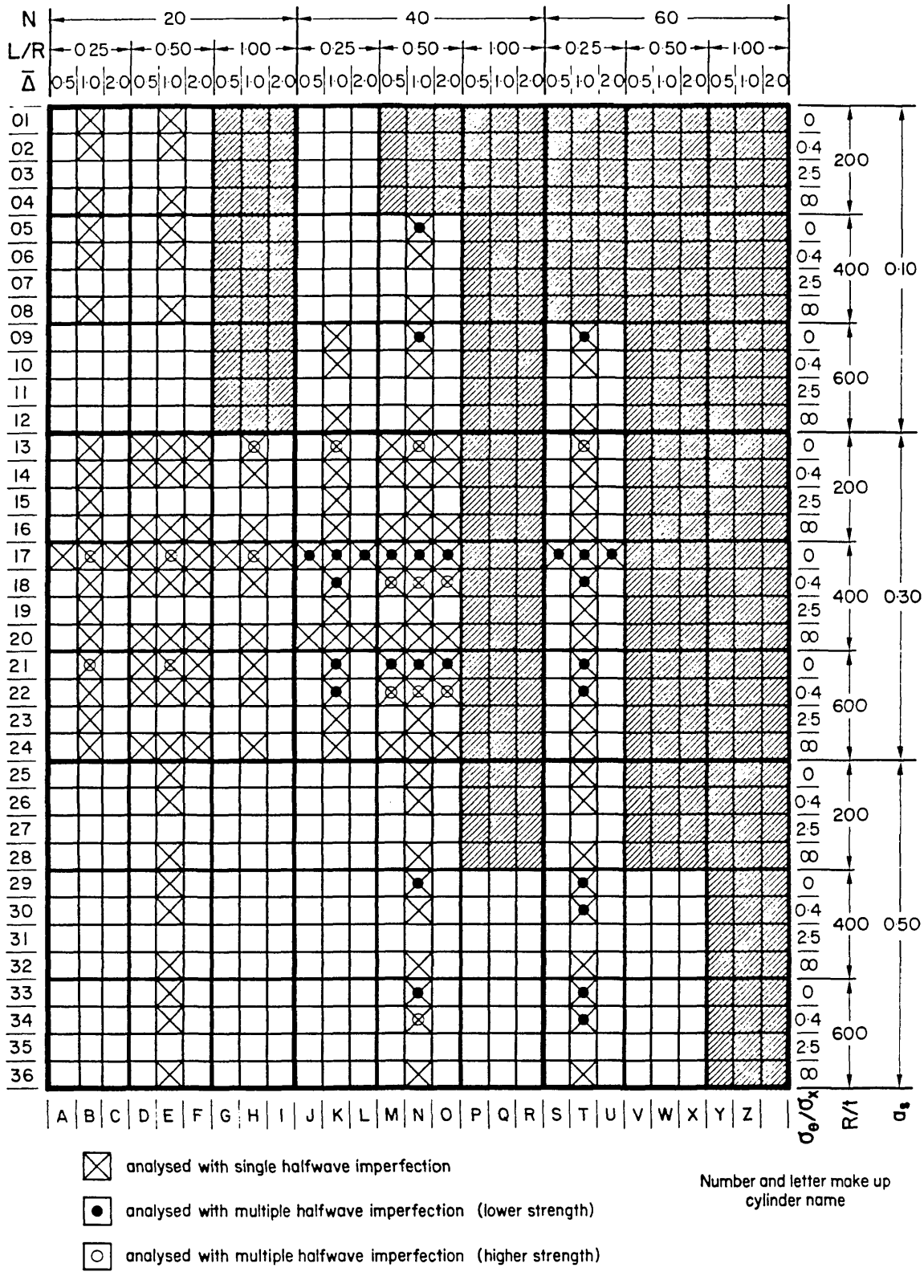
NAME	R	N	L	a_s	d/t	σ_r	LOAD	IMPERFECTION SHELL	IMPERFECTION STIFF	IMPERFECTION MODE	σ_{xu}	σ_{x1}	$\bar{\sigma}_{xu}$	$\bar{\sigma}_{x1}$
13E	200	20	100	.300	10	0	AXIAL	.6283	.150	1	229.4		.655	
49E	200	20	100	.300	20	0	AXIAL	.6283	.150	1	224.9		.643	
13N	200	40	100	.300	10	0	AXIAL	.2715	.150	1	339.0		.969	
49N	200	40	100	.300	20	0	AXIAL	.2715	.150	1	269.0		.769	
13T	200	60	50	.300	10	0	AXIAL	.1896	.075	1	307.8		.879	
49T	200	60	50	.300	20	0	AXIAL	.1896	.075	1				
17E	400	20	200	.300	10	0	AXIAL	1.2566	.300	1		117.6		.336
53E	400	20	200	.300	20	0	AXIAL	1.2566	.300	1		113.1		.323
17N'	400	40	200	.300	10	0	AXIAL	.1780	.100	3	243.7		.696	
53N'	400	40	200	.300	20	0	AXIAL	.1780	.100	3	225.6		.645	
14E	200	20	100	.300	10	0	0.4	.6283	.100	1	174.3	132	.498	.377
50E	200	20	100	.300	20	0	0.4	.6283	.100	1	179.4	130	.513	.371
14N	200	40	100	.300	10	0	0.4	.2715	.150	1	312.9		.894	
50N	200	40	100	.300	20	0	0.4	.2715	.150	1	279.2		.798	
14T	200	60	50	.300	10	0	0.4	.1896	.075	1	327.0		.934	
50T	200	60	50	.300	20	0	0.4	.1896	.075	1	240.8		.688	
18E	400	20	200	.300	10	0	0.4	1.2566	.300	1	104.1	58.39	.297	.167
54E	400	20	200	.300	20	0	0.4	1.2566	.300	1		56.80		.162
18N	400	40	200	.300	10	0	0.4	.5430	.300	1	176.1		.503	
54N	400	40	200	.300	20	0	0.4	.5430	.300	1	212.5		.607	
											$\sigma_{\theta u}$	$\sigma_{\theta 1}$	$\bar{\sigma}_{\theta u}$	$\bar{\sigma}_{\theta 1}$
16E	200	20	100	.300	10	0	PRESS	.6283	.150	1	238.0	100	.680	.286
52E	200	20	100	.300	20	0	PRESS	.6283	.150	1	213.3	95	.609	.271
16N	200	40	100	.300	10	0	PRESS	.2715	.150	1	>346	212.6	>.99	.607
52N	200	40	100	.300	20	0	PRESS	.2715	.150	1	>302	240.6	>.86	.687
16T	200	60	50	.300	10	0	PRESS	.1896	.075	1	556.7	520	1.591	1.486
52T	200	60	50	.300	20	0	PRESS	.1896	.075	1	640.5	600	1.830	1.714
20E	400	20	200	.300	10	0	PRESS	1.2566	.300	1	142.0	42	.406	.120
56E	400	20	200	.300	20	0	PRESS	1.2566	.300	1	130.9	44	.374	.126
20N	400	40	200	.300	10	0	PRESS	.5430	.300	1	271.9	100	.777	.286
56N	400	40	200	.300	20	0	PRESS	.5430	.300	1	>230	115	>.66	.329

Table 4.5 PARAMETRIC STUDY OF STIFFENER SLENDERNESS

NAME	R	N	L	a_s	d/t	σ_r	LOAD	IMPERFECTION SHELL	IMPERFECTION STIFF	m	n_5	σ_{xu}	σ_{x1}	$\bar{\sigma}_{xu}$	$\bar{\sigma}_{x1}$
13N	200	40	100	.300	10	0	AXIAL	.2715	.150	1	5	339.0		.969	
13N5	200	40	100	.300	10	0	AXIAL	.2715	.150	1	3	328.8		.939	
13T	200	60	50	.300	10	0	AXIAL	.1896	.075	1	5	307.8		.879	
13T5	200	60	50	.300	10	0	AXIAL	.1896	.075	1	2	305.6		.873	
17H	400	20	400	.300	10	0	AXIAL	1.1383	.600	1	5		122.4		.350
17H5	400	20	400	.300	10	0	AXIAL	1.1383	.600	1	5		124.3		.355
17N'	400	40	200	.300	10	0	AXIAL	.1780	.100	3	5	243.7		.696	
17N5	400	40	200	.300	10	0	AXIAL	.1780	.100	1	3	270.7		.773	
21H	600	20	600	.300	10	0	AXIAL	1.8783	.900	1	5		74.77		.214
21H5	600	20	600	.300	10	0	AXIAL	1.8783	.900	1	6		80.50		.230
21N'	600	40	300	.300	10	0	AXIAL	.2715	.150	3	5	187.4	139.0	.535	.397
21N5	600	40	300	.300	10	0	AXIAL	.2715	.150	1	4		179.9		.514
05N'	400	40	200	.159	10	0	AXIAL	.1780	.100	3	5	237.4		.678	
05N5	400	40	200	.159	10	0	AXIAL	.1780	.100	1	3	223.5		.639	
												$\sigma_{\theta u}$	$\sigma_{\theta 1}$	$\bar{\sigma}_{\theta u}$	$\bar{\sigma}_{\theta 1}$
16N	200	40	100	.300	10	0	PRESS	.2715	.150	1	5	>346	212.6	>.99	.607
16N5	200	40	100	.300	10	0	PRESS	.2715	.150	1	4		208.0		.594
16T	200	60	50	.300	10	0	PRESS	.1896	.075	1	5	556.7	520	1.591	1.486
16T5	200	60	50	.300	10	0	PRESS	.1896	.075	1	4		499.3		1.427
20H	400	20	400	.300	10	0	PRESS	1.1383	.600	1	5	>109	17	>.31	.049
20H5	400	20	400	.300	10	0	PRESS	1.1383	.600	1	6		17		.049
24H	600	20	600	.300	10	0	PRESS	1.8783	.900	1	5	99.0	9	.283	.026
24H5	600	20	600	.300	10	0	PRESS	1.8783	.900	1	5		12		
24N	600	40	300	.300	10	0	PRESS	.8145	.450	1	5	>248	85	>.71	.243
24N5	600	40	300	.300	10	0	PRESS	.8145	.450	1	5		85		.243

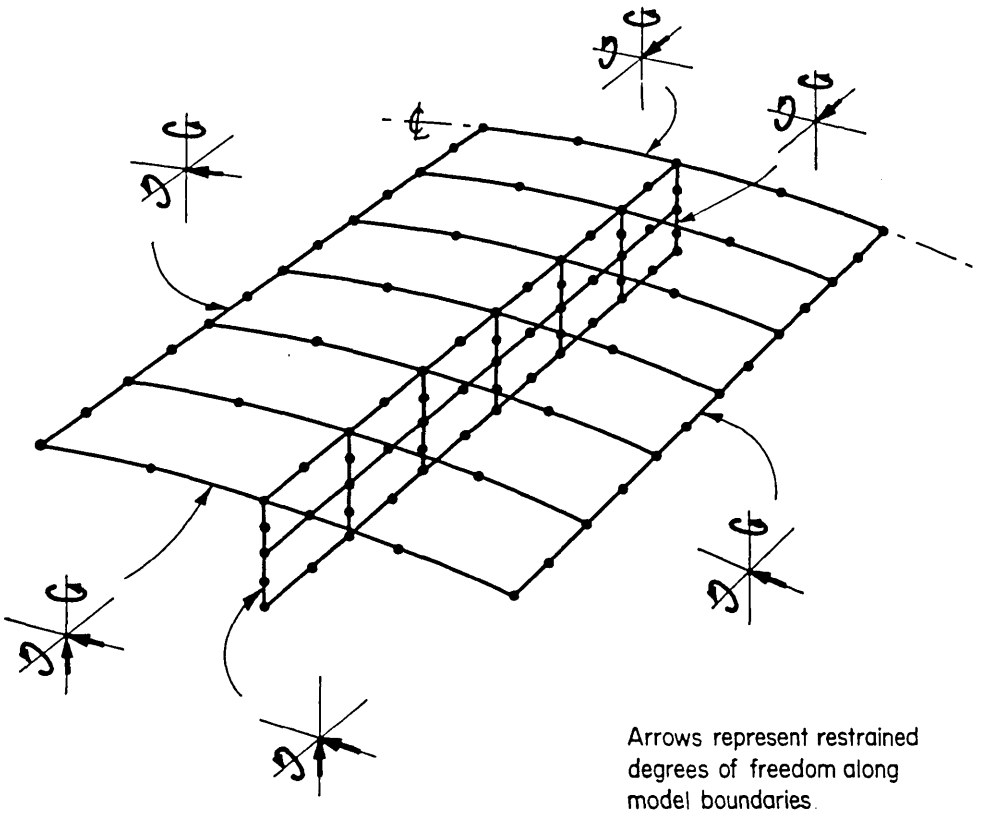
n_5 number of circumferential waves in five panel model

Table 4.6 FIVE PANEL ANALYSES



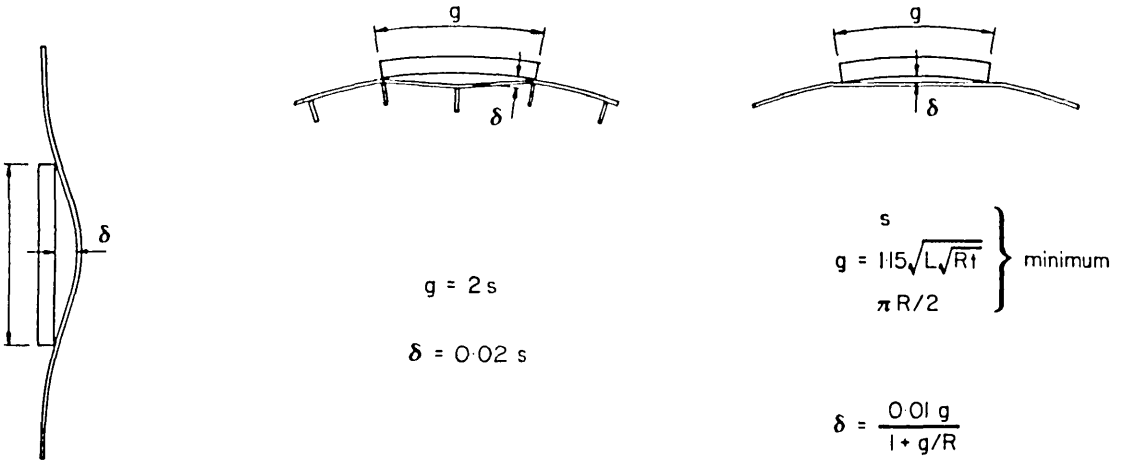
INFORMATION TABLE OF MAJOR VARIABLES IN PARAMETRIC STUDY

Fig. 4.1



Finite element model
(parametric study)

Fig. 4.2



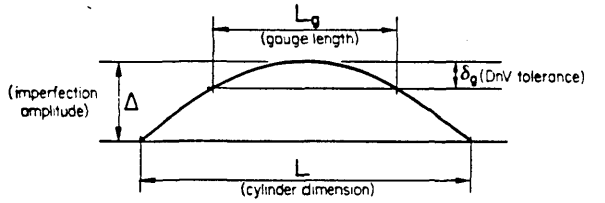
(a) out-of-straightness

(b) misalignment of stiffeners

(c) out-of-roundness

DnV imperfection tolerances

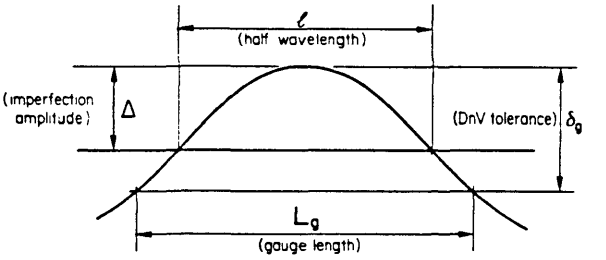
Fig. 4.3



$$\Delta = \frac{\delta_g}{1 - \cos\beta\frac{\pi}{2}}$$

where $\beta = L_g/L$

(a) Single halfwave imperfection



$$\Delta = \frac{\delta_g}{1 - \cos\beta\frac{\pi}{2}}$$

where $\beta = L_g/\ell$ (if $\beta > 2$ $\Delta = \frac{1}{2}\delta_g$)

(b) Multiple halfwave imperfection

Extrapolation of imperfection magnitude

Fig. 4.4

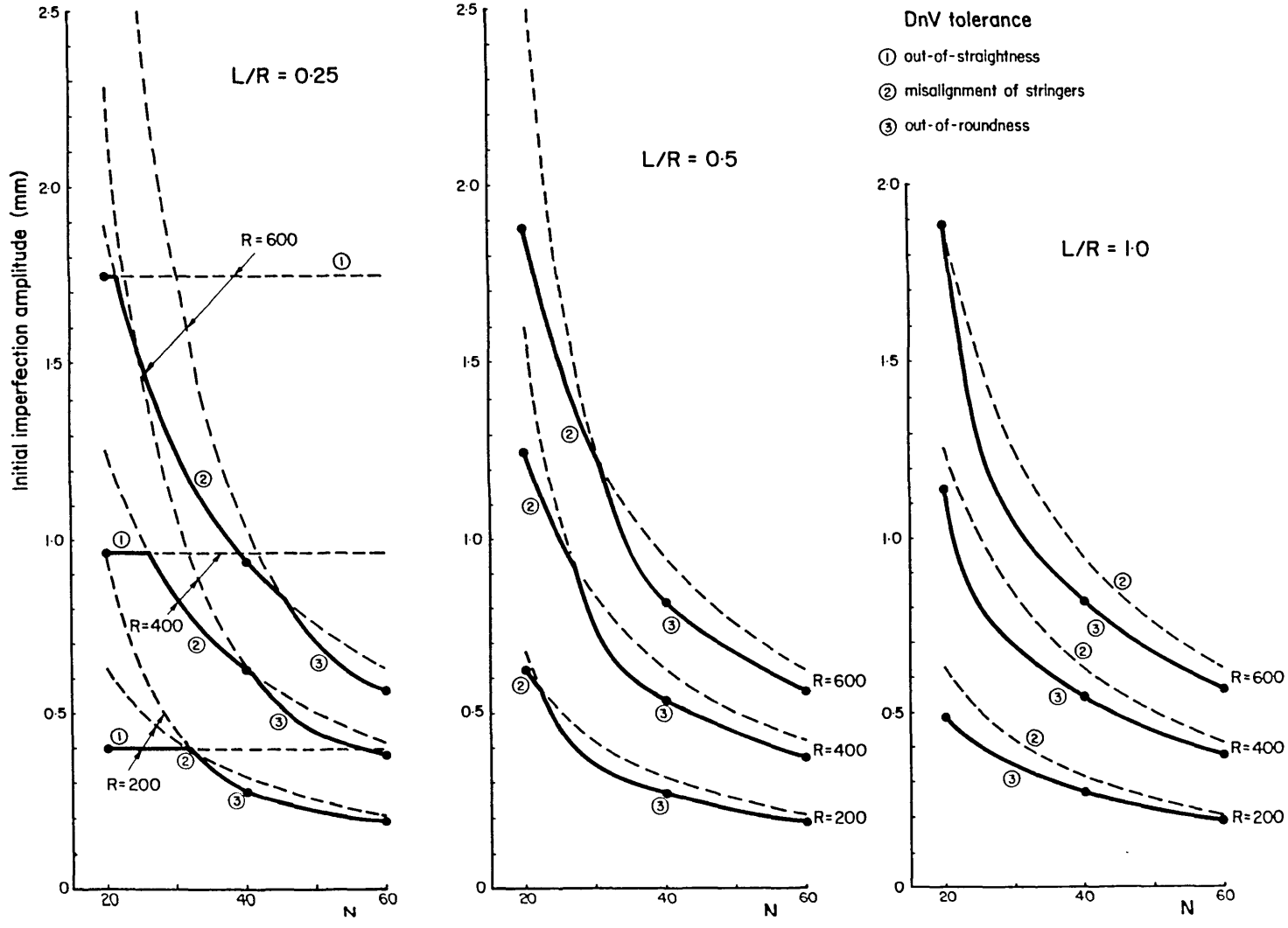

Imperfections for parametric study
DnV tolerance
① out-of-straightness
② misalignment of stringers
③ out-of-roundness
L/R = 0·25
L/R = 0·5
L/R = 1·0
Initial imperfection amplitude (mm)
R=600
R=400
R=200
N
2·5
2·0
1·5
1·0
0·5
0
20
40
60

Fig. 4.5

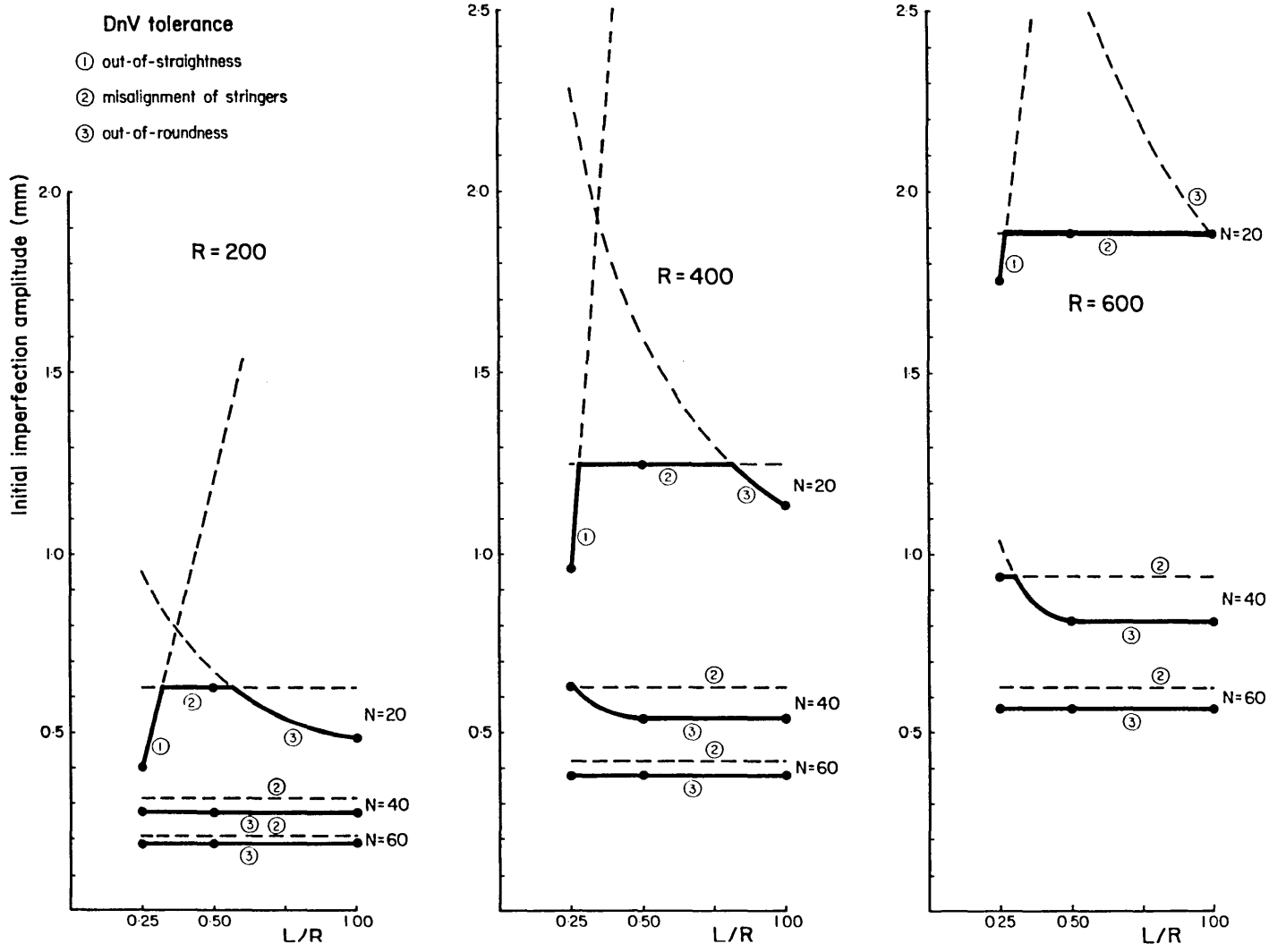
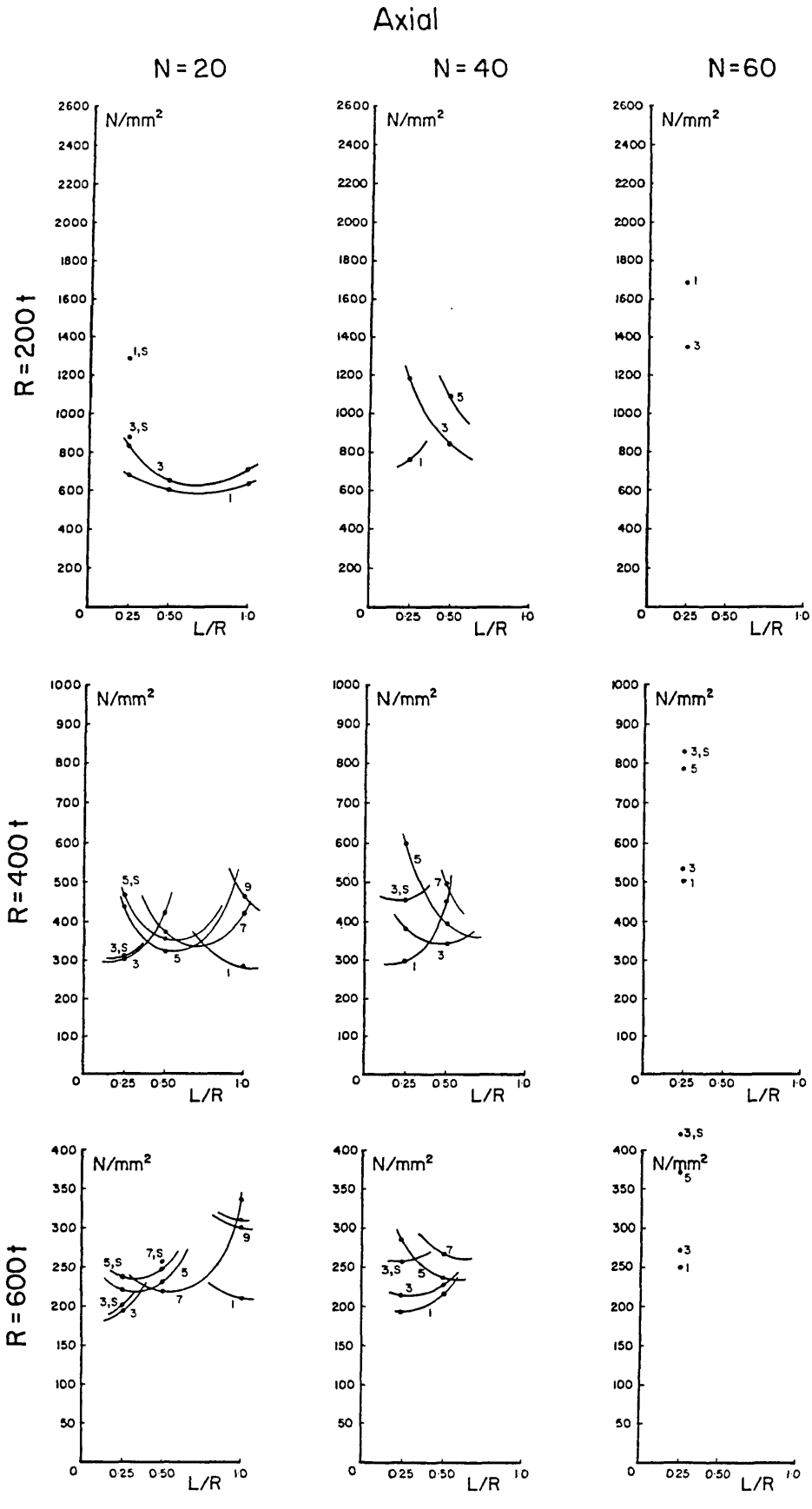

Imperfections for parametric study
DnV tolerance
① out-of-straightness
② misalignment of stringers
③ out-of-roundness
Initial imperfection amplitude (mm)
R = 200
R = 400
R = 600
N=20
N=40
N=60
L/R
0·25
0·50
1·00
0·5
1·0
1·5
2·0
2·5

Fig. 4.6

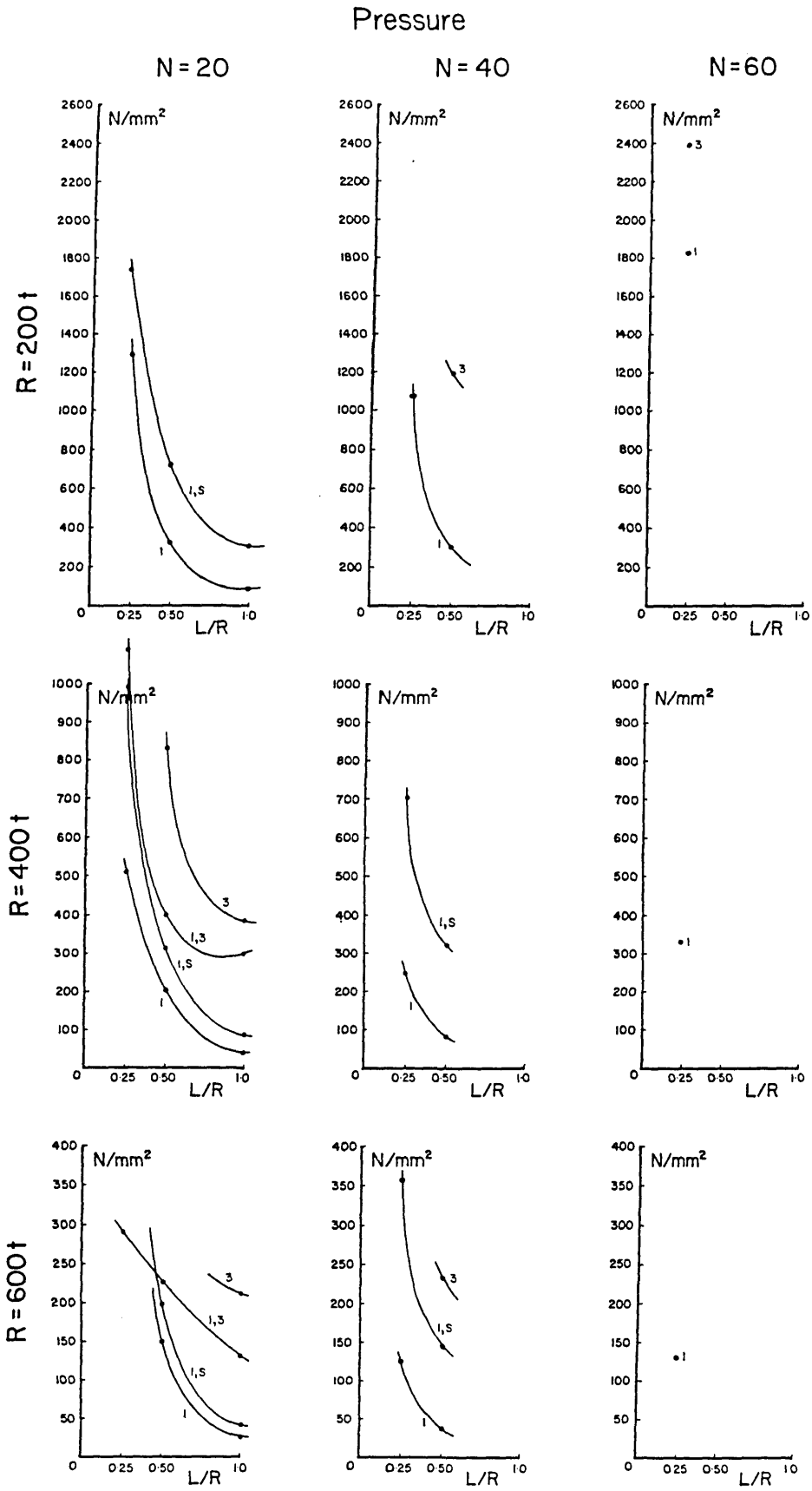
Eigenvalues



Notes: where one number appears it refers to the halfwaves in the longitudinal direction
there is one halfwave in the the transverse direction unless noted otherwise (second no.)
the mode shape is antisymmetric unless the letter S (symmetric) appears

Fig. 4.7

Eigenvalues

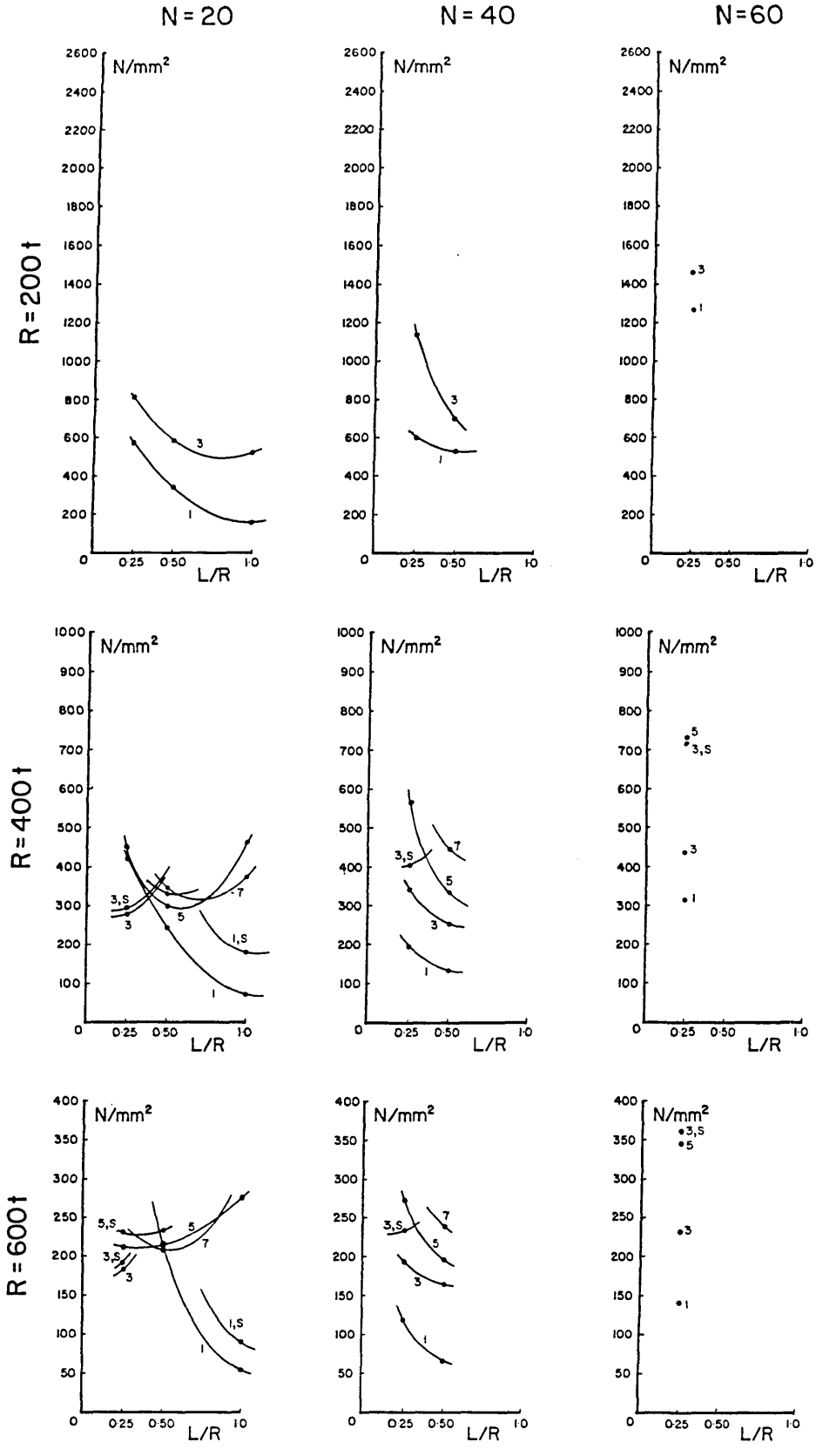


Notes: where one number appears it refers to the halfwaves in the longitudinal direction
there is one halfwave in the the transverse direction unless noted otherwise (second no.)
the mode shape is antisymmetric unless the letter S (symmetric) appears

Fig. 4.8

Eigenvalues

$\sigma_\theta/\sigma_x = 0{\cdot}4$



Notes: where one number appears it refers to the halfwaves in the longitudinal direction
there is one halfwave in the the transverse direction unless noted otherwise (second no.)
the mode shape is antisymmetric unless the letter S (symmetric) appears

Fig. 4.9

LOAD-DEFLECTION PATHS

Axial load

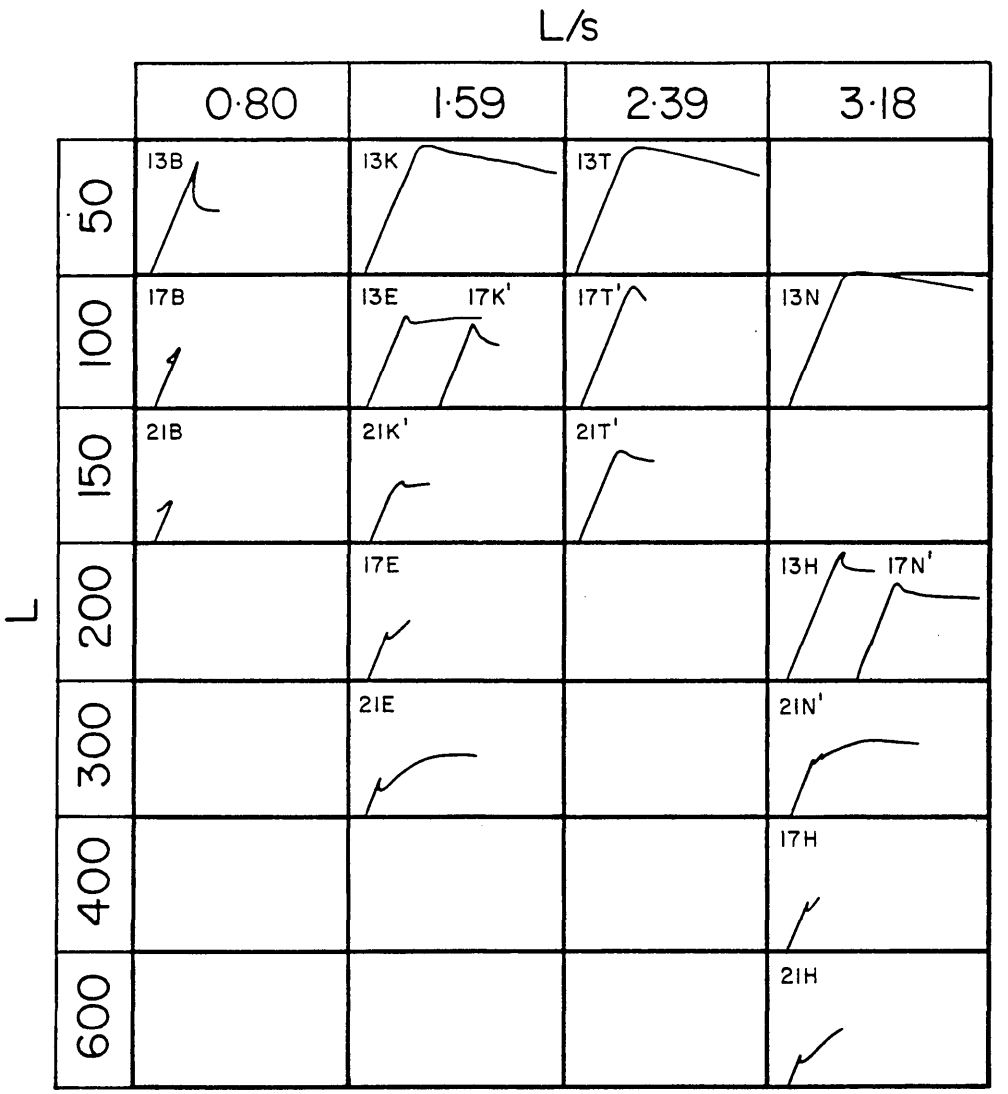


Fig. 4.10

DEFLECTION MODE

Axial load

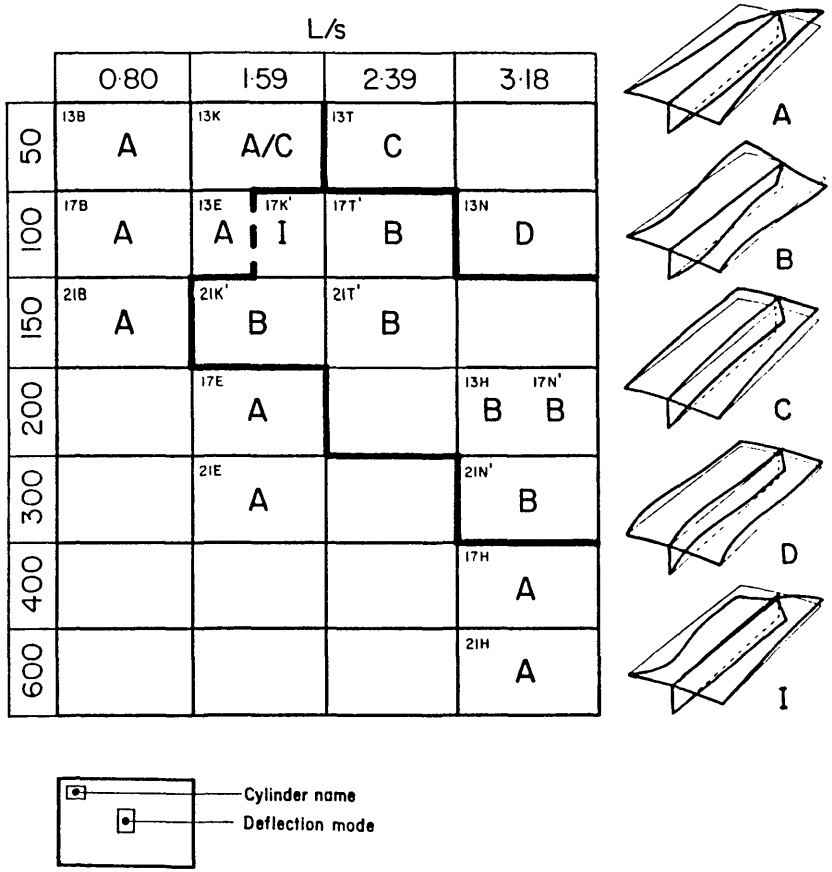


Fig. 4.12

FIRST YIELD

Axial load

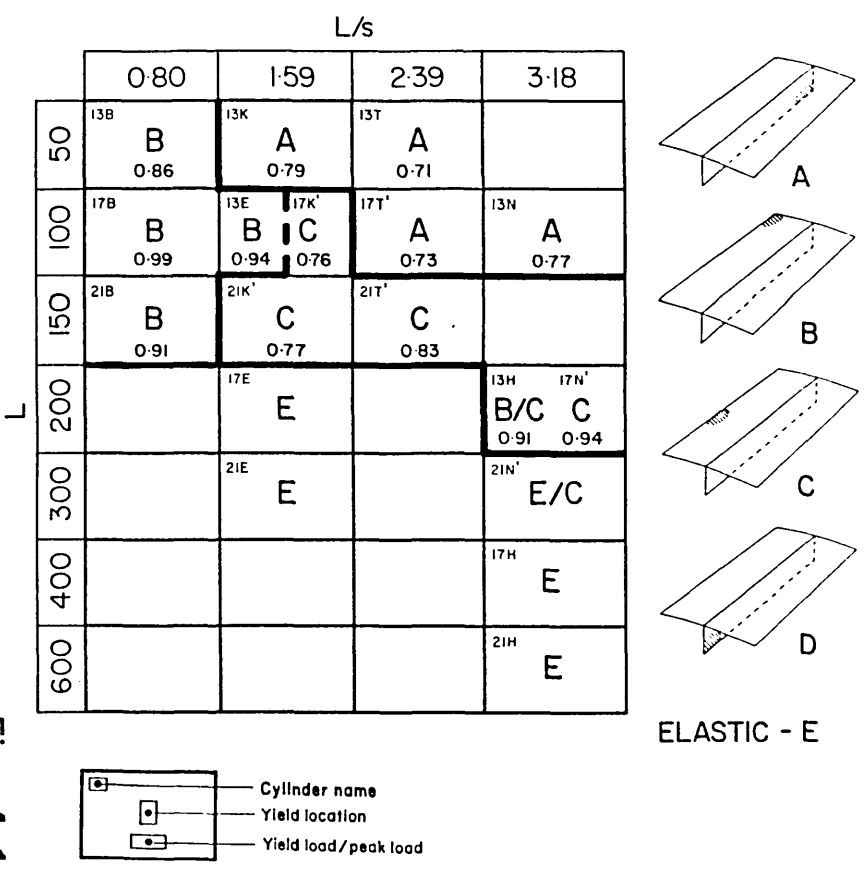


Fig. 4.11

LOAD-DEFLECTION PATHS

Pressure load

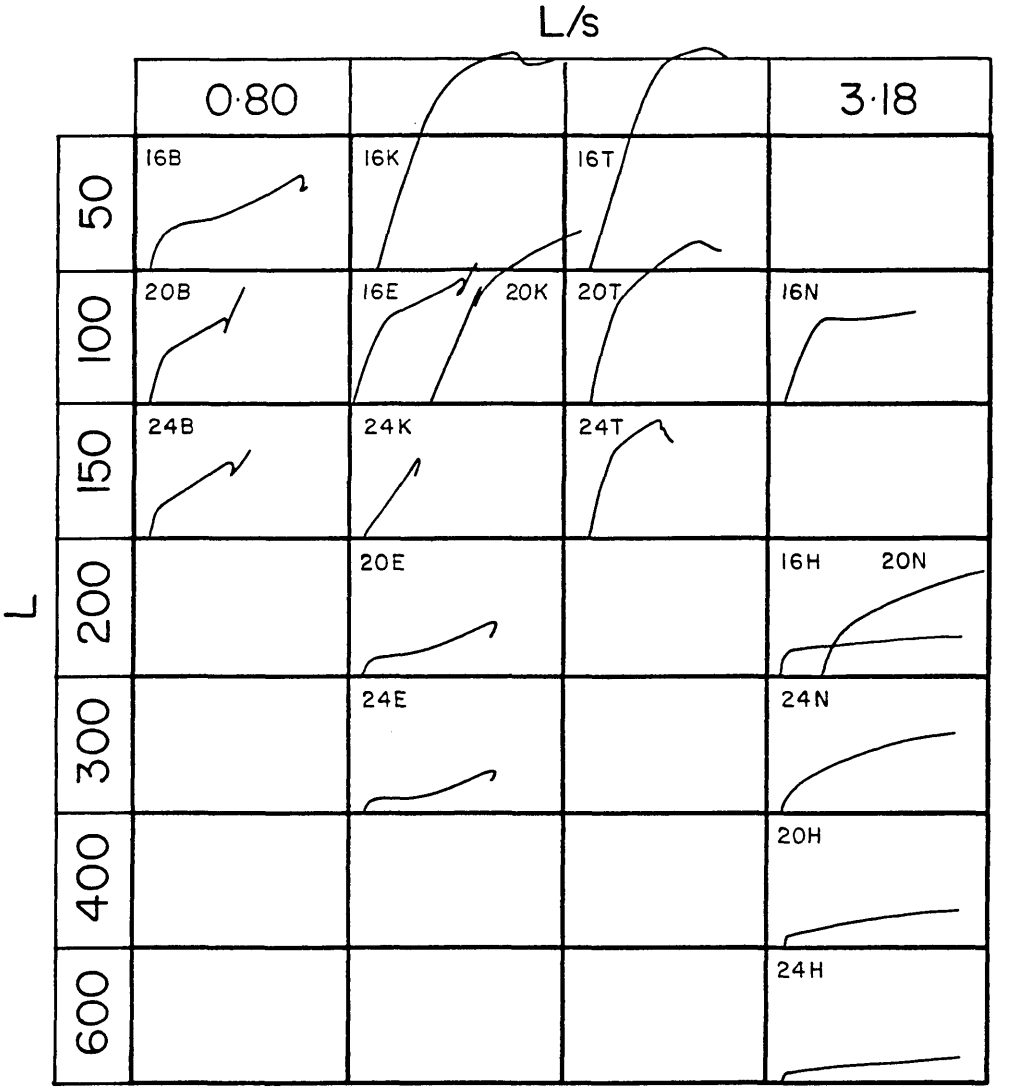
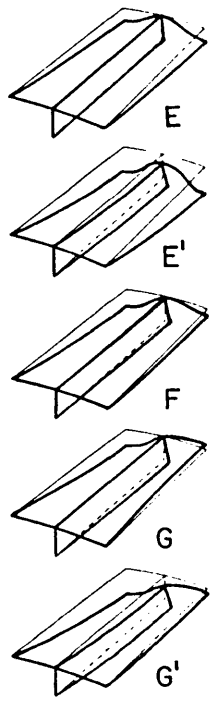


Fig. 4.13

DEFLECTION MODE

Pressure load

L \ L/s	0·80	1·59	2·39	3·18
50	16B F-E	16K F-E'	16T G'-E'	
100	20B F-E	16E F-E 20K F-E	20T G'-E'	16N G-G'
150	24B F-E	24K G-E	24T G'-E'	
200		20E G-E		16H G-G' 20N G-G'
300		24E G-E		24N G-G'
400				20H G-G'
600				24H G-G'



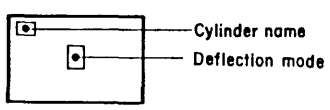
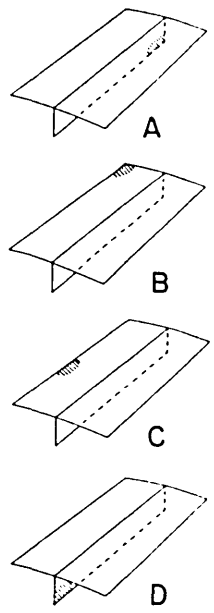


Fig. 4.15

FIRST YIELD

Pressure load

L \ L/s	0·80	1·59	2·39	3·18
50	16B B 0·76	16K B 0·59	16T A 0·58	
100	20B B 1·14	16E B 1·00 20K B 0·45	20T A/B 0·76	16N B 0·71
150	24B B 1·62	24K B 0·60	24T B 0·68	
200		20E B 1·19		16H B 0·73 20N B ·75
300		24E E/C 1·67		24N B 0·75
400				20H B 1·41
600				24H C 2·78



ELASTIC - E

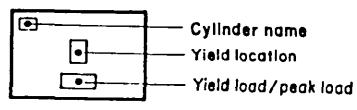


Fig. 4.14

LOAD-DEFLECTION PATHS

$\sigma_\theta/\sigma_x = 0{\cdot}4$

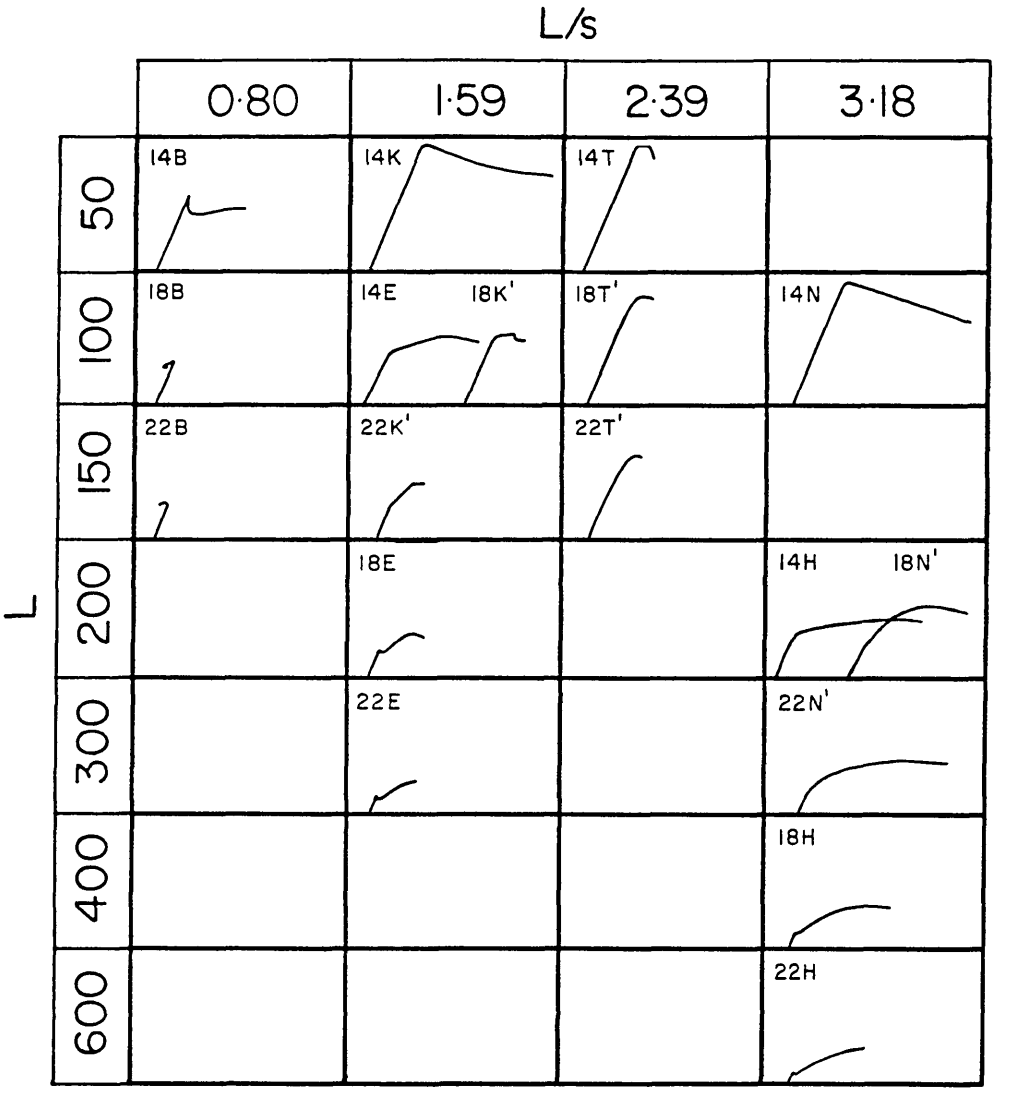
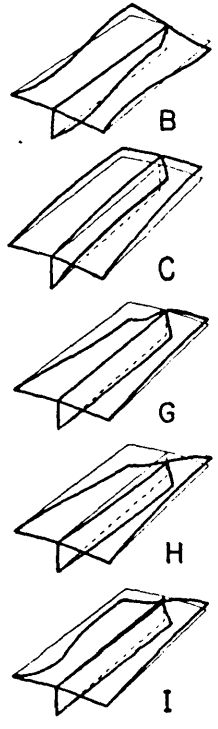


Fig. 4.16

DEFLECTION MODE

$\sigma_\theta/\sigma_x = 0{\cdot}4$

L \ L/s	0·80	1·59	2·39	3·18
50	14B G	14K G	14T C	
100	18B G	14E G | 18K' I	18T' B	14N H
150	22B G	22K' I	22T' I	
200		18E G		14H H 18N H
300		22E G		22N H
400				18H H
600				22H H



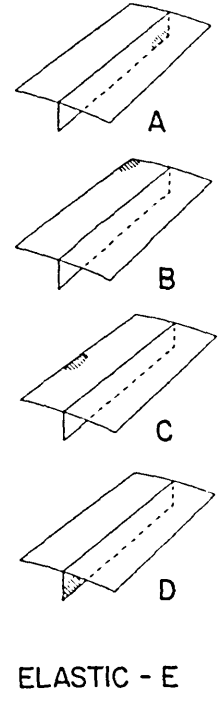
Cylinder name
Deflection mode

Fig. 4.18

FIRST YIELD

$\sigma_\theta/\sigma_x = 0{\cdot}4$

L \ L/s	0·80	1·59	2·39	3·18
50	14B B 0·93	14K B 0·69	14T D 0·86	
100	18B B 0·98	14E B 0·72 18K' C 0·90	18T' C 0·81	14N B 0·77
150	22B B 0·95	22K' E/C	22T' C 0·72	
200		18E E		14H B 0·74 18N B 0·68
300		22E E		22N C 0·61
400				18H E/B
600				22H E



ELASTIC - E

Cylinder name
Yield location
Yield load/peak load

Fig. 4.17

LOAD-DEFLECTION PATHS

$\sigma_\theta/\sigma_x = 2{\cdot}5$

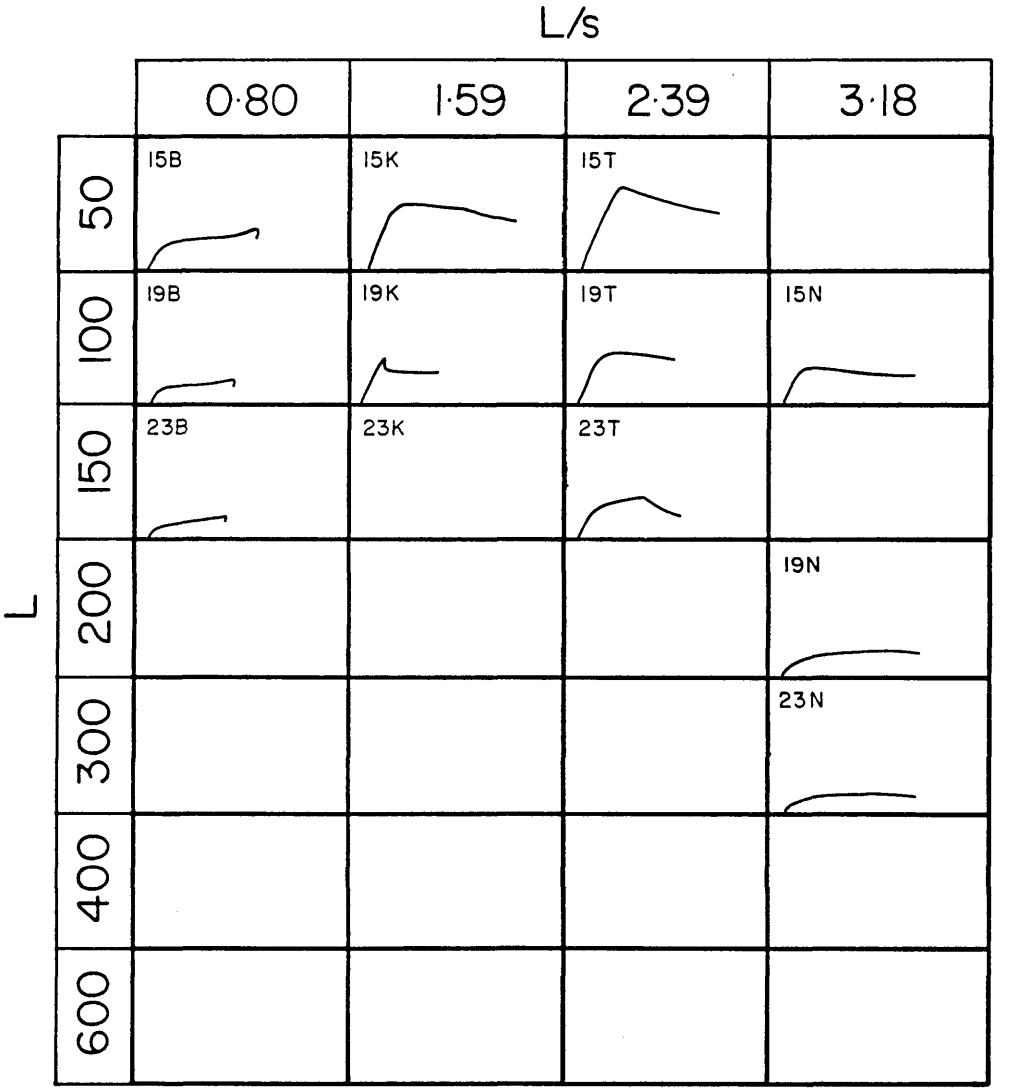
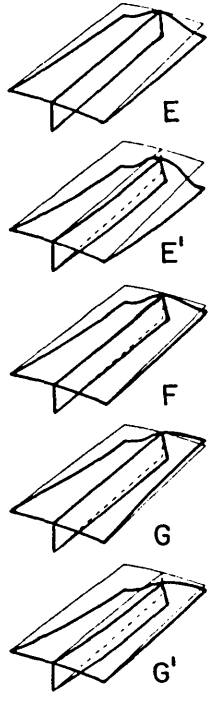


Fig. 4.19

DEFLECTION MODE

$\sigma_\theta/\sigma_x = 2{\cdot}5$

L \ L/s	0·80	1·59	2·39	3·18
50	15B F-E	15K F-E'	15T G-G'	
100	19B F-E	19K F-E'	19T G-G'	15N G-G'
150	23B F-E	23K F-E'	23T G-G'	
200				19N G-G'
300				23N G-G'
400				
600				



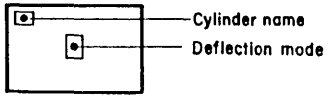
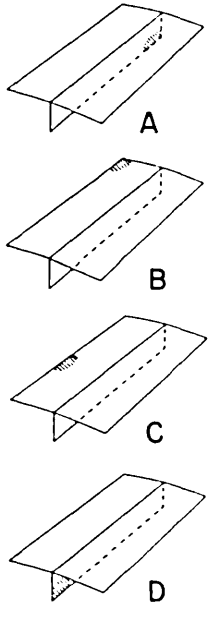


Fig. 4.21

FIRST YIELD

$\sigma_\theta/\sigma_x = 2{\cdot}5$

L \ L/s	0·80	1·59	2·39	3·18
50	15B B 0·55	15K B 0·53	15T B 0·57	
100	19B B 0·58	19K B 0·43	19T B 0·59	15N B 0·69
150	23B E/B	23K B 0·51	23T B 0·59	
200				19N B 0·70
300				23N B 0·75
400				
600				



ELASTIC - E

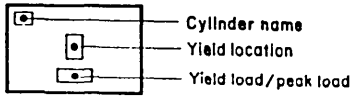


Fig. 4.20

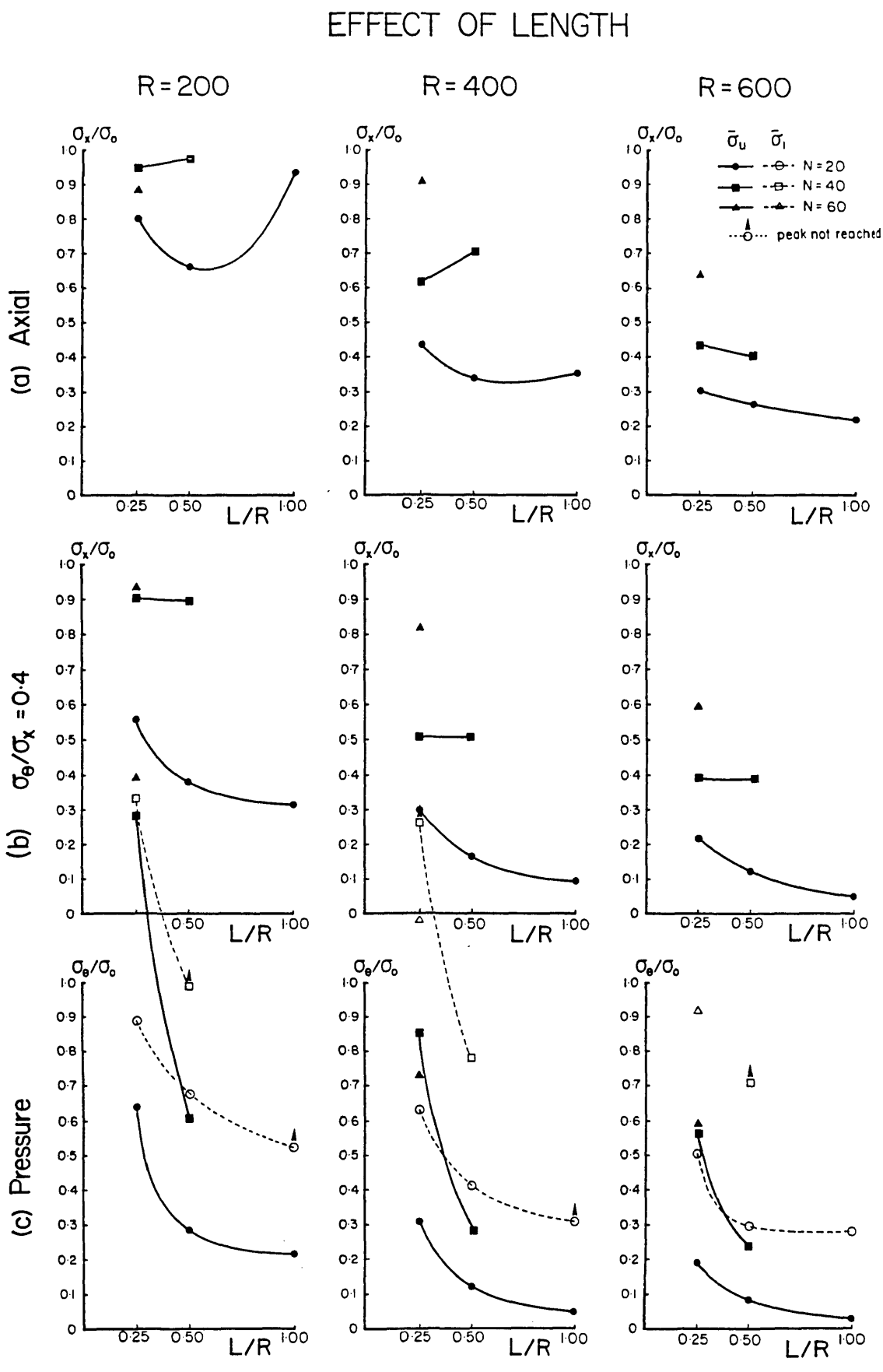

EFFECT OF LENGTH
R = 200
R = 400
R = 600
(a) Axial
(b) $\sigma_\theta/\sigma_x = 0.4$
(c) Pressure
σ_x/σ_o
σ_θ/σ_o
L/R
0·25
0·50
1·00
$\bar{\sigma}_u$ $\bar{\sigma}_l$
N = 20
N = 40
N = 60
peak not reached

Fig. 4.22

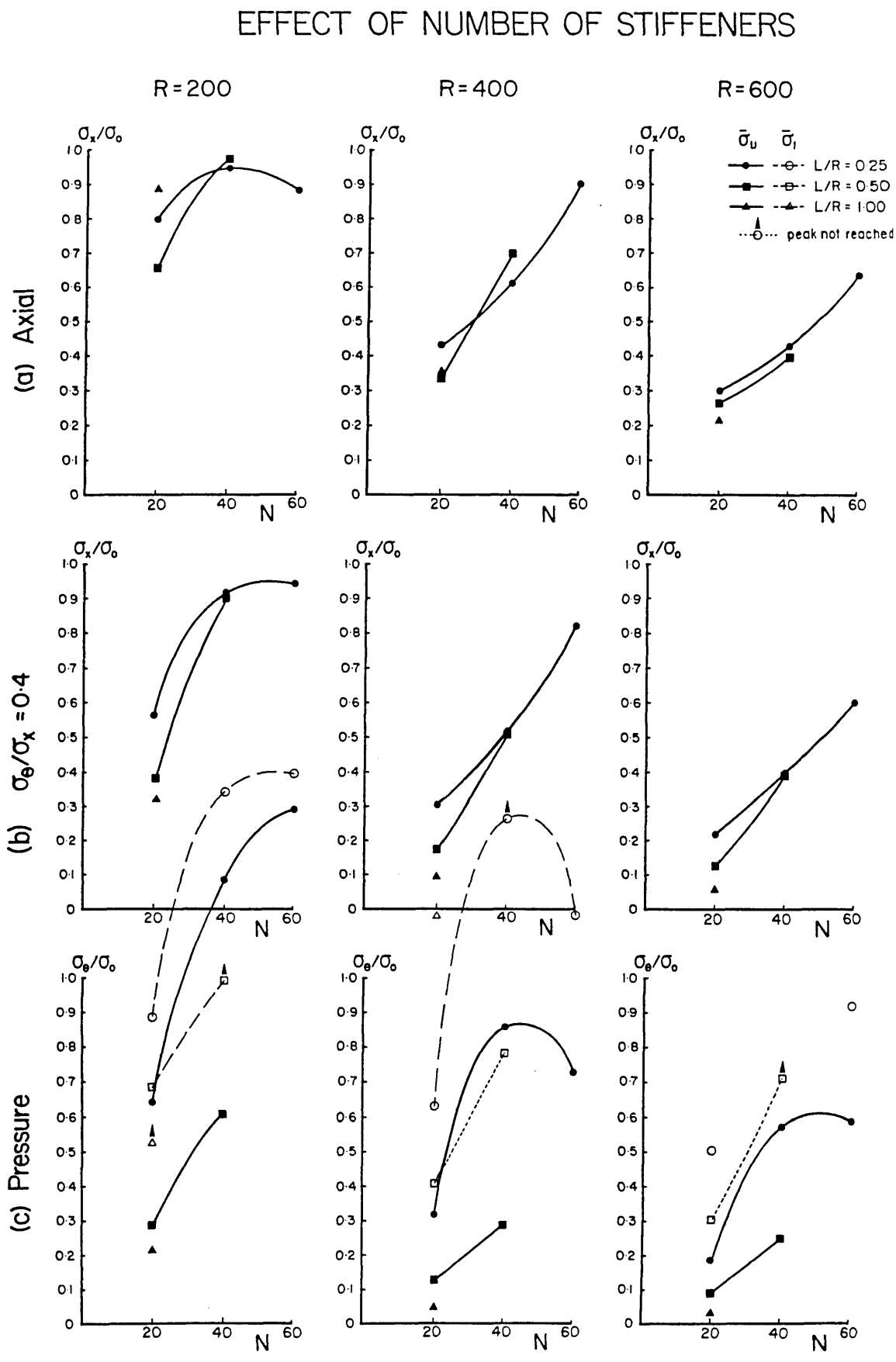

EFFECT OF NUMBER OF STIFFENERS
R = 200
R = 400
R = 600
(a) Axial
(b) $\sigma_\theta/\sigma_x = 0.4$
(c) Pressure
σ_x/σ_o
σ_θ/σ_o
$\bar{\sigma}_u$ $\bar{\sigma}_l$
L/R = 0.25
L/R = 0.50
L/R = 1.00
peak not reached
N

Fig. 4.23

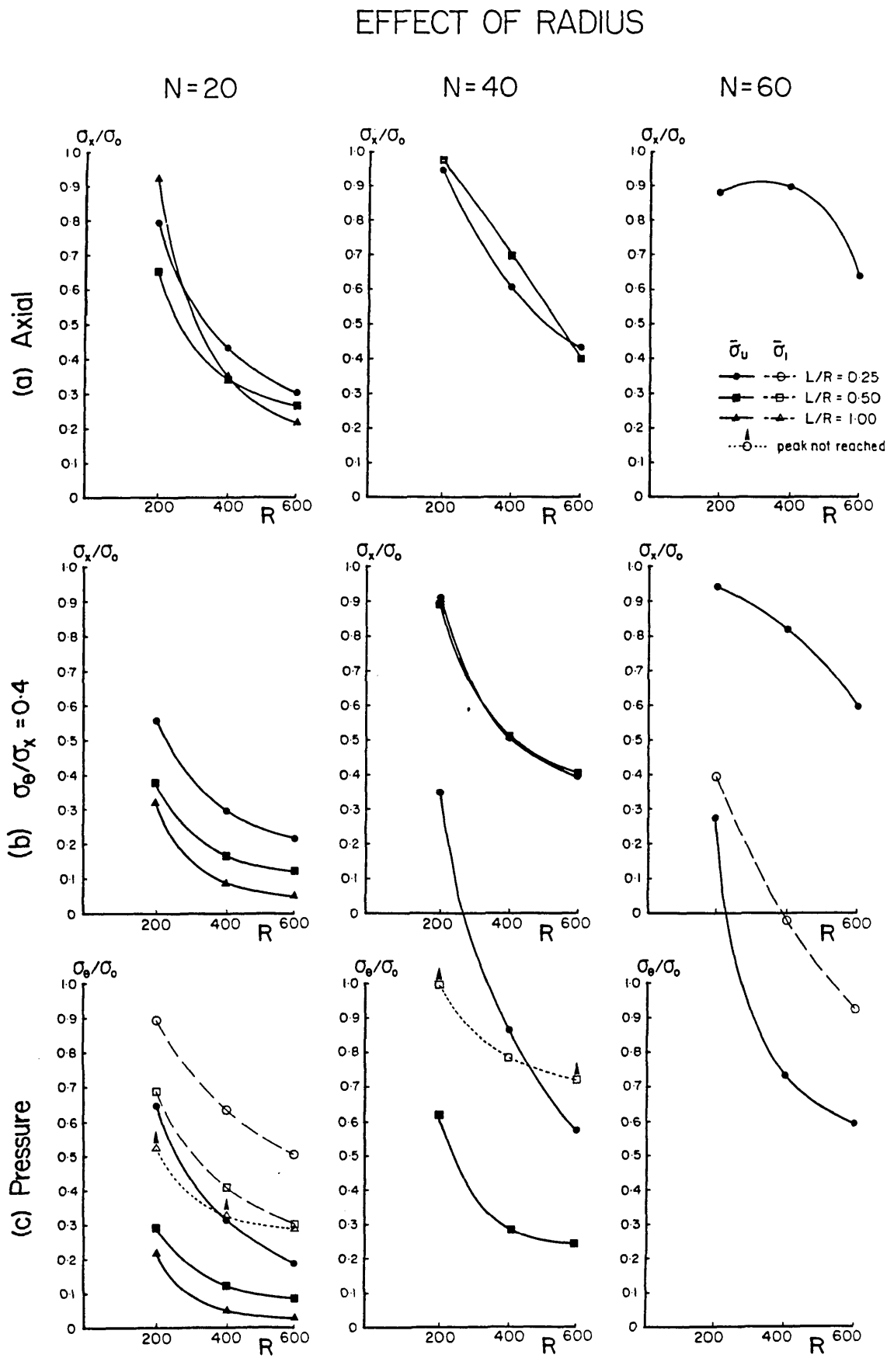

EFFECT OF RADIUS
N=20
N=40
N=60
(a) Axial
(b) $\sigma_\theta/\sigma_x = 0.4$
(c) Pressure
σ_x/σ_o
σ_θ/σ_o
R
200
400
600
$\bar{\sigma}_u$ $\bar{\sigma}_l$
L/R = 0·25
L/R = 0·50
L/R = 1·00
peak not reached

Fig. 4.24

$\sigma_\theta/\sigma_x = 2{\cdot}5$

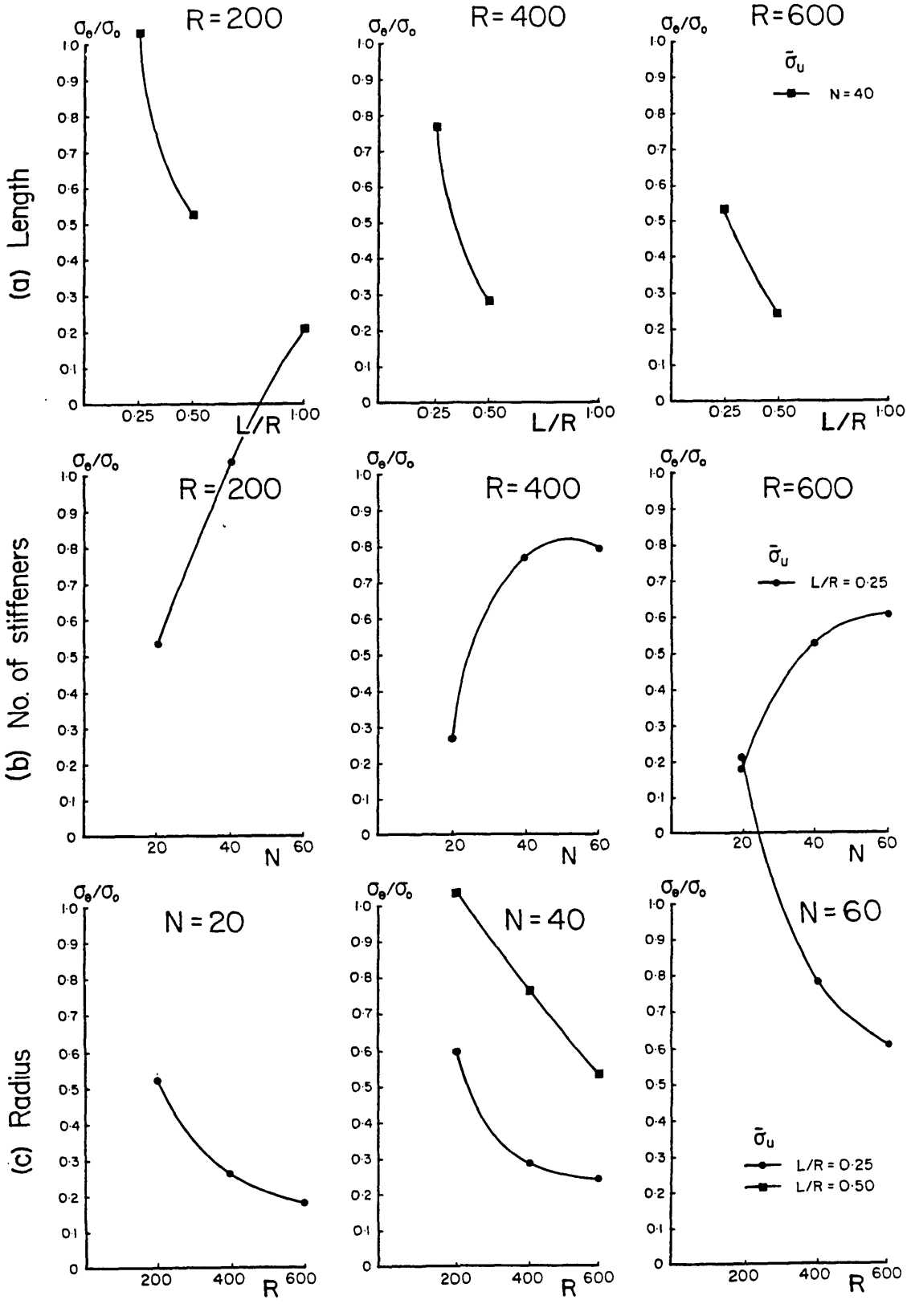
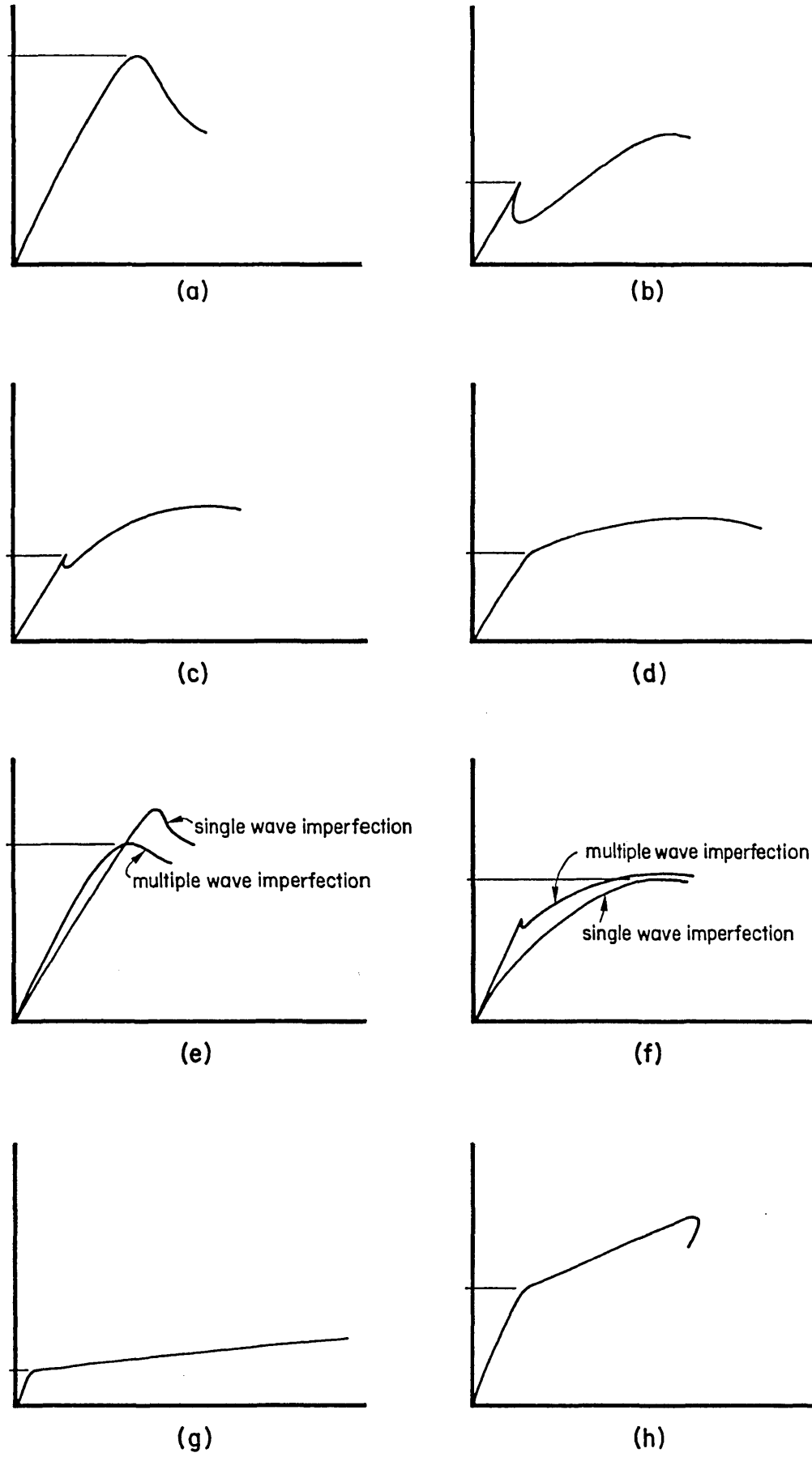


Fig. 4.25



CYLINDER STRENGTH IN TYPICAL CASES

Fig. 4.26

INTERACTION CURVES

R = 200

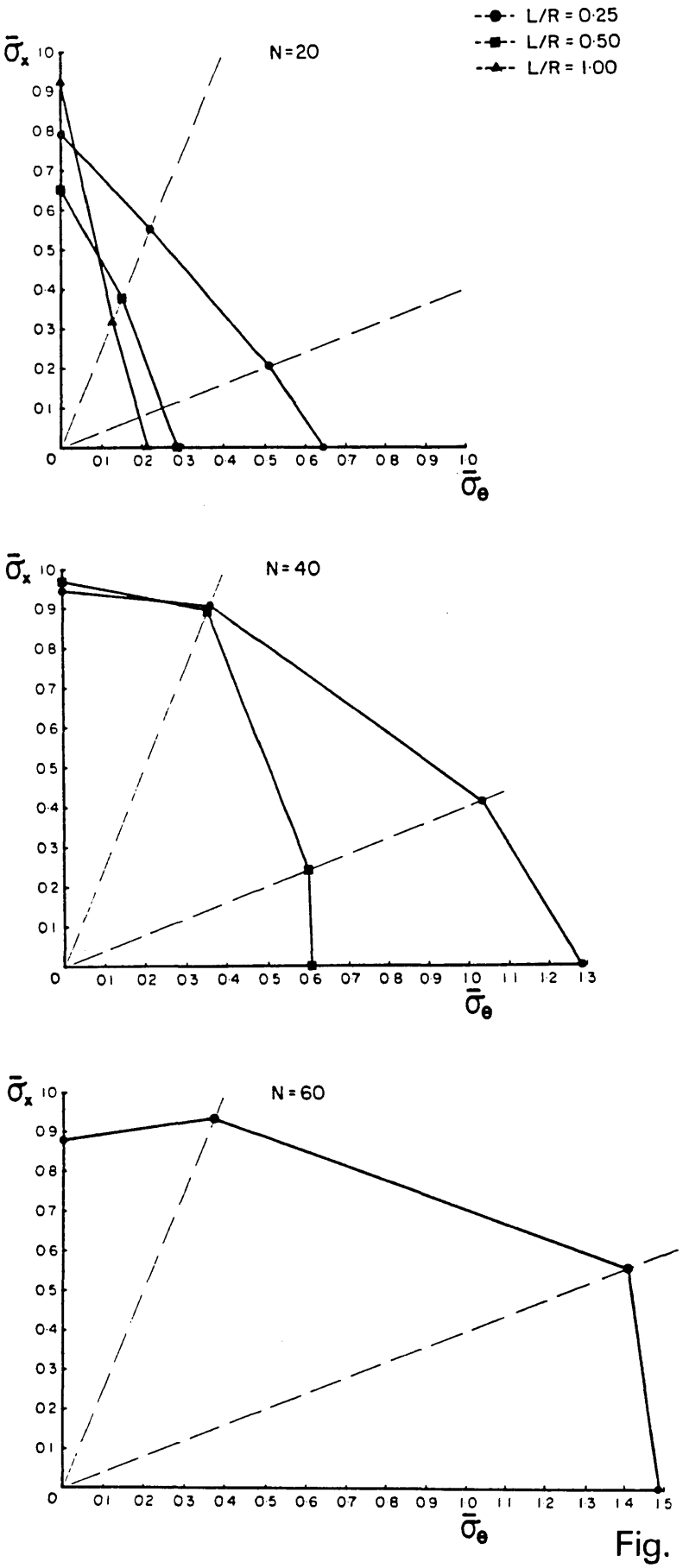


Fig. 4.27

INTERACTION CURVES

R = 400

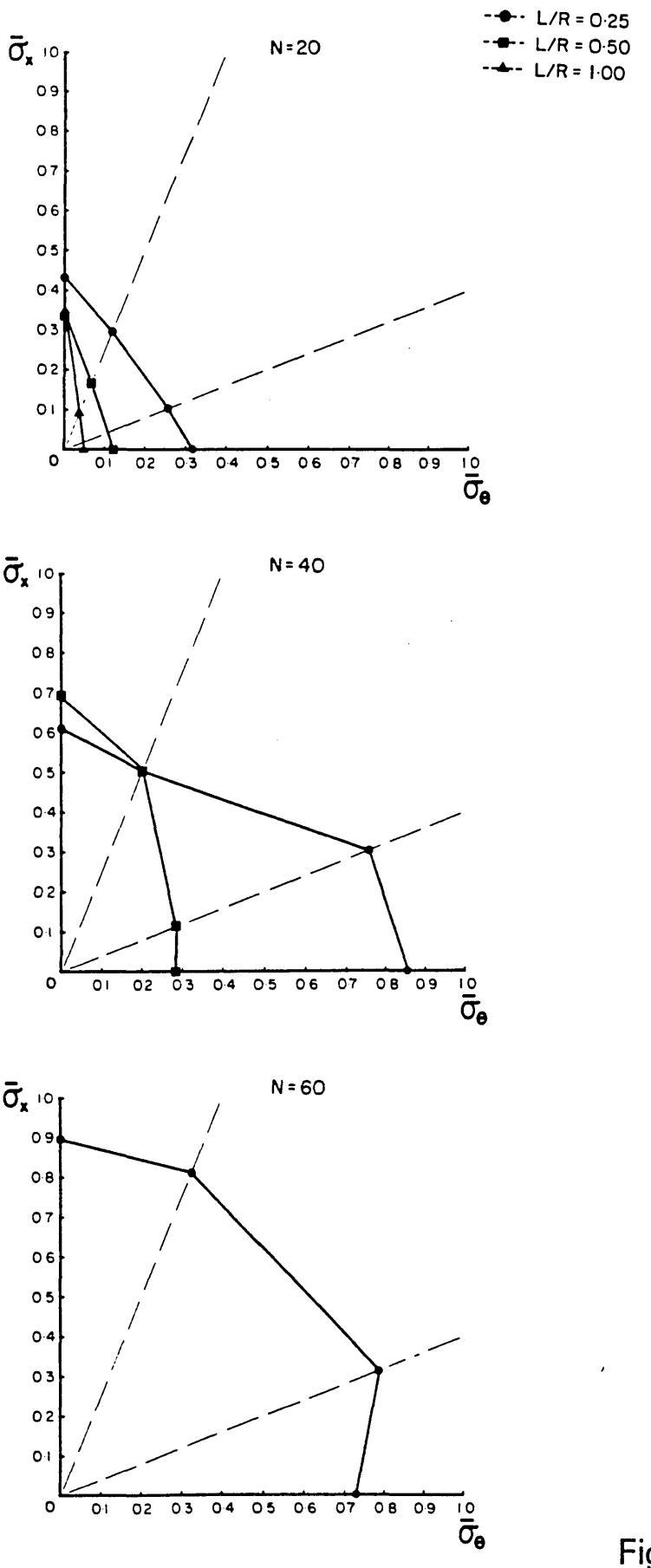


Fig. 4.28

INTERACTION CURVES

R = 600

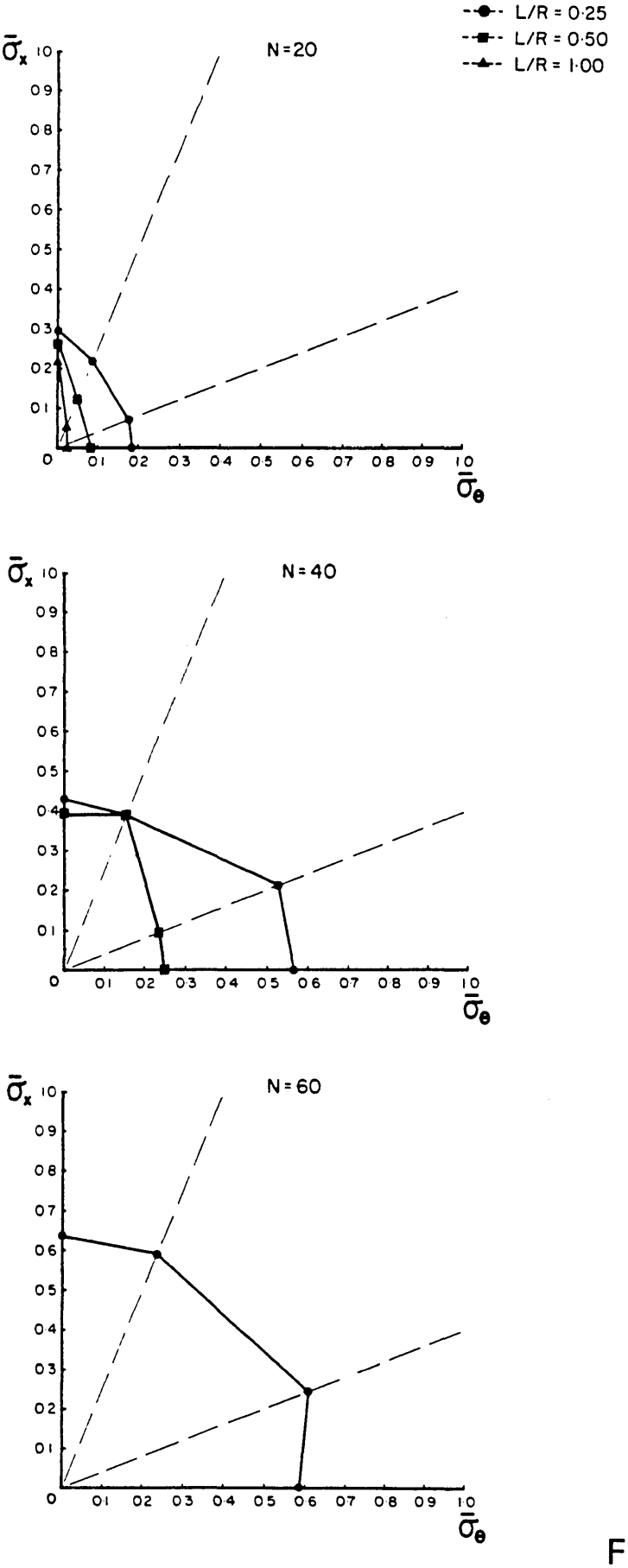


Fig. 4.29

INTERACTION CURVES

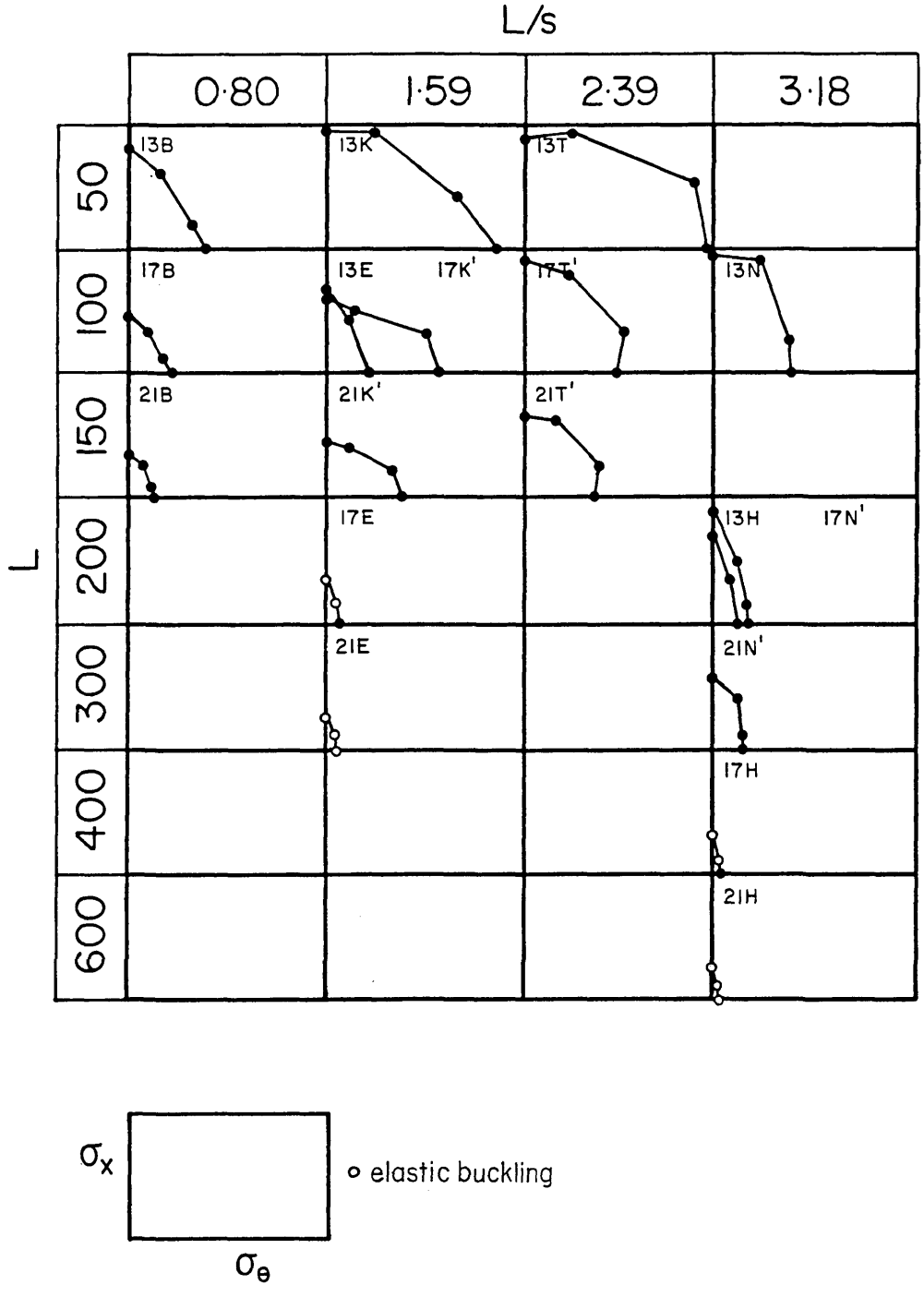
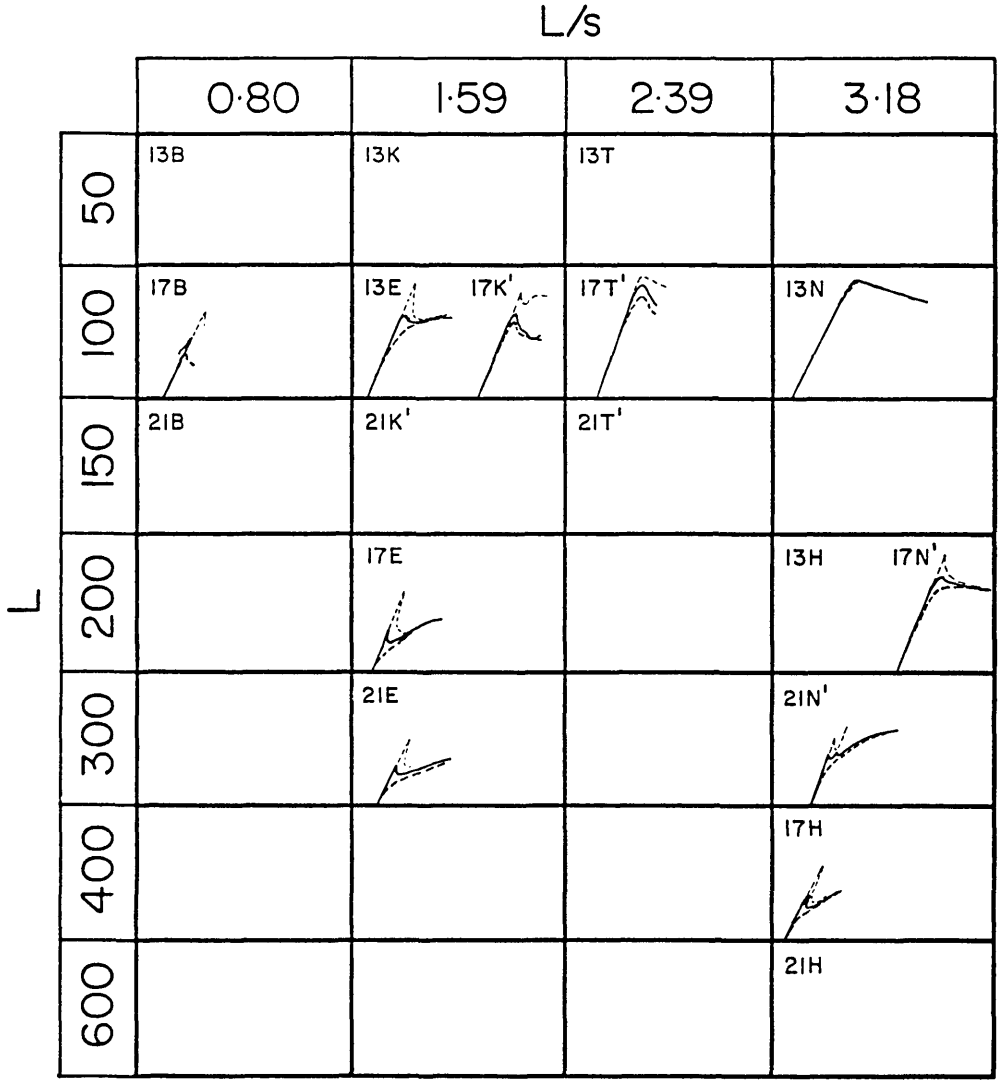


Fig. 4.30

INFLUENCE OF INITIAL IMPERFECTIONS ON LOAD-DEFLECTION PATHS

Axial load



---- $\bar{\Delta}$ = 0.5

—— $\bar{\Delta}$ = 1.0

---- $\bar{\Delta}$ = 2.0

Fig. 4.31

INFLUENCE OF INITIAL IMPERFECTIONS ON DEFLECTION MODE

Axial load

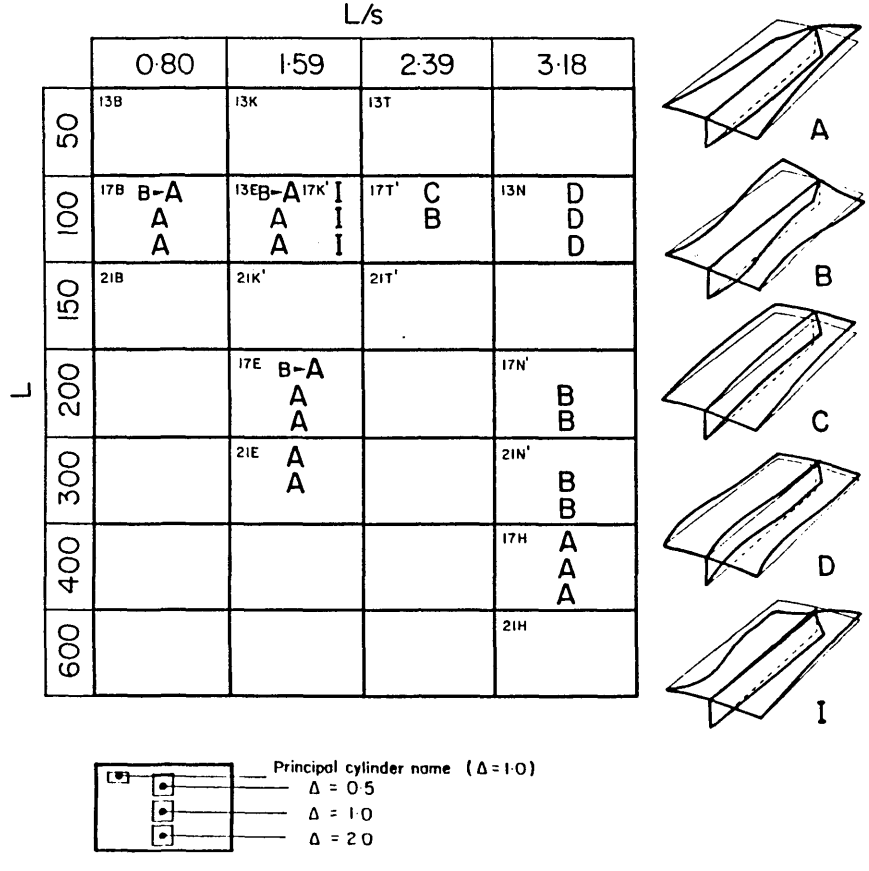


Fig. 4.33

INFLUENCE OF INITIAL IMPERFECTIONS ON FIRST YIELD

Axial load

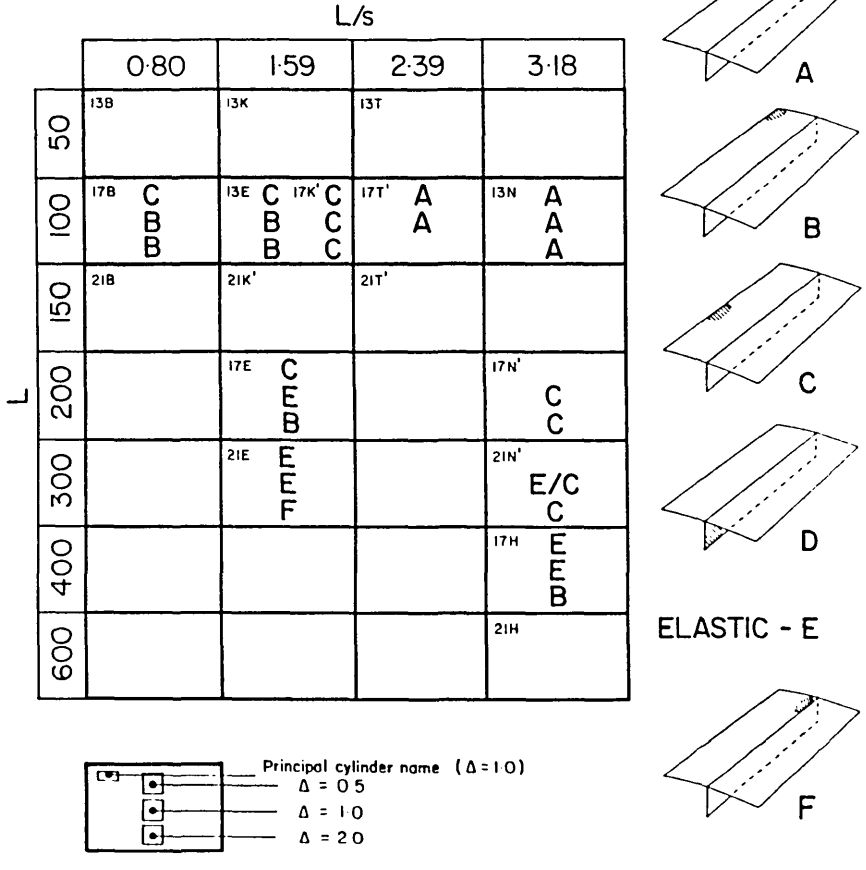


Fig. 4.32

INFLUENCE OF INITIAL IMPERFECTIONS ON LOAD-DEFLECTION PATHS

Pressure load

L/s

L	0·80	1·59	2·39	3·18
50	16B	16K	16T	
100	20B	16E 20K	20T	16N
150	24B	24K	24T	
200		20E		16H 20N
300		24E		24N
400				20H
600				24H

---- $\bar{\Delta}$ = 0.5

—— $\bar{\Delta}$ = 1.0

---- $\bar{\Delta}$ = 2.0

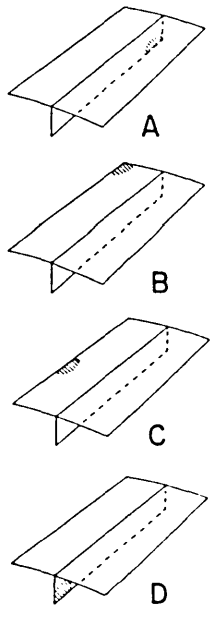
Fig. 4.34

INFLUENCE OF INITIAL IMPERFECTIONS ON FIRST YIELD

Pressure load

L/s

L \ L/s	0·80	1·59	2·39	3·18
50	16B	16K	16T	
100	20B	16E B B B	20T	16N B B B
150	24B	24K	24T	
200		20E E B B		20N B B B
300		24E E E/C C		24N B B A
400				20H
600				24H



ELASTIC - E

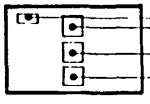


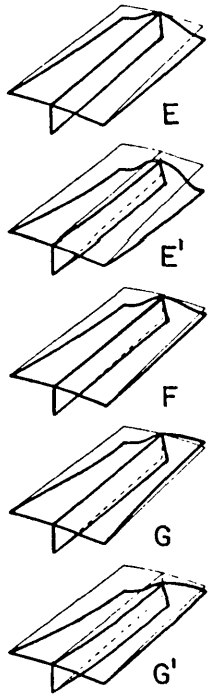
Fig. 4.35

INFLUENCE OF INITIAL IMPERFECTIONS ON DEFLECTION MODE

Pressure load

L/s

L \ L/s	0·80	1·59	2·39	3·18
50	16B	16K	16T	
100	20B	16E F→E F→E G→E	20T	16N G→G' G→G' G→G'
150	24B	24K	24T	
200		20E G→E G→E G→E		20N G→G' G→G' G→G'
300		24E G→E G→E G→E		24N G→G' G→G' G→G'
400				20H
600				24H



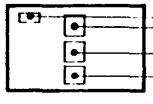


Fig. 4.36

INFLUENCE OF INITIAL IMPERFECTIONS ON LOAD-DEFLECTION PATHS

$\sigma_\theta/\sigma_x = 0{\cdot}4$

L/s

L	0·80	1·59	2·39	3·18
50	14B	14K	14T	
100	18B	14E 18K'	18T'	14N
150	22B	22K'	22T'	
200		18E		14H 18N'
300		22E		22N'
400				18H
600				22H

---- $\bar{\Delta}$ = 0.5

—— $\bar{\Delta}$ = 1.0

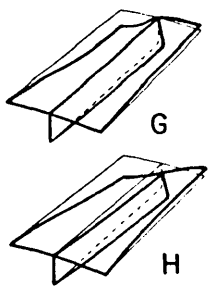
---- $\bar{\Delta}$ = 2.0

Fig. 4.37

INFLUENCE OF INITIAL IMPERFECTIONS ON DEFLECTION MODE

$\sigma_\theta/\sigma_x = 0{\cdot}4$

L \ L/s	0·80	1·59	2·39	3·18
50	14B	14K	14T	
100	18B	14E G G G	18T'	14N H H H
150	22B	22K'	22T'	
200		18E G G G		18N H H H
300		22E G G G/H		22N H H H
400				18H
600				22H



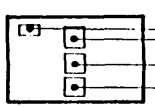
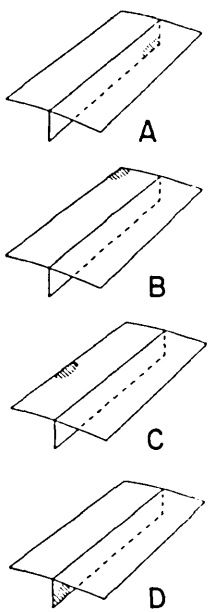


Fig. 4.39

INFLUENCE OF INITIAL IMPERFECTIONS ON FIRST YIELD

$\sigma_\theta/\sigma_x = 0{\cdot}4$

L \ L/s	0·80	1·59	2·39	3·18
50	14B	14K	14T	
100	18B	14E B B B	18T'	14N B B B
150	22B	22K'	22T'	
200		18E E E B		18N B B B
300		22E E E C		22N C C C
400				18H
600				22H



ELASTIC - E

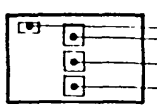


Fig. 4.38

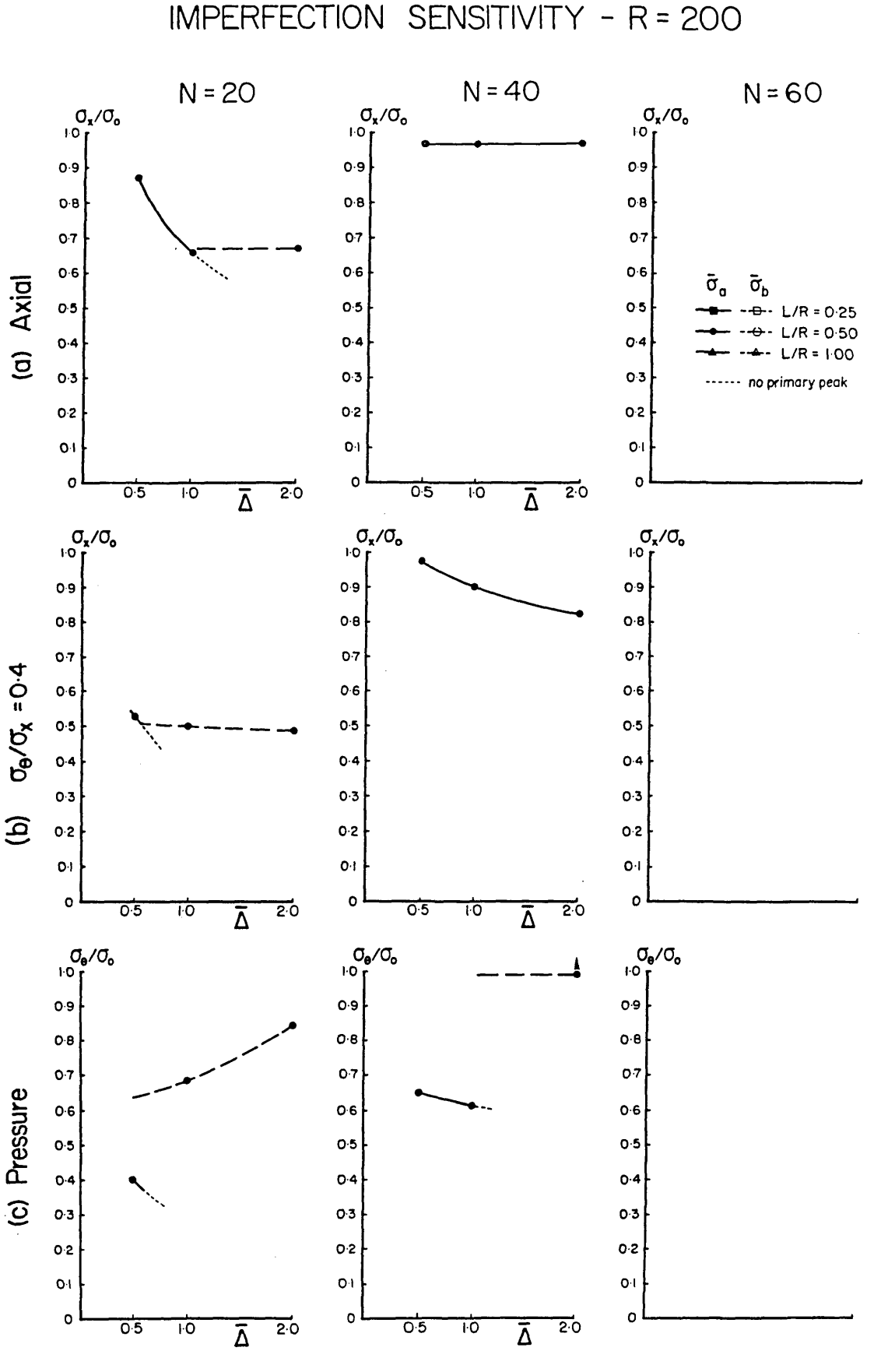

IMPERFECTION SENSITIVITY - R = 200
N = 20
N = 40
N = 60
(a) Axial
(b) $\sigma_\theta/\sigma_x = 0.4$
(c) Pressure
σ_x/σ_o
σ_θ/σ_o
$\bar{\Delta}$
$\bar{\sigma}_a$ $\bar{\sigma}_b$
L/R = 0·25
L/R = 0·50
L/R = 1·00
no primary peak

Fig. 4.40

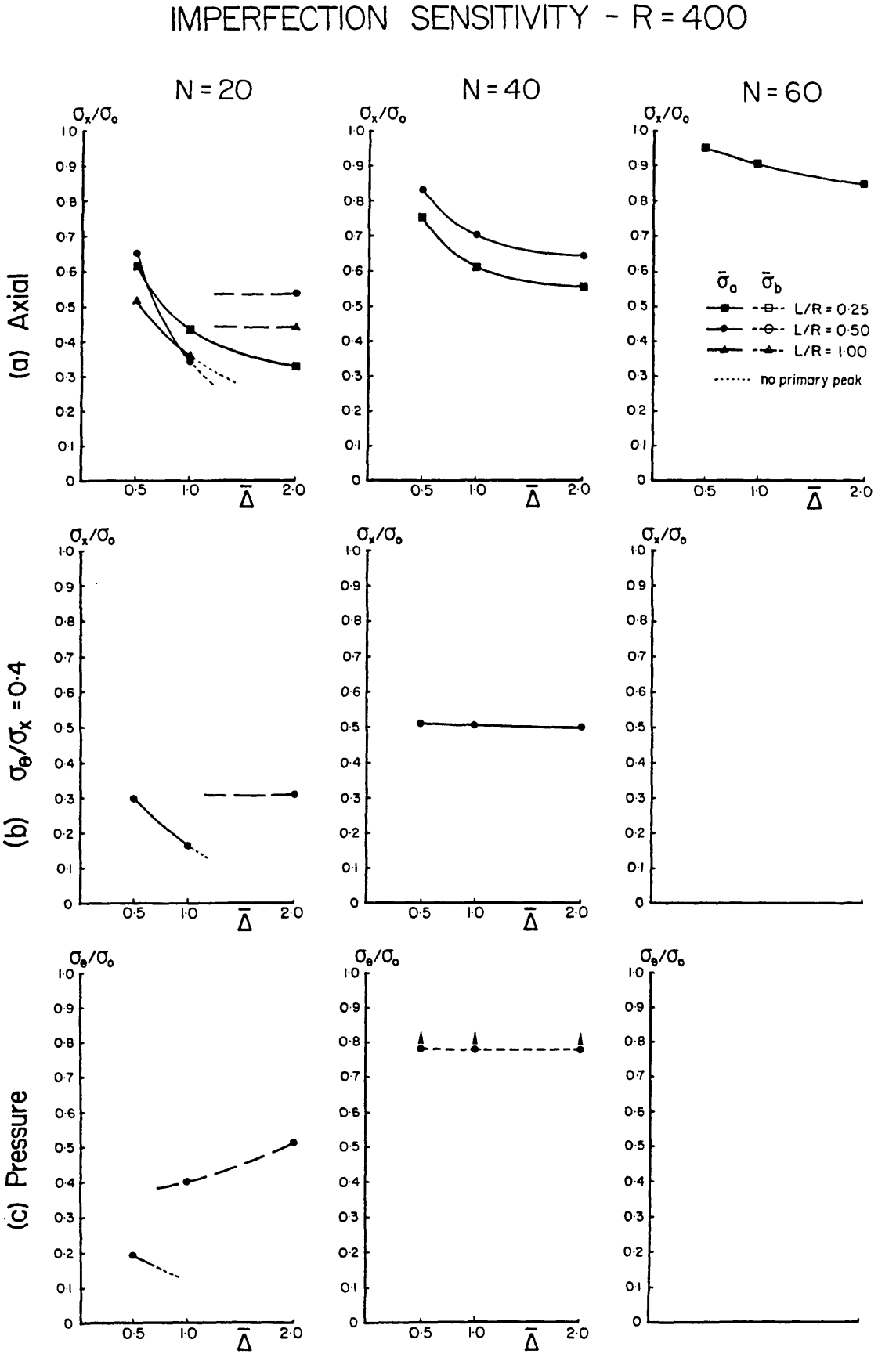

IMPERFECTION SENSITIVITY - R = 400
N = 20
N = 40
N = 60
(a) Axial
(b) σθ/σx = 0·4
(c) Pressure
σx/σo
σθ/σo
Δ̄
σ̄a σ̄b
L/R = 0·25
L/R = 0·50
L/R = 1·00
no primary peak

Fig. 4.41

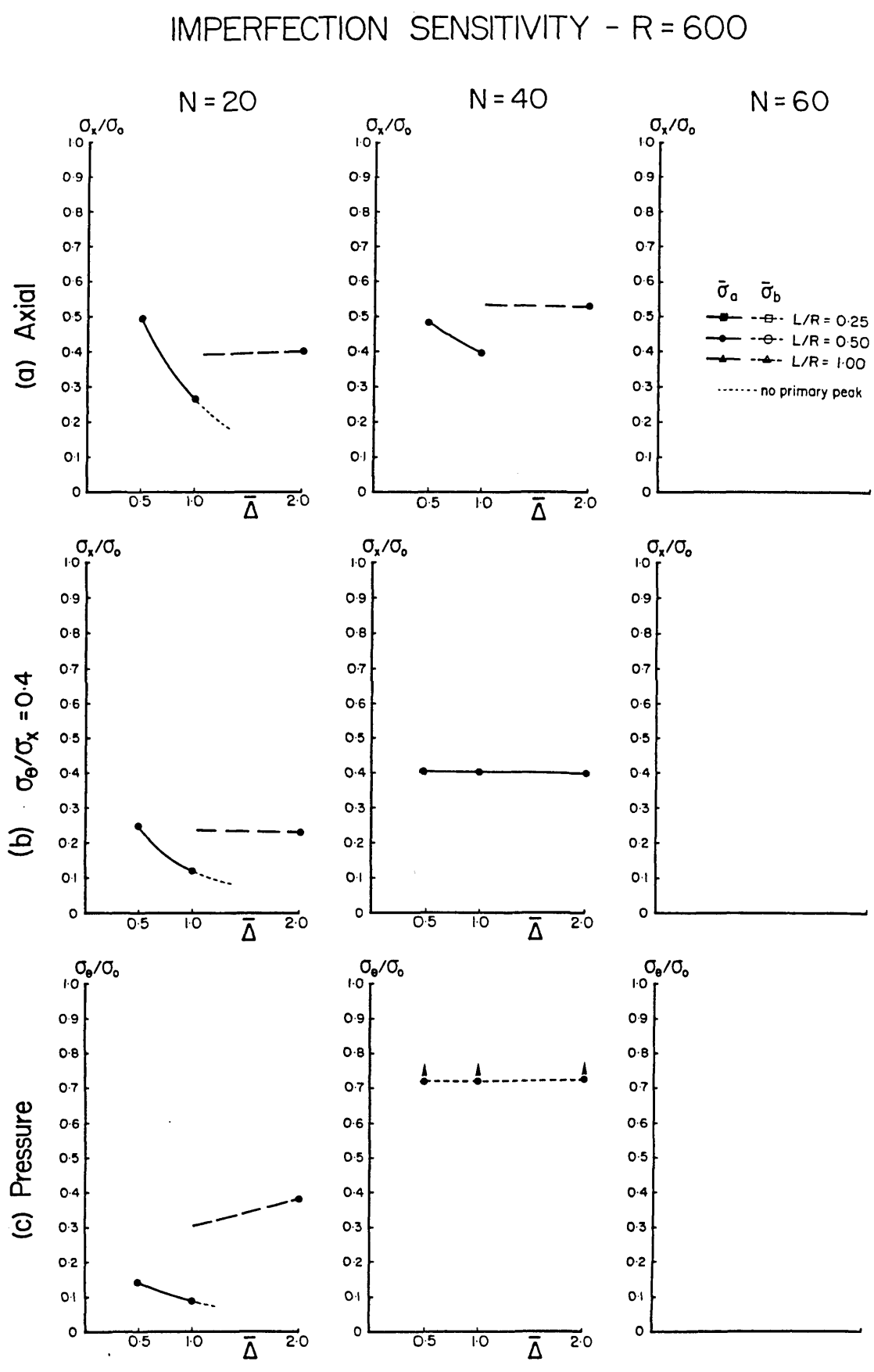
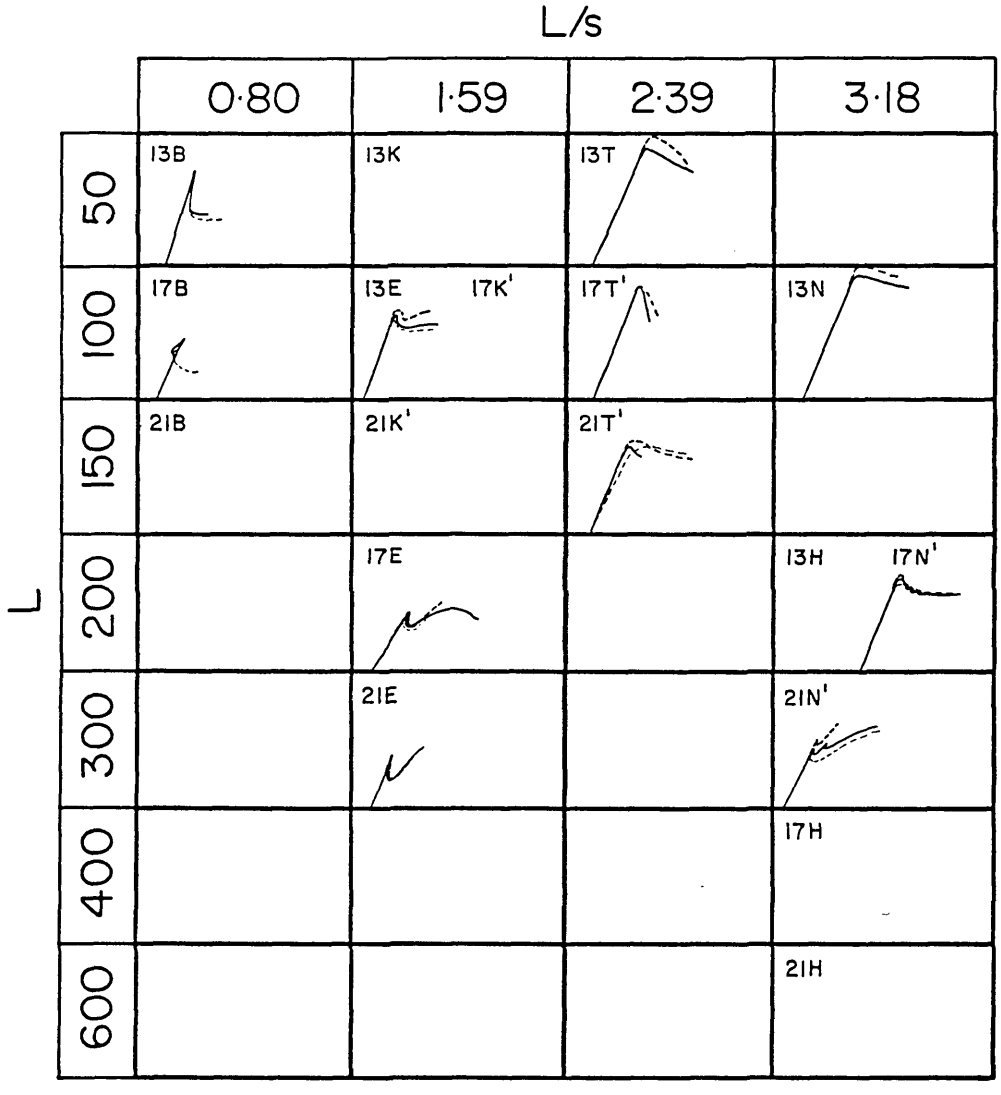

IMPERFECTION SENSITIVITY - R = 600
N = 20
N = 40
N = 60
(a) Axial
(b) $\sigma_\theta/\sigma_x = 0.4$
(c) Pressure
σ_x/σ_0
σ_θ/σ_0
$\bar{\Delta}$
$\bar{\sigma}_a$ $\bar{\sigma}_b$
L/R = 0·25
L/R = 0·50
L/R = 1·00
no primary peak

Fig. 4.42

INFLUENCE OF STIFFENING RATIO ON LOAD-DEFLECTION PATHS

Axial load



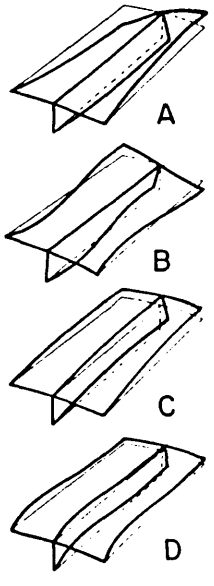
---- a_s = 0.100
—— a_s = 0.300
---- a_s = 0.500

Fig. 4.43

INFLUENCE OF STIFFENING RATIO ON DEFLECTION MODE

Axial load

L \ L/s	0·80	1·59	2·39	3·18
50	13B A A	13K	13T C C	
100	17B A A	13E A A A	17T' B B	13N D C
150	21B	21K'	21T' B B B	
200		17E A A A		17N' B B B
300		21E A A		21N' B B B
400				17H
600				21H



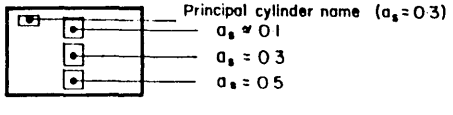
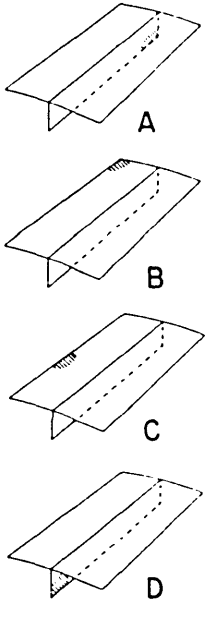


Fig. 4.45

INFLUENCE OF STIFFENING RATIO ON FIRST YIELD

Axial load

L \ L/s	0·80	1·59	2·39	3·18
50	13B A B	13K	13T A A	
100	17B B B	13E B B B	17T' C C	13N A A
150	21B	21K'	21T' C C C	
200		17E E E E		17N' C C C
300		21E E E		21N' E/C E/C B
400				17H
600				21H



ELASTIC - E

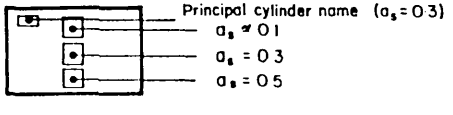
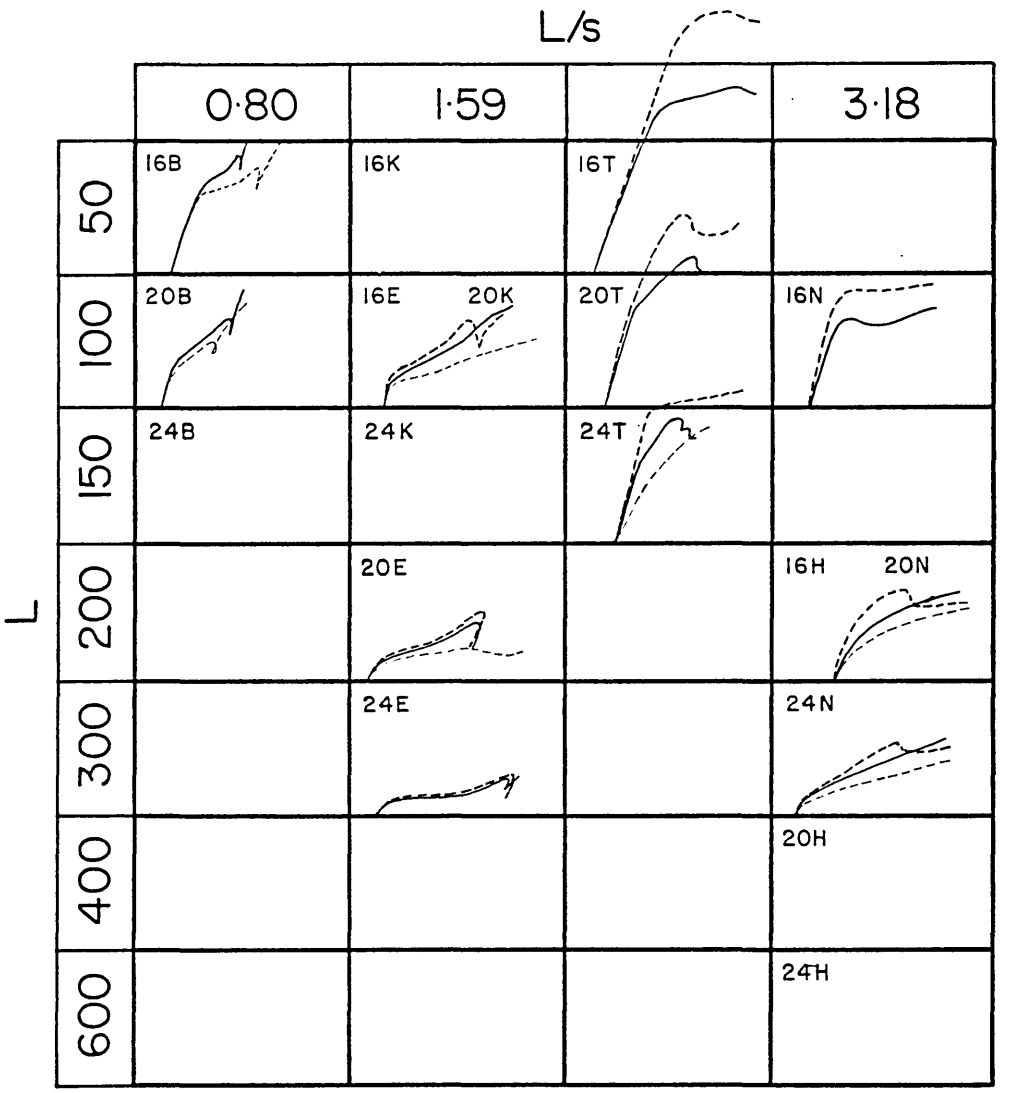


Fig. 4.44

INFLUENCE OF STIFFENING RATIO ON LOAD-DEFLECTION PATHS

Pressure load



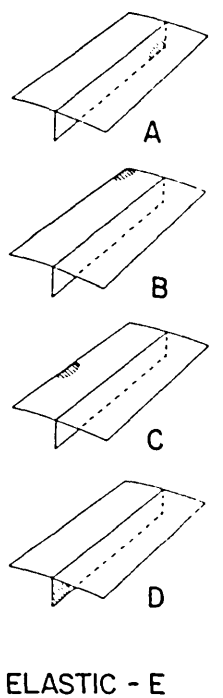
---- a_s = 0.100
—— a_s = 0.300
---- a_s = 0.500

Fig. 4.46

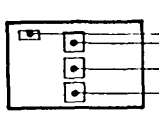
INFLUENCE OF STIFFENING RATIO ON FIRST YIELD

Pressure load

L \ L/s	0·80	1·59	2·39	3·18
50	16B B B	16K	16T A A	
100	20B B B	16E B B B	20T A/B B	16N B B
150	24B	24K	24T A B B	
200		20E B B B		20N B B B
300		24E E/C E/C		24N A B B
400				20H
600				24H



ELASTIC - E



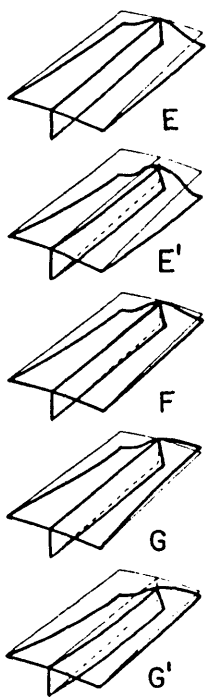
Principal cylinder name ($a_s = 0.3$)
$a_s = 0.1$
$a_s = 0.3$
$a_s = 0.5$

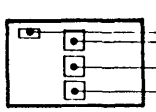
Fig. 4.47

INFLUENCE OF STIFFENING RATIO ON DEFLECTION MODE

Pressure load

L \ L/s	0·80	1·59	2·39	3·18
50	16B F-E' F-E	16K	16T G'-E' G'-E'	
100	20B F-E F-E	16E G-G' F-E F-E	20T G'-E' G'-E'	16N G-G' G-G'
150	24B	24K	24T G-G' G'-E' G'-E'	
200		20E G-G' G-E G-E		20N G-G' G-G' G'-E'
300		24E G-E G-E		24N G-G' G-G G'-E'
400				20H
600				24H



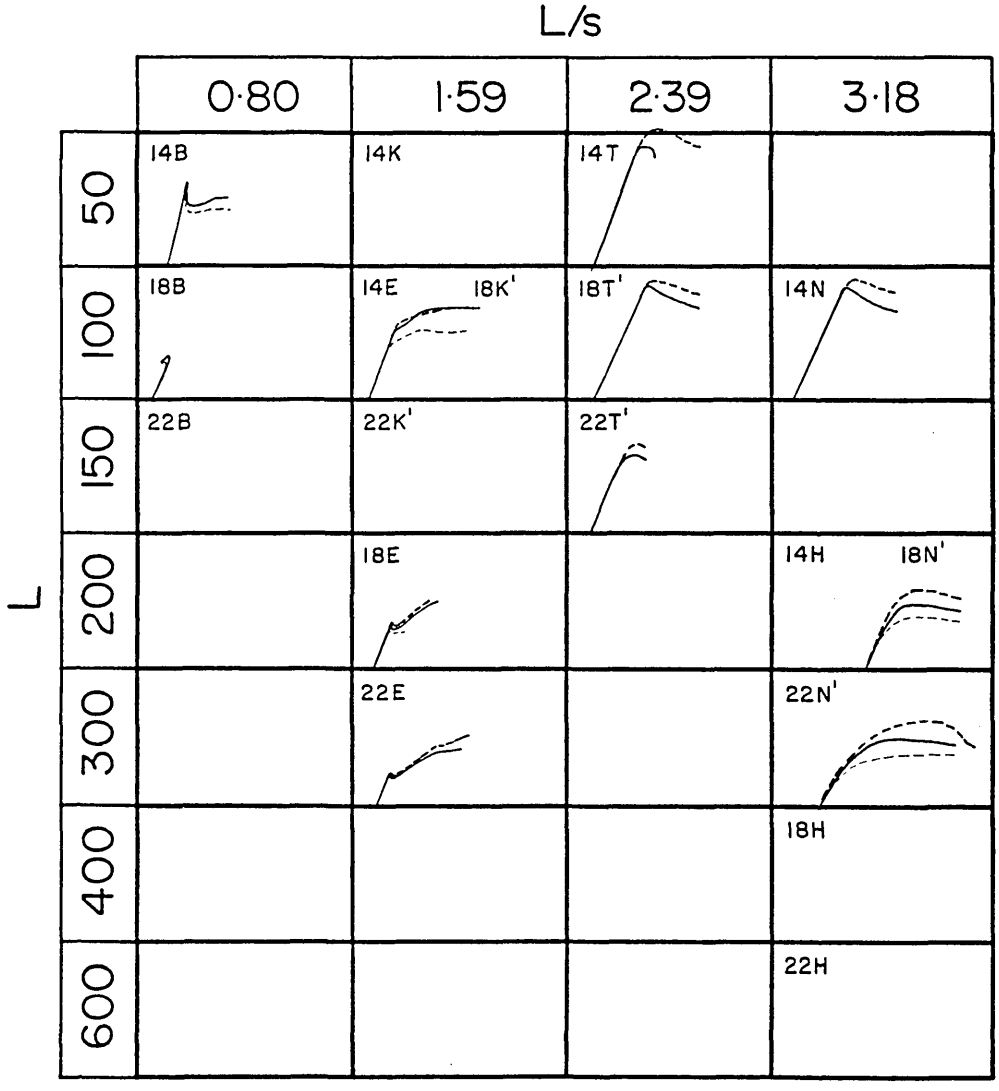


Principal cylinder name ($a_s = 0.3$)
$a_s = 0.1$
$a_s = 0.3$
$a_s = 0.5$

Fig. 4.48

INFLUENCE OF STIFFENING RATIO ON LOAD-DEFLECTION PATHS

$\sigma_\theta/\sigma_x = 0{\cdot}4$



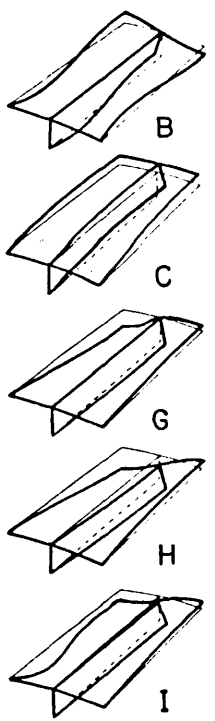
---- a_s = 0.100
—— a_s = 0.300
---- a_s = 0.500

Fig. 4.49

INFLUENCE OF STIFFENING RATIO ON DEFLECTION MODE

$\sigma_\theta/\sigma_x = 0{\cdot}4$

L \ L/s	0·80	1·59	2·39	3·18
50	14B G G	14K	14T C G	
100	18B G G	14E H G G	18T' B B	14N H H
150	22B	22K'	22T' I B	
200		18E H G G		18N H H H
300		22E G G		22N H H H
400				18H
600				22H



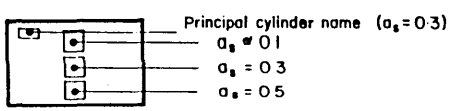
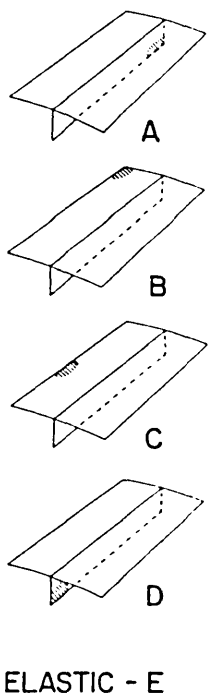


Fig. 4.51

INFLUENCE OF STIFFENING RATIO ON FIRST YIELD

$\sigma_\theta/\sigma_x = 0{\cdot}4$

L \ L/s	0·80	1·59	2·39	3·18
50	14B B B	14K	14T D B	
100	18B B B	14E B B B	18T' C C	14N B B
150	22B	22K'	22T' C C	
200		18E E E E		18N B B B
300		22E E E		22N B/C C C
400				18H
600				22H



ELASTIC - E

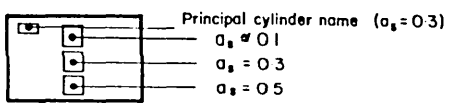


Fig. 4.50

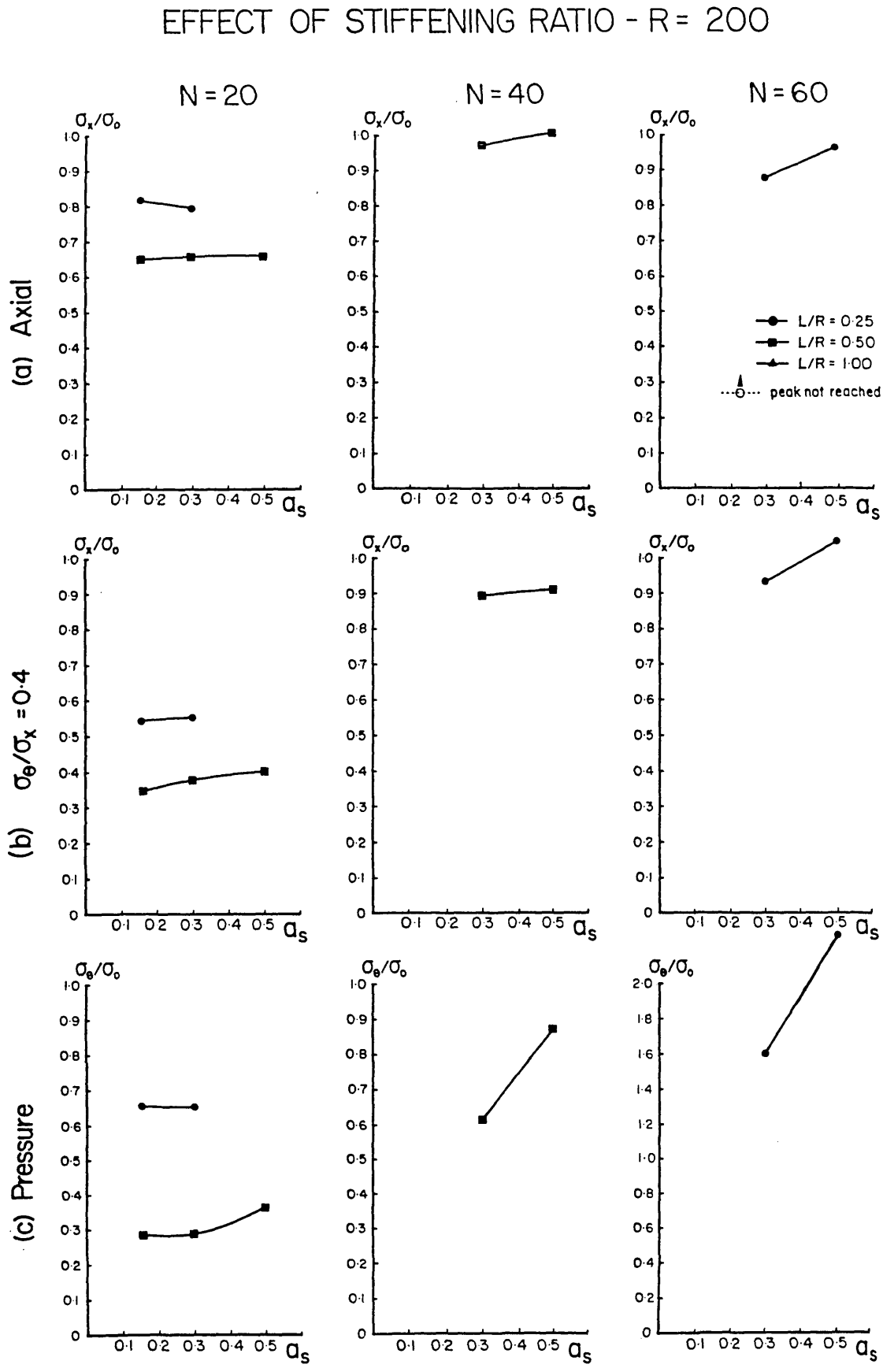

EFFECT OF STIFFENING RATIO - R = 200
N = 20
N = 40
N = 60
(a) Axial
(b) σ_θ/σ_x = 0·4
(c) Pressure
σ_x/σ_o
σ_θ/σ_o
a_s
L/R = 0·25
L/R = 0·50
L/R = 1·00
peak not reached

Fig. 4.52

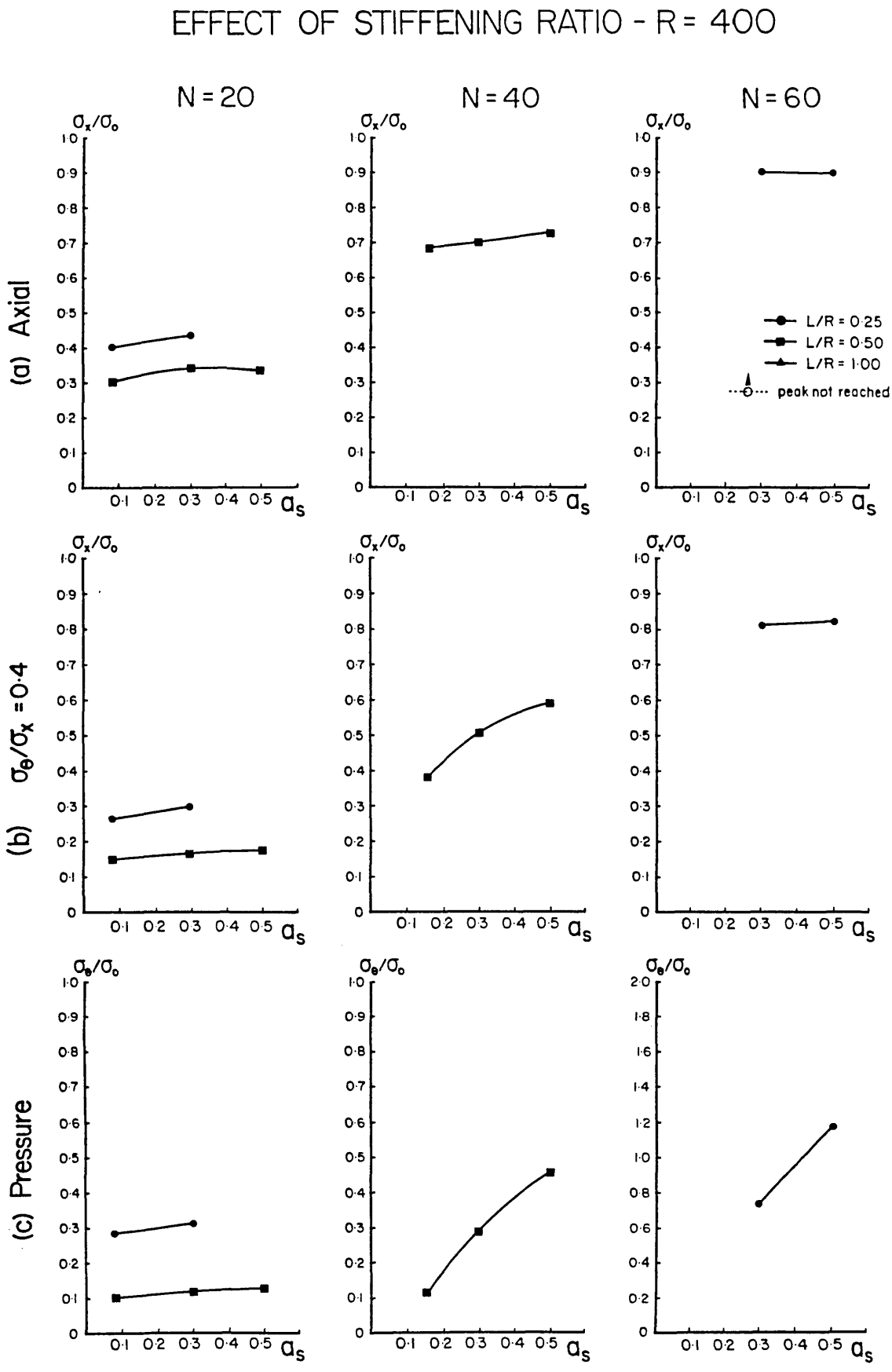

EFFECT OF STIFFENING RATIO - R = 400
N = 20
N = 40
N = 60
(a) Axial
(b) $\sigma_\theta/\sigma_x = 0.4$
(c) Pressure
σ_x/σ_o
σ_θ/σ_o
a_s
L/R = 0.25
L/R = 0.50
L/R = 1.00
peak not reached

Fig. 4.53

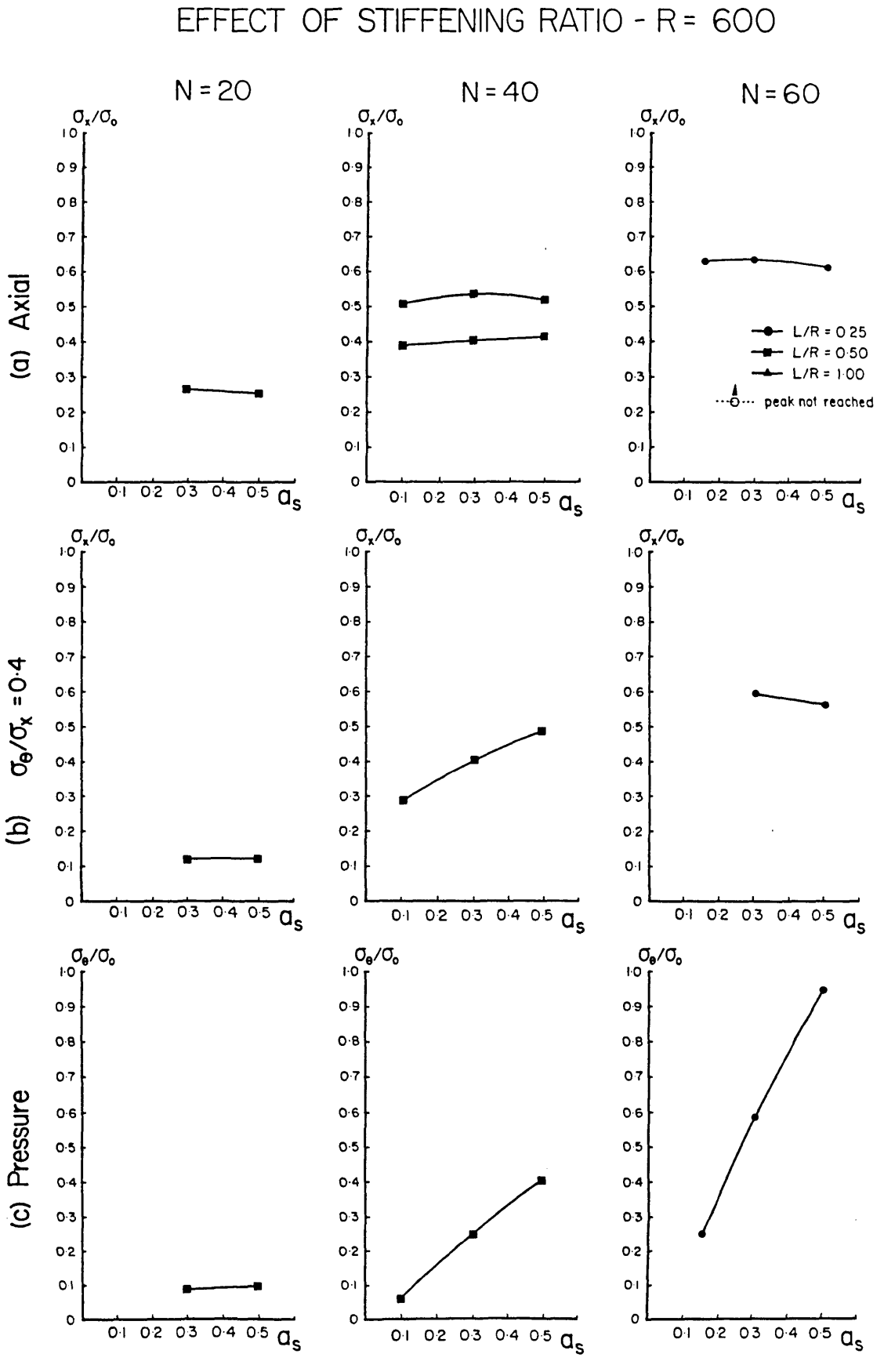

EFFECT OF STIFFENING RATIO - R = 600
N = 20
N = 40
N = 60
(a) Axial
(b) σ_θ/σ_x = 0·4
(c) Pressure
σ_x/σ_o
σ_θ/σ_o
a_s
L/R = 0·25
L/R = 0·50
L/R = 1·00
peak not reached

Fig. 4.54

INTERACTION CURVES

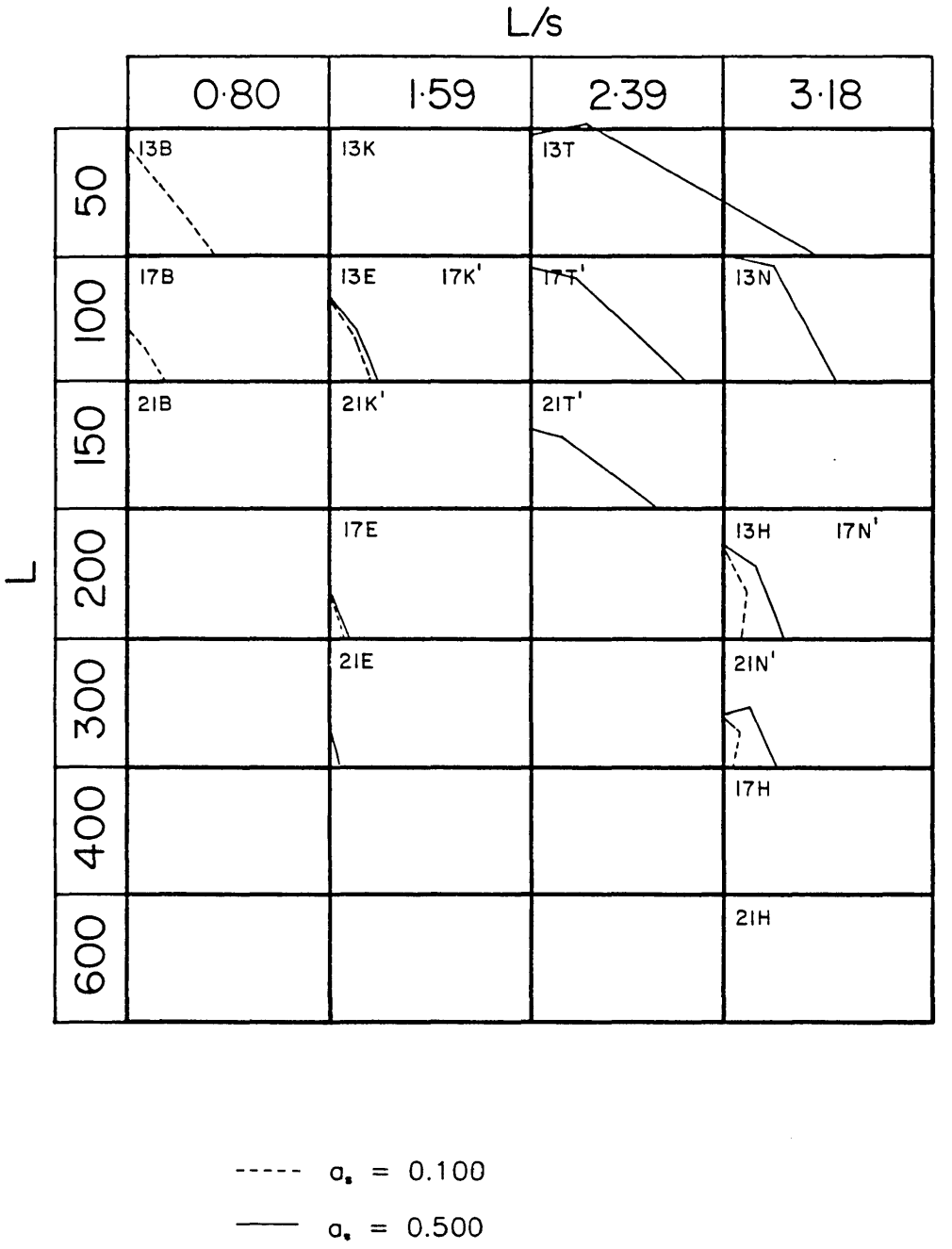
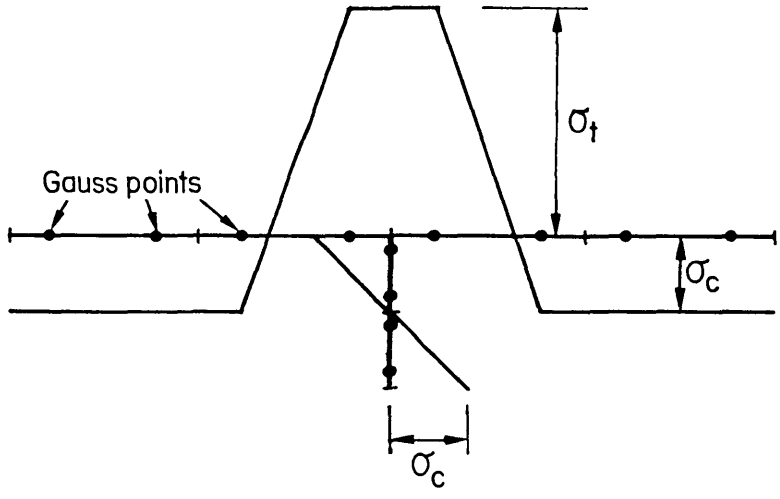


Fig. 4.55

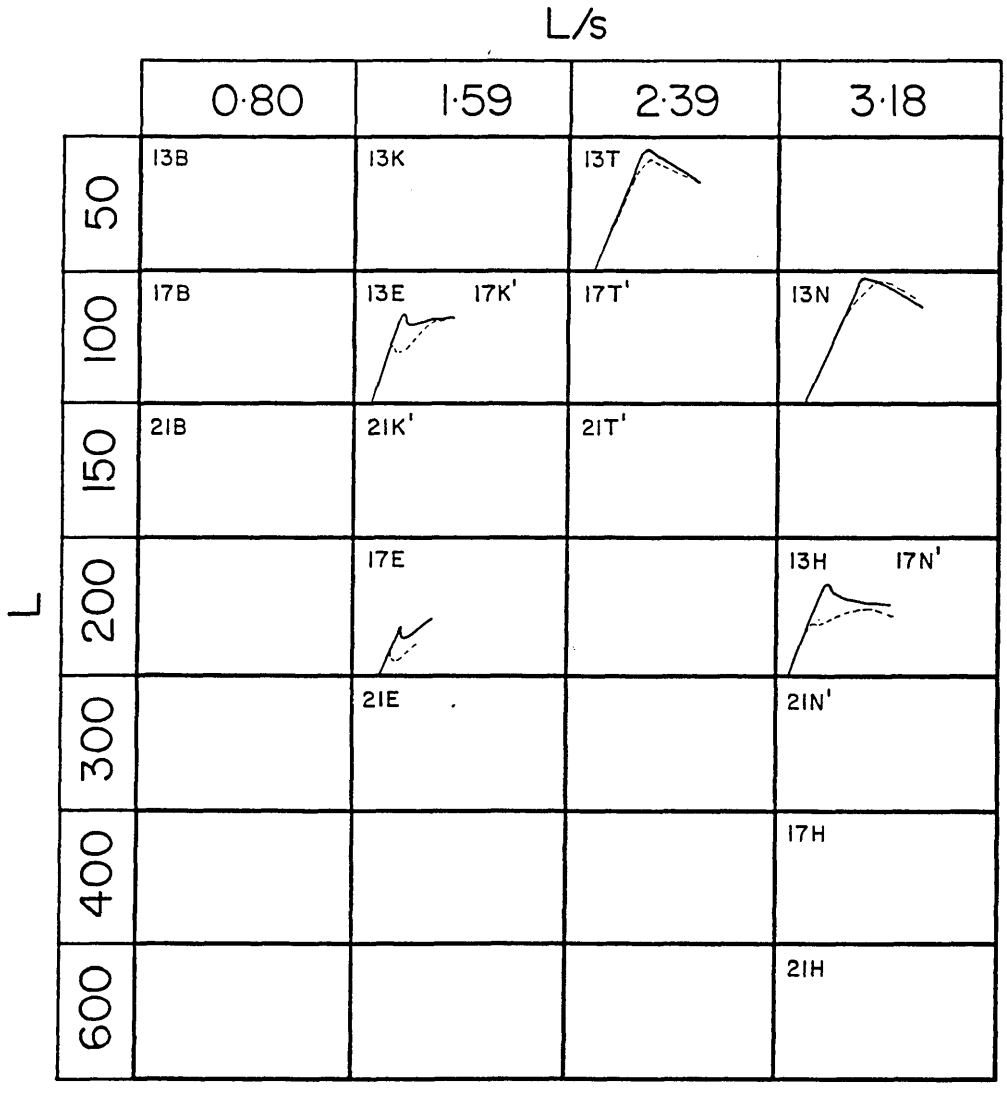


RESIDUAL STRESS DISTRIBUTION

Fig. 4.56

INFLUENCE OF RESIDUAL STRESSES ON LOAD-DEFLECTION PATHS

Axial load



—— $\sigma_r = 0.$

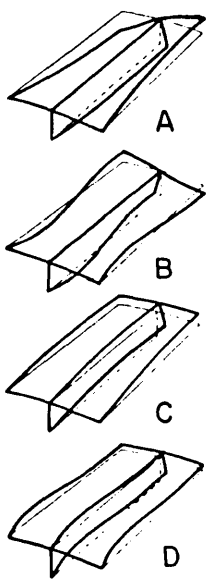
------ $\sigma_r = 0.30$

Fig. 4.57

INFLUENCE OF RESIDUAL STRESSES ON DEFLECTION MODE

Axial load

L \ L/s	0·80	1·59	2·39	3·18
50	13B	13K	13T C C	
100	17B	13E A A	17T'	13N D C
150	21B	21K'	21T'	
200		17E A A		17N' B B
300		21E		21N'
400				17H
600				21H



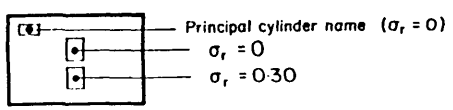
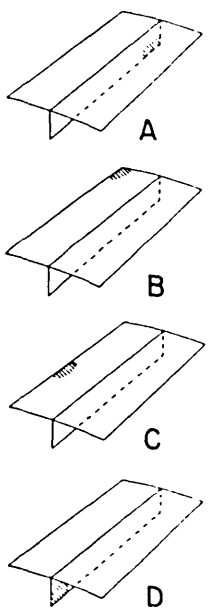


Fig. 4.59

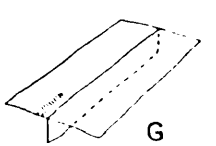
INFLUENCE OF RESIDUAL STRESSES ON FIRST YIELD

Axial load

L \ L/s	0·80	1·59	2·39	3·18
50	13B	13K	13T A G/A	
100	17B	13E B B	17T'	13N A G/A
150	21B	21K'	21T'	
200		17E E E		17N' C B
300		21E		21N'
400				17H
600				21H



ELASTIC - E



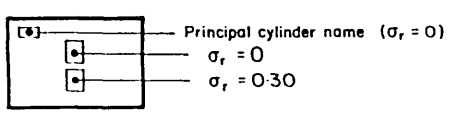
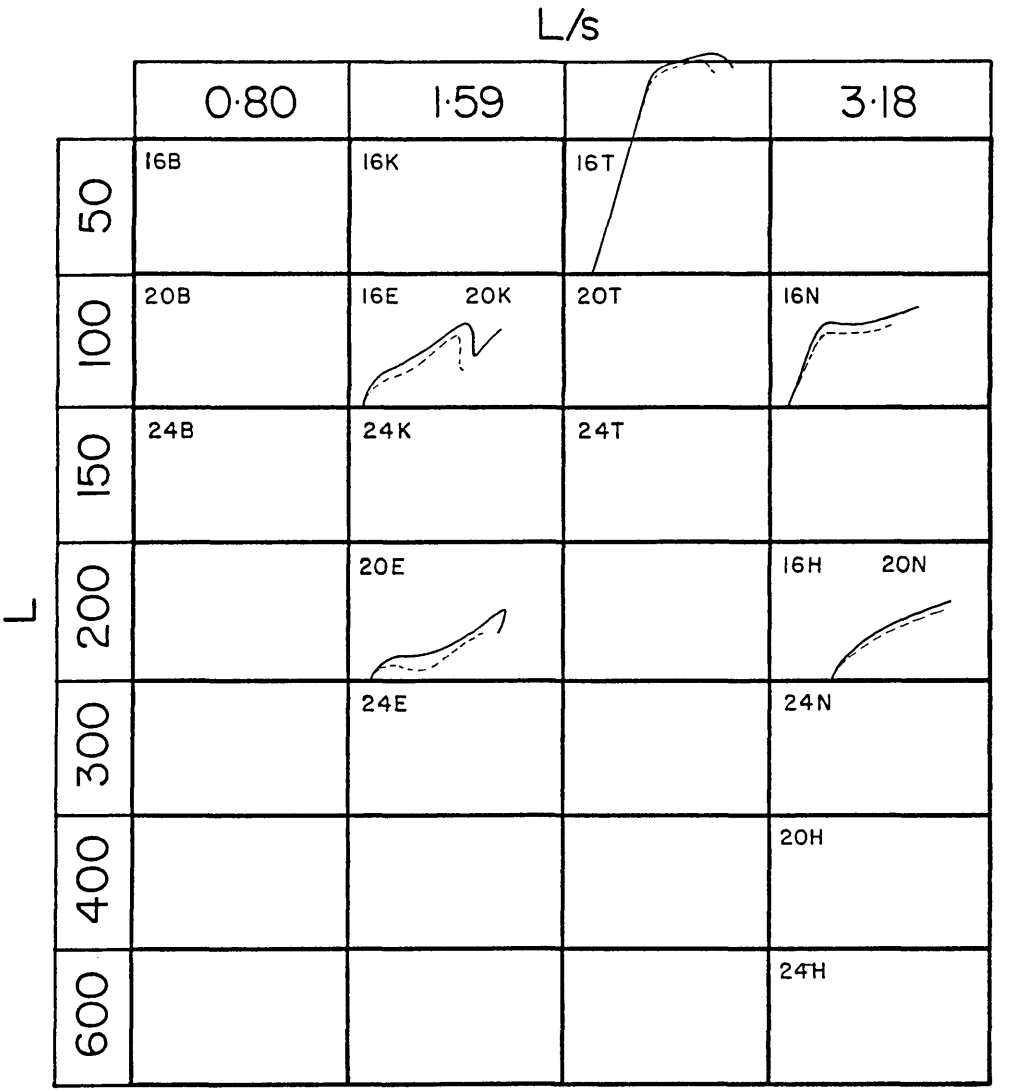


Fig. 4.58

INFLUENCE OF RESIDUAL STRESSES ON LOAD-DEFLECTION PATHS

Pressure load



—— $\sigma_r = 0.$

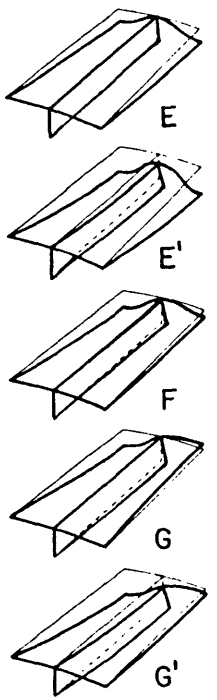
------ $\sigma_r = 0.30$

Fig. 4.60

INFLUENCE OF RESIDUAL STRESSES ON DEFLECTION MODE

Pressure load

L \ L/s	0·80	1·59	2·39	3·18
50	16B	16K	16T G'-E' G'-E'	
100	20B	16E F-E G-E	20T	16N G-G' G-G'
150	24B	24K	24T	
200		20E G-E G-E		20N G-G' G-G'
300		24E		24N
400				20H
600				24H



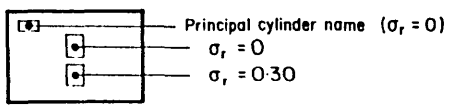
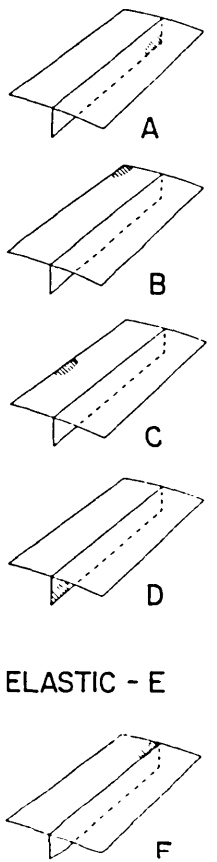


Fig. 4.62

INFLUENCE OF RESIDUAL STRESSES ON FIRST YIELD

Pressure load

L \ L/s	0·80	1·59	2·39	3·18
50	16B	16K	16T A F	
100	20B	16E B F	20T	16N B F
150	24B	24K	24T	
200		20E B E		20N B F
300		24E		24N
400				20H
600				24H



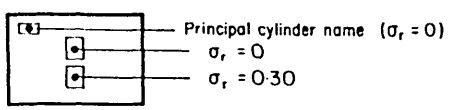
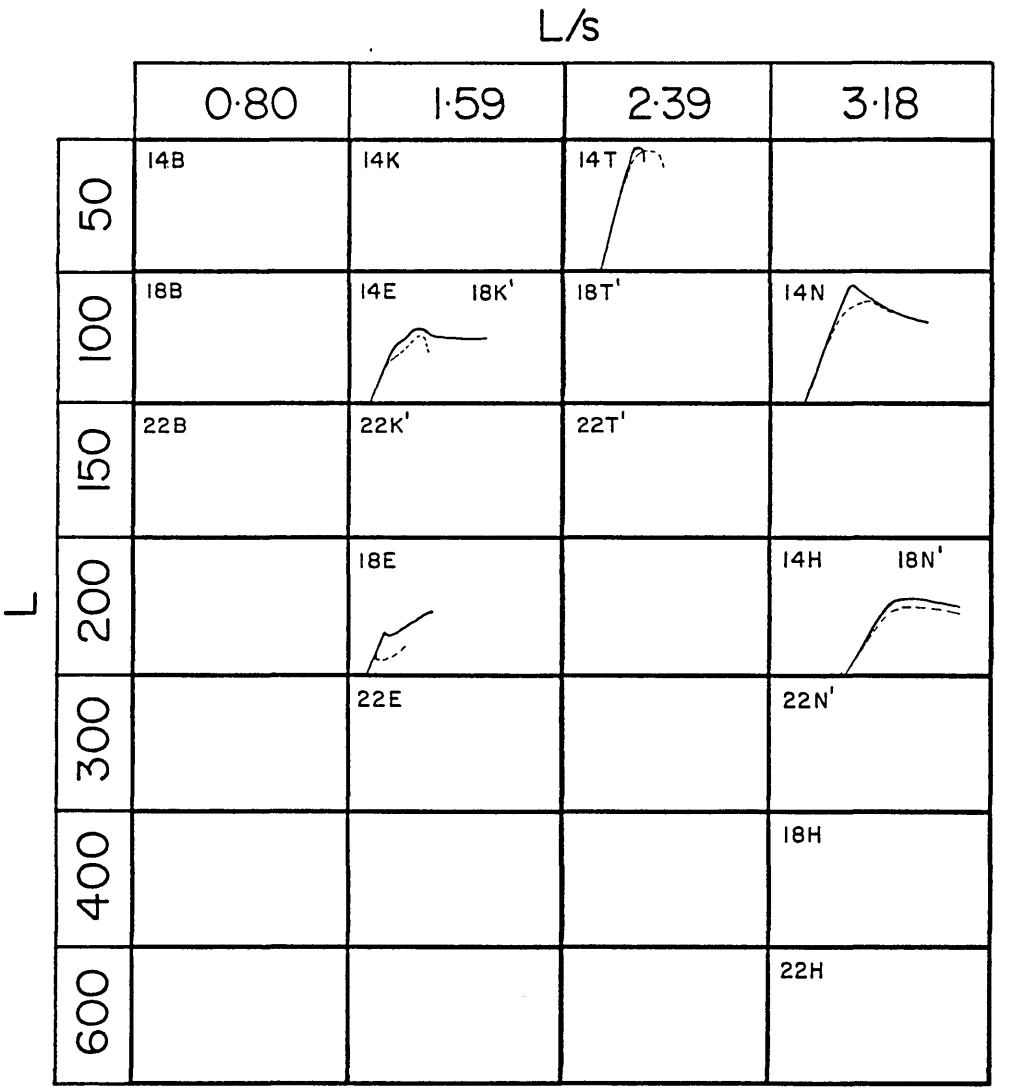


Fig. 4.61

INFLUENCE OF RESIDUAL STRESSES ON LOAD-DEFLECTION PATHS

$\sigma_\theta/\sigma_x = 0{\cdot}4$



—— $\sigma_r = 0.$

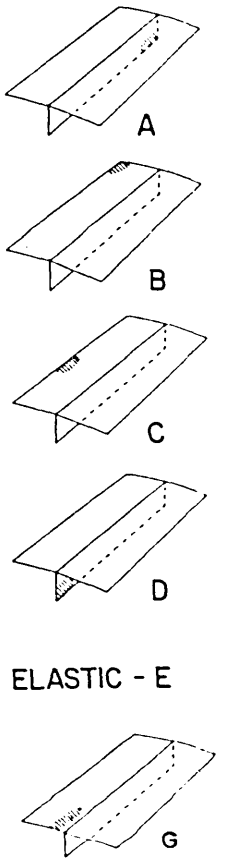
------ $\sigma_r = 0.30$

Fig. 4.63

INFLUENCE OF RESIDUAL STRESSES ON FIRST YIELD

$\sigma_\theta/\sigma_x = 0{\cdot}4$

L \ L/s	0·80	1·59	2·39	3·18
50	14B	14K	14T D G	
100	18B	14E B B	18T'	14N B B
150	22B	22K'	22T'	
200		18E E E		18N B B
300		22E		22N'
400				18H
600				22H



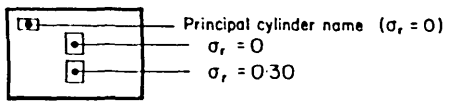
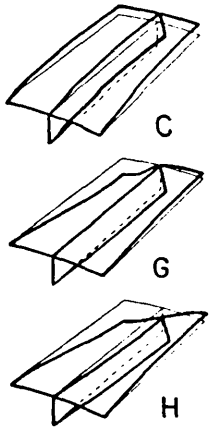


Fig. 4.64

INFLUENCE OF RESIDUAL STRESSES ON DEFLECTION MODE

$\sigma_\theta/\sigma_x = 0{\cdot}4$

L \ L/s	0·80	1·59	2·39	3·18
50	14B	14K	14T C G-C	
100	18B	14E G G	18T'	14N H H
150	22B	22K'	22T'	
200		18E G G		18N H H
300		22E		22N'
400				18H
600				22H



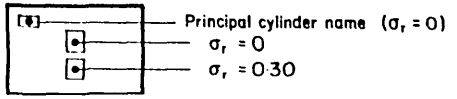
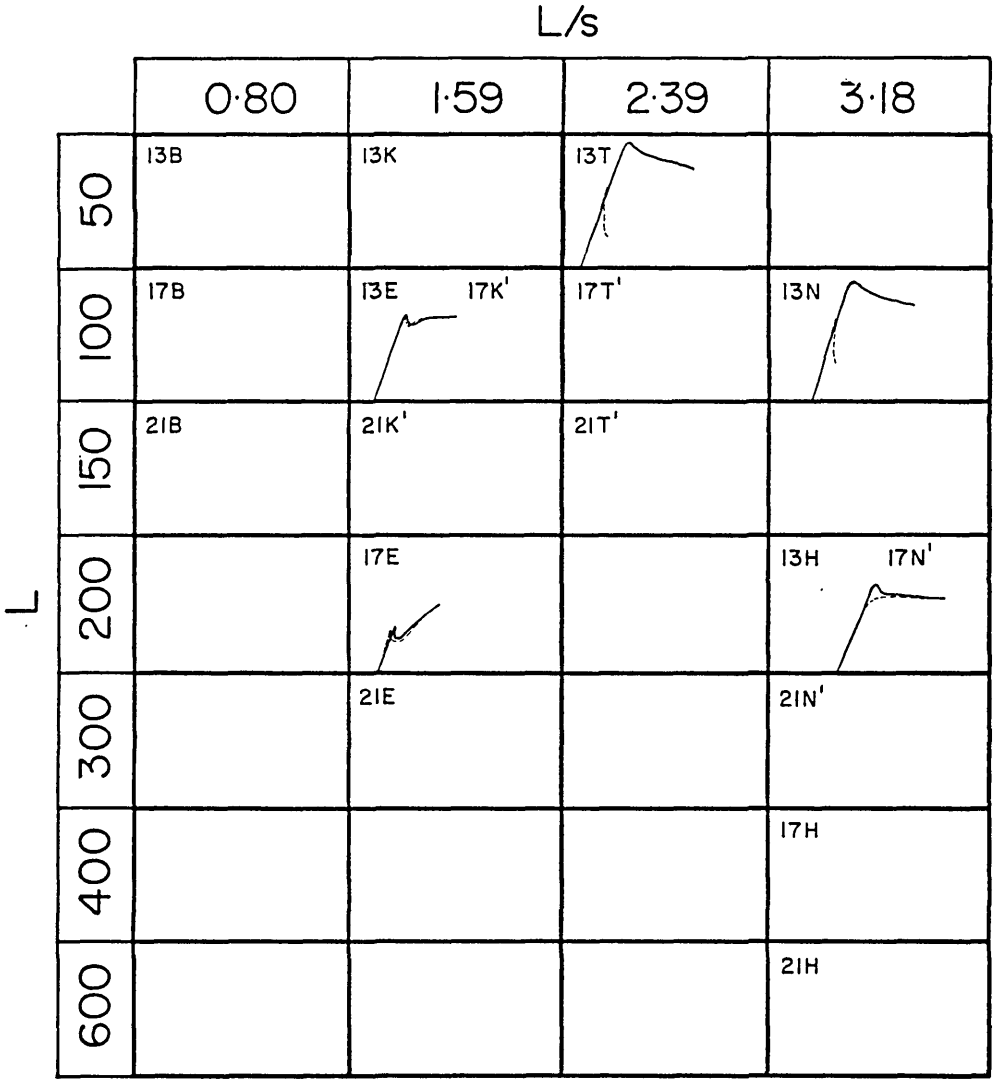


Fig. 4.65

INFLUENCE OF STIFFENER SLENDERNESS ON LOAD-DEFLECTION PATHS

Axial load



—— d_s/t_s = 10

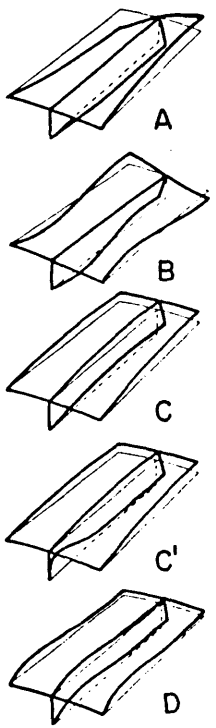
----- d_s/t_s = 20

Fig. 4.66

INFLUENCE OF STIFFENER SLENDERNESS ON DEFLECTION MODE

Axial load

L \ L/s	0·80	1·59	2·39	3·18
50	13B	13K	13T C C'	
100	17B	13E A A	17T'	13N D C'
150	21B	21K'	21T'	
200		17E A A		17N' B B
300		21E		21N'
400				17H
600				21H



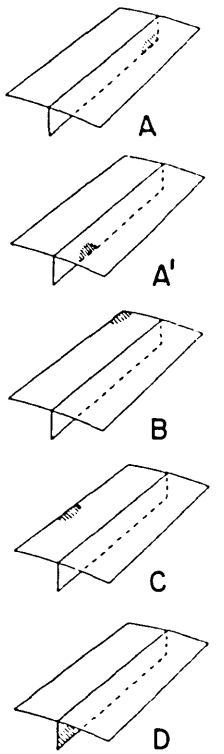
Principal cylinder name (d/t = 10)
d/t = 10
d/t = 20

Fig. 4.68

INFLUENCE OF STIFFENER SLENDERNESS ON FIRST YIELD

Axial load

L \ L/s	0·80	1·59	2·39	3·18
50	13B	13K	13T A A-A'	
100	17B	13E B B	17T'	13N A A'
150	21B	21K'	21T'	
200		17E E E		17N' C C
300		21E		21N'
400				17H
600				21H



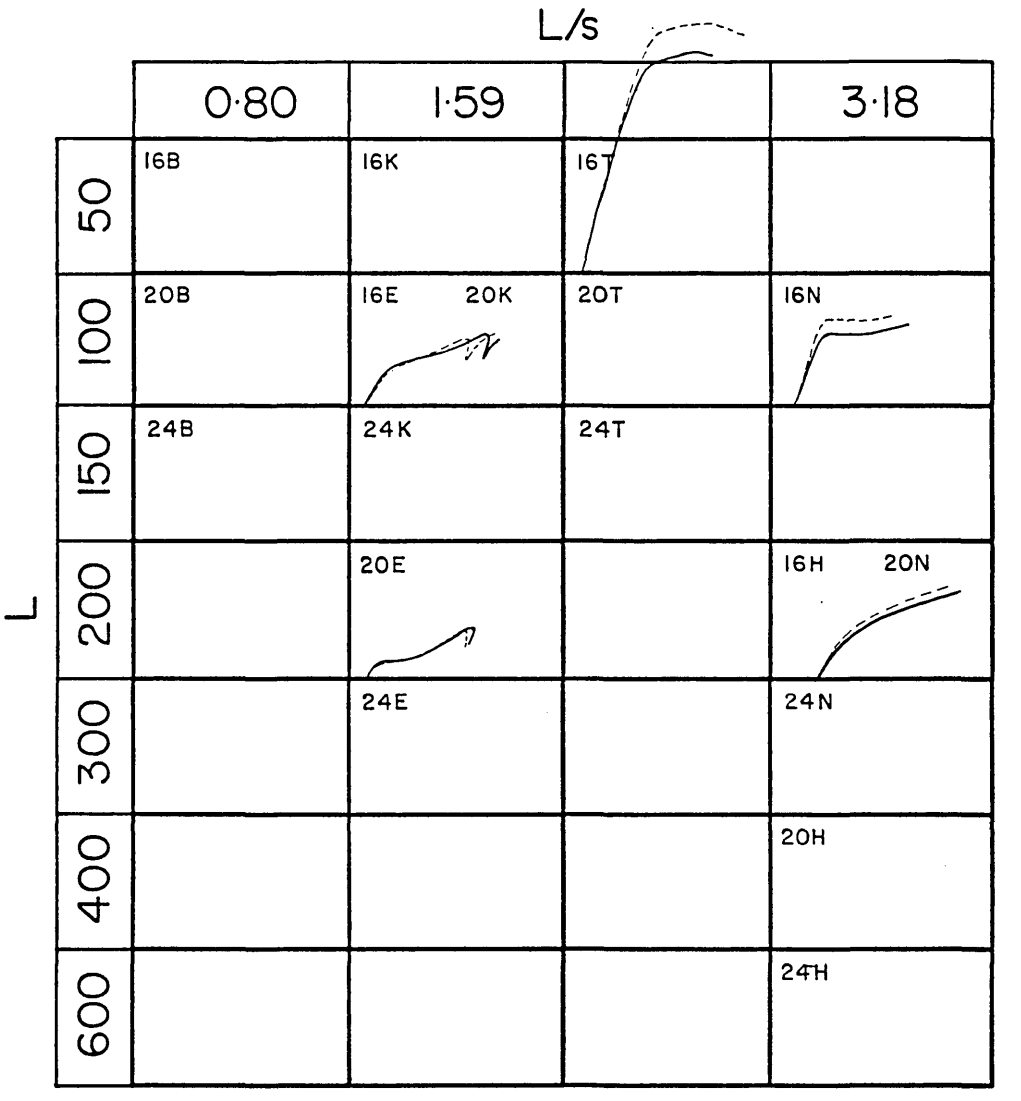
Principal cylinder name (d/t = 10)
d/t = 10
d/t = 20

ELASTIC - E

Fig. 4.67

INFLUENCE OF STIFFENER SLENDERNESS ON LOAD-DEFLECTION PATHS

Pressure load



—— $d_s/t_s = 10$

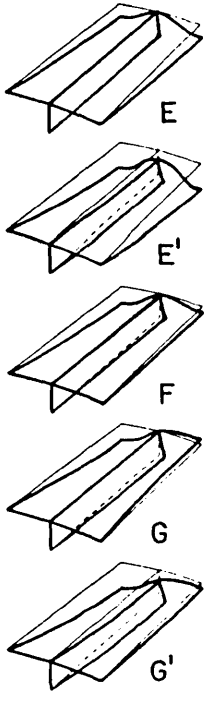
----- $d_s/t_s = 20$

Fig. 4.69

INFLUENCE OF STIFFENER SLENDERNESS ON DEFLECTION MODE

Pressure load

L \ L/s	0·80	1·59	2·39	3·18
50	16B	16K	16T G'-E' G'-E'	
100	20B	16E F'-E G-E	20T	16N G-G' G-G'
150	24B	24K	24T	
200		20E G-E G-E		20N G-G' G-G'
300		24E		24N
400				20H
600				24H



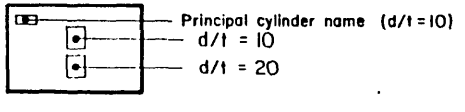
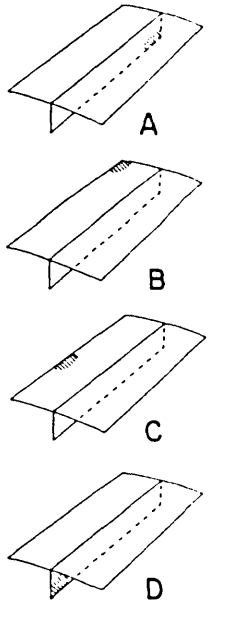


Fig. 4.71

INFLUENCE OF STIFFENER SLENDERNESS ON FIRST YIELD

Pressure load

L \ L/s	0·80	1·59	2·39	3·18
50	16B	16K	16T A A	
100	20B	16E B B	20T	16N B B
150	24B	24K	24T	
200		20E B B/E		20N B B
300		24E		24N
400				20H
600				24H



ELASTIC - E

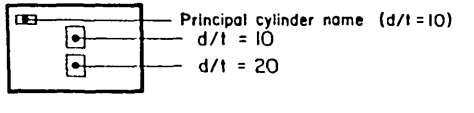
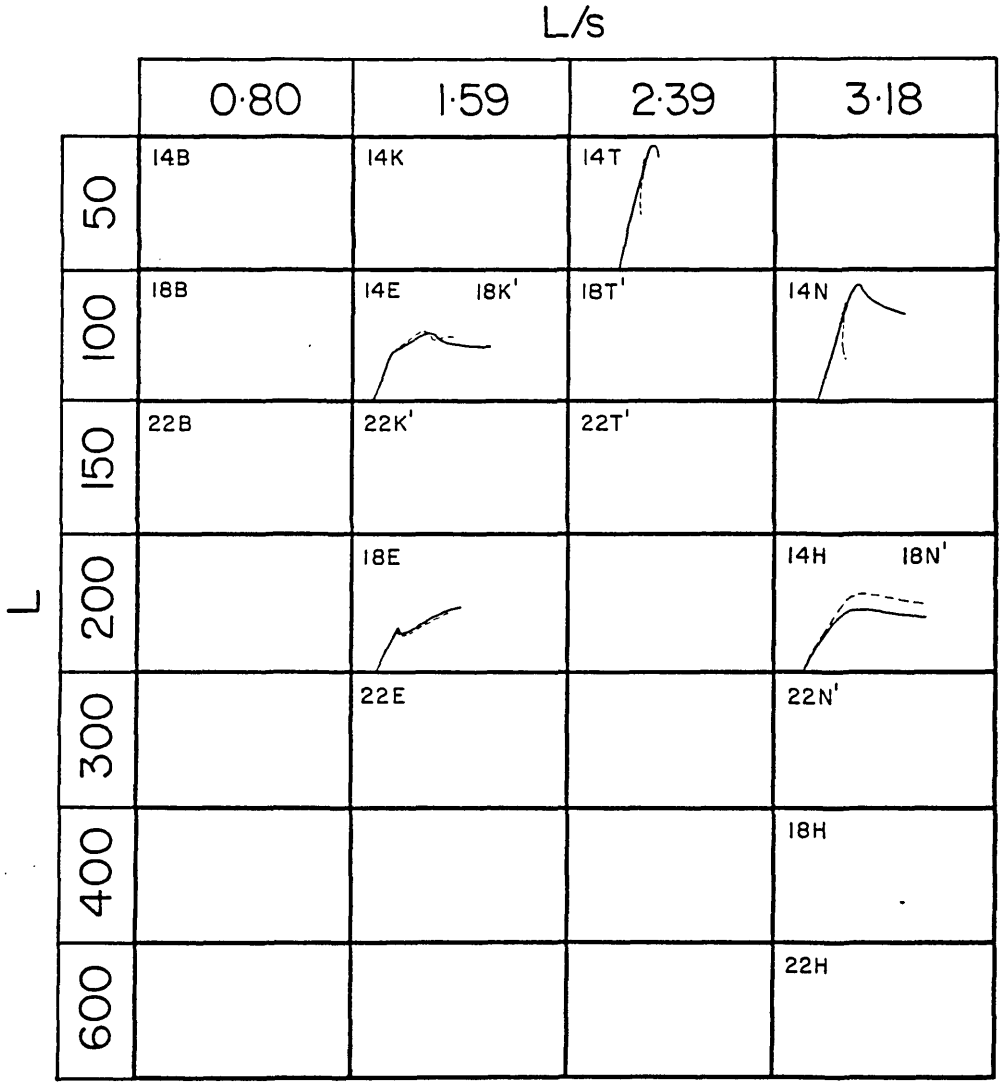


Fig. 4.70

INFLUENCE OF STIFFENER SLENDERNESS ON LOAD-DEFLECTION PATHS

$\sigma_\theta/\sigma_x = 0{\cdot}4$



—— $d_s/t_s = 10$

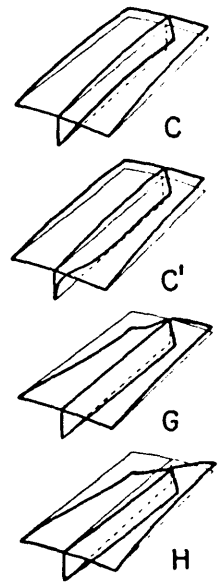
----- $d_s/t_s = 20$

Fig. 4.72

INFLUENCE OF STIFFENER SLENDERNESS ON DEFLECTION MODE

$\sigma_\theta/\sigma_x = 0{\cdot}4$

L \ L/s	0·80	1·59	2·39	3·18
50	14B	14K	14T C C'	
100	18B	14E G G	18T'	14N H C'
150	22B	22K'	22T'	
200		18E G G		18N H H
300		22E		22N
400				18H
600				22H



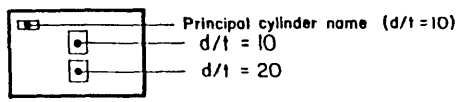
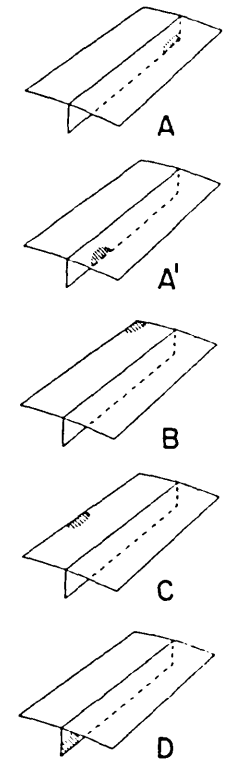


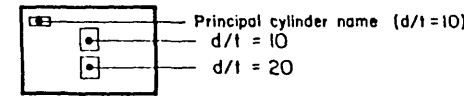
Fig. 4.74

INFLUENCE OF STIFFENER SLENDERNESS ON FIRST YIELD

$\sigma_\theta/\sigma_x = 0{\cdot}4$

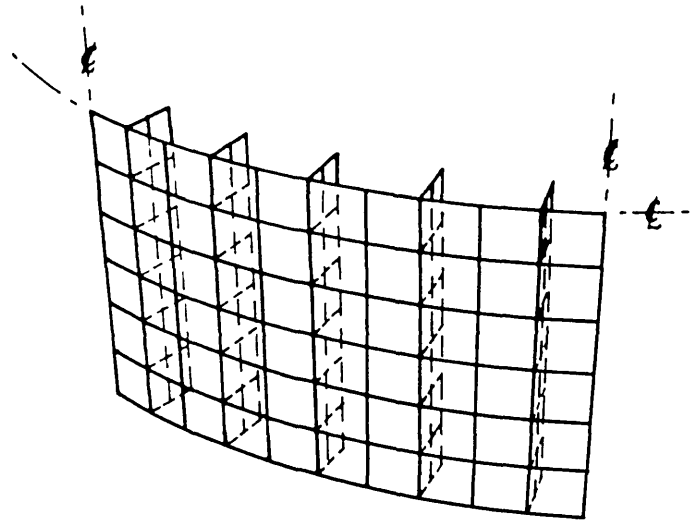
L \ L/s	0·80	1·59	2·39	3·18
50	14B	14K	14T D A'	
100	18B	14E B B	18T'	14N B A'
150	22B	22K'	22T'	
200		18E E E		18N B B
300		22E		22N
400				18H
600				22H





ELASTIC - E

Fig. 4.73



FIVE PANEL FINITE ELEMENT MESH

Fig. 4.75

NUMBER OF
CIRCUMFERENTIAL HALFWAVES
IN OVERALL MODE
OF FIVE PANEL MODELS

Axial load

L \ L/s	0·80	1·59	2·39	3·18
50	13B 6	13K 3	13T 2	
100	17B 9	13E 5 17K' 4	17T' 3	13N 3
150	21B 10	21K' 5	21T' 3	
200		17E 7		13H 4 17N' 3
300		21E 8		21N' 4
400				17H 5
600				21H 6

(Using eqn A.5)

Pressure load

L \ L/s	0·80	1·59	2·39	3·18
50	16B 17	16K 7	16T 4	
100	20B 20	16E 9 20K 9	20T 5	16N 4
150	24B 22	24K 9	24T 6	
200		20E 11		16H 5 20N 5
300		24E 12		24N 5
400				20H 6
600				24H 7

(Using eqn A.9)

Fig. 4.76

CHAPTER FIVE

ASSESSMENT OF CURRENT DESIGN RULES

5.1 INTRODUCTION

A large amount of data was generated and presented in the previous chapter, which, it is hoped, will provide a useful source of information for other workers. Its most obvious application is in the assessment and calibration of current and proposed design formulations. This chapter will briefly review the various design rules currently in use applicable to axially-loaded and pressure-loaded stringer-stiffened cylinders. The finite element and experimental results will be used to assess the predictions of the various methods and to offer suggestions where their performance is poor.

The principal design documents dealing with stringer-stiffened shells that are considered here are the DnV Rules [153], the DnV Classification Notes [154], the ECCS Draft Rules [155] and the ASME Code Case N-284 [156]. In using these rules, safety factors to be applied to the loads and partial safety factors on the material properties or structural strength have been omitted in order to obtain ultimate strength predictions for direct comparison with the numerical and experimental results.

5.2 AXIALLY-LOADED CYLINDERS

5.2.1 LOCAL BUCKLING

The DnV [153] and ECCS [155] rules approach the prediction of the

local buckling strength of cylindrical panels from slightly different directions.

The ECCS Draft Rules consider two categories of behaviour, dependent upon the Z_s ($=\sqrt{1-\nu^2}\,\frac{s^2}{Rt}$) of the panel. For low values of Z_s the effect of curvature is neglected and the elastic critical stress of the flat panels is used (Curve A in Fig 5.1). In this range of behaviour the imperfection sensitivity is relatively low, and a small and constant knockdown is used to account for its effect, yielding curve B.

For panels of higher Z_s the elastic critical stress of a complete unstiffened cylinder is used. The curves labelled C are the predicted values for the radii investigated in the parametric study. The effect of imperfections is greater and is reflected in the larger reduction which is applied to the critical stress. This knockdown factor, α, is dependent upon the R/t ratio of the cylinder and is an empirical quantity providing a lower bound to the scatter band of experimental points. It depends upon the geometry, imperfections and type of loading.

A further partial safety factor, $\gamma = 4/3$, is applied to account for the unfavourable postbuckling response of these panels; this is the range of geometries in which the greatest scatter in experimental results is observed and the additional reduction factor is deemed necessary in order to reduce the possibility that a particular structure will fail at a load below the lower bound of experimental results. The resulting strengths are shown as curves D.

The higher of the two strengths (flat plate and curved panel) is taken to be the elastic critical stress of the imperfect panel. If it exceeds half of the yield stress a further reduction is applied to

account for plasticity. A modified form of the Johnson-Ostenfeld equation is used to define a parabola joining the yield stress to the elastic critical stress at $\sigma = 0.5\sigma_o$ (Curve E). The reduction factor is a function of the reduced slenderness, $\bar{\lambda}$ $(=\sqrt{\sigma_o/\sigma_e})$.

The DnV Rules [153] and Notes [154] implicitly recognize the two types of cylindrical panel behaviour through the use of an empirical expression dependent upon both the R/t ratio and Z_s to give the elastic critical stress of an imperfect panel directly. The buckling strength coefficient is presented graphically in the Rules and explicitly in the Notes. The strengths so obtained are shown as Curves A in Fig 5.2 and can be compared with Curves D in Fig 5.1.

The Rules specify a minimum panel aspect ratio (L/s) of 0.5 for which the method is valid, which includes all the cases considered here. The Notes, however, limit this value to 1.0, below which they suggest that the strength of an unstiffened cylinder be used. Consequently, for the three broadest-panelled geometries of the parametric study slightly different predictions of the local buckling strengths are obtained from the two sets of rules.

A reduction to account for plasticity is applied to all cases irrespective of their elastic critical stress, although its value is small for the lower critical stress cases. The reduction factor is obtained using a simple interaction approach to relate the yield stress, the elastic critical stress and the failure stress in the form of a Merchant-Rankine equation. This yields a reduction factor $\varphi = 1/\sqrt{1+\lambda^4}$, by which the yield stress is multiplied to give the elastoplastic failure stress (Curve B in Fig 5.2).

The values predicted by the various methods are given in Table 5.1. The procedure to be followed in the presentation of these and

subsequent tabulated code predictions will be to present the estimated loads for all geometries, but to enclose within brackets the values for the cases in which the particular method is not strictly valid. The ECCS and DnV predictions are plotted against the parametric results in Figs 5.3 and 5.4 respectively. The DnV predictions are, in general, slightly higher than those of the ECCS rules, and in almost all cases give conservative strength estimates.

The major difference between the two methods is in the intermediate range of panel widths at the transition between flat plate and cylindrical behaviour. The DnV approach yields a smooth transition while the ECCS rules, based as they are on the superposition of two curves, contain a discontinuity, in the region of which more conservative results are produced. Nevertheless, both methods are satisfactory and gave acceptably conservative strength estimates.

5.2.2 IMPERFECTION SENSITIVITY

Koiter [98] investigated the elastic buckling of cylindrical panels and found that they exhibited stable or unstable postbuckling paths depending upon their degree of curvature. He defined a curvature parameter,

$$\theta = \frac{1}{2\pi}\,[12(1-\nu^2)]^{1/4}\,\frac{s}{\sqrt{Rt}}$$

which he found to be equal to 0.64 when the postbuckling response was neutral (i.e. $s/\sqrt{Rt} = 2.2$). For curvatures less than this the cylindrical panel behaved like a flat plate, possessing a stable postbuckling path and little sensitivity to imperfections; panels which were more curved had unstable postbuckling paths similar to unstiffened cylinders and were imperfection sensitive. Although flat plates buckling elstoplastically do display a sensitivity to imperfections, it is of lesser magnitude than that of curved panels.

The ECCS rules also distinguish between flat plate and cylindrical panel behaviour, and separate the two by equating the elastic critical stresses, in which case the transition occurs at $s/\sqrt{Rt} = 2.44$.

The parametric results can be used to assess the degree of imperfection sensitivity. In order that the results can be presented graphically, it is convenient to define a sensitivity parameter, ψ, as the ratio of the cylinder strength for $\bar{\Delta} = 1$ to the strength for $\bar{\Delta} = 0.5$. As was mentioned in Sect 4.4.2.4, this parameter compares the basic strength with that of the more perfect cylinder to avoid the change in the form of the load-deflection path which often occurred when the imperfection was doubled.

ψ has been plotted against $s/\sqrt{Rt}$ in Fig 5.5, and the behaviour is, in fact, of the type predicted. Geometries with $s/\sqrt{Rt}$ approximately equal to 2 were insensitive to imperfections, but the sensitivity grew rapidly as the curvature was increased.

The ECCS rules provide a very basic approach for the design of panels with imperfections larger than the standard tolerance. If the behaviour is of the flat plate type no penalty is imposed. If, however, the panel has a $s/\sqrt{Rt}$ value which places it in the cylindrical shell range of behaviour, its elastic critical stress is halved if the imperfection is up to twice the tolerance. Whilst the method is rather simplistic, it does offer some guidance where other methods do not. Since it is able to handle the more imperfect cases analysed in the parametric study, these results have also been included in Table 5.1 and the comparison of Fig 5.3.

The imperfection sensitivity plot of Fig 5.5 shows that the ECCS approach of halving the strength is not unreasonable; this value

corresponds to the worst cases observed. It may, however, be possible to use a variable knockdown for poor cylinders based upon the Z_s value of the panel, in order to avoid the discontinuity in the magnitude of the reduction factor applied to the different panels. In addition, the neglect of any imperfection sensitivity for slightly curved panels may be somewhat unconservative.

Only the cylinders with larger imperfections have been included in the comparison of Fig 5.3. All methods are valid if the imperfections are reduced, but it is unreasonable to expect the analyses to offer a strength increase in these cases. Consequently, the comparisons have been based on the poorest cylinders that still satisfy the preconditions of each method.

5.2.3 OVERALL BUCKLING

Most of the cylinders analysed in the parametric study did not buckle in overall modes (with the exception of the two shortest stocky cylinders which failed axisymmetrically). The overall buckling predictions are, therefore, not of direct relevance, although it is still important that the design rules do not find an overall mode to be critical.

The ECCS rules use a complex formula, based on the work by Block et al [65] and applicable to stringer-stiffened and orthogonally-stiffened cylinder buckling. It is based on a smeared stiffener theory, in which the eccentricity of the stiffeners is included. An effective width approach is used to account for the possible coincidence of local panel buckling. The equation must be minimized with respect to the wave numbers defining the buckling mode in each direction, and limitations are placed on the minimum number of stringers within each circumferential wave for the smearing assumption

to be valid. Since the effective width is a function of the predicted strength, an iterative technique must be employed in addition to the minimization process. A computer solution is therefore necessary. This procedure yields the elastic critical stress for a perfect cylinder, which is then reduced to allow for the effect of imperfections and plasticity in a manner similar to that described for cylindrical panels.

The method yielded overall buckling loads higher than local for all the cylinders of the parametric study, except 13N and 13T; for those an axisymmetric failure was predicted, as it had been by the finite element method. In the comparison of Fig 5.3 the overall buckling strengths were plotted for these two cases.

The DnV rules use the extremely conservative approach of neglecting the curvature of the shell and treating the cylinder as a flat stiffened plate. This is too great a simplification and the results are, consequently, poor. All the stocky cylinders (R/t = 200) and several of the others were predicted, incorrectly, to fail in overall modes.

Attempts have been made, however, by workers at DnV to improve the method by including the effect of curvature. This modification has been carried out by Valsgard and Steen [162], who follow the basic approach of the DnV Rules to obtain a Perry-Robertson type formula, in which the elastic critical stress of the curved panel is incorporated. An effective width approach is used to account for simultaneous local shell buckling. The analysis is valid for narrow-panelled cylinders with a Z_s less than approximately 7.0. This limitation means that the method is applicable to only a small number of the cases considered in the parametric study.

This is not necessarily a drawback, provided the method predicts the correct failure mode in all the cases in which it is valid. The results are presented in Table 5.1, and show that for both of the models that failed axisymmetrically lower buckling loads were obtained in the overall modes. However, the method also predicted overall failures in several other cases, which in the finite element analyses had failed locally.

Finally, the DnV Notes offer a somewhat different approach. They identify three categories of behaviour: category A contains broad-panelled cylinders with a Z_s greater than 8.6, whose strengths are assumed to be equal to those of the unstiffened cylinders. Category B comprises narrow-panelled, heavily-stiffened cylinders ($Z_s < 8.6$), which are analysed as flat stiffened plates, according to the approach of the DnV Rules. If the additional requirement of $R/t > 0.25\ E/\sigma_o$ is also met, the cylinder falls into category C, for which a semi-empirical approach similar to that used for cylindrical panels is followed.

A considerable number of the cylinders in the parametric study were in the first group; all had their strengths significantly underestimated by the method. The limit of $Z_s > 8.6$, above which unstiffened cylinder behaviour is assumed, is too low. This is the range in which local panel buckling is likely to occur, and the method would be less conservative, but still safe, if the boundary of this first category were raised significantly, and cylinders in this range were handled by the local shell panel buckling rules which already exist. In the comparison of the predictions of the DnV Notes with the finite element results, the estimates for category A have been neglected.

The distinction between category B (closely spaced, heavy

stiffeners) and category C (closely spaced, light stiffeners) is made only on the basis of the R/t ratio, without defining any criterion for the stiffeners themselves. This seems a somewhat paradoxical approach, unless the intention is that the designer should decide himself whether the stiffeners are "light" or "heavy". However, this is not how the rule reads. It is true that a particular size of stringer will provide light or heavy stiffening depending on the R/t ratio of the cylinder to which it is attached. Conversely, however, a particular cylinder may be lightly or heavily-stiffened according to the size of stiffeners attached to it, and to neglect this aspect seems to be an oversimplification.

For the material properties used in the parametric study, the limiting value of R/t is 150, placing all the closely-stiffened cylinders into the lightly-stiffened category. Of the two short, stocky cylinders which failed axisymmetrically, only one (13T) was predicted by the DnV Notes to have a lower strength in an overall mode, although two other cylinders were also predicted to fail in overall modes.

5.2.4 EXPERIMENTAL MODELS

Six of the experimental cylinders had been tested under axial compression and were now analysed using the design methods described above. The results are presented in Table 5.2.

Both the DnV and ECCS rules gave reasonable, conservative predictions of the local buckling strengths of the models. However, the overall buckling strengths calculated by the various methods differed greatly. The DnV Rules gave extremely conservative results, especially for the lightly-stiffened cylinders, A and E, and the longest of the more heavily-stiffened cylinders, 10, (Fig 5.6).

Neglecting the effect of curvature in these cases makes it impossible to obtain realistic strength estimates. For all the experimental models the DnV rules predicted an overall failure to be critical by a large margin.

For the three cylinders mentioned above, the strengths predicted by the flat plate approach were considerably less than those found for the unstiffened cylinders. The unstiffened cylinder strengths must represent the lower bounds to any conservative approach and should be explicitly recognized as such in the rules; instead, it is merely stated that stringer-stiffened shell buckling should be analysed by the stiffened flat plate rules.

The DnV Notes gave somewhat better results (Fig 5.7); however, they too predicted an overall failure mode in each case.

The most satisfactory results were obtained using the ECCS rules, and are presented in Table 5.2 and Fig 5.8. A local mode was predicted for the shortest cylinder of the DnV series; for the midlength cylinder a local mode was predicted to slightly precede an n = 10 overall mode, while for the longest cylinder an n = 8 mode was found to occur first. An almost simultaneous local and overall mode was estimated for the sparsely-stiffened slender cylinder, A, and an overall n = 9 mode for the closely-stiffened cylinder, E. The large-scale model was predicted to fail in a local mode. In all cases the calculated modes were in close agreement with the experimental observations.

The ECCS rules were successful, therefore, both in their estimates of strength and in their accurate prediction of the failure modes. It is not a straightforward matter to incorporate the same level of conservatism into the various components of a design

formulation. By correctly distinguishing between the local and overall modes of failure for all the cases investigated here, the ECCS Rules appear to approach this situation most closely.

5.2.5 RESIDUAL STRESSES

Very little guidance is given in the various design codes regarding the strength deterioration produced by residual stresses. The semi-empirical approaches of the various rules are claimed to allow for practical levels of residual stress in the knockdown factors.

This can be assessed by comparing the predicted strengths with those obtained from the finite element results. If this is done, it is seen that the code predictions often overestimate the cylinder buckling strengths. It should be remembered, however, that the rules do not allow a specified level of residual stress to be incorporated in the analysis, but try to ensure that the strengths of practical structures will not fall below the lower bound curve.

It is important to determine whether the constant residual stress level used in the parametric study is likely to occur in all the cylinders in practice. It was mentioned in Sect 4.6.2 that for a particular welding process the tendon force would be constant and the compressive residual stress inversely proportional to the cross-sectional area of the shell and stiffener. If it is assumed that a compressive residual stress of 30% of yield is a relatively severe case in practice, and this value is assigned to the model with the smallest cross-sectional area, residual stress levels of corresponding severity can be calculated for the remaining cylinders (Table 5.3).

In the parametric study, residual stresses produced the greatest strength reductions in the weaker cylinders; these were the broader-

panelled models, in which the residual stress of 0.30 σ_o was probably a significant overestimate of the level to be expected in practice. Linear interpolation can be used to obtain strength estimates for these models with the reduced residual stress level. The values are shown in the last column of Table 5.3.

Plotting these values against the strengths predicted by the ECCS rules, Fig 5.3, shows that in almost all cases the rules are conservative. The exception is geometry 13T for which a 5.5% overestimate was obtained. The correlation with the DnV Notes is similar, Fig 5.4, although unconservative predictions are slightly more frequent.

Although both sets of rules seem to give reasonable estimates of the strength of fabricated cylinders, a definitive assessment requires the experimental testing of more cylinders with residual stresses.

5.2.6 SUMMARY

There appears to be little to distinguish between the local buckling predictions of the three sets of rules considered. The ECCS rules are slightly more complex and conservative, but provide a better understanding of the likely behaviour by distinguishing between flat plate and curved panel behaviour. They enable, if only in a very simple fashion, strength estimates to be obtained for cylinders with larger imperfections than the specified tolerance. The slightly greater conservatism of the ECCS rules ensured that safe predictions were made for cylinders with residual stresses. On the other hand, the DnV approach is simpler, in that it requires the application of two rules in all cases. Nevertheless, the differences between the various methods were relatively small.

For overall buckling, however, the ECCS rules provide superior

results, and justify the more complex calculations necessary for their application. In the relatively small number of overall buckling cases considered the ECCS Rules gave accurate predictions of both the strength and buckling mode.

5.3 PRESSURE-LOADED CYLINDERS

The ECCS rules do not cover stringer-stiffened cylinders under pressure loading, while the DnV Rules, once again, tackle the problem from an oversimplified viewpoint. The local buckling strength of the shell panels is assumed to be equal to the strength of the unstiffened cylinder. The implicit assumption is that the number of circumferential halfwaves in the buckling mode of the unstiffened cylinder is approximately equal to the number of stringers in the stiffened cylinder. In narrow-panelled models, for which this assumption may be far from accurate, very conservative results will be produced. The estimates obtained by this method are given in Table 5.4 and Fig 5.9.

Overall buckling is handled in the DnV Rules by neglecting the curvature of the shell and analysing a laterally-loaded, flat stiffened plate. The cylinder strength is limited by the plastic moment capacity of the shell-stiffener unit. The analysis is, by implication, valid only in those cylinders that buckle elastoplastically. Since several of the parametric and experimental results buckled elastically, it is inappropriate to apply the method generally to all cases. However, no guidance is given as to the extent of application of this approach.

A beam-column method is considered in a later section (5.3.1) and a more detailed discussion will be postponed until then. However, at this point it should be noted that as the Rules stand the pressure

capacity in almost all cases of the parametric study was still limited by the local buckling strength of the shell panel.

The DnV Notes use a semi-empirical approach, similar to those outlined previously, for both the local and overall buckling modes. The local buckling strength is taken to be the higher of two values: the first is the strength of a flat panel with in-plane compression applied to its longer edges; the second, which is applied to broad-panelled cylinders, is the buckling strength of the unstiffened cylinder.

The calculation of the overall buckling strength requires the distinction between the A, B and C categories mentioned previously; once again, the same criticisms regarding these groupings can be made. The predicted strengths for the cylinders of the parametric study are given in Table 5.4, and in some cases the low strength found for category A suggested an overall mode, which did not develop in the finite element analyses. As before, in the correlation between the numerical results and the DnV Notes in Fig 5.10 the predicted values for the unstiffened cylinders (Category A) have been ommitted.

Finally, the ASME Rules [156] were also applied. The approach is an empirical one, in which coefficients have been determined to provide a lower bound to experimental results. Local and overall buckling are considered in an approach that first calculates the elastic critical stresses for a perfect structure and then applies empirical knockdown factors to account for the effects of imperfections and plasticity.

The local shell buckling critical stress is calculated as that of a curved panel or unstiffened cylinder depending upon the $s/\sqrt{Rt}$ ratio. The overall buckling strength is determined using an equation of the

form employed in the ECCS Rules for overall buckling under axial compression. A constant value of effective panel length is used, which does not require an iterative solution of the strength equation. In all cases local buckling was predicted to be critical (Table 5.4).

The estimates of the DnV Notes and the ASME Rules are presented graphically in Figs 5.10 and 5.11 respectively. For weak cylinders, failing at a hoop stress of less than approximately one third of yield, both methods predicted strengths which followed the general trend of the numerical results. The correlation with the DnV Notes was marginally better and more consistently conservative. Both methods, however, were very over-conservative in their estimates for shorter cylinders with many stiffeners (especially the "K" and "T" geometries) and produced an almost random scatter of points in the upper parts of Figs 5.10 and 5.11.

5.3.1 LATERALLY-LOADED BEAM MODE

In these cases the principal mode of action of the shell-stiffener unit is that of a laterally-loaded beam, whose strength is limited by its plastic moment capacity. This will be the type of behaviour provided the shell panel is relatively narrow (i.e. Z_s is small) and the panel is relatively short (i.e. Z is small). An inspection of the finite element and experimental results shows that the laterally-loaded beam mode governed the failure when Z_s was less than approximately 15 and Z was less than approximately 40.

The plastic moment capacities of these cross-sections were calculated assuming that the shell becomes plastic when the axial stress reaches the uniaxial yield stress. In other words, the effect of the compressive hoop stress, whose presence will tend to increase the axial compressive stress necessary to reach yield, was neglected.

Considering the shell-stiffener unit to be a simply supported beam allows the determination of the external pressure required to produce the plastic moment. The nominal hoop stress (=pR/t) at this pressure has been given in Table 5.4; the results are presented graphically in Fig 5.12 for the geometries that meet the limits on the Z values mentioned above, and in each case a line connects this strength with the buckling strength predicted by the DnV Notes. A great improvement in the correlation is produced, although in a few cases the results are slightly unconservative. In the two strongest cylinders even the beam model significantly underestimated the pressure capacity. This was most probably due to the neglect of the simultaneous resistance to the external pressure by the hoop mode, which in these stocky models would be significant.

It can be seen from Table 5.4 that when the failure load is determined using the laterally-loaded beam approach, the nominal hoop stress, σ_θ, significantly exceeds the predicted local buckling stress under hoop compression. It may not be immediately apparent why the plastic beam failure is not preceded, therefore, by local shell buckling. The reason is simply that the actual level of hoop stress is considerably less than the nominal stress. The applied pressure is resisted primarily by the shell-stiffener beam through the development of bending stresses in the cross-section. Because the hoop stiffness is relatively small, only a small proportion of the applied pressure is resisted by hoop stresses.

The beam mode will develop only if the panel is relatively narrow; otherwise, the magnitude of the radial shell panel deflections will be governed, not by the stiffness of the beam unit, but by the local stiffness of the shell panel between stringers. The deflections of the shell may, therefore, be considerably larger at the midpanel

than at the stiffener line and induce local shell buckling before the shell-stiffener unit has reached its limiting strength in the beam mode. This can be avoided by imposing an upper limit on the Z_s value of the panel.

The capacity of a cylinder that meets this requirement will be governed by the strength of the shell-stiffener beam. Can it be assumed, however, that the beam will reach its fully-plastic moment? Is it not possible, for example, that the shell will fail in axial compression before the plastic moment of the section is developed?

When the shell-stiffener cross-section is elastic, its neutral axis lies in the upper part of the stiffener and the shell is in compression through its entire thickness. As the pressure is increased, the stiffener tip will begin to yield in tension and the neutral axis will move upwards. Provided the stiffening ratio is less than unity, the neutral axis will eventually enter the shell itself.

An alternative limit to the strength of the shell-stiffener can be determined by assuming that it can be loaded until the axial stress in the midplane of the shell reaches the buckling stress in axial compression. If the buckling stress is very low, the neutral axis will be within the stringer and the moment capacity will be considerably less than the plastic moment. However, even for moderate local axial buckling strengths of the shell the neutral axis will have moved into the shell and little difference between the capacity calculated by this method and the fully-plastic moment will be obtained. In any case, once the neutral axis is near the shell midsurface, the shell is loaded primarily in bending and it is inappropriate to limit its strength to the axial buckling stress.

The cylinders from the parametric study that met the requirement

on Z_s were analysed using the simple beam model to determine the position of the neutral axis and hence the applied bending moment when the shell midsurface stress reached the local buckling stress under axial compression determined from the DnV Rules. Several cases needed to be considered depending upon the position of the neutral axis. The results have been expressed as a nominal hoop stress and presented in Table 5.4.

In almost all cases, the required position of the neutral axis was so close to the equal area axis that the moment capacity was very nearly equal to the fully-plastic moment. Only in one case, 24K, was the compressive strength of the shell low enough for there to be a reduction in the moment capacity of any significance.

The plastic moment appears, therefore, to be a valid strength estimate provided that it is employed only for cylinders with sufficiently narrow panels that the beam mode can develop. Although a minimum Z_s value was suggested, it is not certain that this is the governing parameter, and more work would be needed to determine the precise range of geometries for this mode of behaviour. This is particularly important because the predicted strength is allowed to exceed the local buckling strength of the shell, and the designer must be assured that the cylinder is of such proportions that the full beam capacity can be mobilized.

It is not necessary to define a minimum length parameter (e.g. Z); provided the Z_s limit is met, the cylinder strength can be taken to be the greater of the strengths determined by assuming that the pressure is resisted either by hoop compression or beam bending.

It is often stated that stringers are ineffective in raising the capacity of pressure-loaded cylinders. The parametric study has shown

that a large strength enhancement can be produced in short, narrow-panelled cylinders, and the analysis above has outlined a method by which the magnitude of the effect can be determined. Stringer-stiffened cylinders of the proportions investigated here are unlikely to be used in practice to resist only external pressure. However, an accurate assessment of their pressure capacity may still be important if they are to be subjected to combined loading and their interaction behaviour needs to be determined.

5.3.2. EXPERIMENTAL MODELS

The relevant experimental cylinders were analysed for external pressure using both the DnV Notes and the ASME Rules and the results are given in Table 5.5. Cylinders B and F of the slender series were tested under hydrostatic loading, but their interaction diagrams (Fig 3.15) were so steep that little change in their strengths would be expected for the pure pressure cases. The predictions from both rules are very similar (Figs 5.13 and 5.14), with the ASME values being slightly less conservative.

The strengths of the cylinders were also calculated using the beam approach and presented in Table 5.5. The maximum applied pressure was determined assuming the beam to be fully clamped at its ends. In most cases the beam mode was not critical, either because the method was inappropriate ($Z_s < 15$), or because it gave lower strength estimates than the overall buckling predictions.

For cylinder 3, however, a slightly higher pressure was predicted to cause failure in the beam mode. Although this was the mode of failure observed in the experiment [203], the predicted strength was still significantly less than the experimental failure pressure. Once again, this was probably due to the neglect of the load sharing

between the beam mode and the hoop mode.

5.4 INTERACTION BEHAVIOUR

Up to this point the strengths of cylindrical shells under a single state of applied stress have been considered. In general, the cylinder will be loaded by a combination of loads. Most design rules tackle the problem through the use of an interaction equation, which relates the various components of the applied load to the cylinder strength for each acting individually. The advantage of this approach is not only its simplicity, but also that it allows the prediction to be based on the current state of knowledge for each type of loading.

The most common form is:

$$\left(\frac{\sigma_x}{\sigma_{cx}}\right)^m + \left(\frac{\sigma_\theta}{\sigma_{c\theta}}\right)^n \leq 1.0 \qquad 5.1$$

where the ratios are between the applied stress and the characteristic elastoplastic strength for axial compression and hoop compression respectively. The ECCS Rules for unstiffened cylinders use a linear interaction (m=n=1), which is conservative in all cases. In the DnV Rules m and n are set equal to 2 to produce an elliptical interaction curve, which is often unconservative. Alternative shapes have also been suggested, e.g. Faulkner et al [160], by assigning other values to the indices.

The interaction diagrams obtained in the parametric study (Figs 4.27 - 4.29) and from the experiments (Figs 3.5 and 3.15) showed that the shape of the curve may vary significantly depending primarily upon whether failure is elastic or plastic. An interaction formula that reflects these changes is desirable.

The ASME Rules take the rather extreme course when buckling takes place inelastically of disregarding any interaction between axial and

hoop compression. The parametric and experimental results show this to be an unconservative approach.

The most appropriate method to date seems to be that suggested by Odland [166] and incorporated in the DnV Notes. The interaction equation between axial and hoop compression is:

$$\left(\frac{\sigma_x}{\sigma_{ex}} + \frac{\sigma_\theta}{\sigma_{e\theta}}\right)^2 + \left(\frac{\bar{\sigma}}{\sigma_o}\right)^2 \leq 1.0 \qquad 5.2$$

where $\bar{\sigma}$ is the equivalent von Mises stress given by:

$$\bar{\sigma}^2 = \sigma_x^2 + \sigma_\theta^2 - \sigma_x\sigma_\theta. \qquad 5.2(a)$$

The equation normalizes each applied load by the corresponding elastic critical stress and the equivalent stress by the yield stress. Incorporating the ratio of the equivalent stress to the yield stress in the interaction equation changes the shape of the curve depending upon the stress level. For very stocky cylinders, the first bracketed term will be negligible and the equation will approximate the yield criterion; when buckling is elastic, the equivalent stress term is small and the equation approaches a linear interaction.

For a single stress loading condition this equation reduces to:

$$\sigma_x = \sigma_o/\sqrt{1+\lambda^4} \quad \text{where } \lambda^2 = \sqrt{\sigma_o/\sigma_{ex}}, \qquad 5.3$$

which is the elastoplastic strength formulation used in the DnV Rules and Notes.

The interaction equation 5.2 can also be recast in a similar form:

$$\bar{\sigma} = \sigma_o/\sqrt{1+\lambda^4} \quad \text{where } \lambda^2 = \frac{1}{\sigma_o}(\sigma_x\bar{\lambda}_x^2 + \sigma_\theta\bar{\lambda}_\theta^2) \qquad 5.4$$

$$\text{and } \bar{\lambda}_x = \sqrt{\sigma_o/\sigma_{ex}} \qquad \bar{\lambda}_\theta = \sqrt{\sigma_o/\sigma_{e\theta}}.$$

The predicted strengths under the single stress states of pure axial compression and hoop compression have already been compared with the finite element and experimental results. In this section a comparison of the shapes of the interaction curves is desired. It

will be assumed that the method has predicted the strengths under axial and hoop compression exactly and the analytical interaction curve will be drawn which connects these points.

For example, let the experimental or F.E. strength under axial compression be $(\sigma_x)_{exp} = \sigma_o/k_x$. The DnV Notes predict a value of $\sigma_x = \sigma_o/\sqrt{1+\bar{\lambda}_x^4}$, where $\bar{\lambda}_x = \sqrt{\sigma_o/\sigma_{ex}}$. The predicted strength will be exact if $\bar{\lambda}_x^2 = \sqrt{k_x^2-1}$, which requires that:

$$\sigma_{ex} = \sigma_o/\sqrt{k_x^2-1}. \qquad 5.5$$

Similarly, the equality of the experimental and predicted strengths under pure pressure would require that:

$$\sigma_{e\theta} = \sigma_o/\sqrt{k_\theta^2-1}. \qquad 5.6$$

To determine the predicted strength for a cylinder with a loading ratio defined by:

$$\sigma_\theta = \alpha\sigma_x, \qquad 5.7$$

equations 5.5, 5.6 and 5.7 can be substituted into 5.2 to give:

$$\left[\frac{\sigma_x}{\sigma_o}(k_x^2 - 1) + \frac{\alpha\sigma_x}{\sigma_o}(k_\theta^2 - 1)\right]^2 + \left(\frac{\sigma_x}{\sigma_o}\right)^2(1 + \alpha^2 - \alpha) \leq 1.0 \qquad 5.8$$

Putting $b_x = \sqrt{k_x^2-1}$ and $b_\theta = \sqrt{k_\theta^2-1}$ and simplifying gives:

$$\sigma_x = \frac{\sigma_o}{\sqrt{(b_x + b_\theta)^2 + 1 + \alpha^2 - \alpha}} \qquad 5.9$$

This expression gives the axial component of the specified combined loading predicted by the interaction expression of the DnV Notes between specified points on the axial and pressure axes. The results so obtained are presented in Figs 5.15, 5.16 and 5.17 for the cylinders of the parametric study. In general, the agreement is good, and certainly better than would be achieved using any other code procedure. The transition between the straight line interaction of the elastic cases and the concave interaction of the elastoplastic cases is achieved.

The strength under external pressure of two of the short stocky models exceeded the nominal yield pressure. In the interaction expression the maximum value that can be introduced for σ_θ is σ_o, and this was the value used in these cases. For this reason the predicted interaction curve does not intersect the pressure axis at the same point as the finite element results.

Often, the shape of the interaction was conservative; i.e. it was straighter than the numerical results; in some cases, however, the interaction was significantly unconservative (e.g. R = 200, N = 40, L/R = 0.25). It seems that the finite element analyses predicted interaction curves of more consistent shape for cylinders of varying radius. For example, the finite element interaction curves for the N = 60, L/R = 0.25 cylinders have, more or less, the same shape, even though their scale varies. The DnV Notes, however, predict a significant change in the shape of the interaction curves due to the difference in the strengths of the cylinders. This suggests that the stress level is not the only variable affecting the shape of the curve.

It should be remembered that the actual strength predictions of the DnV Notes for combined loading cases will be significantly less than have been shown here, since the interaction curve will join conservative predicted values for the single stress loading cases. The final interaction curve will not only be displaced towards the origin, but will also become straighter as the equivalent stress term in eqn 5.2 is reduced.

For example, the most unconservative curve (R = 200, N = 40, L/R = 0.25) will become conservative when the strengths predicted by the DnV Notes for the axial and pressure cases are used. However, an interaction equation should not rely on this effect in order to give

conservative predictions. In fact, one of the advantages of using an interaction approach is that use can be made of the current state of knowledge for each single stress case. If it depends on a high level of conservatism in the single stress predictions in order to give acceptable results, it would restrain the development of more accurate analyses for the single stress cases; the curve should ideally yield predictions with the same degree of conservatism as the end points it joins.

The experimental interaction curves are compared with the DnV Notes in Figs 5.18 and 5.19. Good and consistent agreement is obtained for all the cylinders of the stocky series, amongst which the only variable was the length. In the slender series, where the cylinder cross-section was varied, the relationship between the experimental and code interaction curves was less uniform. This reinforces the assertion that it may not be possible to obtain a more accurate prediction of the interaction behaviour by including only an equivalent stress term.

An alternative approach to the prediction of strength under combined loading has recently been suggested by Steen et al [164]. They begin by determining the local and overall elastic critical stresses under axial load and external pressure. The initial imperfections are amplified by factors which depend on the ratios of the applied stresses to the elastic buckling stresses. The additional bending stresses which these imperfections will produce at the outer fibre of the shell are then calculated and added to the design stresses. The von Mises yield criterion is used to check that the yield stress has not been exceeded.

If the cylinder is stocky and therefore has high critical buckling stresses the amplification factors and additional stresses

are small and the method reduces to the von Mises yield criterion. In very slender cylinders the solution is governed by the ratio of the applied stress to the critical stress, which is determined using a linear interaction.

For the checking of designs the series of steps described above is followed sequentially. For strength predictions, however, an iterative method requiring a computer solution is necessary, since the amplification factors are functions of the applied stress levels.

Harding et al [165] applied this method in a comparison with the stocky series of small-scale models described in this thesis and obtained good agreement.

5.5 C O N C L U S I O N S

The brief review of current design rules related to stringer-stiffened cylinders undertaken in this chapter has highlighted a number of strengths and weaknesses in the various methods.

Axially-loaded cylinders can be handled reasonably satisfactorily. The local buckling predictions of the various design rules are similar and provide adequate strength estimates in most cases. The degree of conservatism is in some cases fairly large, but the imperfection sensitive nature of the problem makes this unavoidable. Although a certain amount of "fine-tuning" of the empirical coefficients may still be possible, major improvements are probably unattainable.

Satisfactory predictions of the overall buckling behaviour were obtained by using the ECCS Rules; in each case they distinguished correctly between local and overall buckling, predicted the appropriate buckling mode in the overall buckling cases and gave

acceptable strength estimates.

In contrast, the pressure-loaded cylinders were not handled as well. The difficulty arises because of the two different modes of load resistance developed in the cylinders: hoop compression, which predominates in the longer and more lightly-stiffened geometries and shell-stiffener bending in the short heavily-stiffened cylinders. Most codes disregard the latter mode and, therefore, significantly underestimate the capacities of the stronger cylinders.

The exception is the DnV Rules, which neglects the effect of curvature in its approach to most stringer-stiffened cylinder problems. The cylinder strength is calculated as the plastic moment capacity of the shell-stiffener unit, but is still not allowed to exceed the local buckling stress of the shell panel under hoop compression. The assumption that bending is the mode of action in one case and hoop compression in the other is inconsistent and unsatisfactory.

The parametric study showed that the cylinder strength under external pressure often exceeded the local buckling strength of the panel by a large amount. The appropriate course is to limit the cylinder capacity either to the bending strength of the shell-stiffener beam or to the local shell buckling strength by establishing which mode will predominate. A tentative proposal for this boundary was made ($Z_s \cong 15$), but further work is needed to define its precise form and location. Even this approach will be conservative in the cases in which both load carrying mechanisms contribute significantly to the cylinder strength.

Of the various simple interaction equations, the one used in the DnV Notes appears to be the best, since it approximates the form of

the interaction curves over a broad range of geometries. However, this approach is not always conservative, and a more accurate prediction will probably require a detailed analysis which takes account of the specific geometry and loading.

NAME	R	N	L	a_s	Z	Z_s	$\bar{\sigma}_{FE}$	DnV Rules local	DnV Rules over.	DnV Rules Valsgard & Steen	DnV Notes local	DnV Notes overall A	DnV Notes overall C	ECCS Rules local	ECCS Rules over.	$\bar{\Delta}$=2.0 $\bar{\sigma}_{FE}$	$\bar{\Delta}$=2.0 ECCS local	$\bar{\sigma}_r$=.3 $\bar{\sigma}_{FE}$
01B	200	20	50	0.159	11.92	18.83	.815	.634	.576	(.509)	.543	.543	(.851)	.552	.810			
13B	200	20	50	0.300	11.92	18.83	.793	.634	.606	(.573)	.543	.543	(.994)	.552	.931			
01E	200	20	100	0.159	47.70	18.83	.647	.634	.446	(.534)	.634	.522	(.703)	.552	.700			
13E	200	20	100	0.300	47.70	18.83	.655	.634	.595	(.574)	.634	.552	(.922)	.552	.875	.655	.454	.579
25E	200	20	100	0.500	47.70	18.83	.659	.634	.621	(.604)	.634	.522	(.983)	.552	.914			
13H	200	20	200	0.300	190.8	18.83	.922	.634	.546	(.585)	.634	.521	(.734)	.552	.786			
13K	200	40	50	0.300	11.92	4.71	.942	.916	.887	.894	.916	(.543)	.977	.862	.906			
13N	200	40	100	0.300	47.70	4.71	.969	.916	.789	.836	.916	(.522)	.824	.862	.835	.968	.862	.966
25N	200	40	100	0.500	47.70	4.71	1.003	.916	.873	.886	.916	(.522)	.941	.862	.885			
13T	200	60	50	0.300	11.92	2.09	.879	.981	.888	.900	.981	(.543)	.954	.939	.886			.833
25T	200	60	50	0.500	11.92	2.09	.963	.981	.935	.938	.981	(.543)	.990	.939	.922			
05B	400	20	100	0.080	23.85	37.66	.397	.269	.315	(.275)	.242	.242	(.610)	.235	.669			
17B	400	20	100	0.300	23.85	37.66	.430	.269	.378	(.352)	.242	.242	(.975)	.235	.880	.320	.118	
05E	400	20	200	0.080	95.39	37.66	.297	.269	.194	(.299)	.269	.237	(.441)	.235	.460			
17E	400	20	200	0.300	95.39	37.66	.336	.269	.360	(.354)	.269	.237	(.763)	.235	.809	.336	.118	.303
29E	400	20	200	0.500	95.39	37.66	.331	.269	.409	(.400)	.269	.237	(.935)	.235	.869			
17H	400	20	400	0.300	381.6	37.66	.350	.269	.275	(.335)	.267	.236	(.475)	.235	.667	.350	.118	
17K	400	40	100	0.300	23.85	9.41	.609	.515	.595	(.567)	.515	.242	(.913)	.454	.857	.550	.454	
05N	400	40	200	0.159	95.39	9.41	.678	.515	.190	(.522)	.515	.237	(.477)	.454	.404			
17N	400	40	200	0.300	95.39	9.41	.696	.515	.546	(.560)	.515	.237	(.584)	.454	.748	.635	.454	.612
29N	400	40	200	0.500	95.39	9.41	.721	.515	.596	(.591)	.515	.237	(.810)	.454	.826			
17T	400	60	100	0.300	23.85	4.18	.896	.783	.767	.745	.783	(.242)	.839	.755	.834	.844	.755	
29T	400	60	100	0.500	23.85	4.18	.890	.783	.784	.767	.783	(.242)	.962	.755	.883			
21B	600	20	150	0.300	35.77	56.50	.298	.150	.293	(.275)	.140	.140	(.945)	.129	.829			
21E	600	20	300	0.300	143.1	56.50	.263	.150	.270	(.276)	.150	.138	(.617)	.129	.757	.263	.065	
33E	600	20	300	0.500	143.1	56.50	.252	.150	.330	(.328)	.150	.136	(.869)	.129	.837			
21H	600	20	600	0.300	572.4	56.50	.214	.150	.175	(.285)	.150	.137	(.338)	.129	.573			
21K	600	40	150	0.300	35.77	14.12	.428	.270	.443	(.422)	.270	.140	(.829)	.202	.814			
09N	600	40	300	0.106	143.1	14.12	.383	.270	.093	(.370)	.270	.138	(.301)	.202	.298			
21N	600	40	300	0.300	143.1	14.12	.397	.270	.372	(.416)	.270	.136	(.431)	.202	.675	.397	.202	
33N	600	40	300	0.500	143.1	14.12	.415	.270	.449	(.457)	.270	.138	(.677)	.202	.778			
09T	600	60	150	0.159	35.77	6.28	.631	.493	.288	.480	.493	(.140)	.325	.454	.475			
21T	600	60	150	0.300	35.77	6.28	.634	.493	.576	.557	.493	(.140)	.714	.454	.787			
33T	600	60	150	0.500	35.77	6.28	.616	.493	.611	.593	.493	(.140)	.919	.454	.848			

Table 5.1 CODE PREDICTIONS FOR AXIALLY-LOADED CYLINDERS - PARAMETRIC STUDY

NAME	R	N	L	a_s	Z	Z_s	$\bar{\sigma}_{exp}$	DnV Rules local	DnV Rules over.	DnV Notes local	DnV Notes overall A	DnV Notes overall C	ECCS Rules local	ECCS Rules over.	ECCS Rules n
1	190	40	76	0.267	29.42	4.48	.95	.926	.798	.926	.837	(.540)	.872	.947	
7	190	40	152	0.267	116.3	4.48	1.01	.926	.558	.926	.708	(.536)	.872	.892	
10	190	40	229	0.267	287.5	4.48	1.06	.926	.344	.926	.695	(.536)	.872	.857	8
A	254	20	254	0.072	242.3	23.91	.78	.474	.039	.474	(.576)	.394	.577	(.569)	
E	254	40	254	0.143	242.3	5.98	1.10	.809	.104	.809	.576	(.394)	.769	.723	9
IC4	170	20	189	0.255	199.8	16.00	.87	.785	.642	.785	(.822)	.665	.805	.934	

Table 5.2 CODE PREDICTIONS FOR AXIALLY-LOADED CYLINDERS - EXPERIMENTAL MODELS

NAME	AREA	$\bar{\sigma}_r$	$(\bar{\sigma}_x)_{r=0}$	$(\bar{\sigma}_x)_{r=.3}$	$\bar{\sigma}'_x$
13E	81.7	0.10	.655	.428	.579
13N	40.8	0.20	.969	.961	.966
13T	27.3	0.30	.879	.833	.833
17E	163.4	0.05	.336	.138	.303
17N	81.7	0.10	.696	.445	.612

$(\bar{\sigma}_x)_{r=0}$ = strength when $\bar{\sigma}_r = 0$

$(\bar{\sigma}_x)_{r=.3}$ strength when $\bar{\sigma}_r = 0.3$

$\bar{\sigma}'_x$ strength for intermediate $\bar{\sigma}_r$ (see Sect 5.2.5)

Table 5.3 INTERPOLATION OF STRENGTHS FROM RESIDUAL STRESS RESULTS

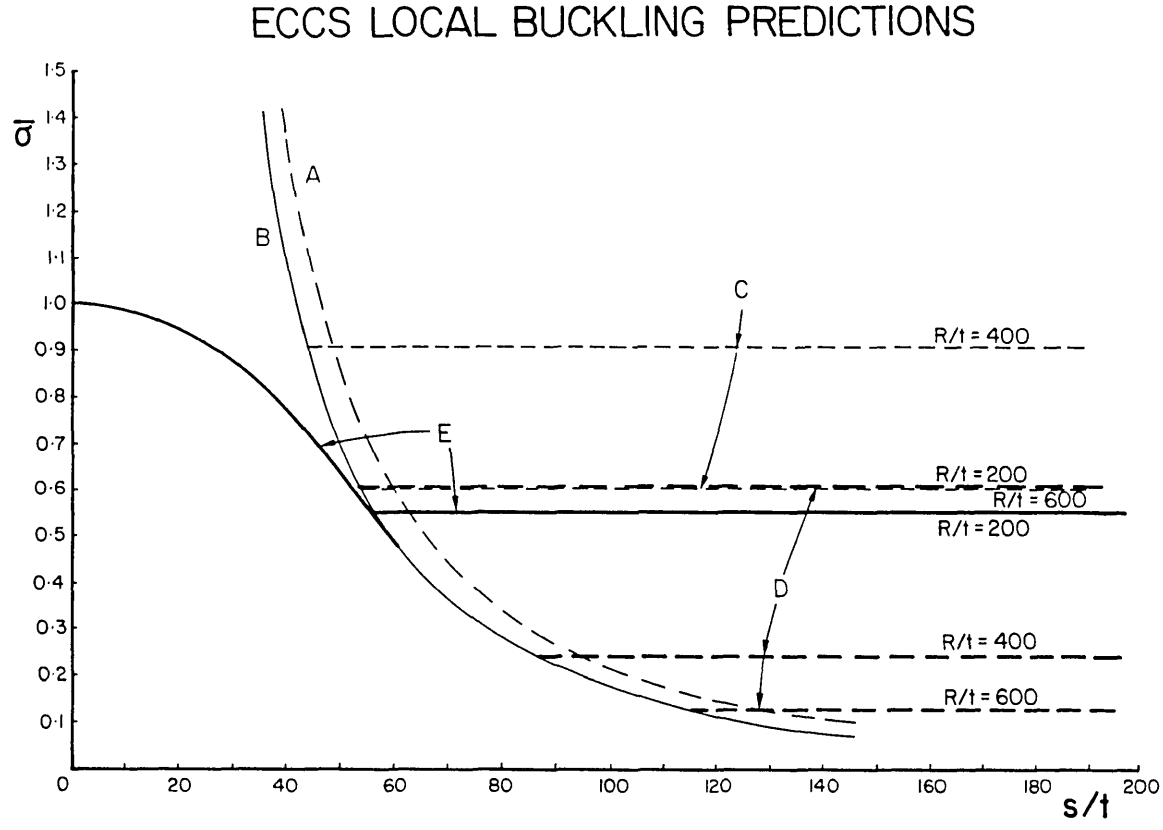
Table 5.4 See over

NAME	R	N	L	a_s	Z	Z_s	$\bar{\sigma}_{exp}$	DnV Rules local	DnV Notes local	DnV Notes overall A	DnV Notes overall C	ASME Rules local	ASME Rules over.	shell-stiffener beam mode max. axial shell stress	shell-stiffener beam mode fully-plastic moment
3	190	40	76	0.267	29.42	4.48	1.055	.354	.620	(.433)	.699	.652	.652	.806	.807
6	190	40	152	0.267	116.3	4.48	.535	.160	.539	(.178)	.269	.512	.336	.189	.192
11	190	40	229	0.267	287.5	4.48	.352	.115	.523	(.112)	.145	.490	.175	.084	.080
B	254	20	254	0.072	242.3	23.91	.153	.086	.098	.085	(.091)	.113	.099	(.031)	(.029)
F	254	40	254	0.143	242.3	5.98	.164	.088	.324	(.085)	(.095)	.275	.117	.046	.044

Table 5.5 CODE PREDICTIONS FOR PRESSURE-LOADED CYLINDERS - EXPERIMENTAL MODELS

NAME	R	N	L	a_s	Z	Z_s	$\bar{\sigma}_{FE}$	DnV Rules local	DnV Notes local	DnV Notes overall A	DnV Notes overall C	ASME Rules local	ASME Rules over.	shell-stiffener beam mode max. axial shell stress	shell-stiffener beam mode fully-plastic moment
04B	200	20	50	0.159	11.92	18.83	.646	.619	.675	.703	(.852)	.753	.903	(.443)	(.443)
16B	200	20	50	0.300	11.92	18.83	.643	.619	.675	.703	(.964)	.753	1.007	(1.548)	(1.550)
04E	200	20	100	0.159	47.70	18.83	.286	.249	.258	.306	(.415)	.374	.537	(.111)	(.111)
16E	200	20	100	0.300	47.70	18.83	.286	.249	.258	.306	(.679)	.374	.787	(.387)	(.388)
28E	200	20	100	0.500	47.70	18.83	.357	.249	.258	.306	(.819)	.374	.854	(.770)	(.779)
16H	200	20	200	0.300	190.8	18.83	.214	.126	.164	.129	(.245)	.170	.295	(.097)	(.097)
16K	200	40	50	0.300	11.92	4.71	1.286	.619	.730	(.703)	.939	.753	.972	1.168	1.168
16N	200	40	100	0.300	47.70	4.71	.607	.249	.553	(.306)	.579	.539	.724	.292	.292
28N	200	40	100	0.500	47.70	4.71	.863	.249	.553	(.306)	.727	.539	.793	.564	.570
16T	200	60	50	0.300	11.92	2.09	1.486	.619	.868	(.703)	.919	.839	.953	.998	.999
28T	200	60	50	0.500	11.92	2.09	2.717	.619	.868	(.703)	.961	.839	.993	1.890	1.915
08B	400	20	100	0.080	23.85	37.66	.286	.210	.223	.264	(.460)	.288	.647	(.271)	(.274)
20B	400	20	100	0.300	23.85	37.66	.314	.210	.223	.264	(.775)	.288	.888	(.964)	(1.052)
08E	400	20	200	0.080	95.39	37.66	.100	.088	.079	.099	(.147)	.125	.179	(.068)	(.069)
20E	400	20	200	0.300	95.39	37.66	.120	.088	.079	.099	(.300)	.125	.371	(.241)	(.263)
32E	400	20	200	0.500	95.39	37.66	.129	.088	.079	.099	(.443)	.125	.517	(.399)	(.536)
20H	400	20	400	0.300	381.6	37.66	.049	.048	.041	.044	(.086)	.059	.101	(.060)	(.066)
20K	400	40	100	0.300	23.85	9.41	.857	.210	.258	.264	(.673)	.288	.800	.771	.776
08N	400	40	200	0.159	95.39	9.41	.114	.088	.164	.099	(.127)	.142	.153	.055	.055
20N	400	40	200	0.300	95.39	9.41	.286	.088	.164	.099	(.232)	.142	.271	.193	.194
32N	400	40	200	0.500	95.39	9.41	.457	.088	.164	.099	(.341)	.142	.380	.383	.389
20T	400	60	100	0.300	23.85	9.41	.729	.210	.393	(.264)	.611	.353	.752	.655	.655
32T	400	60	100	0.500	23.85	9.41	1.171	.210	.393	(.264)	.764	.353	.857	1.283	1.297
24B	600	20	150	0.300	35.77	56.50	.186	.105	.101	.132	(.548)	.149	.790	(.554)	(.841)
24E	600	20	300	0.300	143.1	56.50	.086	.048	.043	.051	(.166)	.066	.200	(.138)	(.210)
36E	600	20	300	0.500	143.1	56.50	.094	.048	.043	.051	(.257)	.066	.279	(.186)	(.433)
24H	600	20	600	0.300	572.4	56.50	.026	.027	.022	.024	(.046)	.032	.056	(.035)	(.053)
24K	600	40	150	0.300	35.77	14.12	.567	.105	.118	.132	(.435)	.149	.666	.561	.619
12N	600	40	300	0.106	143.1	14.12	.043	.048	.073	.051	(.067)	.069	.080	.041	.042
24N	600	40	300	0.300	143.1	14.12	.157	.048	.073	.051	(.126)	.069	.150	.140	.141
36N	600	40	300	0.500	143.1	14.12	.397	.048	.073	.051	(.191)	.069	.240	.232	.234
12T	600	60	150	0.159	35.77	6.28	.243	.105	.186	(.132)	.192	.164	.237	.147	.148
24T	600	60	150	0.300	35.77	6.28	.586	.105	.186	(.132)	.377	.164	.520	.513	.518
36T	600	60	150	0.500	35.77	6.28	.929	.105	.186	(.132)	.535	.164	.747	1.020	1.032

Table 5.4 CODE PREDICTIONS FOR PRESSURE-LOADED CYLINDERS - PARAMETRIC STUDY



Curve A flat panel (perfect) $\sigma_{cr} = 3{\cdot}6E\left(\frac{t}{s}\right)^2$

Curve B (imperfect) $\alpha\sigma_{cr}$ where $\alpha = 0{\cdot}83$

Curve C curved panel (perfect) $\sigma_{cr} = 0{\cdot}605E\frac{t}{r}$

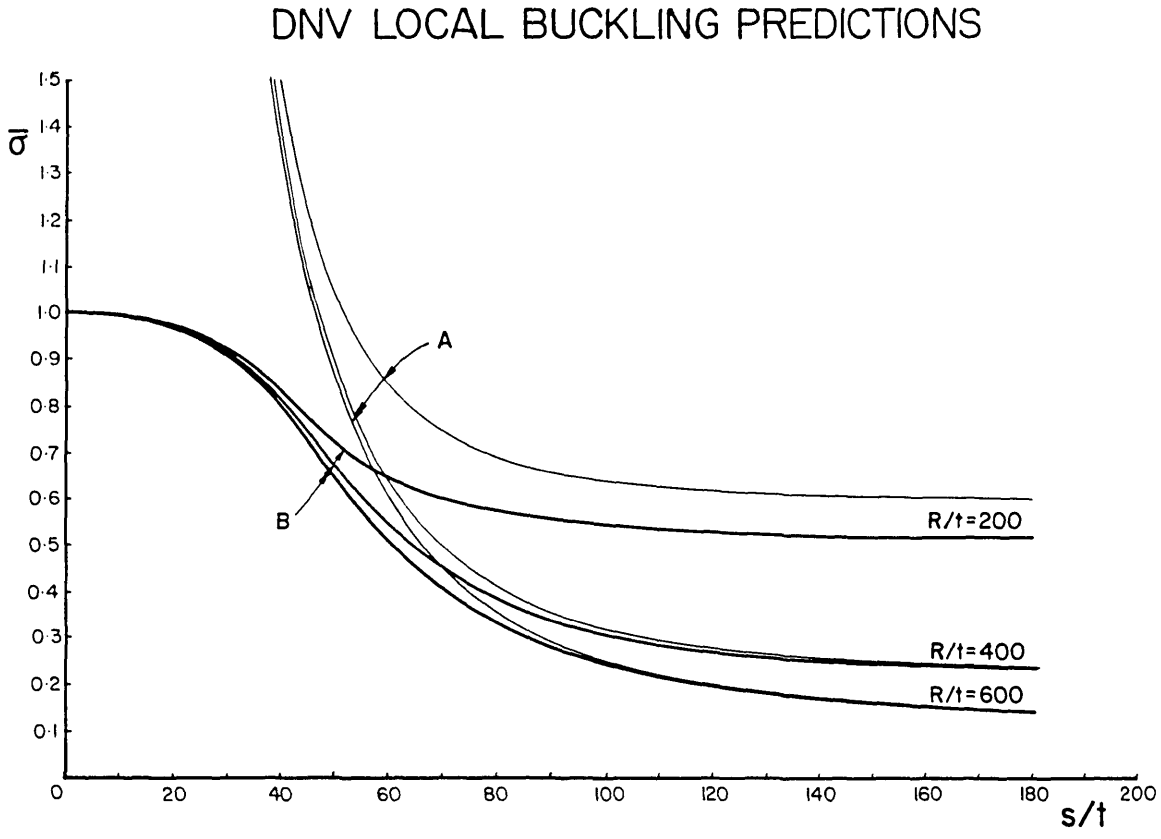
Curve D (imperfect) $\frac{\alpha\sigma_{cr}}{\gamma}$ where $\alpha = \frac{0{\cdot}83}{\sqrt{1+{\cdot}01r/t}}$ for $r/t<212$ $\gamma = 4/3$

$= \frac{0{\cdot}70}{\sqrt{1+{\cdot}01r/t}}$ for $r/t>212$

Curve E plasticity reduction $\sigma_{ul} = \sigma_0\left(1-0{\cdot}4123\left(\frac{\sigma_0}{\alpha\sigma_{cr}}\right)^{0{\cdot}6}\right)$ if $0{\cdot}605\alpha E\frac{t}{r} > 0{\cdot}5\sigma_0$

$= \sigma_0\left(1-0{\cdot}25\frac{\sigma_0}{\alpha\sigma_{cr}}\right)$ if $0{\cdot}83\times3{\cdot}6E\left(\frac{t}{s}\right)^2 > 0{\cdot}5\sigma_0$

Fig. 5.1



Curve A: $\sigma_e = C \cdot \frac{\pi^2 E}{12(1-\nu^2)} \left(\frac{t}{s}\right)^2$

where $C = 4\sqrt{1+(kZ_s)^2}$ and $k = \frac{0{\cdot}09}{\sqrt{1+\frac{r/t}{150}}}$

Curve B: $\sigma = \frac{\sigma_o}{\sqrt{1+\lambda^4}}$ where $\lambda = \sqrt{\sigma_o/\sigma_e}$

Fig. 5.2

COMPARISON OF ECCS RULES
WITH FINITE ELEMENT RESULTS
-AXIAL

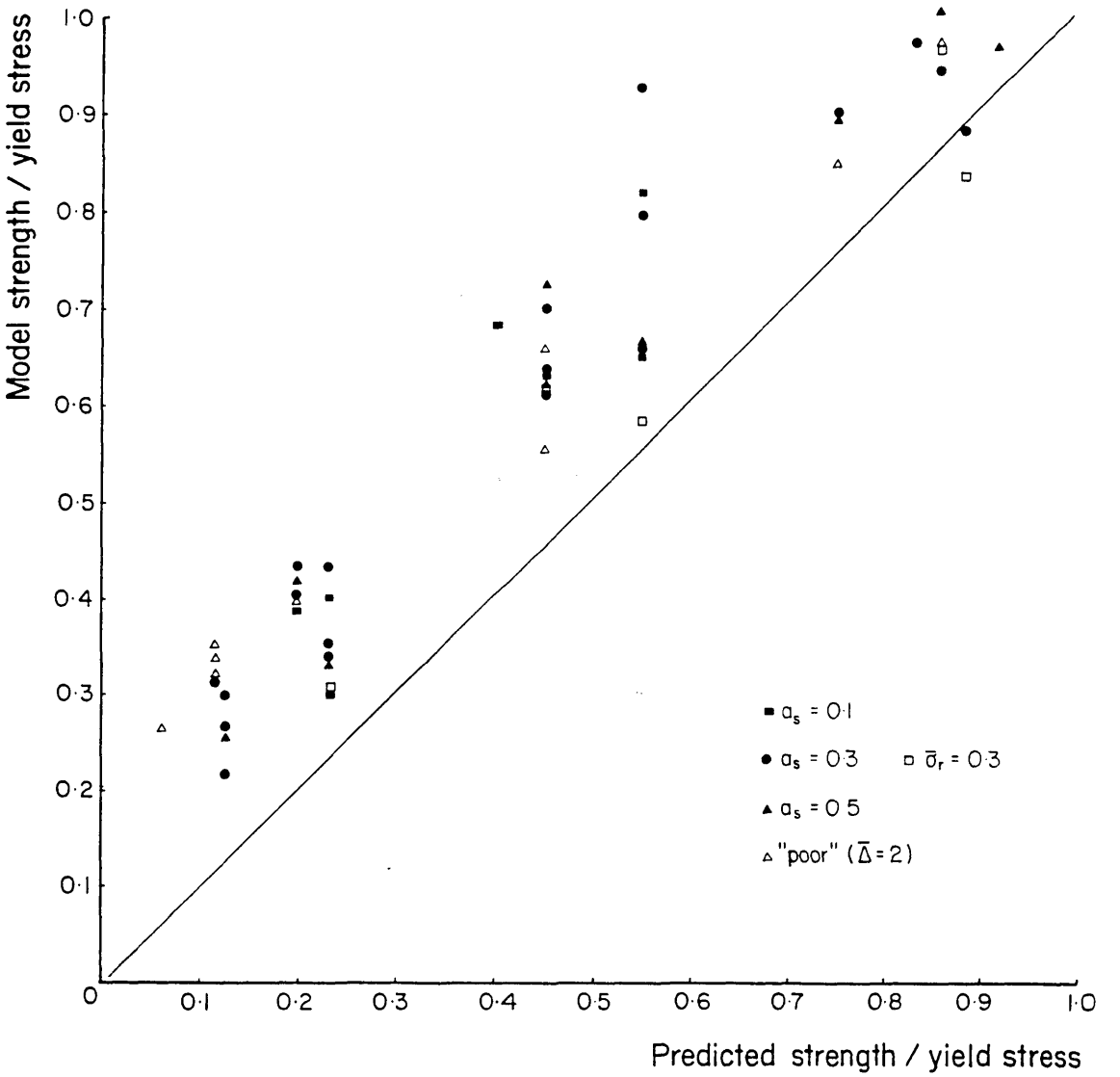


Fig. 5.3

COMPARISON OF DNV NOTES
WITH FINITE ELEMENT RESULTS
-AXIAL

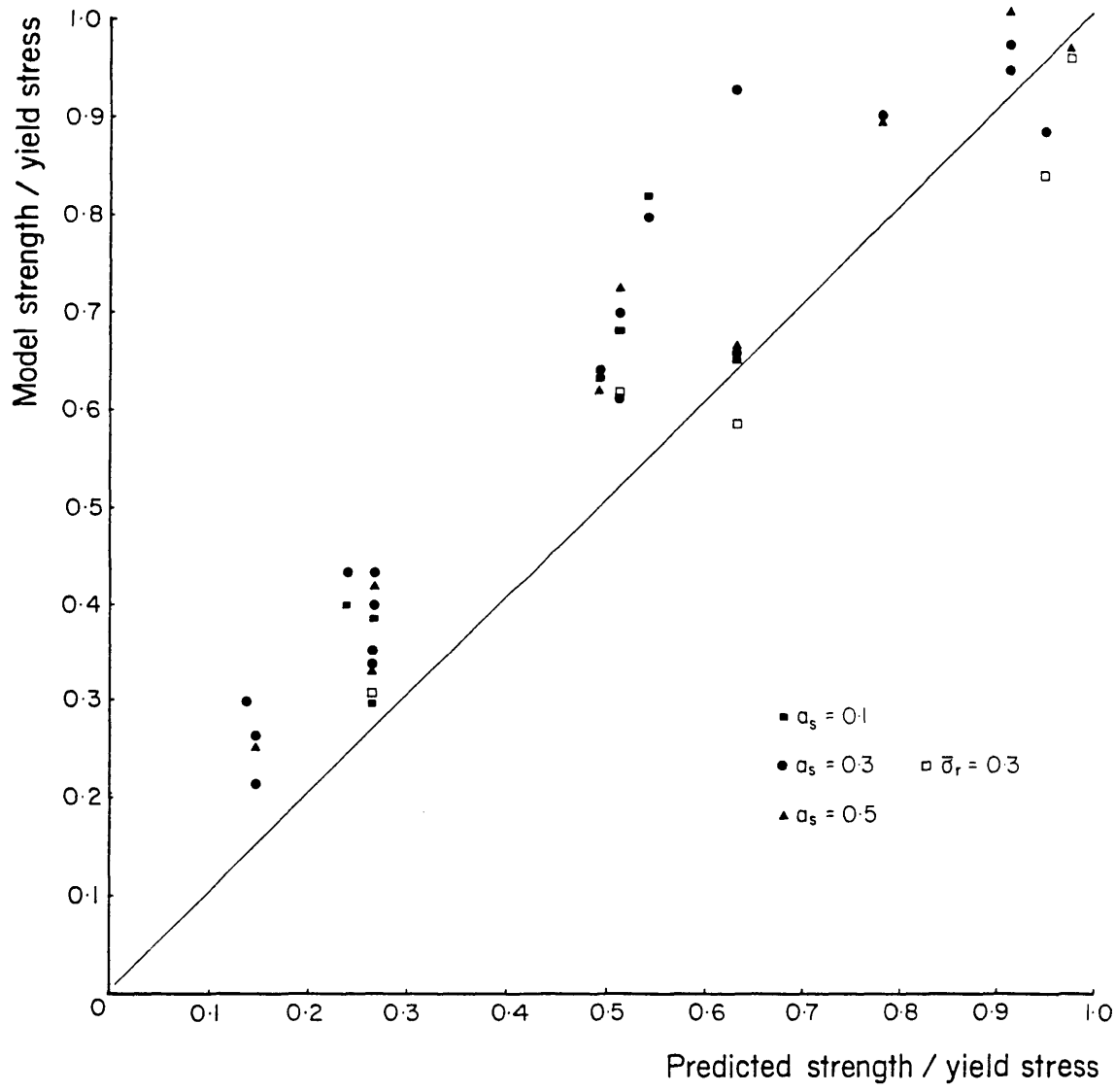


Fig. 5.4

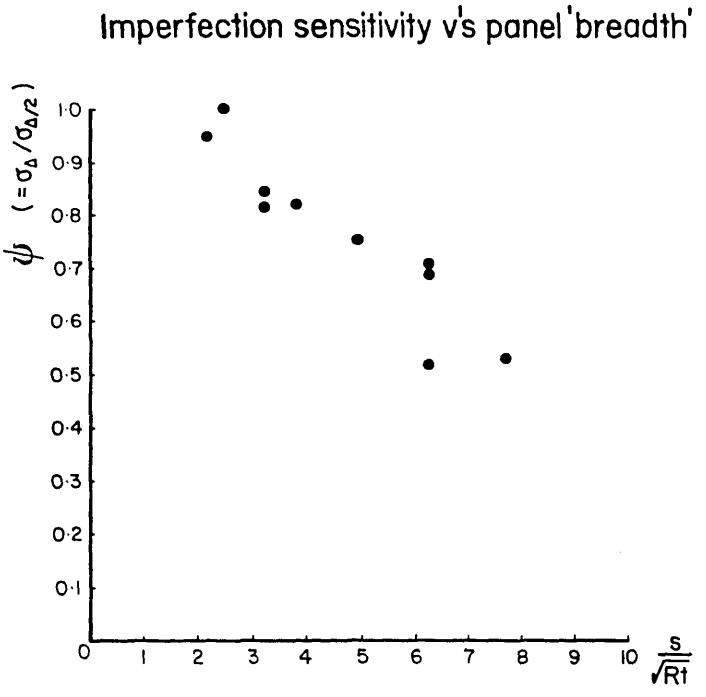

Imperfection sensitivity v's panel 'breadth'
ψ (= σΔ / σΔ/2)
1·0
0·9
0·8
0·7
0·6
0·5
0·4
0·3
0·2
0·1
0
1
2
3
4
5
6
7
8
9
10
s / √Rt

Fig. 5.5

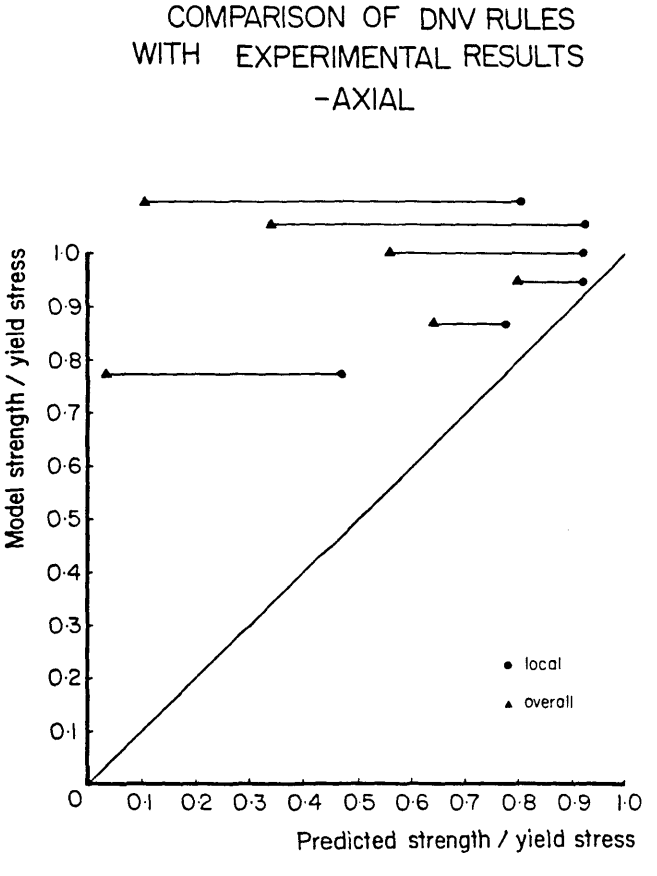

COMPARISON OF DNV RULES
WITH EXPERIMENTAL RESULTS
-AXIAL
Model strength / yield stress
1·0
0·9
0·8
0·7
0·6
0·5
0·4
0·3
0·2
0·1
0
0·1
0·2
0·3
0·4
0·5
0·6
0·7
0·8
0·9
1·0
Predicted strength / yield stress
• local
▲ overall

Fig. 5.6

COMPARISON OF DNV NOTES
WITH EXPERIMENTAL RESULTS
-AXIAL

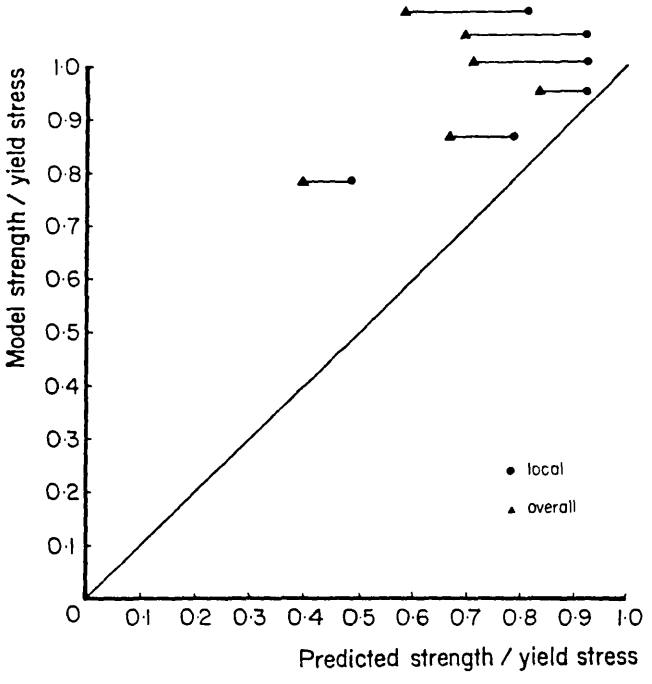


Fig. 5.7

COMPARISON OF ECCS RULES
WITH EXPERIMENTAL RESULTS
-AXIAL

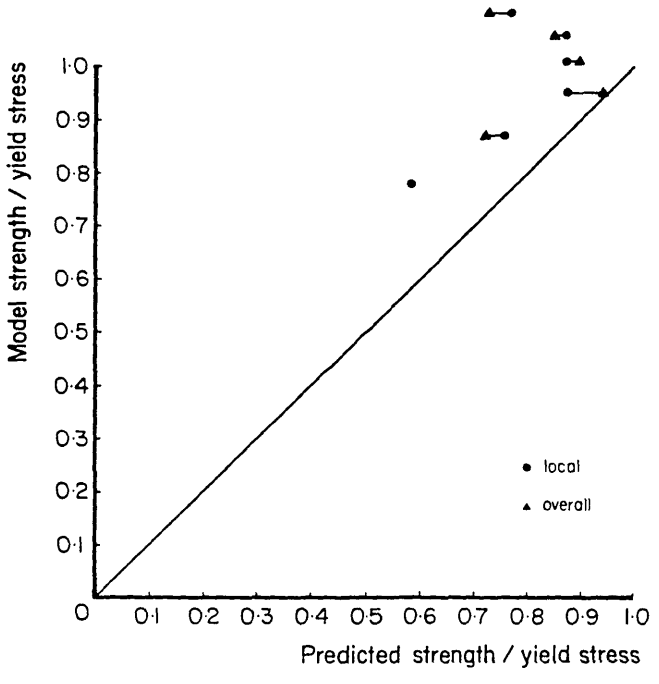


Fig. 5.8

COMPARISON OF DNV RULES
WITH FINITE ELEMENT RESULTS
-PRESSURE

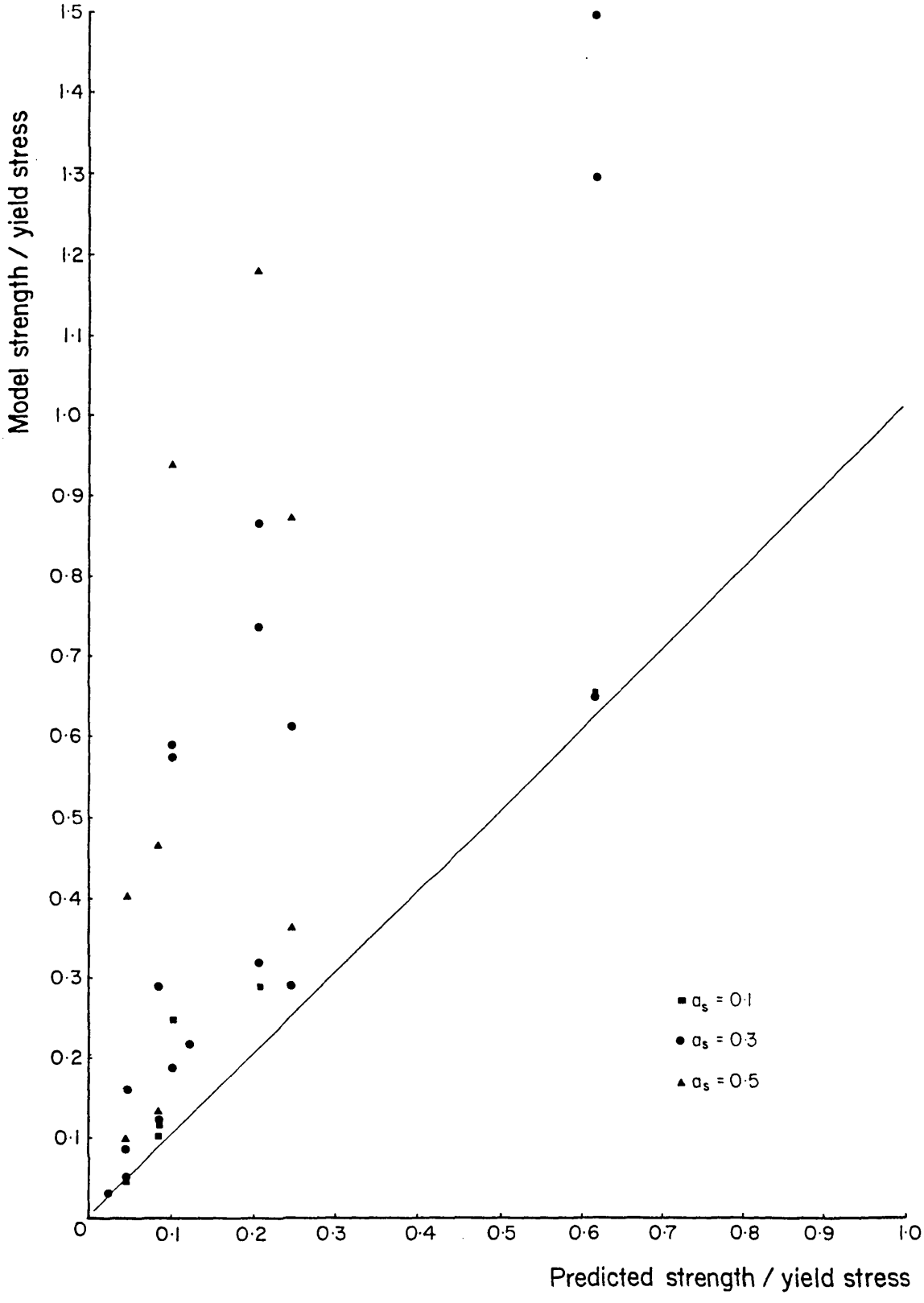


Fig. 5.9

COMPARISON OF DNV NOTES
WITH FINITE ELEMENT RESULTS
-PRESSURE

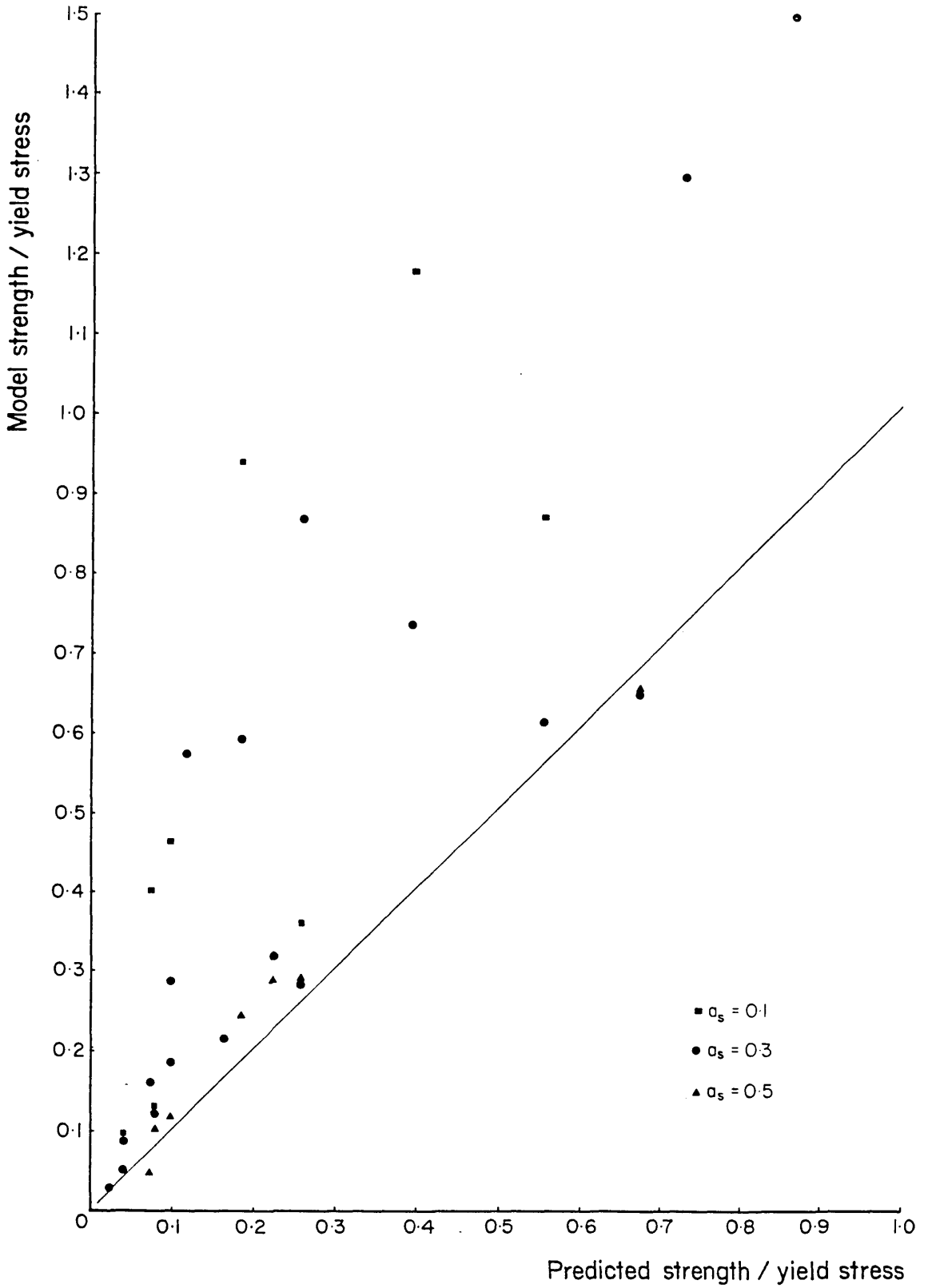


Fig. 5.10

COMPARISON OF ASME RULES
WITH FINITE ELEMENT RESULTS
- PRESSURE

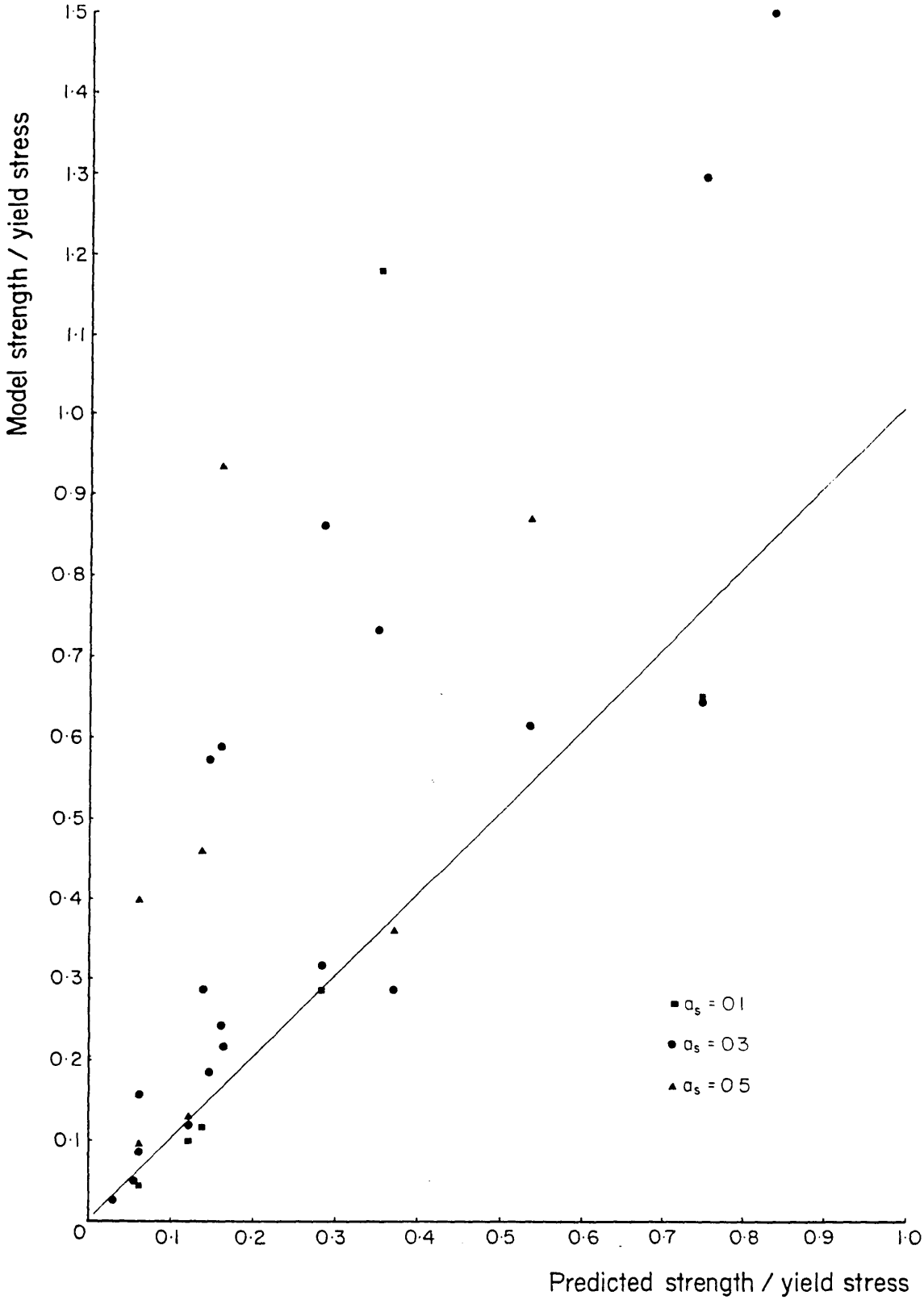


Fig. 5.11

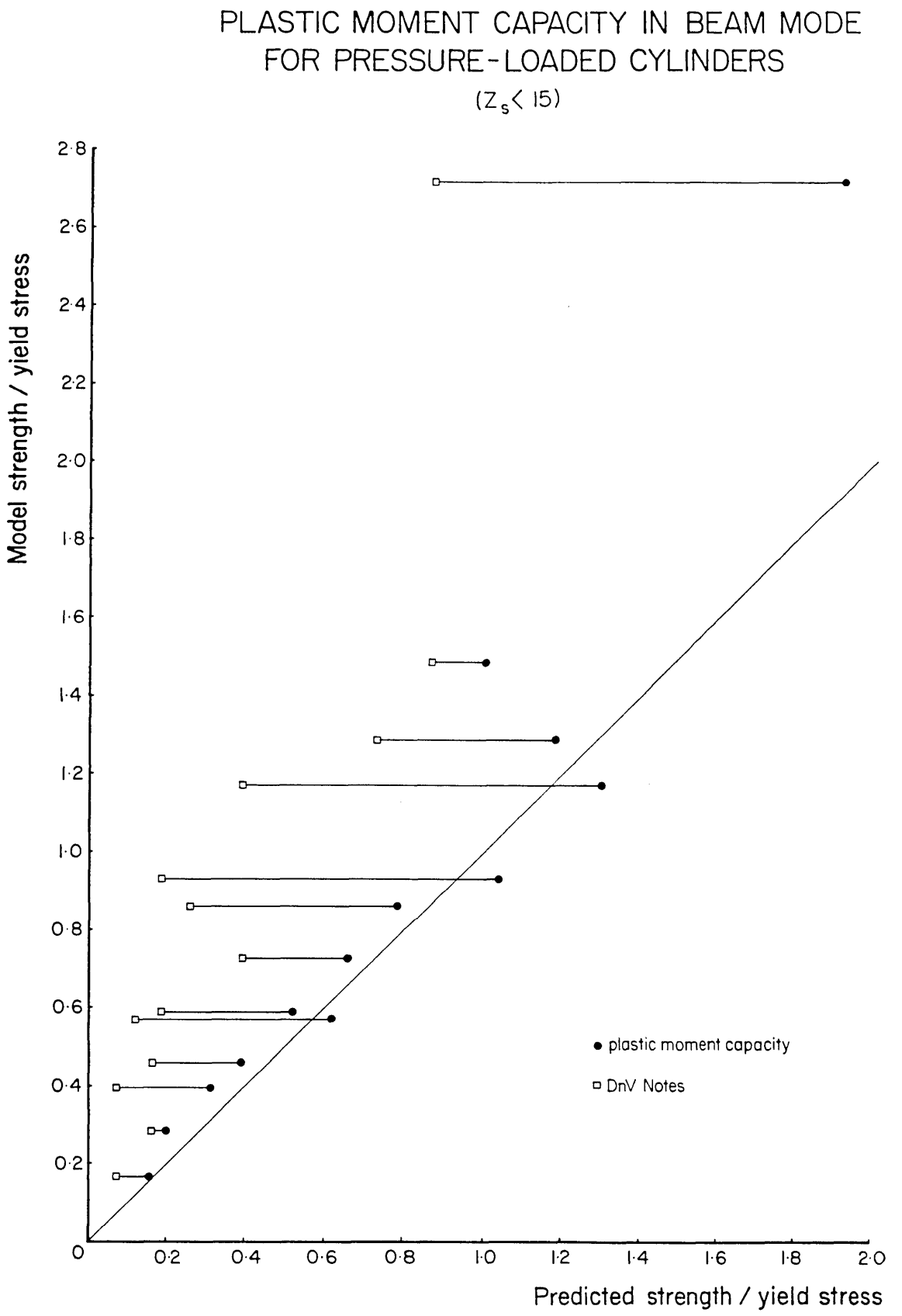

PLASTIC MOMENT CAPACITY IN BEAM MODE
FOR PRESSURE-LOADED CYLINDERS
(Z_s < 15)
Model strength / yield stress
Predicted strength / yield stress
2·8
2·6
2·4
2·2
2·0
1·8
1·6
1·4
1·2
1·0
0·8
0·6
0·4
0·2
0
0·2
0·4
0·6
0·8
1·0
1·2
1·4
1·6
1·8
2·0
• plastic moment capacity
□ DnV Notes

Fig. 5.12

COMPARISON OF DNV RULES
WITH EXPERIMENTAL RESULTS
-PRESSURE

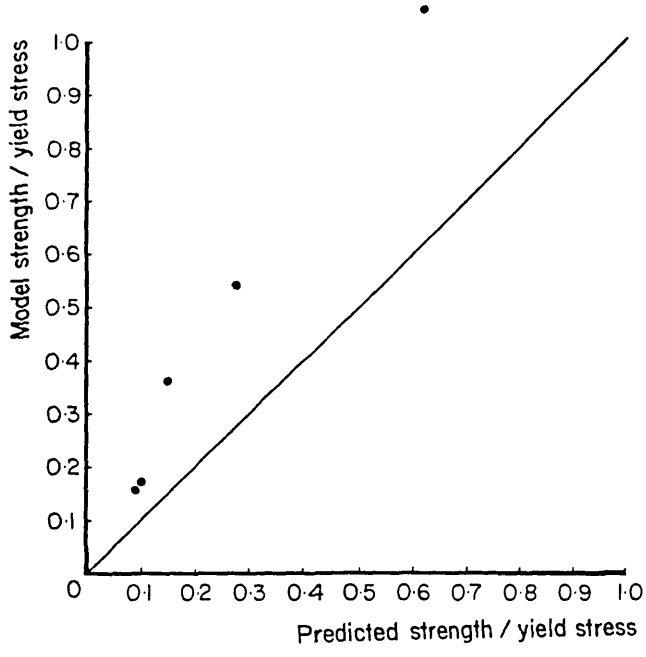


Fig. 5.13

COMPARISON OF ASME RULES
WITH EXPERIMENTAL RESULTS
-PRESSURE

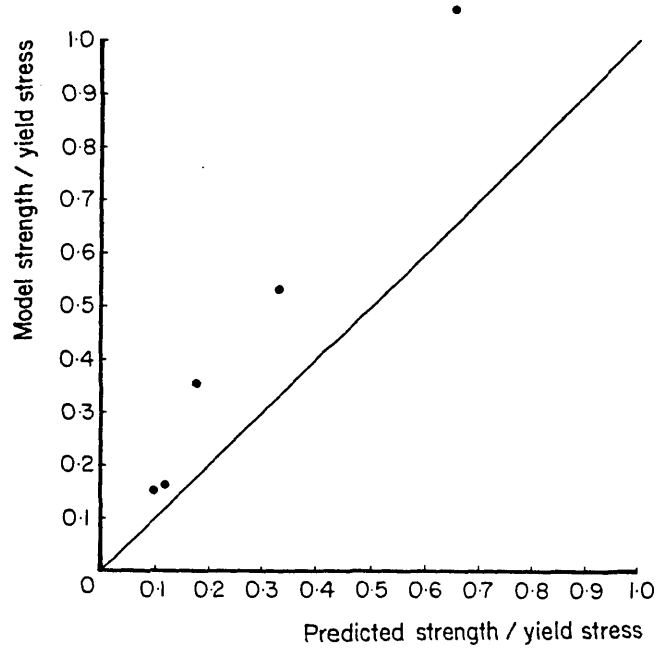


Fig. 5.14

COMPARISON OF DNV NOTES WITH FINITE ELEMENT RESULTS - INTERACTION CURVES

R = 200

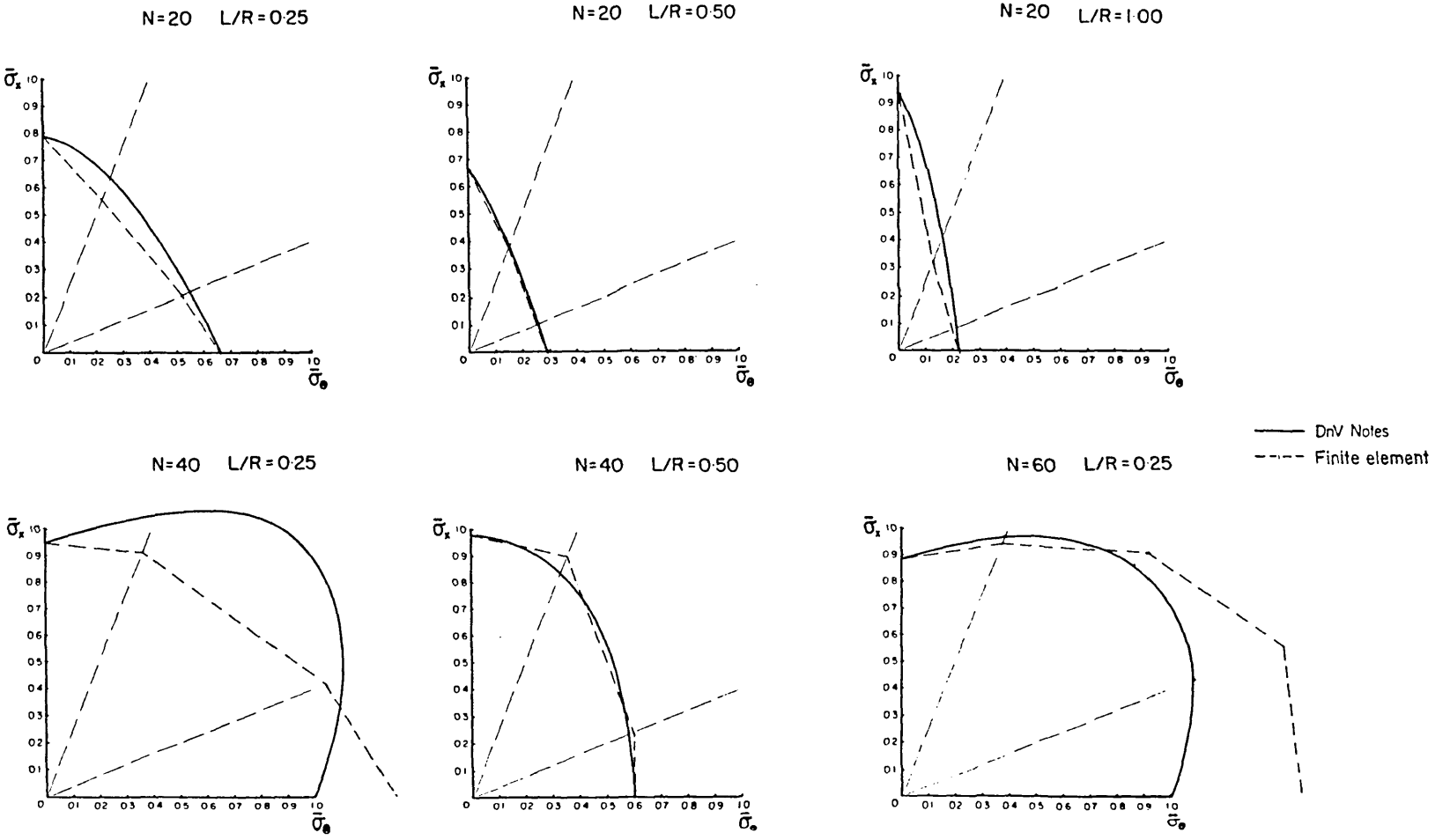
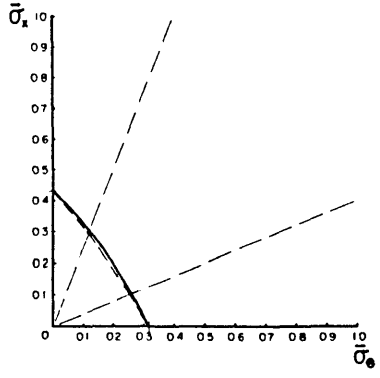


Fig. 5.15

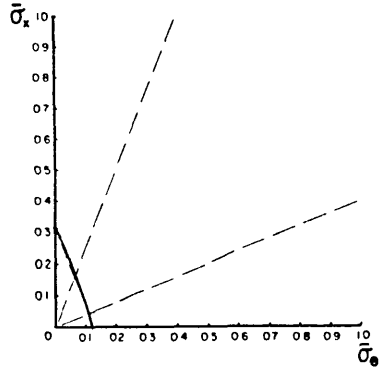
COMPARISON OF DNV NOTES WITH FINITE ELEMENT RESULTS - INTERACTION CURVES

R = 400

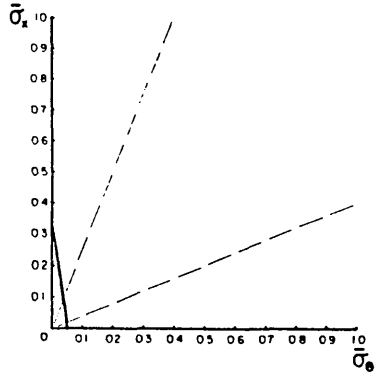
N=20 L/R=0·25



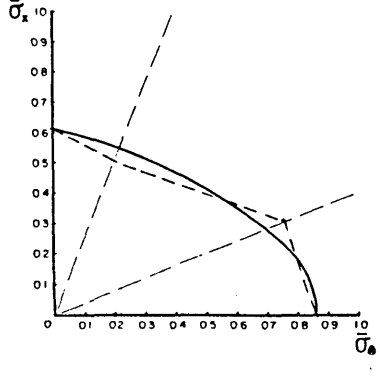
N=20 L/R=0·50



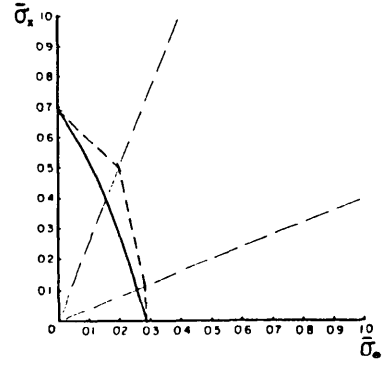
N=20 L/R=1·00



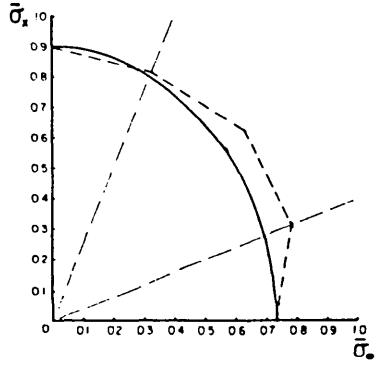
N=40 L/R=0·25



N=40 L/R=0·50



N=60 L/R=0·25



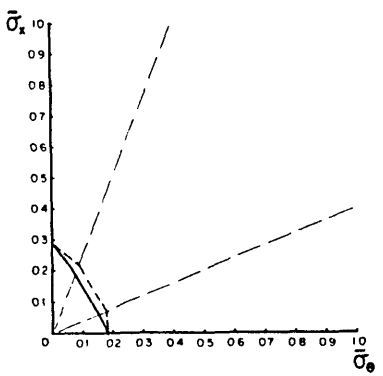
DnV Notes
Finite element

Fig. 5.16

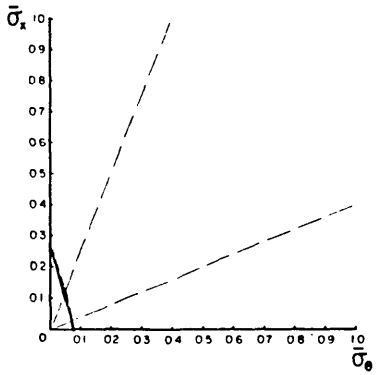
COMPARISON OF DNV NOTES WITH FINITE ELEMENT RESULTS - INTERACTION CURVES

R=600

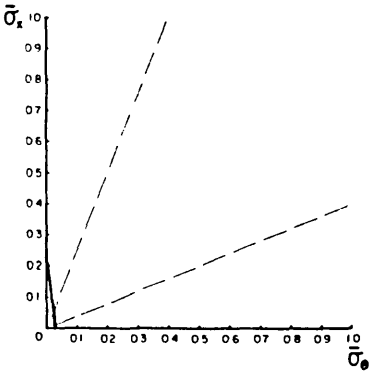
N=20 L/R=0·25



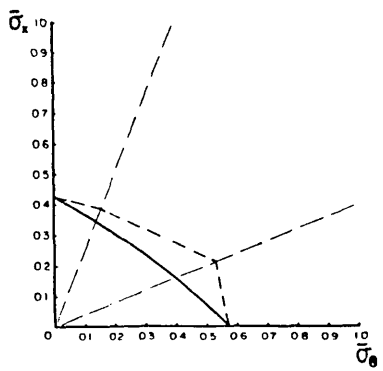
N=20 L/R=0·50



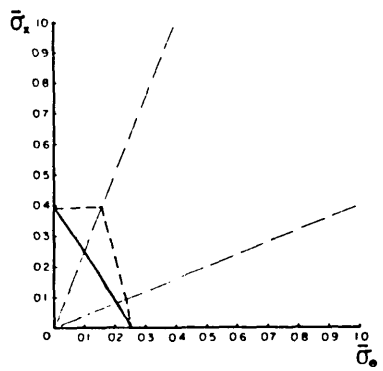
N=20 L/R=1·00



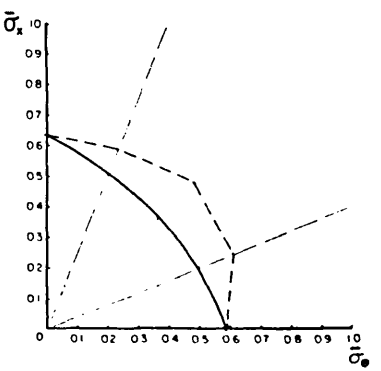
N=40 L/R=0·25



N=40 L/R=0·50



N=60 L/R=0·25

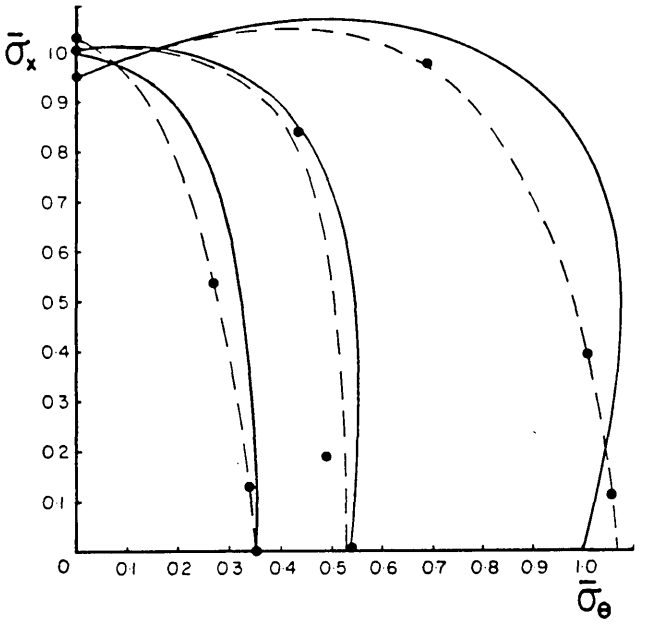


DnV Notes
Finite element

Fig. 5.17

COMPARISON OF DNV NOTES WITH EXPERIMENTAL RESULTS - INTERACTION CURVES

(a) DnV series



DnV Notes
Experimental

(b) Slender series

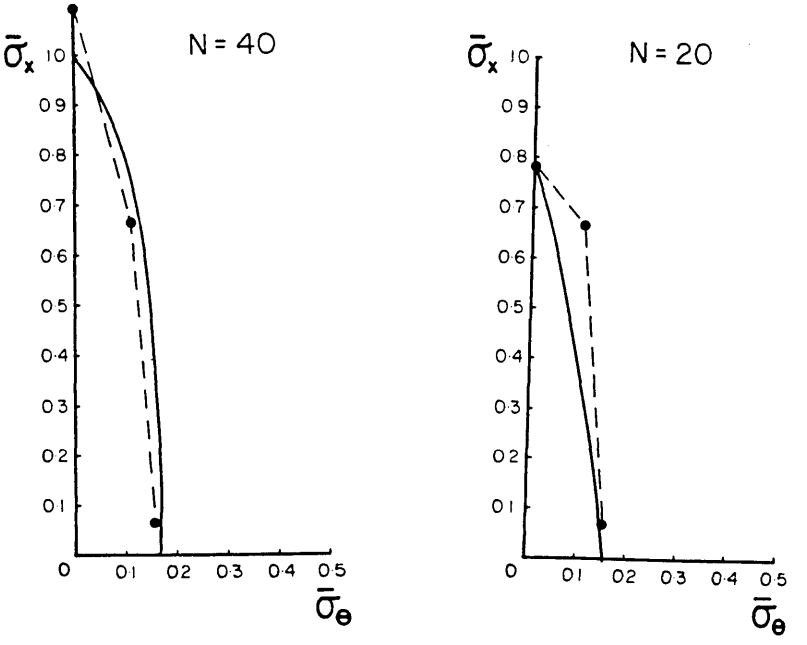


Fig. 5.18

CHAPTER SIX

CONCLUSIONS AND SUGGESTIONS FOR FUTURE WORK

6.1 CONCLUSIONS

The motive for this work sprang from the general scarcity of data on the buckling behaviour of stringer-stiffened cylinders of proportions likely to be encountered in offshore structures. This situation has been improved by the testing of ten experimental models and the execution of an extensive numerical parametric study.

6.1.1 EXPERIMENTAL RESULTS

Several points can be made regarding the manufacture and testing of the experimental models. The conventional welding and forming techniques used in the fabrication of the large-scale cylinder produced a representative model of prototype structures. Typical levels of initial imperfections and residual stresses were incorporated and measured in detail. The initial imperfections of both the shell and stiffeners were within the specified DnV tolerances. The Fourier analysis of the initial shape showed the presence of higher mode imperfections of significant magnitude in the axial direction, which were of similar form to the deflections produced under load. The dominant mode in the circumferential direction was correlated to the fabrication method used, but had little effect on the failure mode.

A comparison of the initial imperfections of all cylinders showed that for the major circumferential mode the magnitude of the Fourier components varied inversely with the axial wave number. This result

was used in the parametric study in the selection of imperfection magnitudes.

At such a relatively large scale of modelling, providing either fully-clamped or simply supported boundaries would be extremely difficult; for this reason continuous end conditions were adopted by using a three bay test specimen, whose central panel was designed to fail.

The small-scale models enabled the study at a more moderate cost of various geometric parameters and loading conditions. The method of manufacture produced high quality specimens, which easily satisfied the DnV tolerances. The difficulty of producing typical residual stresses and measuring them in detail at this scale of modelling was avoided by stress-relieving the cylinders after fabrication.

The most easily achieved and well defined end supports were fully-clamped boundaries, which were adopted for all models. Some doubt exists about the performance of the grooved end rings for predominantely axial loading tests. The alternative two-ring detail used in the axial loading tests of the slender series allowed the mating surfaces of the shell and loading platten to be lapped and provided a superior uniformity of load transfer. Under combined or pressure loading, however, the grooved end rings performed satisfactorily.

The models tested by the author spanned a range of behaviour types, and can best be summarized in terms of the various controlling parameters.

Number of stiffeners (i.e. panel width)

In the large-scale model the twenty stringers subdivided the

cylinder shell into relatively broad panels, which buckled locally at a load slightly below the ultimate load of the cylinder. The stockiness of the shell delayed this local mode until the elastoplastic range of behaviour. The 20 stiffener cylinder of the slender, small-scale series also buckled in a local shell mode prior to collapse, but in this more slender shell this mode was initiated elastically. Once again, a small reserve of strength was available before ultimate collapse.

None of the remaining models, all of which contained forty stiffeners, exhibited this sort of two-stage buckling behaviour: they all collapsed immediately after the onset of buckling, but for different reasons. In the slender model, E, and the longest stocky model, 10, collapse was triggered by the formation of an overall mode, after which no increase in load is possible. The shorter small-scale models, on the other hand, buckled into a local mode at a load so near squash that no reserve of strength was available.

The panel breadth also had an effect on the shape of the prebuckling deflections. For all models the shape of the radial deformations along the stiffener lines was a smooth single halfwave. The spacing of stiffeners determined whether the shell midpanel lines were constrained to follow the same shape or free to take up a higher mode similar to that which would form in an unstiffened cylinder. The effect was most apparent in the longitudinal distribution of hoop stresses.

Length

Length was a variable only in the first set of small-scale models. The failure modes varied from local shell buckling in the short models to an overall mode in the longest model. However, in

these stocky cylinders the variation in length did not produce a marked difference in the peak load or in the shape of the load deflection path. In more slender models, where the local and overall buckling loads may be more widely separated, length could have a more significant effect on the peak load.

The axial distributions of hoop stress were also modified by the change in length. The midheight hoop stress was compressive in the shortest model, but tensile in the longest, reflecting the reduced radial restraint that the more distant end rings could impose.

Shell slenderness

The most apparent effect of the shell slenderness was in the shape of the load deflection path and the suddenness of failure. The slender models buckled at relatively low loads into an elastically-initiated mode and shed a large proportion of their peak load suddenly and dramatically. The stockier models buckled more gradually, in the elasto-plastic regime, and shed load slowly to reach a postbuckling strength representing a higher proportion of their peak load.

6.1.2 NUMERICAL INVESTIGATION

As an extension to the column analogy used for flat stiffened plates, a finite element model was proposed, consisting of a single stiffener and the associated shell, to analyse cylinders failing in local or axisymmetric modes. The conditions of symmetry along the midpanel lines and at midheight and the inclusion of the shell curvature enabled the analysis to model the prebuckling deflections and hoop stresses directly. Convergence studies showed that accurate results could be obtained with a moderately coarse mesh.

The method was compared with the experimental results and gave

accurate predictions of the failure load and the stress and deflection distributions for those cases to which it was applicable. It performed less satisfactorily when used for the slender models that failed in overall modes.

The ability to model cylinder behaviour accurately and efficiently was exploited by conducting a substantial parametric study of cylinder behaviour. It is unlikely that the quantity of data generated in this study could have been accumulated experimentally.

The analysis was carried out for cylinders whose elastic critical stress in the local mode was lower than in the overall mode. This boundary to the extent of the analysis was found to be satisfactory when checked later by analysing larger portions of the cylinder, in which overall modes could develop.

The use of initial eigenvalue analyses to determine the number of halfwaves in the critical mode of each geometry and hence establish the worst initial imperfection shape for the full nonlinear analysis was only moderately successful. The neglect of prebuckling deformations resulted in poor estimates in several cases, which had to be re-analysed using higher mode imperfections.

If a relationship between the amplitudes of the various imperfection modes could be assumed (such as the inverse proportionality used here) a more appropriate way to proceed would be to apply the total required imperfection in the form of a summation of the first few modes.

The parametric study provided detailed information on a considerable number of variables, and the reader is referred to Sect 4.9 for a brief tabulated summary.

The parametric and experimental data was used as the basis of an assessment of a number of design codes. For axially-loaded cylinders it was found that the ECCS Rules were the only method that gave adequate and consistent predictions for both the local and overall modes.

Code predictions were generally much poorer for externally pressurized cylinders, especially for the stronger cases failing in a bending mode rather than hoop compression. The plastic moment capacity of a simple laterally-loaded beam model was found to give very good predictions in the former case, and a tentative proposal was made regarding the geometries in which the beam mode can be assumed to predominate.

The analytical and experimental results showed that the interaction curves obtained for the combined loading behaviour varied in shape. Design methods which assume a constant shape will either often be overconservative, e.g. ECCS Rules [155], or occasionally unconservative, e.g. DnV Rules [153]. The method used in the DnV Notes [154], which tries to include the change in shape through the addition of an effective stress term, has much to commend it: it is simple and mirrors the general trend in the results. However, this also does not always give accurate results. It is unlikely that significant improvements can be expected through the use of this type of simple interaction equation. More accurate predictions of the strength under combined loading will probably require a more comprehensive approach, such as that of Steen et al [164].

6.2 SUGGESTIONS FOR FUTURE WORK

More experimental tests are always valuable, and several extensions to the experimental work can be suggested. Tests of large-

scale fabricated cylinders under combined or pressure loading would provide useful confirmation of the small-scale results and information on the effect of residual stresses under these types of loads. It will be interesting to compare the results of recent tests described by Miller et al [173], when they are published in detail, with the predictions of the finite element analyses.

Also, information on the magnitudes and modes of initial imperfections produced in full-scale structures would be of great value. This would allow decisions regarding imperfection shapes, such as the inverse proportionality displayed by the experimental models, to be based on a broader range of experimental information.

Much useful information remains to be extracted from the testing of alternative geometries at the smaller scale, particularly if higher levels of instrumentation can be incorporated into the combined loading tests.

A difficult but useful task would be to investigate in greater detail the boundary conditions which exist along the circumferential edges of an internal panel and establish whether constant stress or constant strain loading is the more appropriate analytical representation. In a stiffened cylinder the area of interest is the panel that will ultimately initiate failure. As this is not known beforehand, equally refined measurements must be obtained for the entire circumference. In addition, significant differences may only develop shortly before failure, making this an extremely difficult investigation to perform experimentally. Perhaps a detailed finite element study, comprising several bays of the cylinder but possibly only one panel wide, may be a more appropriate method.

The parametric study can be easily extended to look in more

detail at variables only briefly studied here. In particular, the effect of varying the yield stress and the level of residual stresses seem to be two areas that require more detailed investigation. In addition, the extension to multi-bay analyses would be straightforward and useful. In many cases simple supports at the intermediate ring positions would be sufficient to establish the effect of continuity of the shell. In others it may be necessary to incorporate the properties of the rings themselves; for example, in order to determine the size of rings required to mobilize the full strength of the beam mode under pressure.

A more detailed investigation of the beam mode for pressure-loaded cylinders would enable its range of occurrence to be established with greater confidence.

The amount of data now available enables the undertaking of a quantitative reliability approach to the problem of shell buckling. Such a project has been initiated at Imperial College.

Finally, it would be valuable to apply the finite element analysis to the overall buckling behaviour of stringer-stiffened cylinders. The much larger model which must be studied makes it unlikely that this problem could be handled in an equally comprehensive way, but a more moderate study would still be extremely useful.

REFERENCES

1. Love, A.E.H. 'A Treatise on the Mathematical Theory of Elasticity,' Dover Publ., New York, 1944.

2. Budiansky, B. and Sanders, J.L. 'On the "best" first-order linear shell theory,' in Progress in Applied Mechanics (Prager Anniversary Volume), MacMillan, New York, 1963, pp. 129-140.

3. Koiter, W.T. 'A consistent first approximation in the general theory of thin elastic shells,' in Theory of Thin Elastic Shells, Proc. IUTAM Symp., W.T. Koiter (Ed.), Delft, North-Holland Publ. Co., 1960, pp. 12-33.

4. Donnell, L.H. 'Stability of thin walled tubes under torsion,' NACA Report 479, 1933.

5. Flugge, W. 'Die Stabilitat der Kreiszylinderschale,' Ingenieur-Archiv, vol. 3, 1932, pp. 463-506.

6. Koiter, W.T. 'Foundations and basic equations of shell theory - a survey of recent progress,' in Theory of Thin Shells, Proc. 2nd IUTAM Symp., F.I. Niordson (Ed.), Copenhagen, Springer-Verlag, 1967, pp. 93-105.

7. Reissner, E. 'Stress strain relations in the theory of thin elastic shells,' J. Math. Phys., vol. 31, 1952, pp. 109-119.

8. Mindlin, R.D. 'Influence of rotaty inertia and shear on flexural motions of isotropic, elastic plates,' J. Appl. Mech., vol. 18, no. 1, March 1951, pp. 31-38.

9. Naghdi, P.M. 'On the theory of thin elastic shells,' Q. Appl. Math., vol. 14, 1956, pp. 369-380.

10. Donnell, L.H. 'A new theory for the buckling of thin cylinders under axial compression and bending,' Trans. ASME, vol. 56, no. 11, Nov. 1934, pp. 795-806.

11. Vlasov, V.Z. 'General Shell Theory and Its Applications in Engineering,' Nat. Tech. Info. Service, N64-19883, 1964.

12. Reissner, E. 'On symmetrical deformations of thin shells of revolution,' Proc. Symp. Appl. Math., McGraw-Hill, New York, 1950, vol. 3, pp. 27-52.

13. Novozhilov, V.V. 'Foundations of the Nonlinear Theory of Elasticity,' Greylock Press, Rochester, N.Y., 1953.

14. Sanders, J.L. 'Nonlinear theories for thin shells,' Q. Appl. Math., vol. 21, 1963, pp. 21-36.

15. Budiansky, B. 'Notes on nonlinear shell theory,' J. Appl. Mech., vol. 35, no. 2, June 1968, pp. 392-401.

16. Koiter, W.T. 'On the nonlinear theory of thin elastic shells,'

Proc. Koninkijke Nederlandische Akademie van Wetenschappen, Series B, vol. 69, no. 1, 1966, pp. 1-54.

17. Lorenz, R. 'Die nichtachsensymmetrische Knickung duennwandiger Hohlzylinder,' Physikalische Zeitschrift, vol. 13, 1911, pp. 241-260.

18. Southwell, R.V. 'On the general theory of elastic stability,' Philosophical Trans. of the Royal Soc. of London, Series A, vol. 213, 1914, pp. 187.

19. Timoshenko, S. Bull. Electrotech. Inst., St. Petersburg, vol. 11, 1914.

20. von Mises, R. 'Der kritische Aussendruck zylindrischer Rohre,' Z. Ver. Deutsch. Ing., vol. 58, 1914, pp. 750-755.

21. Lundquist, E.E. 'Strength tests of thin-walled Duralumin cylinders in compression,' NACA Report 473, 1933.

22. von Karman, T. and Tsien, H.S. 'The buckling of thin cylindrical shells under axial compression,' J. Aeron. Sci., vol. 8, no. 8, June 1941, pp. 303-312.

23. Tsien, H.S. 'A theory for the buckling of thin shells,' J. Aeron. Sci., vol. 9, no. 10, Oct. 1942, pp. 373-384.

24. Leggett, D.M.A. and Jones, R.P.N. 'The behaviour of a cylindrical shell under axial compression when the buckling load has been exceeded,' Aero. Res. Council London, Rep. & Mem. no. 2190, Aug. 1942.

25. Michielsen, H.F. 'The behaviour of thin cylindrical shells after buckling in axial compression,' J. Aeron. Sci., vol. 15, no. 12, Dec. 1948, pp. 738-744.

26. Kempner, J. 'Postbuckling behaviour of axially compressed circular cylindrical shells,' J. Aeron. Sci., vol. 21, no. 5, May 1954, pp. 329-335.

27. Almroth, B.O. 'Postbuckling behaviour of axially compressed circular cylinders,' J. AIAA, vol. 1, no. 3, March 1963, pp. 630-633.

28. Hoff, N.J., Madsen, W.A. and Mayers, J. 'Postbuckling equilibrium of axially compressed circular cylindrical shells,' J. AIAA, vol. 4, no. 1, Jan. 1966, pp. 126-133.

29. Esslinger, M. and Geier, B. 'Calculated postbuckling loads as lower limits for the buckling loads of thin-walled circular cylinders,' in Buckling of Structures, Proc. of IUTAM Symp., B. Budiansky (Ed.), Harvard Univ., Springer-Verlag, 1976, pp. 274-290.

30. Batista, R.C. and Croll, J.G.A. 'A design approach for axially compressed unstiffened cylinders,' in Stability Problems in Engineering Structures and Components, T.H. Richards and P. Shanley (Eds.), App. Sci. Publ., London, 1979, pp 377-399.

31. Koiter, W.T. 'On the stability of elastic equilibrium,' Thesis, Delft Univ., H.J. Paris, Amsterdam, 1945, (in Dutch).

32. Koiter, W.T. 'Elastic stability and postbuckling behaviour,' in Nonlinear Problems, R.E. Langer (Ed.), Univ. Wisconsin Press, 1963, pp. 257-273.

33. Koiter, W.T. 'The effect of axisymmetric imperfections of the buckling of cylindrical shells under axial compression,' Proc. Koninkijke Nederlandische Akademie van Wetenschappen, Series B, vol. 66, no. 5, 1963, pp. 265-279.

34. Hutchinson, J.W. and Koiter, W.T. 'Postbuckling theory,' Appl. Mech. Reviews, vol. 23, no. 12, Dec. 1970, pp. 1353-1366.

35. Hutchinson, J.W. 'Axial buckling of pressurized imperfect cylindrical shell,' J. AIAA, vol. 3, no. 8, Aug. 1965, pp. 1461-1466.

36. Roorda, J. 'Stability of structures with small imperfections,' Proc. ASCE, Eng. Mech. Div., vol. 91, no. EM1, Feb. 1965, pp. 87-106.

37. Tennyson, R.C. and Muggeridge, D.B. 'Buckling of axisymmetric imperfect circular cylindrical shells under axial compression,' J. AIAA, vol. 7, no. 11, Nov. 1969, pp. 2127-2131.

38. Hutchinson, J.W., Tennyson, R.C. and Muggeridge, D.B, 'Effect of a local axisymmetric imperfection on the buckling behaviour of a circular cylindrical shell under axial compression,' J. AIAA, vol. 9, no. 1, Jan. 1971, pp. 48-52.

39. Donnell, L.H. and Wan, C.S. 'Effect of imperfections on buckling of thin cylinders and columns under axial compression,' J. Appl. Mech., vol. 17, no. 1, March 1950, pp. 73-83.

40. Almroth, B.O., Holmes, A.M.C. and Brush, D.O. 'An experimental study of cylinders under axial compression,' Experimental Mech., vol. 4, no. 9, Sept. 1964, pp. 263-270.

41. Yoshimura, Y. 'On the mechanism of buckling of a circular cylindrical shell under axial compression,' Reports of the Institute of Sci. and Tech. of the Univ. of Tokyo, vol. 5, 1951, (in Japanese), English translation available as NACA TM 1390, 1955.

42. Hoff, N.J. and Soong, T.C. 'Buckling of circular cylindrical shells in axial compression,' Int. J. Mech. Sci., vol. 7, no. 7, July 1965, pp. 489-520.

43. Stein, M. 'The effect on the buckling of perfect cylinders of prebuckling deformations and stresses induced by edge supports,' in Collected Papers on Instability of Shell Structures, NASA TN D-1510, Dec. 1962, pp. 217-227.

44. Almroth, B.O. 'Influence of edge conditions on the stability of axially compressed cylindrical shells,' J. AIAA, vol. 4, no. 1, Jan. 1966, pp. 132-140.

45. Cohen, G.A. 'Effect of a nonlinear prebuckling state on the postbuckling behaviour and imperfection sensitivity of elastic structures,' J. AIAA, vol. 6, no. 8, Aug. 1968, pp. 1616-1619.

46. Bijlaard, P.P. 'Theory and tests on the plastic stability of plates and shells,' J. Aeron. Sci., vol. 16, no. 9, Sept. 1949, pp. 529-541.

47. Gerard, G. 'Plastic stability theory of thin shells,' J. Aero. Sci., vol. 24, no. 4, April 1957, pp. 269-274.

48. Lee, L.N.H. 'Inelastic buckling of initially imperfect cylindrical shells subject to axial compression,' J. Aero. Sci., vol. 29, no. 1, Jan. 1962, pp. 87-95.

49. Hutchinson, J.W. 'Plastic Buckling,' Advances in Appl. Mech., vol. 14, 1974, pp. 67-144.

50. Batterman, S.C. 'Plastic buckling of axially compressed cylindrical shells,' J. AIAA, vol. 3, no. 2, Feb. 1965, pp. 316-325.

51. Murphy, L.M. and Lee, L.N.H. 'Inelastic buckling process of axially compressed cylindrical shells subjected to edge constraints,' Int. J. Solids and Struct., vol. 7, no. 9, Sept. 1971, pp. 1153-1170.

52. Sobel, L.H. and Newman, S.Z. 'Plastic buckling of cylindrical shells under axial compression,' J. Press. Vessel Tech., vol. 102, no. 1, Feb. 1980, pp. 40-44.

53. Gellin, S. 'Effect of an axisymmetric imperfection on the plastic buckling of an axially compressed cylindrical shell,' J. Appl. Mech., vol. 46, no. 1, March 1979, pp. 125-131.

54. Tvergaard, V. 'Buckling behaviour of plate and shell structures,' in Theoretical and Applied Mechanics, Proc. 14th Int. Cong. of Theor. and Appl. Mech., W.T. Koiter (Ed.), North-Holland Publ. Co., New York, 1976, pp. 233-247.

55. Nimmer, R.P. and Mayers, J. 'Limit point buckling loads of axially compressed, circular cylindrical shells - the effect of nonlinear material behaviour,' J. Appl. Mech., vol. 46, no. 2, June 1979, pp. 386-392.

56. Gerard, G. and Becker, H. 'Handbook of structural stability, Part III - Buckling of curved plates and shells,' NACA TN 3783, 1957.

57. Harding, J.E. 'The elasto-plastic analysis of imperfect cylinders,' Proc. Instn. Civil Engrs., Part 2, vol. 65, Dec. 1978, pp. 875-892.

58. Singer, J. 'Buckling of integrally stiffened cylindrical shells - a review of experiment and theory,' in Contributions to the Theory of Aircraft Structures, Delft Univ. Press, 1972, pp. 325-357.

59. Becker, H. and Gerard, G. 'Elastic stability of orthotropic shells,' J. Aero. Sci., vol. 29, no. 5, May 1962, pp. 505-515.

60. Gerard, G. 'Compressive stability of orthotropic cylinders,' J. Aero. Sci., vol. 29, no. 10, Oct. 1962, pp. 1171-1179.

61. Milligan, R., Gerard, G. and Lakshmikantham, C. 'General instability of orthotropically stiffened cylinders under axial

compression,' J. AIAA, vol. 4, no. 11, Nov. 1966, pp. 1906-1913.

62. van der Neut, A. 'The general instability of stiffened cylindrical shells under axial compression,' National Luchtvaatlaboratorium, Reports and Trans., vol. 13, 1947, pp. S57-S84.

63. Baruch, M. and Singer, J. 'Effect of eccentricity of stiffeners on the general instability of stiffened cylindrical shells under hydrostatic pressure,' J. Mech. Eng. Sci., vol. 5, no. 1, March 1963, pp. 23-27.

64. Singer, J., Baruch, H. and Harari, O. 'On the stability of eccentrically stiffened cylindrical shells under axial compression,' Int. J. Solids and Structures, vol. 3, no. 4, April 1967, pp. 445-470.

65. Block, D.L., Card, M.F. and Mikulas, M.M. 'Buckling of eccentrically stiffened orthotropic cylinders,' NASA TN D-2960, Aug. 1965.

66. Hedgepeth, J.M. and Hall, D.B. 'Stability of stiffened cylinders,' J. AIAA, vol. 3, no. 12, Dec. 1965, pp. 2275-2286.

67. Card, M.F. and Jones, R.M. 'Experimental and theoretical results for buckling of eccentrically stiffened cylinders,' NASA TN D-3639, Oct. 1966.

68. Burns, A.B. 'Structural optimization of axially compressed cylinders, considering ring-stringer eccentricity effects,' J. Spacecraft and Rockets, vol. 3, no. 8, Aug. 1966, pp. 1263-1268.

69. Soong, T.C. 'Influence of boundary constraints on the buckling of eccentrically stiffened orthotropic cylinders,' in 7th Int. Symp. on Space Tech. and Sci., Tokyo, May 1967.

70. Singer, J., Arbocz, J. and Babcock, C.D. 'Buckling of imperfect cylindrical shells under axial compression,' J. AIAA, vol. 9, no. 1, Jan. 1971, pp. 68-75.

71. Singer, J. and Rosen, A. 'The influence of boundary conditions on the buckling of stiffened cylindrical panels,' in Buckling of Structures, Proc. IUTAM Symp., B. Budiansky (Ed.), Harvard Univ., Springer-Verlag, 1976, pp. 227-250.

72. Stuhlman, C., DeLuzio, A. and Almroth, B.O. 'Influence of stringer eccentricity and end moment on stability of cylinders in compression,' J. AIAA, vol. 4, no. 5, May 1966, pp. 872-877.

73. Block, D.L. 'Influence of discrete ring stiffeners and prebuckling deformations on the buckling of eccentrically stiffened orthotropic cylinders,' NASA TN D-4283, Jan. 1968.

74. Weller, T., Singer, J. and Batterman, S.C. 'Influence of eccentricity of loading on buckling of stringer stiffened cylindrical shells,' in Thin Shell Structures, Y.C. Fung and E.E. Sechler (Eds.), Prentice-Hall, 1974, pp. 305-324.

75. van der Neut, A. 'General instability of orthogonally stiffened cylindrical shells,' in Collected Papers on Instability of Shell Structures, NASA TN D-1510, Dec. 1962, pp. 309-321.

76. Singer, J. 'The influence of stiffener geometry and spacing on the buckling of axially compressed cylindrical and conical shells,' in Theory of Thin Shells, Proc. 2nd IUTAM Symp., F.I. Niordson (Ed.), Copenhagen, Springer-Verlag, 1967, pp. 234-262.

77. Arbocz, J. and Babcock, C.D. 'The effect of general imperfections on the buckling of cylindrical shells,' J. Appl. Mech., vol. 36, no. 1, March 1969, pp. 28-38.

78. Arbocz, J. and Sechler, E.E. 'On the buckling of stiffened imperfect cylindrical shells,' J. AIAA, vol. 14, no. 11, Nov. 1976, pp. 1611-1617.

79. Stein, M. 'Some recent advances in the investigation of shell buckling,' J. AIAA, vol. 6, no. 12, Dec. 1968, pp. 2339-2345.

80. Hutchinson, J.W. and Frauenthal, J.C. 'Elastic postbuckling behaviour of stiffened and barreled cylindrical shells,' J. Appl. Mech., vol. 36, no. 4, Dec. 1969, pp. 784-790.

81. Huthcinson, J.W. and Amazigo, J.C. 'Imperfection sensitivity of eccentrically stiffened cylindrical shells,' J. AIAA, vol. 5, no. 3, March 1967, pp. 392-401.

82. Sheinman, I. and Simitses, G.J. 'Buckling analysis of geometrically imperfect stiffened cylinders under axial load,' J. AIAA, vol. 15, no. 3, March 1977, pp. 374-382.

83. Tennyson, R.C. and Booton, M. and Hui, D. 'Changes in cylindrical shell buckling behaviour resulting from system parameter variations,' in Proc. 15th Int. Cong. of Theor. and Appl. Mech., F.P.J. Rimrott and B. Tabarrok (Eds.), North-Holland Publ. Co., 1980, pp. 417-430.

84. Arbocz, J. and Babcock, C.D. 'Prediction of buckling loads based on experimentally measured initial imperfections,' in Buckling of Structures, Proc. IUTAM Symp., B. Budiansky (Ed.), Harvard Univ., Springer-Verlag, 1976, pp. 291-311.

85. Arbocz, J. and Babcock, C.D. 'Stability analysis of shells using the STAGS computer code,' in Buckling of Shells in Offshore Structures, J.E. Harding, P.J. Dowling and N. Agelidis (Eds.), Granada, London, 1982, pp. 549-575.

86. Thielemann, W.F. and Esslinger, M.E. 'On the postbuckling equilibrium and stability of thin walled circular cylinders under axial compression,' in Theory of Thin Shells, Proc. 2nd IUTAM Symp., F.I. Niordson (Ed.), Copenhagen, Springer-Verlag, 1967, pp. 264-292.

87. Ellinas, C.P., Batista, R.C. and Croll, J.G.A. 'Overall buckling of stringer stiffened shells,' Proc. Instn. Civil Engrs., Part 2, vol. 71, no. 2, June 1981, pp. 479-512.

88. Ellinas, C.P. and Croll, J.G.A. 'Experimental and theoretical correlations for elastic buckling of axially compressed stringer stiffened cylinders,' J. Strain Anal., vol. 18, no. 1, 1983, pp. 41-67.

89. Gerard, G. 'Plastic stability theory of geometrically orthotropic plates and cylindrical shells,' J. Aero. Sci., vol. 29, no. 8, Aug. 1962, pp. 956-962.

90. Jones, R.M. 'Plastic buckling of eccentrically stiffened circular cylindrical shells,' J. AIAA, vol. 5, no. 6, June 1967, pp. 1147-1152.

91. Singer, J. and Haftka, R. 'Buckling of discretely ring stiffened cylindrical shells,' Israel J. of Tech., vol. 6, no. 1-2, Jan-March 1968, pp. 125-137.

92. Singer, J. and Haftka, R. 'Buckling of discretely stringer stiffened cylindrical shells and elastically restrained panels,' J. AIAA, vol. 13, no. 7, July 1975, pp. 849-850.

93. Wang, J.T.S. and Lin, Y.J. 'Stability of disretely stringer stiffened cylindrical shells,' J. AIAA, vol. 11, no. 6, June 1973, pp. 810-814.

94. Esslinger, M. and Geier, B. 'Buckling and postbuckling behaviour of discretely stiffened thin walled circular cylinders,' Z. Flugwiss., vol. 18, no. 7, July 1970, pp. 246-253.

95. Syngellakis, S. and Walker, A.C. 'Elastic buckling of stiffened cylindrical shells,' Proc. of Int. Symp. on Integrity of Offshore Structures, Instn. of Engrs. and Shipbuilders in Scotland, Glasgow, 1978, pp. 12/1-12/21.

96. Syngellakis, S. and Walker, A.C. 'Elastic buckling of cylinders with widely spaced stiffeners,' in Theory of Shells, Proc, 3rd IUTAM Symp., W.T. Koiter and G.K. Mikhailov (Eds.), Tbilisi, USSR, 1978, pp. 553-574.

97. Reddy, B.D. 'Buckling of elastic-plastic discretely stiffened cylinders in axial compression,' Int. J. Solids and Structures, vol. 16, no. 4, May 1980, pp. 313-328.

98. Koiter, W.T. 'Buckling and postbuckling behaviour of a cylindrical panel under axial compression,' National Luchtvaartlaboratorium, Amsterdam, Reports and Trans., vol. 20, 1955, pp. 71-84.

99. Stephens, W.B. 'Imperfection sensitivity of axially compressed stringer reinforced cylindrical panels under internal pressure,' J. AIAA, vol. 9, no. 9, Sept. 1971, pp. 1713-1719.

100. Tvergaard, V. 'Buckling of elastic-plastic cylindrical panel under axial compression,' Int. J. Solids and Structures, vol. 13, no. 10, Oct. 1977, pp. 957-970.

101. Dowling, P.J. and Ho, T.K. 'Effect of initial deformations on the strength of axially compressed cylindrical panels,' Proc. Conf. on Significance of Deviations from Design Shapes, Appl. Mech. Group, Instn. Mech. Engrs., London, 1979.

102. Byskov, E. and Hutchinson, J.W. 'Mode interaction in axially stiffened cylindrical shells,' J. AIAA, vol. 15, no. 7, July 1977, pp. 941-948.

103. Byskov, E. and Hansen, J.C. 'Postbuckling and imperfection

sensitivity analysis of axially stiffened cylindrical panels with mode interaction,' J. Struct. Mech., vol. 8, no. 2, 1980, pp. 205-224.

104. Koiter, W.T. 'General theory of mode interaction in stiffened plate and shell structures,' Delft Univ. of Tech., Report WTHD 91, Sept. 1976.

105. Tsang, S.K. and Harding, J.E. 'Literature review on the behaviour of circular cylindrical shells under external pressure,' Imperial Coll. Civil Eng. Struct. Lab. Report RS2, August 1983.

106. Levy, M. 'Memoire sur une nouveau cas integrable du probleme de l'elastique et l'une de ses applications,' J. Math. Pures et Appl., Ser. 3, vol. 10, p. 5, 1884.

107. von Mises, R. 'Der Kritische Aussendruck fur allseits belastete zylindrische Rohre,' Fest. zum Geburstag von Prof. Dr. A. Stodola, Zurich, 1929, p. 418.

108. Windenburg, D.F. and Trilling, C. 'Collapse by instability of thin cylindrical shells under pressure,' Trans. ASME, vol. 56, no. 11, 1934, pp. 819-825.

109. Nash, W.A. 'Buckling of multibay ring reinforced cylindrical shells subject to hydrostatic pressure,' J. Appl. Mech., vol. 20, no. 4, Dec. 1953, pp. 469-474.

110. Wenk, E., Slankard, R.C. and Nash, W.A. 'Experimental analysis of the buckling of cylindrical shells subjected to external hydrostatic pressure,' Exp. Stress Anal., vol. 12, no. 1, 1954, pp. 163-180.

111. Bijlaard, P.P. 'Buckling under external pressure of cylindrical shells evenly stiffened by rings only", J. Aero. Sci., vol. 24, no. 6, June 1957, pp. 437-447.

112. Batdorf, S.B. 'A simplified method of elastic stability analysis for thin cylindrical shells,' NACA Report 874, 1947.

113. Loo, T.T. 'An extension of Donnell's equations for a circular cylindrical shell,' J. Aero. Sci., vol. 24, no. 5, May 1957, pp. 390-391.

114. Armenakas, A.E. and Hermann, G 'Buckling of thin shells under external pressure,' Proc. ASCE, vol. 89, no. EM3, June 1963, pp. 131-146.

115. Soong, T.C. 'Buckling of cylindrical shell under pressure by using Sander's theory,' J. AIAA, vol. 5, no. 5, May 1967, pp. 1049-1052.

116. Yamaki, N. 'Buckling of circular cylindrical shells under external pressure,' Report Inst. High Speed Mech., Tohoku Univ., Japan, vol. 20, no. 196, 1968/9, pp. 35-55.

117. Sobel, L.H. 'Effects of boundary conditions on the stability of cylinders subject to lateral and axial pressures,' J. AIAA, vol. 2, no. 8, Aug. 1964, pp. 1437-1440.

118. Yamaki, N. 'Influence of prebuckling deformations on the buckling

of circular cylindrical shells under external pressure,' Report Inst. High Speed Mech., Tohoku Univ., Japan, vol. 21, no. 211, 1969/70, pp. 81-104.

119. Tokugawa, T. 'Model experiment on the elastic stability of closed cross-stiffened circular cylinders under uniform external pressure,' Proc. World Eng. Cong., Tokyo, 1929, vol. 29, pp. 249-279.

120. Bryant, A.R. 'Hydrostatic pressure loading of a ring stiffened tube,' Naval Constr. Res. Estab. Report R-306, 1954.

121. Salerno, V.L. and Levine, B. 'General instability of reinforced shells under hydrostatic pressure,' PIBAL Report no. 189, Polytechnic Inst. of Brooklyn, Sept. 1951.

122. Kendrick, S. 'The buckling under external pressure of circular cylindrical shells with evely spaced, equal strength, circular ring frames - Part I, III,' Naval Constr. Res. Estab. Report nos. R-211, Feb. 1953, and R-244, Sept. 1953.

123. Kendrick, S. 'The buckling under external pressure of ring stiffened circular cylinders,' Trans. Royal Inst. Naval Arch., vol. 107, no. 1, Jan. 1965, pp. 139-152.

124. Reynolds, T.E. and Blumenburg, W.F. 'General instability of ring-stiffened cylindrical shells subject to external hydrostatic pressure,' David Taylor Model Basin, Report 1324, June 1959.

125. Bodner, S.R. 'General instability of a ring-stiffened circular cylindrical shell under hydrostatic pressure,' J. Appl. Mech., vol. 24, no. 2, June 1957, pp. 269-277.

126. Sturm, R.G. 'A study of the collapsing pressure of thin-walled cylinders,' Univ. of Illinois, Eng. Exp. Station Bull. 329, 1941.

127. Bodner, S.R. and Berks, W. 'The effect of imperfections on the stresses in a circular shell under hydrostatic pressure,' PIBAL Report no. 210, Polytechnic Ins. of Brooklyn, Dec. 1952.

128. Galletly, G.D. and Bart, R. 'Effects of boundary conditions and initial out-of-roundness on the strength of thin-walled cylinders subject to external hydrostatic pressure,' J. Appl. Mech., vol. 23, no. 3, Sept. 1956, pp. 351-358.

129. Holt, M. 'A procedure for determining the allowable out-of-roundness for vessels under external pressure,' Trans. ASME, vol. 74, Oct. 1952, pp. 1225-1230.

130. Donnell, L.H. 'Effect of imperfections on buckling of thin cylinders under external pressure,' J. Appl. Mech., vol. 23, Dec. 1956, pp. 569-575.

131. Nash, W.A. 'Effect of large deflections and initial imperfections on the buckling of cylindrical shells subject to hydrostatic pressure,' J. Aero. Sci., vol. 22, no. 4, April 1955, pp. 264-269.

132. Kempner, J., Pandalai, K.A.V., Patel, S.A. and Crouzet-Pascal, J. 'Postbuckling behaviour of circular cylindrical shells under hydrostatic pressure,' J. Aero. Sci., vol. 24, no. 4, April 1957,

pp. 253-264.

133. Budiansky, B. and Amazigo, J.C. 'Initial postbuckling behaviour of cylindrical shells under external pressure,' J. Math. and Phys., vol. 47, 1968, pp. 223-235.

134. Amazigo, J.C. and Frazer, W.B. 'Buckling under external pressure of cylindrical shells with dimple shaped initial imperfections,' Int. J. Solids and Structures, vol. 7, no. 8, Aug. 1971, pp. 883-900.

135. Amazigo, J.C. 'Asymptotic analysis of the buckling of externally pressurized cylinders with random imperfections,' Q. Appl. Math., Jan. 1974, pp. 429-442.

136. Montague, P. 'Experimental behaviour of thin-walled cylindrical shells subjected to external pressure,' J. Mech. Eng. Sci., vol. 11, no. 1, 1969, pp. 40-56.

137. Hodge, P.G. 'Rigid-plastic analysis of symmetrically loaded cylindrical shells,' J. Appl. Mech., vol. 21, no. 4, Dec. 1954, pp. 336-343.

138. Lunchick, M.E. 'Plasticity research on submarine pressure hulls conducted at the David Taylor Model Basin,' Proc. 2nd Symp. on Naval Struct. Mech., E.H. Lee and P.S. Symmonds (Eds.), Pergammon Press, 1960, pp. 347-366.

139. Lunchick, M.E. 'Plastic axisymmetric buckling of ring-stiffened cylindrical shells fabricated from strain-hardening materials and subjected to external hydrostatic pressure,' David Taylor Model Basin Report 1393, Jan. 1961.

140. Reynolds, T.E. 'Inelastic local buckling of cylindrical shells under external hydrostatic pressure,' David Taylor Model Basin Report 1392, Aug. 1960.

141. Reis, A.J. and Walker, A.C. 'Local buckling strength of ring stiffened cylindrical shells under external pressure,' Appl. Ocean Res., vol. 5, no. 2, 1983, pp. 56-62.

142. Lunchick, M.E. 'Plastic general instability pressure of ring stiffened cylindrical shells,' David Taylor Model Basin Report 1587, Sept. 1963.

143. Ellinas, C.P. and Croll, J.G.A. 'Elastic-plastic general buckling of ring-stiffened cylinders,' in Collapse - the buckling of structures in theory and practice, J.M.T. Thompson and G.W. Hunt (Eds.), Cambridge Univ. Press, 1983, pp. 93-109.

144. Timoshenko, S.P. and Gere, J.M. 'Theory of Elastic Stability,' McGraw Hill, 1961.

145. Sharman, P.W. 'A theoretical interaction equation for the buckling of circular shells under axial compression and external pressure,' J. Aero. Sci., vol. 29, no. 7, July 1962, pp. 878-879.

146. Lakshmikantham, C. and Gerard, G. 'Elastic stability of cylindrical shells under axial and lateral loads,' J. Royal Aero. Soc., vol. 68, no. 11, Nov. 1964, pp. 773-775.

147. Krishnamoorthy, G. 'Buckling of thin cylinder under combined external pressure and axial compression,' J. Aircraft, vol. 11, no. 3, Feb. 1974, pp. 65-68.

148. Zyczkowski, M. and Bucko, S. 'A method of stability analysis of cylindrical shells under biaxial compression,' J. AIAA, vol. 9, no. 11, Nov. 1971, pp. 2259-2263.

149. Weingarten, V.I. and Seide, P. 'Elastic stability of thin walled cylindrical and conical shells under combined external pressure and axial compression,' J. AIAA, vol. 3, no. 3, March 1965, pp. 913-920.

150. Hutchinson, J.W. 'Buckling of imperfect cylindrical shells under axial compression and external pressure,' J. AIAA, vol. 3, no. 10, Oct. 1965, pp. 1968-1970.

151. Tennyson, R.C., Booton, M. and Chan, K.H. 'Buckling of short cylinders under combined loading,' J. Appl. Mech., vol. 45, no. 3, Sept. 1978, pp. 574-578.

152. Reis, A.J., Walker, A.C. and Virtuoso, F.E. 'Externally pressurized cylindrical shells: buckling and collapse under combined loading,' in Collapse - the buckling of structures in theory and practice, J.M.T. Thompson and G.W. Hunt (Eds.), Cambridge Univ. Press., London, 1983, pp. 481-491.

153. Det norske Veritas 'Rules for the Design, Construction and Inspection of Offshore Structures,' Høvik, Norway, 1977.

154. Det norske Veritas 'Classification Notes - Buckling Strength Analysis,' Note no. 30.1, Høvik, Norway, 1982.

155. European Convention for Constructional Steelwork 'Buckling of Shells,' Draft Rules, 1984.

156. American Society of Mechanical Engineers 'Boiler and Pressure Vessel Code - Code Case N-284,' New York, 1980.

157. Samuelson, L.A. and Vestergren, P. 'Analysis of axially loaded stringer stiffened circular cylinders,' Aero. Res. Inst. of Sweden, Tech. Note HU-2134, Dec. 1979.

158. Samuelson, L.A. 'Practical analysis methods for design of circular cylinders with longitudinal stiffeners and subjected to axial compression,' in Buckling of Shells - A State-of-the-art Colloquium, E. Ramm (Ed.), Stuttgart, 1982.

159. Walker, A.C. and Sridharan, S. 'Analysis of the behaviour of axially compressed stringer-stiffened cylindrical shells,' Proc. Instn. Civil Engrs., Part 2, vol. 69, 1980, pp. 447-472.

160. Faulkner, D., Chen, Y.N. and de Oliveira, J.G. 'Limit state design criteria for stiffened cylinders of offshore structures,' Proc. 4th Nat. Cong. of Pressure Vessels and Piping Tech., Portland, Oregon, 1983.

161. Croll, J.G.A. and Ellinas, C.P. 'Design formulation for axisymmetric collapse of stiffened and unstiffened cylinders,'

Proc. 3rd Int. Symp. on Offshore Mech. and Arctic Eng., ASME, New Orleans, Feb. 1983, pp. 612-617.

162. Valsgard, S. and Steen, E. 'Simplified strength analysis of narrow panelled stringer stiffened cylinders under axial compression and lateral load,' DnV Report 80-059, Høvik, Norway, Aug. 1980.

163. Steen, E. and Valsgard, S. 'General buckling of orthogonally stiffened cylindrical shells under various load conditions,' DnV Report 81-061, Høvik, Norway, Sept. 1981.

164. Steen, E., Xirouchakis, P. and Valsgard, S. 'Design proposals for buckling of stringer-stiffened cylindrical shells under axial compression and external pressure,' DnV Report 82-0268, Høvik, Norway, March 1982.

165. Harding, J.E., Dowling, P.J., Valsgard, S. and Walker, A.C. 'The buckling design of stringer-stiffened shells subject to combined pressure and axial loading,' Proc. 15th Offshore Tech. Conf., Houston, 1983, pp. 267-276.

166. Odland, J. 'Buckling resistance of unstiffened and stiffened circular cylindrical shell structures,' Norwegian Maritime Res., vol. 3, 1978, pp. 2-22.

167. Harding, J.E. 'Ring-stiffened cylinders under axial and external pressure loading,' Proc. Instn. Civil Engrs., Part 2, vol. 71, Sept. 1981, pp. 863-878.

168. Walker, A.C., Segal, Y. and McCall, S. 'The buckling of thin-walled ring-stiffened steel shells,' in Buckling of Shells - A State-of-the-art Colloquium, E. Ramm (Ed.), Stuttgart, 1982.

169. Tsang, S.K., Harding, J.E., Walker, A.C. and Andronicou, A. 'Buckling of ring stiffened cylinders subjected to combined pressure and axial compressive load,' Proc. 4th Nat. Cong. of Pressure Vessels and Piping Tech., Portland, Oregon, 1983.

170. Galletly, G.D. and Pemsing, K. 'Buckling of cylinders under combined external pressure and axial compression,' in Collapse - the buckling of structures in theory and practice, J.M.T. Thompson and G.W. Hunt (Eds.), Cambridge Univ. Press, London, 1983, pp. 505-527.

171. Galletly, G.D., Pemsing, K. and James, S. 'Buckling of cylinders under biaxial compression,' in Stability of Metal Structures, 3rd Int. Colloquium, CTICM, Paris, 1983, pp.375-382.

172. Miller, C.D. 'Buckling design methods for steel structures - a state of the art,' in Integrity of Offshore Structures, D. Faulkner, M.J. Cowling and P.A. Frieze (Eds.), Appl. Sci. Publ., 1981, pp. 397-418.

173. Miller, C.D., Frieze, P.A., Zimmer, R.A. and Jan, H.Y. 'Collapse tests on fabricated stiffened steel cylinders under combined loads,' Proc. 4th Nat. Cong. of Pressure Vessels and Piping Tech., Portland, Oregon, 1983.

174. Babcock, C.D. 'Experiments in shell buckling,' in Thin Shell Structures, Y.C. Fung and E.E. Sechler (Eds.), Prentice-Hall, 1974,

pp. 345-369.

175. Tsao, C.H. and Chin, A. 'Tests of, and semiempirical formulas for, instability of longitudinally stiffened shells,' J. Spacecraft and Rockets, vol. 5, no. 2, Feb. 1968, pp. 196-201.

176. Thompson, J.M.T. 'Making of thin metal shells for model stress analysis,' J. Mech. Eng. Sci., vol. 2, no. 2, June 1960, pp. 105-108.

177. Babcock, C.D. and Sechler, E.E. 'The effects of initial imperfections on the buckling stress of cylindrical shells,' NASA TN D-2005, July 1963.

178. Tennyson, R.C. 'The effect of shape imperfections and stiffening on the buckling of circular cylinders,' in Buckling of Structures, Proc. IUTAM Symp., B. Budiansky (Ed.), Harvard Univ., Springer-Verlag, 1976, pp. 251-273.

179. Coppa, A.P. 'Measurement of initial geometrical imperfections of cylindrical shells,' J. AIAA, vol. 4, no. 1, Jan. 1966, pp. 172-174.

180. Arbocz, J. and Williams, J.G. 'Imperfection surveys on a 10-ft-diameter shell structure,' J. AIAA, vol. 15, no. 7, July 1977, pp. 949-956.

181. Dowling, P.J., Harding, J.E., Agelidis, N. and Fahy, W. 'Buckling of orthogonally stiffened cylindrical shells used in offshore structures,' in Buckling of Shells - A State-of-the-art Colloquium, E. Ramm (Ed.), Stuttgart, 1982.

182. Fahy, W. 'Collapse of longitudinally stiffened cylinders subject to axial and pressure loading,' PhD Thesis, Imperial College, Univ. of London, to be submitted.

183. Singer, J. 'Vibration correlation techniques for improved buckling predictions of imperfect stiffened shells,' in Buckling of Shells in Offshore Structures, J.E. Harding, P.J. Dowling and N. Agelidis (Eds.), Granada, London, 1982, pp. 285-329.

184. Galletly, G.D., Slankard, R.C. and Wenk, E. 'General instability of ring-stiffened cylindrical shells subject to external hydrostatic pressure - a comparison of theory abd experiment,' J. Appl. Mech., vol. 25, 1958, pp. 259-266.

185. Wilson, W.M. and Newmark, N.M. 'The strength of thin cylindrical shells as columns,' Univ. of Illinois Eng. Exp. Sta. Bull. 255, 1933.

186. Wilson, W.M. 'Tests of steel columns,' Univ. of Illinois Eng. Exp. Sta. Bull. 292, 1937.

187. Marzullo, M.A. and Ostapenko, A. 'Tests on two high-strength short tubular columns,' Proc. 10th Annual Offshore Tech. Conf., Houston, 1978, pp. 327-334.

188. Chen, W.F. and Ross, D.A. 'The axial strength and behaviour of cylindrical columns,' Proc. 9th Annual Offshore Tech. Conf., Houston, 1977, pp. 741-754.

189. Ostapenko, A. and Gunzelman, S.X. 'Local buckling tests on three steel large-diameter tubular columns,' Lehigh Univ., Dept. of Civil Eng., Fritz Eng. Lab. Report 406.7, Bethlehem, Pa., 1977.

190. Miller, C.D. 'Buckling of axially compressed cylinders,' Proc. ASCE, Struct. Div., vol. 103, no. ST3, May 1977, pp. 695-721.

191. Miller, C.D. 'Summary of buckling tests on fabricated steel cylindrical shells in USA,' in Buckling of Shells in Offshore Structures, J.E. Harding, P.J.Dowling and N. Agelidis (Eds.), Granada, London, 1982, pp. 429-471.

192. Dowling, P.J. and Harding, J.E. 'Experimental behaviour of ring and stringer stiffened cylinders,' in Buckling of Shells in Offshore Structures, J.E. Harding, P.J. Dowling and N. Agelidis (Eds.), Granada, London, 1982, pp. 73-107.

193. Walker, A.C., Andronicou, A. and Sridharan, S. 'Experimental investigation of the buckling of stiffened shells using small scale models,' in Buckling of Shells in Offshore Structures, J.E. Harding, P.J. Dowling and N. Agelidis (Eds.), Granada, London, 1982, pp. 45-71.

194. Walker, A.C. and Davies, P. 'The collapse of stiffened cylinders,' in Steel Plated Structures, P.J. Dowling, J.E. Harding and P.A. Frieze (Eds.), Crosby Lockwood Staples, 1976, pp. 791-808.

195. Dowling, P.J., Harding, J.E., Fahy, W. and Agelidis, N. 'Report on the testing of large and small scale stiffened shells under axial compression,' Imperial Coll. Civil Eng. Struct. Lab. Report SS1, 1981.

196. Green, D.R. and Nelson, H.M. 'Compression tests on large-scale, stringer-stiffened tubes,' in Buckling of Shells in Offshore Structures, J.E. Harding, P.J. Dowling and N. Agelidis (Eds.), Granada, London, 1982, pp. 25-43.

197. Kinra, R.K. 'Hydrostatic and axial collapse tests of stiffened cylinders,' Proc. 10th Annual Offshore Tech. Conf., Houston, 1978, pp. 765-788.

198. Ellinas, C.P., Supple, W.J. and Walker, A.C. 'Buckling of Offshore Structures,' Granada, 1984.

199. Dowling, P.J. and Harding, J.E. 'Current research into the strength of cylindrical shells used in steel jacket construction,' Proc. 2nd Int. Conf. on Behaviour of Offshore Structures, Imperial College, London, Aug. 1979, pp. 327-339.

200. Lloyds Register of Shipping Private communication

201. Transport and Road Research Laboratory 'Recommended standard practices for structural testing of steel models,' Supp. Report 254, 1977.

202. Denston, R.J. and White, J.D. 'An electrical demountable extensometer,' Cambridge Univ. Dept. of Eng. Report CUED/C-Struct/TR 61, 1977.

203. McCall, S. and Walker, A.C. 'Buckling tests on stringer stiffened cylinder models subject to load combinations,' Report to DnV from Dept. of Mech. Eng., Univ. of Surrey, Dec. 1981, also DnV Report 82/0299.

204. Agelidis, N., Harding, J.E. and Dowling, P.J. 'Final report on buckling tests on stringer stiffened cylinder models subject to load combinations,' Vol. 1, London Centre for Marine Technology Report, Imperial College, London, Jan. 1982, also DnV Report 82/0298.

205. Owens, G.W. 'Experimental nonlinear modelling for composite structures applied to a bifurcated bridge,' PhD thesis, Imperial College, London, May 1979.

206. Roark, R.J. and Young, W.G. 'Formulas for stress and strain,' McGraw Hill, 5th Ed., 1975.

207. Moolani, F.M. and Dowling, P.J. 'Ultimate load behaviour of stiffened plates in compression,' Proc. Int. Symp. on Steel Plated Structures, Imperial College, London, 1976.

208. Diack, A. and Ramm, E. 'A parametric study on the stability of stringer-stiffened cylindrical shells under axial load,' in Stability of Metal Structures, CTICM, Paris, Nov. 1983, pp. 357-366.

209. Trueb, U. 'Stability problems of elasto-plastic plates and shells by finite elements,' PhD thesis, Imperial College, London, Sept. 1983.

210. Bates, D.N. 'Nonlinear finite element analysis of curved beams and shells,' PhD thesis, Imperial College, London, (to be submitted)

211. Valsgard, S., Wen-Jiao, S. and Steen, E. 'Data collection on geometry and design loads for stiffened cylindrical shells in marine structures,' DnV Report 80-0156, Høvik, Norway, Feb. 1980.

212. Dwight, J.B. and Moxham, K.E. 'Welded steel plates in compression,' Structural Engineer, vol. 47, no. 2, Feb. 1969.

213. Kamtekar, A.G., White, J.D. and Dwight, J.B. 'Shrinkage stresses in a thin plate with a central weld,' J. Strain Anal., vol. 12, no. 2, April 1977.

214. White, J.D. and Dwight, J.B. 'Residual stresses in large stiffened tubulars,' Cambrige Univ. Dept. of Civil Eng. Report CUED/C-Struct/TR 67, 1978.

APPENDIX A

APPROXIMATE DETERMINATION OF MINIMUM STIFFENING RATIO FOR LOCAL BUCKLING MODE

A.1 GENERAL

Steen et al [164] used the principle of stationary potential energy to derive an elastic interaction formula for a stringer-stiffened cylinder under a combination of axial compression and external pressure. They assumed the cylinder to be simply supported and neglected the strain energy contribution from the torsional deformation of the stringers and the in-plane bending of the shell to yield the formula:

$$(\frac{t}{r})^2[\bar{m}^{-2}+n^2]^2 + 12(1-\nu^2)\bar{m}^{-4}/[\bar{m}^{-2}+n^2]^2 + \gamma_s(\frac{t}{r})^2\bar{m}^{-4}$$
$$= 12(1-a_s)\bar{m}^{-2}\Phi_x + 12n^2\Phi_\theta \qquad \text{A.1}$$

in which the symbols are as defined below:

$\bar{m} = m\pi r/l$

m = number of axial halfwaves between rings

n = number of circumferential waves

t = shell thickness

r = radius

$a_s = A_s/st$ where A_s = area of stiffener

$\gamma_s = 12(1-\nu^2)\ I_s/(st^3)$ I_s = moment of inertia of stiffener

$\Phi_x = \sigma_x(1-\nu^2)/E$

$\Phi_\theta = \sigma_y(1-\nu^2)/E$

This general formula can be simplified for specific loading cases and assumed buckling mode shapes.

A.2 AXIAL COMPRESSION ($\Phi_\theta = 0$)

A.2.1 Local buckling

The circumferential buckling mode, n, is equal to the number of stiffeners, N, and it is assumed that the shell panel subdivides into square buckles, giving $\bar{m} = \pi r/s$ (ie $l/m = s$). Substitution into eqn A.1 and simplification yields the following expression for the elastic buckling stress for local buckling under axial load:

$$\sigma_{xl} = C_{xl} \frac{\pi^2 E}{12(1-\nu^2)} \left(\frac{t}{s}\right)^2 \qquad \text{A.2}$$

where $C_{xl} = 4 + \frac{3}{\pi^4} Z_s^2 \qquad$ for $Z_s < 11.4$ A.2(a)

If $Z_s > 11.4$ the unstiffened cylinder buckling stress is used:

$$\sigma_{xl} = \frac{E}{\sqrt{3(1-\nu^2)}} \frac{t}{r} \qquad \text{A.3}$$

A.2.2 Overall buckling

In this case it is assumed that the buckling mode contains only a single halfwave in the axial direction, (ie m = 1). Substitution into eqn A.1 yields an equation which can be minimized with respect to n, and then used to determine the buckling stress:

$$\sigma_{xo} = C_{xo} \frac{\pi^2 E}{12(1-\nu^2)} \left(\frac{t}{l}\right)^2 \qquad \text{A.4}$$

where $C_{xo} = \frac{4\sqrt{3}}{\pi^2} \frac{Z}{(1+a_s)} + \frac{\gamma_s}{(1+a_s^2)}$ A.4(a)

The buckling mode parameter $\bar{n}$ ($= \frac{nl}{\pi r}$) was given by:

$$\bar{n} = [0.59\sqrt{Z} - 1]^{1/2} \qquad \text{A.5}$$

A.2.3 Equate local and overall buckling stresses

Putting σ_{xl} equal to σ_{xo} for $Z_s < 11.4$ results in:

$$C_{xo} = C_{xl} \left(\frac{l}{s}\right)^2 \qquad \text{A.6}$$

where the right hand side is independent of the stiffening ratio.

Assuming rectangular stiffeners with $d_s = 10.t_s$ gives a stiffener area, A_s of $10.t_s^2$. The stiffener ratio is, therefore, $a_s = 10.t_s^2/s$ giving $t_s = \sqrt{s.a_s/10}$ and $d_s = \sqrt{10.s.a_s}$. The other stiffener section properties can now be expressed in terms of a_s and substituted into eqn A.4(a) and then A.6 to yield a quadratic equation in a_s. This can be solved to give the following expression:

$$a_s = \frac{A \pm \sqrt{A^2 - 4C(A-B)}}{2C} \qquad \text{A.7}$$

where $A = C_{xl} \left(\frac{l}{s}\right)^2$

$B = 4\sqrt{3}\, Z/\pi^2$

$C = 10(1-\nu^2)s$

When $Z_s > 11.4$ the procedure and eqn A.7 remain unchanged but

$$A = \frac{4\sqrt{3(1-\nu^2)}}{\pi^2} \left(\frac{l}{r}\right)^2$$

A.3 EXTERNAL PRESSURE ($\Phi_x = 0$)

A.3.1 Local buckling

A buckling mode shape with m = 1 and n = N/2 was assumed by Steen et al, but it is possible that for wide-panelled cylinders n = N will yield a lower buckling stress, and both modes were investigated here. This results in:

$$\sigma_{\theta l} = C_{\theta l} \frac{\pi^2 E}{12(1-\nu^2)} \left(\frac{t}{l}\right)^2 \qquad \text{A.8}$$

where $C_{\theta l} = \left(a_s + \frac{12}{\pi^2} \frac{Z^2}{a}\right) / \left(\frac{l}{s}\right)^2$

and $a_2 = [1+(l/s)^2]^2$ for n = N/2

or $[1+(2l/s)^2]^2$ for n = N

A.3.2 Overall buckling

As in the case of overall buckling under axial load, substitution of m = 1 into A.1 yields an expression to be minimized with respect to $\bar{n}$ ($= \frac{nl}{\pi r}$). An explicit solution for $\bar{n}$, valid for the entire range of geometries cannot be found, and simplifying assumptions are made for particular ranges of geometries. The cylinders to be studied in the parametric analysis fall into the "moderately long" category, for which $\bar{n}^2 > 1$ and $\bar{n}^4 >> 1$ are valid assumptions. This yields:

$$\sigma_{\theta o} = C_{\theta o} \frac{\pi^2 E}{12(1-\nu^2)} \left(\frac{t}{l}\right)^2 \qquad \text{A.9}$$

where $C_{\theta o} = (\bar{n}^2+2) + \frac{12Z^2}{(\pi\bar{n})^4(\bar{n}^2+2)} + \frac{\gamma_s}{\bar{n}^2}$

and $\bar{n} = \bar{n}_o + \Delta\bar{n}$

$$\bar{n}_o = \left(\frac{1}{2}\gamma_s\bar{Z}\right)^{1/4}$$

$$\Delta\bar{n} = \frac{4}{3}\frac{1}{\bar{n}_o\{1+(3\gamma_s-5\bar{n}_o^{-4})(\bar{n}_o^{-2}\pi^2/6Z)\}}$$

$$\bar{Z} = 1+(1+\beta^2)^2$$

$$\beta = \frac{12}{\pi^2}\frac{Z}{\gamma_s}$$

A.3.3 Equate local and overall buckling stresses

Equating A.8 and A.9 yields $C_{\theta l} = C_{\theta o}$. Once again, the stiffener properties are expressed in terms of a_s; however, the resulting equation is more complex than before and an iterative solution was employed to determine a_s for each cylinder geometry.

For each cylinder, stiffening ratios less than the values calculated would represent models whose overall buckling stress was less than the local buckling stress. These models were consequently excluded from the single panel finite element studies.

APPENDIX B

LOAD-DEFLECTION CURVES FROM PARAMETRIC STUDY

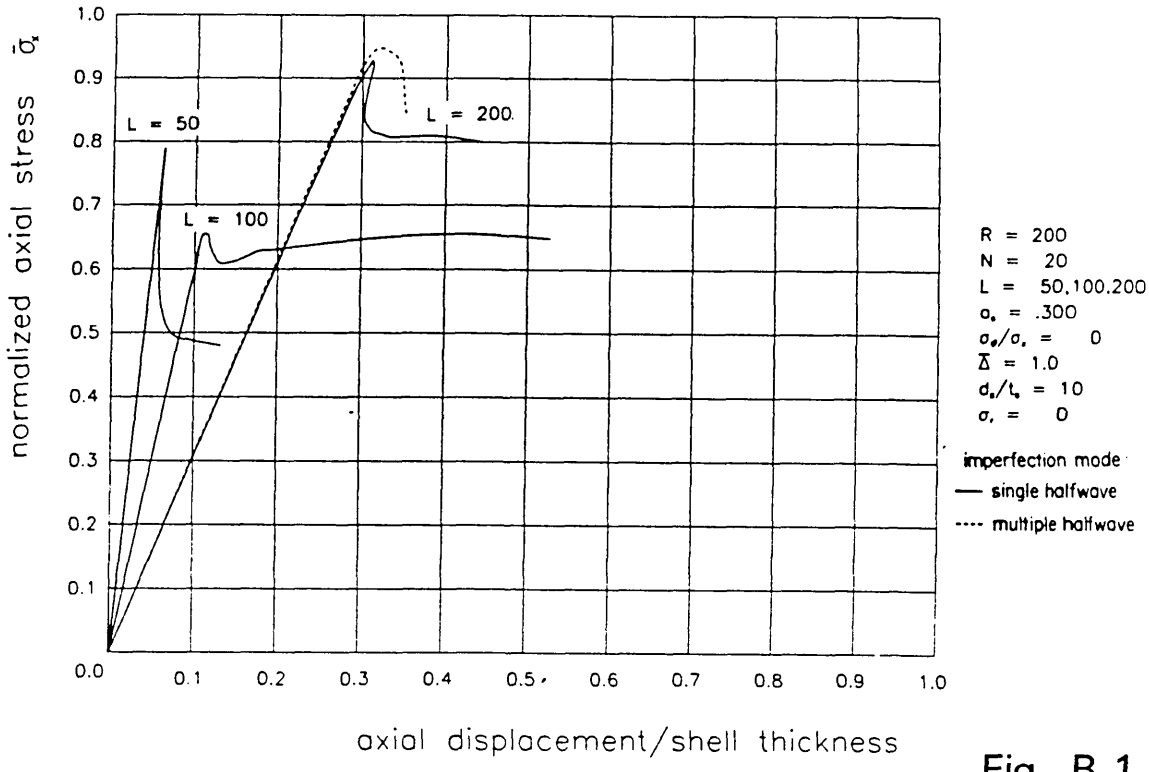


Fig. B.1

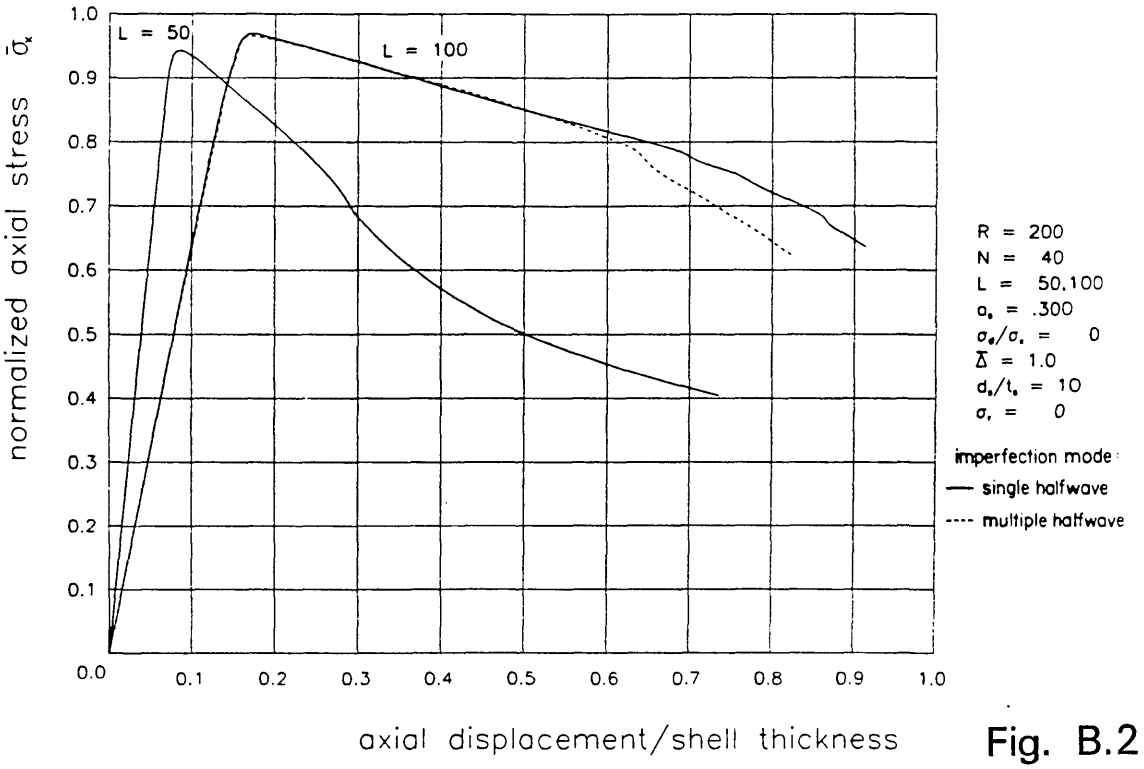


Fig. B.2

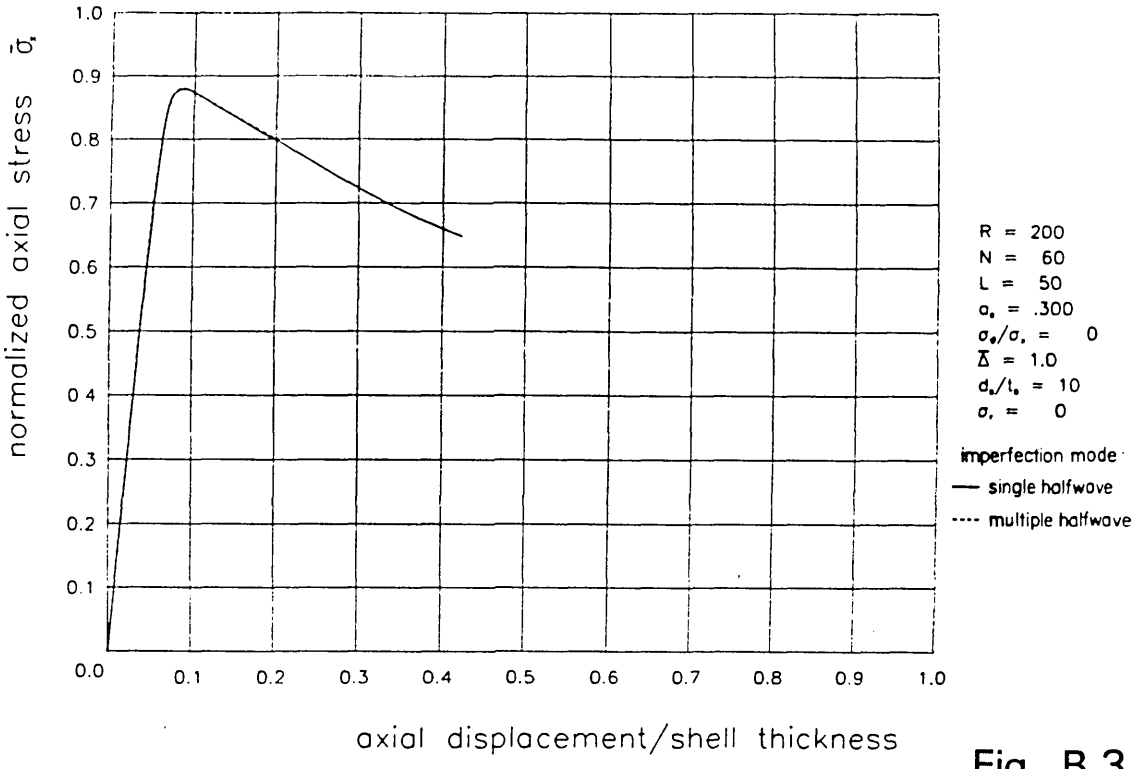

normalized axial stress $\bar{\sigma}_x$
1.0
0.9
0.8
0.7
0.6
0.5
0.4
0.3
0.2
0.1
0.0
0.1
0.2
0.3
0.4
0.5
0.6
0.7
0.8
0.9
1.0
axial displacement/shell thickness
R = 200
N = 60
L = 50
a_o = .300
σ_o/σ_x = 0
$\bar{\Delta}$ = 1.0
d_o/t_o = 10
σ_r = 0
imperfection mode
single halfwave
multiple halfwave

Fig. B.3

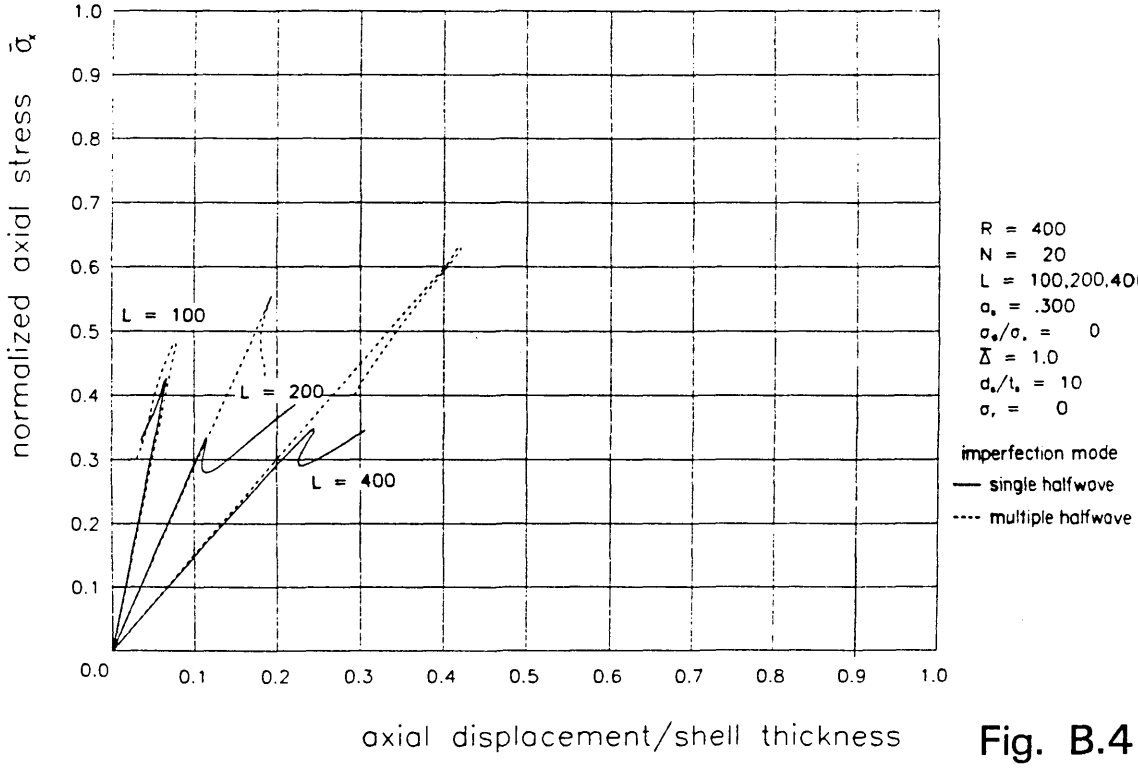

normalized axial stress $\bar{\sigma}_x$
1.0
0.9
0.8
0.7
0.6
0.5
0.4
0.3
0.2
0.1
0.0
0.1
0.2
0.3
0.4
0.5
0.6
0.7
0.8
0.9
1.0
L = 100
L = 200
L = 400
axial displacement/shell thickness
R = 400
N = 20
L = 100,200,400
a_o = .300
σ_o/σ_x = 0
$\bar{\Delta}$ = 1.0
d_o/t_o = 10
σ_r = 0
imperfection mode
single halfwave
multiple halfwave

Fig. B.4

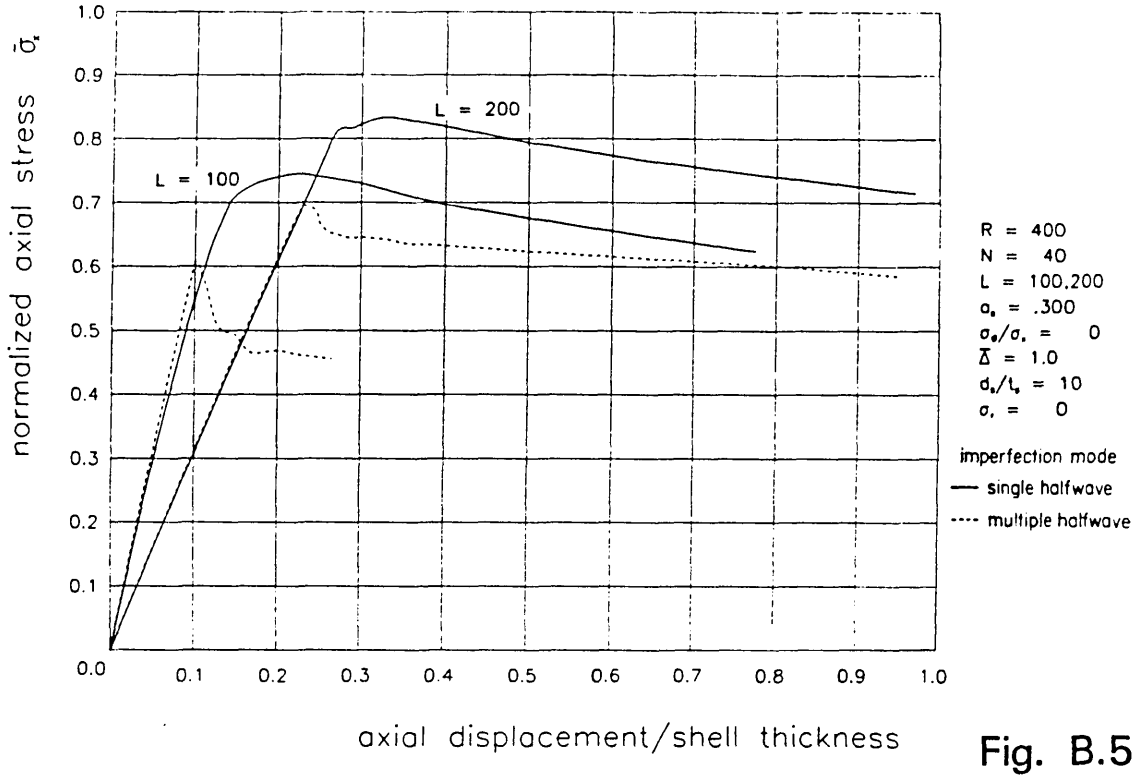

normalized axial stress $\bar{\sigma}_x$
1.0
0.9
0.8
0.7
0.6
0.5
0.4
0.3
0.2
0.1
0.0
0.1
0.2
0.3
0.4
0.5
0.6
0.7
0.8
0.9
1.0
L = 200
L = 100
axial displacement/shell thickness
R = 400
N = 40
L = 100,200
$\alpha_* = .300$
$\sigma_*/\sigma_* = 0$
$\bar{\Delta} = 1.0$
$d_*/t_* = 10$
$\sigma_r = 0$
imperfection mode
single halfwave
multiple halfwave

Fig. B.5

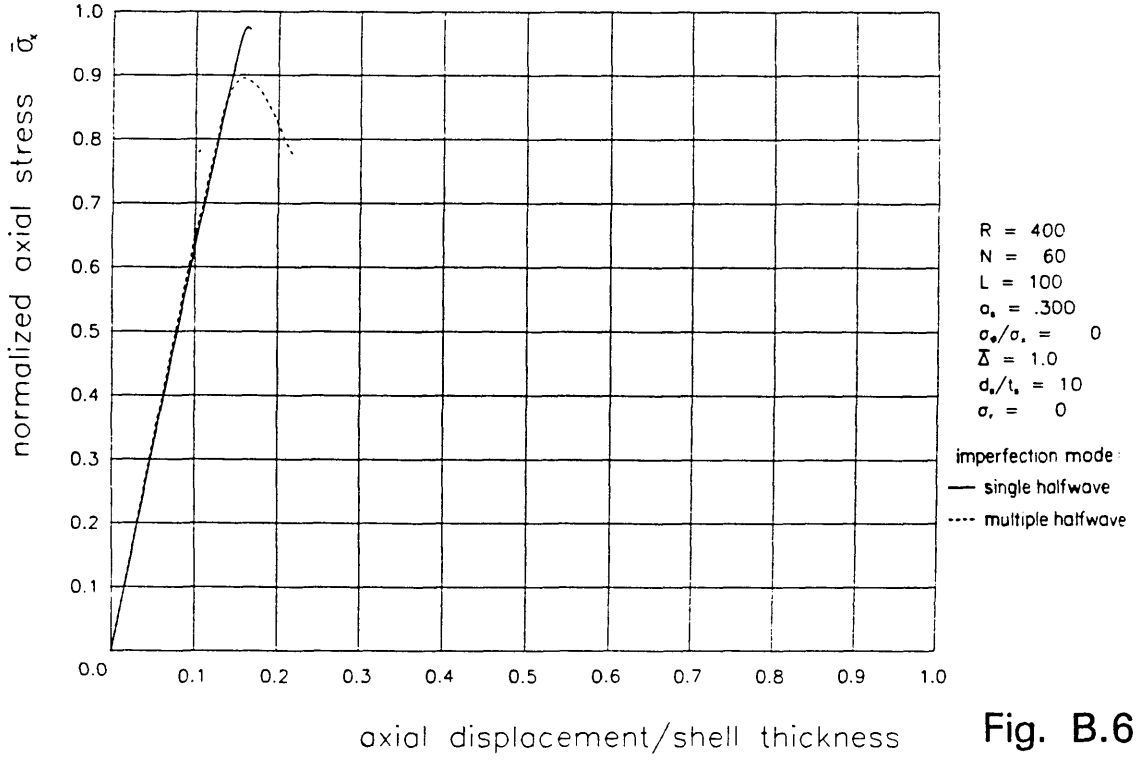

normalized axial stress $\bar{\sigma}_x$
1.0
0.9
0.8
0.7
0.6
0.5
0.4
0.3
0.2
0.1
0.0
0.1
0.2
0.3
0.4
0.5
0.6
0.7
0.8
0.9
1.0
axial displacement/shell thickness
R = 400
N = 60
L = 100
$\alpha_* = .300$
$\sigma_*/\sigma_* = 0$
$\bar{\Delta} = 1.0$
$d_*/t_* = 10$
$\sigma_r = 0$
imperfection mode
single halfwave
multiple halfwave

Fig. B.6

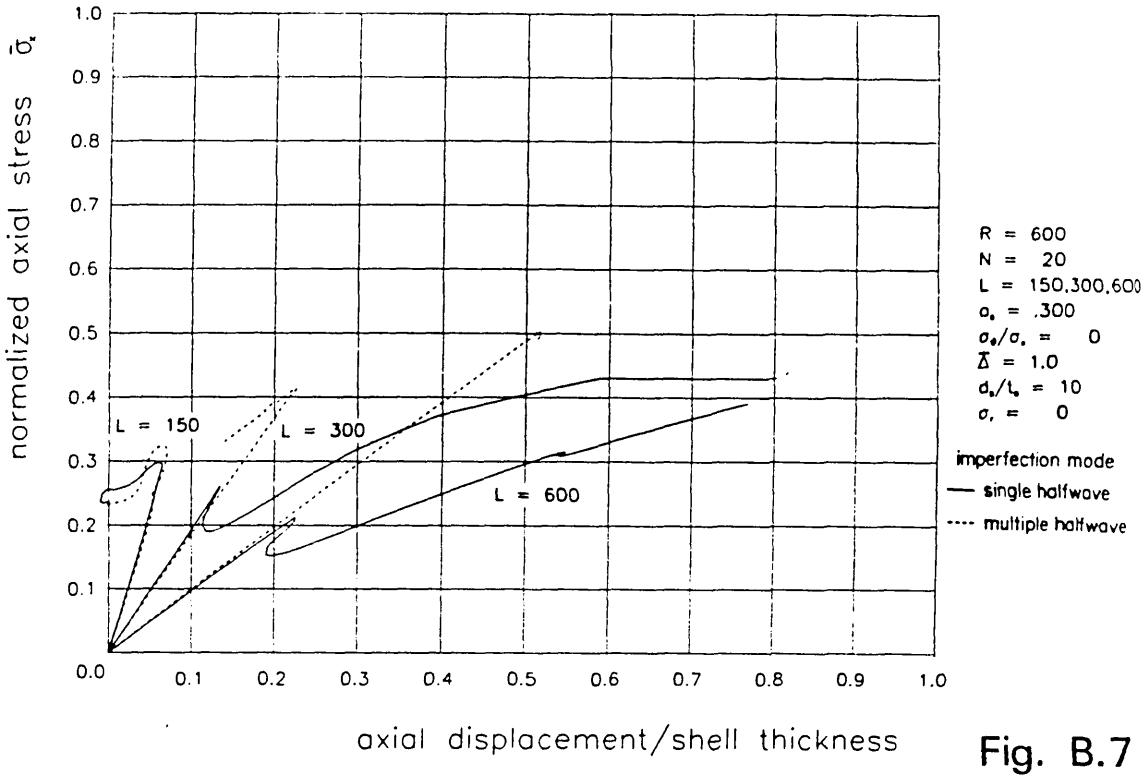

normalized axial stress $\bar{\sigma}_x$
1.0
0.9
0.8
0.7
0.6
0.5
0.4
0.3
0.2
0.1
0.0
0.1
0.2
0.3
0.4
0.5
0.6
0.7
0.8
0.9
1.0
L = 150
L = 300
L = 600
axial displacement/shell thickness
R = 600
N = 20
L = 150,300,600
α_0 = .300
σ_ϕ/σ_x = 0
$\bar{\Delta}$ = 1.0
d_0/t_0 = 10
σ_r = 0
imperfection mode
single halfwave
multiple halfwave

Fig. B.7

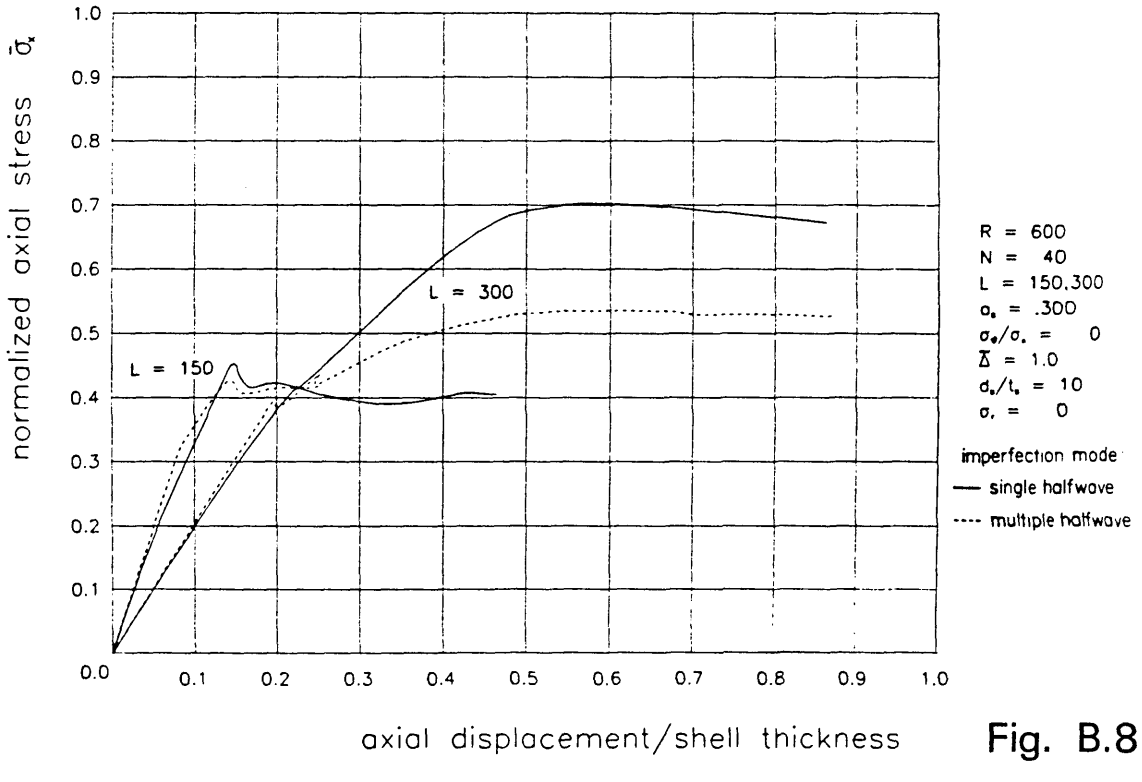

normalized axial stress $\bar{\sigma}_x$
1.0
0.9
0.8
0.7
0.6
0.5
0.4
0.3
0.2
0.1
0.0
0.1
0.2
0.3
0.4
0.5
0.6
0.7
0.8
0.9
1.0
L = 150
L = 300
axial displacement/shell thickness
R = 600
N = 40
L = 150,300
α_0 = .300
σ_ϕ/σ_x = 0
$\bar{\Delta}$ = 1.0
d_0/t_0 = 10
σ_r = 0
imperfection mode
single halfwave
multiple halfwave

Fig. B.8

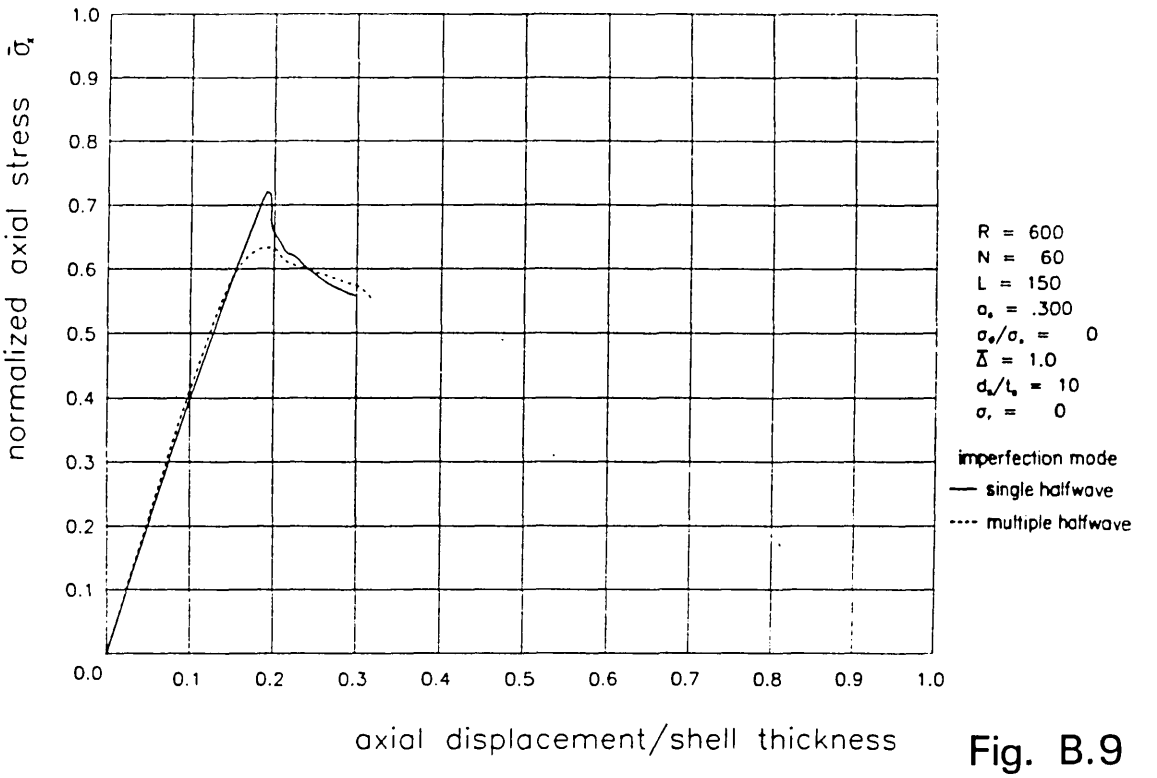


Fig. B.9

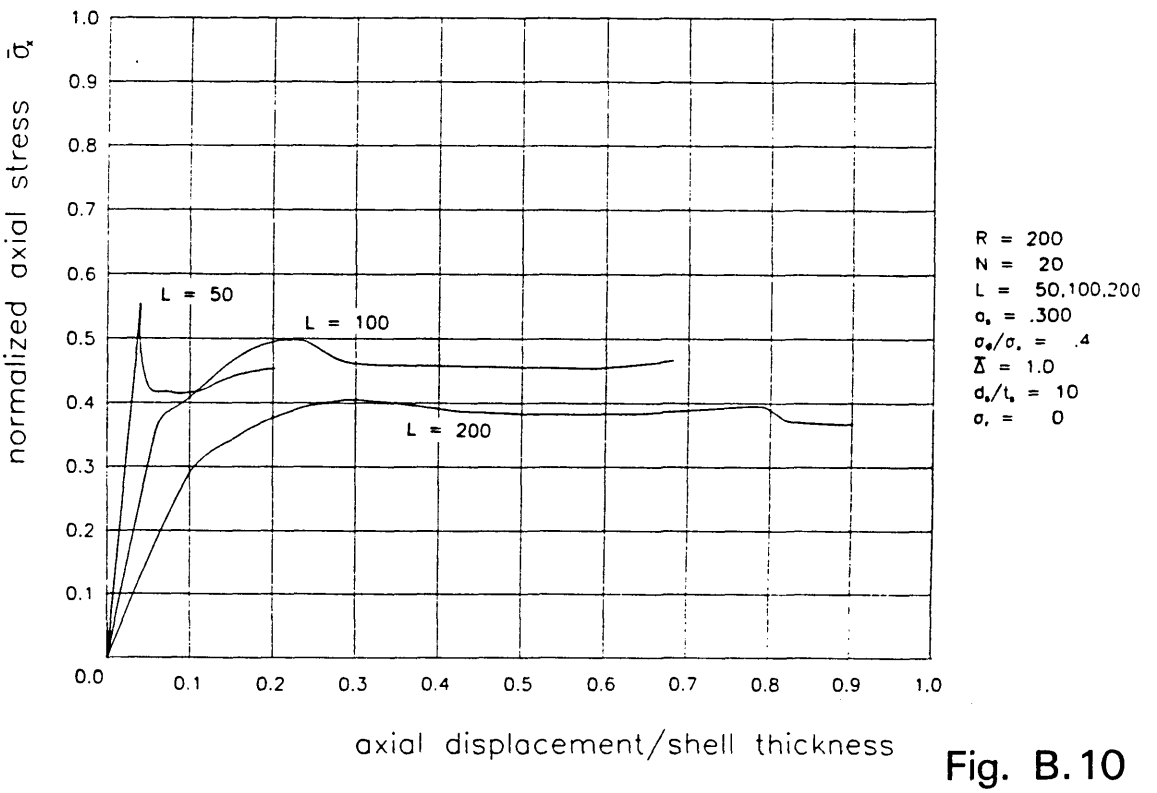


Fig. B.10

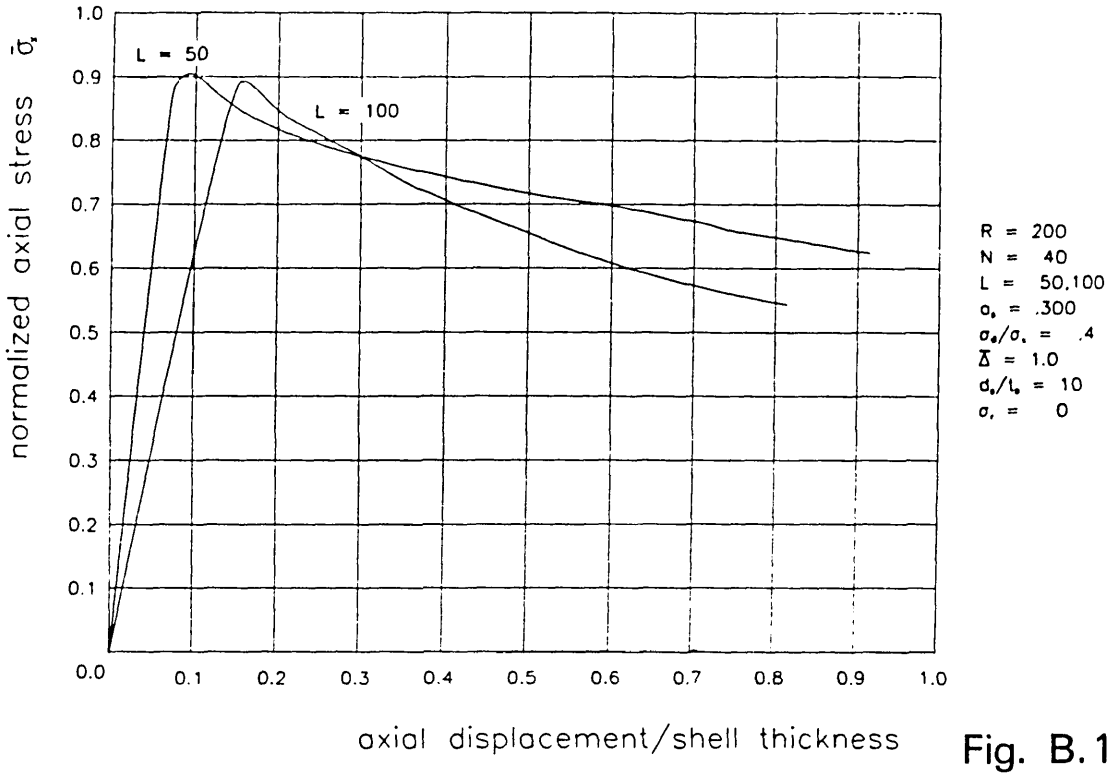


Fig. B.11

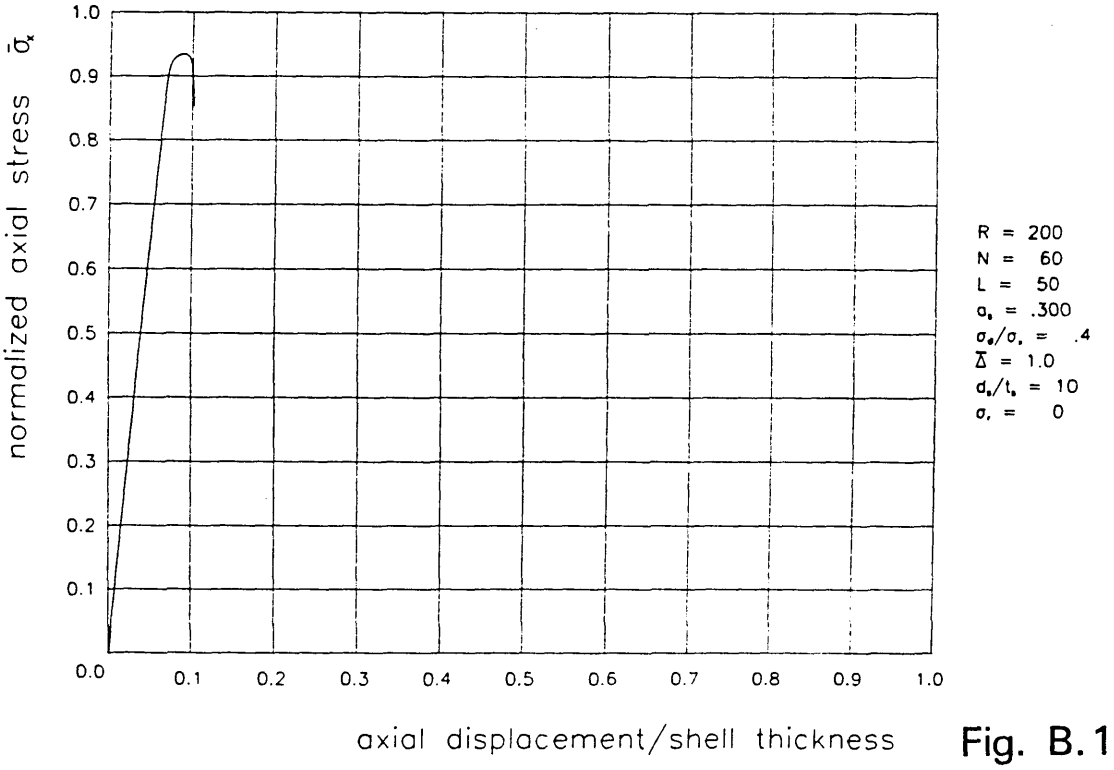


Fig. B.12

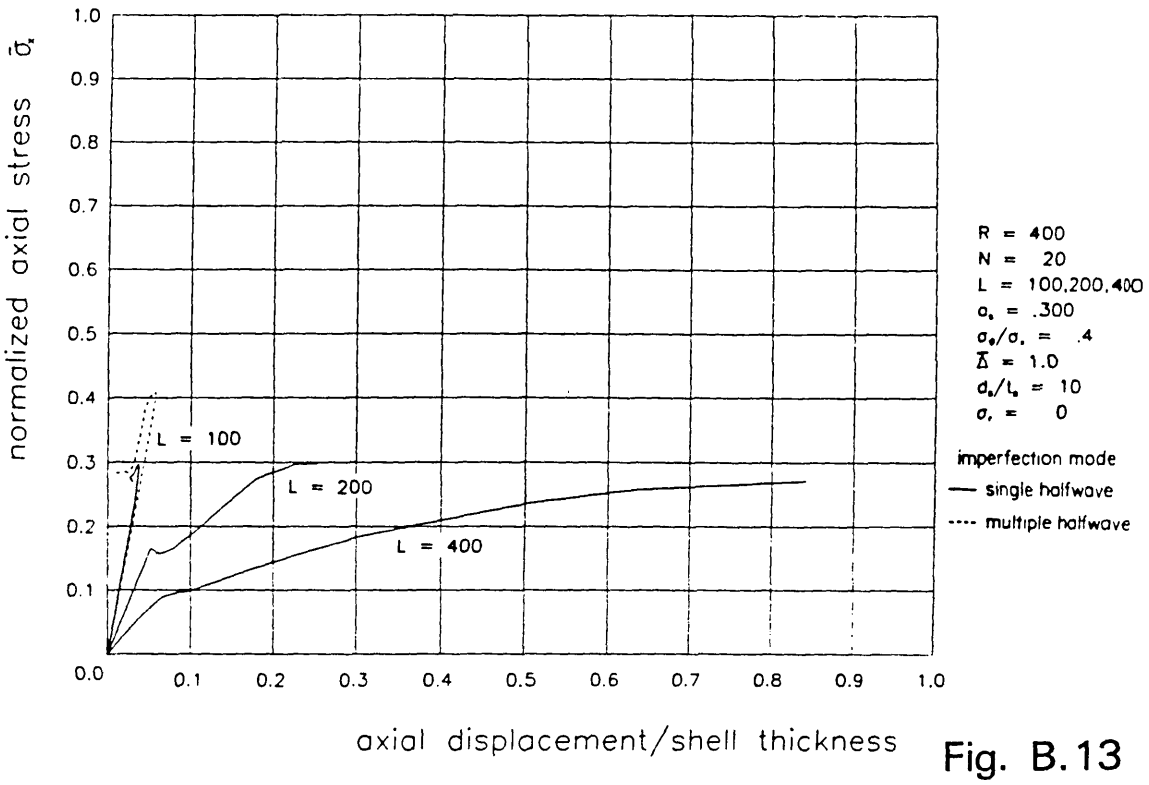


Fig. B.13

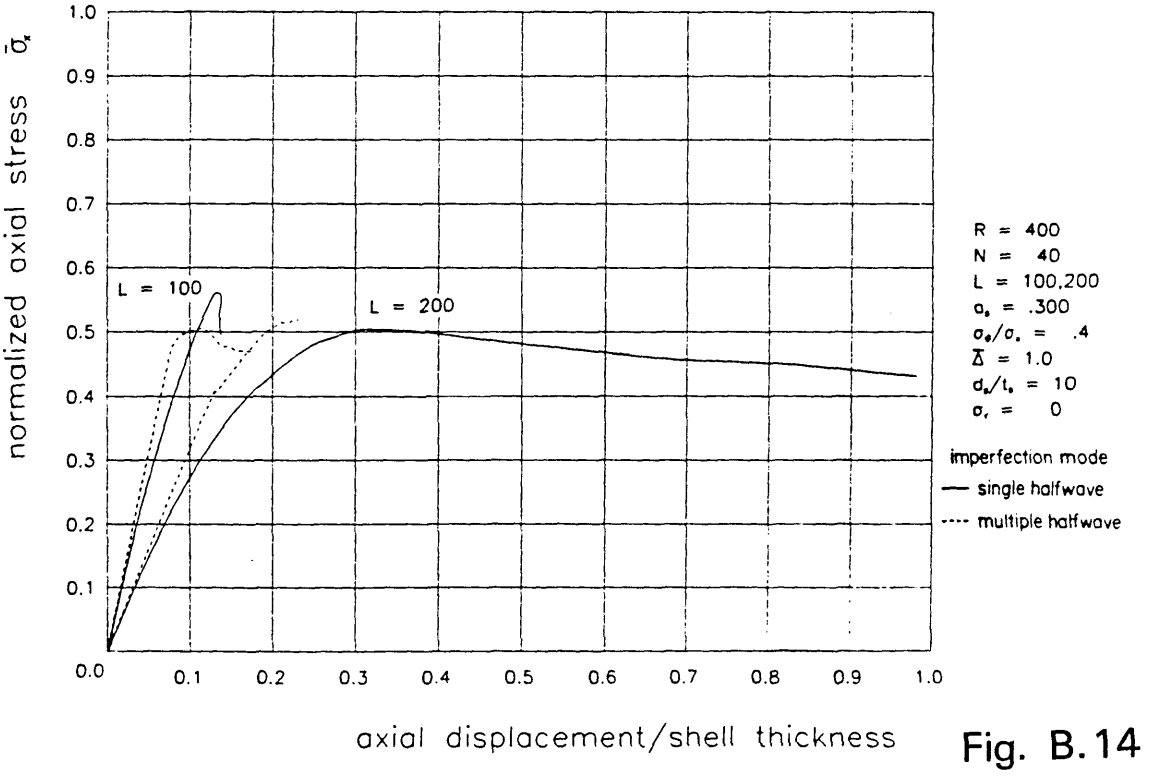


Fig. B.14

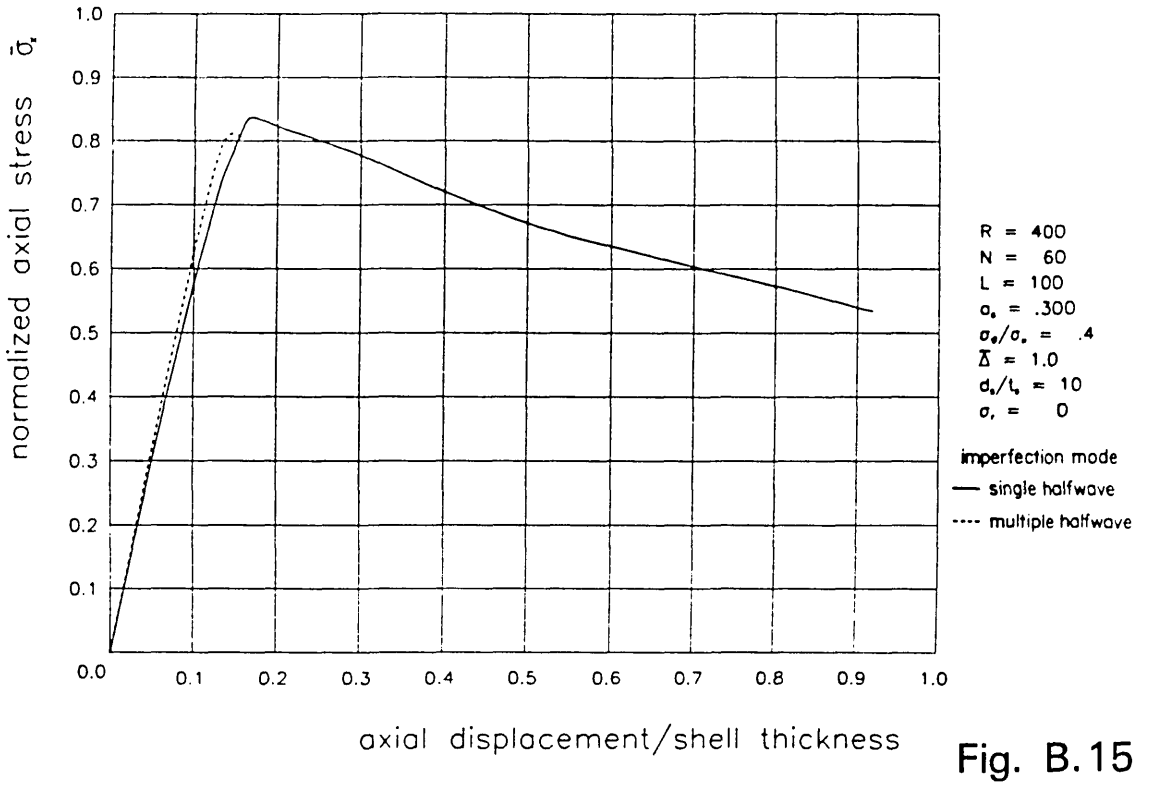


Fig. B.15

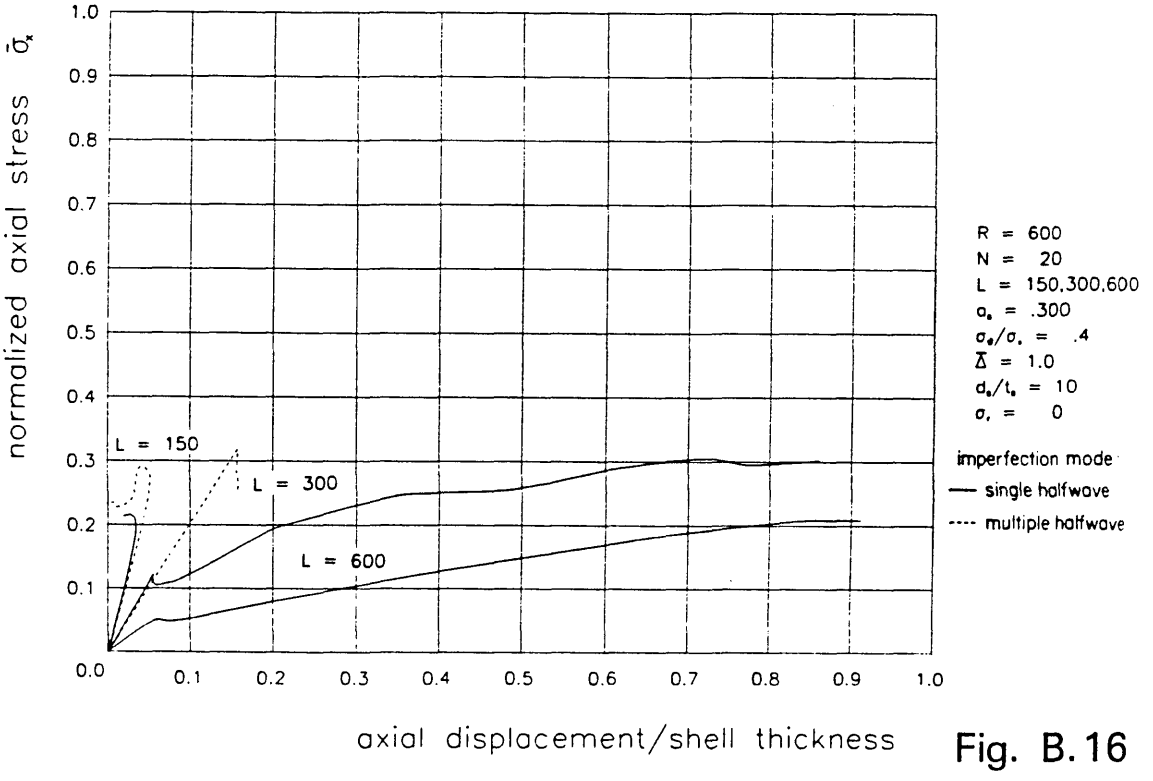


Fig. B.16

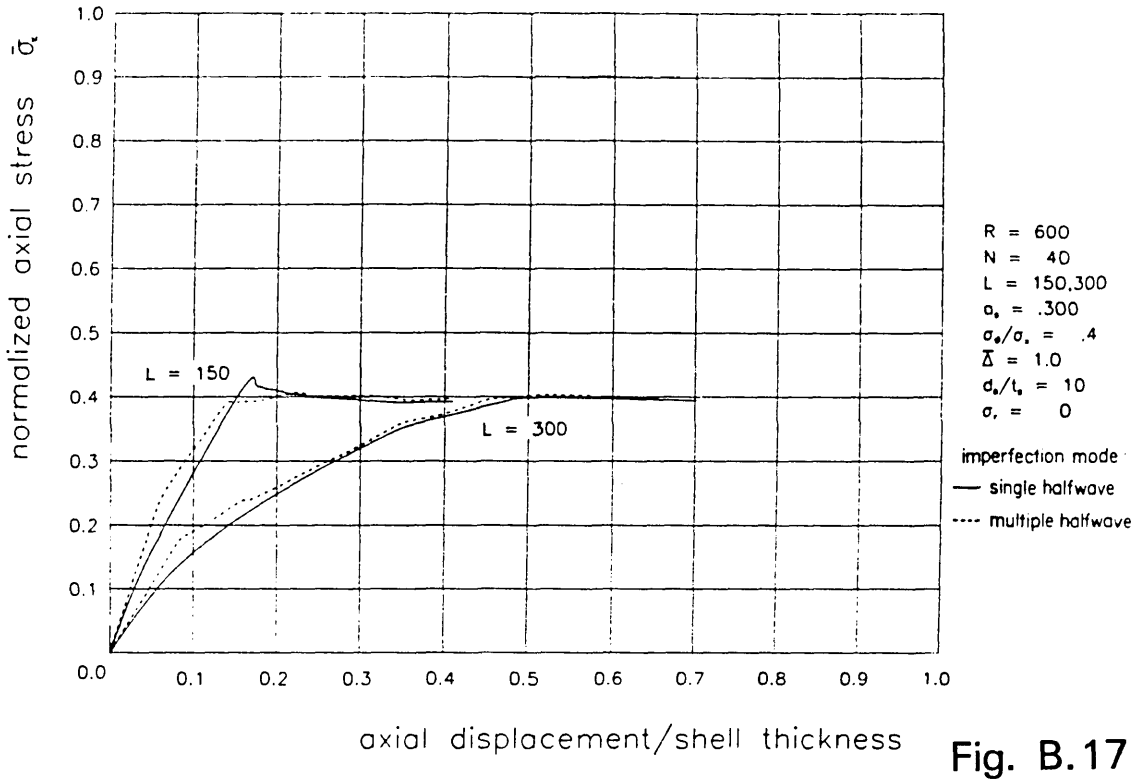


Fig. B.17

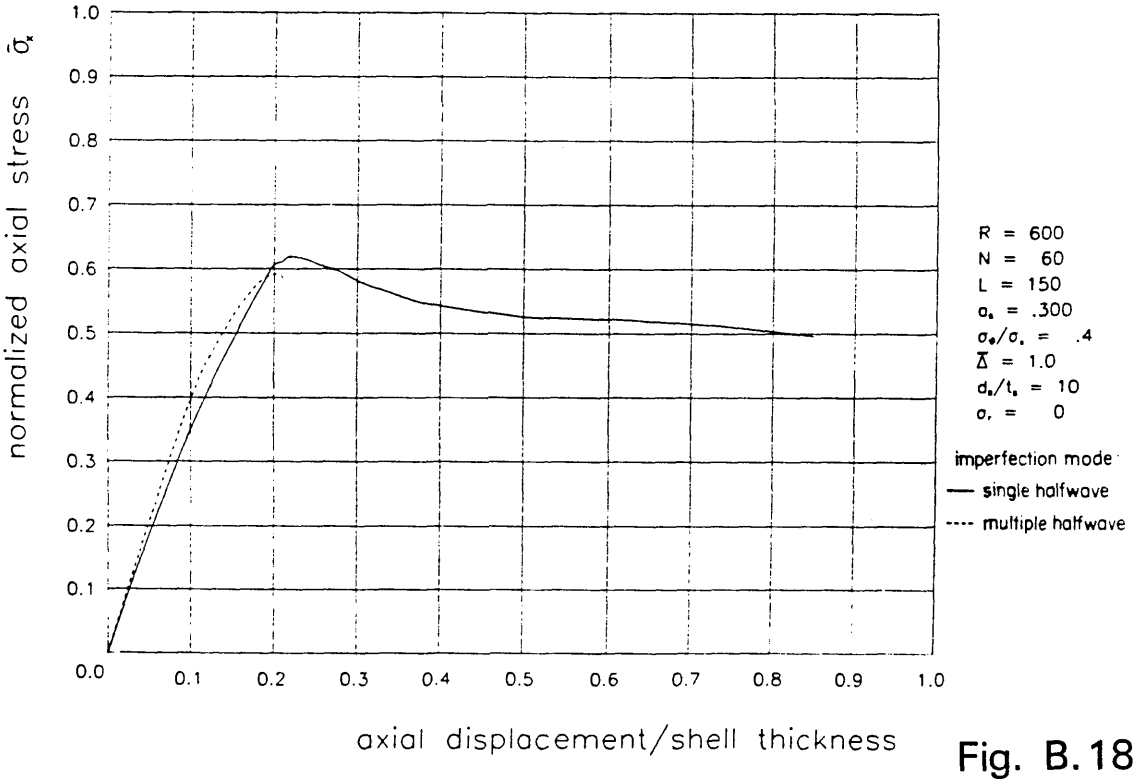


Fig. B.18

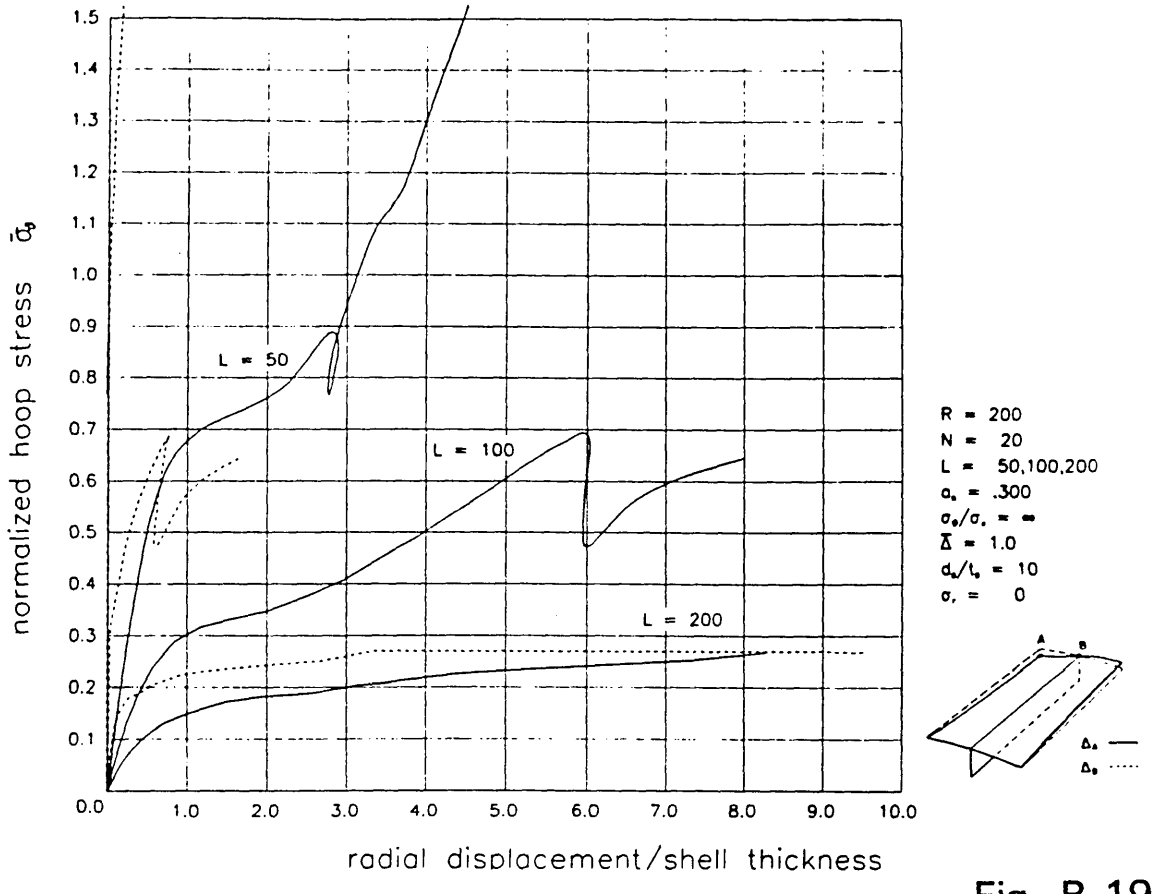


Fig. B.19

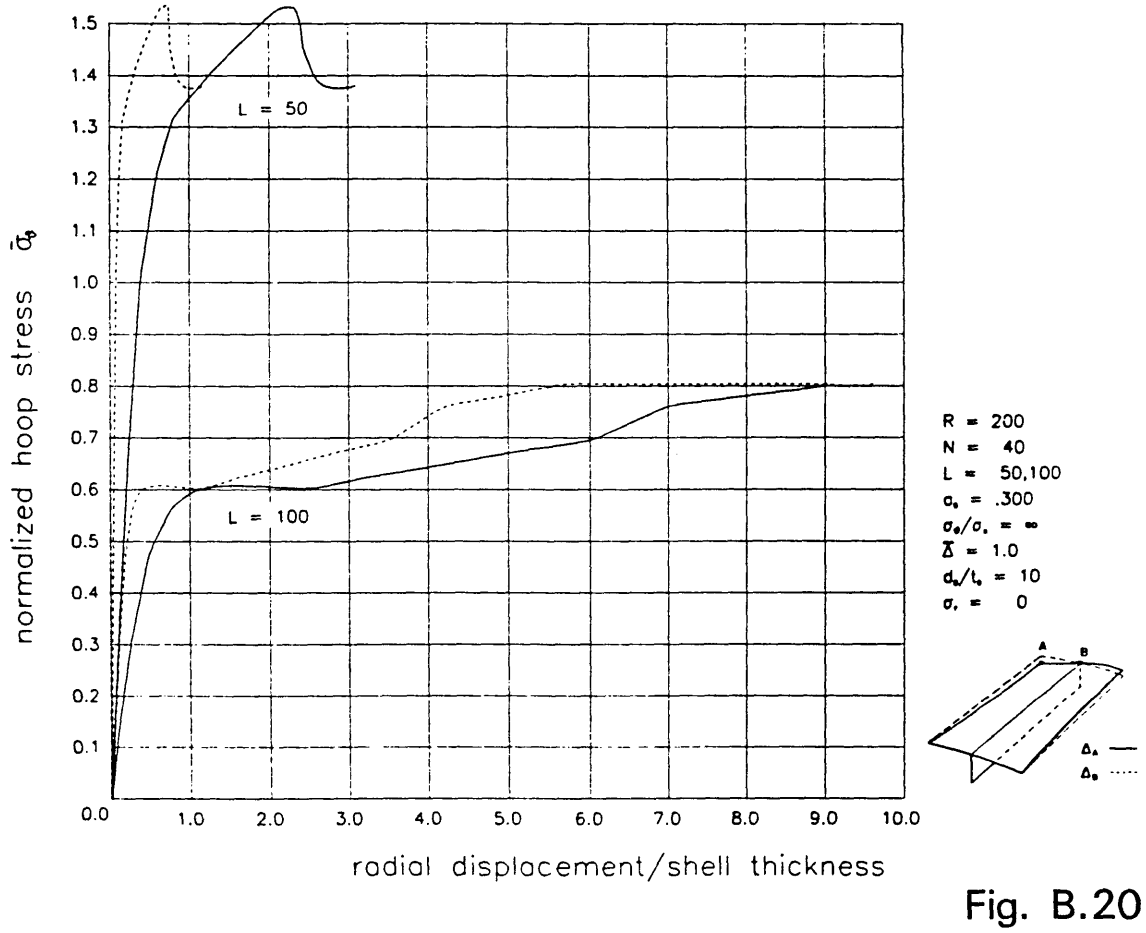


Fig. B.20

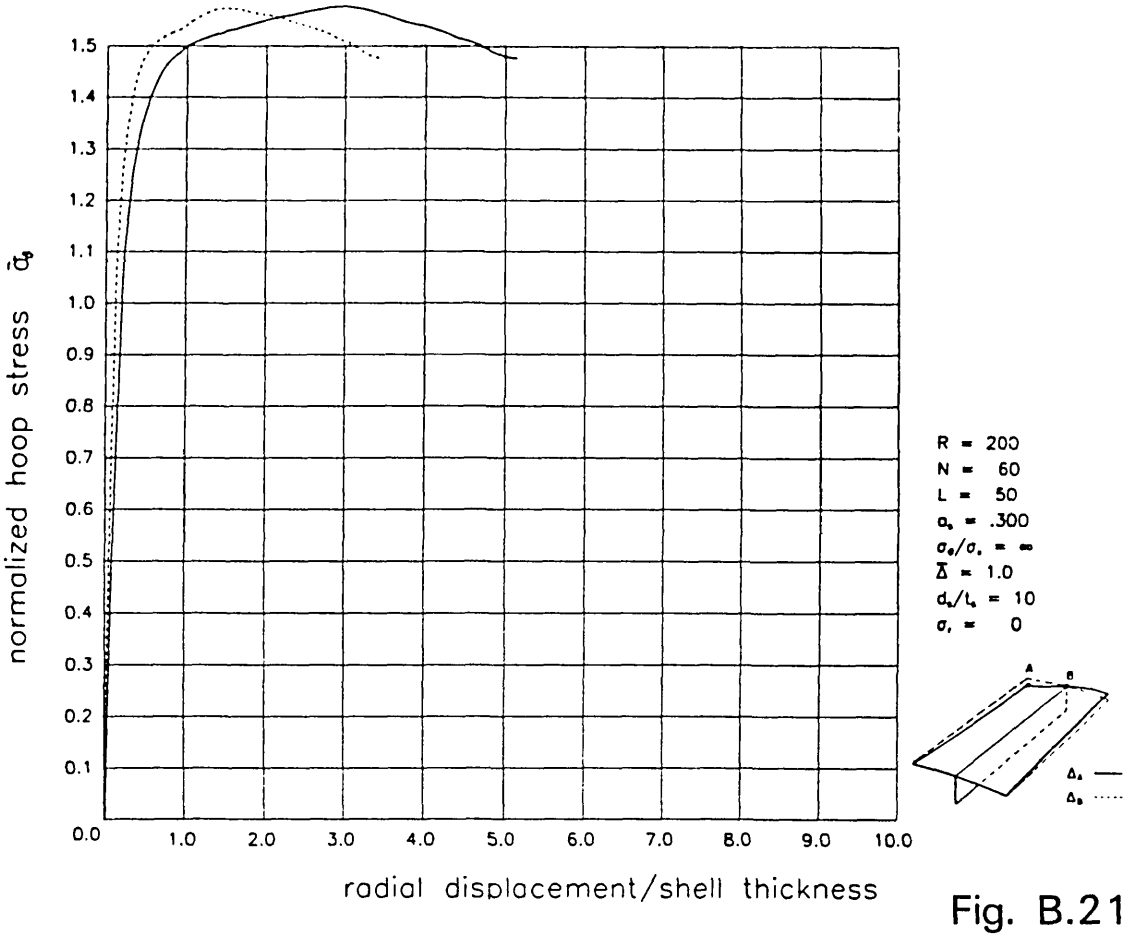


Fig. B.21

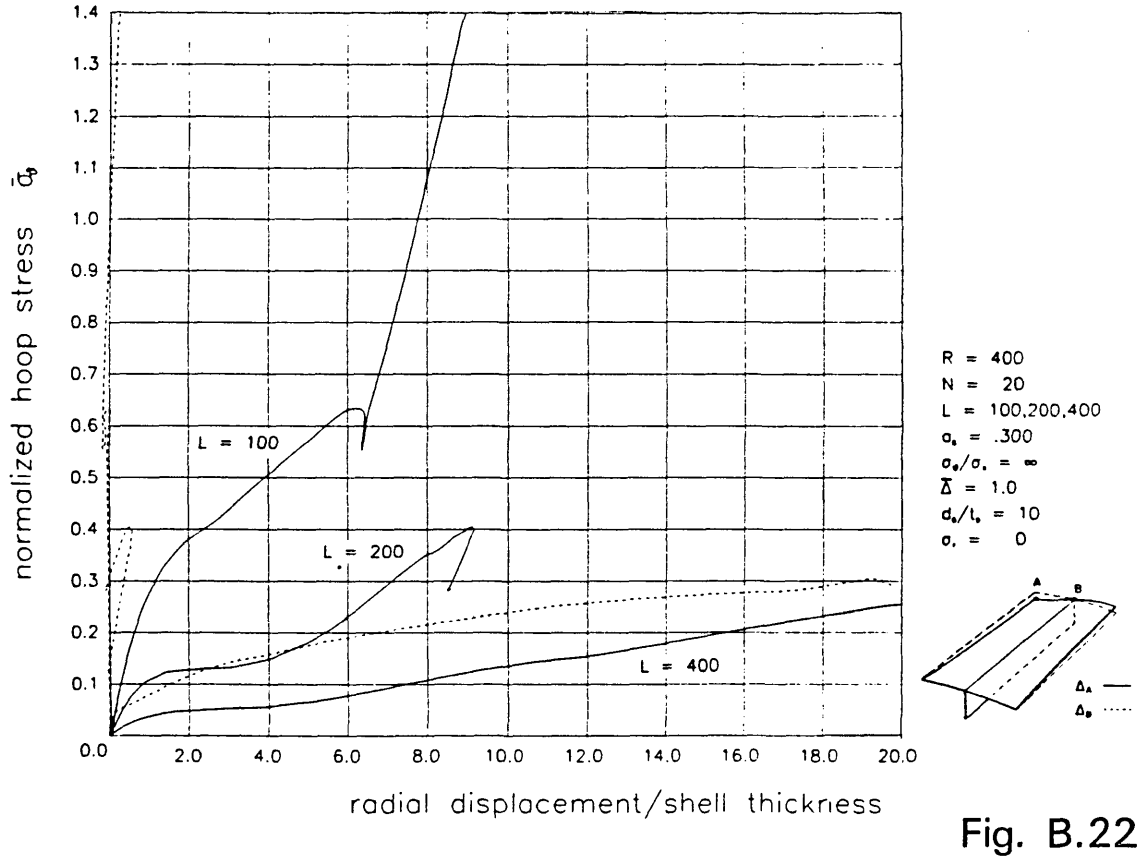


Fig. B.22

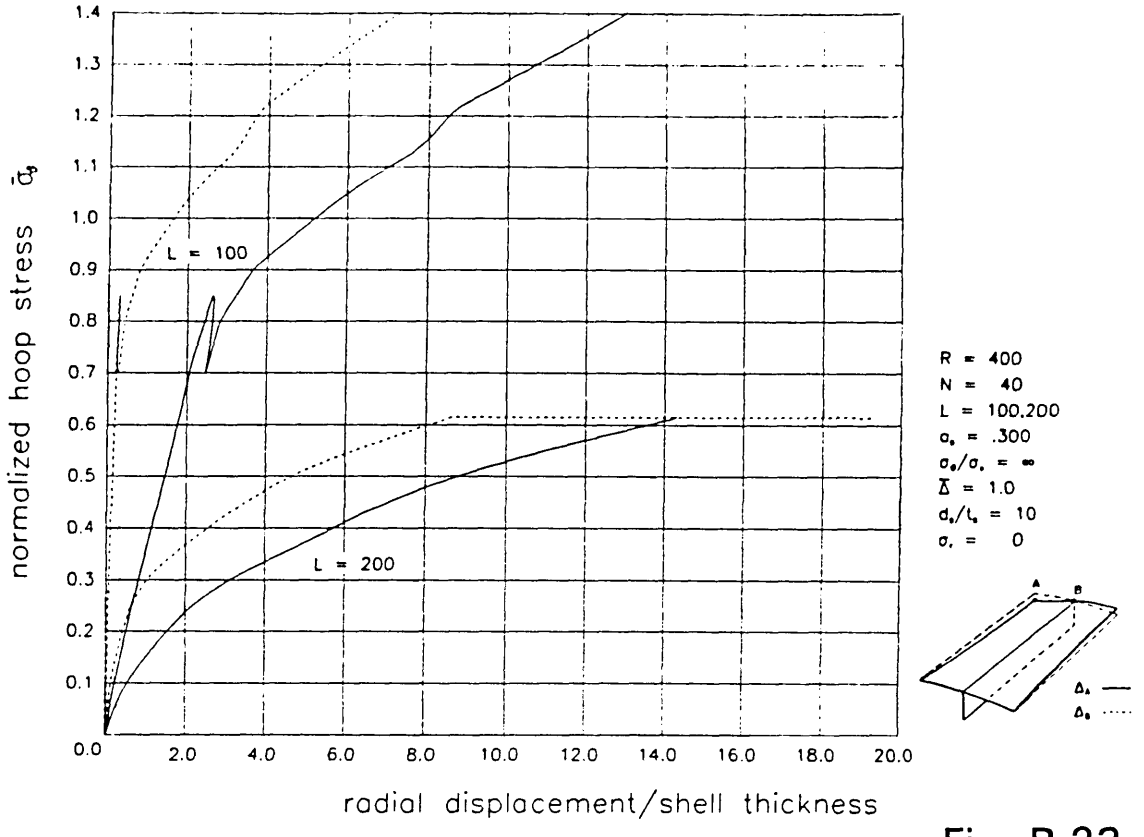


Fig. B.23

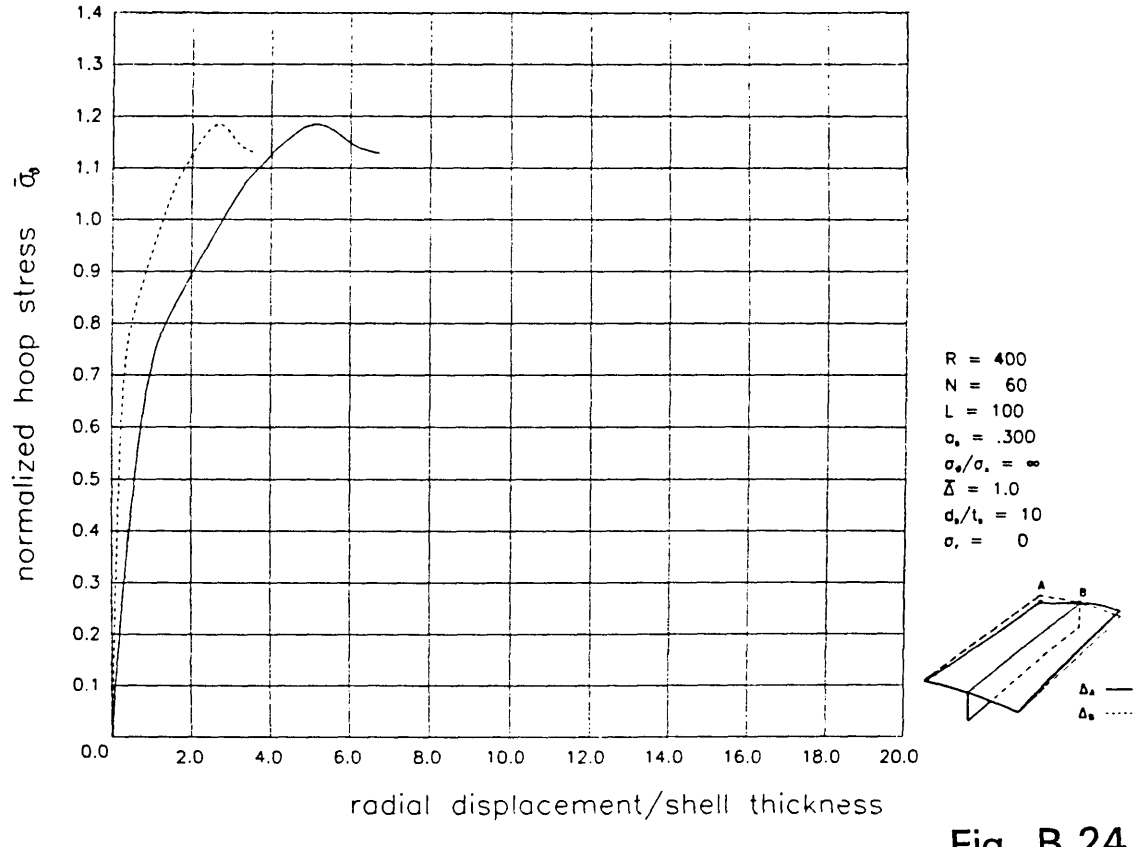


Fig. B.24

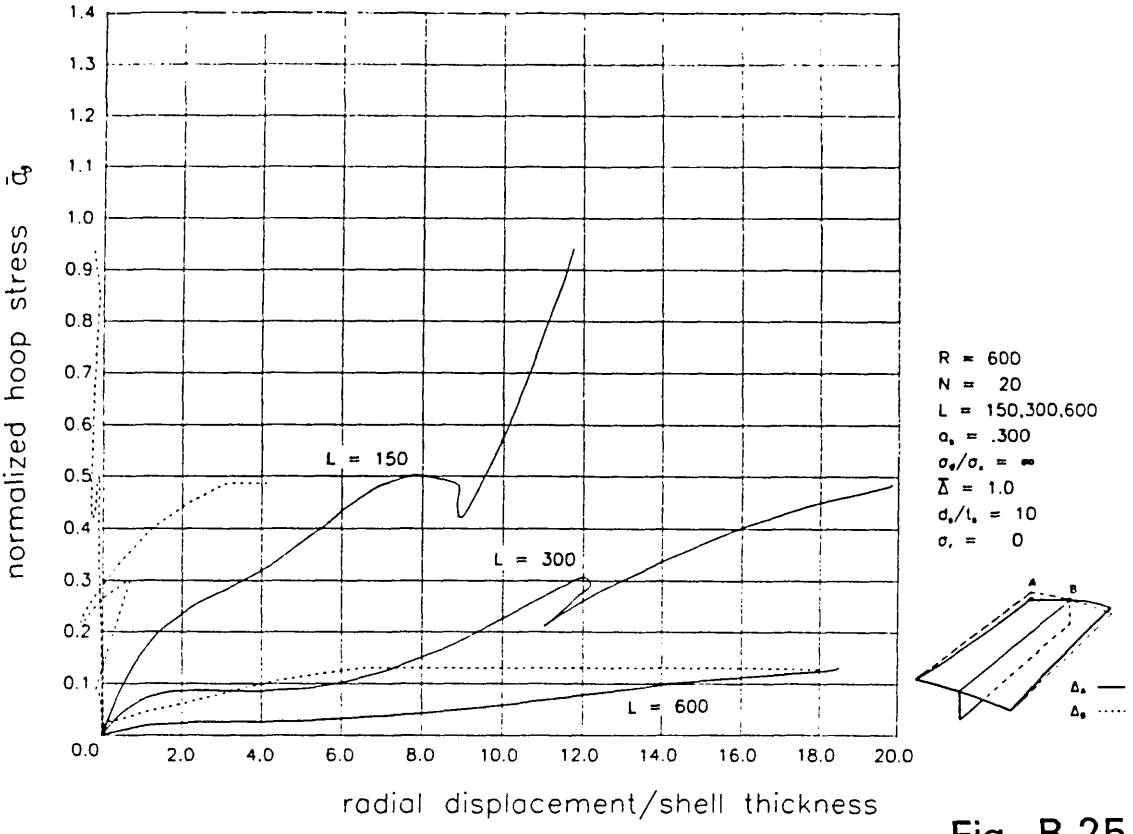


Fig. B.25

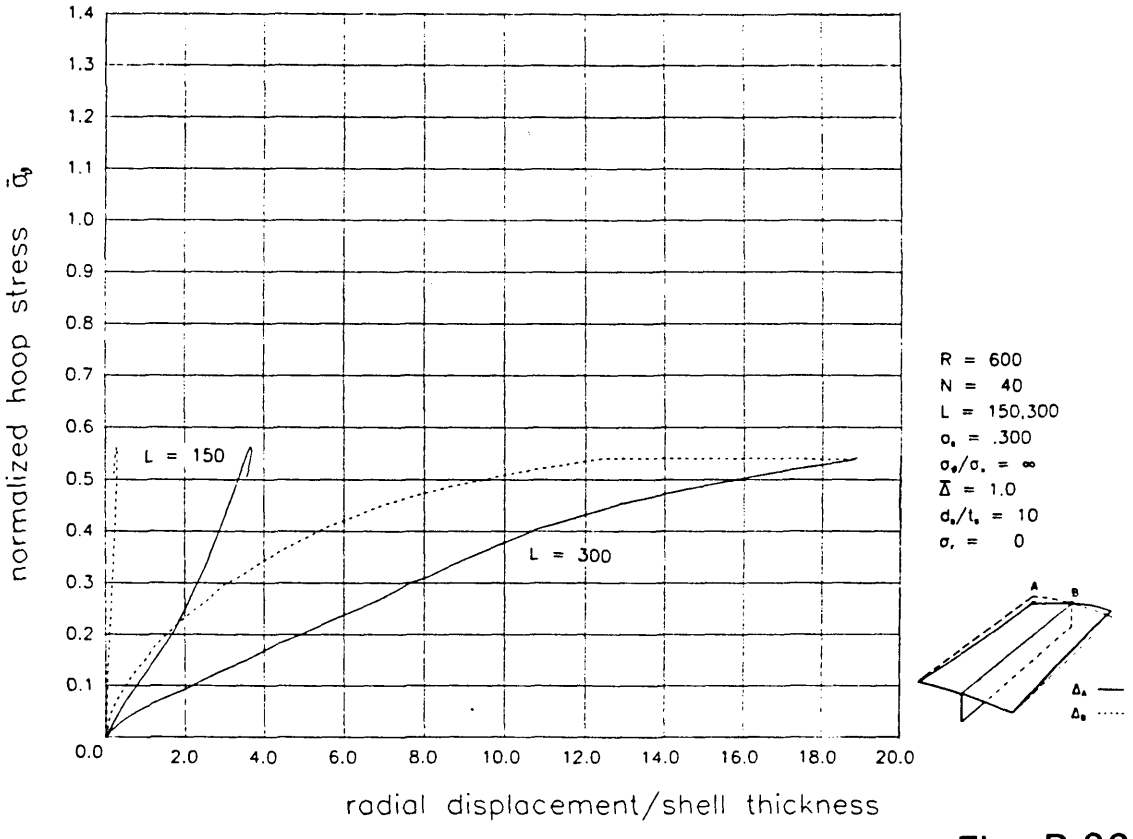


Fig. B.26

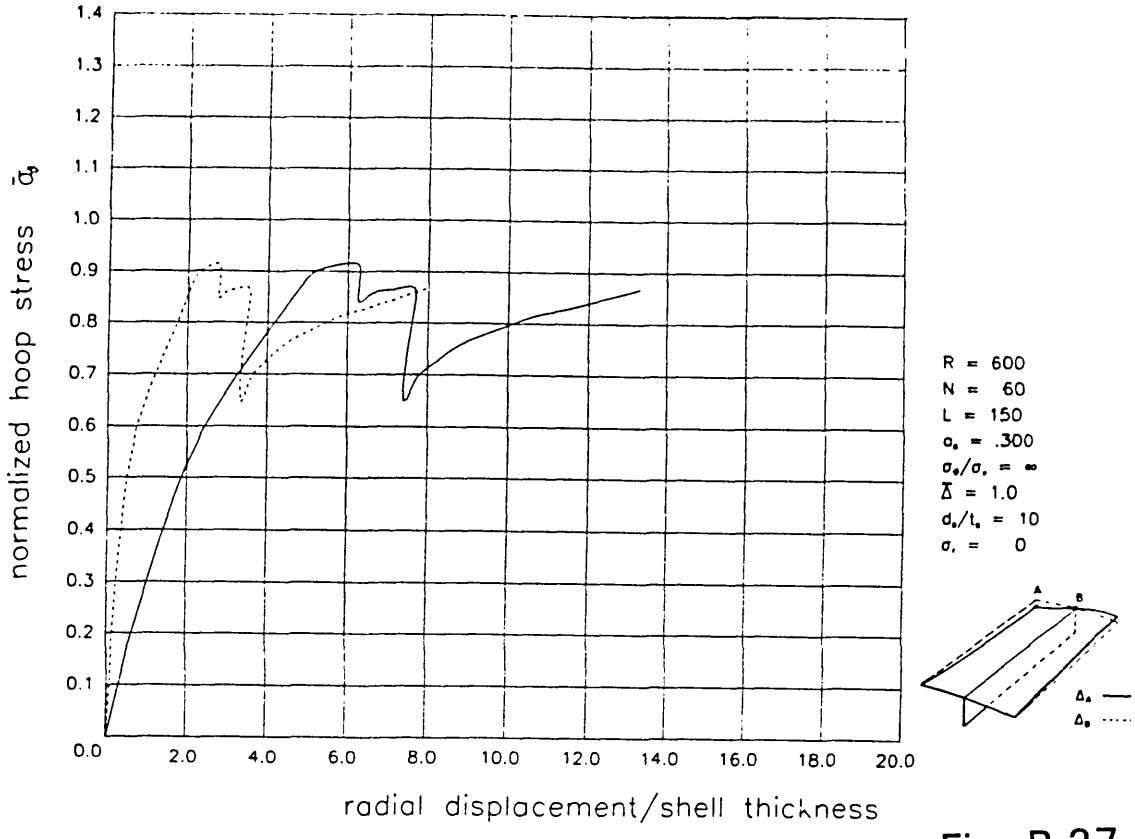


Fig. B.27

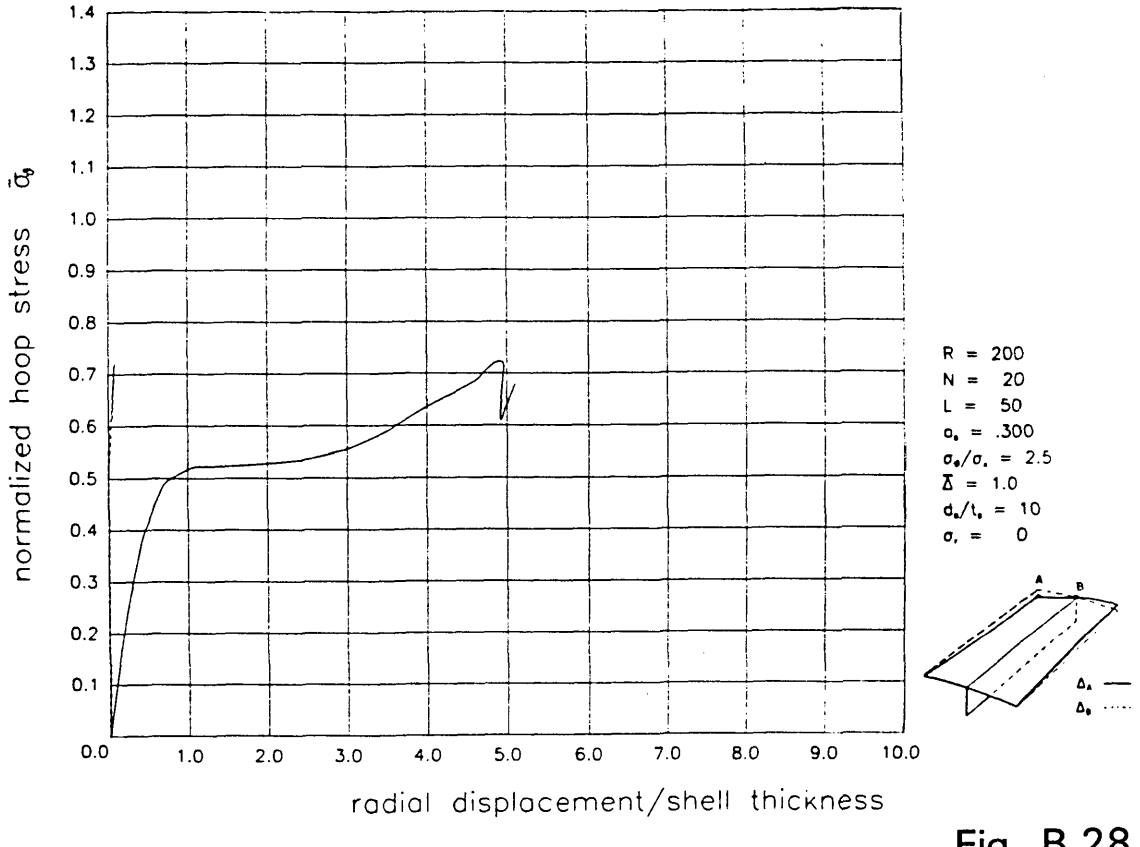


Fig. B.28

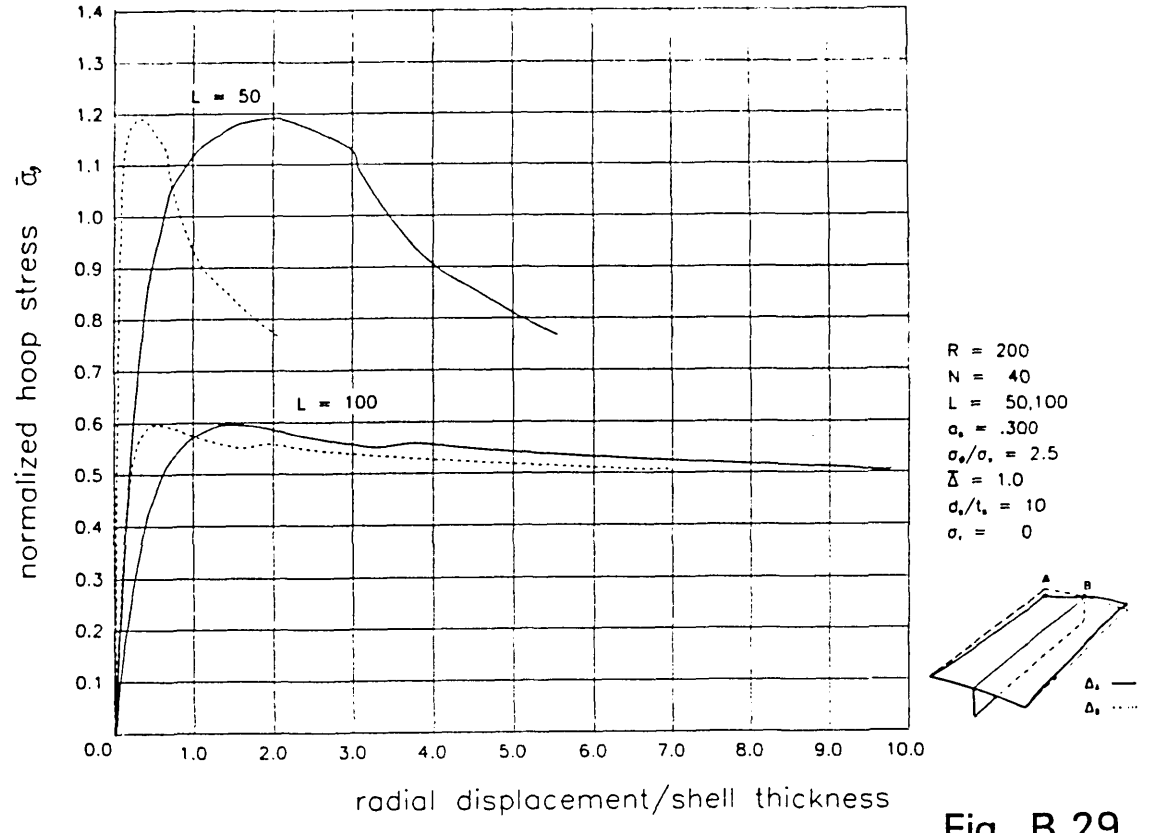


Fig. B.29

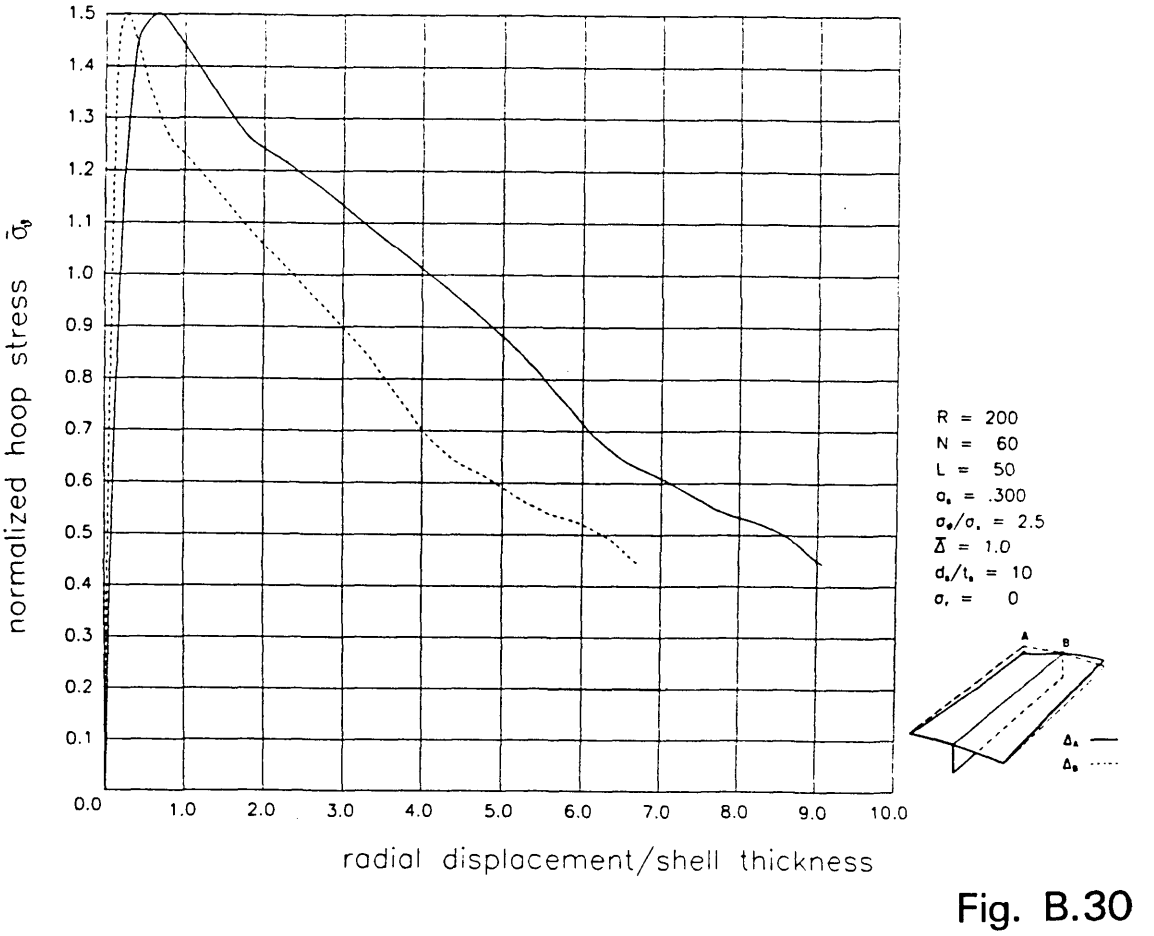


Fig. B.30

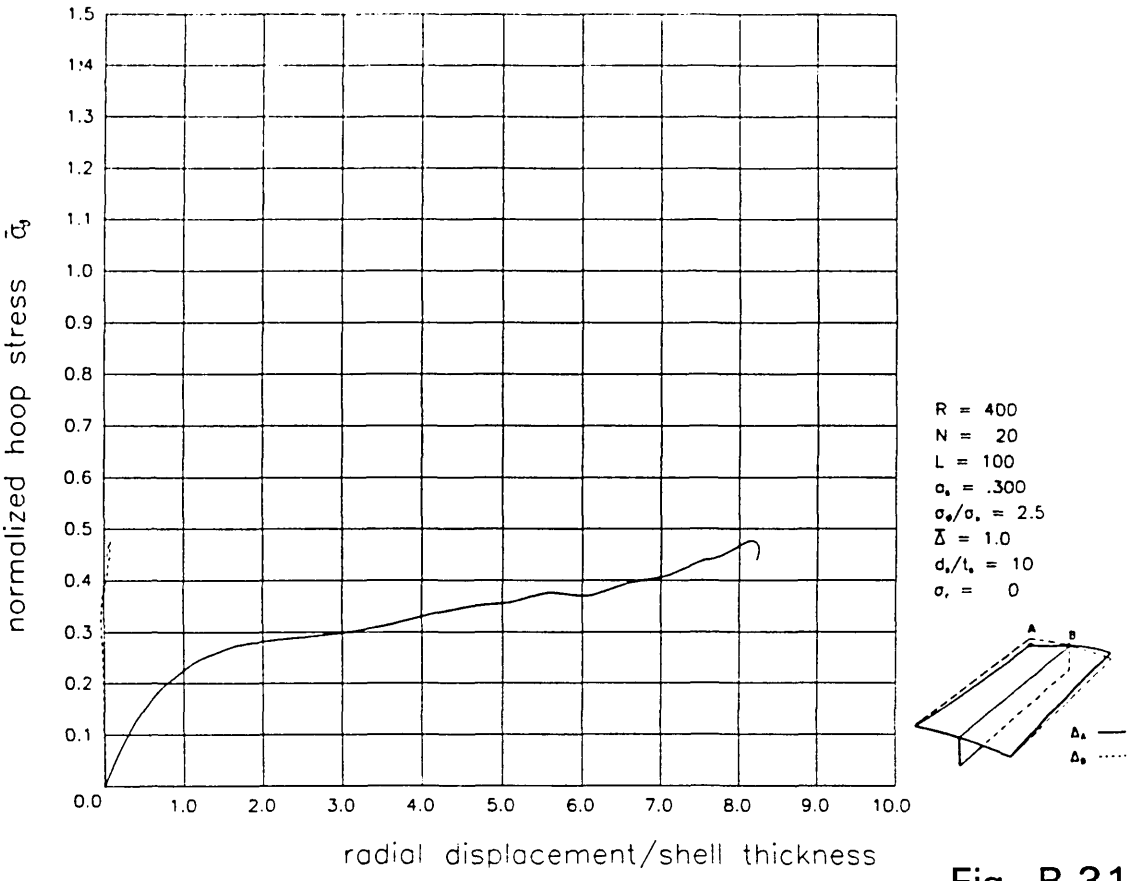


Fig. B.31

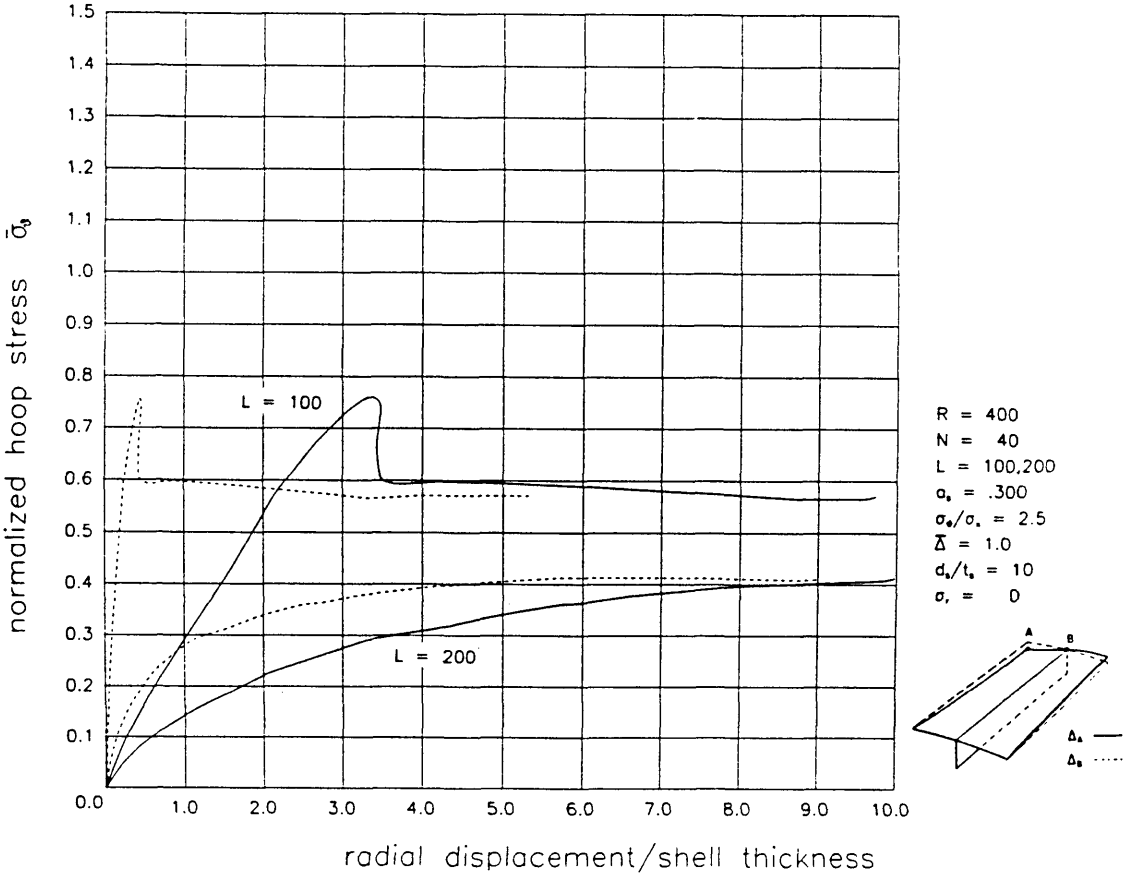


Fig. B.32

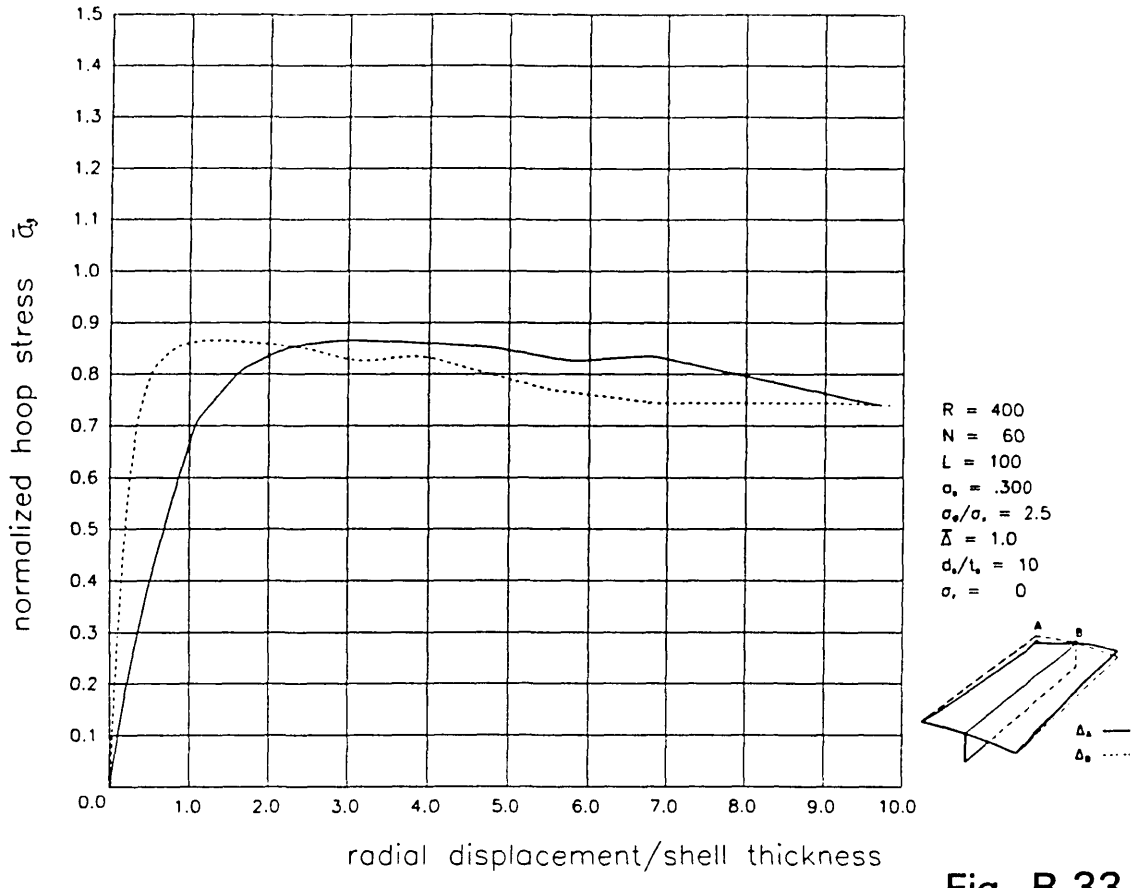


Fig. B.33

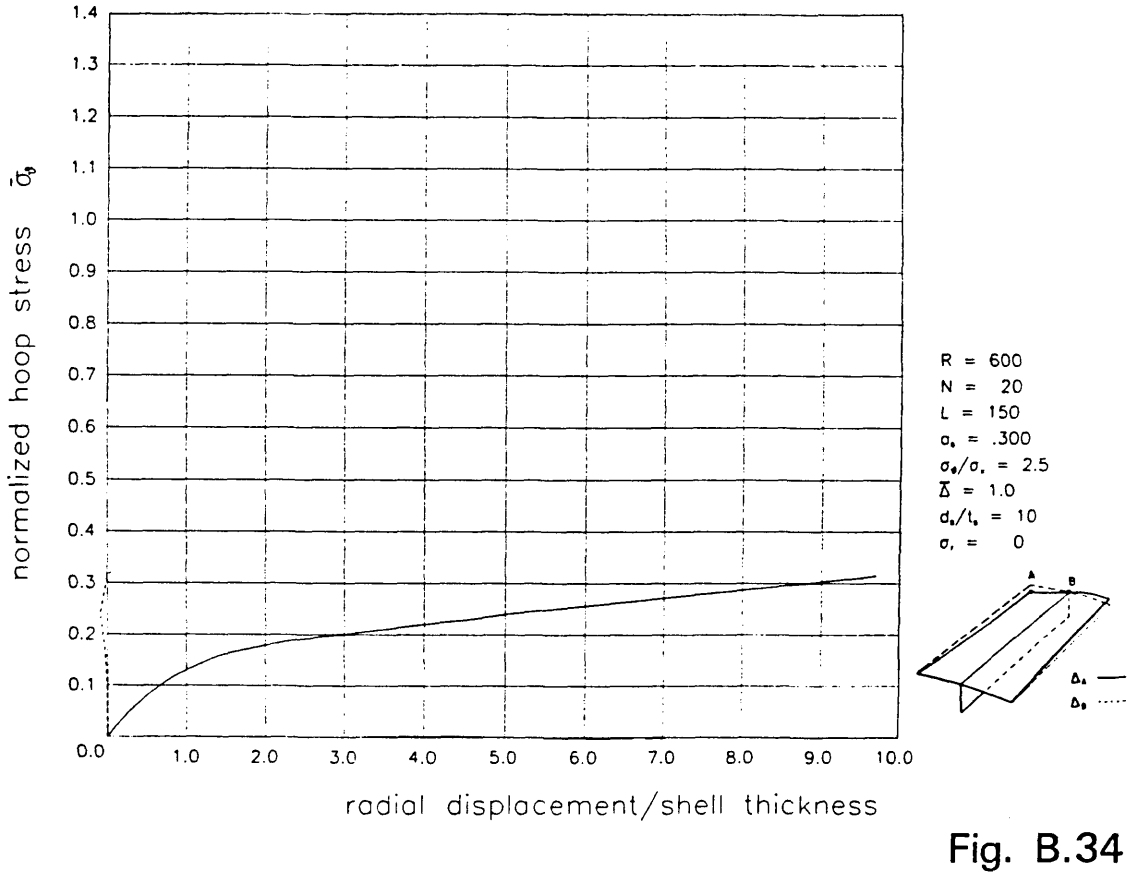


Fig. B.34

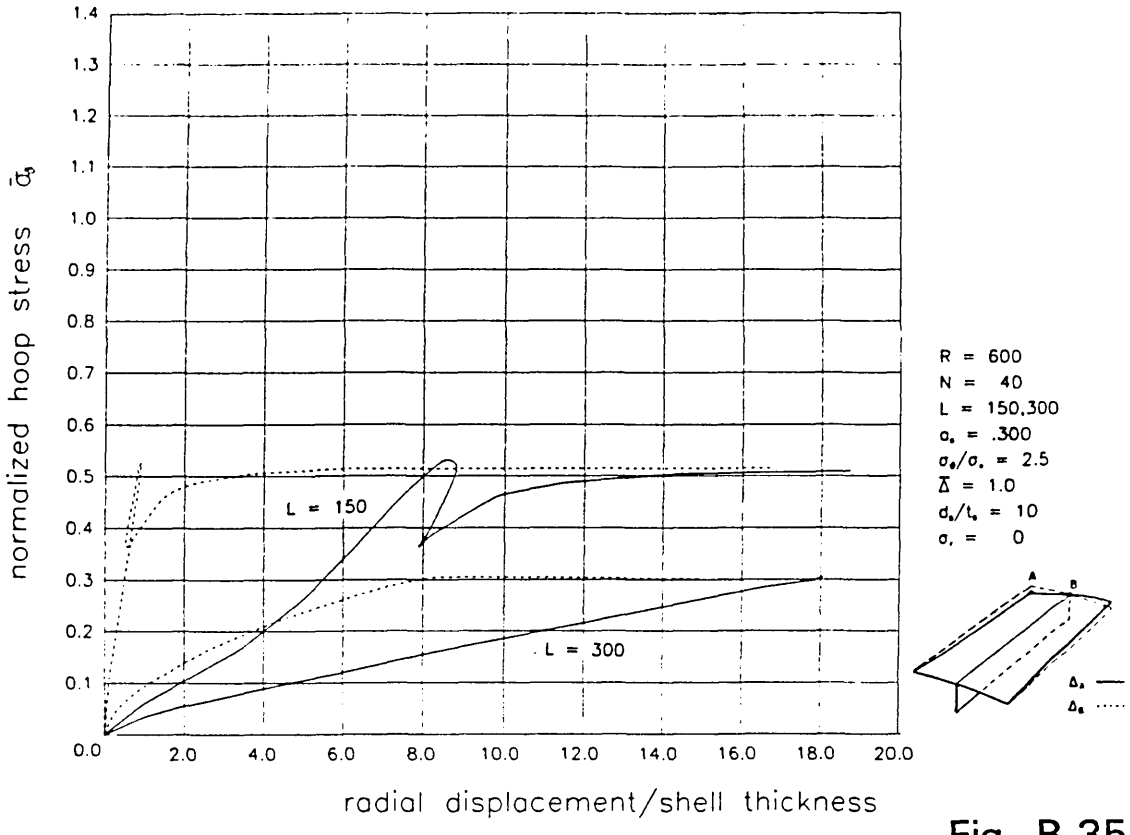


Fig. B.35

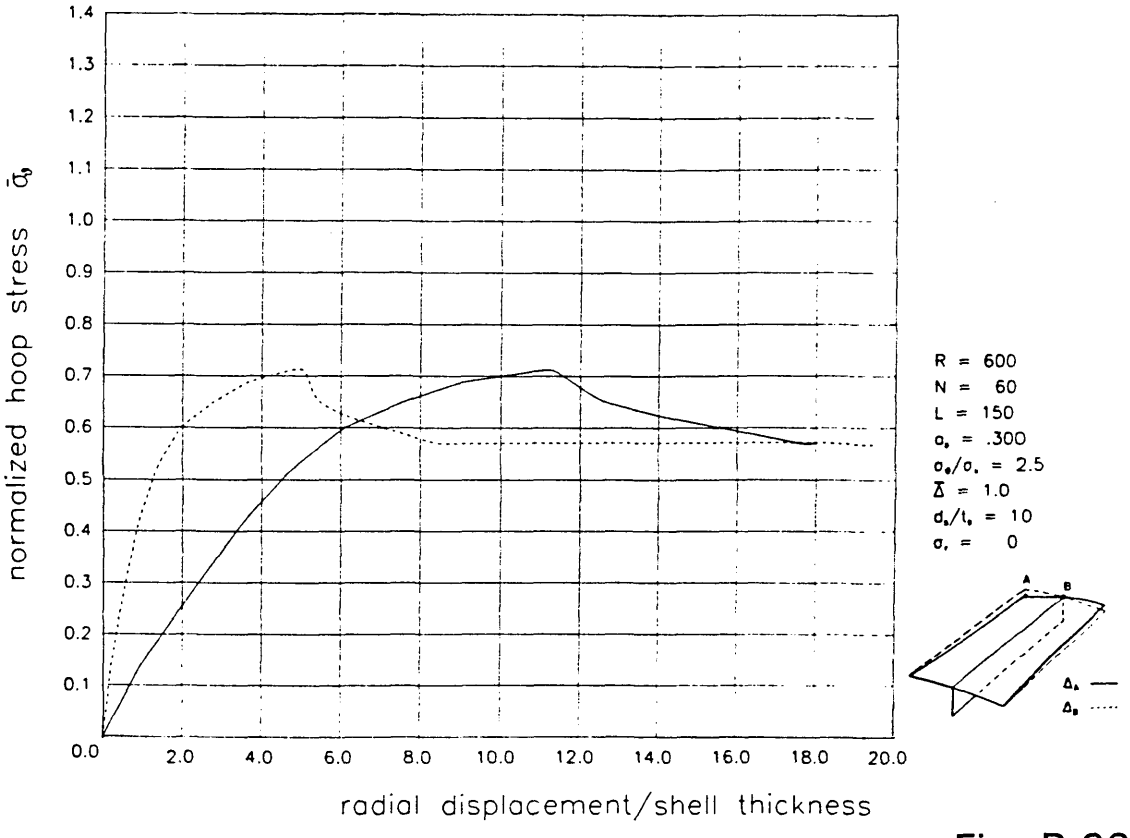


Fig. B.36

EFFECT OF INITIAL IMPERFECTIONS

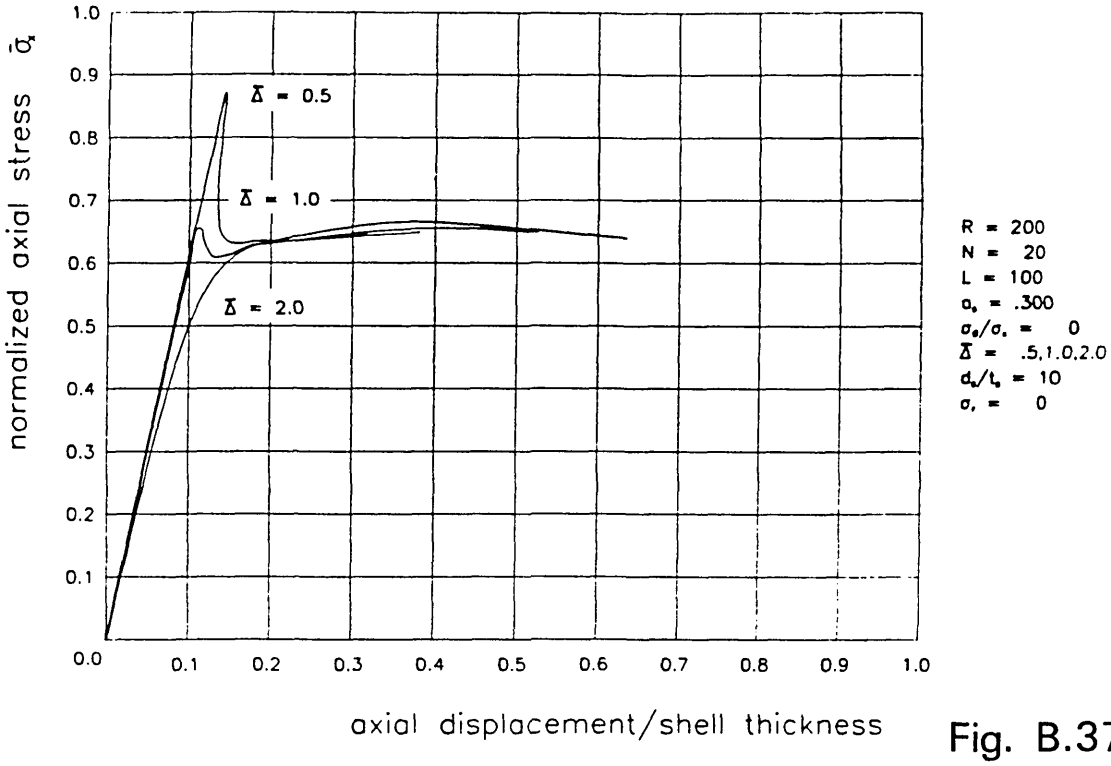


Fig. B.37

EFFECT OF INITIAL IMPERFECTIONS

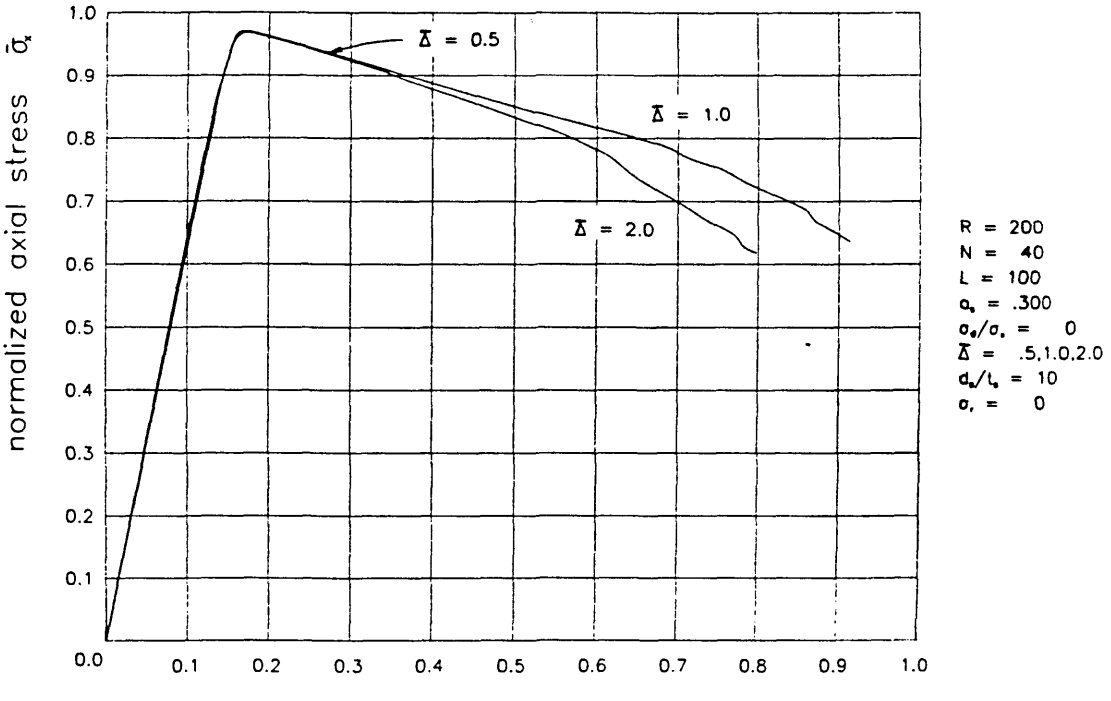


Fig. B.38

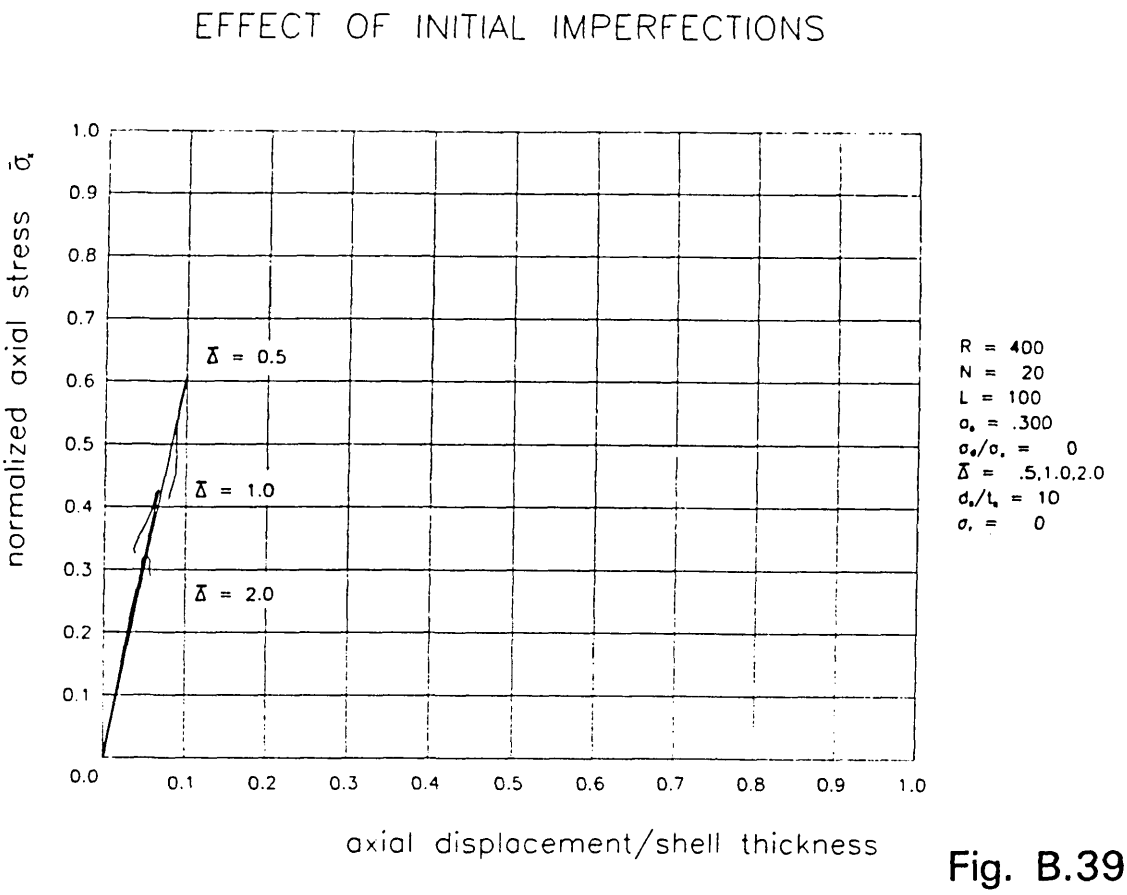


Fig. B.39

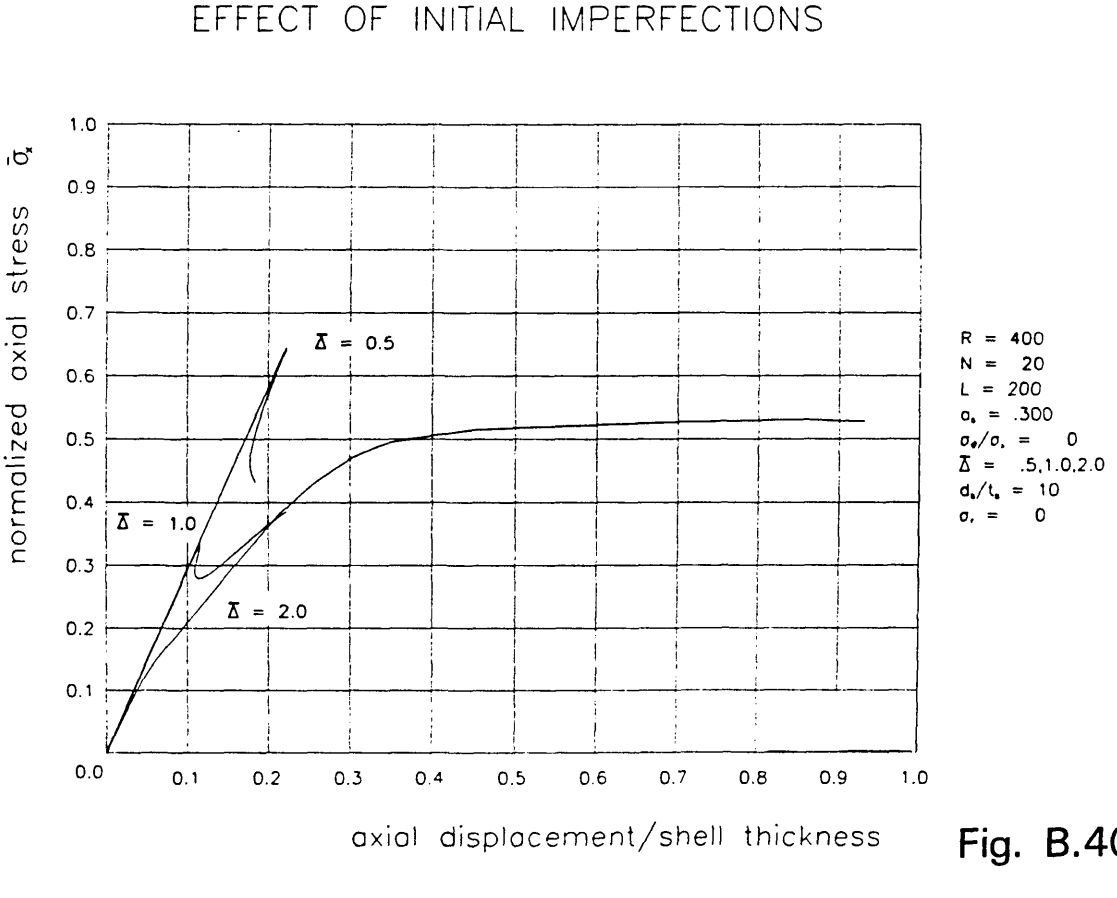
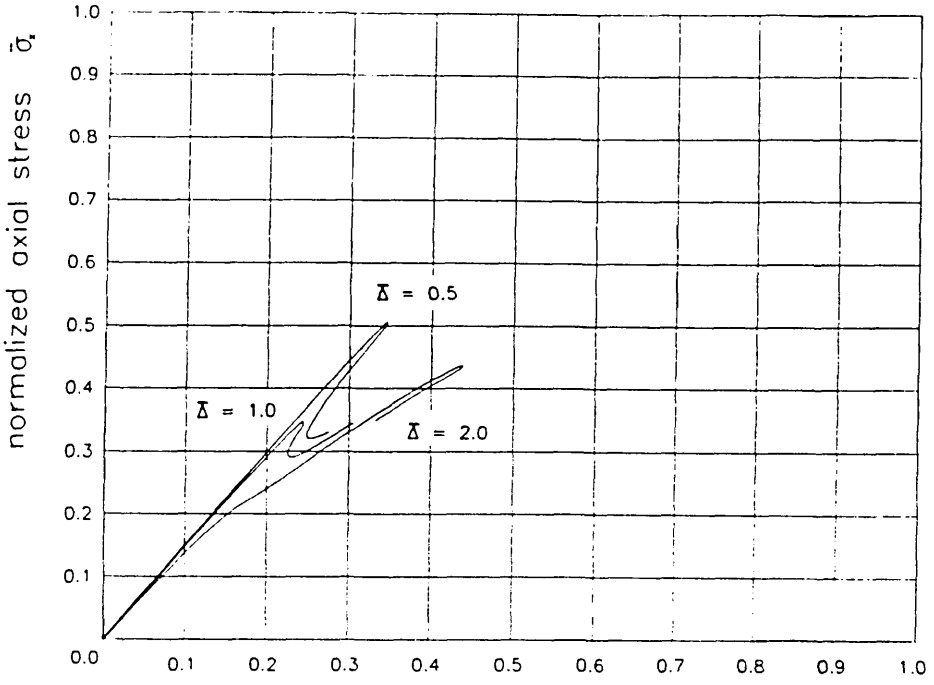


Fig. B.40

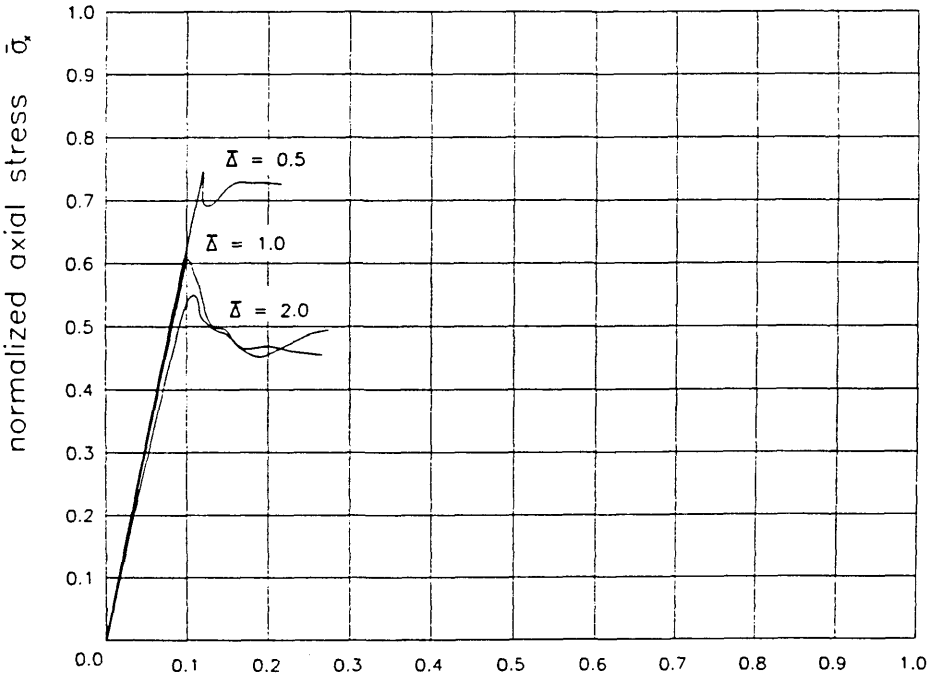
EFFECT OF INITIAL IMPERFECTIONS



R = 400
N = 20
L = 400
a_o = .300
σ_ϕ/σ_o = 0
$\bar{\Delta}$ = .5,1.0,2.0
d_o/t_o = 10
σ_r = 0

Fig. B.41

EFFECT OF INITIAL IMPERFECTIONS



R = 400
N = 40
L = 100
a_o = .300
σ_ϕ/σ_o = 0
$\bar{\Delta}$ = .5,1.0,2.0
d_o/t_o = 10
σ_r = 0

Fig. B.42

EFFECT OF INITIAL IMPERFECTIONS

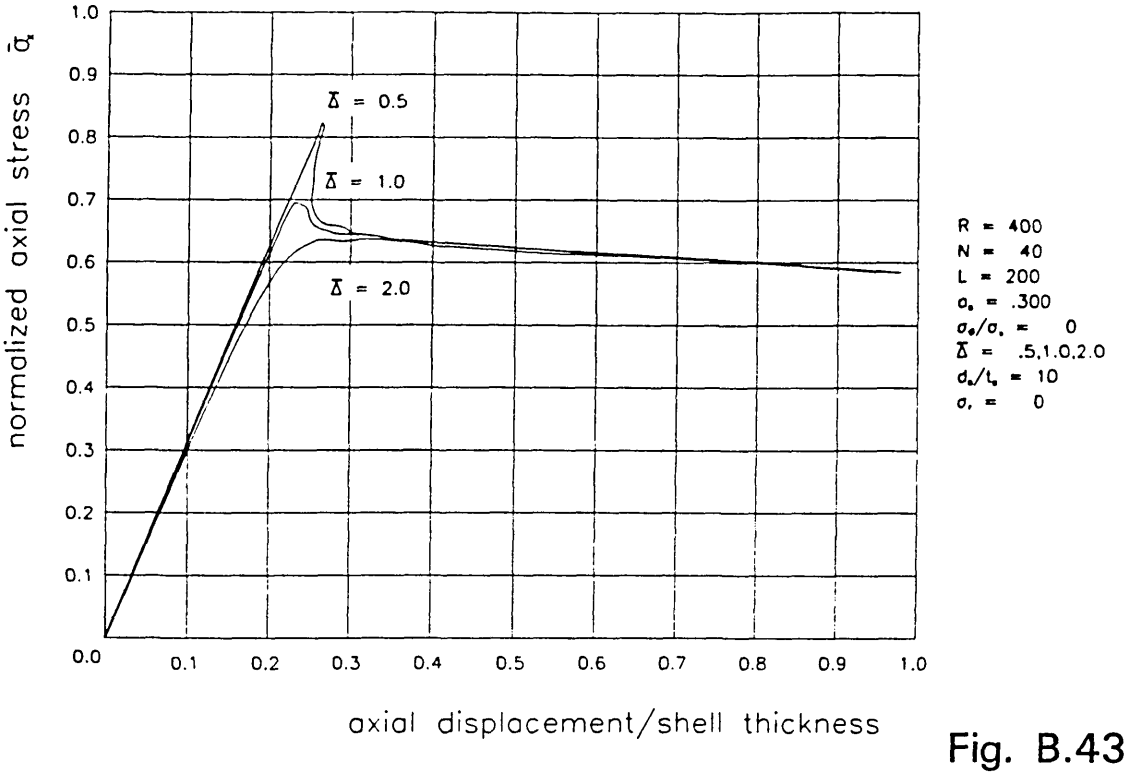


Fig. B.43

EFFECT OF INITIAL IMPERFECTIONS

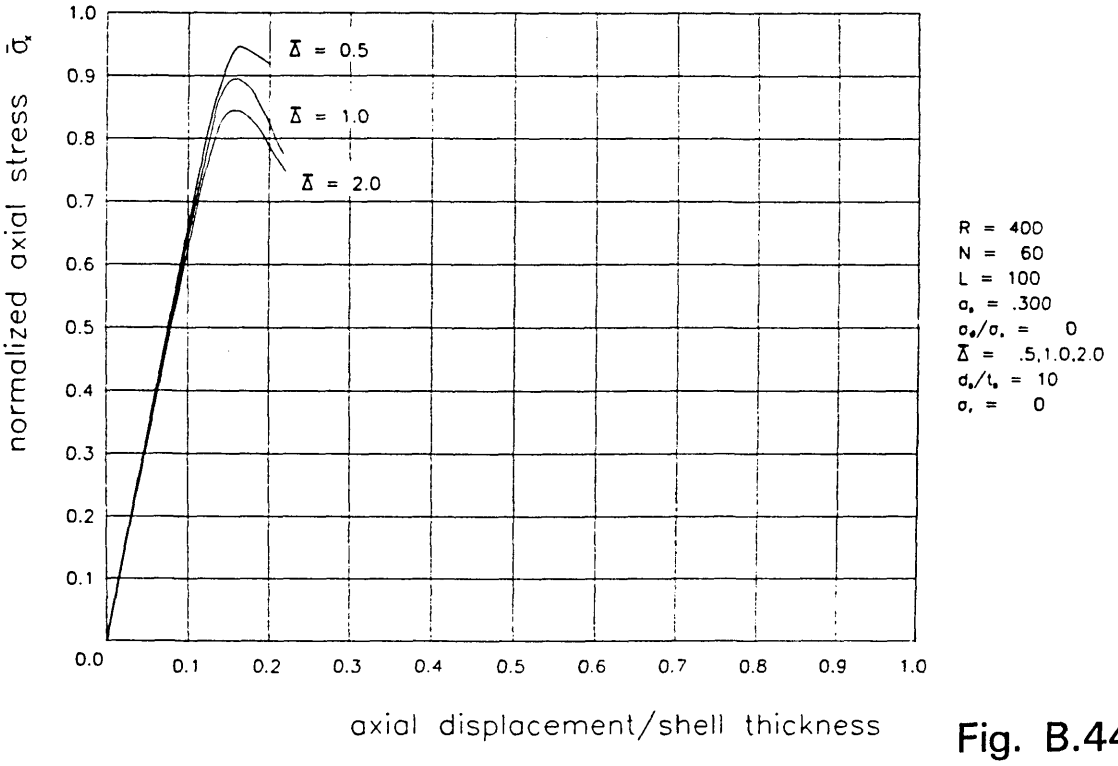


Fig. B.44

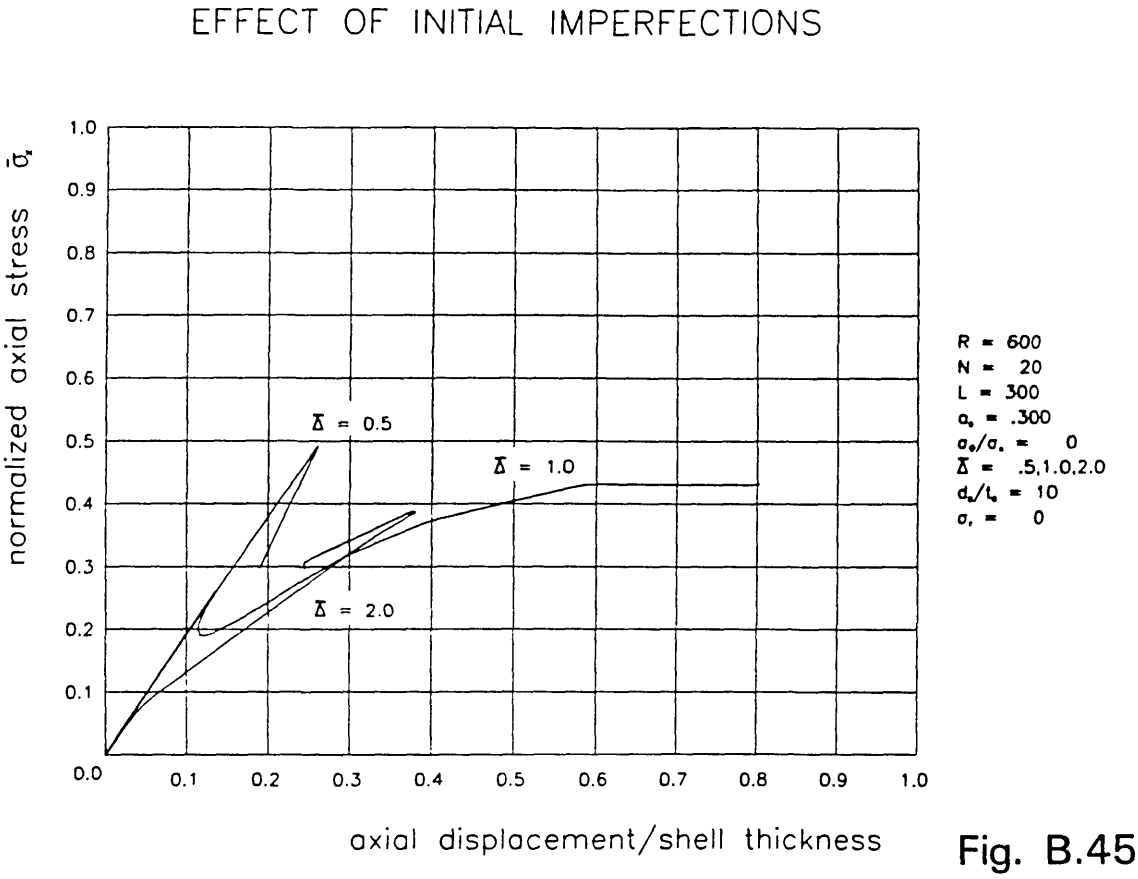


Fig. B.45

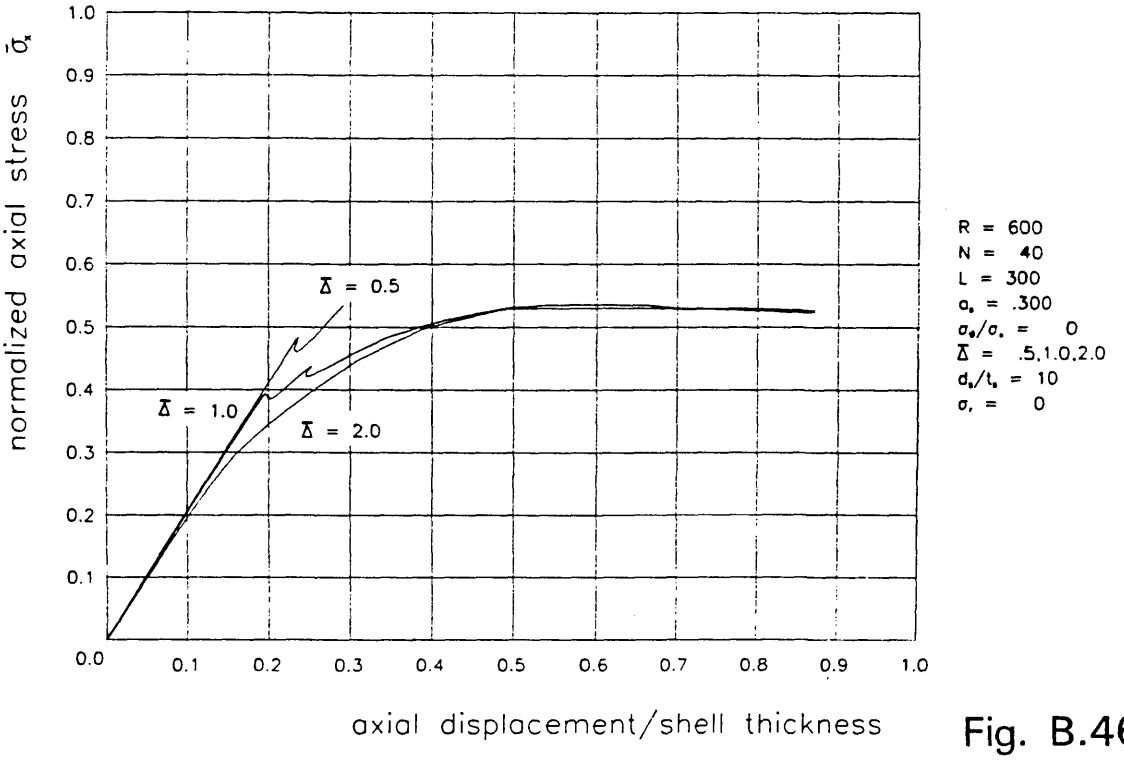
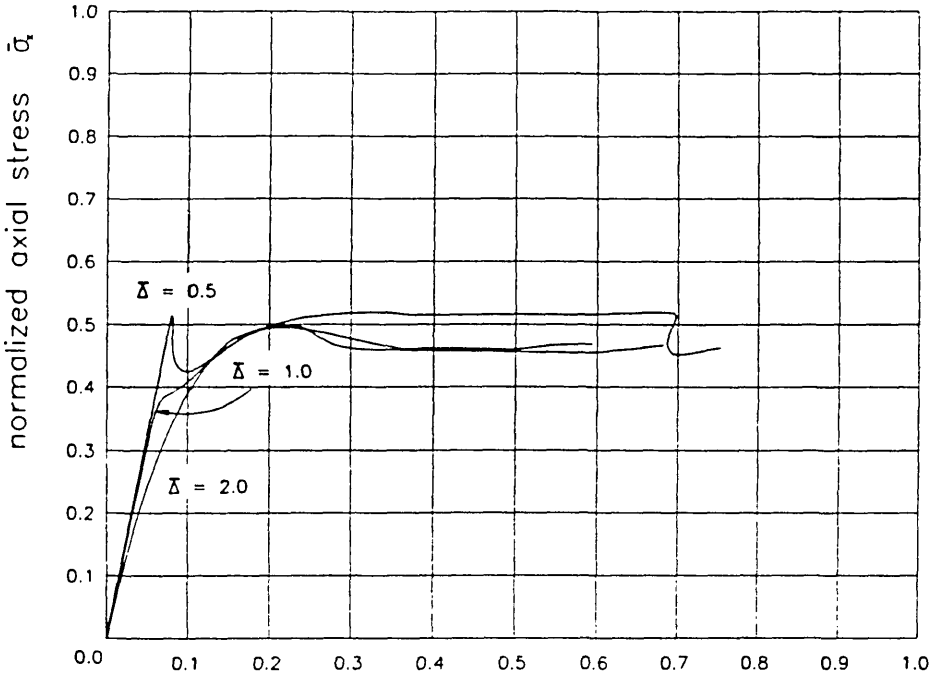


Fig. B.46

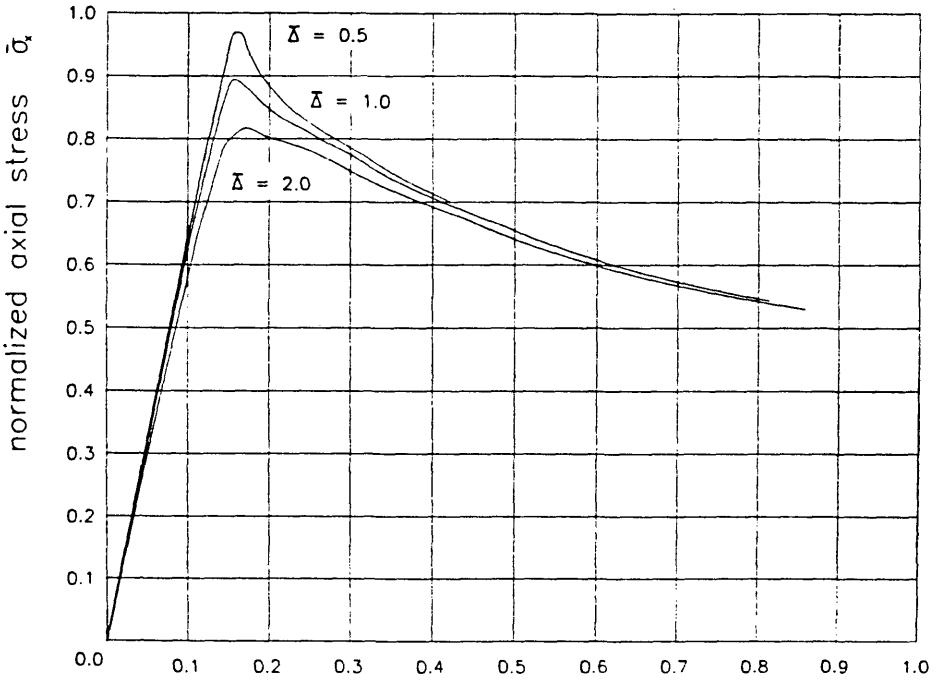
EFFECT OF INITIAL IMPERFECTIONS



R = 200
N = 20
L = 100
a_o = .300
σ_o/σ_x = .4
$\bar{\Delta}$ = .5,1.0,2.0
d_o/t_o = 10
σ_r = 0

Fig. B.47

EFFECT OF INITIAL IMPERFECTIONS



R = 200
N = 40
L = 100
a_o = .300
σ_o/σ_x = .4
$\bar{\Delta}$ = .5,1.0,2.0
d_o/t_o = 10
σ_r = 0

Fig. B.48

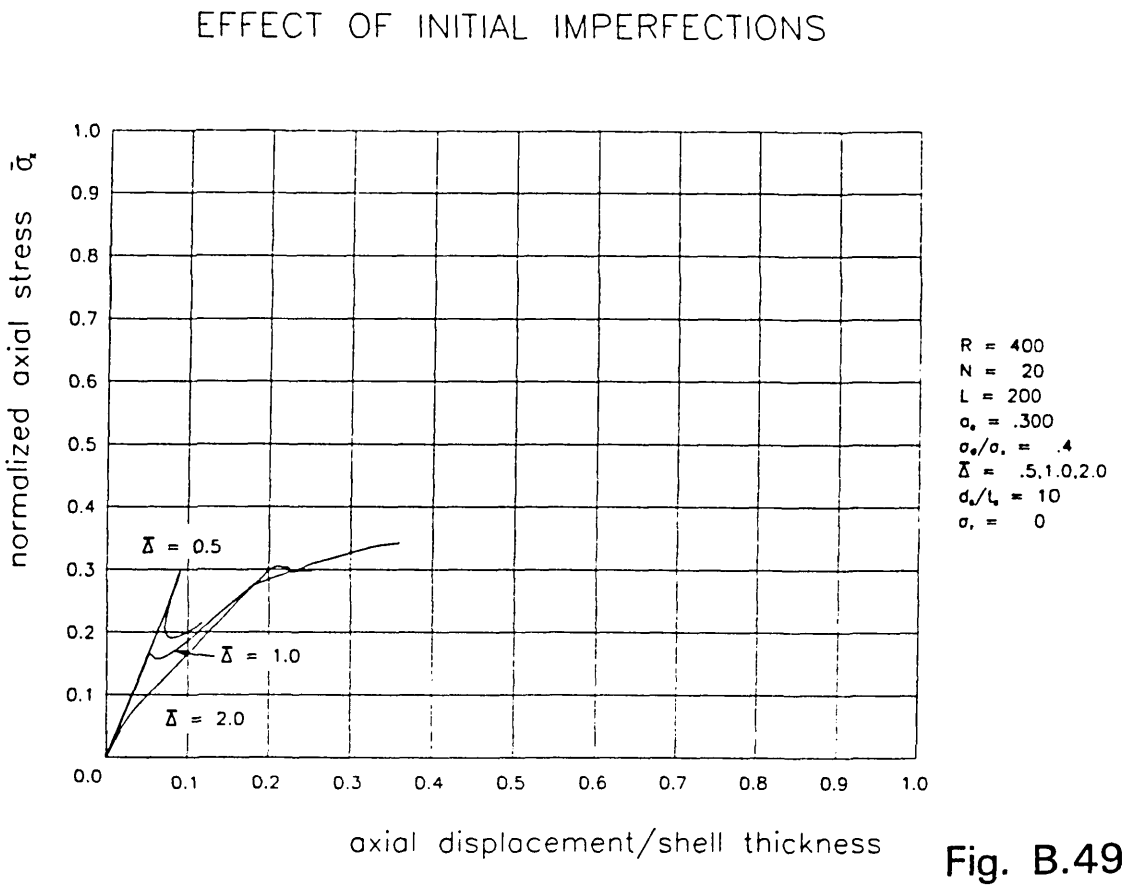


Fig. B.49

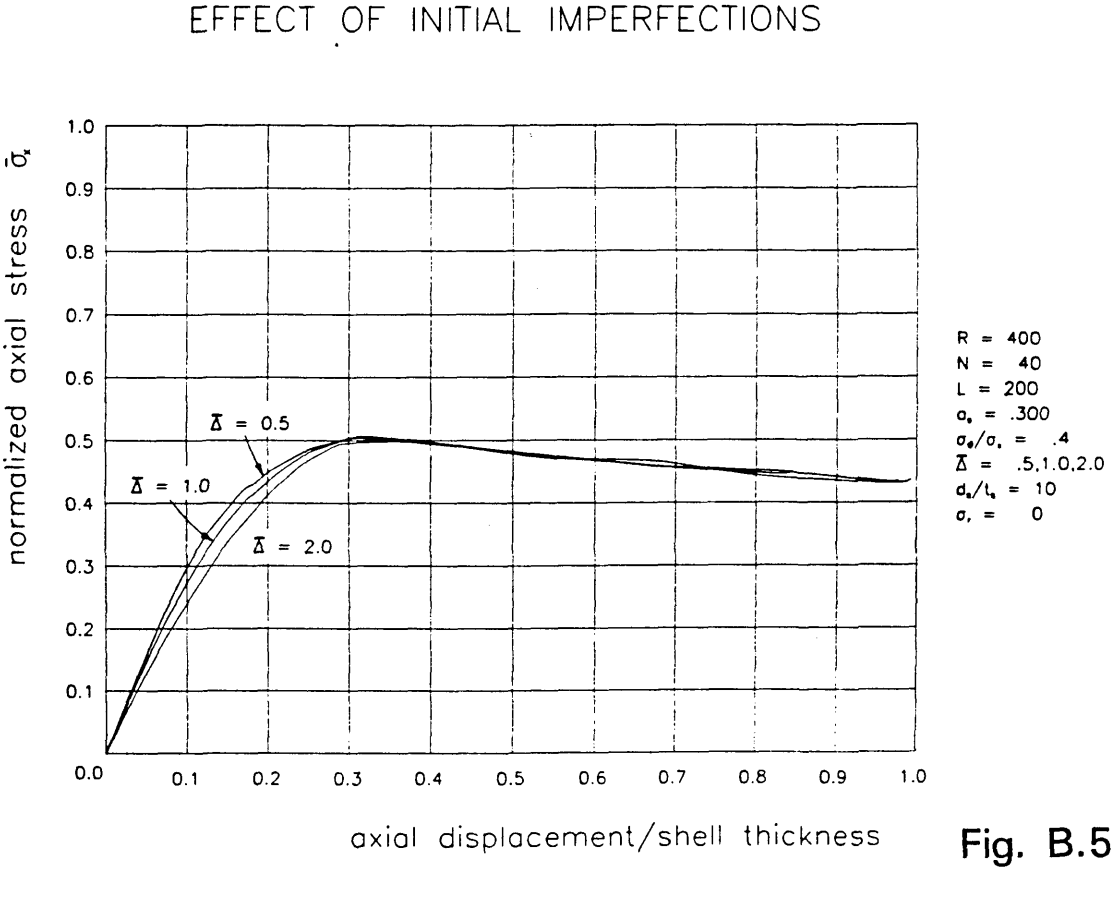


Fig. B.50

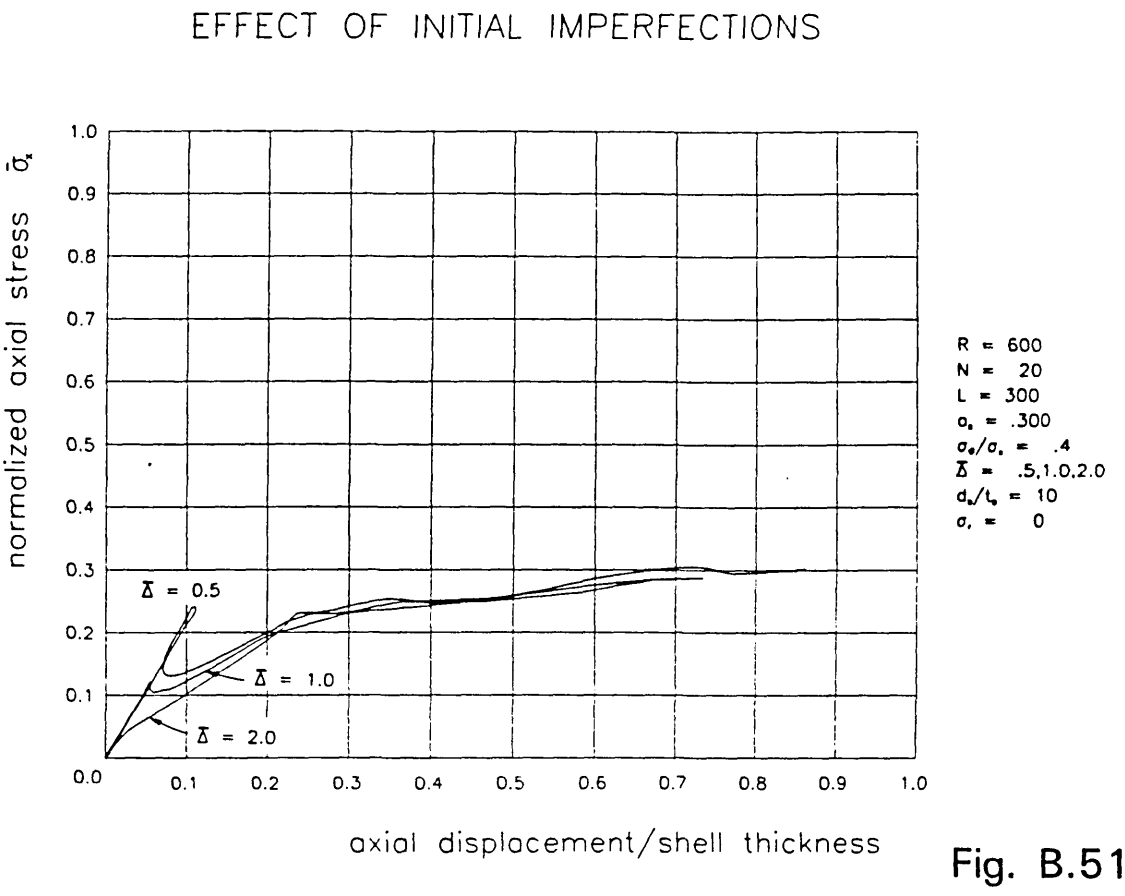


Fig. B.51

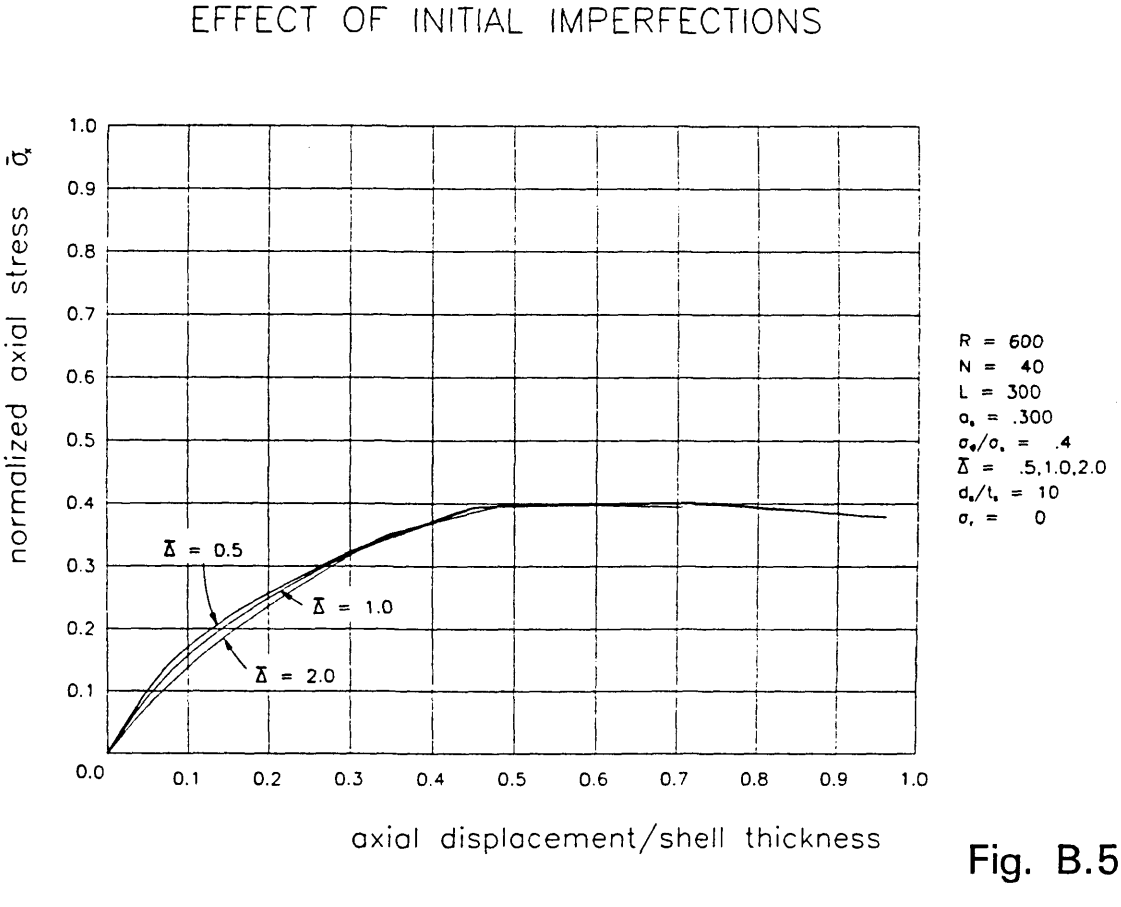


Fig. B.52

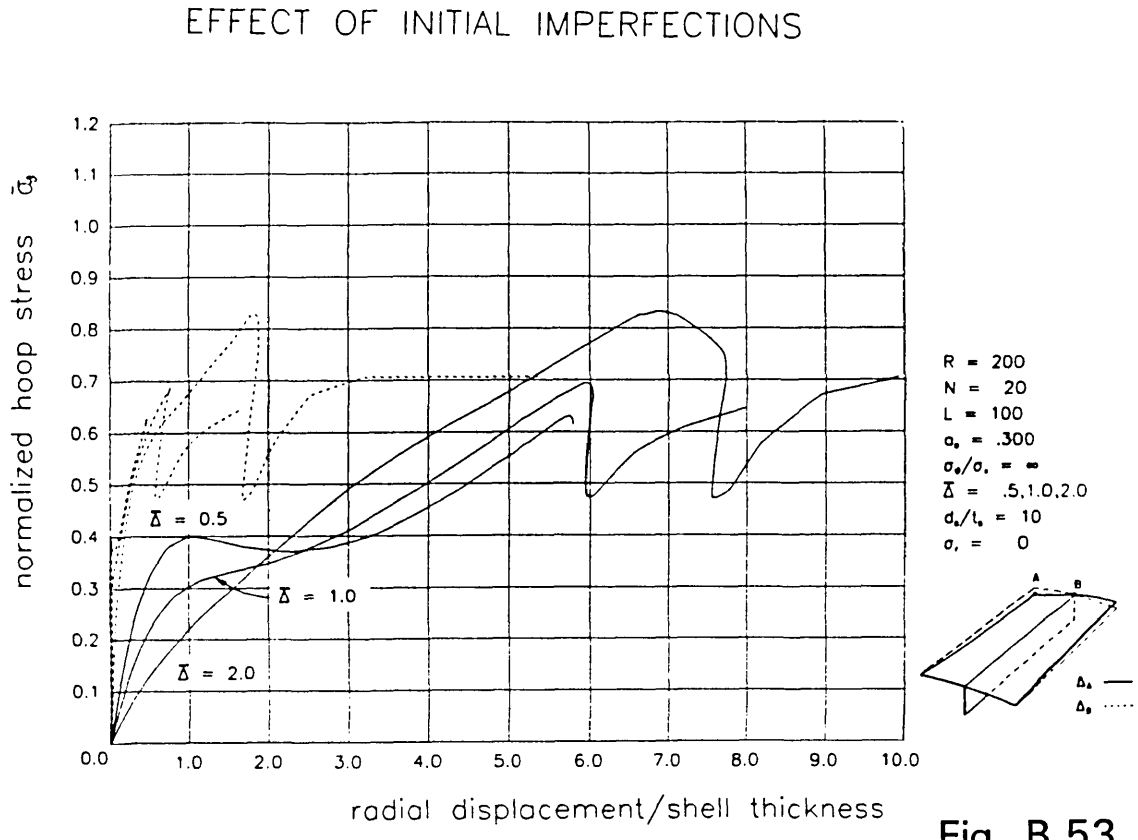


Fig. B.53

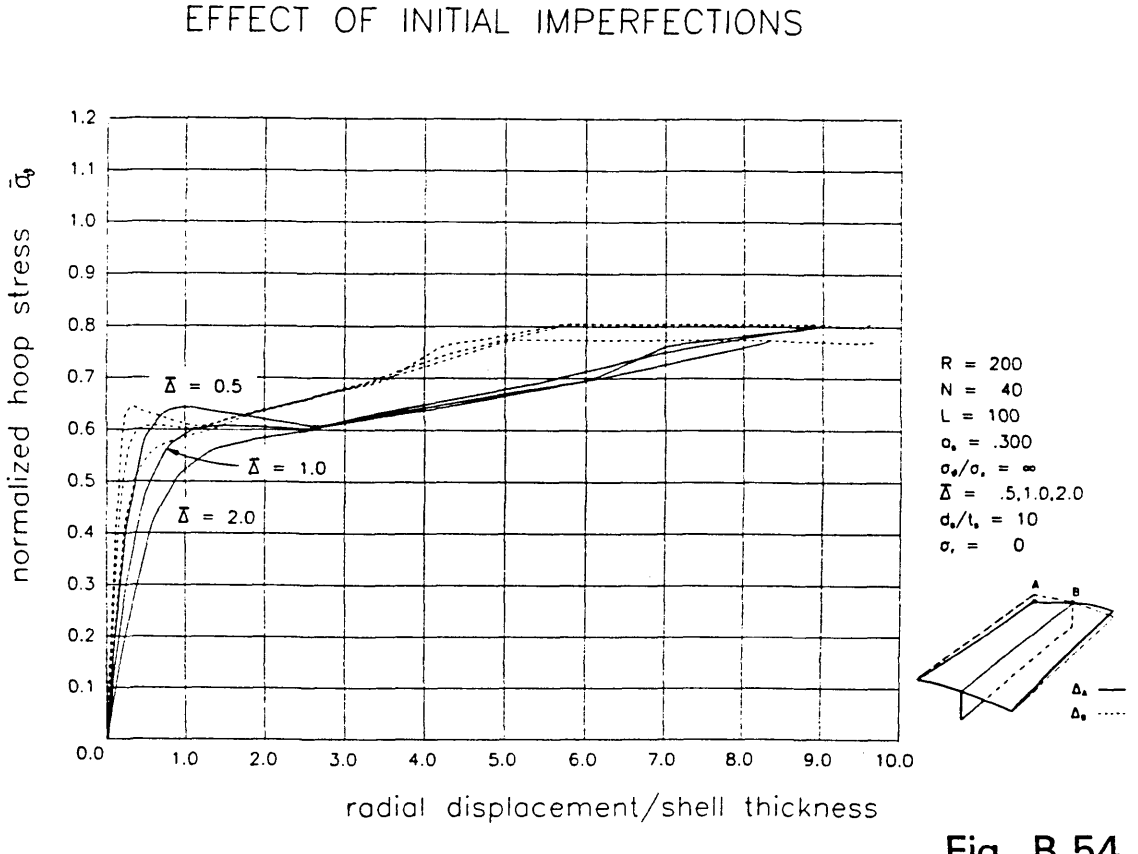


Fig. B.54

EFFECT OF INITIAL IMPERFECTIONS

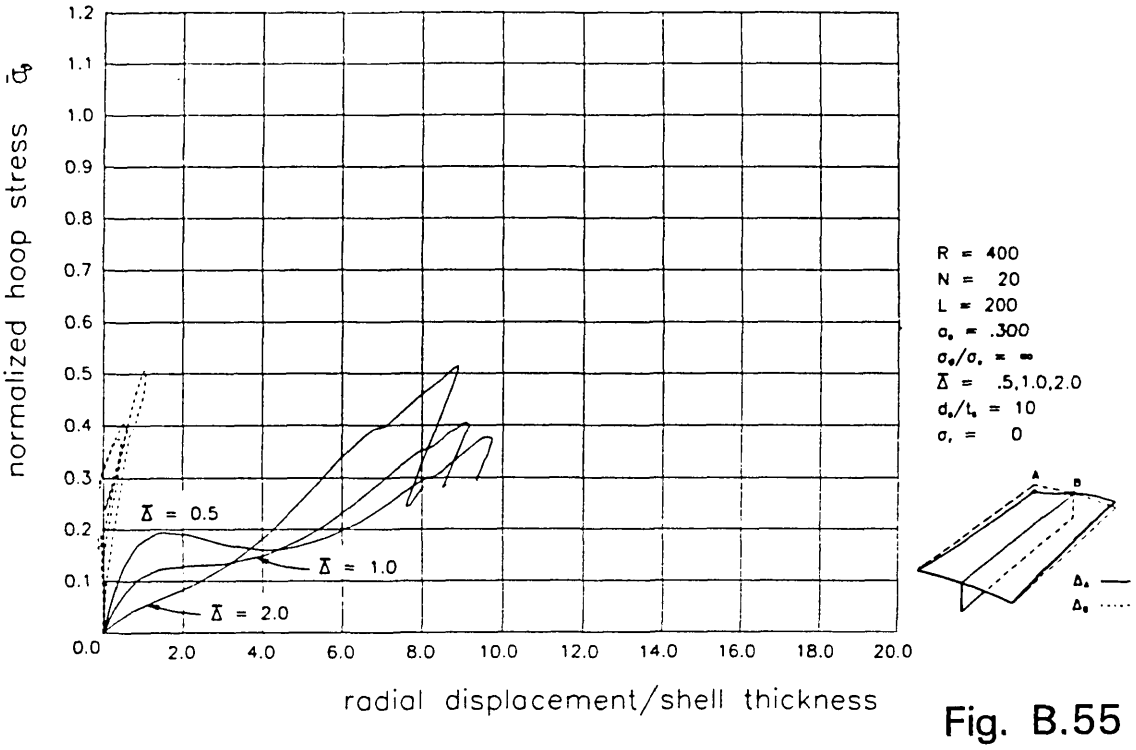


Fig. B.55

EFFECT OF INITIAL IMPERFECTIONS

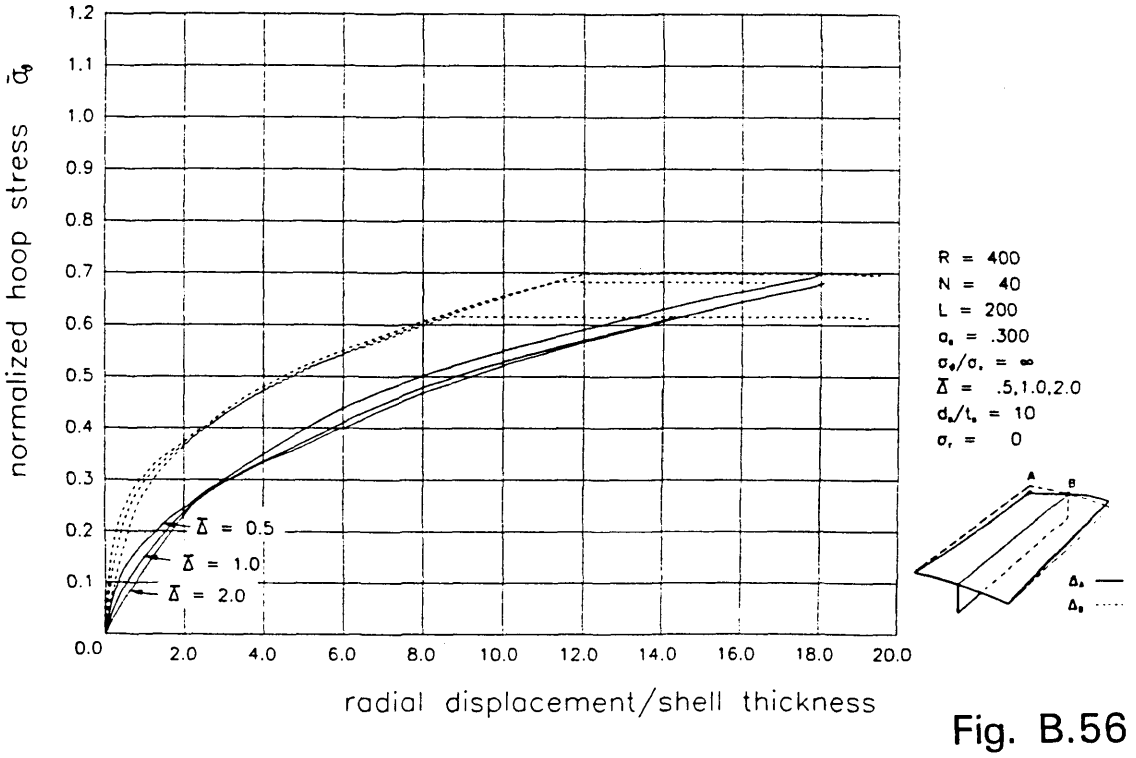


Fig. B.56

EFFECT OF INITIAL IMPERFECTIONS

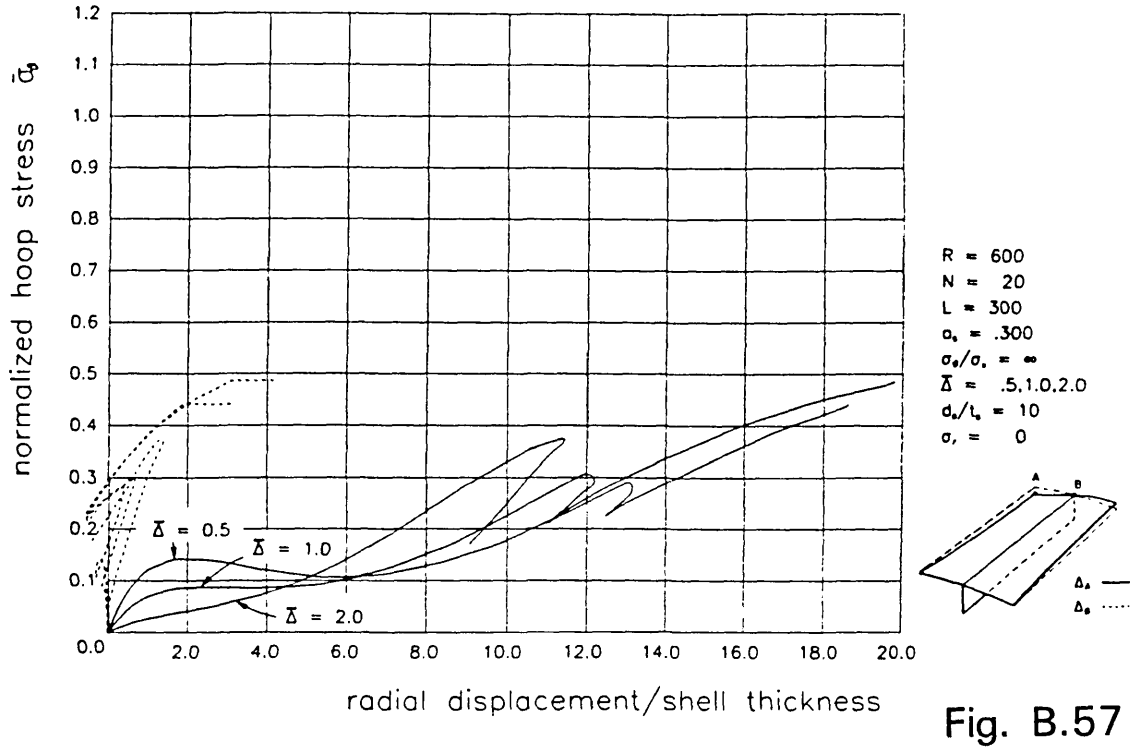


Fig. B.57

EFFECT OF INITIAL IMPERFECTIONS

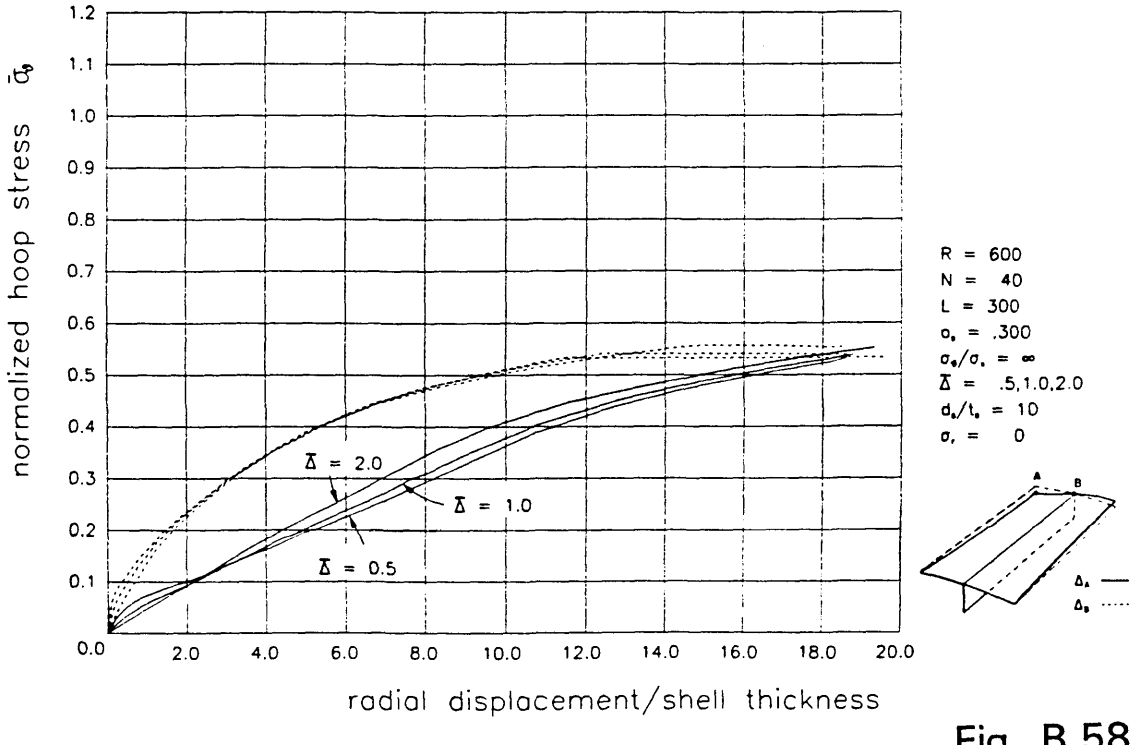


Fig. B.58

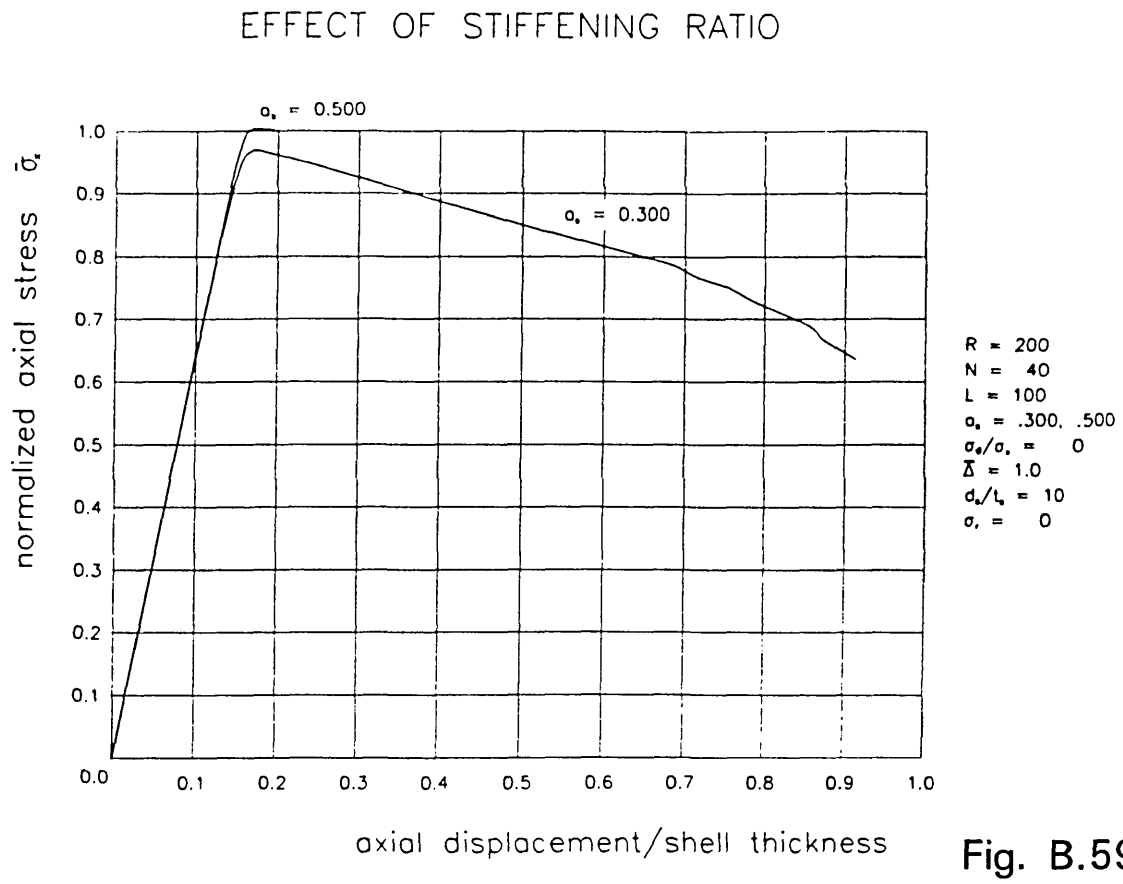


Fig. B.59

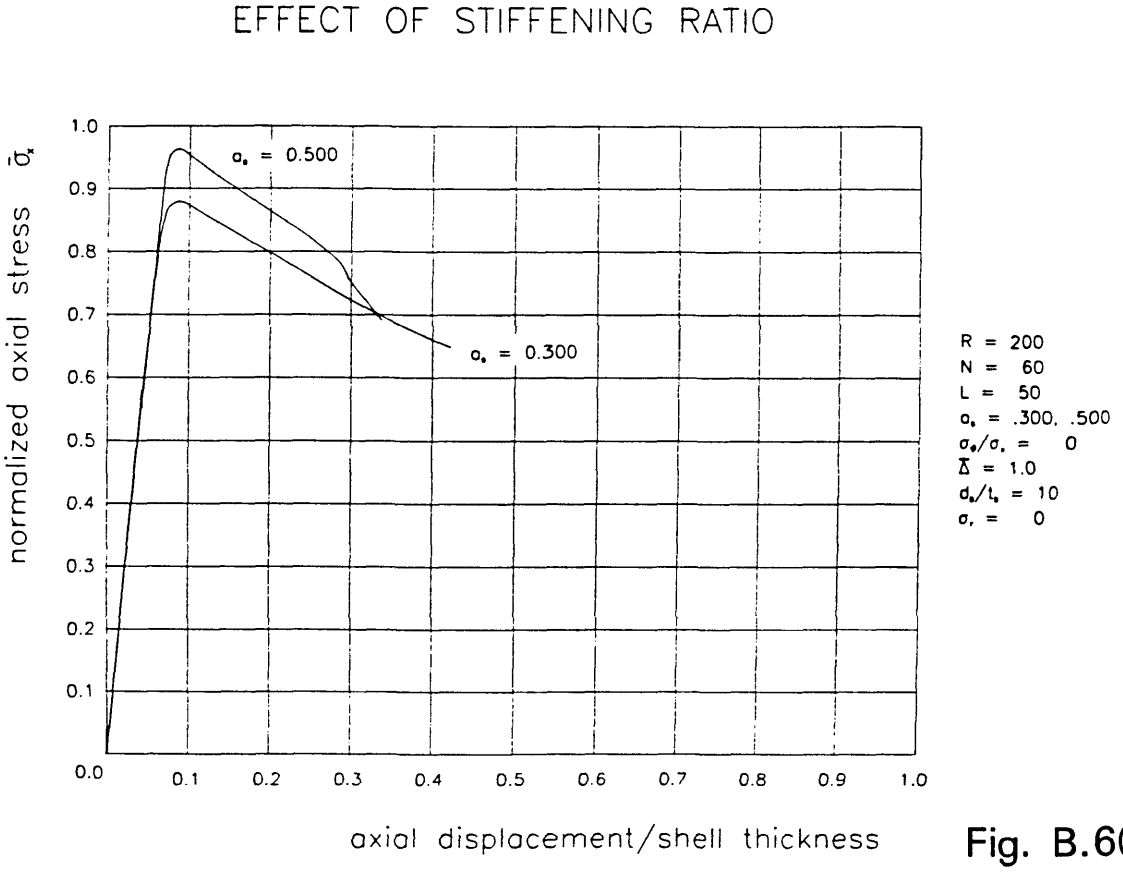
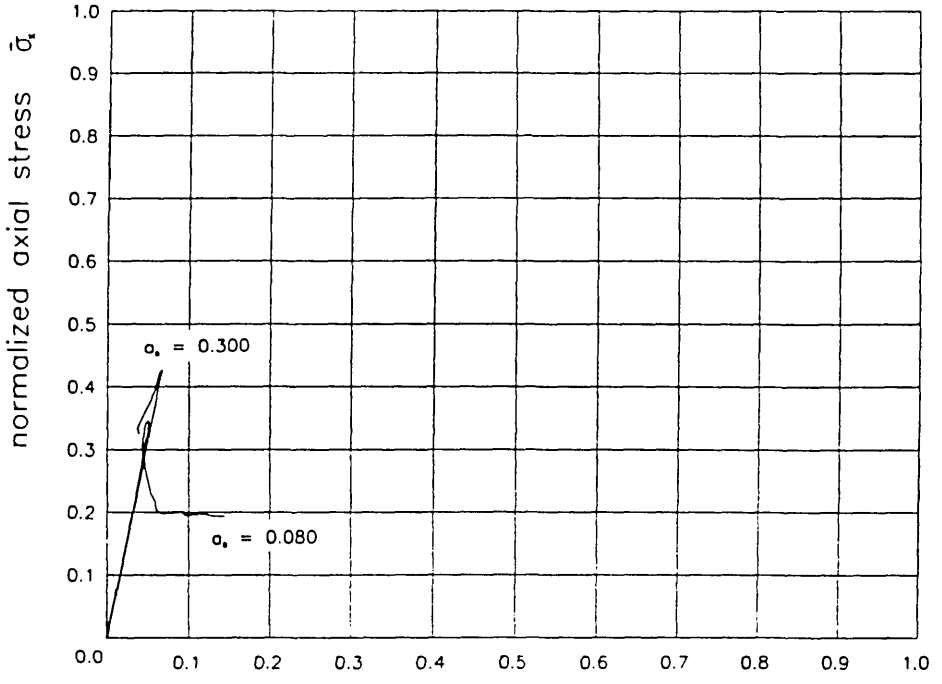


Fig. B.60

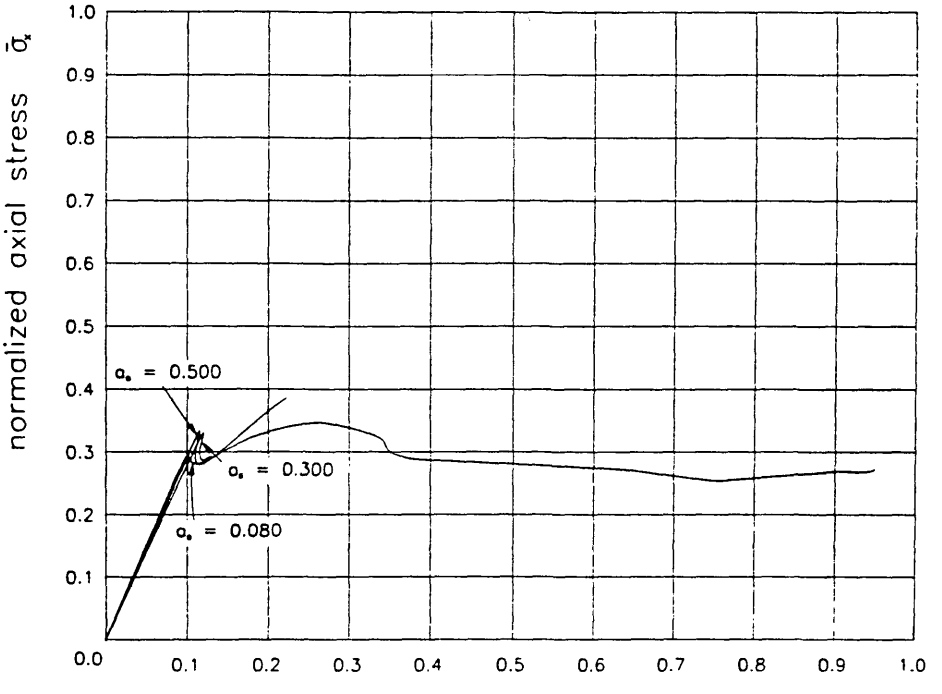
EFFECT OF STIFFENING RATIO



R = 400
N = 20
L = 100
a_o = .080, .300
σ_ϕ/σ_x = 0
$\bar{\Delta}$ = 1.0
d_o/t_o = 10
σ_r = 0

Fig. B.61

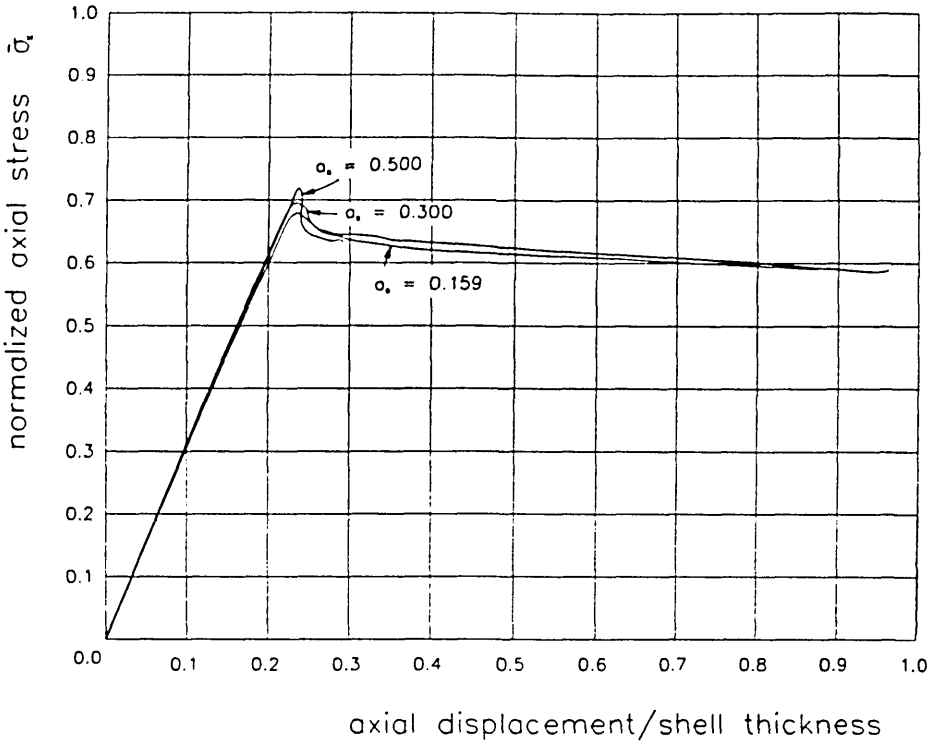
EFFECT OF STIFFENING RATIO



R = 400
N = 20
L = 200
a_o = .080, .300, .500
σ_ϕ/σ_x = 0
$\bar{\Delta}$ = 1.0
d_o/t_o = 10
σ_r = 0

Fig. B.62

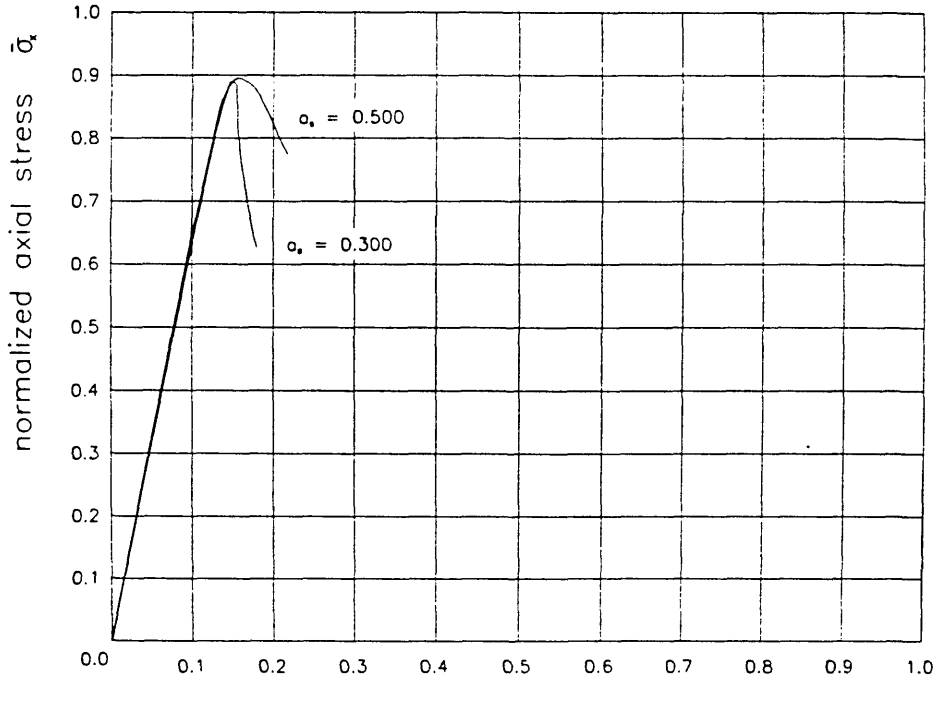
EFFECT OF STIFFENING RATIO



R = 400
N = 40
L = 200
α_s = .159, .300, .500
σ_ϕ/σ_x = 0
$\bar{\Delta}$ = 1.0
d_s/t_s = 10
σ_r = 0

Fig. B.63

EFFECT OF STIFFENING RATIO



R = 400
N = 60
L = 100
α_s = .300, .500
σ_ϕ/σ_x = 0
$\bar{\Delta}$ = 1.0
d_s/t_s = 10
σ_r = 0

Fig. B.64

EFFECT OF STIFFENING RATIO

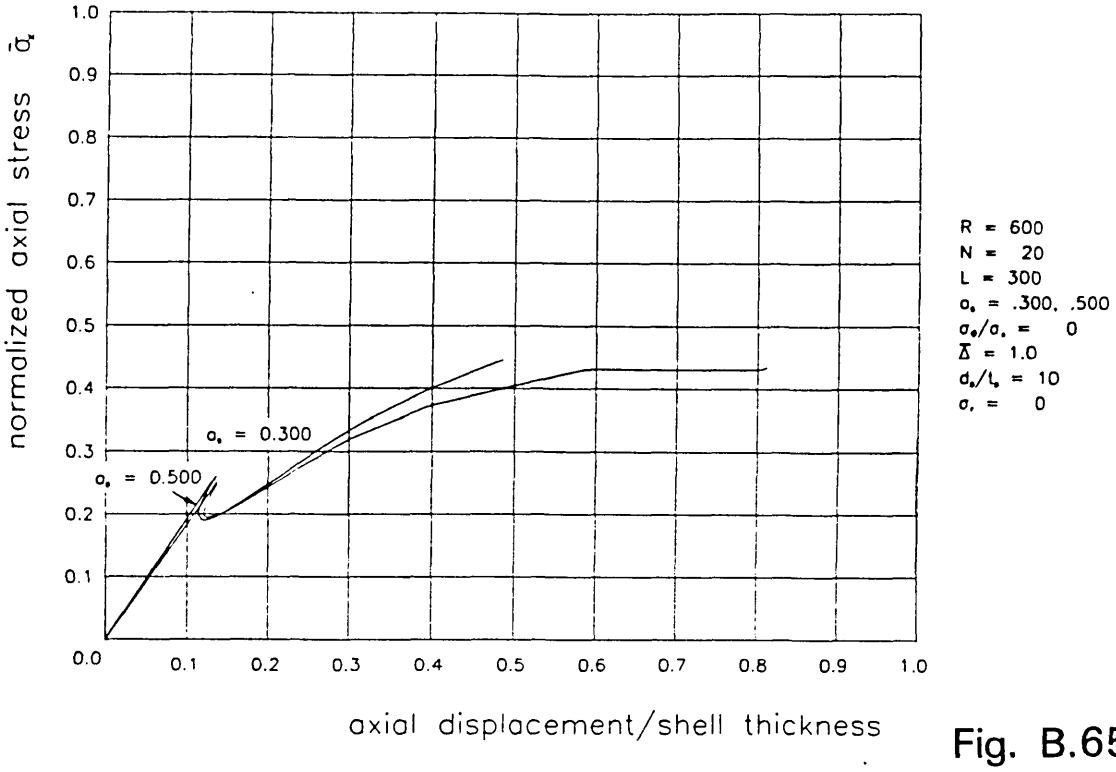


Fig. B.65

EFFECT OF STIFFENING RATIO

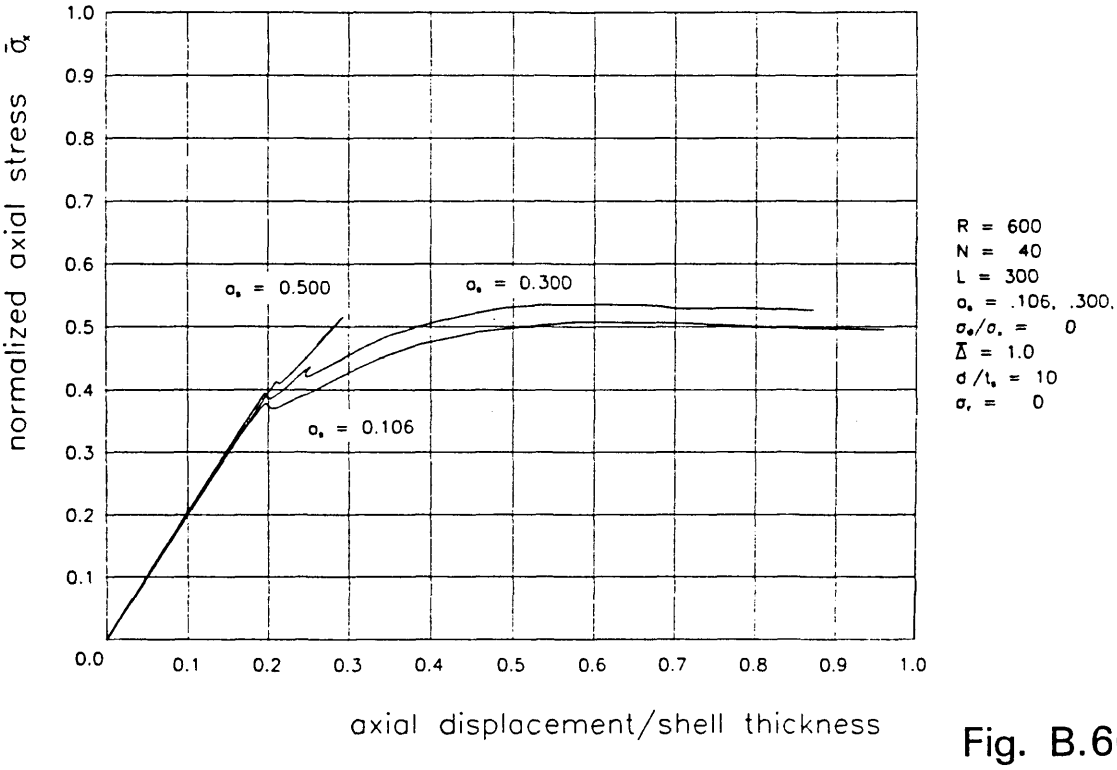
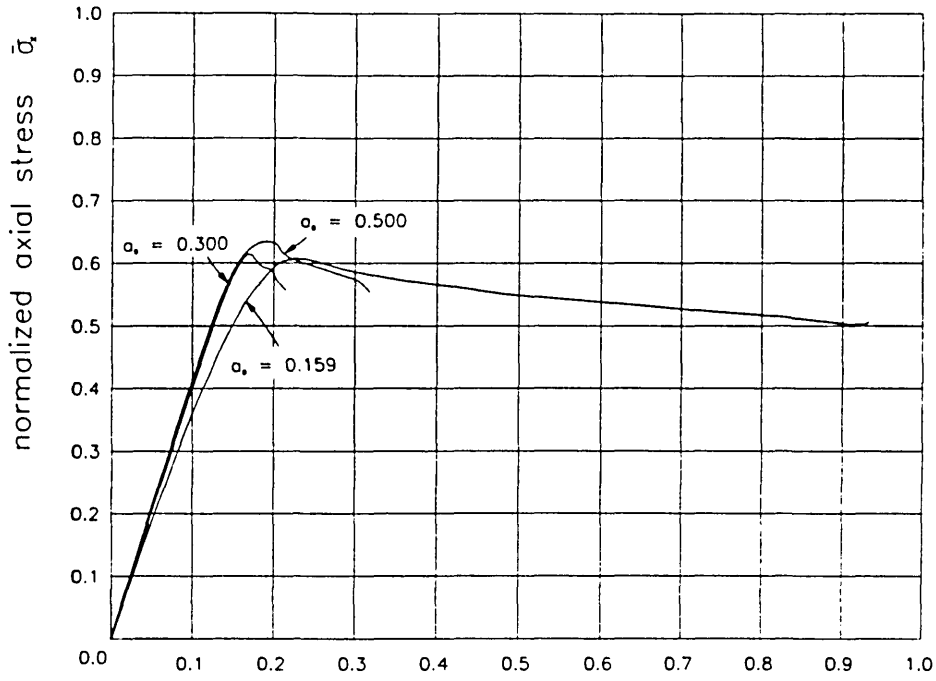


Fig. B.66

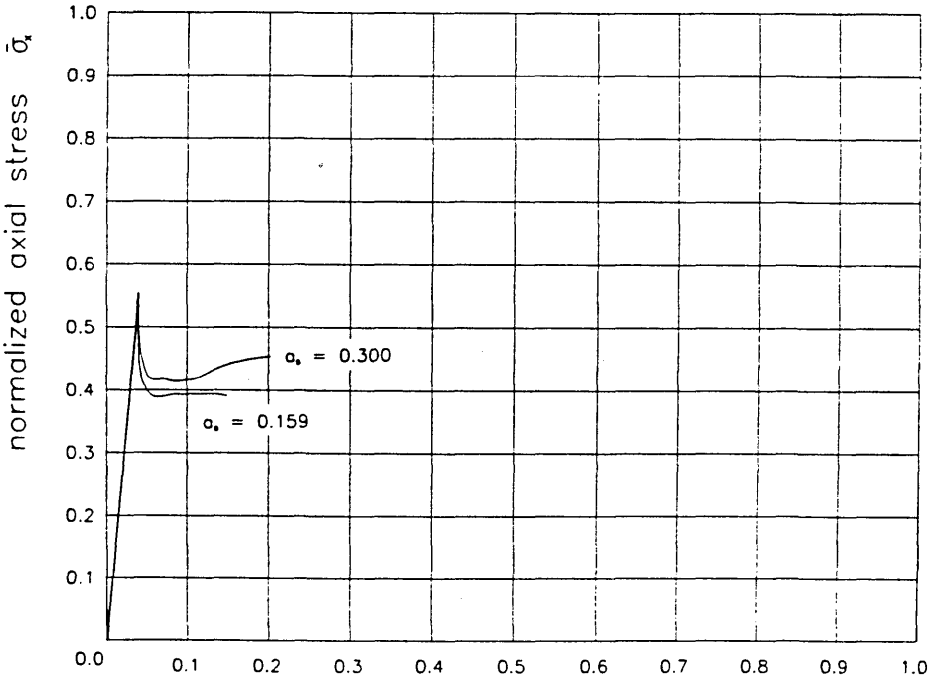
EFFECT OF STIFFENING RATIO



R = 600
N = 60
L = 150
a_o = .159, .300, .500
σ_e/σ_o = 0
$\bar{\Delta}$ = 1.0
d_o/t_o = 10
σ_r = 0

Fig. B.67

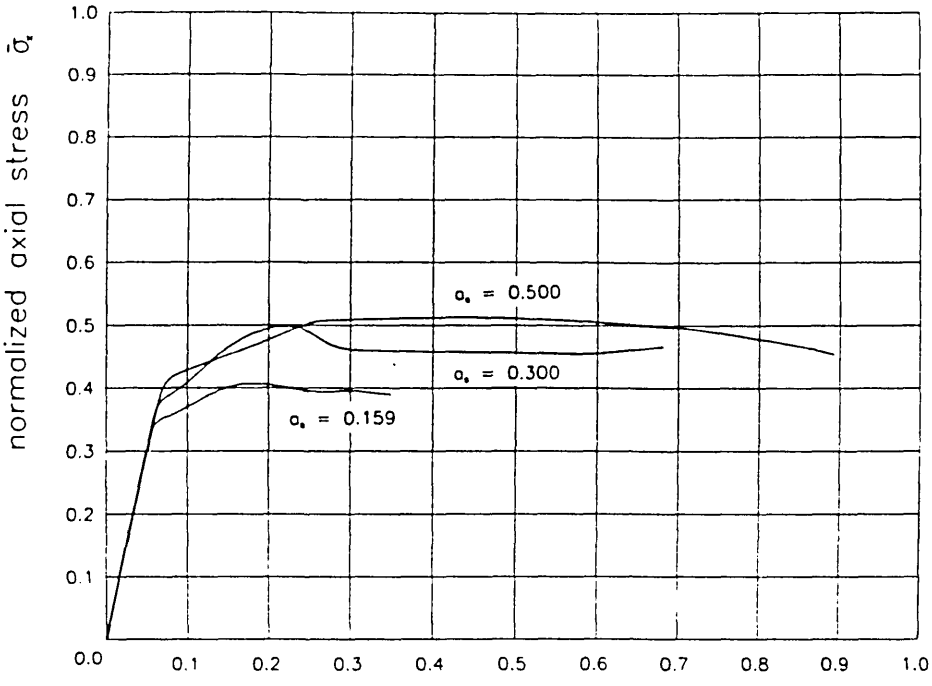
EFFECT OF STIFFENING RATIO



R = 200
N = 20
L = 50
a_o = .159, .300
σ_e/σ_o = .4
$\bar{\Delta}$ = 1.0
d_o/t_o = 10
σ_r = 0

Fig. B.68

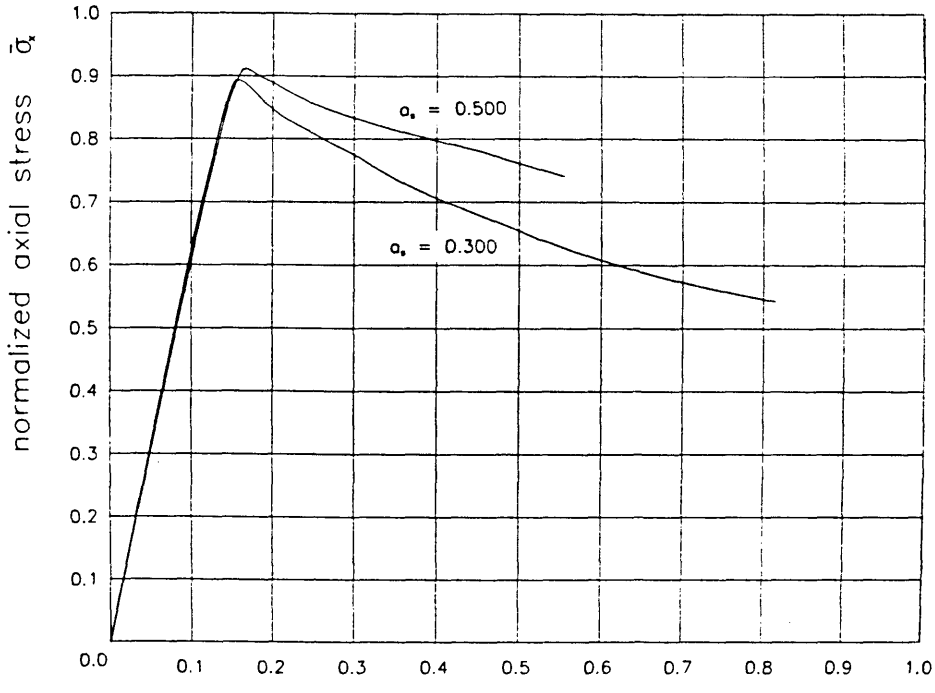
EFFECT OF STIFFENING RATIO



R = 200
N = 20
L = 100
a_s = .159, .300, .500
σ_ϕ/σ_x = .4
$\bar{\Delta}$ = 1.0
d_s/t_s = 10
σ_r = 0

Fig. B.69

EFFECT OF STIFFENING RATIO



R = 200
N = 40
L = 100
a_s = .300, .500
σ_ϕ/σ_x = .4
$\bar{\Delta}$ = 1.0
d_s/t_s = 10
σ_r = 0

Fig. B.70

EFFECT OF STIFFENING RATIO

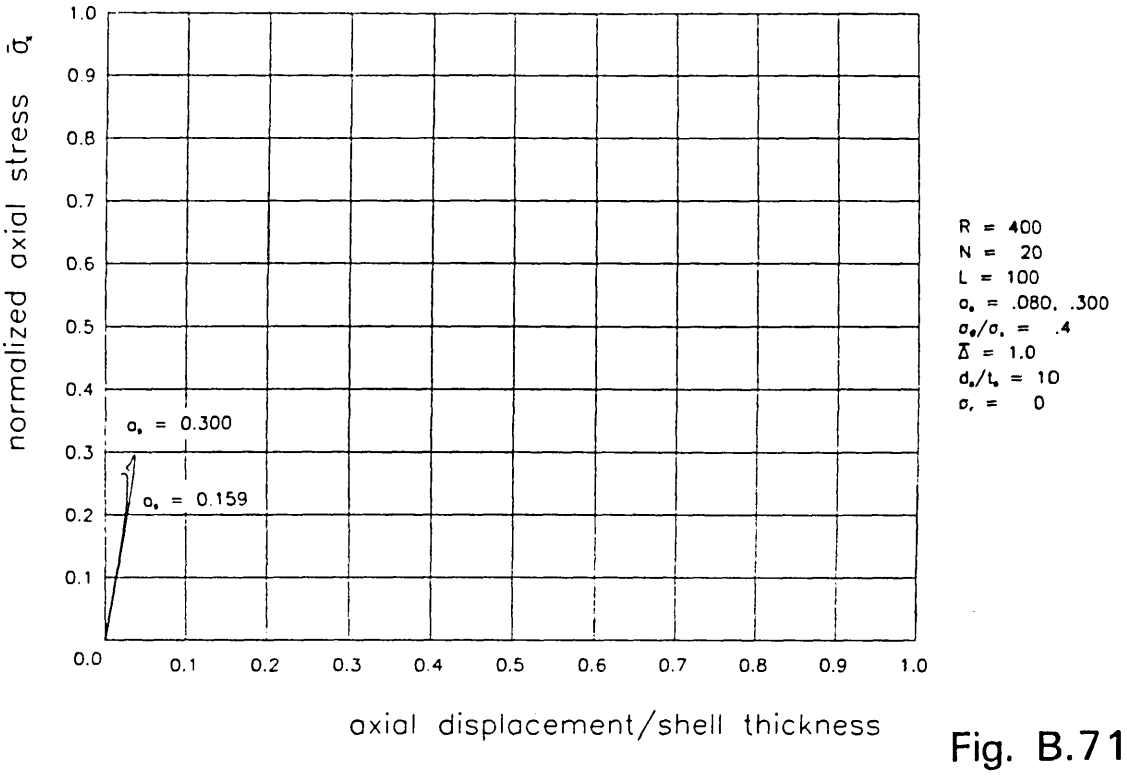


Fig. B.71

EFFECT OF STIFFENING RATIO

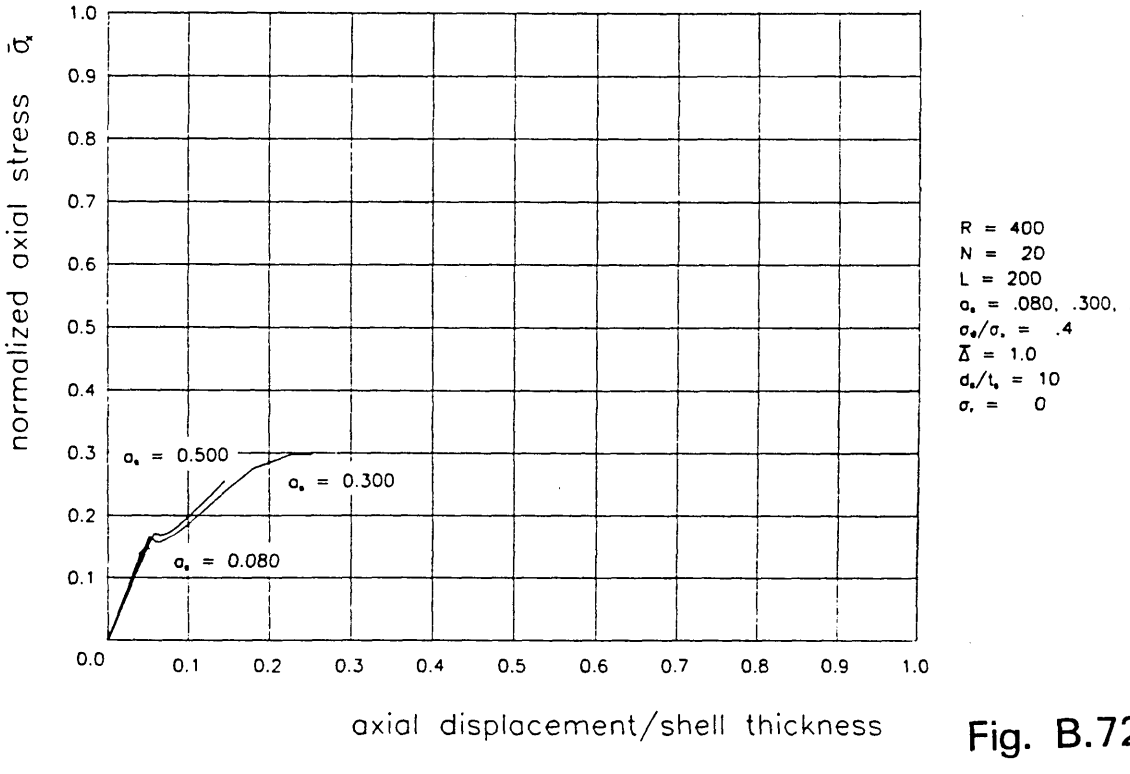
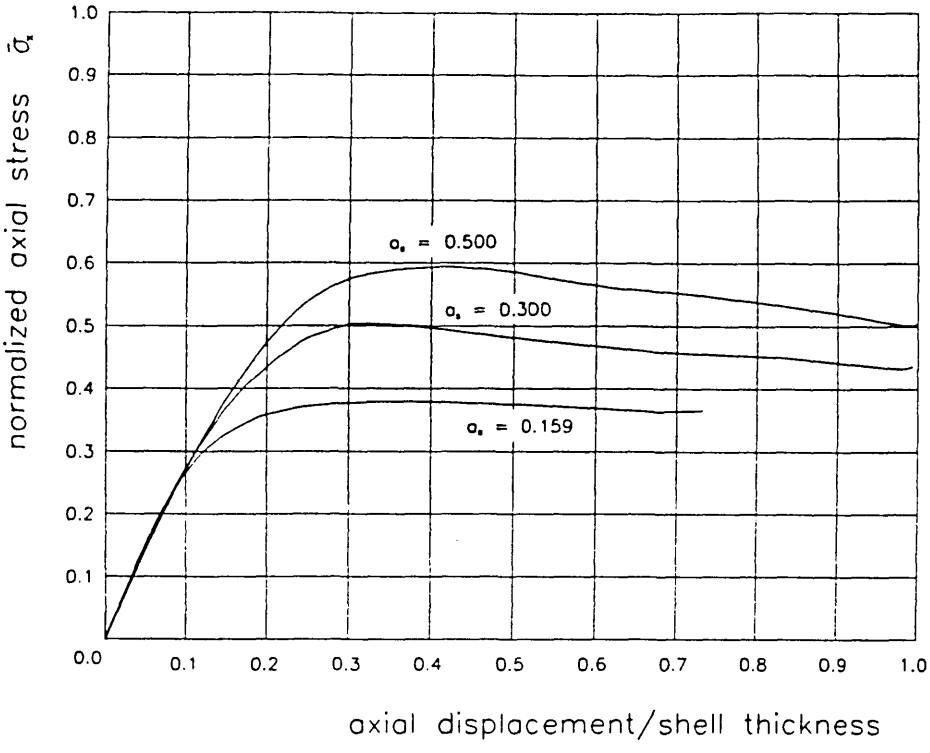


Fig. B.72

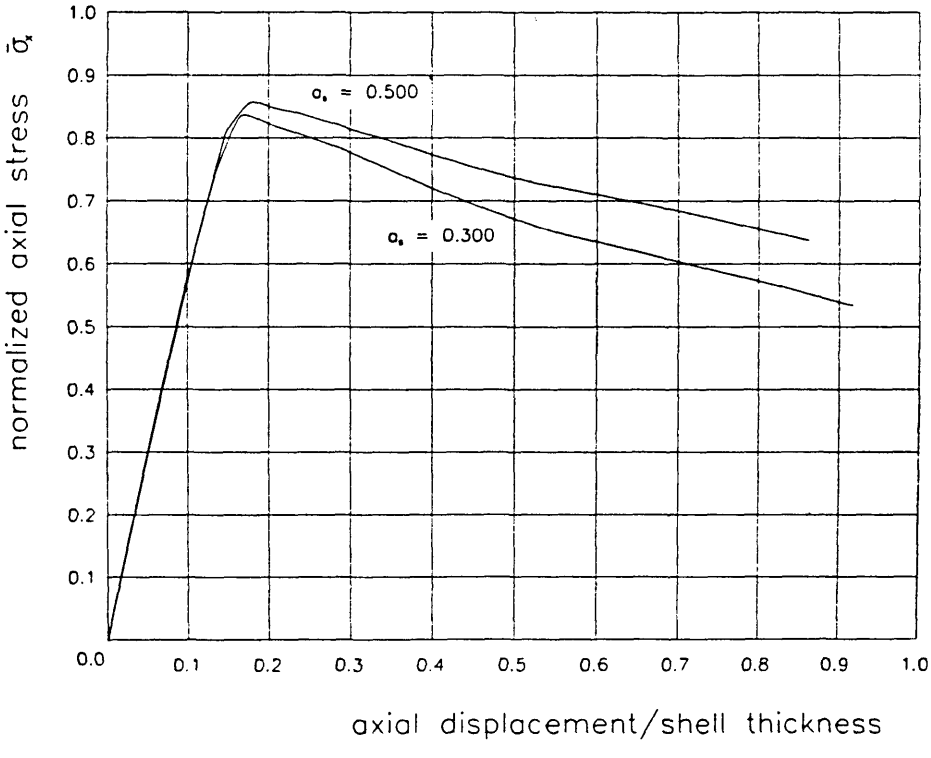
EFFECT OF STIFFENING RATIO



R = 400
N = 40
L = 200
α_s = .159, .300, .500
σ_θ/σ_x = .4
$\bar{\Delta}$ = 1.0
d_s/t_s = 10
σ_r = 0

Fig. B.73

EFFECT OF STIFFENING RATIO



R = 400
N = 60
L = 100
α_s = .300, .500
σ_θ/σ_x = .4
$\bar{\Delta}$ = 1.0
d_s/t_s = 10
σ_r = 0

Fig. B.74

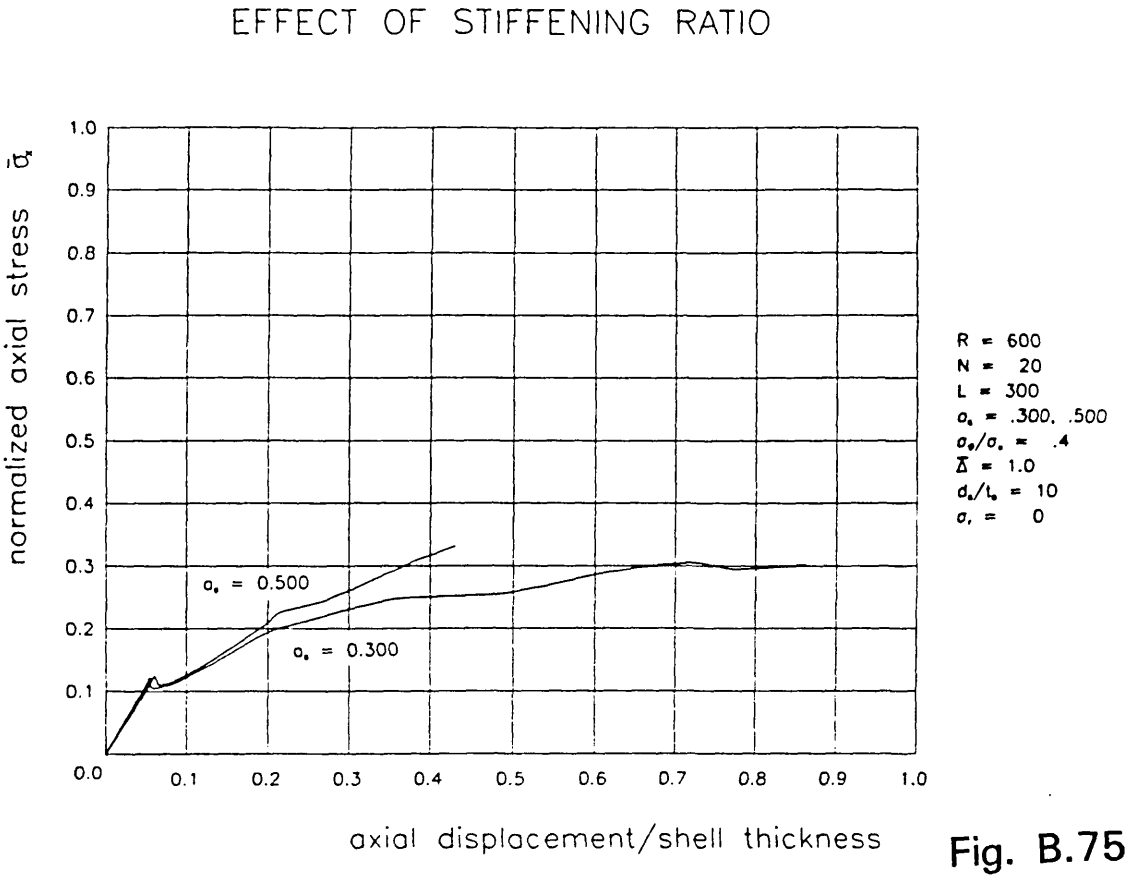


Fig. B.75

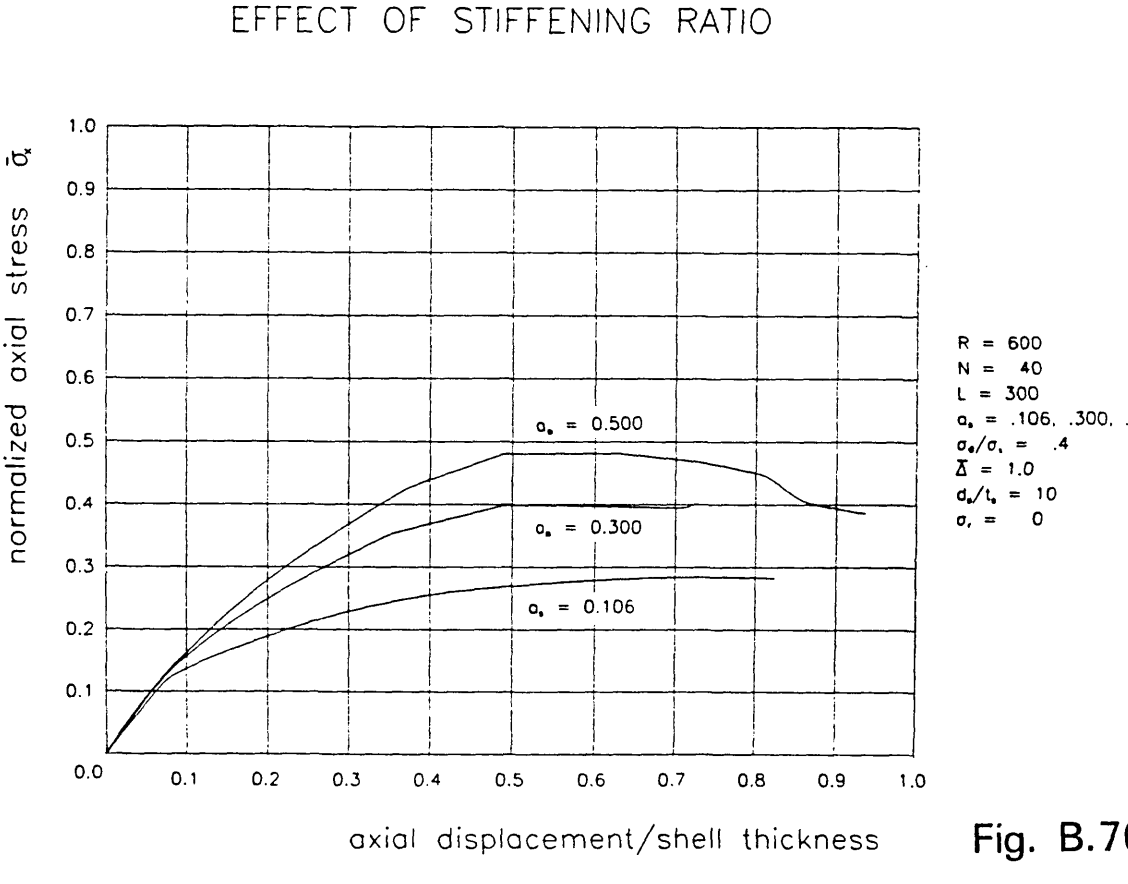


Fig. B.76

EFFECT OF STIFFENING RATIO

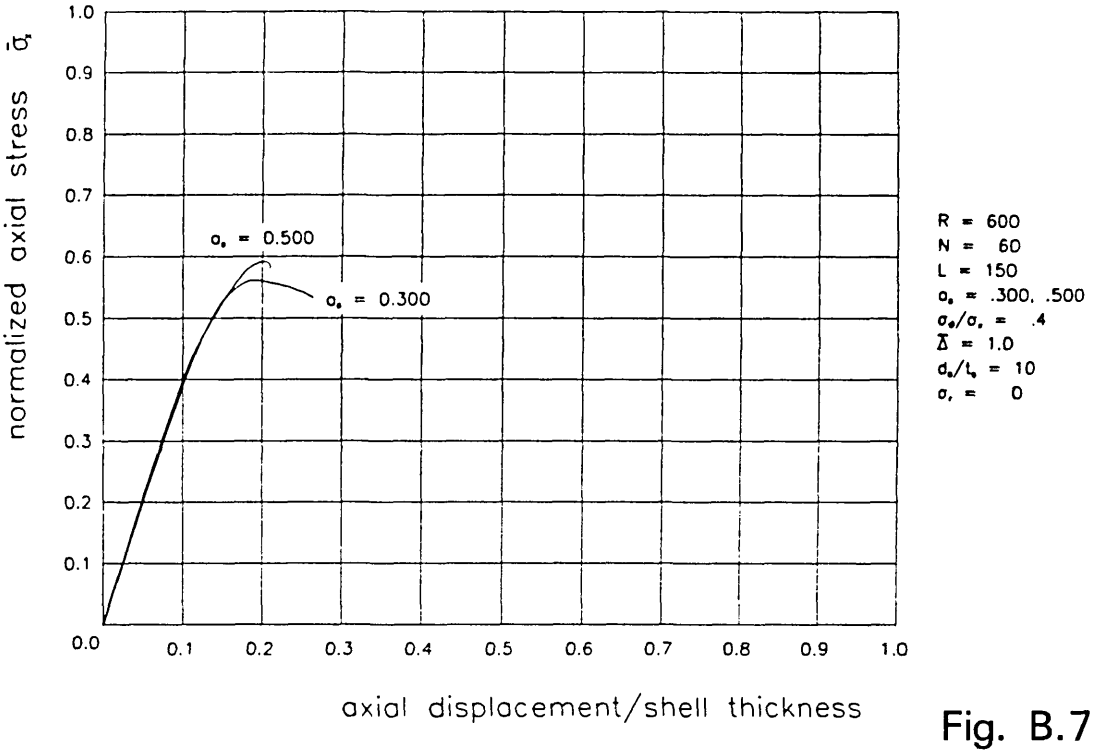


Fig. B.77

EFFECT OF STIFFENING RATIO

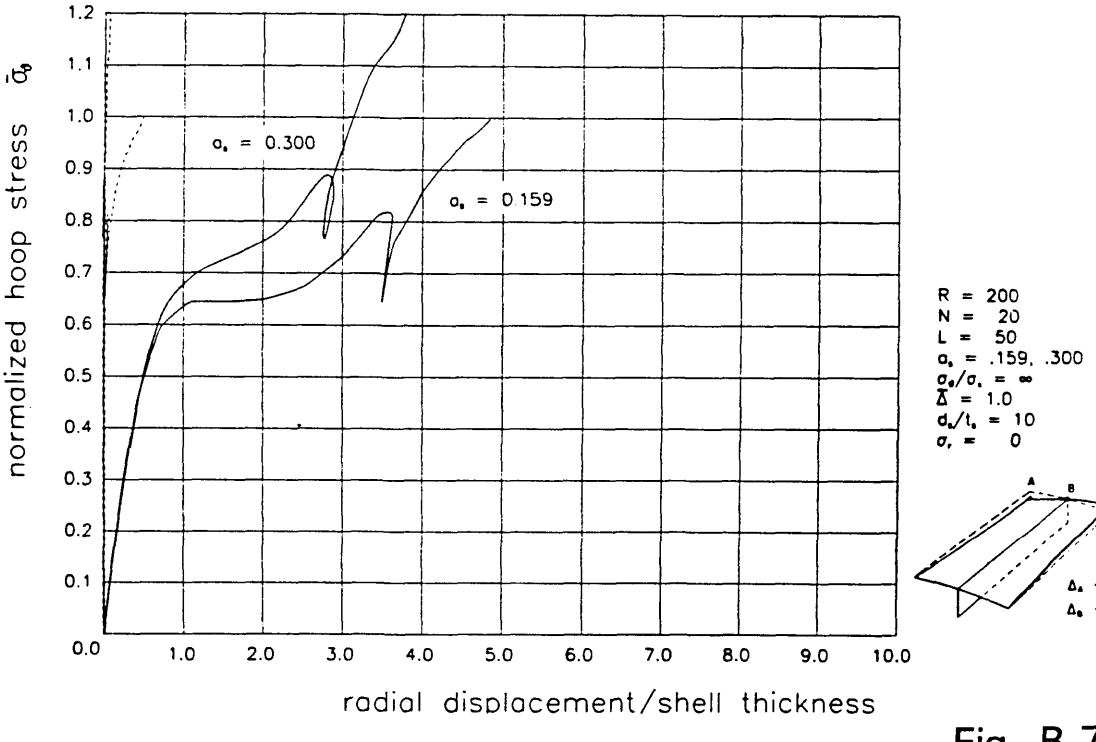


Fig. B.78

EFFECT OF STIFFENING RATIO

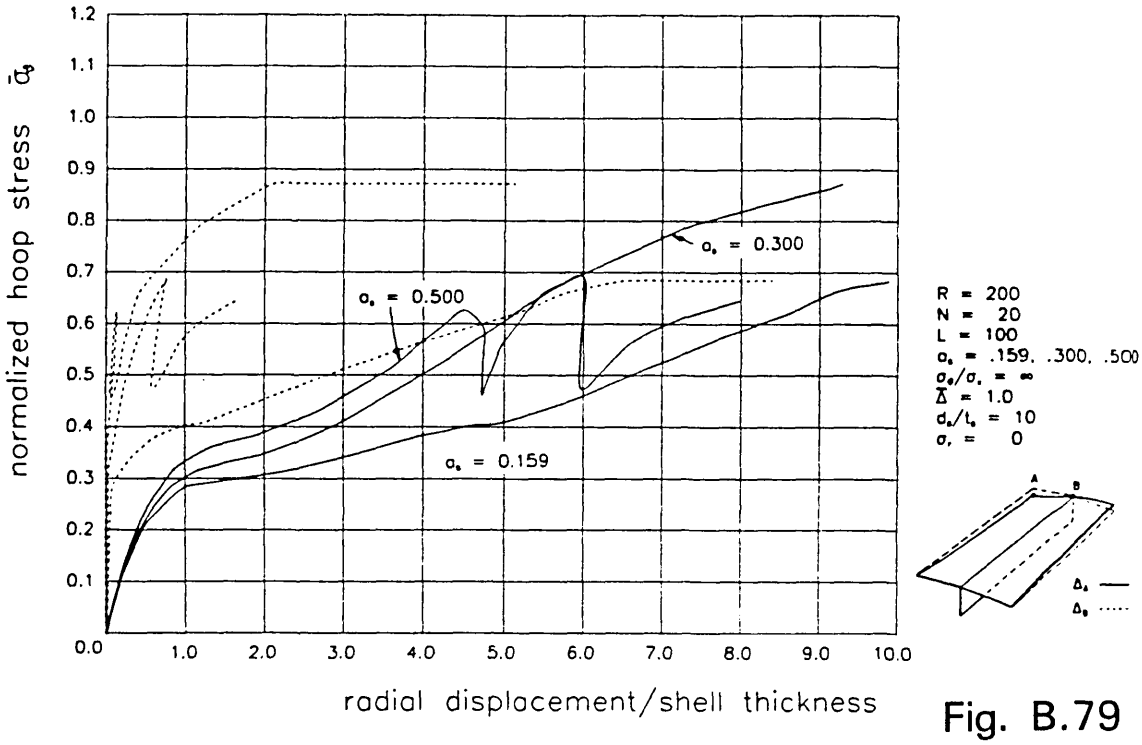


Fig. B.79

EFFECT OF STIFFENING RATIO

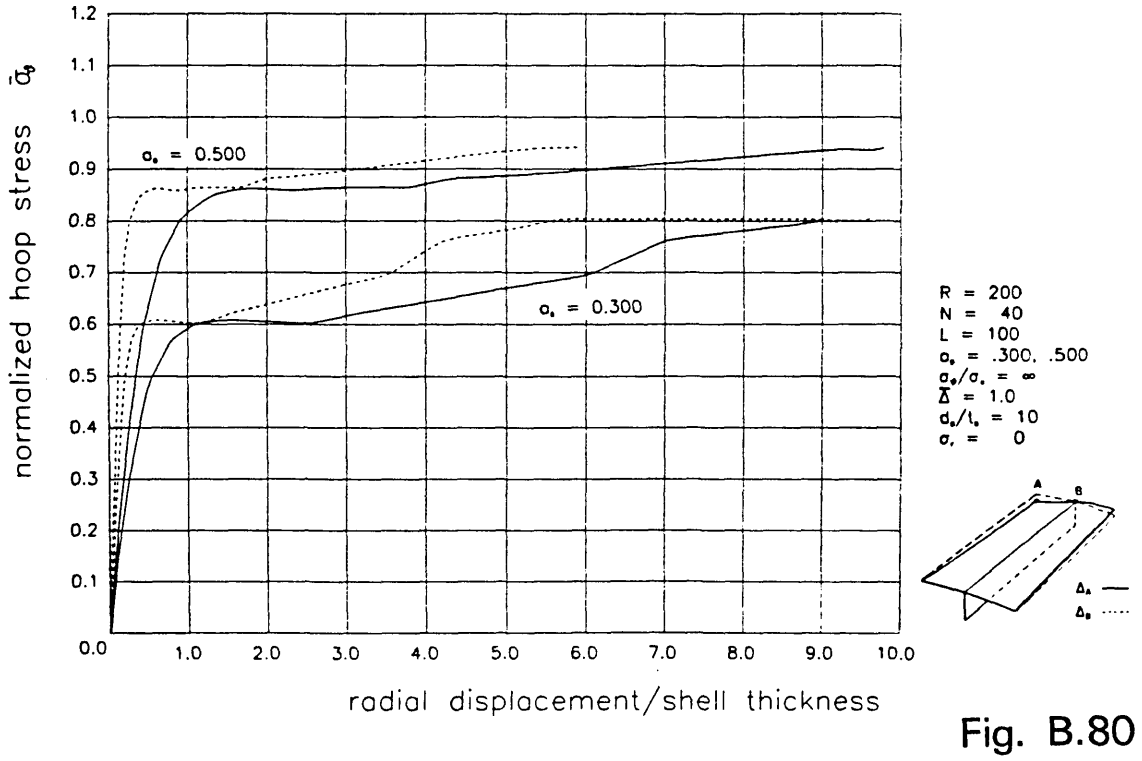


Fig. B.80

EFFECT OF STIFFENING RATIO

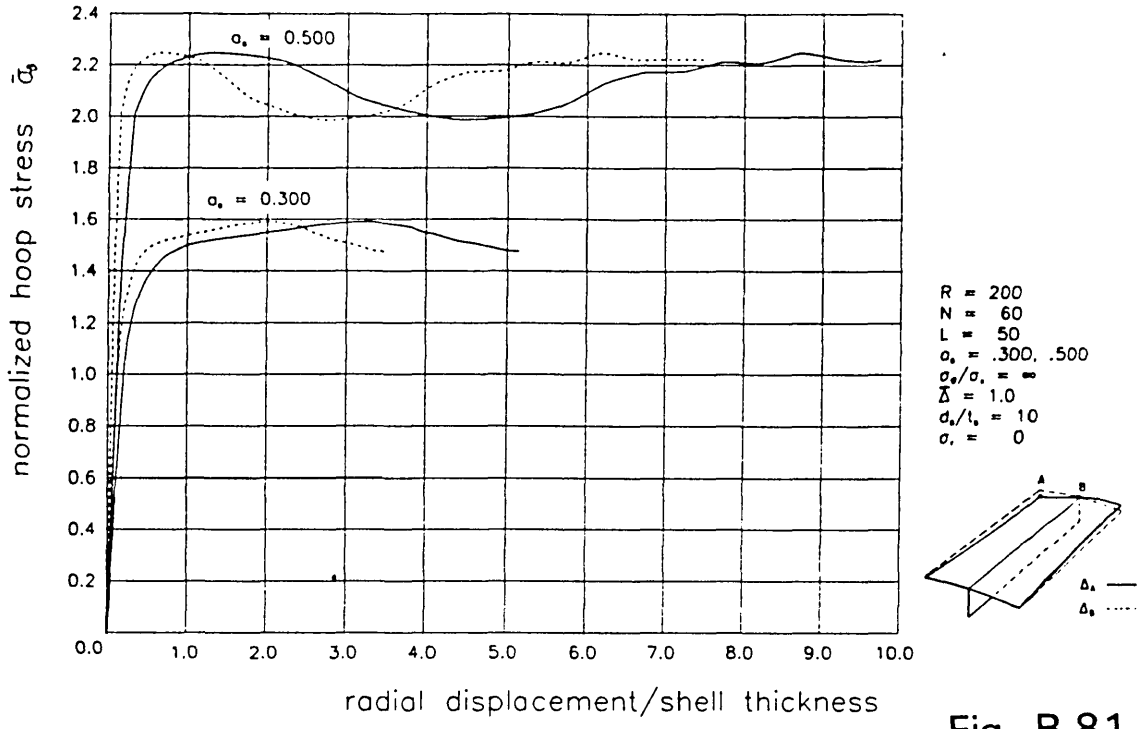


Fig. B.81

EFFECT OF STIFFENING RATIO

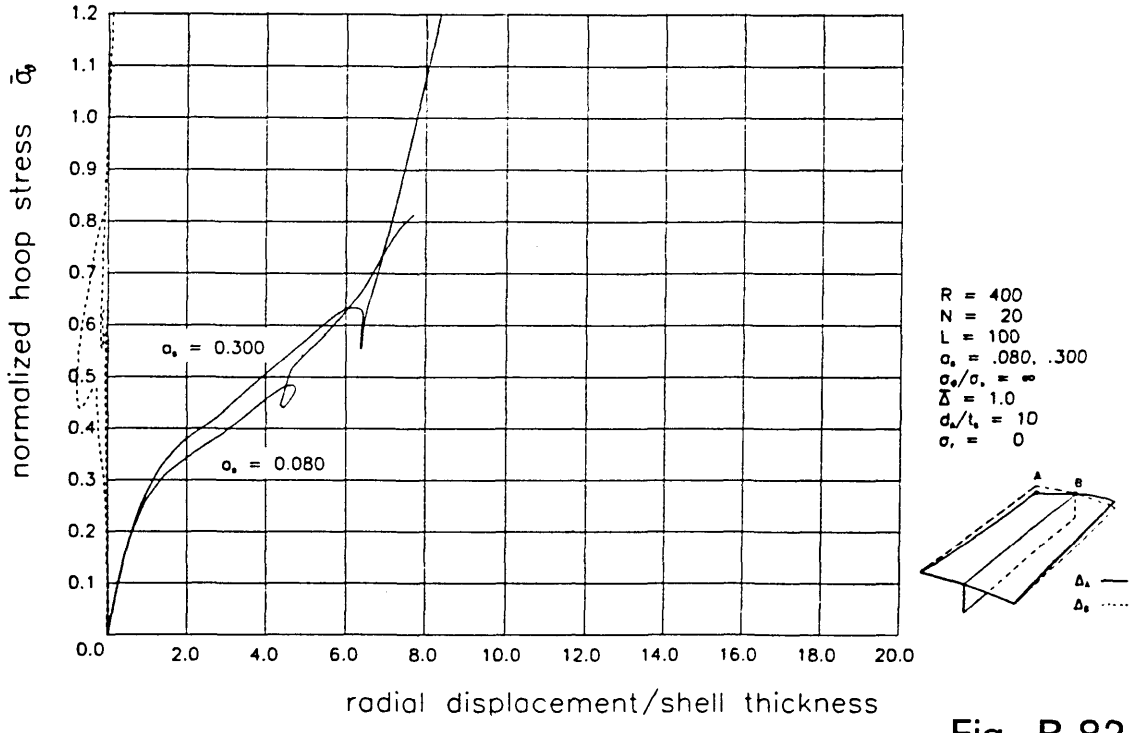


Fig. B.82

EFFECT OF STIFFENING RATIO

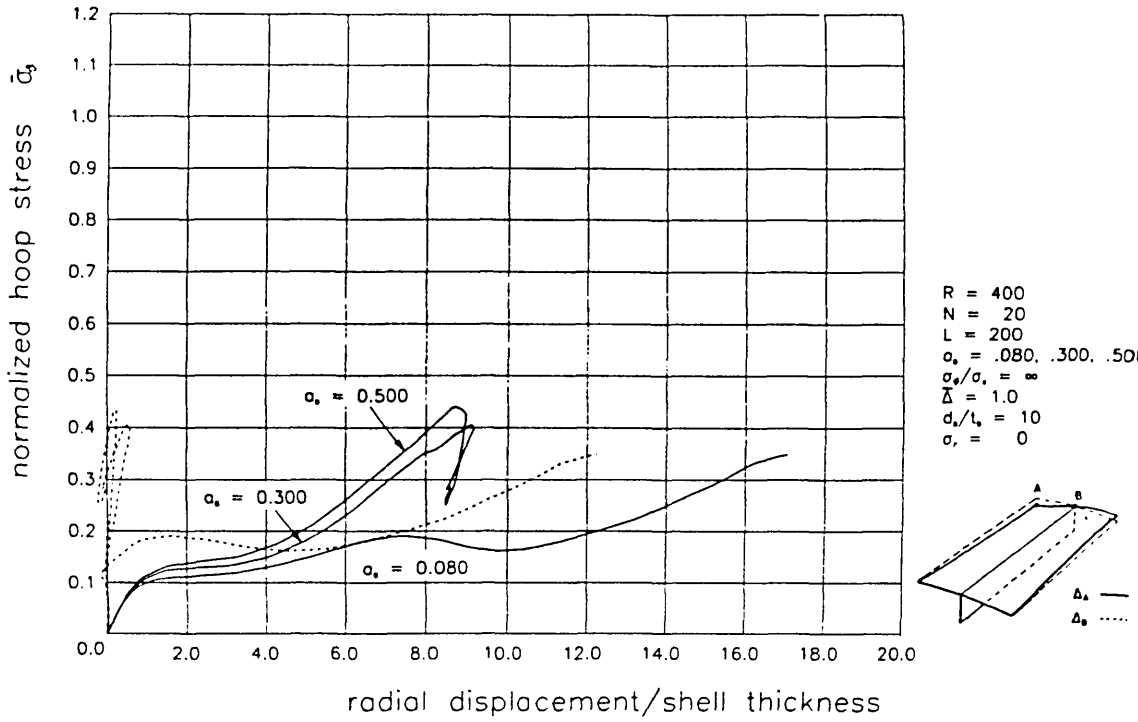


Fig. B.83

EFFECT OF STIFFENING RATIO

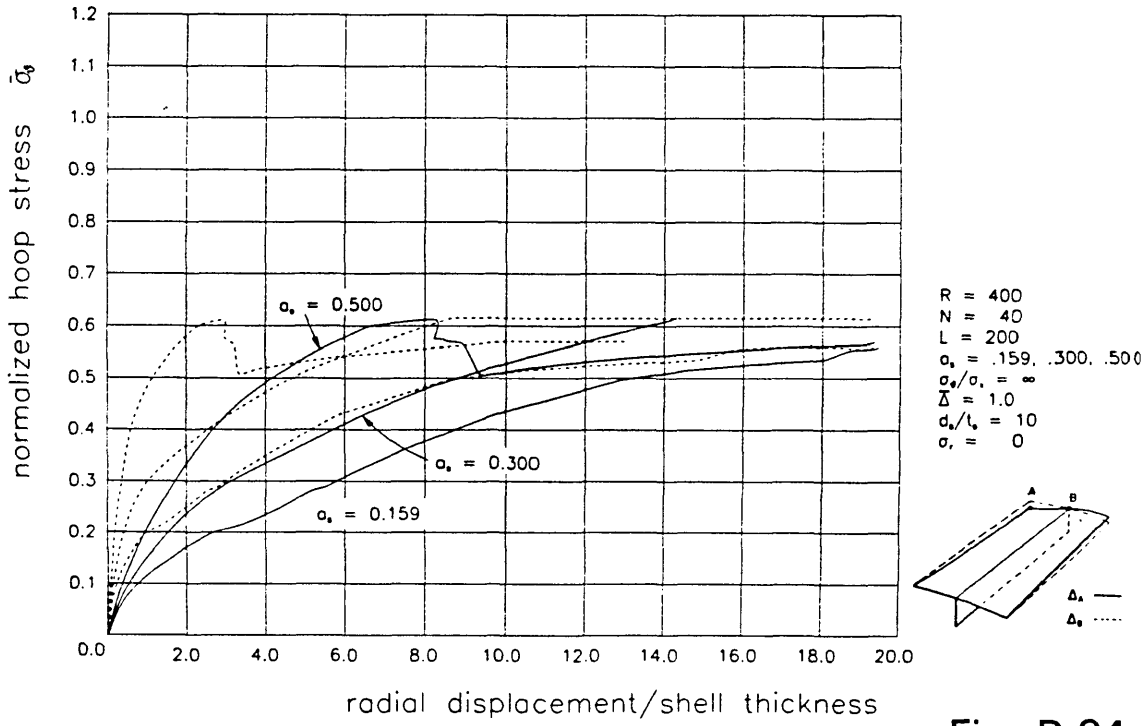


Fig. B.84

EFFECT OF STIFFENING RATIO

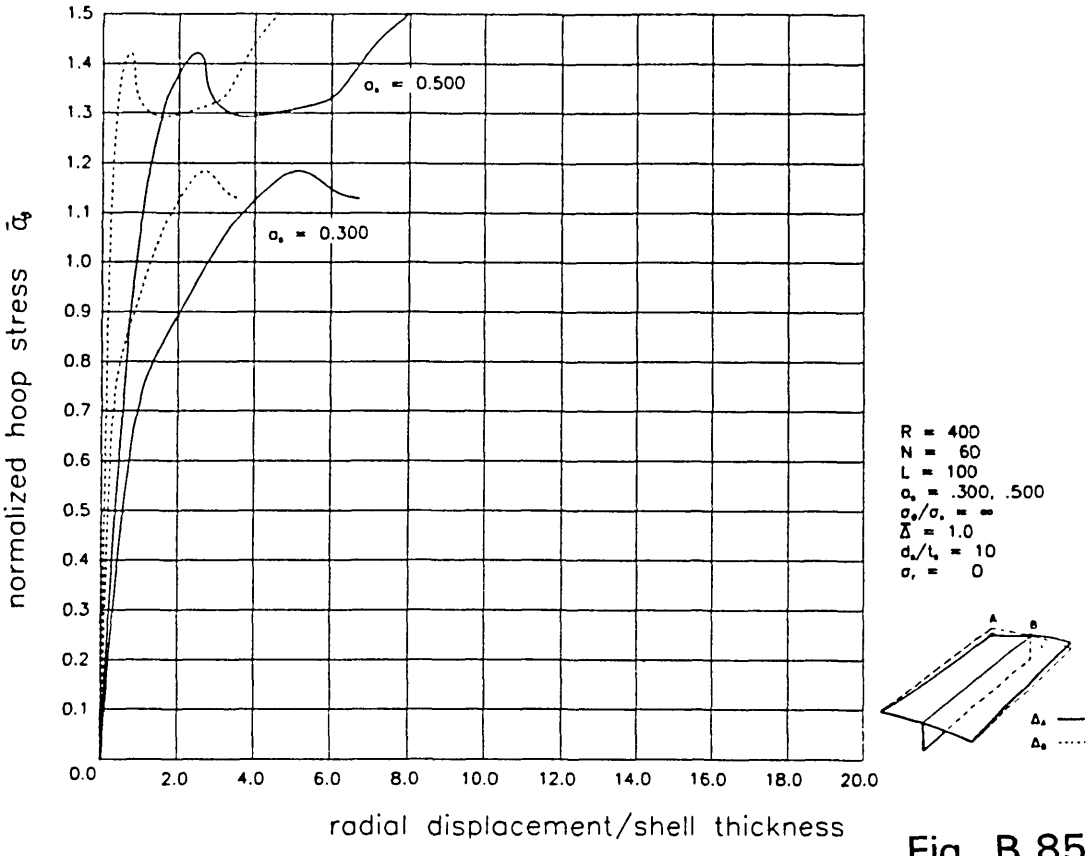


Fig. B.85

EFFECT OF STIFFENING RATIO

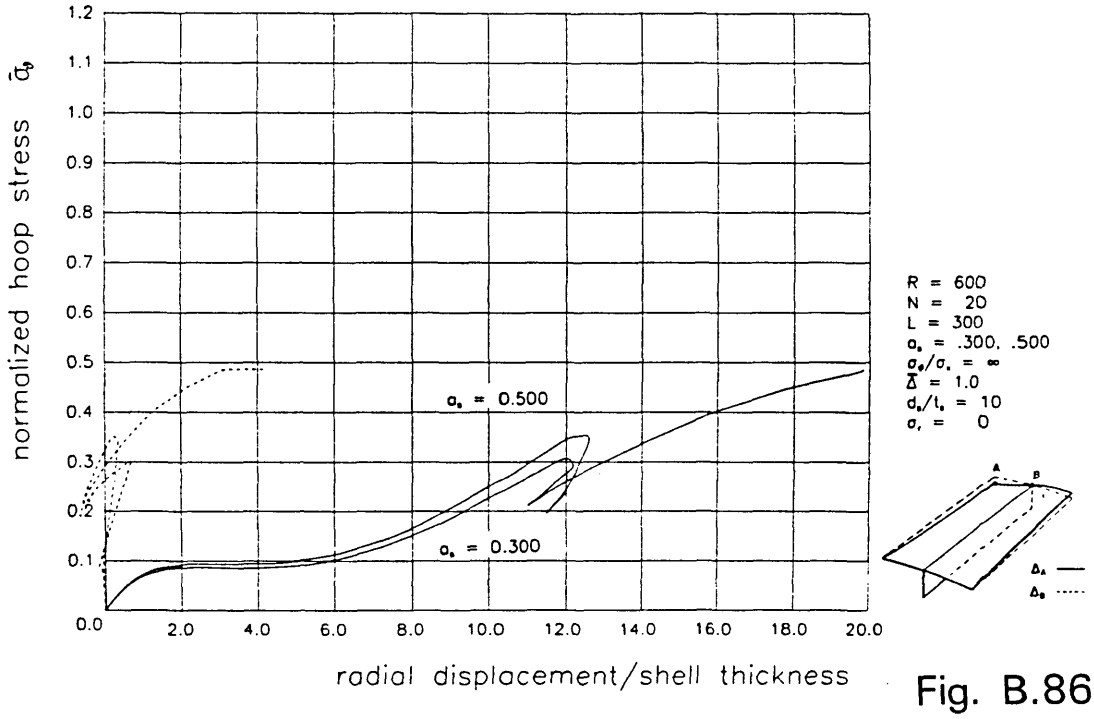


Fig. B.86

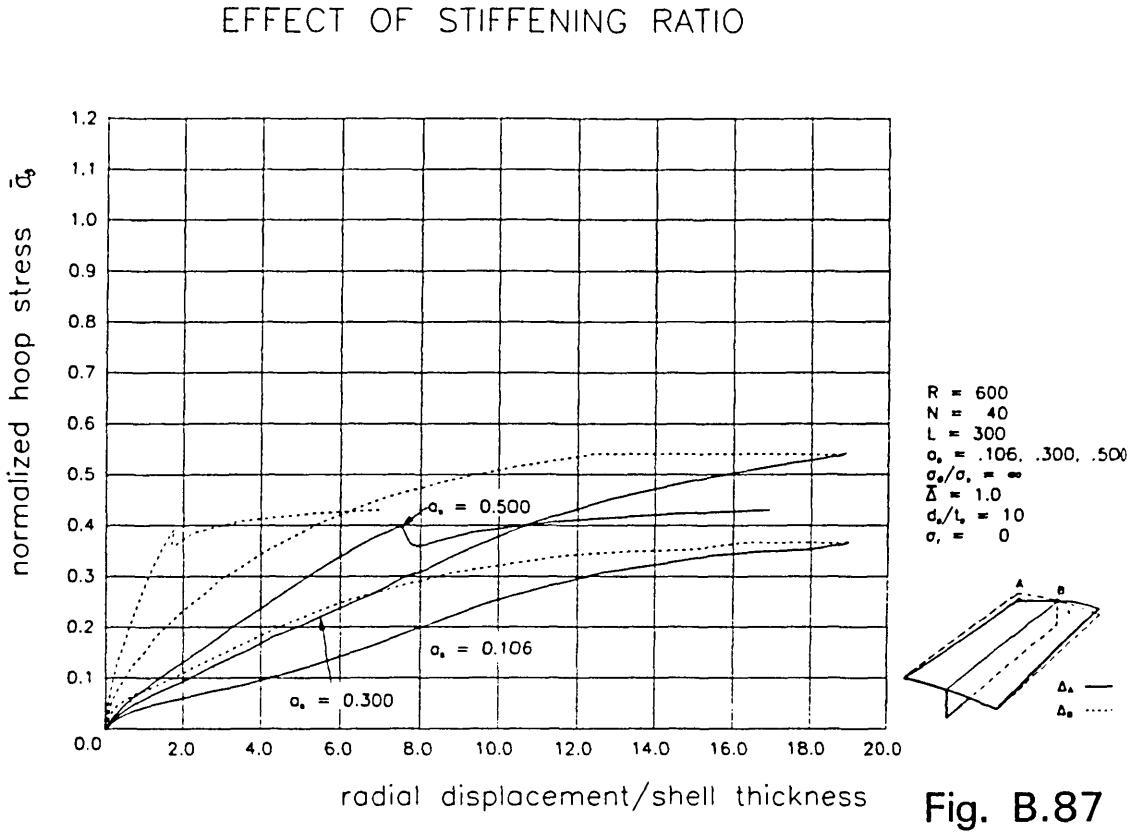


Fig. B.87

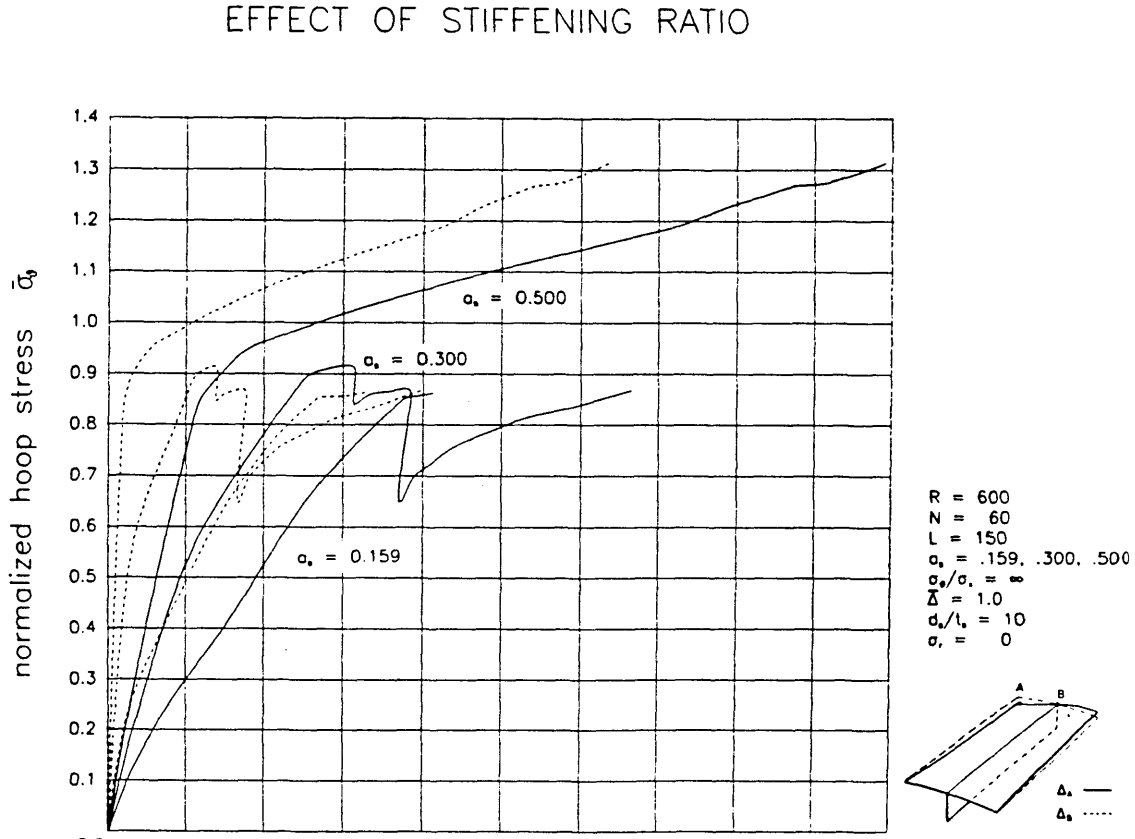


Fig. B.88

EFFECT OF RESIDUAL STRESS

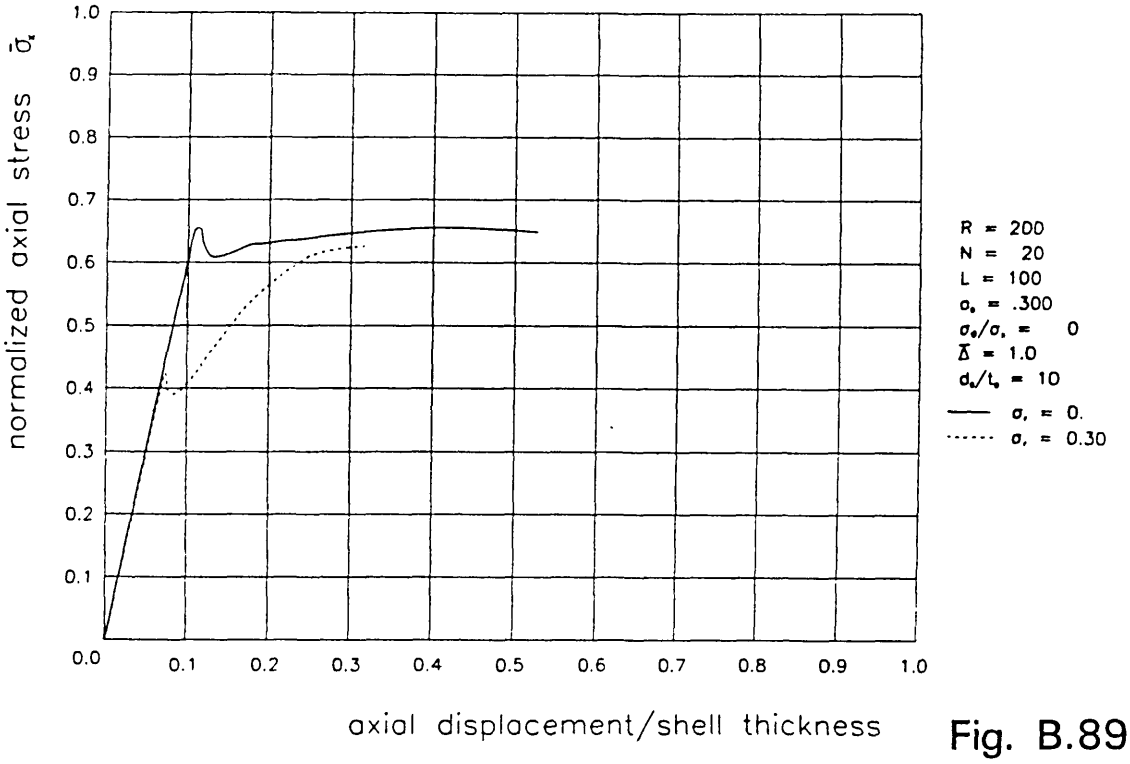


Fig. B.89

EFFECT OF RESIDUAL STRESS

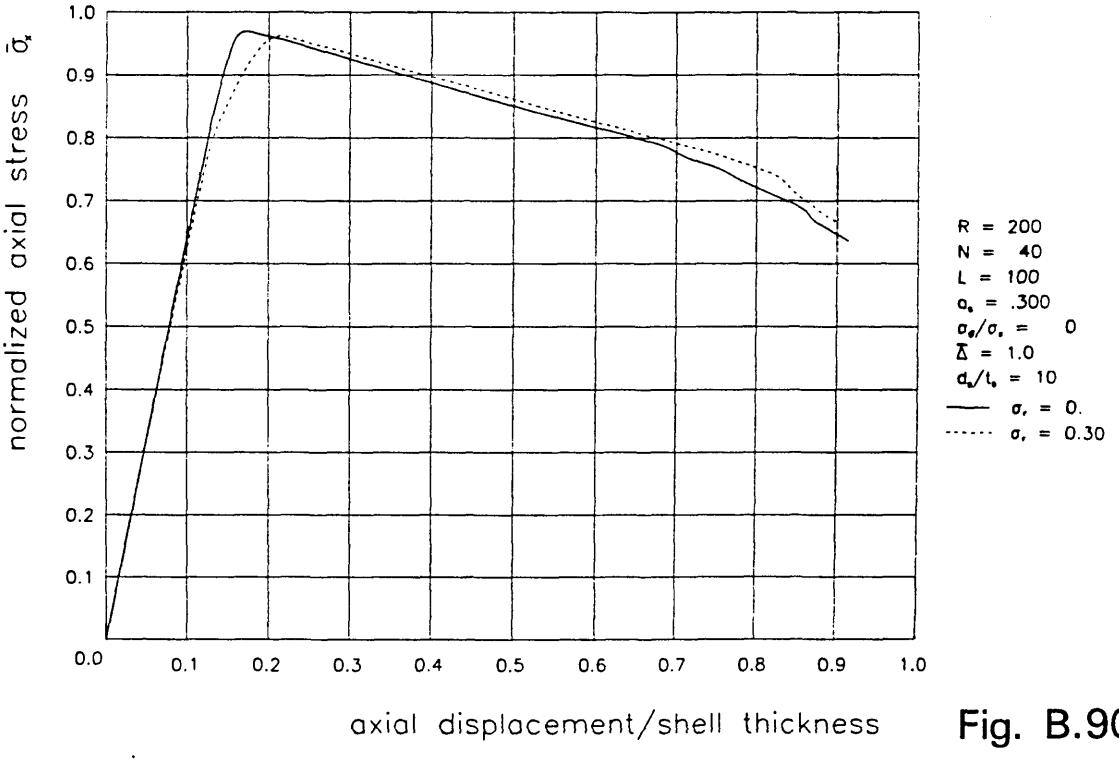


Fig. B.90

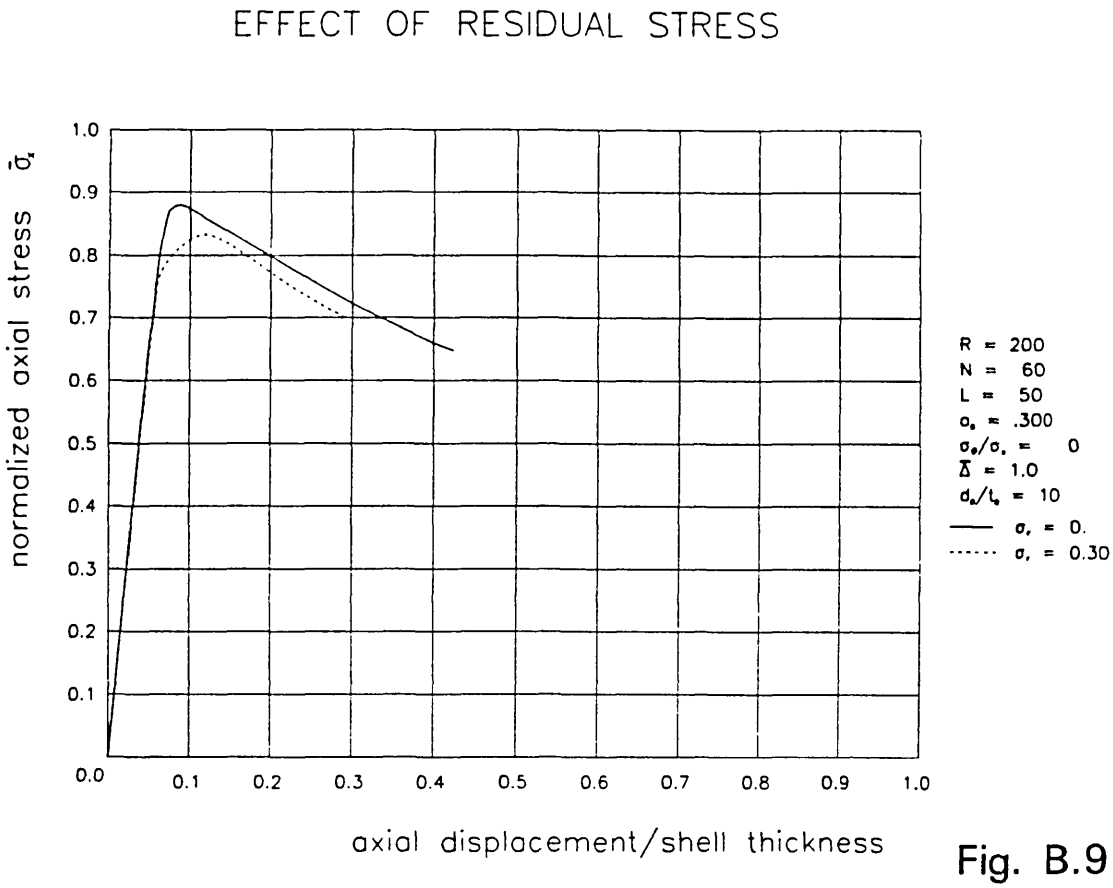


Fig. B.91

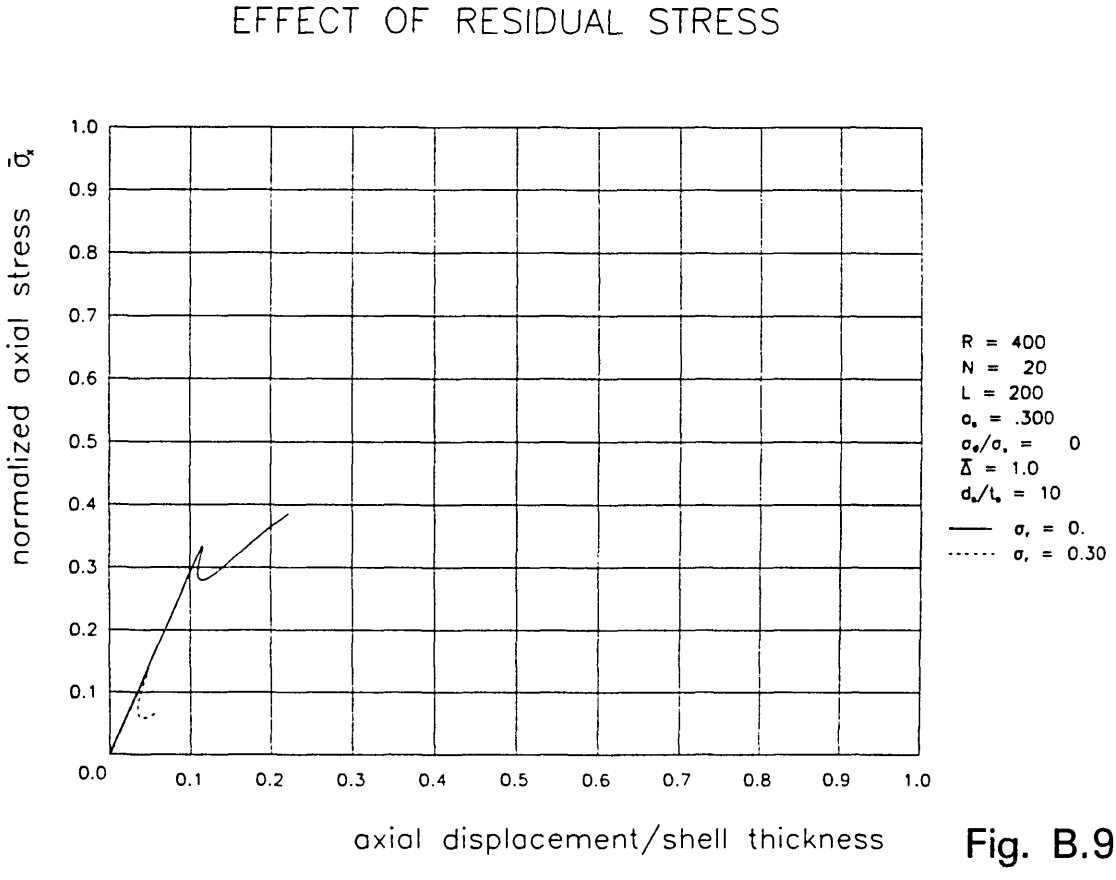


Fig. B.92

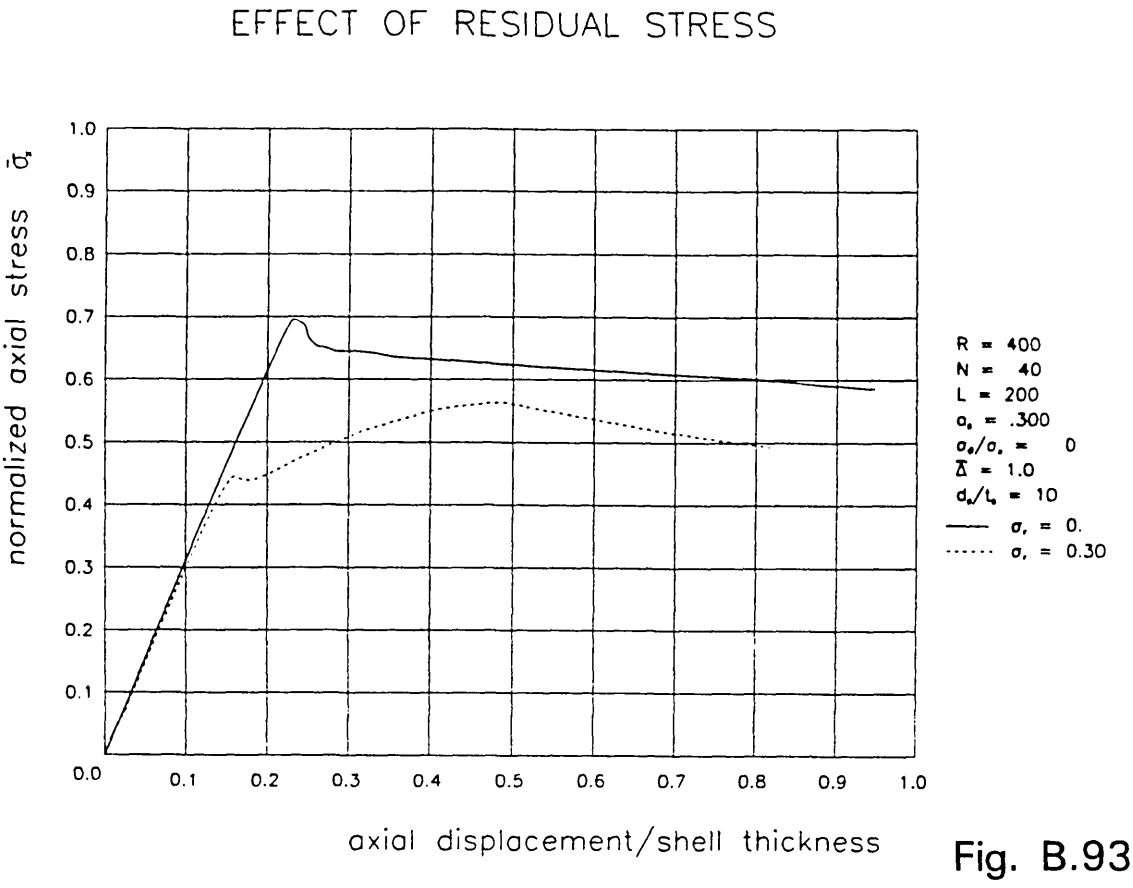


Fig. B.93

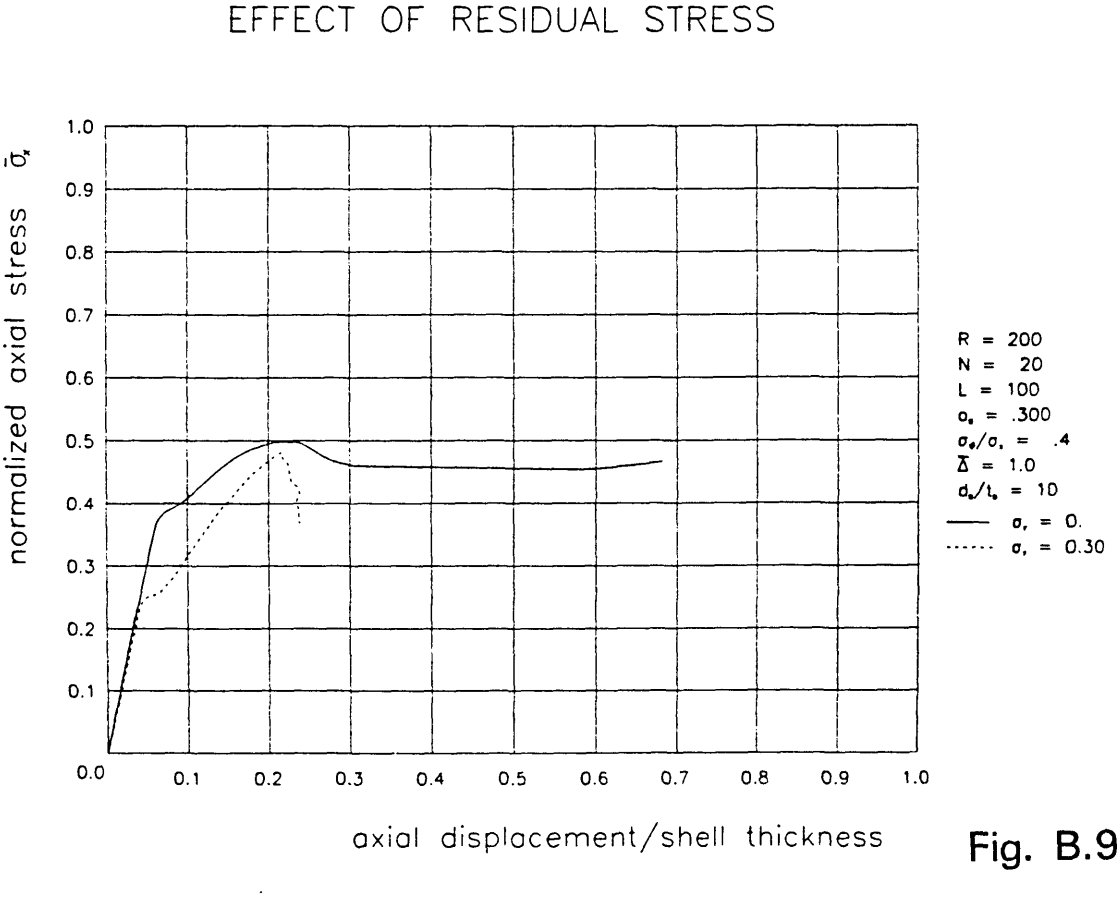


Fig. B.94

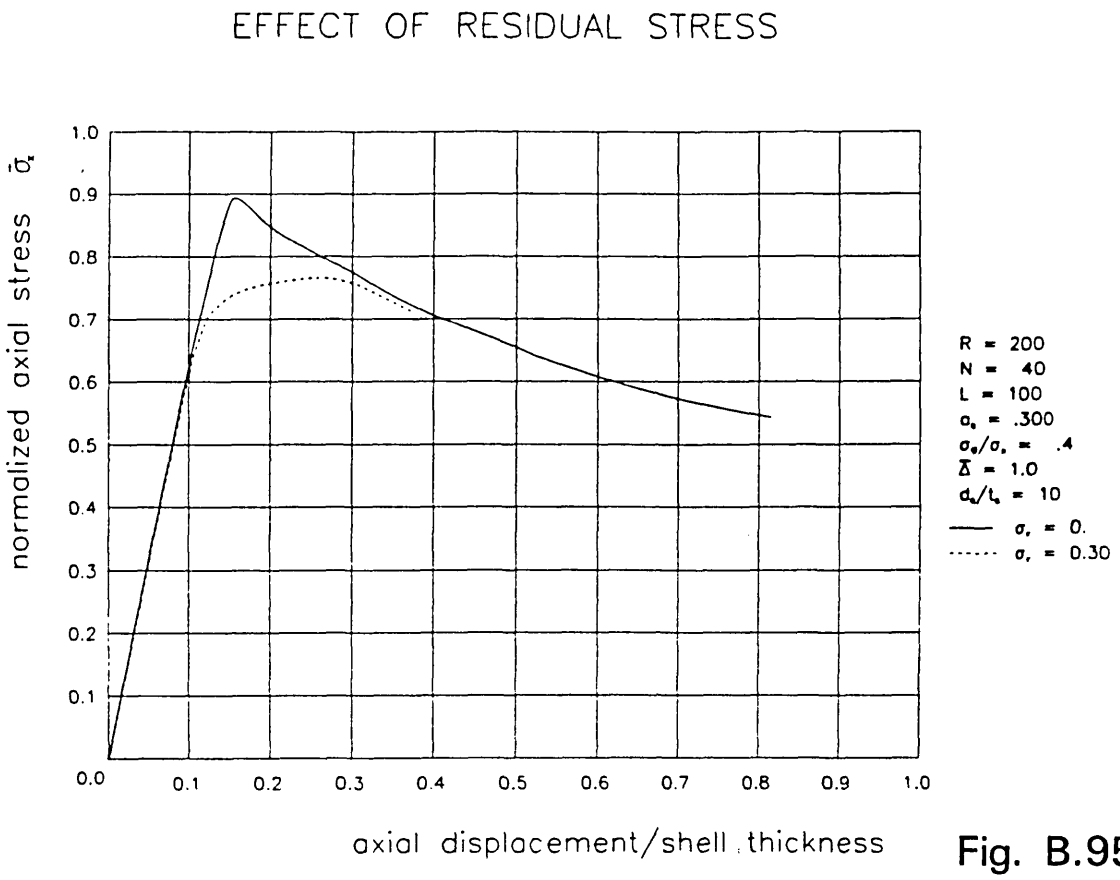


Fig. B.95

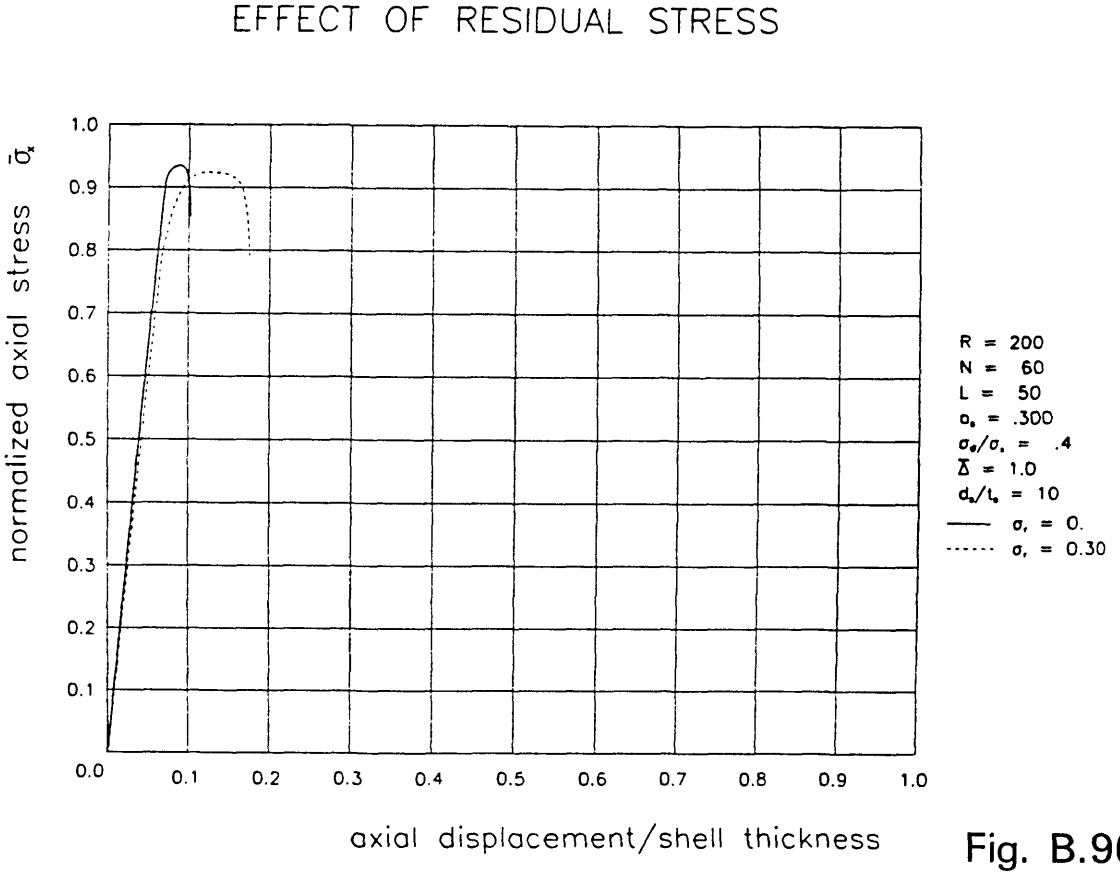


Fig. B.96

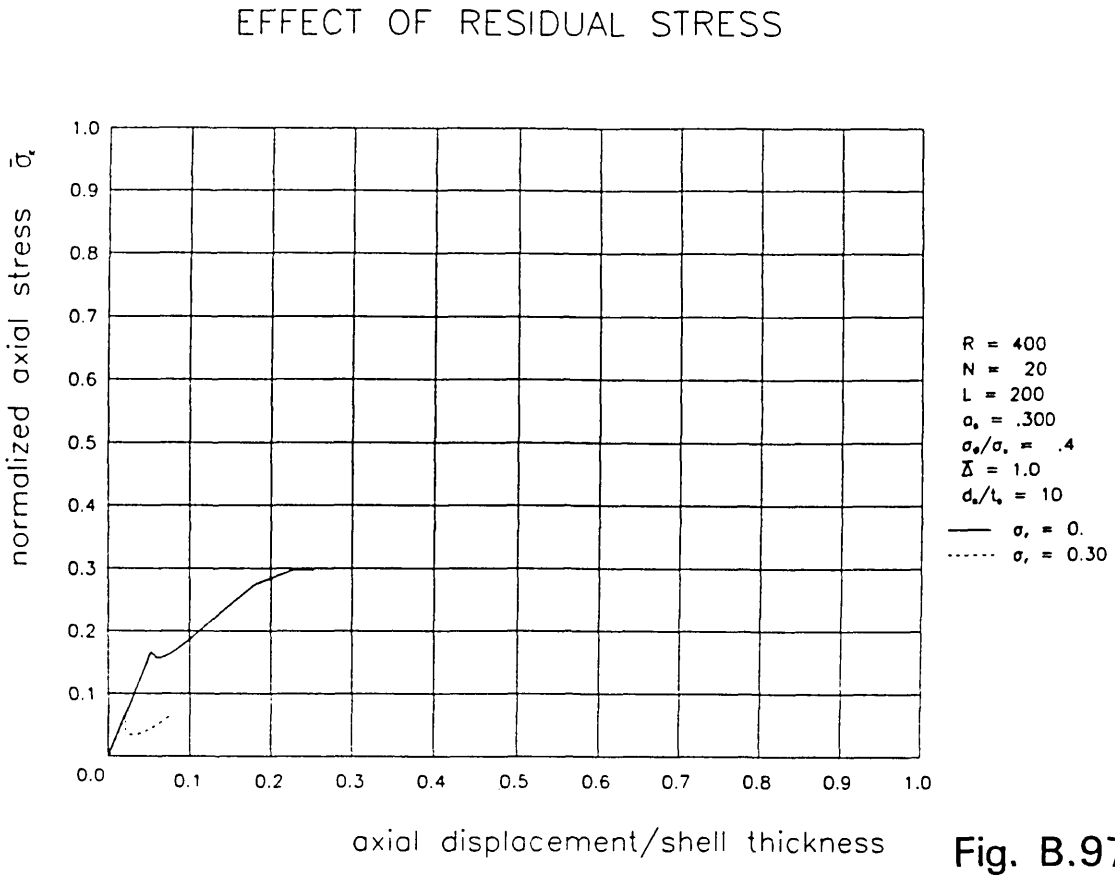


Fig. B.97

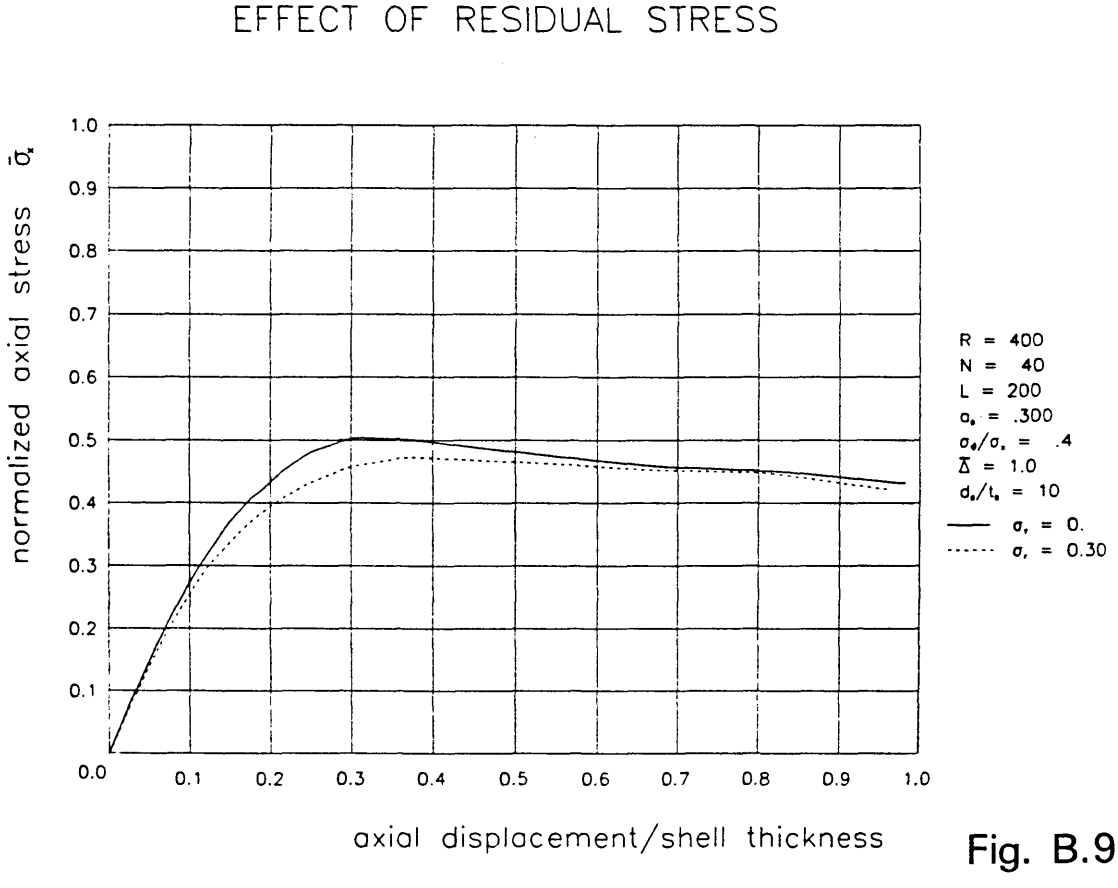


Fig. B.98

EFFECT OF RESIDUAL STRESS

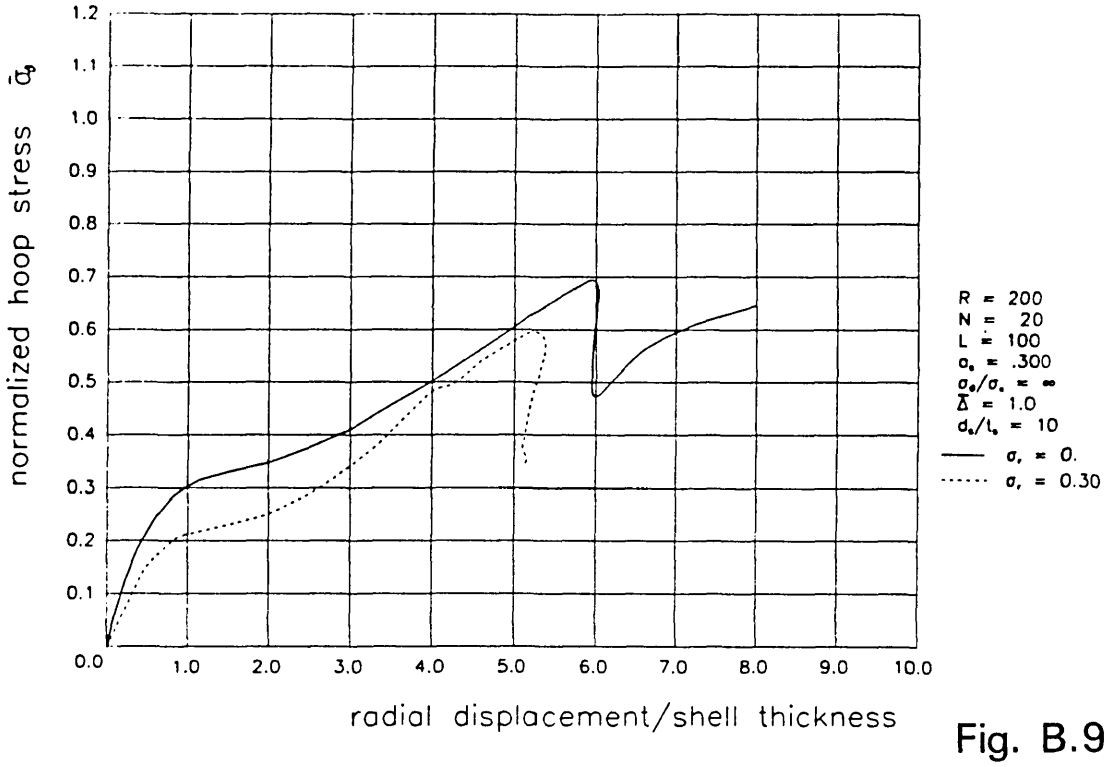


Fig. B.99

EFFECT OF RESIDUAL STRESS

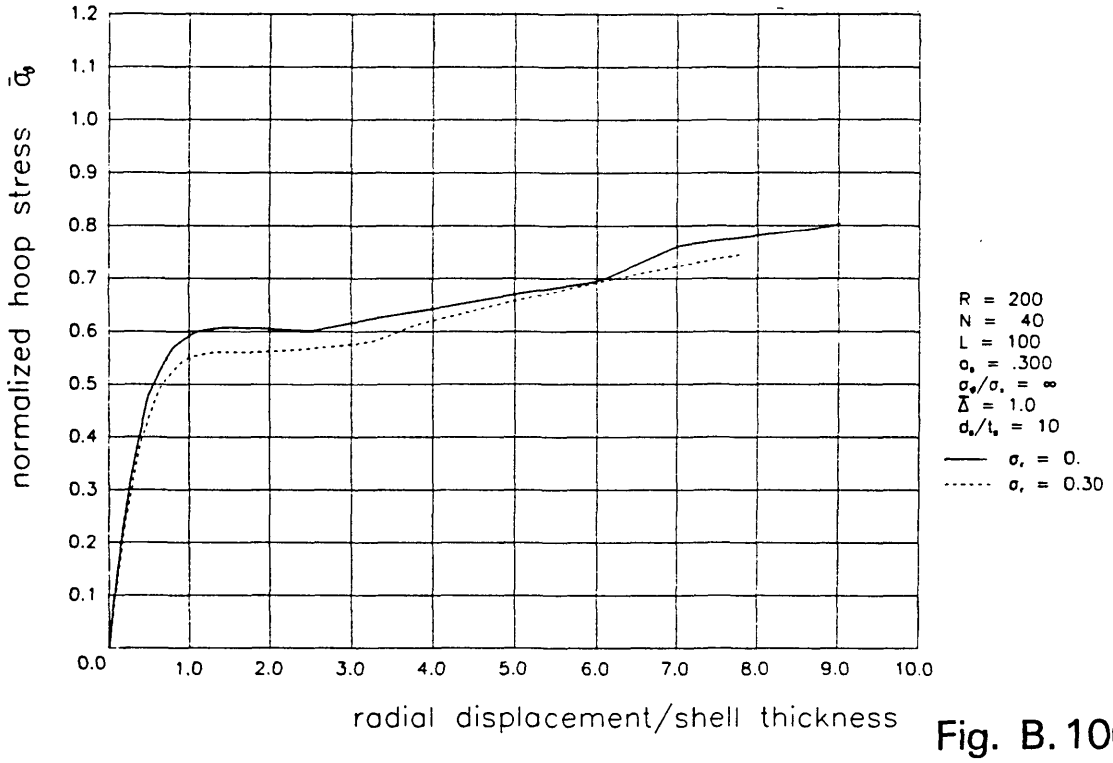


Fig. B.100

EFFECT OF RESIDUAL STRESS

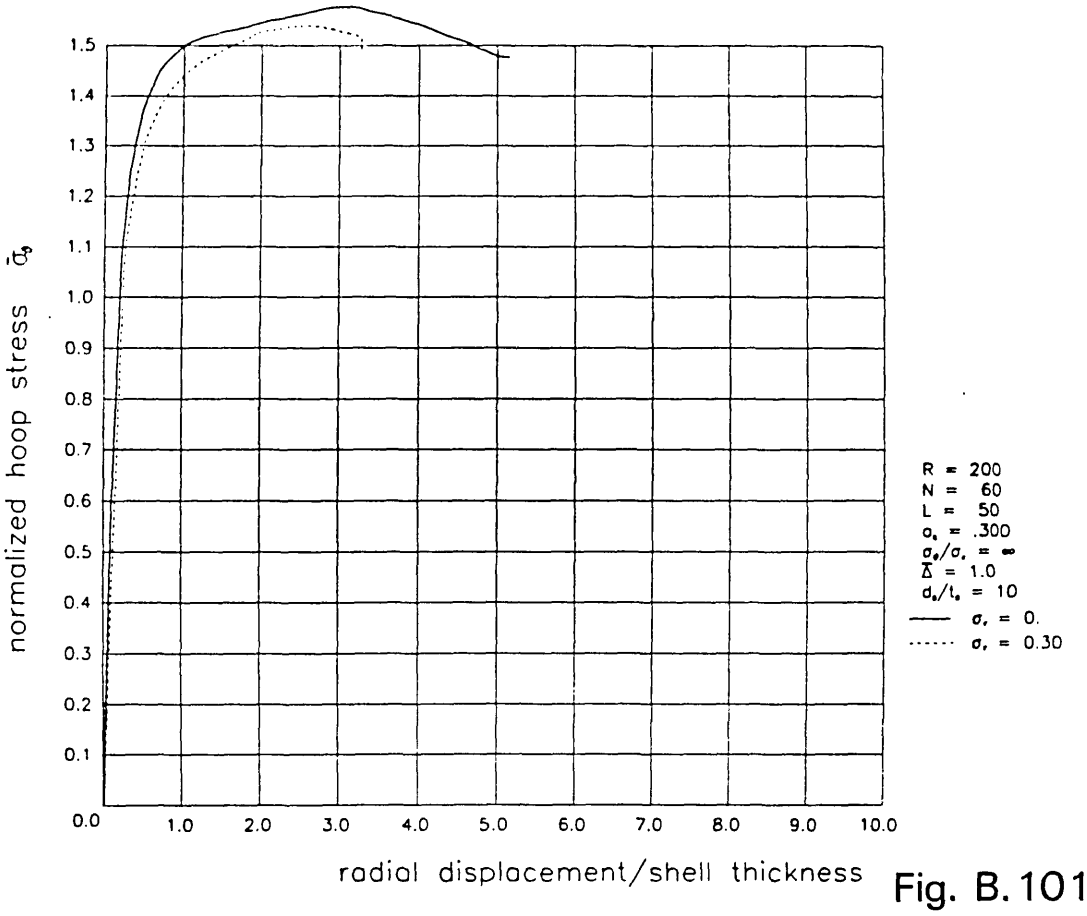


Fig. B.101

EFFECT OF RESIDUAL STRESS

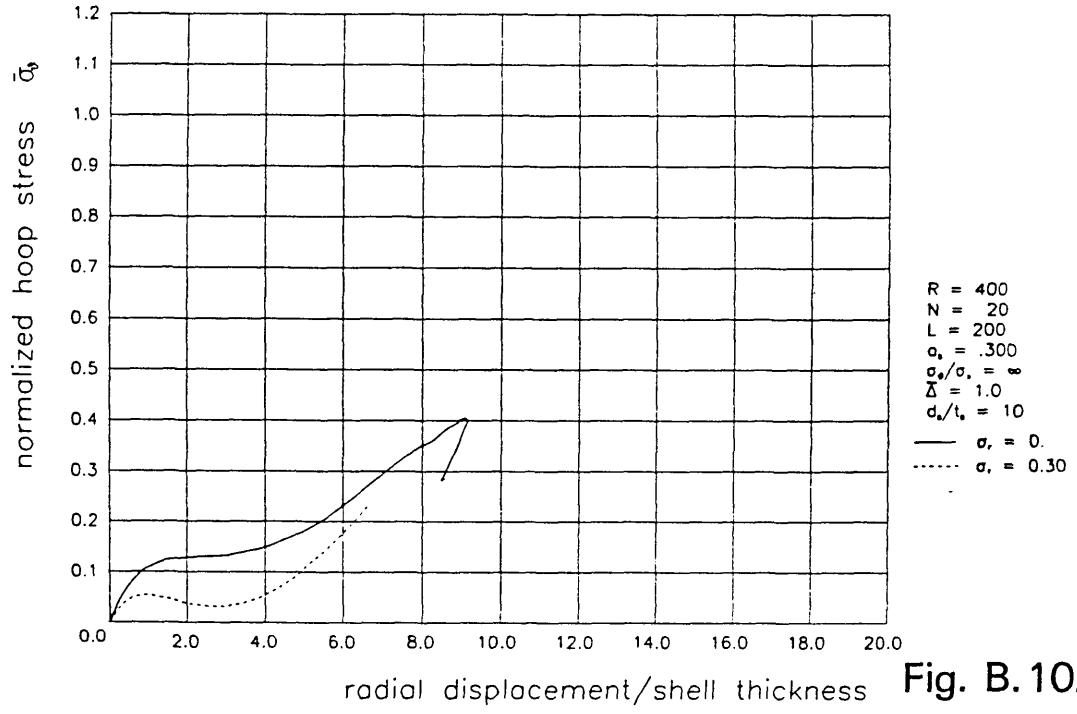


Fig. B.102

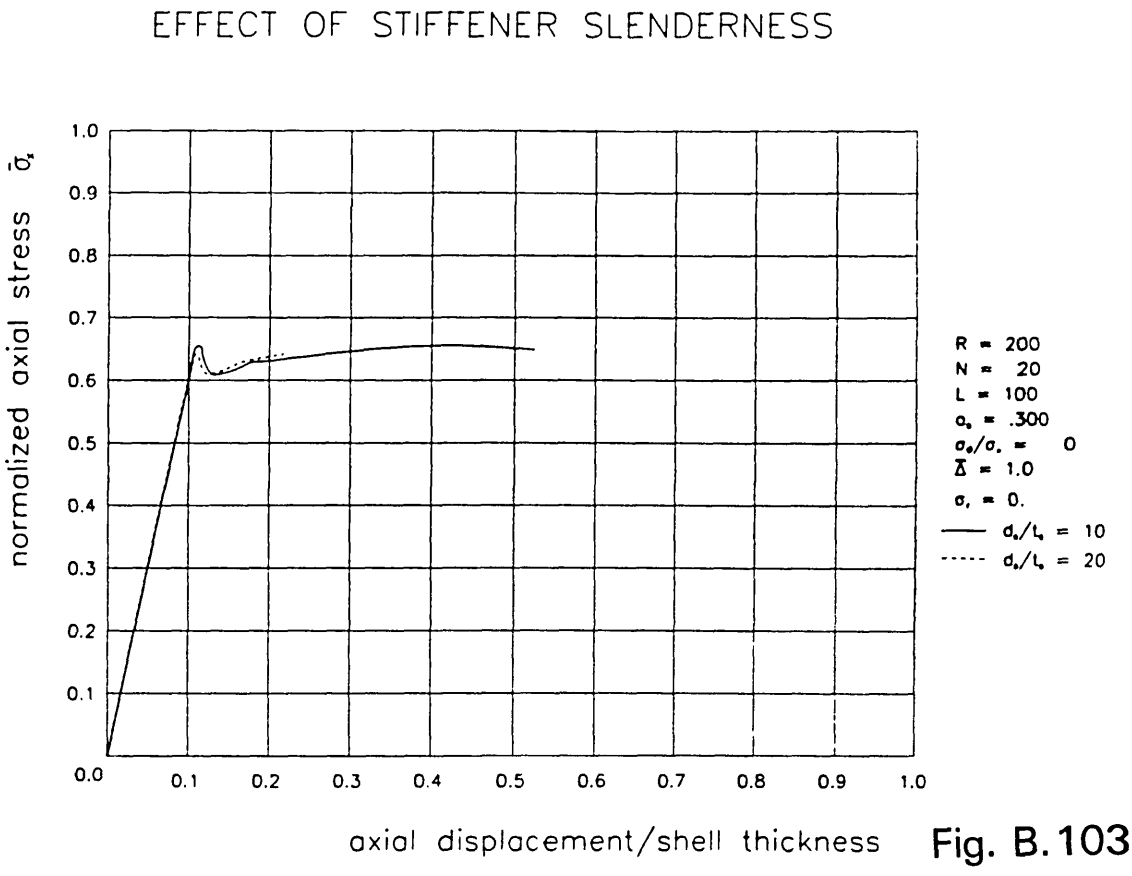


Fig. B.103

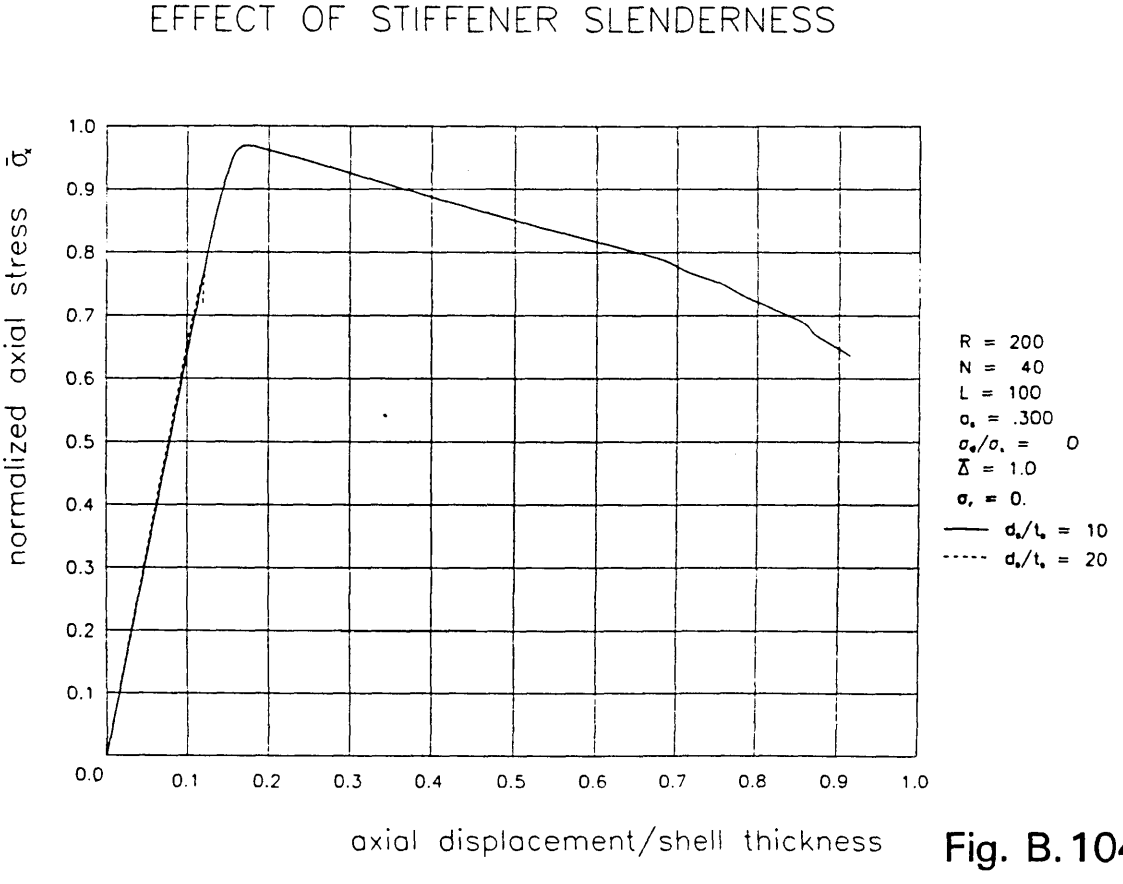


Fig. B.104

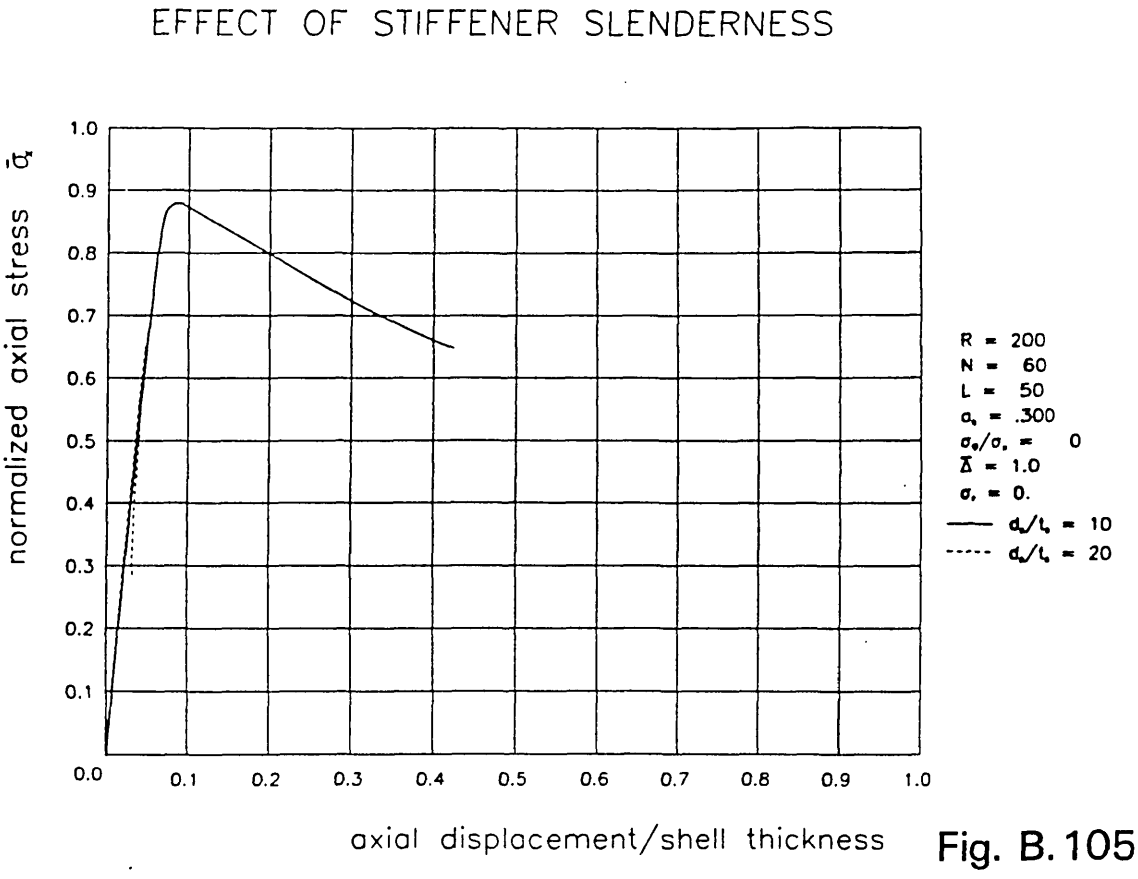


Fig. B.105

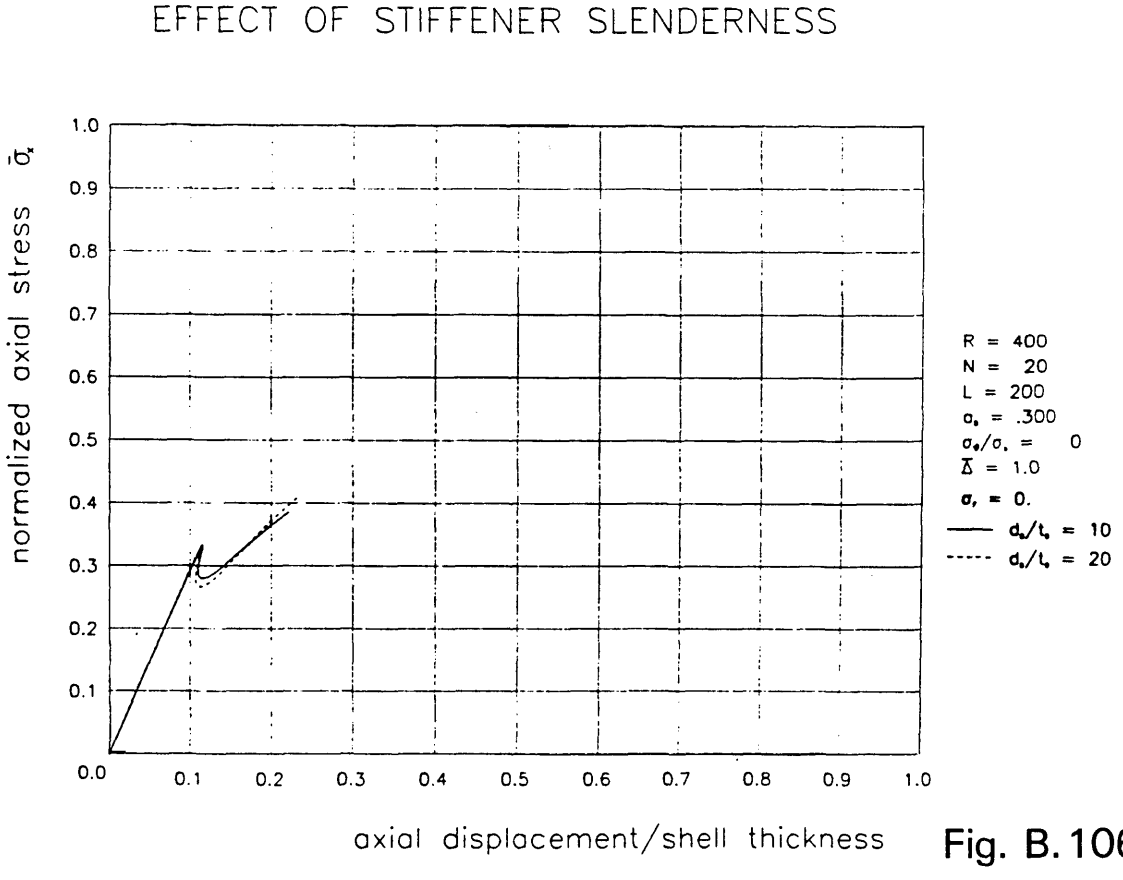


Fig. B.106

EFFECT OF STIFFENER SLENDERNESS

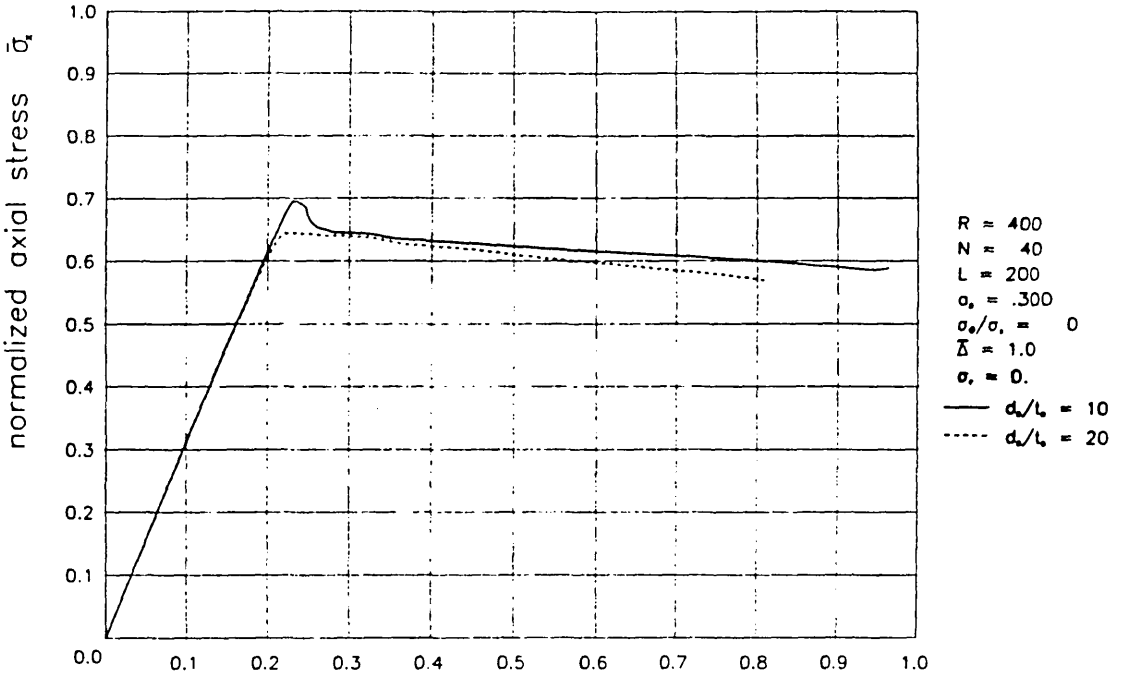


Fig. B.107

EFFECT OF STIFFENER SLENDERNESS

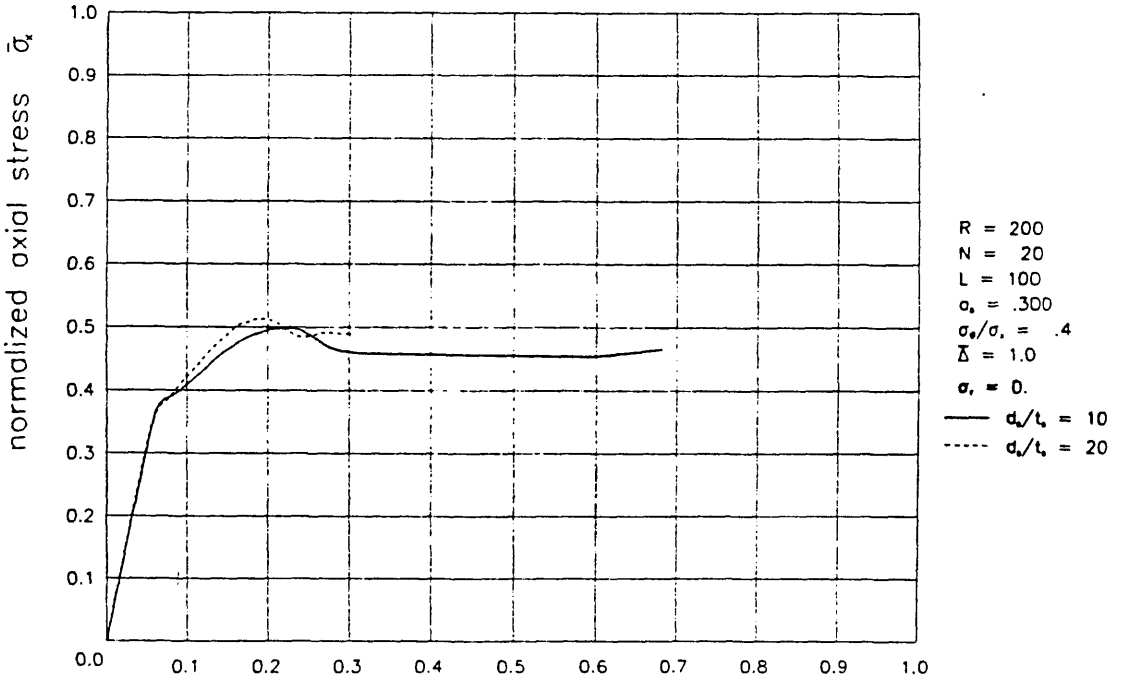


Fig. B.108

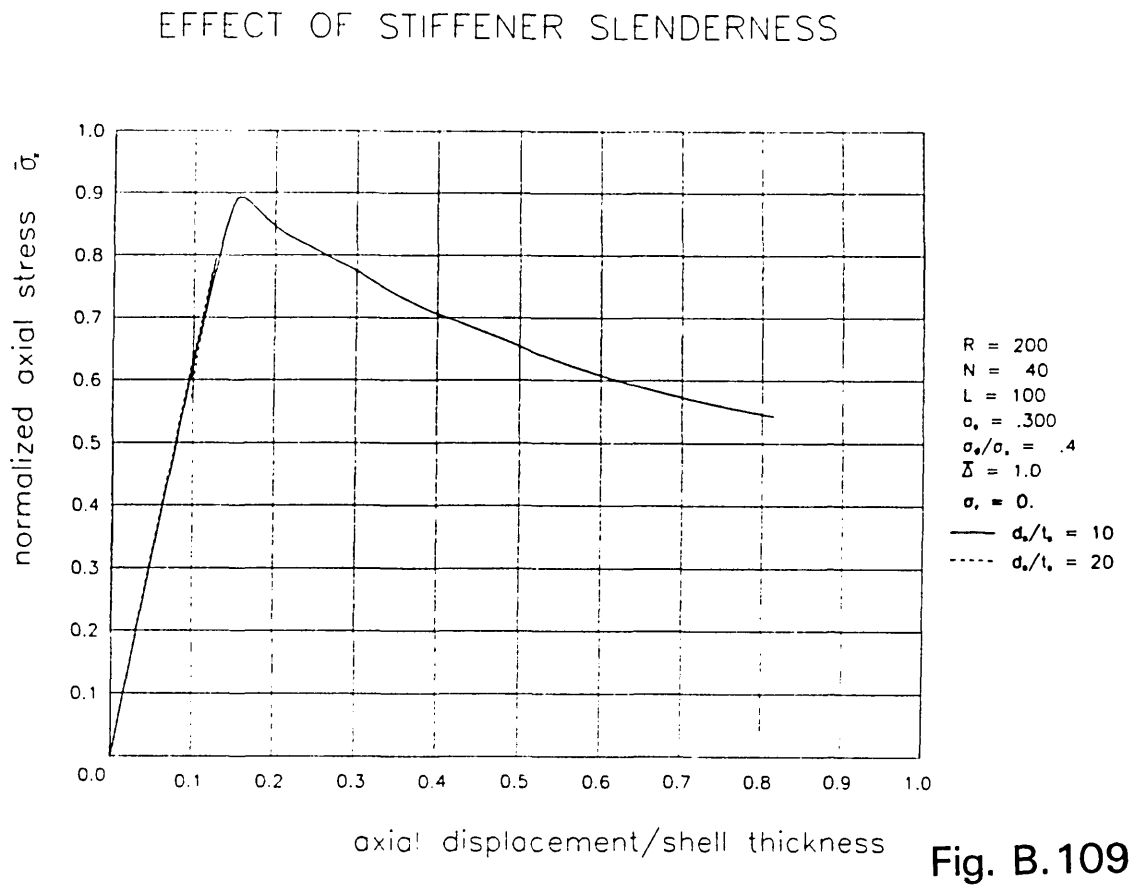


Fig. B.109

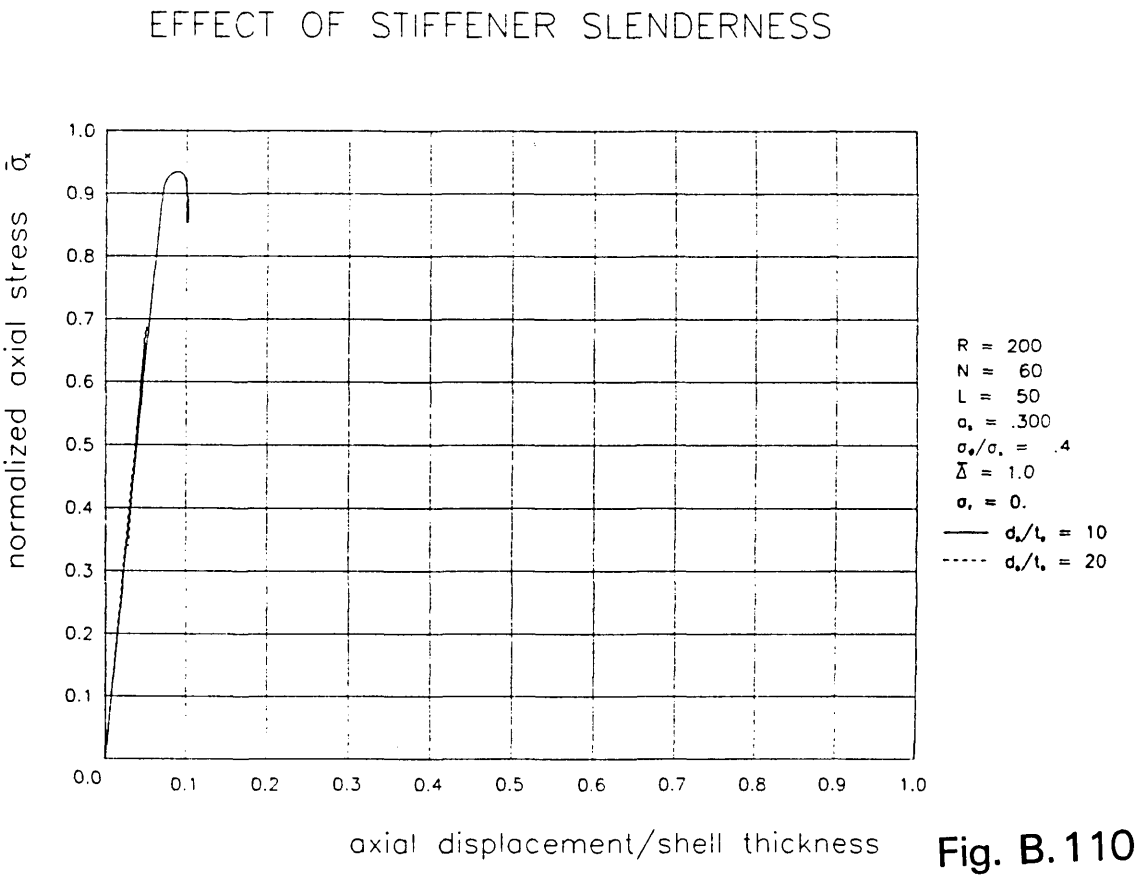


Fig. B.110

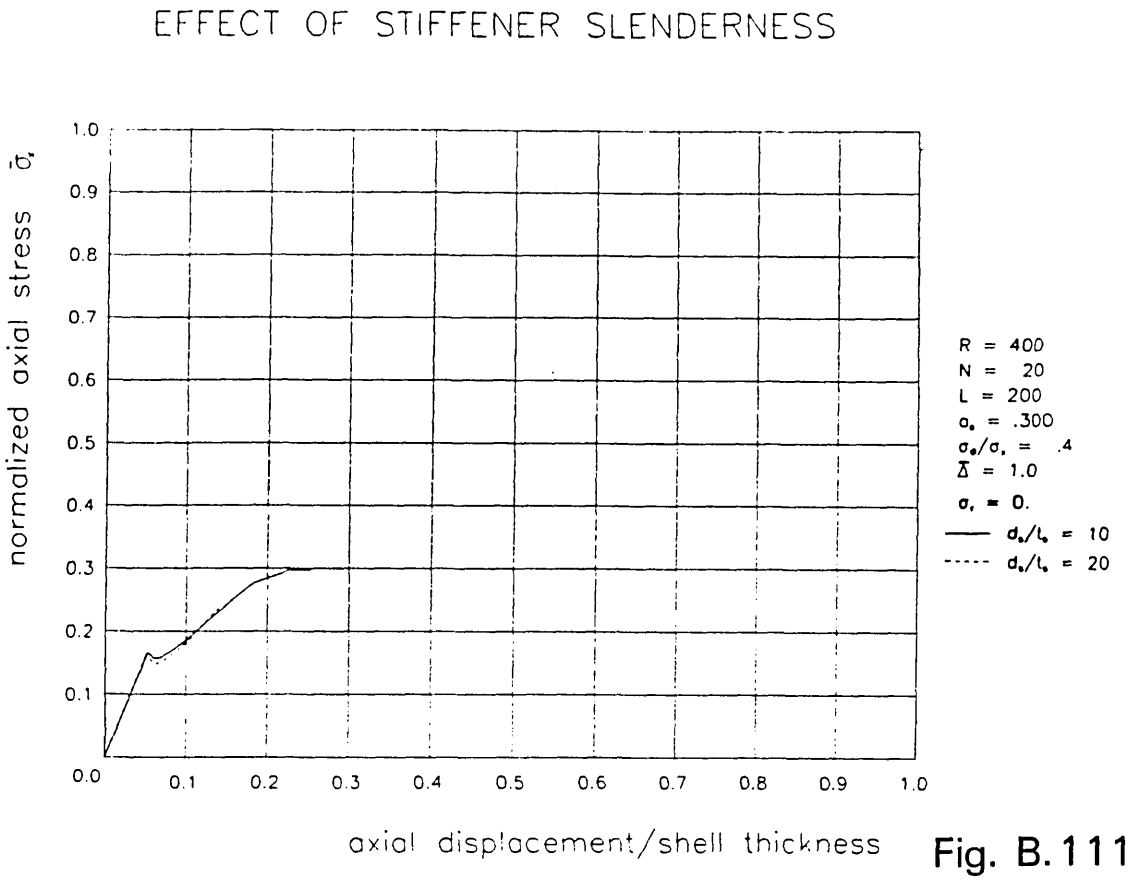


Fig. B.111

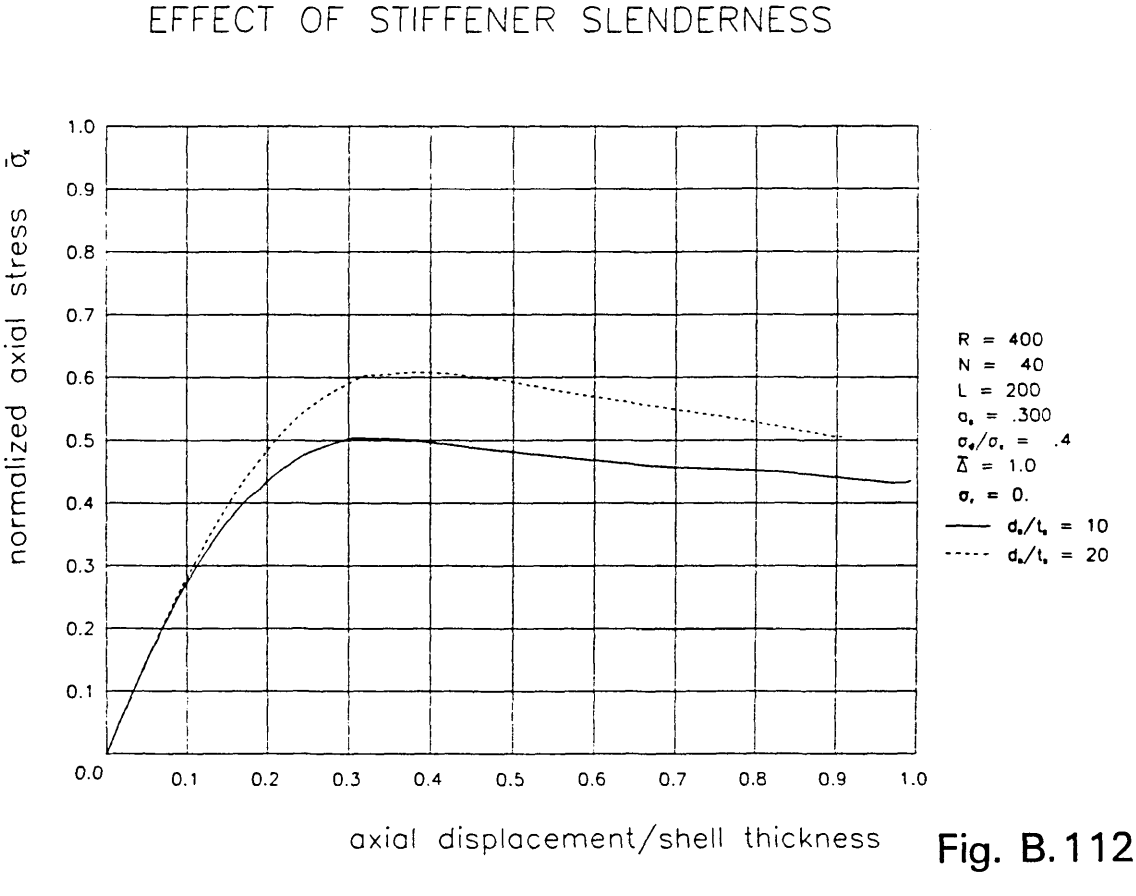


Fig. B.112

EFFECT OF STIFFENER SLENDERNESS

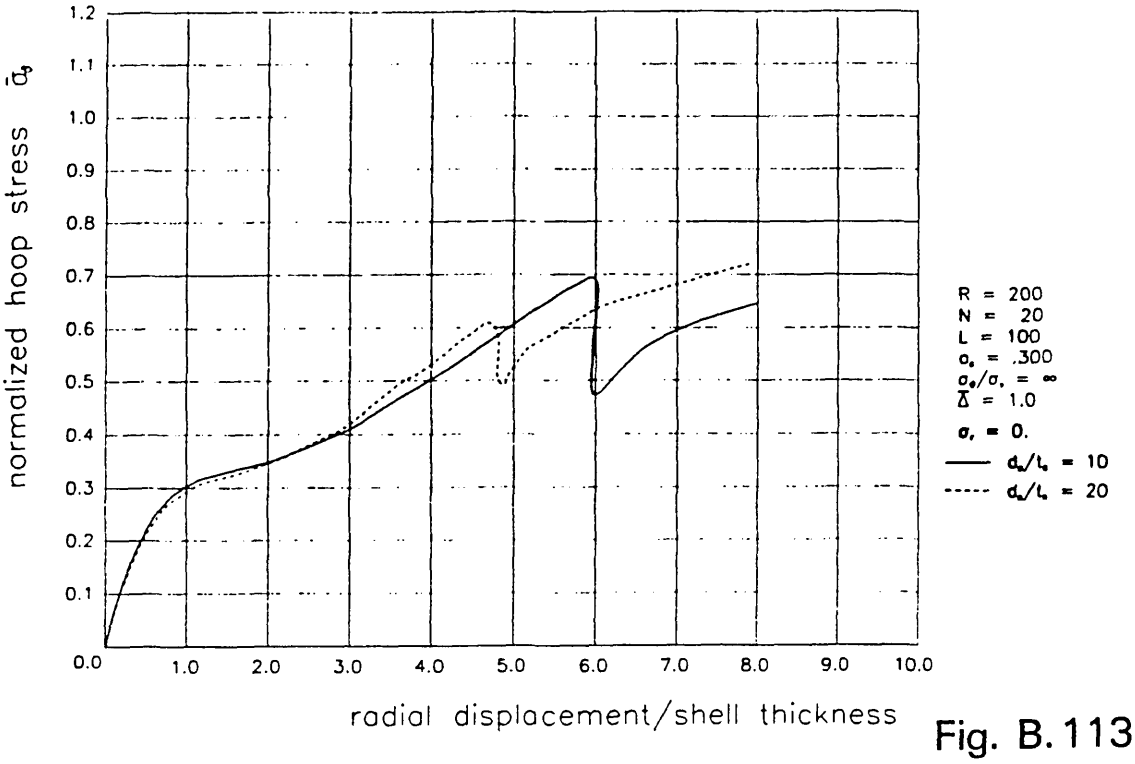


Fig. B.113

EFFECT OF STIFFENER SLENDERNESS

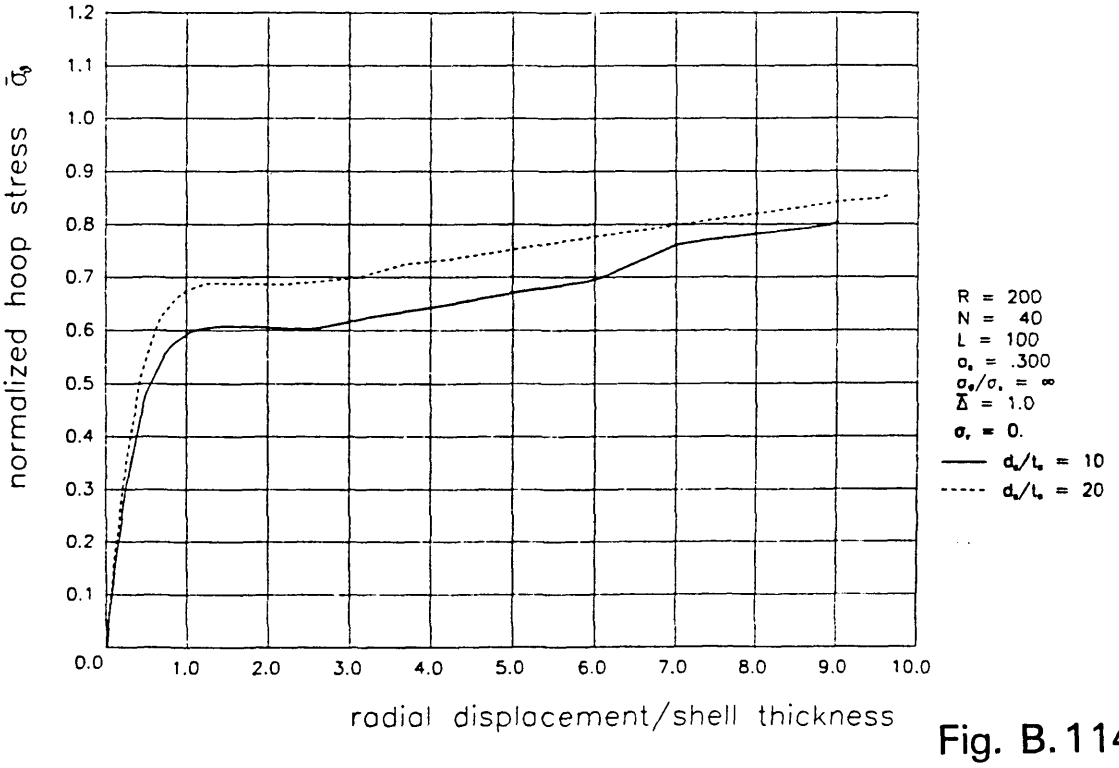


Fig. B.114

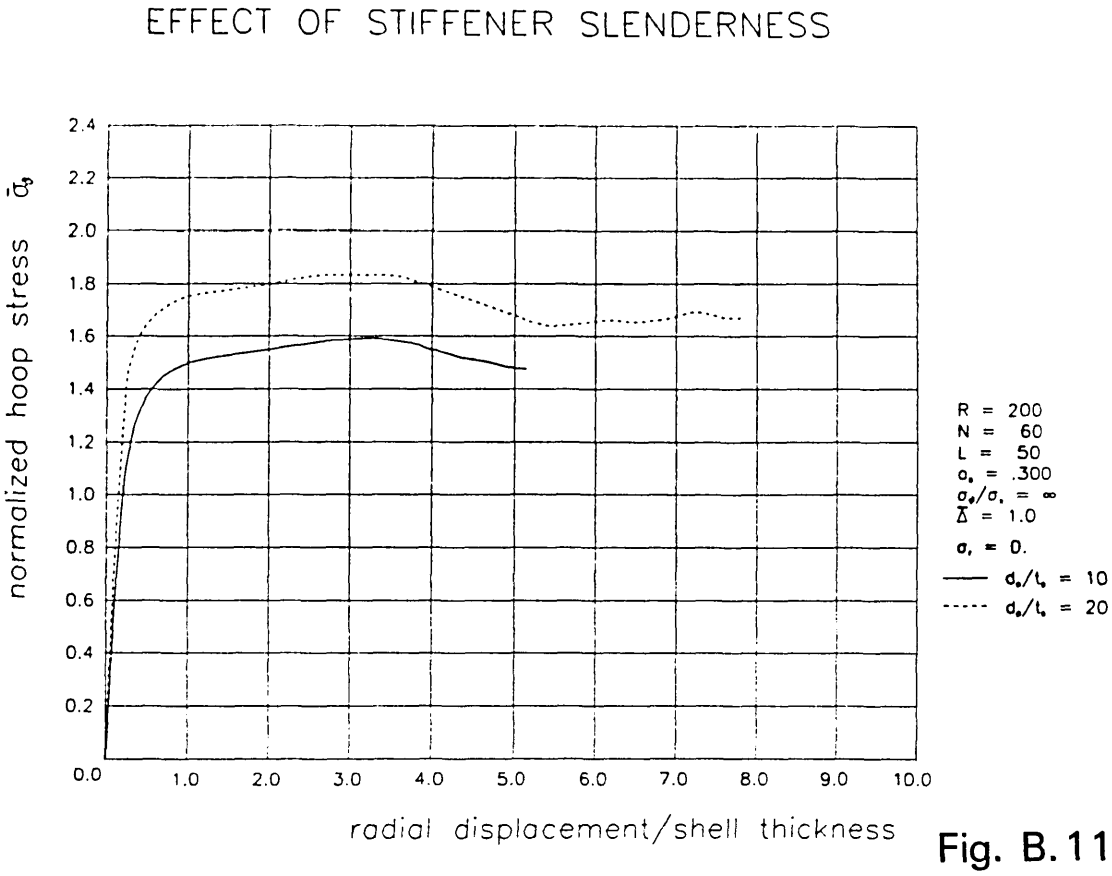


Fig. B.115

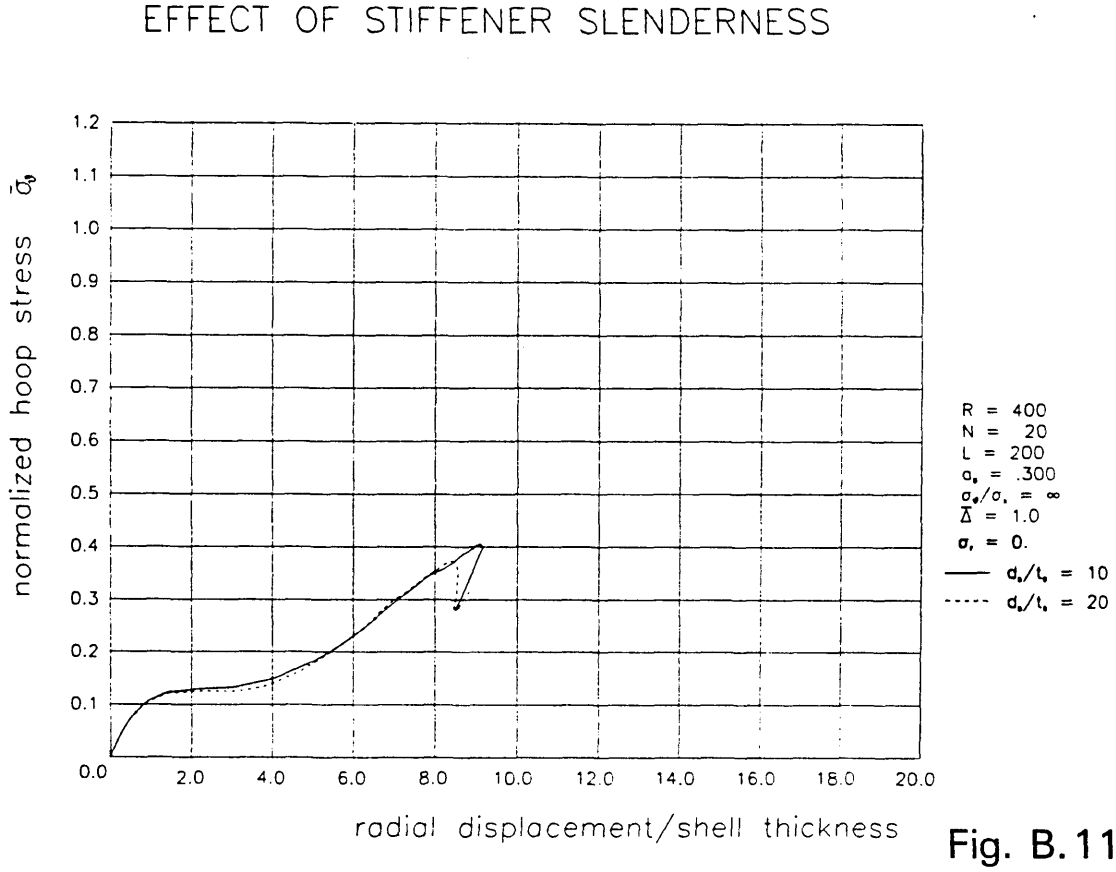


Fig. B.116

EFFECT OF STIFFENER SLENDERNESS

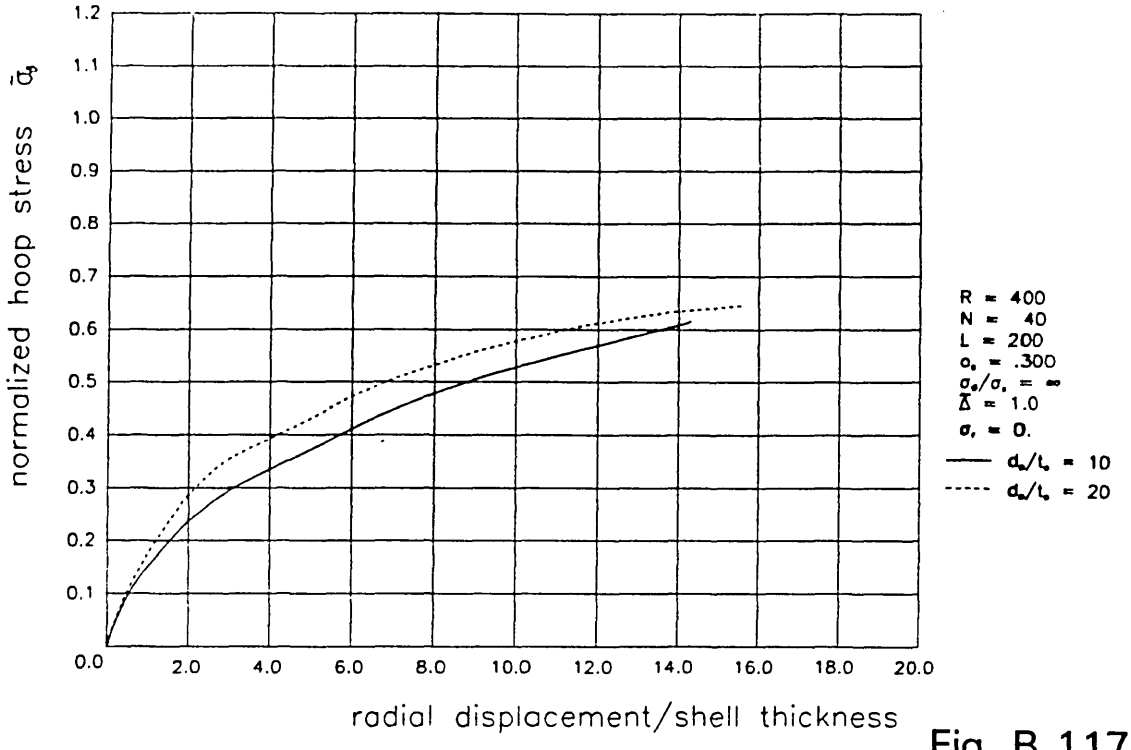


Fig. B.117

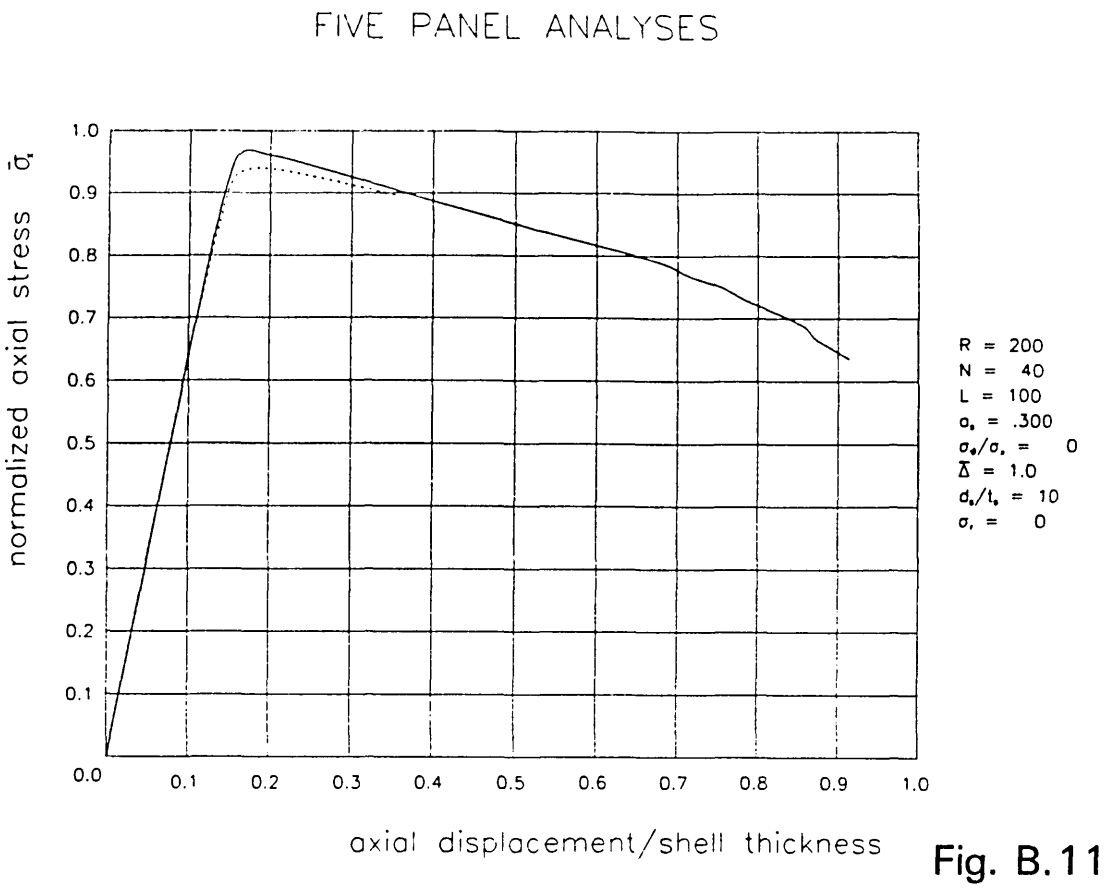


Fig. B.118

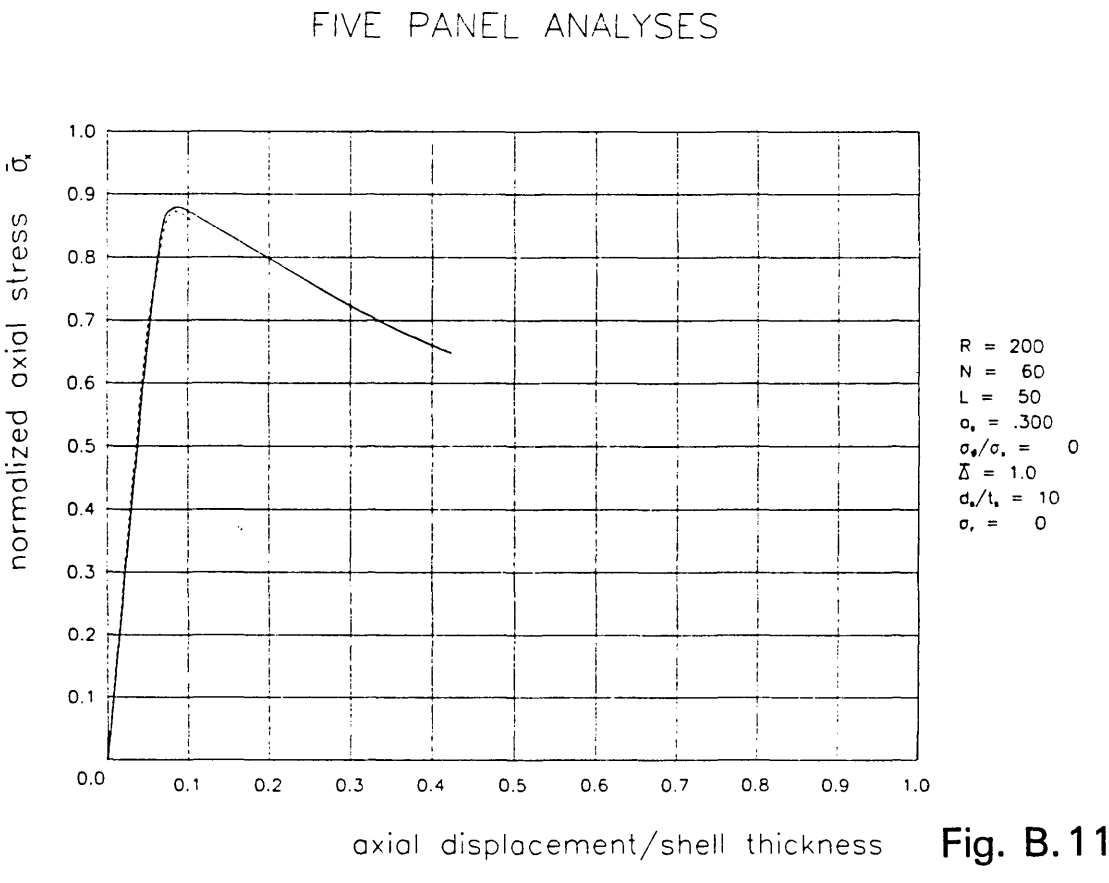


Fig. B.119

FIVE PANEL ANALYSES

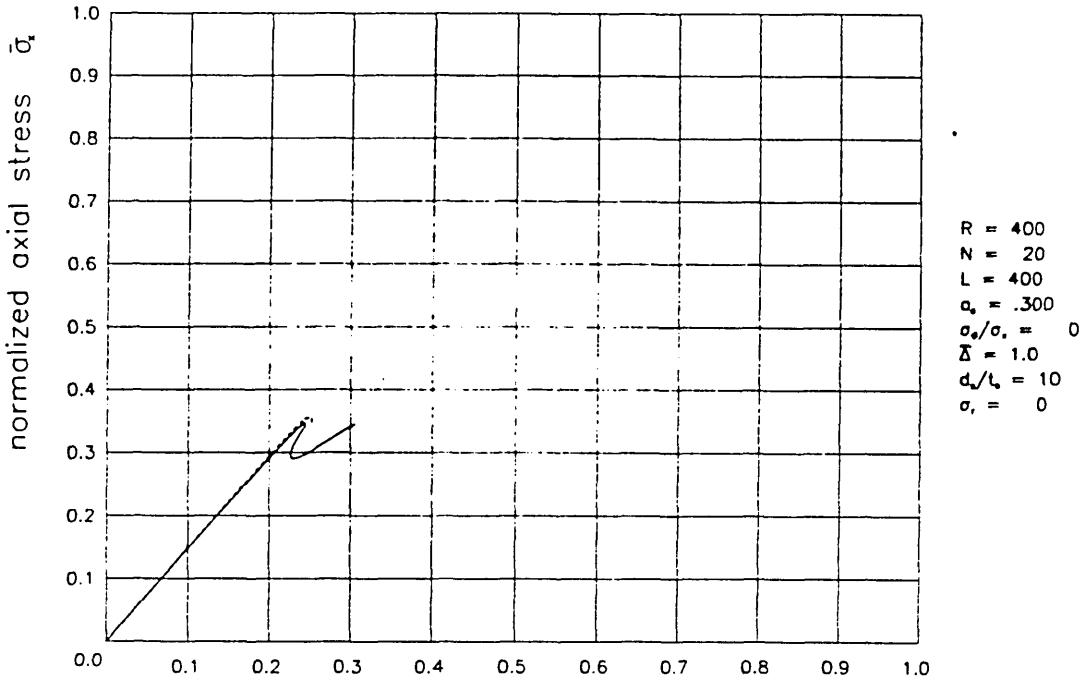


Fig. B.120

FIVE PANEL ANALYSES

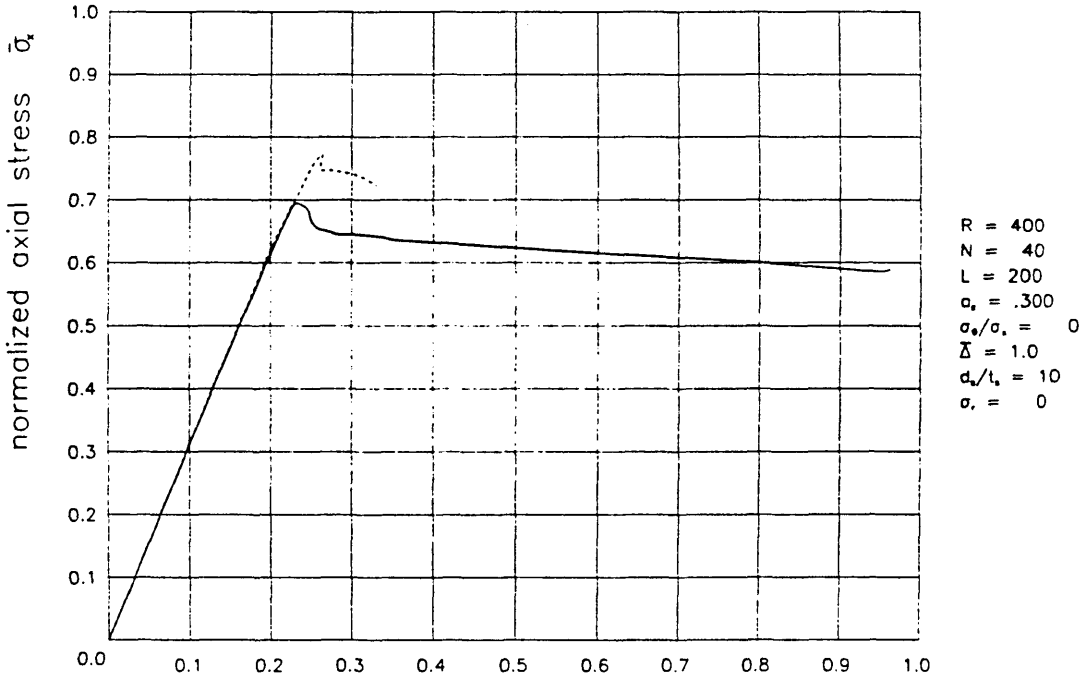


Fig. B.121

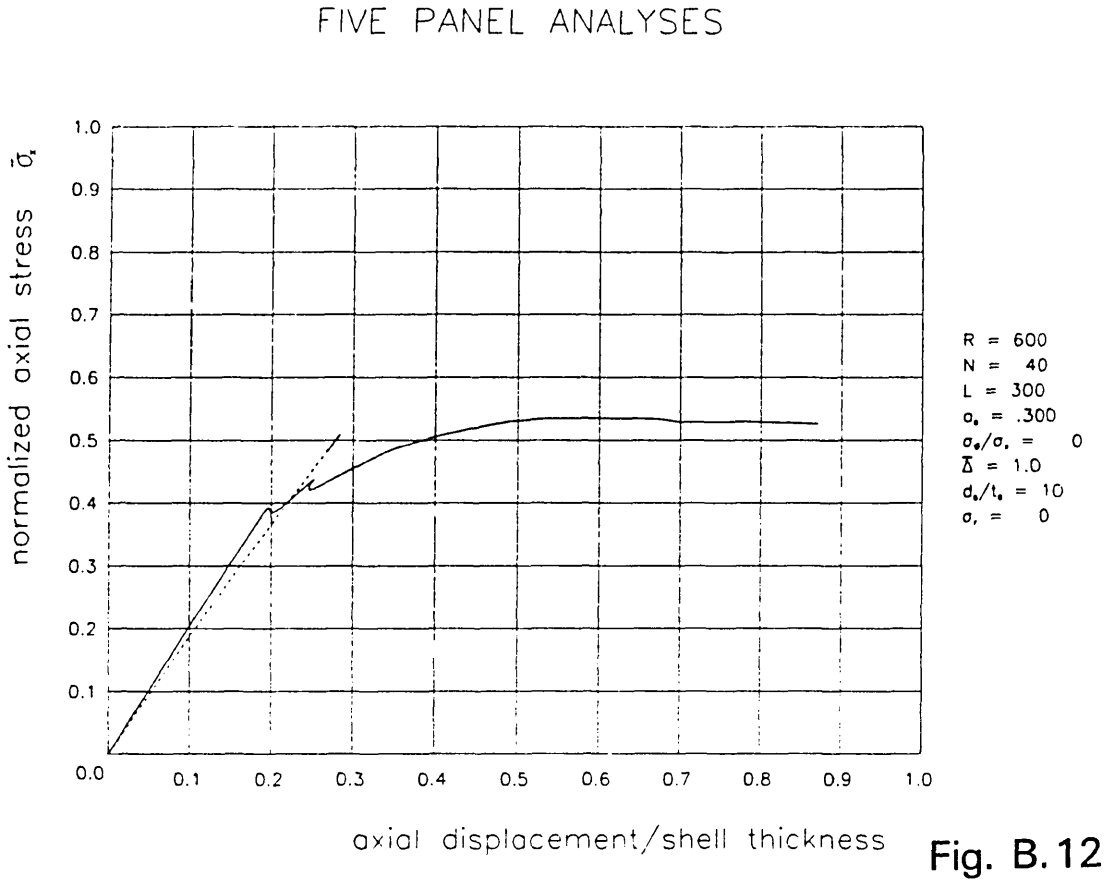


Fig. B.122

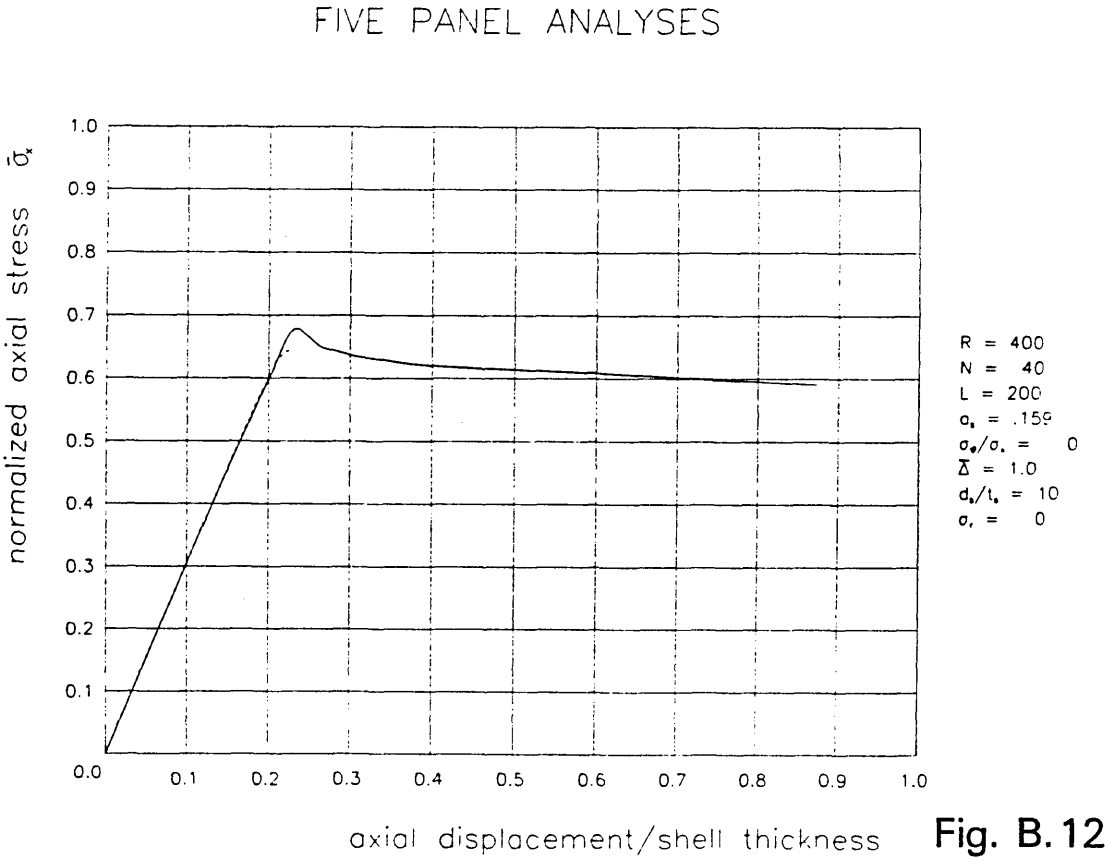


Fig. B.123

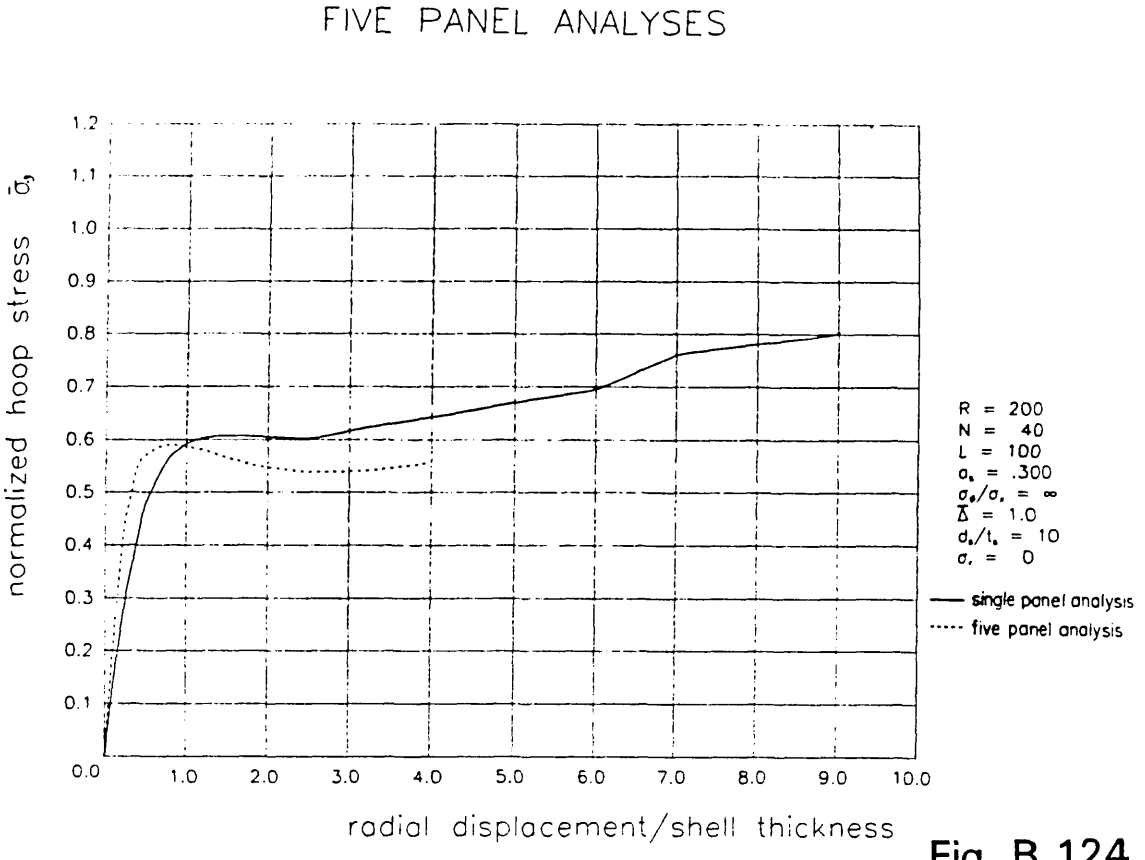


Fig. B.124

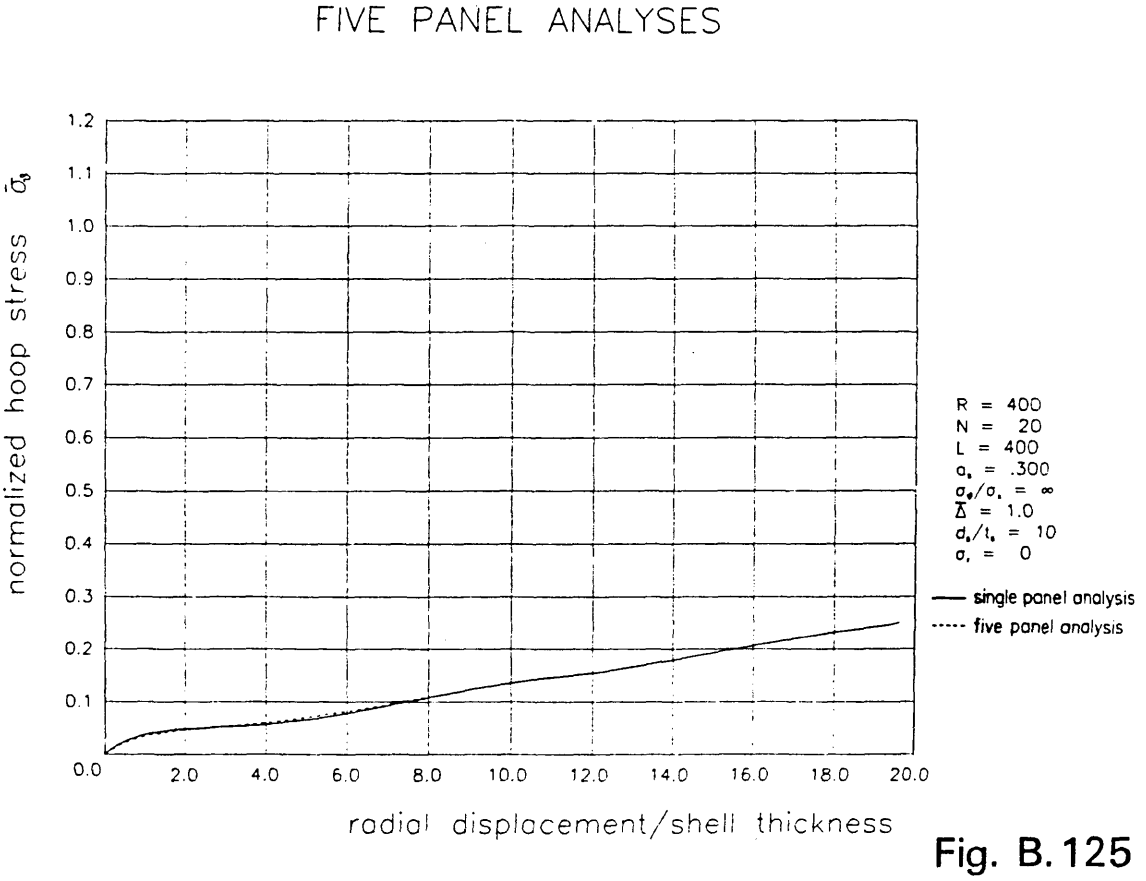


Fig. B.125

FIVE PANEL ANALYSES

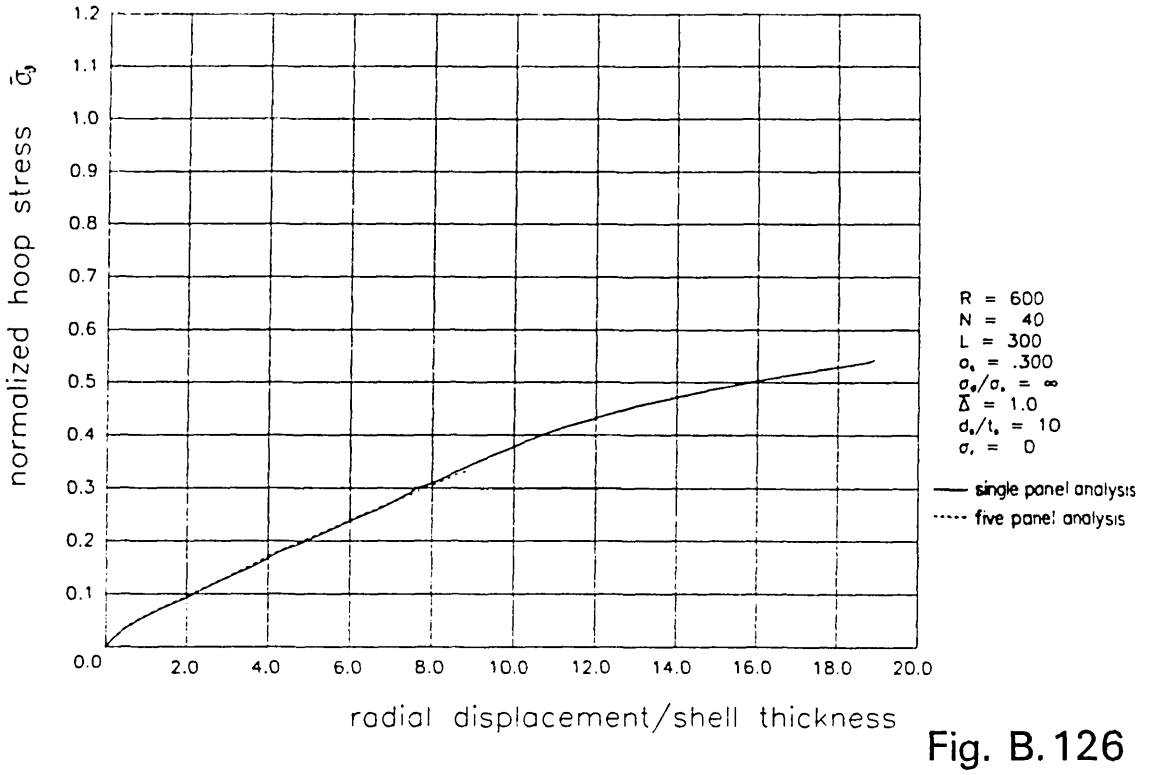
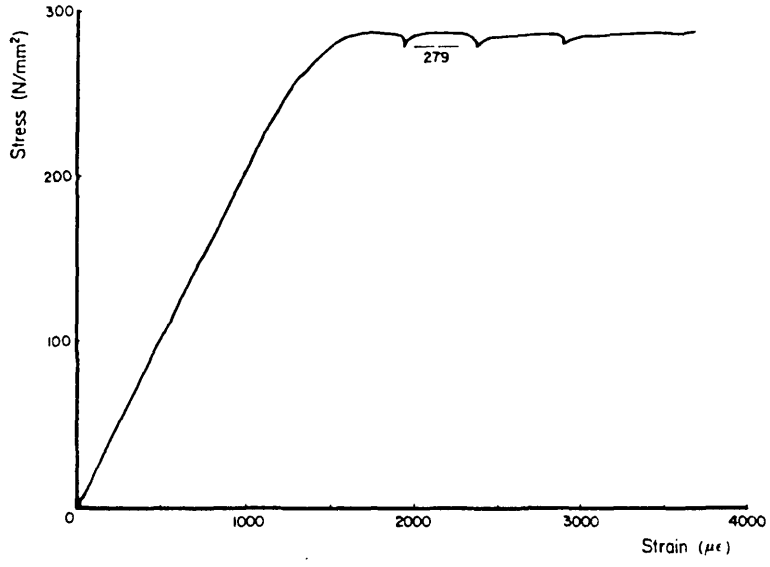


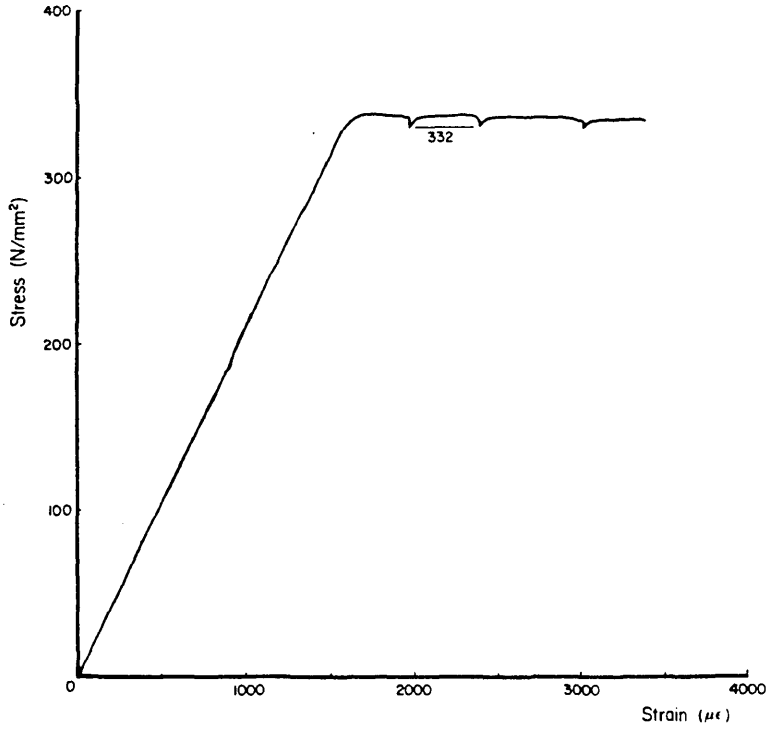
Fig. B.126

APPENDIX C

MATERIAL STRESS-STRAIN CURVES



TYPICAL STRESS-STRAIN CURVE – 3·53 mm SHEET



TYPICAL STRESS-STRAIN CURVE – 0·63 mm SHEET